

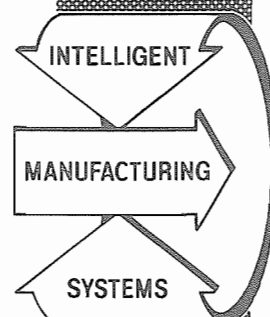
# Engineering Research Center for Intelligent Manufacturing Systems

## CHARACTERIZATION OF UHF FACTORY MULTIPATH CHANNELS

Theodore S. Rappaport  
Clare D. McGillem

TR - ERC 88-12  
June 1988

Schools of Engineering  
Purdue University  
West Lafayette, Indiana 47907





# **CHARACTERIZATION OF UHF FACTORY MULTIPATH CHANNELS**

*Theodore S. Rappaport and Clare D. McGillem*

*School of Electrical Engineering  
Purdue University  
West Lafayette, Indiana 47907*

**TR-ERC 88-12**

**A Technical Report for the  
Purdue Engineering Research Center for  
Intelligent Manufacturing Systems**

**June 1988**



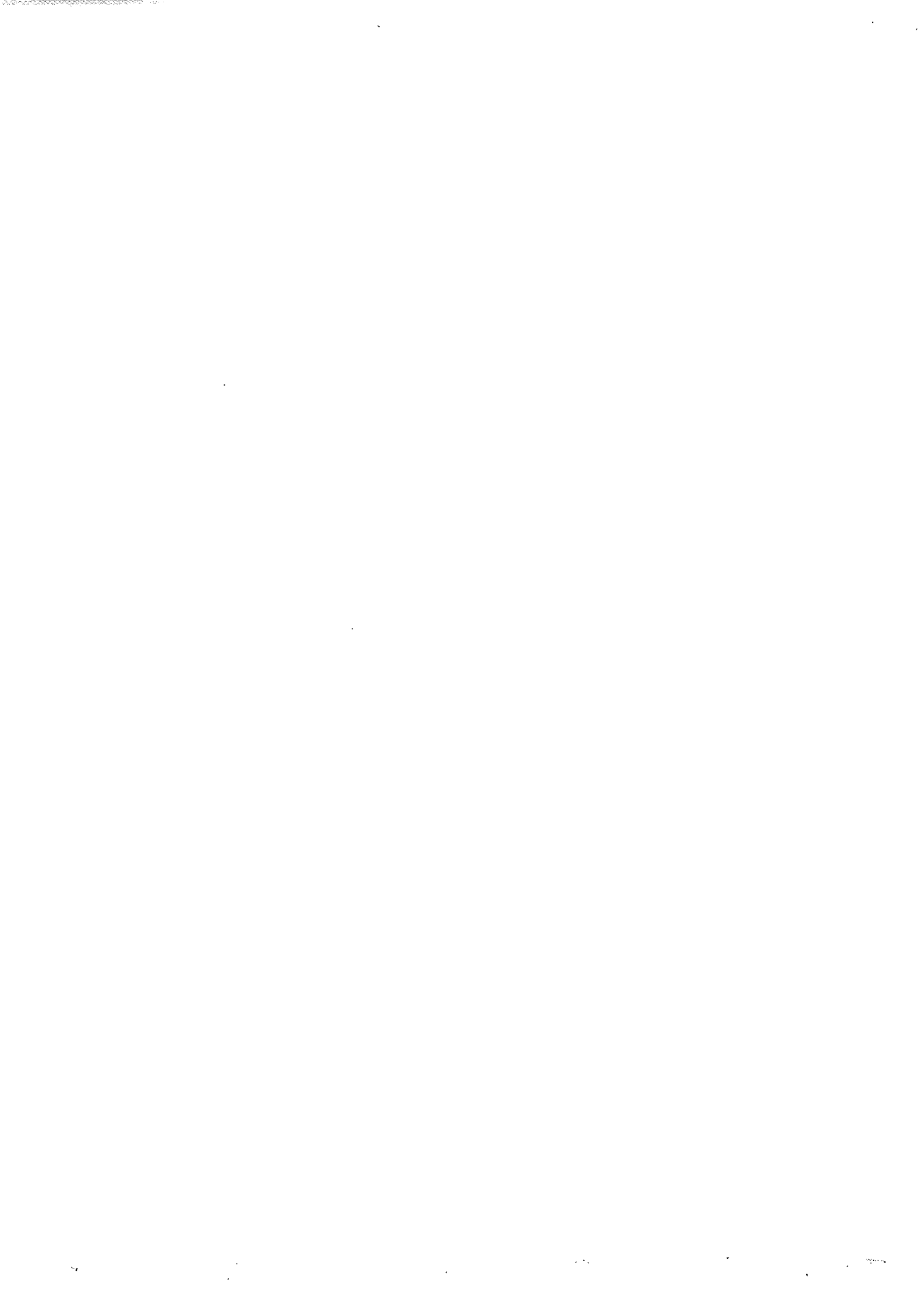
## TABLE OF CONTENTS

	Page
LIST OF TABLES .....	vi
LIST OF FIGURES.....	vii
ABSTRACT .....	xiii
CHAPTER I - INTRODUCTION .....	1
1.1 Definition of Problem.....	1
1.2 The Multipath Problem .....	4
1.2.1 Overview.....	4
1.2.2 Definition of Terms .....	10
1.3 Previous Work.....	12
1.4 Goals of this Work .....	18
CHAPTER 2 - EXPERIMENTAL DESIGN.....	22
2.1 Objective of Experiments .....	22
2.2 Development of Measurement Apparatus .....	24
2.3 Description of Factory Sites.....	32
2.4 Experimental Procedure.....	48
CHAPTER 3 - CHANNEL FORMULATION AND DATA REDUCTION ...	54
3.1 Impulse Response Model.....	54
3.1.1 Multipath Power Delay Model.....	54
3.1.2 CW Fading Model.....	58
3.2 Important Multipath Channel Parameters .....	62
3.3 Data Organization and Storage .....	65
3.3.1 File Handling .....	65
3.3.2 Data Processing .....	67

	Page
CHAPTER 4 - NARROW BAND MEASUREMENT RESULTS .....	73
4.1 Introduction.....	73
4.1.1 Detailed Description of Measurement Sites .....	74
4.2 Large Scale Path Loss .....	76
4.3 Shadowing .....	94
4.4 Small Scale Signal Fluctuations .....	97
4.5 Temporal Fading.....	109
CHAPTER 5 - WIDE BAND MEASUREMENT RESULTS.....	120
5.1 Introduction.....	120
5.1.1 Review of the Data .....	120
5.2 Large Scale Signal Attenuation.....	126
5.3 R.M.S. Delay Spread ( $\sigma$ ) and Mean Excess Delay ( $\bar{\tau}$ ).....	130
5.4 Impulse Response Statistical Model .....	149
5.4.1 Assumptions.....	152
5.4.2 Mean Square Value of Path Amplitudes .....	155
5.4.3 Distribution of Path Voltage Gains ( $\alpha_k$ 's).....	158
5.4.4 Using the Model.....	162
CHAPTER 6 - CONCLUSION.....	164
6.1 Summary .....	164
6.2 Possible Extensions of this Work .....	167
LIST OF REFERENCES.....	169
APPENDICES	
Appendix A -- Discone Design Using Simple N-Connector Feed.....	178
Appendix B -- Computer Programs.....	191
Appendix C -- CW Envelope Measurements .....	249
Appendix D -- Pulse Measurements - Raw Data.....	267
Appendix E -- Spatially Averaged Multipath Power Delay Profiles.....	376
Appendix F -- Spatial Fluctuations of Multipath over a Local Area.....	383
VITA .....	432

## LIST OF TABLES

Table	Page
4.1 Path loss exponent as function of factory site.....	83
4.2 Path loss exponent as function of geography.....	83
4.3 Path loss exponent as function of antenna position .....	92
4.4 Shadowing effects of some common factory equipment.....	96
4.5 Fading extremes from median level (10-25 m path).....	98
4.6 Fading extremes from median level (25-40 m path).....	98
4.7 Fading extremes from median level (40-75 m path).....	98
5.1 R.M.S. delay spread data (10-25 m path) .....	133
5.2 R.M.S. delay spread data (25-40 m path) .....	133
5.3 R.M.S. delay spread data (40-75 m path) .....	133
5.4 Mean excess delay data (10-25 m path) .....	134
5.5 Mean excess delay data (25-40 m path) .....	134
5.6 Mean excess delay data (40-75 m path) .....	134
A1.1 Antenna cone dimensions.....	181





## LIST OF FIGURES

Figure	Page
1.1 Communication system performance for typical multipath channels .....	5
1.2 Geometry of scattering channel.....	6
1.3 Experimental data: probability of path occupancy .....	14
1.4 Signal fading as a function of receiver antenna height.....	17
1.5 Set-up for wide band building multipath measurements .....	19
1.6 Graphical representation of two-tier indoor multipath model.....	20
2.1 Block diagram of factory multipath measurement system .....	25
2.2 Transmitted multipath probing pulse .....	28
2.3 Power spectrum envelope of multipath probing pulse .....	28
2.4 Transfer function of narrow band receiver cascade.....	30
2.5 Factory multipath measurement apparatus .....	31
2.6 Site B: Food Processing Plant, multi floor structure .....	33
2.7 Site C: Engine Manufacturing Plant, new single floor structure .....	33
2.8 Site D: Aluminum Manufacturing Facility, single floor structure.....	34
2.9 Site E: Casting Foundry, single floor structure.....	34

Figure	Page
2.10 Site F: Engine Machine and Assembly Shop, single floor structure .....	35
2.11 Layout of factory site B .....	37
2.12 Floor layout of site C .....	39
2.13 Floor layout of site D .....	42
2.14 Floor layout of site E.....	43
2.15 Floor layout of site F.....	47
2.16 Example of LOS light clutter geography.....	50
2.17 Example of LOS heavy clutter geography.....	50
2.18 Example of obstructed path light clutter geography .....	51
2.19 Example of obstructed path heavy clutter geography .....	51
3.1 Linear channel models for multipath channel.....	55
3.2 Cumulative Rayleigh, Rician and log-normal distributions .....	61
3.3 Performance curves for DPSK in fading channels .....	63
3.4 File naming system for raw data .....	66
3.5 Listing of raw data files from Site C.....	66
3.6 An example of raw data format (eb2ac).....	68
3.7 Flow chart of data processing.....	69
4.1 Large scale path loss at site B.....	77
4.2 Large scale path loss at site C.....	78
4.3 Large scale path loss at site D.....	79
4.4 Large scale path loss at site E.....	80
4.5 Large scale path loss at site F .....	81

Figure	Page
4.6 Large scale path loss at all sites .....	82
4.7 Large scale path loss in LOS light clutter paths .....	85
4.8 Large scale path loss in LOS heavy clutter paths .....	86
4.9 Large scale path loss in obstructed light clutter paths .....	87
4.10 Large scale path loss in obstructed heavy clutter paths.....	88
4.11 Large scale path loss with 2 m antenna in center of aisle .....	89
4.12 Large scale path loss with 1.5 m antenna in center of aisle .....	90
4.13 Large scale path loss with 2 m antenna on side of aisle .....	91
4.14 Cumulative distribution of large scale signal levels about the mean....	93
4.15 Typical small scale spatial signal fluctuations .....	102
4.16 Worst case small scale spatial signal fluctuations.....	103
4.17 Best case small scale spatial signal fluctuations.....	104
4.18 Cumulative distributions for some spatial fading measurements.....	105
4.19 CDF's for three measurements and their fit to various distributions.....	108
4.20 CDF of small scale spatial fading as function of factory site .....	110
4.21 CDF of small scale spatial fading as function of geography .....	111
4.22 CDF of spatial fading measurements over all factories and geographies .....	112
4.23 Temporal fading in core room aisle .....	113
4.24 Temporal fading in core room across pep-set line .....	113
4.25 Temporal fading in engine assembly aisle .....	114
4.26 Temporal fading in engine assembly area across wash line .....	114

Figure	Page
4.27 Cumulative distribution for 200 seconds of fading data .....	116
4.28 Cumulative distribution for fading data in various locations .....	118
5.1 Typical individual multipath delay profiles from various geographies .....	121
5.2 Typical spatially-averaged multipath delay profiles from various geographies .....	122
5.3 Typical spatial fluctuations of a multipath delay profile over $4.3\lambda$ track on LOS path .....	124
5.4 Typical spatial fluctuations of a multipath delay profile over a $4.3\lambda$ track on obstructed path .....	125
5.5 Large scale path loss over all factories using wide band measurements .....	127
5.6 Large scale path loss over factory geographies using wide band measurements .....	131
5.7 Scatter plot of excess mean delay vs. r.m.s. delay spread as a function of factory geography .....	135
5.8 CDF of $\sigma$ for site B LOS paths .....	137
5.9 CDF of $\sigma$ for site C LOS paths .....	137
5.10 CDF of $\sigma$ for site D LOS paths.....	138
5.11 CDF of $\sigma$ for site E LOS paths.....	138
5.12 CDF of $\sigma$ for site F LOS paths.....	139
5.13 CDF of $\sigma$ for site B obstructed paths .....	139
5.14 CDF of $\sigma$ for site C obstructed paths.....	140
5.15 CDF of $\sigma$ for site D obstructed paths.....	140
5.16 CDF of $\sigma$ for site E obstructed paths .....	141

Figure	Page
5.17 CDF of $\sigma$ for site F obstructed paths .....	141
5.18 CDF of $\sigma$ for LOS paths at all sites .....	142
5.19 CDF of $\sigma$ for obstructed paths at all sites .....	142
5.20 CDF of $\sigma$ for all wide band factory data.....	143
5.21 Scatter plot of R.M.S. delay spread vs. received power as a function of factory site .....	147
5.22 Scatter plot of R.M.S. delay spread vs. received power as a function of geography.....	147
5.23 Scatter plot of R.M.S. delay spread vs. T-R separation as a function of factory site.....	148
5.24 Scatter plot of R.M.S. delay spread vs. T-R separation as a function of geography.....	148
5.25 Discretized power impulse response formed from spatially averaged profile in LOS path .....	151
5.26 Discretized power impulse response formed from spatially averaged profile in obstructed path .....	151
5.27 Averaged power delay profile for all LOS paths.....	153
5.28 Averaged power delay profile for all obstructed paths.....	153
5.29 Probability of path arrival (from 27 locations) at a particular excess time delay in LOS geographies.....	154
5.30 Probability of path arrival (from 23 locations) at a particular excess time delay in obstructed geographies.....	154
5.31 Log-normal fit to LOS multipath power behavior as a function of excess delay.....	157
5.32 Log-normal fit to OBS multipath power behavior as function of excess delay.....	157

Figure	Page
5.33 Weighted average power profile in LOS paths using detected paths only.....	159
5.34 Weighted average power profile in OBS paths using detected paths only.....	159
5.35 CDF of normalized path gains over all spatially averaged profiles.....	161
A1.1 Photograph of several discone antennas designed by the author.....	176
A1.2 The discone antenna.....	181
A1.3 Loading characteristics of discone antennas.....	185
A1.4 Loading characteristics as function of disc feed diameter.....	185
A1.5 Loading characteristics of discone antennas.....	185
A1.6 Loading characteristics of discone antennas (w/clamp nut).....	187
A1.7 45° discone loading optimized for 1.1-1.4 GHz.....	187

## ABSTRACT

Futuristic flexible manufacturing facilities will likely use radio to provide portable communications and mobile robot control. In the factory environment, deleterious effects caused by reflections and refractions of the transmitted signal from the surrounding building structure and inventory cause intersymbol interference and signal fading, thus limiting radio system performance. A portable UHF factory multipath measurement apparatus which uses pulsed and CW transmissions has been developed and used to measure narrow band fading and multipath power delay profiles to 10 ns resolution in five large factories throughout Indiana. Four distinct factory geographies common to all manufacturing facilities have been identified and characterized by extensive multipath measurements. Results indicate that multipath distributions are similar in shape to the urban mobile radio channel, with delay spreads ranging from 50 - 150 ns in line of sight (LOS) paths to 100 -250 ns for obstructed paths. Path loss is largely dependent upon surrounding clutter and varies with distance as  $d^{1.5}$  to  $d^{2.8}$ . Shadowing effects of common factory machinery are presented, along with distributions on spatial and temporal fading. The data indicates large scale path losses are log-normally distributed, small scale fading is primarily Rayleigh (although log-normal and Rician distributions fit some of the data well), and temporal fading is Rician with  $K=10$  dB. A simple multipath statistical model, based in principle on a model recently proposed by Saleh and Valenzuela for office buildings, is suggested here. This thesis provides measurements and results for an indoor radio channel not considered previously in the open literature.





## CHAPTER I INTRODUCTION

### 1.1. Definition of Problem

Ever since Marconi's demonstration of radio transmission to a tugboat in the English Channel in the 1890's, wireless communication has been used for a multitude of applications. For each new application, the user must know the capabilities and limitations of the radio communication system. Predicting the propagation of radio waves in unfamiliar environments is generally not easy. However, through experimentation and analysis, radio investigators can develop models that adequately describe the time- and spatially- varying channel which separates the transmitter from the receiver. These models then serve as important tools for predicting the performance of radio communication systems, and also serve to permit analysis of future systems designed for the particular environment.

With a "good" channel model, an accurate prediction of system performance may be carried out through analysis or simulation, providing bounds on important parameters such as maximum data transmission rate and minimum transmission power levels for a given Signal-to-Noise (SNR) Ratio or Bit Error Rate (BER). Anomalous effects such as signal fading due to multipath propagation are accounted for with a good model. Inevitably, *the goodness of the channel model is determined by its agreement with empirical data gathered in the operating environment of the radio system.* Over the past 40 years, the vast majority of modeling has dealt with channels encountered in conventional mobile systems (in which reliable communications must be provided for distances of up to 20 miles in an urban/suburban environment), short wave terrestrial radio systems, line-of-sight microwave radio links, or satellite-earth links. Some specific channel studies have dealt with empirical and theoretical modeling of noise [1,2]; signal propagation through the ionosphere [3-8]; signal refraction from the

ionosphere, trees, and large buildings [9-31,80,86,87]; attenuation in tunnels [32], and deleterious effects of weather. Only recently has interest been placed on studying the propagation of radio signals in and around office and residential buildings [9,10,52,53,58-64,71-72,75-80].

In a seemingly unrelated engineering discipline, there is currently a worldwide thrust to develop intelligent manufacturing centers; factories which use state of the art technologies to improve small and medium batch manufacturing processes of durable goods, electronics, and small metal products. In this country, the National Science Foundation (NSF) has provided a multi-million dollar Engineering Research Center (ERC) grant to Purdue University for development of new technology which will leapfrog existing automated manufacturing systems. It has been shown at Purdue that with a well designed "factory of the future", order of magnitude cost reductions could be realized for many batch processing operations [33,34]. With such a cost saving incentive, it is not surprising that many existing domestic factories are currently being renovated with automated machinery, and new sites will be built with a high degree of intelligent automation [35].

The future factory communication problem becomes non-trivial when one considers the need to network many computers with many automated machines. Four years ago, the Manufacturing Automation Protocol (MAP) was developed by leaders in the manufacturing industry, and pilot projects are currently underway in several American factories [36-38]. Under the standards set forth by MAP, data is transmitted over coaxial cable at a rate of 10 Megabits per second. Other types of communication currently used in factories include low rate data transmissions over radio links (for computer interfaces and dedicated control) and low rate data transmission over acoustical/ultrasonic links (for guided vehicle control and collision avoidance) [38].

A key element in Purdue's proposed intelligent manufacturing center is the use of small, agile autonomous vehicles that transfer work-in-process throughout the factory. As an integral part of the intelligent manufacturing system, these vehicles will need to be included in the communications network. Since coaxial cable is no longer a feasible means of linking such components to the manufacturing system, a radio link is a viable alternative. Radio is also attractive because of the communications flexibility it

offers in a dynamic, reconfigurable work place. To date, no published work has appeared in the open literature that determines the propagation characteristics of the wide band channel in a factory environment. Clearly, due to the high metal content of a factory, the multipath problem can be expected to be severe, and will most likely be a primary factor in limiting radio system performance. In addition, autonomous vehicles would presumably experience signal fading while traveling through the factory, thus data rates and bit error probabilities would be bounded. The work here strives to provide the empirical data which will allow such bounds to be determined, and which will identify key factors in maximizing the efficiency of a UHF factory radio system.

This report is arranged in 6 chapters. In Chapter 1, a brief overview of the general multipath problem is given, some previous channel experiments and resulting channel models are reviewed, and the goals of this research are stated. Chapter 2 details the measurement apparatus developed for the data collection, and describes the experiments and the five factory sites at which data were collected. Chapter 3 presents the multipath channel formulation used and explains the data reduction and management techniques used to process the large quantity of experimental data. Chapter 4 presents results of the narrow band measurements, and provides models for large scale path loss, signal fluctuations in a local area, and temporal fading. Additionally, shadow losses caused by common factory equipment are tabulated. Chapter 5 presents the wide band measurement results, and provides values for delay spread, excess delay, and path loss as functions of factory and geography. Additionally, a model for multipath power profiles in various geographies is presented, and small scale spatial variations in the received profiles are discussed. Chapter 6 concludes this work with a summary of the results, and suggests areas of future research for the factory radio channel.

## 1.2. The Multipath Problem

### 1.2.1 Overview

It is well known that radio multipath is caused by the reflection and diffraction of radio waves between transmitter and receiver. A very general plot comparing the performance of ideal (white noise) channels to fading dispersive channels is shown in Figure 1.1. The figure demonstrates that for a specific transmitter power level, one must anticipate degradation when using a multipath channel. Degradation becomes more pronounced at low SNR. The plot does not show the additional limitations that multipath imposes upon the channel; namely, that even for a very slowly time varying channel, the data transmission rate is bounded above, and that the BER cannot exceed a nonzero lower bound regardless of transmitter power [39,40,51]. Much work has been done to generalize the multipath channel; it is either modeled as a time varying filter or a channel cluttered by electromagnetic scatterers.

The scattering approach to channel characterization is detailed in Chapter 2 of [39]. A channel model for a scattering channel is shown in Figure 1.2. The transmitted signal may be conveniently written as

$$s(t) = \text{Re}[u(t)e^{j\omega_0 t}] \quad (1.1)$$

where  $\text{Re}$  denote the real part,  $u(t)$  is the low pass complex envelope of  $s(t)$ , and  $\omega_0$  is the carrier radian frequency.

Each scatterer is assumed to introduce a propagation time delay of the form  $T_i(t) = \tau_i + \dot{\tau}_i t$  where  $\tau_i$ , the initial propagation delay, and  $\dot{\tau}_i$ , the rate of change of delay, are time-invariant constants. Then the received signal contribution from the  $i$ -th scatterer is (see Figure 1.2)

$$y_i(t) = A\rho_i \text{Re}[u(t - \tau_i - \dot{\tau}_i t)e^{j\omega_0(t - \tau_i - \dot{\tau}_i t)}] \quad (1.2)$$

where  $\rho_i$  is the square root of the cross sectional reflected energy of the  $i$ -th scatterer. When the rate of change of the propagation delay is much less than the bandwidth of  $u(t)$ , then the received envelope can be approximated as

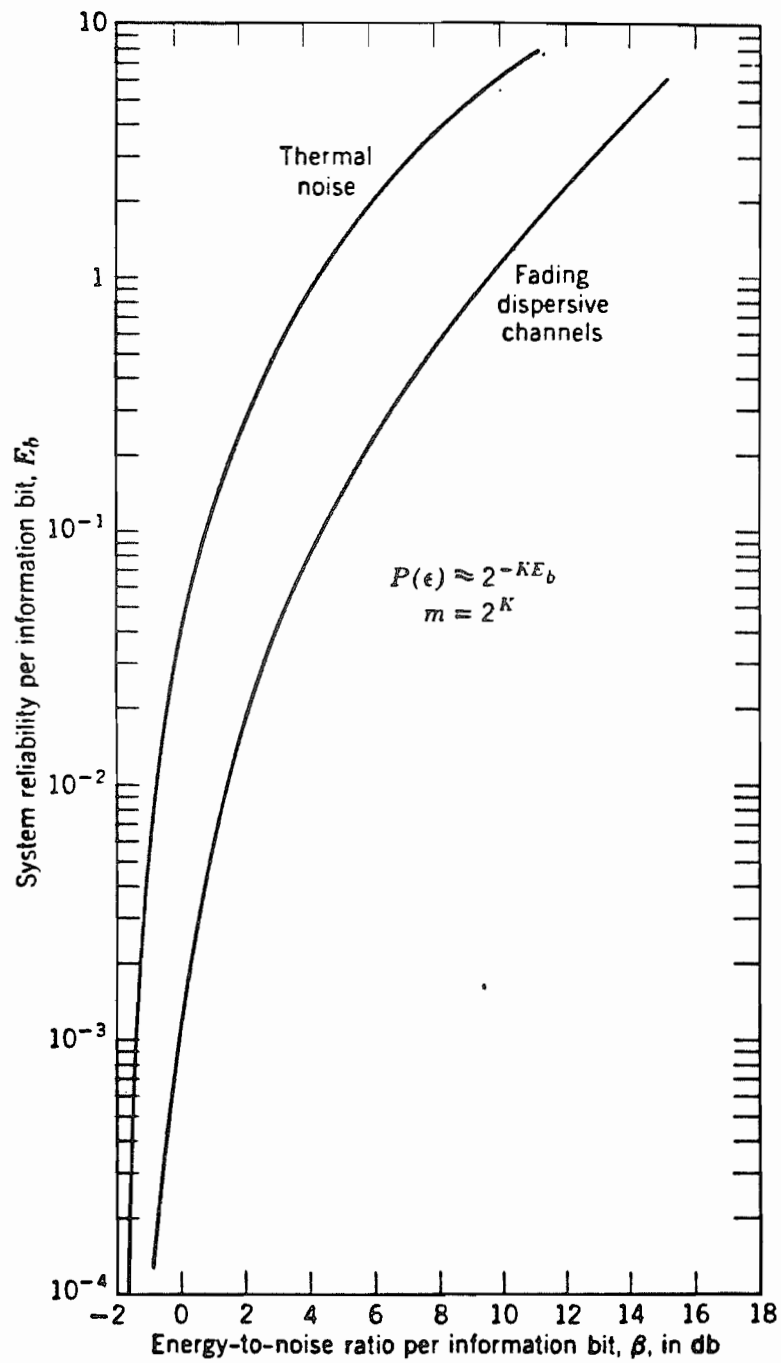


Figure 1.1 Communication system performance for typical multipath channels. (From [39])

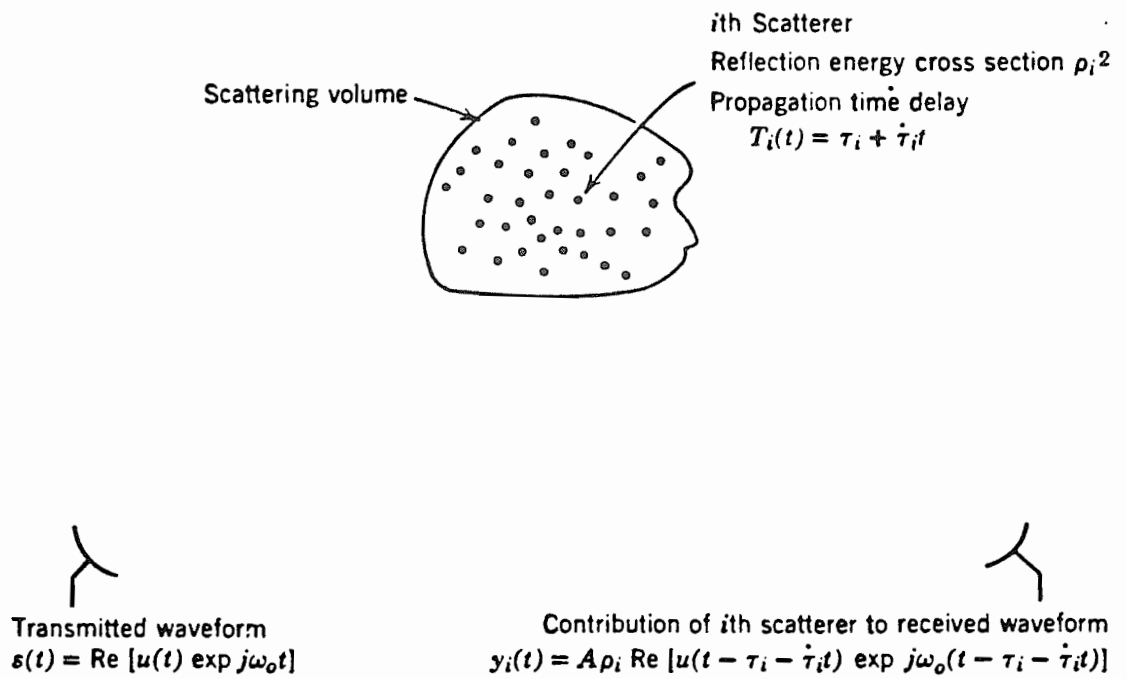


Figure 1.2 Geometry of scattering channel. (From [39])

$$u(t-\tau_i-\dot{\tau}_i t) \simeq u(t-\tau_i) \quad (1.3)$$

If  $\tau_i$  is expressed as

$$\tau_i = r_i + \frac{\theta_i}{\omega_0} \quad (1.4)$$

where  $r_i$  is the gross value of  $\tau_i$  and  $\frac{\theta_i}{\omega_0}$  accounts for minute variations in time about  $r_i$ , and if it is further assumed that  $\theta_i$  is deterministic on  $[-\pi, \pi]$  and the channel in all practicality is time invariant (i.e. no Doppler shift), then the total received signal may be expressed as

$$y(t) = A \operatorname{Re} \left[ \sum_i \rho_i u(t-r_i) e^{j(\omega_0 t - \omega_0 r_i - \theta_i)} \right] \quad (1.5)$$

Note that the low-pass impulse response of the channel,  $h_b(t)$ , may be directly obtained from (1.5) when  $u(t)$  is made to approach  $\delta(t)$  in (1.1).

$$h_b(t) = A \sum_i \rho_i e^{-j\theta_i} \delta(t-r_i) \quad (1.6)$$

The derivation of the deterministic scattering channel is useful in that it demonstrates the kinds of reasonable simplifications that are necessary to keep the model tractable. For the problem at hand, however, the scatterers are too numerous to facilitate use of the above expressions and are randomly distributed throughout the channel. A statistical scattering model is therefore worth considering.

For the scatterers of Figure 1.2, each of the  $\theta_i$  might be assumed to be independent and uniformly distributed over the range of  $[-\pi, \pi]$ . This is a natural assumption for most channels, since scatterers tend to add travel distances of several thousands of wavelengths [39,40,54]. In a factory it is reasonable to assume that at UHF/microwave frequencies, some multipaths might result in hundreds of wavelengths of additional travel. Since the  $\theta_i$  take on their full range over just  $\lambda/2$  while the random multipaths are distributed over a much greater range than this, the uniform distribution assumption seems justified. The reflection energy cross sections  $\rho_i^2$  might also be treated as independently and perhaps identically distributed random variables. Under these assumptions the mean value of the received signal  $y(t)$  can be shown to be zero while the autocorrelation function of  $y(t)$  is

given by [39]

$$R_y(t, \tau) = 0.5 \sum_i A^2 \overline{\rho_i^2} \operatorname{Re} [u(t-r_i) u^*(\tau-r_i) e^{j\omega \tau}] \quad (1.7)$$

where  $u^*$  denotes the complex conjugate of the baseband modulation and the  $\overline{\rho_i^2}$  are the ensemble mean square values of the scatterer cross sections. When  $\rho_i^2$  are identically distributed chi-square random variables with two degrees of freedom, then the  $\rho_i$  are Rayleigh distributed with variance  $\sigma^2$  [41]. For this special case, the received signal is a Gaussian process having zero mean and a variance of

$$R_y(t, t) = \sum_i A^2 \sigma^2 |u(t-r_i)|^2$$

The Gaussian channel assumption has been used in many channel modeling studies to eliminate the need for expressions of third and fourth order statistical moments. It can be shown from the central limit theorem that if the discrete channel has an exceedingly large number of scatterers with similar energy cross section, then  $y(t)$  is a zero mean Gaussian random process [39]. Indeed, for ionospheric modeling, the Gaussian assumption has provided excellent agreement with empirically observed conditions [4,44].

Identical results are derived when the channel is considered to be a time varying filter. Assuming that each of the multiple propagation paths has an associated propagation delay and attenuation factor, then for a transmitted signal having the form of (1.1), the received signal may be represented by

$$y(t) = \sum_i \alpha_i(t) s[t-\tau_i(t)] \quad (1.8)$$

where  $\alpha_i$  is the attenuation factor of the signal received on the  $i$ -th path and  $\tau_i$  is the propagation delay of the  $i$ -th path. Using (1.4) and (1.8), and letting  $u(t) = \delta(t)$  in (1.1), the low pass impulse response of the channel is found to be

$$h_b(\tau, t) = \sum_i \alpha_i(t) e^{-j\theta_i(t)} \delta[\tau - \tau_i(t)] \quad (1.9)$$

When the channel is time invariant, (1.9) is identical in form to the low pass scattering impulse response given by (1.6). For the case when there are many paths of comparable attenuation, and when the  $\theta_i$  of the received paths are considered to be uniformly distributed and independent, the



central limit theorem shows that (1.9) is a Gaussian random process. Assuming that the channel is wide-sense stationary, the autocorrelation function of the low pass impulse response may be expressed as

$$R_{h_b}(\tau_1, \tau_2; \Delta t) = 0.5E[h_b^*(\tau_1; t)h_b(\tau_2; t + \Delta t)] \quad (1.10)$$

where  $E[ ]$  denotes the expected value with respect to time ( $t$ ). (Cox loosely showed wide-sense-stationarity by taking several received impulse response samples and noting their similarities over time [56,76]). When the  $\alpha_i, \theta_i$  are uncorrelated with every other  $\alpha_j, \theta_j$ , the channel is called WSSUS (wide-sense stationary, uncorrelated scatterers) and (1.10) becomes identical to the low pass part of (1.7) [44]. Under the WSSUS assumption, the low pass channel autocorrelation function is given by

$$R_h(\tau; \Delta t) = 0.5E[h^*(\tau; t)h(\tau; t + \Delta t)] \quad (1.11)$$

Equation (1.11) is termed the multipath intensity profile, otherwise called the channel power delay profile [66]. For a time invariant channel,

$$R_{h_b}(\tau; \Delta t) = R_{h_b}(\tau; 0) = R_{h_b}(\tau) = 0.5|h_b(\tau)|^2 = \frac{1}{2}A^2 \sum_i \rho_i^2 \delta(\tau - \tau_i) \quad (1.12)$$

where  $R_{h_b}(\tau)$  is random if the  $\rho_i$  or  $\tau_i$  of (1.6) are random.

The subtle difference between the scattering and filter models is that the former strives to tediously characterize the physical channel, which is sometimes an impossible feat, while the latter uses received signal samples and attempts to characterize the channel phenomenologically. Bello [44], Baghdady [65] and Proakis [66] have done work on the general problem of describing multipath channels from the filter point of view. Kennedy [39], Cooper and McGillem [67] and other researchers in the areas of radar target tracking and target identification have successfully employed scattering channel principles.

Once the received signal (a stochastic process) is characterized in a manner similar to the above ( (1.7) or (1.11) ), it is possible to construct diversity receivers that maximize communication performance by taking advantage of knowledge of the channel statistics. Much work has been done in this area [7,11,39,40,49,50,64,68].

There are many forms of distortion imposed by a multipath factory radio channel. If the transmitter and receiver are stationary, then the time varying effects of the channel (movement of machinery, personnel, or inventory) will cause slow signal fading. Placement of either transmitter or receiver at a different location in the factory will cause different local fading characteristics to be observed. When one or both stations are in motion, there will be a faster fading effect due to movement in and out of heavy fading zones caused by changes in orientations of the scatterers.

The work here approaches the multipath problem from the filter point of view. Empirical data will be recorded from channel sounding experiments performed in five factories. Clearly, all of the assumptions made in (1.1) - (1.9) may not hold in the factory. Many times, a strong distinct line-of-sight path may dominate the multipath components, suggesting a Rician (rather than Rayleigh) distribution on the received signal envelope. Certain distributions may well describe the multipath power delay profiles of the factory channel. At times, it may only be possible to loosely correlate the channel characteristics with particular types of factory geography. Nevertheless, important communication parameters such as delay spread and attenuation characteristics will be found; these will be of use in developing a statistical model for the factory radio channel.

### 1.2.2 Definition of Terms

The following terms are commonly used to describe multipath channel characteristics:

*fading*- Fading is the variation in received radio field intensity caused by changes in the transmission path. Fading is most often produced by changes in position of the receiver or transmitter. Additionally, the change in position of reflecting objects, or the dynamic change of any object or condition that affects the propagation of radio waves in the channel will cause fading.

*Doppler spread*- The maximum frequency shift or frequency broadening that is imposed on the transmitted signal by the channel due to motion of the transmitter, receiver, or objects in the channel.

*coherence time*- Interval of time in which two transmitted signals will undergo similar fading. The coherence time is approximately the reciprocal of the Doppler spread.

*fast fading*- Fast fading implies that the channel is changing rapidly compared to one signaling (bit) interval. This implies that the Doppler spread of the channel is larger than the baseband bandwidth of the transmitted signal.

*slow fading*- Slow fading implies that the channel scarcely changes during one signaling (bit) interval. This implies that the Doppler shift of the channel is much smaller than the baseband bandwidth of the transmitted signal.

*multipath intensity profile*- Sometimes called the *power delay profile* or *delay power spectrum*. It is the autocorrelation function of the channel impulse response that indicates the average power output from a channel as a function of time delay. The duration of the multipath intensity profile is called the *delay spread*.

*Doppler power spectrum*- The Fourier transform of the multipath delay profile. Power spectrum that indicates the signal intensity as a function of the Doppler spread frequency.

*delay spread*- The maximum duration of the multipath delay profile. This parameter is important in determining the maximum data rate which may be passed through a channel. The reciprocal of the delay spread defines an approximate (conservative) upper limit on data rate.

*coherence bandwidth*- Coherence bandwidth is the maximum frequency difference for which signal amplitudes are still strongly correlated. Two sinusoids will be affected similarly by the multipath spread of the channel if their frequency difference is less than the coherence bandwidth.

*frequency selective fading*- Dispersion caused by the channel when the RF signal bandwidth is larger than the coherence bandwidth of the channel. Dispersion is caused by the constructive or destructive interference of cer-

tain frequency components of the transmitted signal due to the multipath spread. This is the most common type of fading in high data rate microwave line-of-sight links.

*frequency nonselective (flat) fading*- Case where coherence bandwidth is larger than the RF signal bandwidth. Baseband signal is not distorted by the multipath structure of the channel, but is still subject to time-varying fading in the channel.

*spread factor*- The product of delay spread and the Doppler spread. When the spread factor is less than 1, the channel is termed *underspread*, and the channel may be frequency-nonselective and slowly fading. When the spread factor is much greater than 1, the channel is *overspread*, and the channel causes the signal to disperse in time, frequency or both.

### 1.3. Previous Work

Work done at the University of California, Berkeley, in the mid 1970's dealt with characterizing the urban radio propagation channel. Extensive wide band data collection and initial modeling of the San Francisco urban/suburban mobile radio channel was performed by G. L. Turin and co-workers for three UHF/microwave frequencies [11,54]. Subsequent work by Suzuki [18] and Hashemi [19,20] dealt with fitting the data to more refined statistical models and developing a simulation program for urban mobile radio systems. Transmitters with carrier frequencies of 488, 1280, and 2920 MHz were used to simultaneously transmit pulses having r.m.s. durations of 100 ns. The high bandwidth pulses, which were dispersed by the multipath environment, were received in a mobile van containing three receivers and a three-trace oscilloscope. The transmitting and receiving stations were equipped with rubidium frequency standards so that synchronization accuracy of 10 ns could be maintained. Every second, a pulse was transmitted, and the oscilloscope was set by the standard to trigger slightly before the line of sight (LOS) delay time thereafter. A camera then captured the scope display, and an optical scanning table was used to analyze the empirical data.

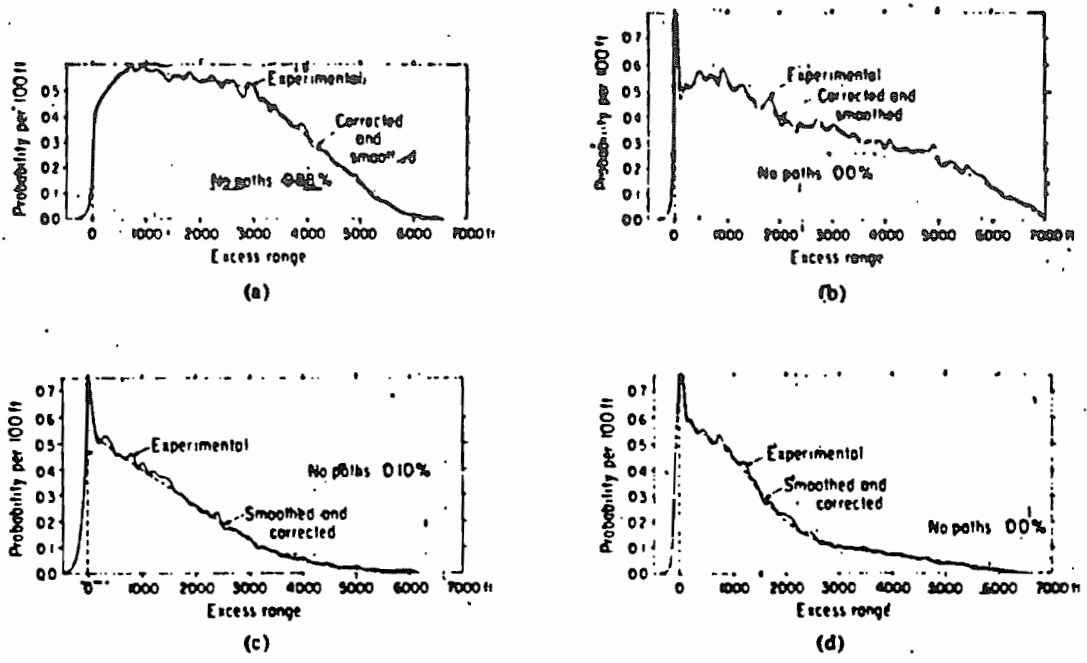
Four distinct reception areas, representative of a large city (area A), the downtown district of a medium sized city (area B), the downtown area of a small town (area C), and a typical residential area (area D), were studied. In each area, 50 reception points were designated a priori. These points represented places on a reasonable vehicle path. The reception points were chosen so that there were roughly an equal number of intersection and mid-block points. Each path was traversed 20 times so that 1000 data frames were logged in each area for each of the three carrier frequencies. Upon each path traversal, data was taken randomly within a 30 foot neighborhood of each of the predesignated points. In this way, the accumulated data represented 20 frames of data from each of 50 ensembles, whereby each point on a path represented an ensemble from the given area.

The data was reduced and discretized by keeping only the peaks or inflection points of the received signals. The received signal was represented as  $\text{Re}[p(t)e^{j\omega_c t}]$ , where  $p(t)$  is the baseband information given by

$$p(t) = \sum_i \alpha_i u(t-\tau_i) e^{j\theta_i} \quad (1.13)$$

and  $u(t)$  is the complex envelope of the modulating pulse. From this representation, the impulse response description given by (1.9) follows directly, since  $u(t)$  could be approximated as an impulse. Equation (1.9) is a classical filter model for both time-varying and time-invariant multipath channels.

The discretized data was quantized into 100 ns time bins, with bin 0 representing the LOS arrival time. Because of the duration of the transmitted pulse, it was impossible to distinguish if more than one multipath signal had arrived within a given bin. The channels in each of the 4 geographical areas were described by the path variables  $\left\{ \alpha_i, \tau_i, \theta_i \right\}$ , where  $i$  denotes the  $i$ -th bin after LOS reception. Several statistics were compiled from the 1000 path profiles in each of the 4 geographical areas. Turin's work was useful in describing channel characteristics in gross geographical areas of the urban radio channel, but it did not consider local statistics within a particular geography. Figure 1.3 shows some of the experimental results.



Probability-of-occupancy curves; 1280 MHz. (a) Area A. (b) Area B. (c) Area C. (d) Area D.

Figure 1.3 Experimental data: probability of path occupancy. (From [54])

Suzuki [18] analyzed the data collected by Turin, and strived to fit the data to well known distributions. Using the two moment method, Suzuki studied the log normal, Rician, Rayleigh, and Nakagami distributions for fit to the path amplitude data. He discovered that the Rayleigh distribution did not fit the data well. This suggested that the local multipath environment had affected the received signal in a biased fashion (i.e., the zero-mean Gaussian channel assumption cannot be applied). The log normal and Nakagami distributions provided the best fit for most of the data. The path arrival probabilities were found to fit a modified Poisson distribution, with the mean dependent upon the time within the multipath profile. Hashemi [19] used the data and the refined statistical models of Suzuki to design an acclaimed computer program called SURP (simulation of urban radio propagation). The program generates values for  $\left\{ \alpha_i, \tau_i, \theta_i \right\}$  in a specified geographical reception area. Using the time-invariant form of (1.9), the low pass channel impulse response is modeled as

$$h_b(t) = \sum_i \alpha_i e^{j\theta_i} \delta(t - \tau_i) \quad (1.14)$$

By forming the convolution of (1.14) with any specified transmitted signal, SURP is able to simulate a (discretized) received signal. In this way, it is possible to predict important quantities such as SNR, channel dispersion, BER, etc. by conventional analysis.

Recent interest in developing low power portable radio systems for indoor use has prompted research on this channel by Motorola and Bell Laboratories. Donald Cox of Bell Laboratories has pioneered the efforts being made to determine radio propagation effects in and around houses and office buildings [9,10,56,60-62,64,72]. Other researchers have conducted similar work [53,58,59,63,71,77,78]. Using a CW signal in the 900 MHz band, Cox showed that when a receiver is moved about in a vacant metal building, the multipath effects can cause large signal fluctuations over spatial distances on the order of a half wavelength (0.3 m). The statistics of the narrow band received envelope appear to follow a Rayleigh distribution, although, since the building was vacant, the effects of metal object clustering (such as machinery) in the vicinity of the transmitter and receiver were not determined. It is likely that the envelope distribution will be different within different areas of a cluttered building, due to the local environment.

Devasirvatham employed a spread-spectrum type of channel sounding apparatus to explore the wide band characteristics of 850 MHz propagation in building environments [58,71,78]. He found r.m.s. delay spreads to range between 100 ns and 600 ns depending on the structure and surroundings of various buildings. This information is of important value in determining the information capacity of the channel [40].

Antenna diversity and cross-polarization coupling in a metal building has been shown by Cox to provide significant communication improvement over small distances [9,10]. Figure 1.4 shows the dramatic difference in received signal amplitude which occurred when the antenna height of the receiver was adjusted. By equipping a mobile receiver with antennas at two heights and selecting the strongest signal from either antenna at each time instant, Cox has shown through a Rayleigh fading simulation that a 5-10 dB signal improvement may be obtained at low SNR.

Data collected in and around eight houses, averaged over 1.3 m square areas, has shown that signal variations over large (30 m) distances loosely fit a log normal distribution about the mean [60]. The mean channel loss was found to vary as inverse distance to the 3.2 power (as opposed to the free space inverse square law).

Work at Motorola has involved attenuation studies of RF signals in the 150 MHz (VHF), 450, and 850 MHz bands within a two story office building [52]. Portable transmitters for each of these three frequency bands were mounted on a rotating mechanical arm at a height of 6 feet above the floor. The supporting structure was made out of PVC pipe and was rotated in a circle with a battery powered motor. The purpose of the rotation was to permit calculation of the local average signal level at each transmission point. The transmitters and the supporting structure were moved to 146 predetermined data sites throughout the building. These sites included corridors, offices, and laboratories located on both floors of the building. The receiving apparatus and the three receiving antennas were located in a fixed, clear location on the top floor. An HP-85 computer was used to control a digital voltmeter and an attenuator, and recorded the received signal level data. Interestingly, the research showed that at distances greater than 30 m, the path loss gradient decreases when compared with closer transmitter-receiver (T-R) separations.



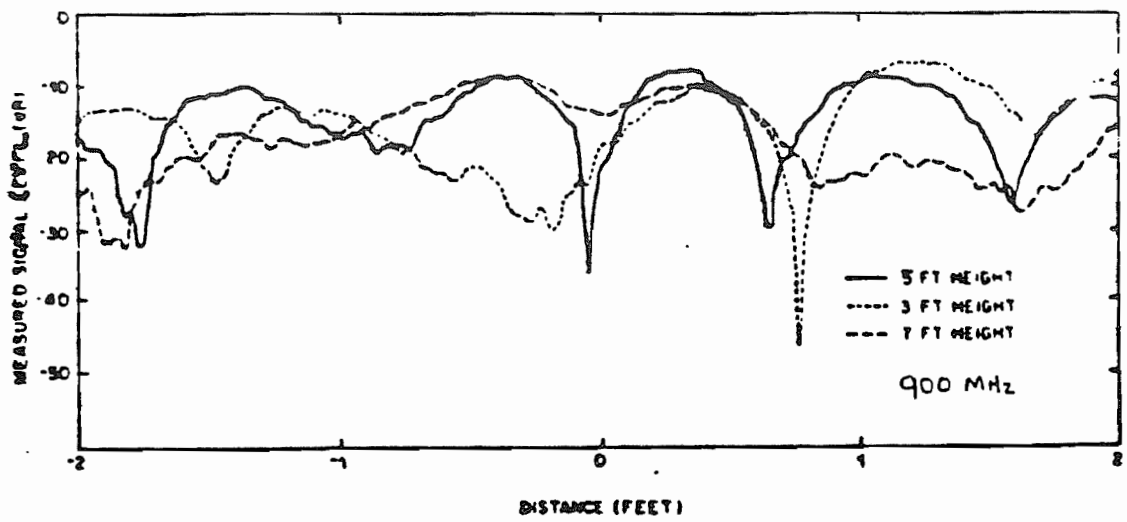


Figure 1.4 Signal fading as a function of receiver antenna height. (From [62])

Important work has recently been reported by Saleh and Valenzuela [53]. Using 10 ns radar-like pulses with swept carrier, multipath data profiles with path resolutions down to 5 feet have been found. The measurement set-up, shown in Figure 1.5 was used to perform the wide band channel sounding in an average two story office building. The carrier frequency used was 1.5 GHz, although it was swept through a total bandwidth of 200 MHz about the carrier. The measurement procedure required that a 10 ns pulse be repetitively transmitted at 600 ns interval, a duration much longer than the delay spread of any point in the building. The carrier was swept while the receiving apparatus recorded and averaged the received profiles. It is easy to show that for the carrier sweep technique, the common assumption of iid uniform  $\theta_i$ 's in (1.13) is valid. The technique even enhances the resolution of the experiment so that multipaths may be resolved to a time duration of approximately half of the transmitted pulse width.

Based on the numerous multipath profiles, Saleh and Valenzuela have proposed a simple statistical model of the indoor channel. In the model, the rays of the received signal arrive in clusters. The rays have amplitudes which are independent Rayleigh random variables with variances that decay exponentially with cluster delay as well as with delays within a cluster. The clusters, as well as rays within a cluster, form Poisson arrival processes with fixed but different rates. Figure 1.6 graphically depicts the two-tier multipath model. For an arbitrary indoor channel, the authors suggest it should be possible to use the model by properly fitting four parameters from experimental channel sounding data. This model has yet to be confirmed or refuted.

#### 1.4 Goals of this Work

An extensive review of the literature shows that no work has been done pertaining to the factory multipath channel or the performance of wide band RF communication systems in the factory environment. The goal of this work is to collect radio propagation data from typical factories so that the characteristics of the factory radio channel may be identified.

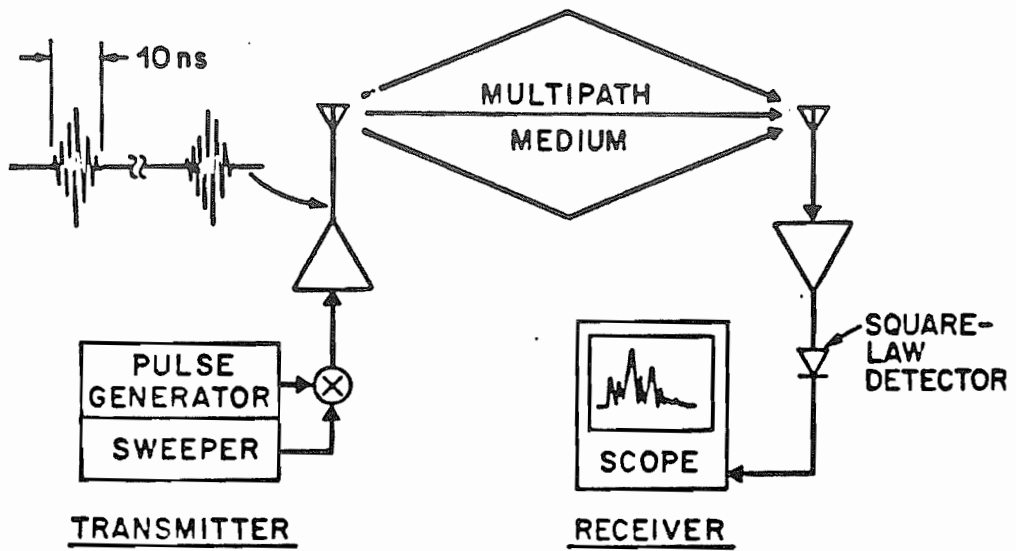


Figure 1.5 Set-up for wide band building multipath measurements. (From [53])

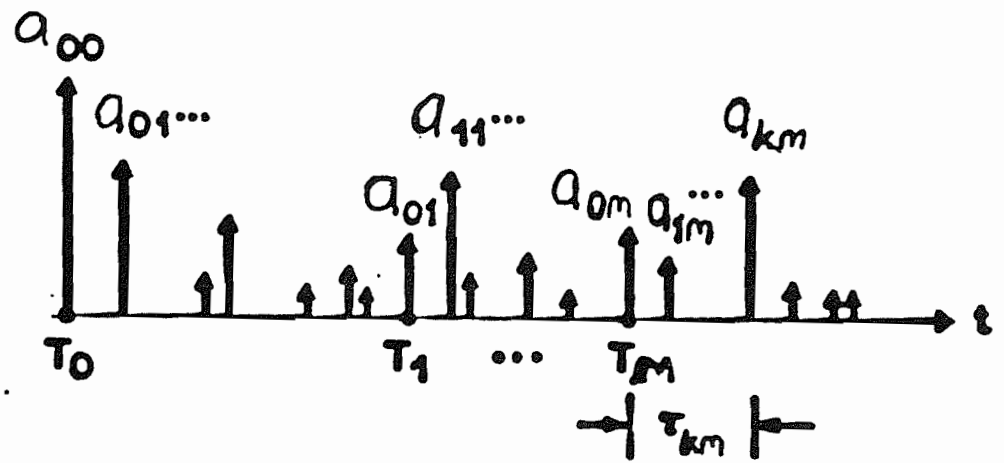
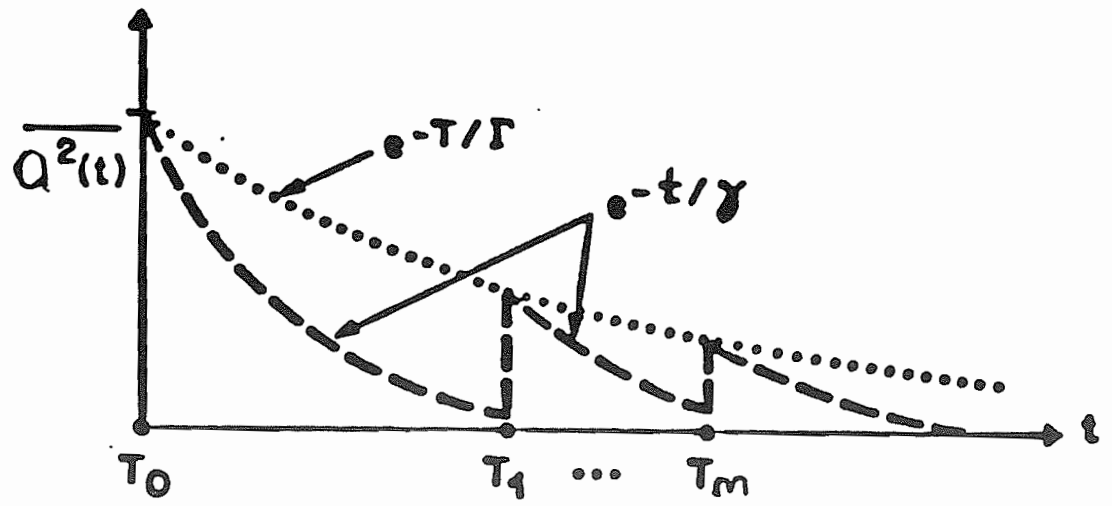


Figure 1.6 Graphical representation of two-tier indoor multipath model. (From [53])

It is envisioned that the factory of the future will make use of radio for point-to-point data communications as well as mobile communications with robotic vehicles. For this reason, both the wide band multipath characteristics and signal fading characteristics of the factory channel will be investigated. Through the collection of empirical data from a series of experiments performed at several factories in the Lafayette, Indiana area, important wide band channel parameters, such as delay spread, multipath amplitude and delay behavior, and their variations over different factories and different geographies within each factory will be found. Fading channel information such as signal attenuation with distance and local envelope distributions will also be found.

This body of data should provide valuable insight for the design of a UHF factory radio communication system, and will be useful in the development of a suitable statistical model of factory radio communication. The data will also be of interest to those studying the use of portable radio communication in buildings.

## CHAPTER 2 EXPERIMENTAL DESIGN

### 2.1 Objective of Experiments

Since radio propagation data has never before been collected in the factory environment, several experiments which give insight into the communication channel were performed. The experiments were designed to determine typical multipath delay profiles of locations throughout factories, typical factory attenuation characteristics, the time varying characteristics of the factory radio channel, local fading characteristics of radio signals, and the effect antenna diversity (namely, antenna height) has upon the received signal strength.

Previous researchers have used many methods to obtain the multipath delay spreads of various channels. These techniques include generating a very short duration RF pulse and using a wide band receiver to collect the experimental data [53,54,73], or generating a high code rate pseudo-random spread spectrum signal and receiving the channel response with a spread spectrum receiver [14,58,70,71,78]. Alternatively, the power delay spread may be measured by monitoring the channel over a wide RF bandwidth, keeping track of the amplitude and phase (or group delay) of the received signal as a function of frequency [5,21,25]. Researchers have used the latter method to develop frequency selective models for terrestrial microwave radio links, which are well described by two or three ray multipath models. Because only a couple of specular scatterers create the multipath distortion, it is relatively easy to fit the frequency and phase information to low order polynomials in frequency. The inverse Fourier transform then yields the time domain representation of the multipath channel.

Recent investigators have used crystal based transmitters and calibrated receivers to perform narrow band path loss measurements in

buildings [52,60-63,72]. Receiver power readings are obtained in local ( $\sim 10\lambda$ ) regions at varying line of sight distances from the transmitter. The power loss factor may then be determined by plotting least square error regression lines of signal attenuation (in dB) as a function of distance (on a log scale). The large portion of building propagation studies have been made in the 800 - 900 MHz spectrum [52,59-63,71-72]. The Japanese have been looking at the 1.3 GHz band for possible portable radio telephone use [59].

The time varying characteristics of the factory radio channel may be obtained by receiving a steady carrier and observing how the signal envelope varies over time. This data is useful in determining the stationarity of the channel over an observation interval, and provides data which indicates the slow fading rate of the channel. One would expect the channel to be slowly varying because of the lack of rapidly moving objects, yet constantly varying because of the continuous motion of personnel and machines in many localized parts of the factory. The data also allows us to find a distribution function which best describes the likelihood of deep fades due to time variations.

Local (spatial) fading characteristics of signals in factories may be measured by taking an adequate number of delay profiles or envelope readings within a small neighborhood. The number of samples taken in a given neighborhood must be such that the fast fading variations (due to changes in scatterer orientation) are smaller than half the spatial frequency between samples. For measurements made in a moving vehicle, it is common practice to assume that the channel is time invariant such that the only fast fading components are due to vehicle motion (Doppler shift) [12,70]. For this case it is easy to show that aliasing is avoided provided successive samples are taken at spatial intervals no larger than  $\lambda/4$ . Other experimenters have used sample spacings as small as  $\lambda/10$  [14,59,62,72].

Antenna diversity measurements have been performed by Cox inside of a vacant metal building [62]. In the factory, it seems reasonable to believe that scattering effects due to machinery and equipment could be mitigated by judicious selection of antenna height. A simple method for performing antenna diversity measurements is to adjust the vertical height of the receiving antenna. This may be accomplished with a sliding antenna mast.

Data may then be taken at identical locations with differing antenna heights.

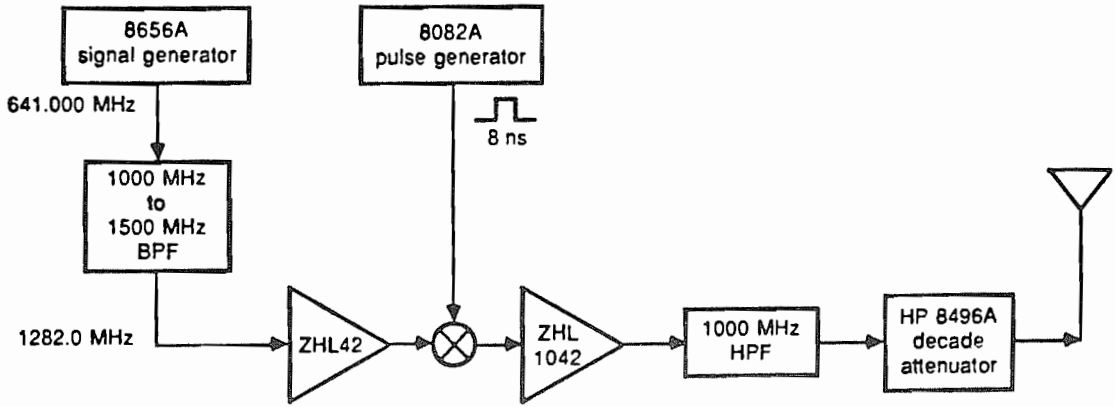
## 2.2 Development of Measurement Apparatus

The selection of 1300 MHz carrier frequency was made as a compromise between the recent indoor propagation studies conducted in the 800-900 MHz [52,59-63,71-72,77], 1300 MHz [59], and 1500 MHz bands [53]. Because virtually no 1.0 - 2.0 GHz equipment existed at Purdue prior to this research, dedicated hardware was purchased with careful consideration given to the usefulness of the equipment upon completion of this thesis. Consequently, the multipath measurement apparatus was developed using a straight-forward building block approach.

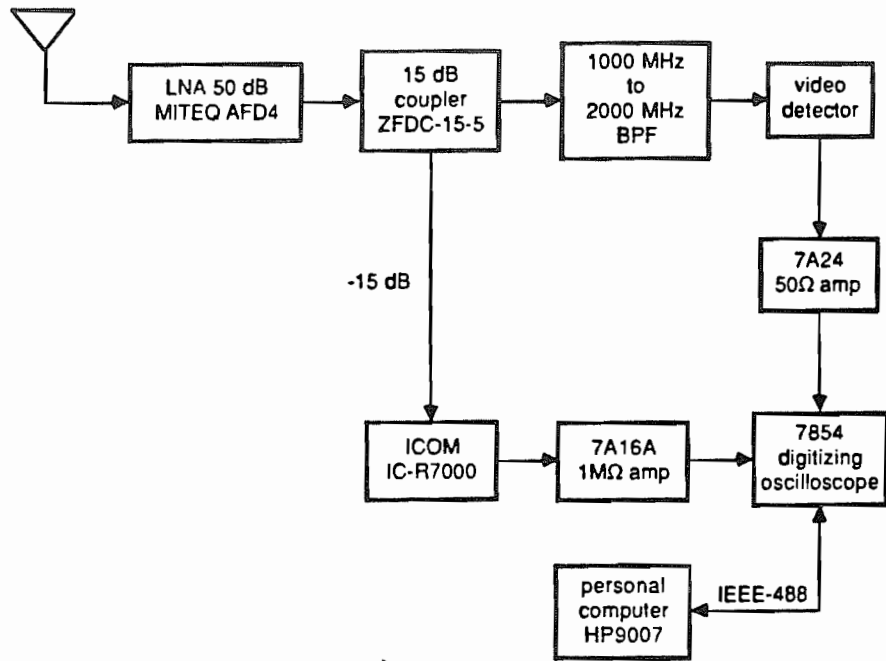
The measurement apparatus (shown in block diagram form in Figure 2.1) is capable of generating either a stable CW carrier or a repetitive probing pulse having a half-power duration of approximately 5 ns. In the pulsed mode, the first harmonic of an ultra stable 641.00 MHz signal is filtered and mixed with a repetitive 10 ns probing pulse. The resulting DSB-SC signal is then filtered and amplified to an average output power level of 14 dBm at 500 ns repetition period. This corresponds to a peak power of about 30 dBm. The radar-like probing pulse is generated at a nominal 2 MHz rate, thus providing a 500 ns delay spread window. However, the repetition rate is fully adjustable on the HP 8082A pulse generator so that measurements may be performed in environments with various delay spreads. All transmitted harmonic and intermodulation components are more than 40 dB below sideband levels. To remove "ghost" pulses due to reflections, attenuators were judiciously placed throughout the transmitting circuit.

Discone antennas, which are well known for their broad band characteristics, were designed on standard N connectors, and used at both the transmitter and receiver [75]. Appendix A details the design of the antennas which were conveniently disassembled during transport of the apparatus.





a) Transmitter.



b) Receiver.

Figure 2.1 Block diagram of factory multipath measurement system.

For CW transmission, the stable first harmonic was mixed with a DC bias provided by the external gate mode of the pulse generator. Thus, selecting CW or pulse mode was accomplished by merely moving a slide switch on the pulse generator. The resulting final RF output level was controlled by both the signal generator drive level and the decade attenuator, and was typically operated in a range from -10 dBm to 10 dBm, with a maximum transmitter power of 30 dBm. Care had to be taken to avoid excess RF radiation due to leakage from the signal generator and other components. We found that an early model Wavetek 2500 signal generator radiated as much as -30 dBm when in the stand by mode! Although line cord radiation was not a problem, RF line filters were installed at the transmitter and receiver as a precaution.

The receiver consisted of a discone antenna followed by a Miteq 48 dB gain low noise amplifier (LNA) designed for the 1.0 - 2.0 GHz band. The received signal was then split into two paths by a 15 dB directional coupler (Mini circuits ZFDC-15-5). The direct path provided pulse detection with a true square law envelope detector (Triangle PT-28 video detector). Tests showed that the detector obeyed a true square law for input powers up to 0 dBm into 50 ohms. For levels above 0 dBm, the detector had roughly a linear voltage response until saturation (8 dBm). A Tektronix 7854 oscilloscope, equipped with a 350 MHz 50 ohm amplifier (7A24A), was used to record and digitize the multipath power delay profiles produced by the video detector. Detector linearity was guaranteed by adjusting the transmitter for a full scale scope display with the vertical scale set at or below 20 mV/division. Because the scope display represents a power measurement, 6 dB of dynamic range (in addition to that provided by the decade attenuator at the transmitter) was provided by selecting between the 5 m/div., 10 mV/div. and 20 mV/div. settings on the 7A24 amplifier. Multipath profiles were formed by averaging between 15 and 50 consecutive sampling waveform sweeps depending on the SNR. Each profile was digitized to 128 points and sent over IEEE 488 bus to an HP 9007 Integral Personal Computer and stored on flexible disc for latter processing on the Engineering Computer Network (ECN). The recording and storing process required about 5 seconds per multipath profile. Software programs written for various data logging and processing chores are given in Appendix B and are discussed in Chapter 3.

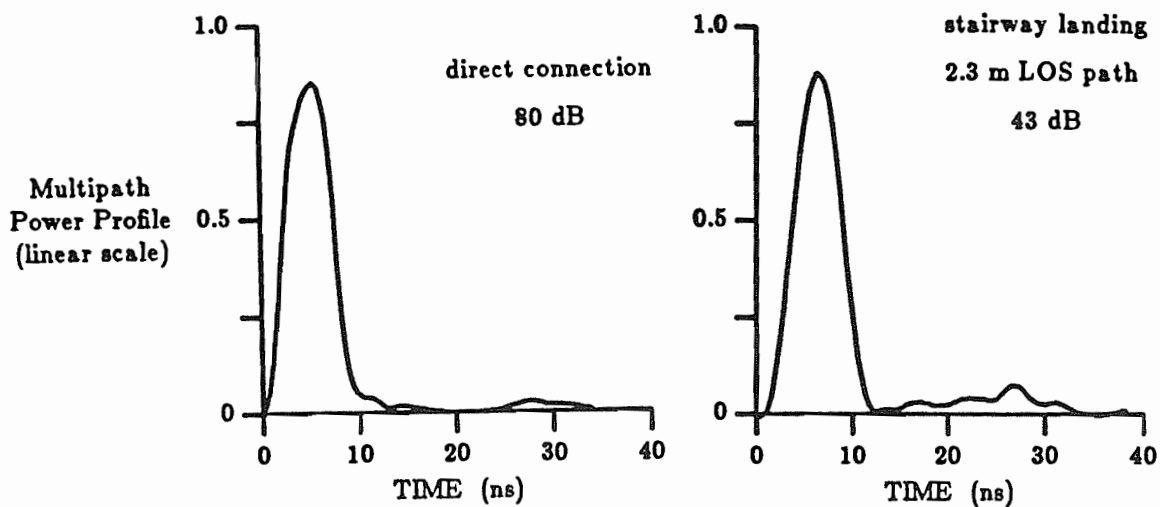
The transmitted pulse is shown in Figure 2.2 with the attenuation setting shown in the upper right hand corner. The envelope of the transmitted spectrum (at 500 ns repetition rate) is shown in Figure 2.3. The measurements shown in Figure 2.2 were taken in a spacious stairway landing in Purdue's Electrical Engineering building and demonstrate the inverse square law relationship

$$P_r = \frac{P_t G_t G_r \lambda^2}{(4\pi)^2 R^2} \quad (2.1)$$

between power and distance in free space, where  $G_t = G_r = 1.5$  for discone antennas and the theoretical free space path loss is 38.3 dB at a distance of  $10\lambda$ . (The measurements were later repeated outside on a sidewalk and were within 2 dB of the first). The clutter at  $\approx 30$  ns excess delay was caused by reflections from the 12' ceiling. Figure 2.3 was obtained using a 7L14 plug-in spectrum analyzer connected to the transmitter output. The slight asymmetry of the spectrum is due to mixer and amplifier flatness characteristics.

The other receiver signal path was fed from the coupler into an ICOM R7000 communications receiver modified to provide a DC voltage corresponding to the received signal power. This was accomplished by tapping the S-meter voltage which is internally provided by the last IF stage of the receiver. The received signal was adjusted for 800 Hz audio tone during all narrow band measurements with the receiver operated in the SSB mode. The receiver AGC attack time was not considered to be a concern since the fading measurements were performed at intervals much longer than the attack time constant. The receiver AGC decay time was decreased to exceed the data sampling rate by changing R113 of the IF board from 1.8 M $\Omega$  to 70 k $\Omega$ . Using a high impedance 7A16A amplifier and the single sweep mode, the Tektronix 7854 oscilloscope was used as a sweeping volt meter to compute instantaneous envelope readings which were immediately written to computer disk. This set-up was convenient because it permitted both pulse and envelope data to be recorded without reconfiguration.

The LNA/coupler/receiver cascade was calibrated so that receiver antenna power could be directly interpreted from the envelope voltage. Careful testing showed that after a 15 minute warm-up, input power measurements could be made repeatably within  $\pm 1.0$  dB over a 60 dB dynamic range. For envelope voltages less than 10 mV, measurements resulted in as



a) Direct Connection

b) Pulse at  $10 \lambda$

Figure 2.2 Transmitted multipath probing pulse.

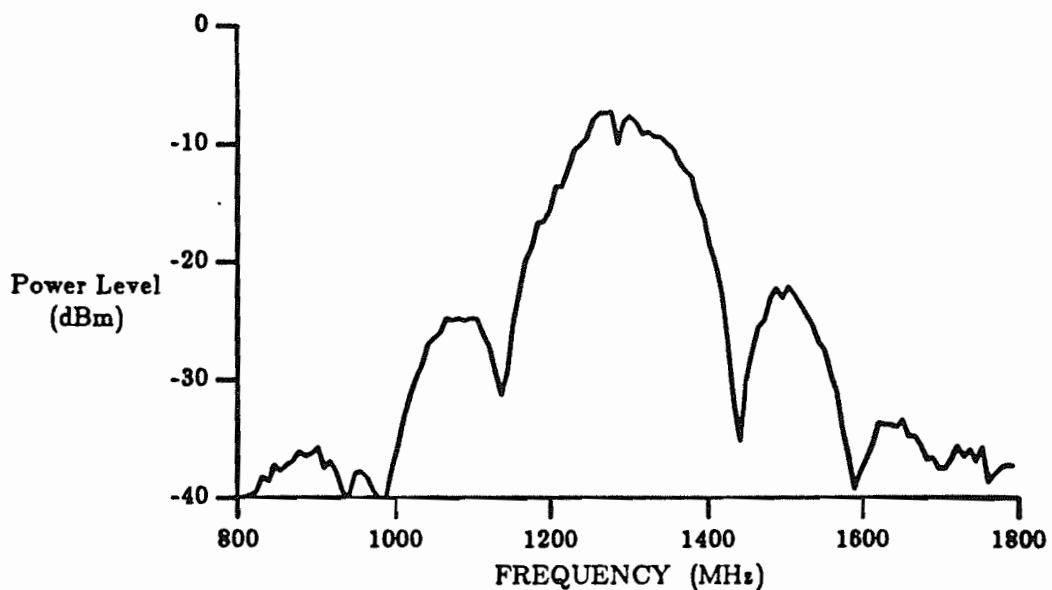


Figure 2.3 Power spectrum envelope of multipath probing pulse.

great as  $\pm 2.0$  dB uncertainty. A plot of the input power/output voltage transfer function for the receiver cascade is given in Figure 2.4. The curve was verified on several occasions at  $25^\circ$  C over the course of one month, and was found to be within  $\pm 1.5$  dB for all input powers. Figure 2.4 shows that the most linear receiver performance occurs for input powers between -50 dBm and -110 dBm. LNA saturation mandated that all useful received signal powers be kept below -40 dBm. An input power of -50 dBm to the LNA corresponds to an S-meter reading of S9 +15, whereas an input power of -110 dBm causes an S-meter reading of S2. By preadjusting the transmitter power for an average S-meter reading of about S7 (-80 dBm), the receiver was always operated in this linear range. The CW path loss over a  $10\lambda$  distance was found to be very close to the expected loss over free space, and was within 2 dB of the received pulse power over an identical path.

The equipment was mounted on two industrial strength push carts equipped with pneumatic tires and 50 ft. extension cords. The antennas were mounted to PVC pipe fastened to the corners of the carts and were adjustable from 1.5 m to 2.0 m in height. Figure 2.5 shows the complete factory measurement apparatus. The carts were transported to each factory site by an 8 passenger van provided by Purdue.

Our apparatus is similar to that used by Saleh and Valenzuela [53] except for two important differences. The first difference is that we found it impractical to run a triggering cable throughout a factory. Fork lift trucks and other factory equipment posed a real danger to the cable. Also, the participating factories expressed their concern with the cable, citing that employees could be tripped. Because of the triggering sensitivity of the 7854, we could not maintain display trigger throughout a frequency sweep. It was not difficult, however, to achieve trigger using a fixed carrier frequency. Trigger timing jitter was much less than the resolution of the measurement apparatus since the SNR was reasonably large at all measurement locations. Consequently, our multipath profiles are much like Turin's [10] in that multipaths within the sounding pulse duration of 10 ns are not directly resolvable. There are, however, signal processing techniques which in many cases are successful in identifying individual multipath components within a sounding pulse duration [74]. These techniques would be worth exploring if one desires even greater resolution of the indoor factory radio

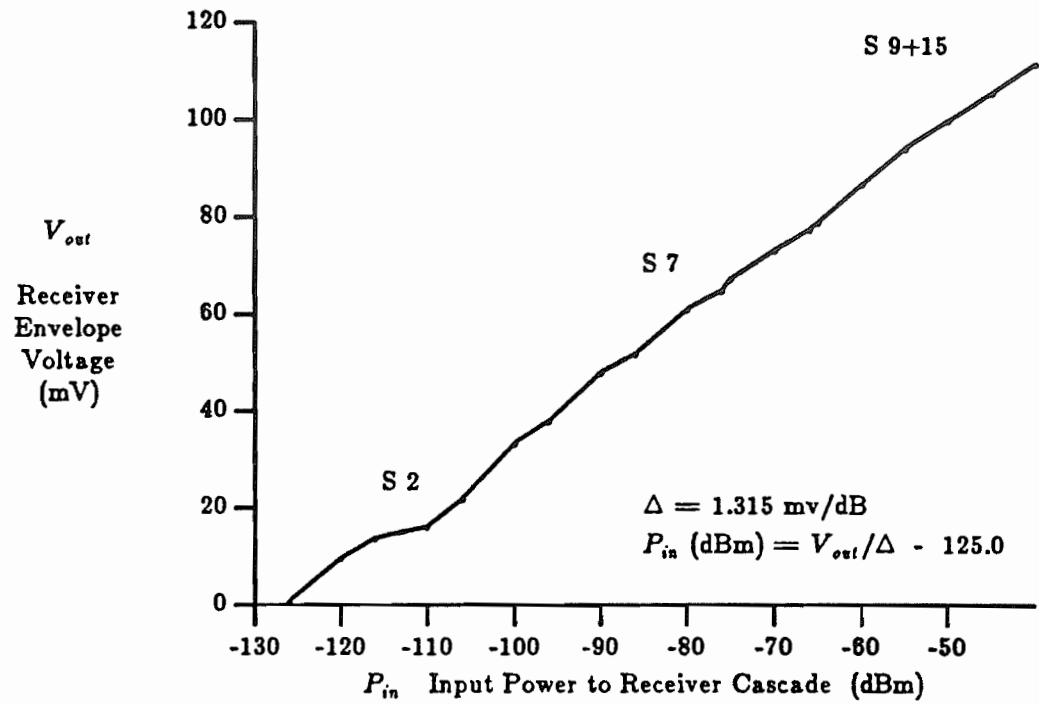
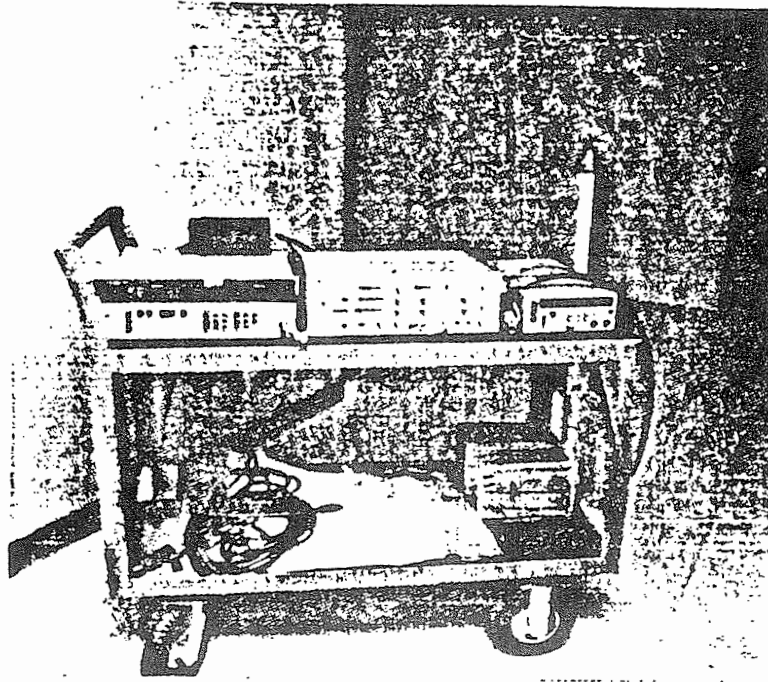
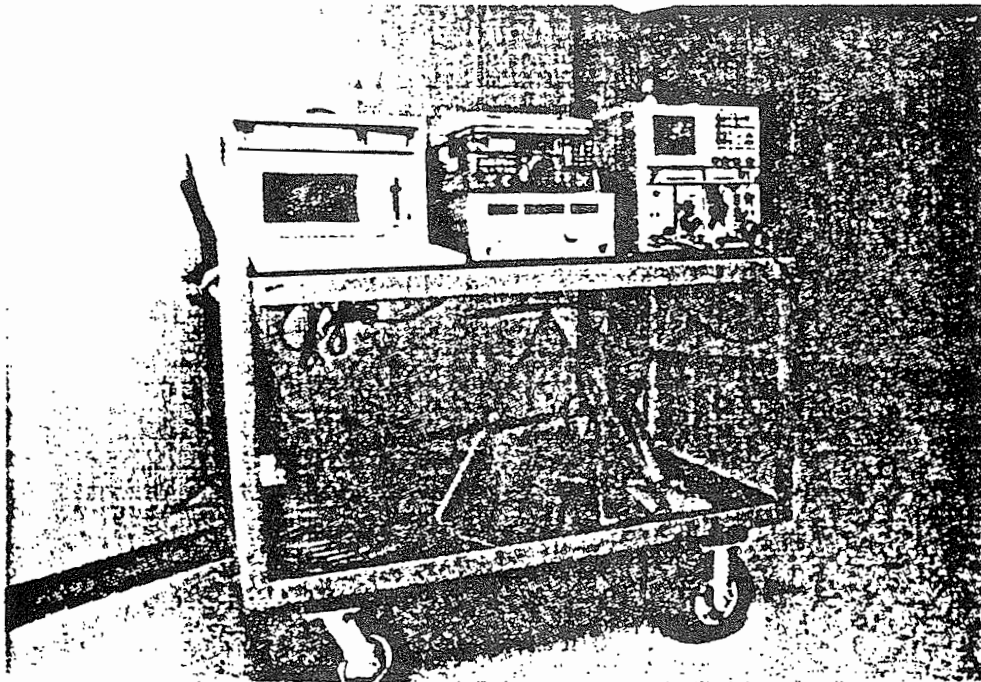


Figure 2.4 Transfer function of narrow band receiver cascade.



a) transmitting cart.



b) receiving cart.

Figure 2.5 Factory multipath measurement apparatus.

scattering channel. Since our apparatus is not synchronized with the transmitter, we cannot be sure that the first received path in a profile is a LOS path. Nevertheless, provided that the first path is not significantly delayed relative to the LOS path (if it existed), accurate delay spread data and excess delay data may be computed while time registration can be maintained between profiles by observing the relative amplitudes of the first few multipaths among successive profiles.

Our apparatus also differs from [53] in that we provide a calibrated narrow band receiver which we believe provides a more accurate power measurement than can be hoped for by summing powers of the individual multipath components with the pulse detection method. The dynamic range of the pulse receiver is poor due to the linear display of the Tektronix 7854 oscilloscope. With the addition of the calibrated receiver, we may be confident of power/distance laws provided by our data, and more importantly, can expeditiously perform diversity and fading measurements.

### 2.3 Description of Factory Sites

Multipath measurements were conducted at 5 fully equipped and operational factory sites in central Indiana. Details of the construction and layout of each facility are given below. At the request of the companies involved, trade names of the participating factories are intentionally not given here. Rather, the data sites are identified by letter. Figures 2.6 through 2.10 show the exteriors of the buildings visited during the course of this research.

#### Site A: Office Building

The measurement apparatus was developed and tested in Purdue's Electrical Engineering building. Although some measurements were performed throughout the building to ensure the hardware and software were functioning properly, this thesis concentrates on measurement and characterization of the factory radio channel. It was interesting to note, however, that a casual analysis of the Site A data confirmed the waveguiding effects



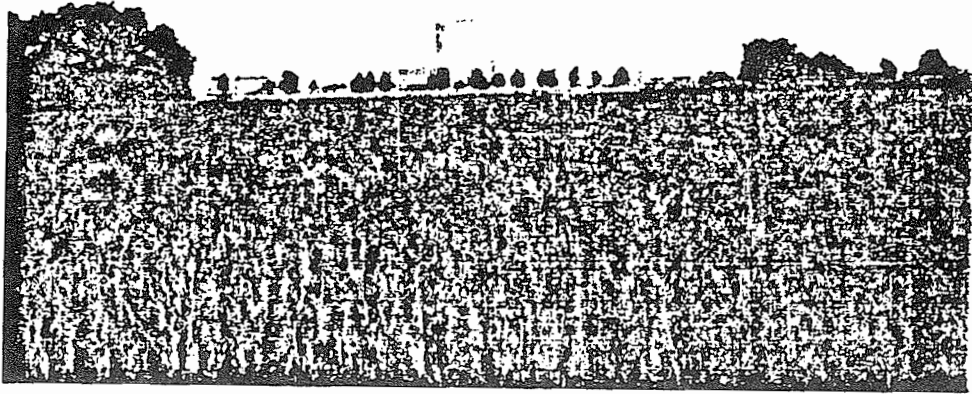


Figure 2.6 Site B: Food Processing Plant, multi floor structure.

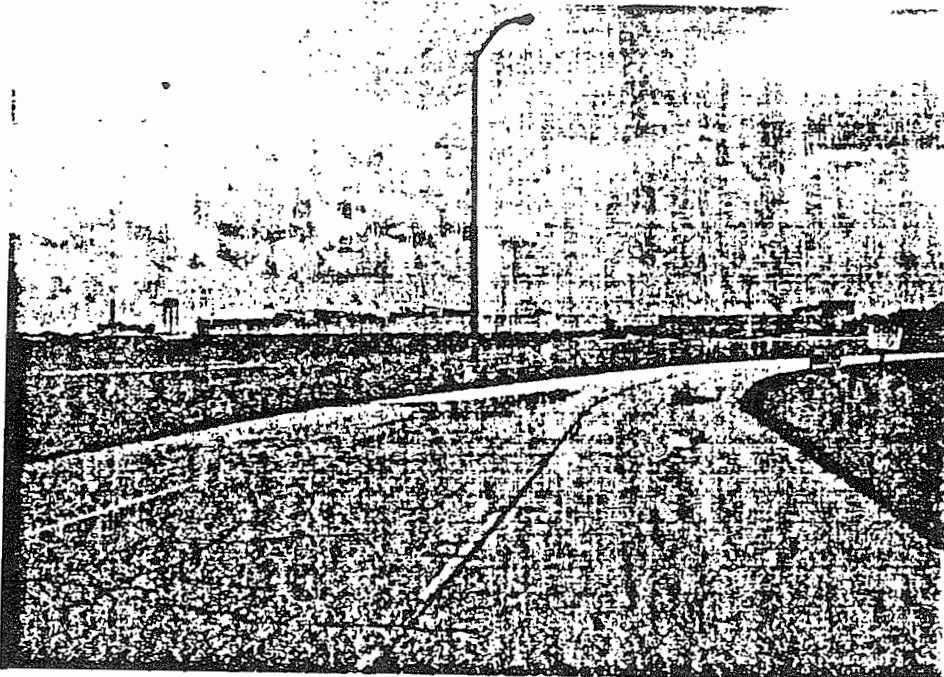


Figure 2.7 Site C: Engine Manufacturing Plant, new single floor structure.

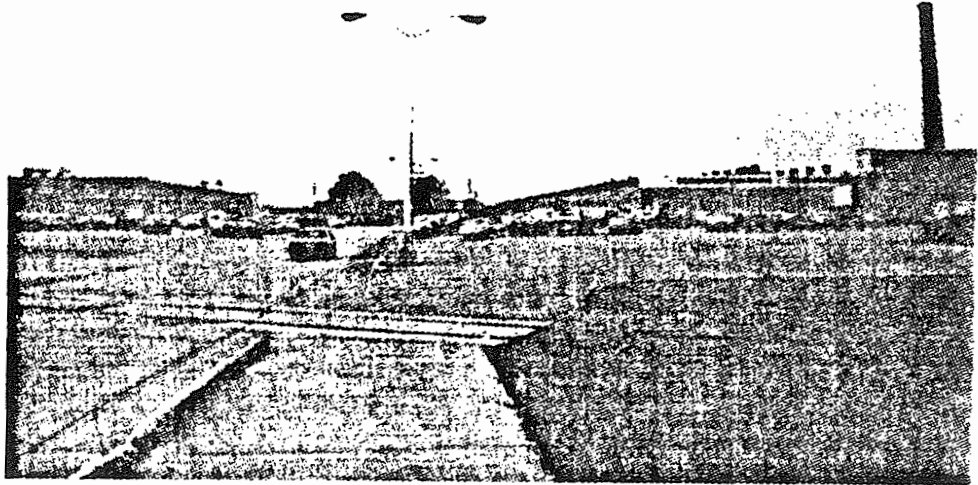


Figure 2.8 Site D: Aluminum Manufacturing Facility, single floor structure.



Figure 2.9 Site E: Casting Foundry, single floor structure.

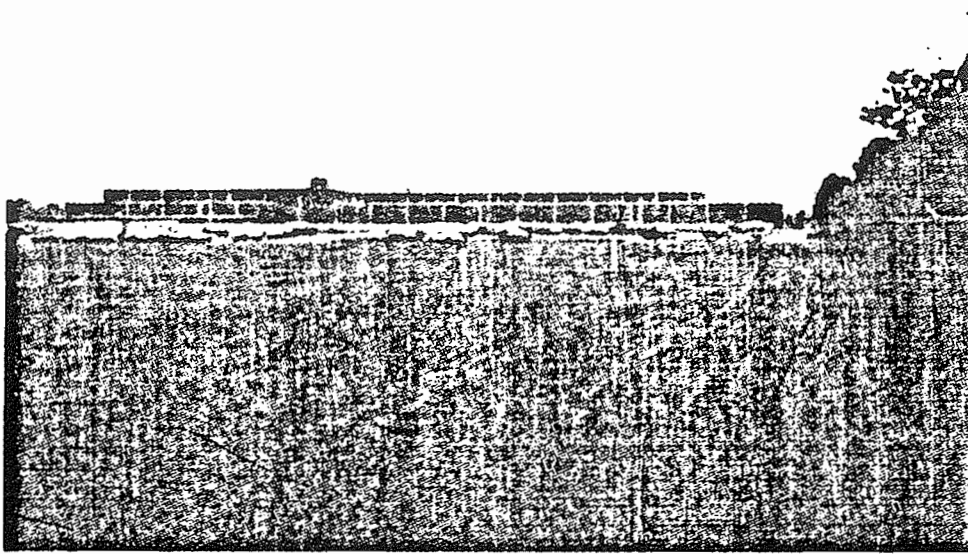


Figure 2.10 Site F: Engine Machine and Assembly Shop, single floor structure.

of hallways reported by others [53,63,72]. We often observed sharp specular reflections caused by metal doors at the end of long hallways. This phenomenon has been reported by others [53].

### **Site B: Food Processing Plant, multi floor structure**

Extensive data was collected at a major food processing/manufacturing company. Factory site B, built in 1970, is used for production and storage of frozen deserts. The 800,000 square foot building is made of thick precast concrete walls, concrete floors and metal ceilings that are reinforced by steel girders. Although the structure contains 5 floors, the first floor of the building represents a large majority of the building space. The 2nd through 5th floors are used primarily for personnel recreation, storage, and power distribution. The main floor is partitioned into five main areas: administration offices; warehouse storage; food processing and production; refrigerated warehouse; and loading dock. The areas are connected by a main 20 ft. wide hallway that runs the length of the building. Figure 2.11 shows the floor layout of building B.

The dry warehouse is typical of most industrial warehouses. The walls are constructed of 6 in. preformed concrete with metal reinforcing rods. The ceiling is made of ribbed steel and is situated 30 ft. above the floor. Steel wide-flange beams from the floor to the ceiling are spaced at 40 ft. X 25 ft. intervals throughout the warehouse. Wide (12 ft. aisles are flanked by large metal shelves that are stocked with dry foodstuffs, aluminum barrels and paper products. The shelves are 16 ft. tall, and, when full, obstruct line-of-sight paths between aisleways. Fork lift trucks, which enter the warehouse through 2 large steel fold-out doors, commonly move about the area.

The food processing and production area consists of many large stainless steel pipes, several huge steel tanks, three conveyor belts, and large metal consoles. A large generator and a steel cat walk hang from the 30 ft. ceiling. The area is manned by approximately 20 employees who constantly move about the area. A mezzanine level, located above a portion of the food production area in the center of the building, contains a small office area for the plant engineering staff. The area contains several modern fiberboard partitions which divide the floor space into several offices.

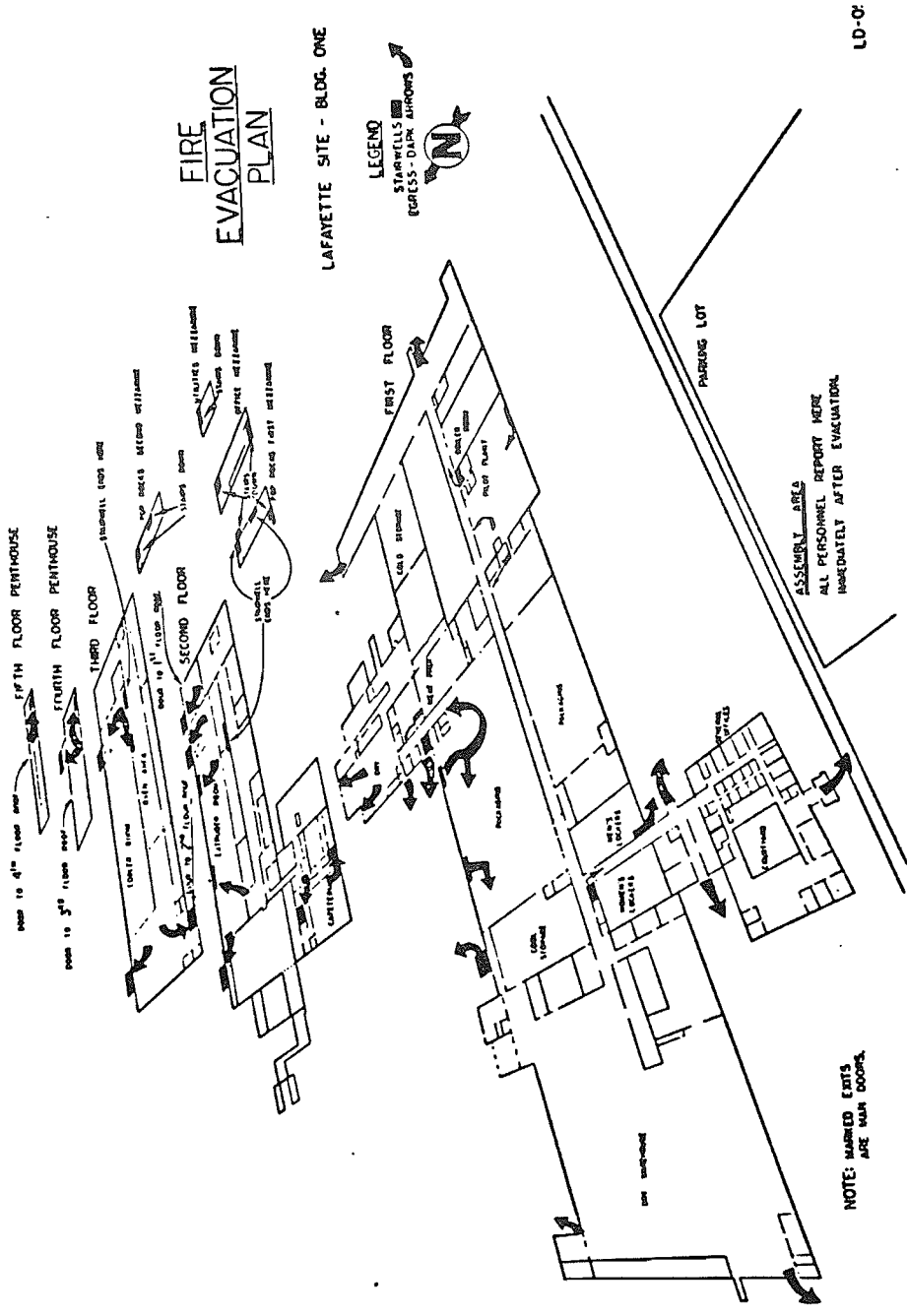


Figure 2.11 Layout of factory site B.

The refrigerated warehouse is very similar in layout to the storage warehouse mentioned above. The most noticeable difference is that room temperature is maintained at 0° F. The entire room has over 8,000 sq. feet of floor space and has insulated walls with an outer metal shell. This area is used to store perishable raw materials as well as inventory, and also serves as a temporary storage for goods to be shipped. Fork lift trucks and personnel frequent the area.

The shipping and packing area is located at the rear of the building and features preformed concrete wall, tall (50 ft.) metal ceilings and 6 large steel docking doors. Several automated packing machines crate the finished products for shipping or inventory storage. Fork lift trucks are in constant use.

#### Site C: Engine Manufacturing Plant, new single floor structure

Data was collected in the manufacturing facility of a a major diesel engine producer. Site C, built in 1985, is used for producing large metal engine products, such as crank shafts, cylinders, and completely assembled engines for world wide customers. The building is 950 ft. X 1320 ft. and features state-of-the art manufacturing technology. An automatic storage retrieval system, modular storage areas, several overhead cranes, and fork lift trucks and trains are used to store and transport parts throughout the plant. Steel trusses support the corrugated steel roof deck, which is exterior coated with 2 in. fiberglass insulation. 4 ply glass fiber roofing felts and flakes of asphalt-based aluminum roof coating material are used on the roof. Busy steel truss work varies in height from 25 ft. to 36 ft. Wooden floors, consisting of 4 in. two-by-fours laid upon concrete, are used in a majority of the plant. The lower segments of walls in the building are made of 7 ft. tall pre-cast reinforced concrete panels. Above 7 ft. the walls are formed from 1.5 in. thick preformed steel sidewalls that are insulated with fiberglass. Wide flange steel beams extend vertically from the floor to the ceiling to form 50 ft. X 50 ft. bays throughout the plant. The steel beams have an 18 in. (on the average) flange width.

The building is separated into three main areas (see Figure 2.12): a manufacturing area, an assembly area, and an office/training area. The manufacturing area occupies roughly half of the building. Here, the ceiling

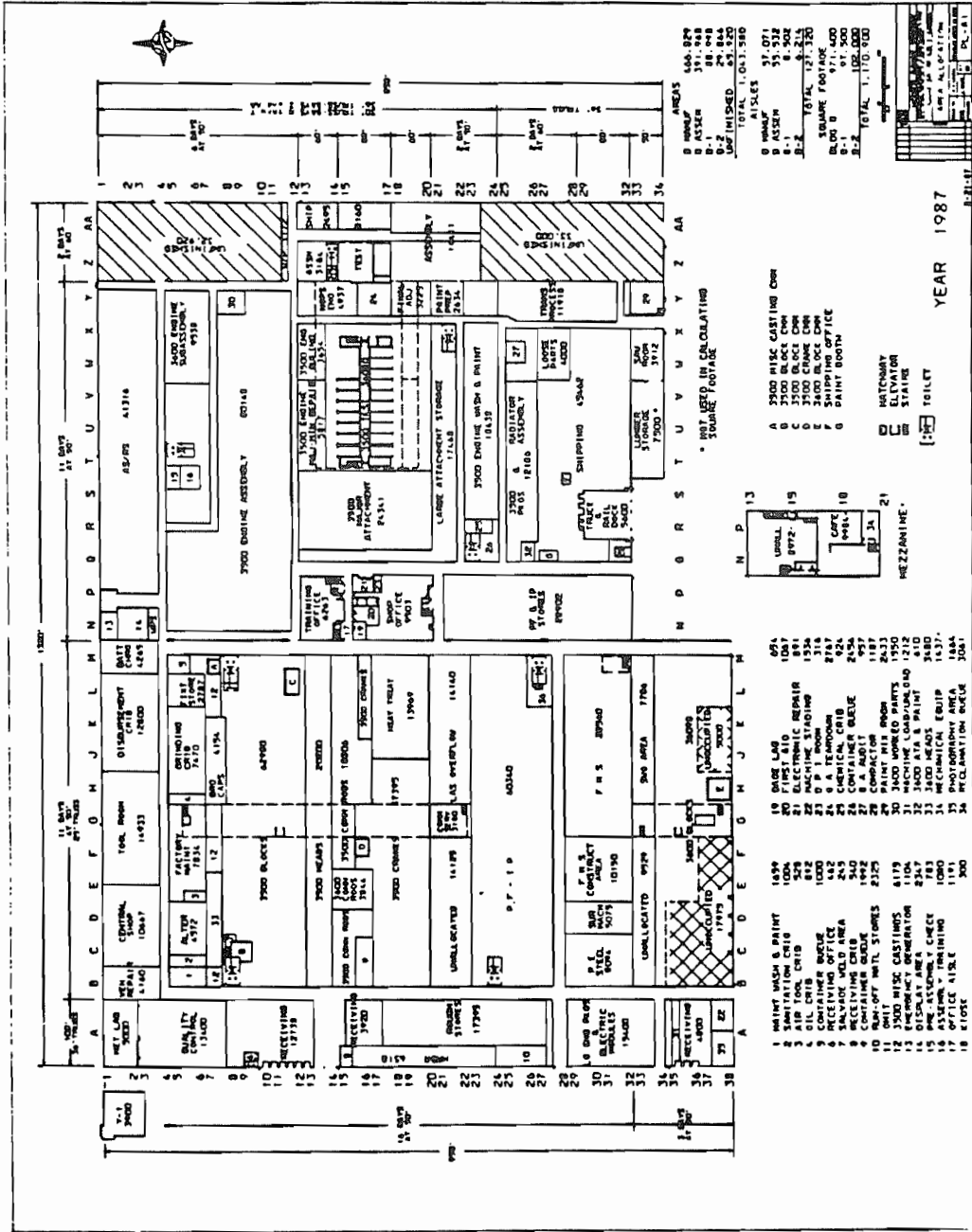


Figure 2.12 Floor layout of site C.

truss work is at a 25 ft. level. This portion of the factory is dedicated to the machining of castings and forgings. Large pieces of equipment and many pieces of metallic work-in-process are located throughout the manufacturing area, which is arranged in a modular fashion and connected with 20 ft. wide aisles. Receiving and quality control departments flank the area. Employees and fork lifts are in constant motion throughout this portion of the plant, and the skyline is very cluttered. Line-of-sight radio paths appear to be difficult because of the large amount of clutter.

The assembly area occupies the majority of the remaining half of the floor space. This portion of the building accommodates the painting, testing and assembly of large pieces of engine equipment. The ceilings are supported by steel trusses at a height of 36 ft. Several overhead crane systems are used to haul large engine components through various phases of assembly. A spacious shipping dock, which features 5 large metal overhead sliding doors, flanks the assembly area and contains several large pieces of inventory. The dock facilitates rail train as well as truck shipments. The assembly area is best described as a lightly cluttered factory area. Line of paths are likely in most locations with antennas mounted above the 6' or 8' level.

The office/training area is located in the center of the building and consists of a two story structure that is entirely enclosed with 8 in. concrete block/ steel rebar walls. In this area there are several offices, an open office area which has several modern metal partitions, and a cafeteria. The surroundings are typical of a modern office building. Poured concrete on a steel frame form the partition between the first and second story of the sub-building. The west end of the office/training building is actually part of the fire wall that divides the factory. The fire wall is 28 in. thick, and consists of steel reinforced (rebar) concrete block.

#### **Site D: Aluminum manufacturing facility, single floor structure**

Factory building D, built in 1938, covers about 40 acres of land and has dimensions 880 ft. X 2020 ft. The single story structure is used for producing extruded aluminum products. Sections of the building are dedicated to ingot fabrication, extrusion, tube milling, heat treating and quenching, and shipping. Large bundles of aluminum tubing, massive quantities of



bulk aluminum ingot, overhead cranes, furnaces, boring machines, lathes and hydraulic tanks and presses are common sites throughout the plant. Figure 2.13 shows an approximate layout of site D.

The factory is laid out in 80 ft. X 20 ft. bays. Aisleways are arranged in perpendicular intersecting fashion and are typically 12 ft. wide. Thick steel I-beams extend from the floor to the ceiling at 50 ft. grid locations. The exterior of the building is made of red brick, and features a roof that has periodic steeping in a saw tooth fashion. Windows are located in the vertical portions of the roof steeples, which are 40 ft. above the factory floor, as well as at eye level in some parts of the building. The tarpaper/gravel roof is supported by sheet steel, which is in turn supported by dense (metal) ceiling truss structures. Ceiling height varies between 40 ft. and 60 ft. while the busy steel truss work is 30 ft. above the floor.

The work floor is formed from 4 in. wooden block on a thick concrete base, whereas aisles are made from poured concrete. The building exterior walls are primarily red brick, although some walls use 3 in. insulated ribbed steel construction. A few of the walls along the side of the building are actually large wooden sliding doors. There is constant motion throughout the factory as employees transport the work-in-process with overhead cranes (mounted 30 ft. above the factory floor) and fork lift trucks. Piles of aluminum inventory and work-in-process may be found throughout the building.

#### **Site E: Casting Foundry, single floor structure**

The foundry of a major engine manufacturing company is denoted by site E. Built in 1937, the grey iron foundry occupies 300,000 square foot of land and has dimensions 300 ft. X 1000 ft. The single story structure is used for all phases of engine metal production, and ranks as one of the five largest foundries in the United States, typically producing 600 engine blocks a day. Figure 2.14 shows a dimensioned layout of the factory. Sections of the building are dedicated to small tool storage, warehouse storage of raw materials, ceramic core mixing and production, molten iron pouring deck, 50/100 ton holding furnaces, cleaning, and inspection.

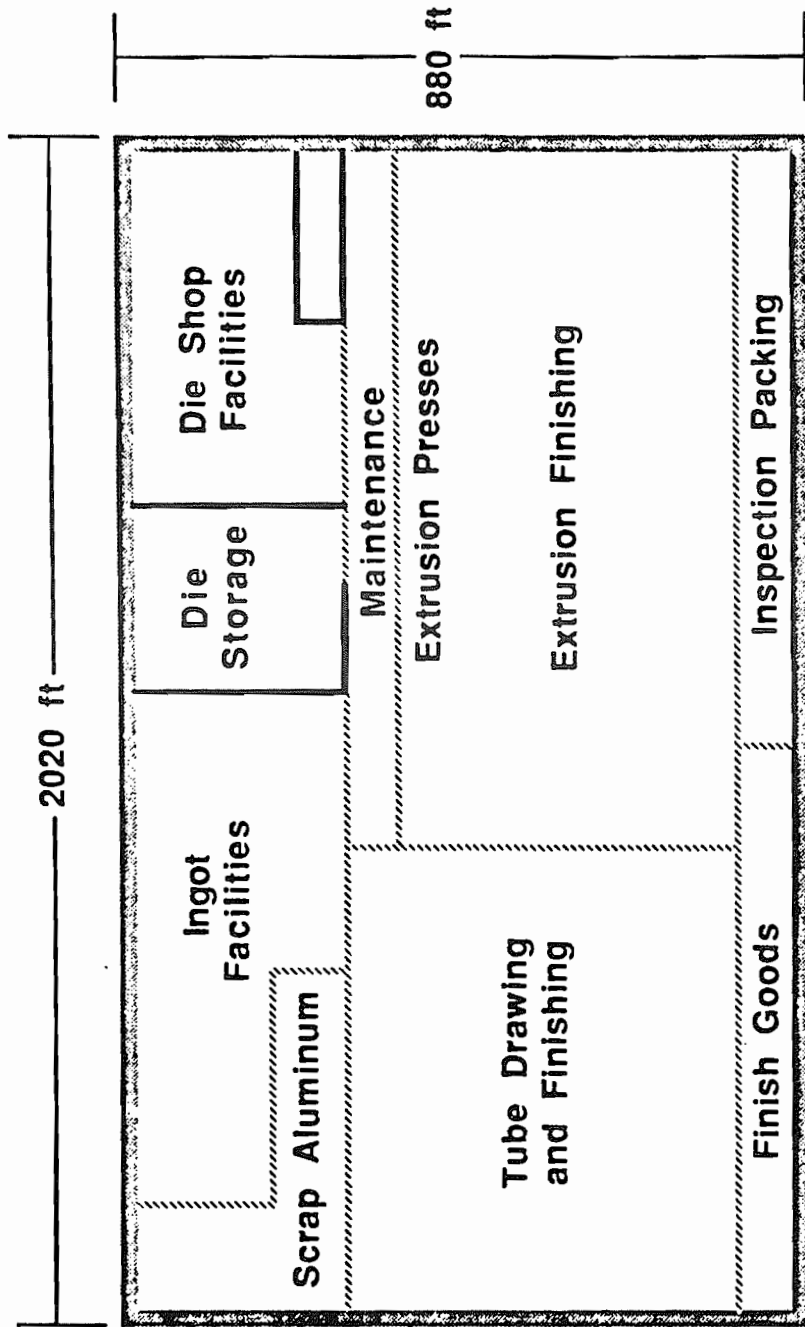


Figure 2.13 Floor layout of site D.

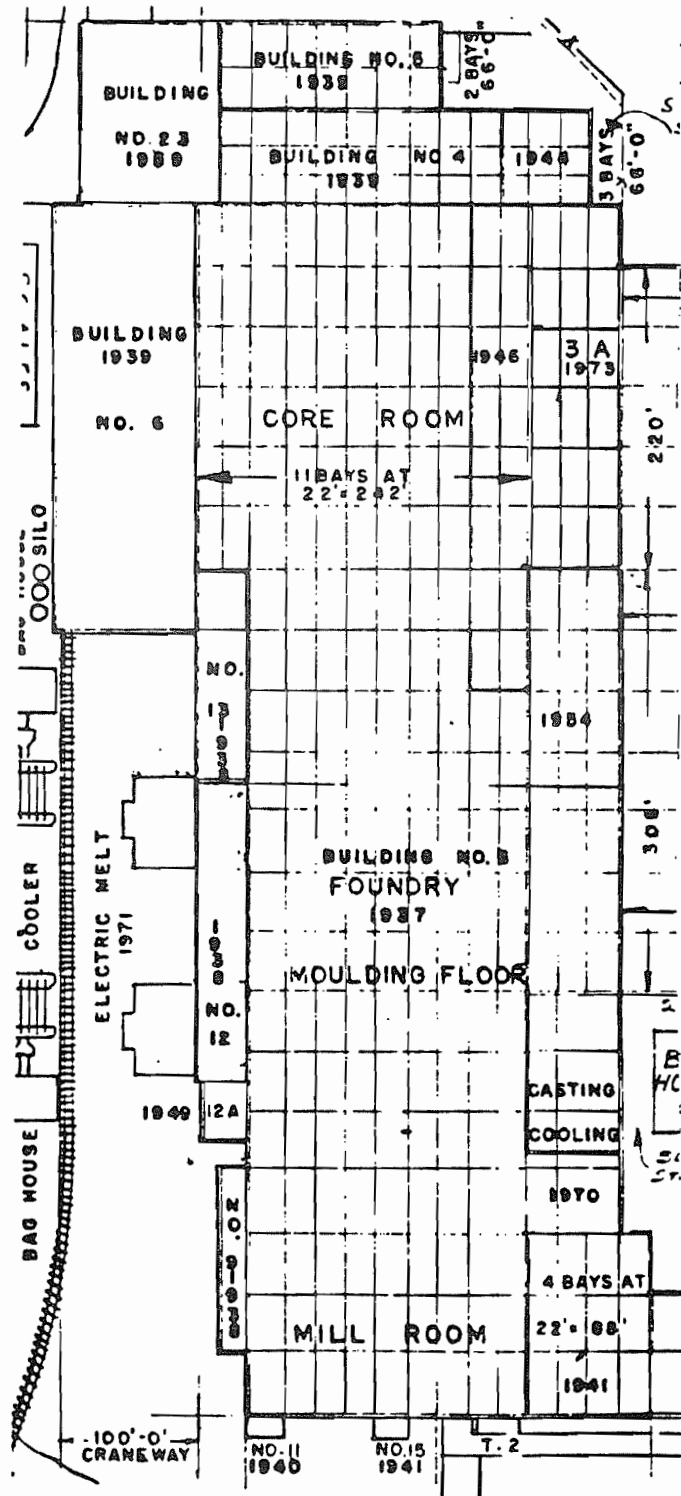


Figure 2.14 Floor layout of site E.

The small tool storage and warehouse storage areas were added later to the main building structure. The small tool storage was built in 1939 whereas the warehouse storage area was added in 1959. Both areas have light ceiling truss work which is located 20 ft. above the concrete floor. Walls are made of 6 in. thick concrete blocks. The roof construction over the newer sections of the building consists of tar and gravel poured on flat sheet steel. Both the tool storage area and warehouse have vertical steel I-beams that form approximately 20 ft. X 20 ft. bays. Exterior building walls are fabricated from 3 in. ribbed aluminum siding. The storage area is densely packed with tooling hardware stacked on large 12 ft. tall metal racks. Each of the racks are very closely spaced; aisle widths are just wide enough to allow a person to walk through. The warehouse storage area is typical of most factories, and consists of 12 ft. wide aisles configured in an orthogonal grid pattern. The inventory consists of bags of sand as well as resin and chemicals that are stored in metal drums. Inventory is typically stacked to a height of 8 ft. and is arranged in rows that flank the aisles. Fork lift trucks and plant personnel frequent the area.

The roof structure throughout the (original) foundry consists of a periodic saw tooth design with large north-facing windows. Roof height typically varies from 25 ft. to 40 ft. reaching a peak height of over 60 ft. in the molten iron pouring and cooling areas. The busy truss work is typically 5 ft. closer to the floor. Roofing material is simple sheet metal covered with tar and gravel. The east exterior wall is formed from 6 in. concrete block while the other exterior walls are formed from 3 in. ribbed aluminum siding. Except for the pouring and furnace areas, the foundry floor is made of wood block. A concrete surface is used on the perimeter aisles. Typical aisle widths are 12 ft. on the perimeter aisles; 8 ft. on interior aisles. Large steel I-beams extend from the floor to the ceiling to form 22 ft. X 44 ft. bays.

The core production area of the foundry features a very dense ceiling truss structure, which typically hangs 25 ft. above the wood block floor. Cat walks support computer controlled sand weighing systems, and serve as power decks for some of the large hydraulic presses and heaters that are used to form the core moldings. There are approximately 60 large core machines of various sizes that are used to weigh, mix, press, form and drill the molded sand cores.

The "hot" area is located in the center of the foundry. This is where the pouring deck and holding furnaces are located. The environment is busy and hostile. Large ceiling-mounted ladles, radio-controlled by operators on the floor below, are used to haul molten steel from the holding furnaces to the pouring deck. Core forms are transported to the pouring deck by tub trains that are suspended from the ceiling. Sparks from splashes of molten iron are frequent, and the heat level is quite high. The floor surface varies between dirt and concrete throughout the pouring and setting deck areas. Up to 200 employees man this portion of the foundry, and are responsible for collecting the slag from ladles, setting the cores in flasks, sand-packing the flasks, and controlling the molten level in the pouring furnace. Underneath the pouring and setting decks are 20 ft. deep tunnels which channel the emptied flasks to the cleaning area. The castings are routed by conveyor belt to the ceiling where they undergo the cool-down process.

Outside of the foundry, directly to the west of the holding furnaces, is a large scrap iron junk yard. A 70 ft. high suspended electromagnetic crane picks up scrap iron and loads it into several 500 KW induction heaters located next to the holding furnace area.

The cleaning and inspection areas have building construction characteristics very similar to the core production area, with the exception of the cat walks. Wood block floors are used throughout both areas. In the cleaning area, large machinery bounce the cooled flasks to free them of sand (shakeout). Sand blasting machinery clean the cooled castings. Fork lift trucks frequent the area to carry cleaned castings to the inspection areas.

The inspection area has a noticeably clear skyline, contrasting the sky-scraper like arrangement of machinery seen elsewhere in the building. Short piles of finished castings are brought in by forklift trucks and are placed in rows throughout the area. Employees operate hand tools to chip unwanted metal from the castings. The finished castings are inspected and sent to the shipping dock, adjacently located at the southern (rear) end of the building.

**Site F: Engine Machine and Assembly Shop, single floor structure**

Site F is a 900,000 square foot single floor structure that is located on the same campus as the casting foundry. The building, built in 1938 and appended in 1973, contains an extensive machine shop area as well as several manual and automated machining and assembly lines. The building may be classified by three distinct areas:

- a) conventional machine shop floor;
- b) conventional assembly line floor;
- c) modern automated assembly line and machine shop floor.

The building layout of site F is shown in Figure 2.15.

The conventional machine shop is arranged by 33 ft. X 22 ft. bays. The roof, which is made of tar built upon a base of insulating board and sheet metal, has a periodic sawtooth structure with north facing windows. Roof height ranges from 16 ft. to 30 ft. Walls throughout the building are made of concrete block or red brick. The machine shop ceiling truss structure includes large steel beams originally designed to hold the belts and pulleys of line shaft machines. The floor is made of wooden blocks, with cement being used for the perimeter aisles.

Large pieces of numerical control equipment are arranged in an orderly fashion throughout the shop. Parts-in-process are transported via electric fork lift trucks that travel throughout the area in 10 ft. aisles. Different sections of the shop are dedicated to the machining of specific engine and automotive components, such as brake drums and exhaust manifolds. In general, there are few tall obstructions that could block a line-of-sight radio path from an antenna mounted at the 2 m or 3 m level.

The assembly line area, located in the middle of the building, is blocked off from the machine shop by a brick wall. In this area, the ceiling trusses are mounted 16 ft. above the wood block floor. Roof construction is identical to the other areas of the building, consisting of tar and gravel upon a deck of sheet steel and insulating paper). Various hand and semi-automated assembly lines are used to build diesel engines. Like the machine shop, there are few obstructions to block a line-of-sight path within the assembly line area.

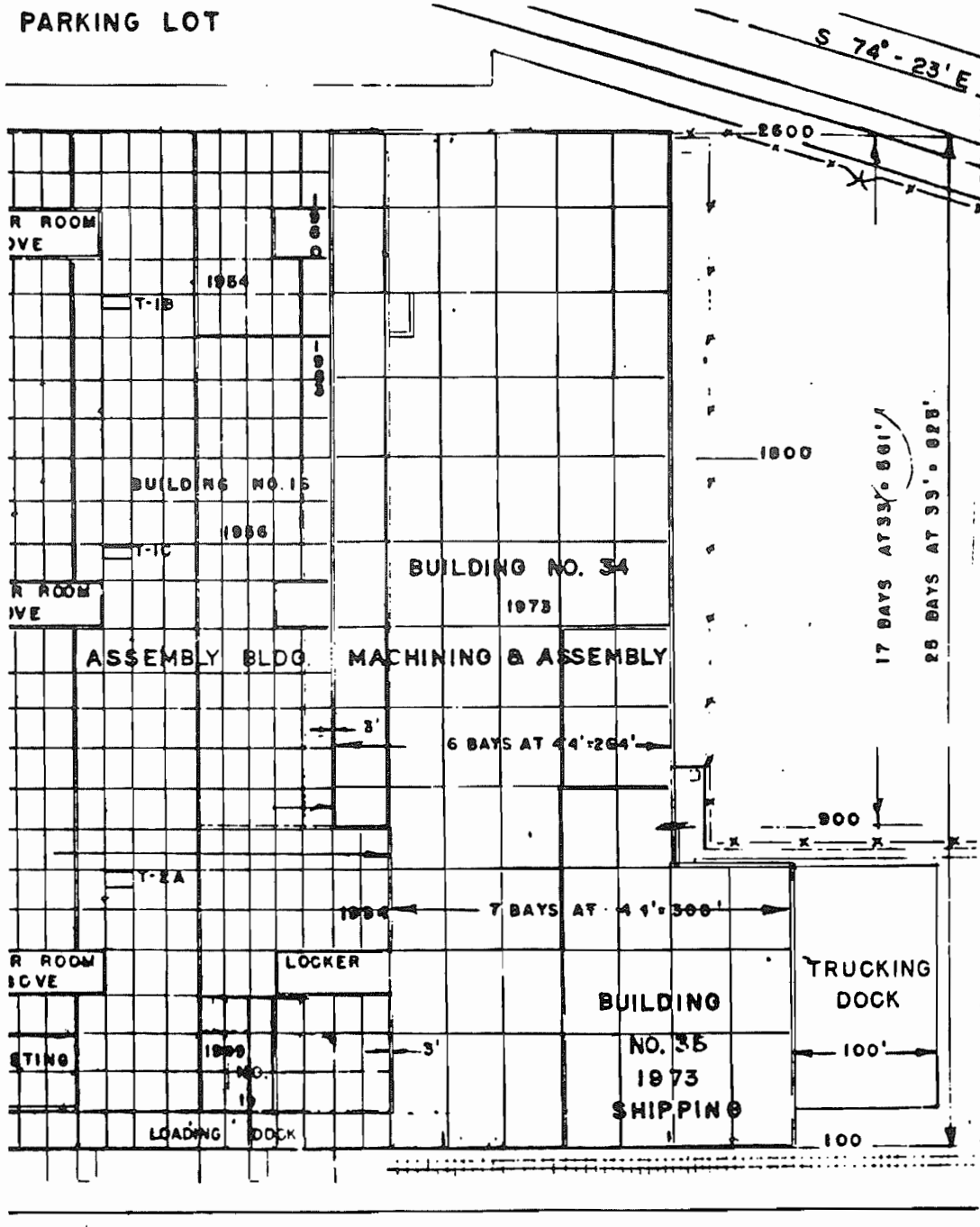


Figure 2.15 Floor layout of site F.

The modern machining and assembly line area is located in a building addition built in 1975. This area of the plant houses state-of-the-art manufacturing technology, and is the site for diesel engine machining. Building characteristics in the modern machine/assembly area include wooden floors, 6 in. thick concrete block walls, 44 ft. X 66 ft. bays, 2 ft. X 2 ft. wide flange steel beams that extend 30 ft. vertically from the floor to the massive ceiling trusses (38 ft. to the steel roof) and several catwalks which support the power supplies for much of the machinery. An automatic storage and retrieval system is located in the southeast corner of the area. Massive machines, such as an automated machining line, and an RF hardening machine make the skyline very busy. Line-of-sight radio paths within the area appear to be difficult.

#### **2.4 Experimental Procedure**

Propagation experiments were conducted in typical areas throughout each of the five aforementioned factories. Several visits to each site indicated that there are at least four general types of geographical settings in all manufacturing facilities. These geographies may be classified as:

**1) Line of sight path with light surrounding clutter**

Such paths are found along major aisles that are surrounded by relatively empty storage areas or low density work areas (such as a machine shop) where most scatterers are lower than the height of the receiver antenna.

**2) Line of sight path with heavy surrounding clutter**

Such paths are found along aisles in a well-stocked warehouse or along the aisles of an automated assembly line area where a significant amount of metal is located at heights greater than the receiver antenna.

**3) Obstructed path-- light surrounding clutter**

Such paths exist when a LOS path is blocked by inventory or machinery that is approximately the same height as the



receiving antenna. Such a radio path would typically exist across a machine shop or a manual assembly area.

#### 4) Obstructed path-- heavy surrounding clutter

Such paths exist throughout areas of the factory where the "skyline" is busy, such as within a metal foundry, across an automated assembly line area, or between aisles in a stocked warehouse.

Figures 2.16 - 2.19 vividly illustrate the four distinct geographical factory settings.

A geography which we could have considered, but did not, is the case where radio paths exist in the vicinity of walls. Such paths exist for radios located along the perimeter of a factory or in aisles adjacent to fire walls. We felt that this geography is similar enough to a line of sight heavy clutter area, and is also similar to hallways in office buildings for which some multipath delay spread and attenuation measurements have already been made [71,72]. Some measurements in such a geographical setting were made at site C. Since the majority of building structures we visited were single storied and had very few partitions, propagation characteristics between floors or through walls were not investigated.

In each factory, measurements were made in the four previously mentioned geographical settings. Arrangements were made with the factories to collect the propagation data during a slow work period so that our measurements would not interfere with normal plant operations. For all measurements, the transmitter cart was positioned in a location clear of immediate obstructions within the desired geography, such as in the middle of the intersection of two main aisles. The transmitting antenna was located 2 m above the floor. For each geographical area within each factory, 3 measurement locations were selected having graduated transmitter-receiver separations (nominally 25 m, 50 m and 75 m). The receiver cart was positioned in an aisle or other sensible vehicle pathway that was typical for the specific geography. Receiver antenna height was 2 m but was lowered to 1.5 m during the fading diversity experiment described below.

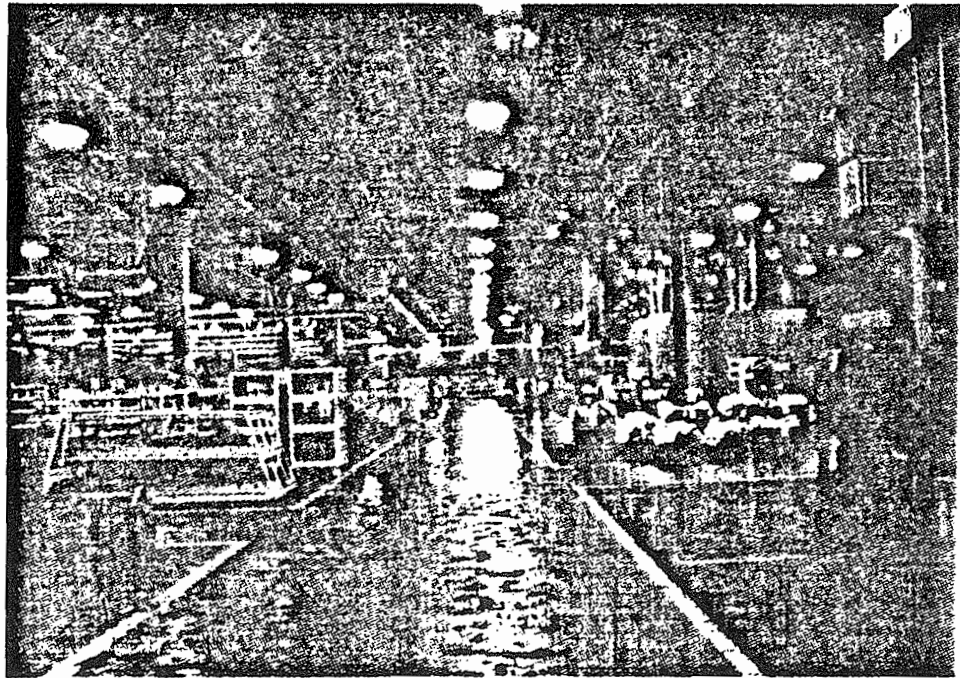


Figure 2.16 Example of LOS light clutter geography (From site C).

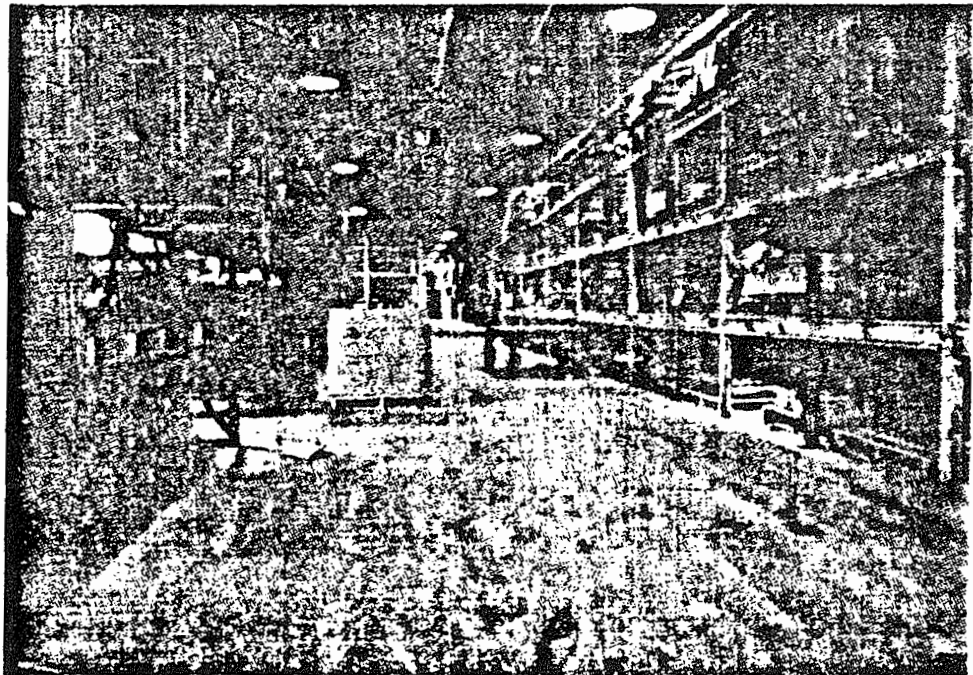


Figure 2.17 Example of LOS heavy clutter geography (From site E).

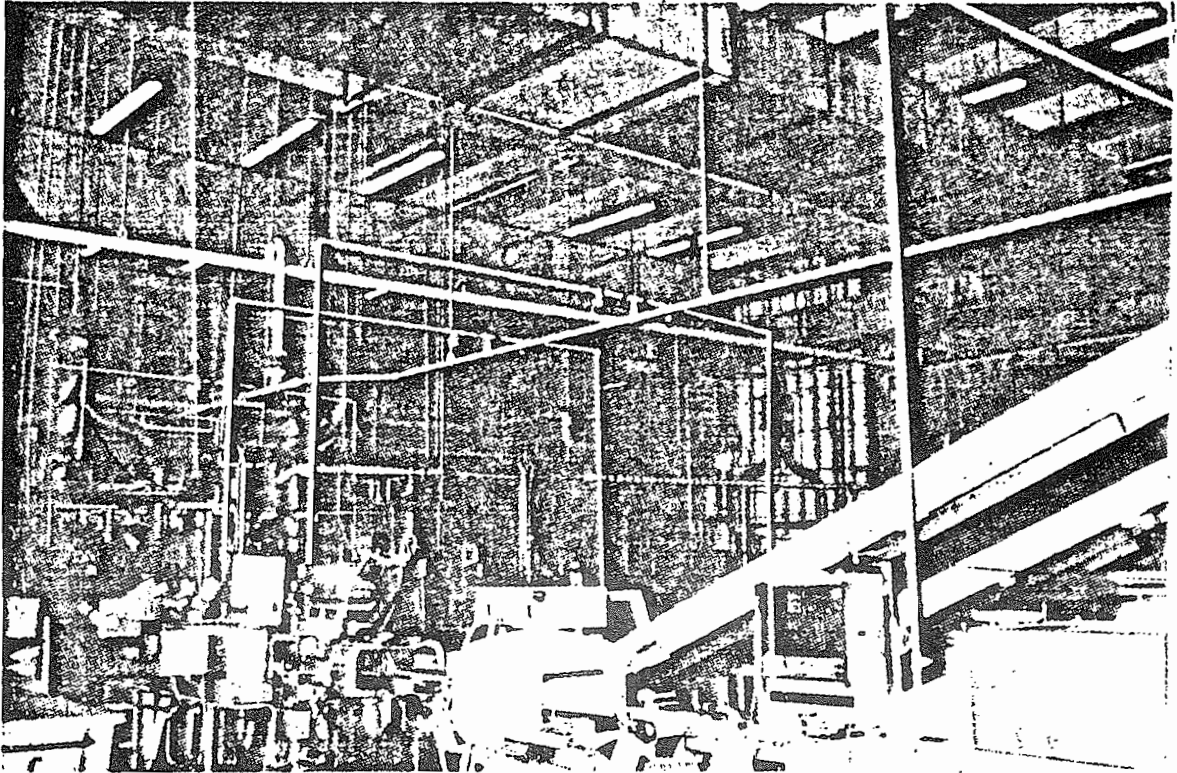


Figure 2.18 Example of obstructed path light clutter geography (From site B).

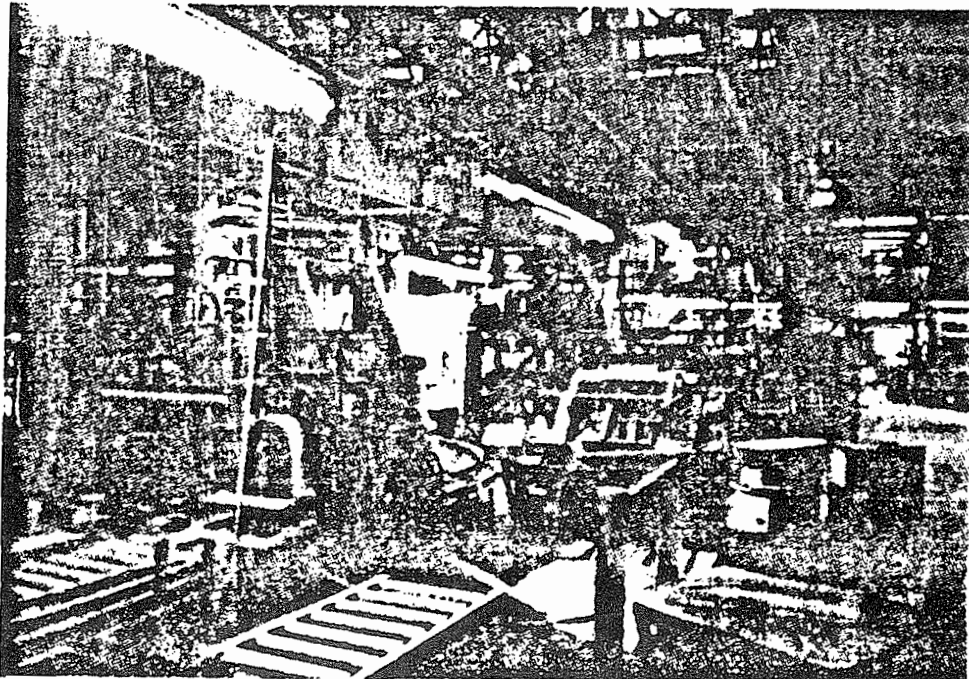


Figure 2.19 Example of obstructed path heavy clutter geography (From site F).

At each measurement location, 4 types of data were collected in a local neighborhood: Wide band multipath power profiles in the center of the aisle, CW fading data in the center of the aisle with antenna heights of 1.5 m and 2 m, and CW fading data at the side of an aisle. In sites E and F, some temporal fading measurements were made with the receiver in the center of the aisle.

Multipath power delay profiles were recorded at  $\lambda/4$  intervals along a 1 m track in the center of the aisle. The measurement was performed by pushing the cart next to a customized meter stick marked in 5.6 cm intervals, and adjusting the scope trigger if necessary before logging a profile at each mark. For all pulse measurements, care was taken to select an oscilloscope display time span great enough to capture all significant paths, yet not excessively great to include receiver noise which artificially increases the delay spread and power gain measurements.

CW fading measurements were performed along 2 paths located in the center and at an arbitrary side of the aisle. It seems reasonable to believe that with similar local surroundings, propagation characteristics on either side of an aisle would be comparable. However, for a ceiling-mounted antenna, received signal characteristics would not necessarily be similar. (For ceiling mounted antennas, one might expect to observe asymmetric shadowing as recent experiments for land mobile-satellite systems have indicated tree shadowing effects differ greatly in opposite lanes of traffic [80]). To collect the fading data for each experiment, the receiver cart was steadily pushed along a 1.3 m track by hand while 128 discrete receiver IF voltage readings were recorded and stored in a 5 second span. A uniform velocity was insured by starting the cart a meter or so before the measurement track. Three such fading measurements were performed at each measurement location. The first measurement was performed in the center of the aisle along the same (but slightly longer) track that was used for the multipath profile measurements. The second measurement used the identical track with the antenna lowered to a height of 1.5 m. The third fading measurement was performed on a track located at the extreme left or right edge of the aisle parallel with the center track. Because most aisle widths are on the order of 3 to 4 m, this corresponded to a distance of 1.5 to 2 m between tracks. Throughout each factory, an equal number of left and right aisle measurements were performed, and an equal number of tracks

which were perpendicular to and radial to a line drawn from the transmitter to receiver were used.

In areas of significant motion, such as beneath a moving overhead fan or near a moving conveyor belt, a 100 s single sweep measurement of the received CW signal level was recorded at a 10.24 Hz sampling rate. Factory sites B, C and D were visited during periods of slow activity and showed very small fluctuations in signal strength during the single sweep measurement. Consequently, single sweep power measurements were retained from the active factories only (sites E and F).

For all measurements, the operators of both transmitter and receiver carts remained still and positioned themselves away from the antennas. Because many members of the research team were amateur radio operators, 144 MHz handi-talkies were used to report information regarding transmitter settings and channel motion. At each factory site, 57 multipath delay profiles and 1152 CW envelope measurements were made in each geographic area (however, the data from a couple of measurement locations was inadvertently destroyed due to carelessness brought on by operator fatigue). Collection of the data typically required six hours per site. At sites B and D, measurements were conducted in all four geographies described on page 48. At site C, measurements were recorded in those four geographies and also in an additional geography (referred to as "LOS wall"). Because of concern that our measurements would interfere with normal factory operations, we were restricted to making measurements in LOS and obstructed heavy clutter path geographies at sites E and F. The experiments resulted in a data pool that contains over 900 factory multipath profiles and 22,500 received CW power measurements.

**CHAPTER 3**  
**CHANNEL FORMULATION**  
**AND**  
**DATA REDUCTION**

**3.1 Impulse Response Model**

**3.1.1 Multipath Power Delay Model**

One of our goals is to characterize the factory channel impulse response. A simple channel representation is illustrated in Figure 3.1a, where  $h(t)$  represents a causal, linear time varying channel. A simple channel model is one in which the received signal  $y(t)$  is an attenuated and time delayed version of the transmitted signal  $x(t)$ . For a discrete channel model, this implies [66]

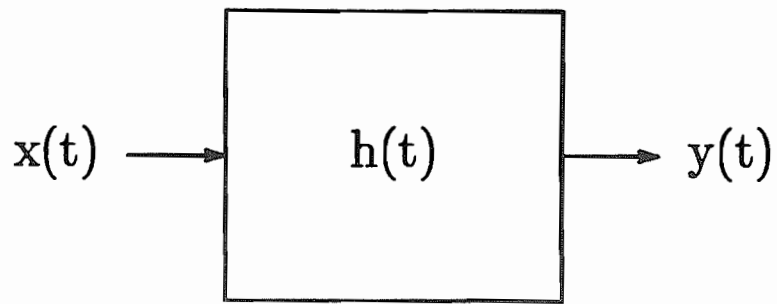
$$y(t) = \sum_k \alpha_k(t) x(t - \tau_k(t)) \quad (3.1)$$

Our digitized experimental data readily lends itself to representation by a discrete channel model. Multipath profile measurements in other radio channels have indicated the discrete model suitably fits the finite and distinct nature of the delayed paths [9,53,54].

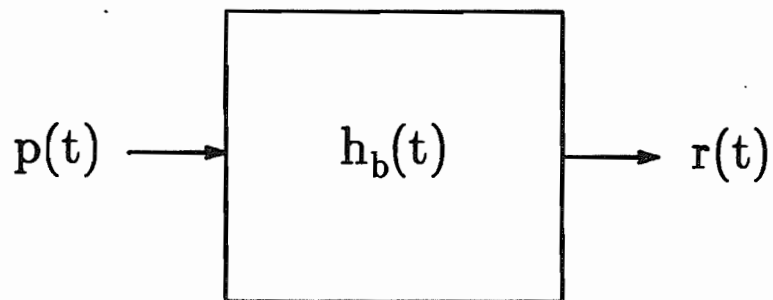
Note that the received signal in (3.1) is a function of both time and excess delay ( $\tau_k$ ). Since our measurements were made during very slow factory activity, the  $\alpha_k$ 's and  $\tau_k$ 's imposed by the channel are virtually independent of time. Using this fact, the impulse response is given by

$$h(t) = \sum_k \alpha_k \delta(t - \tau_k) \quad (3.2)$$

where  $\delta(\ )$  is the Dirac delta function and  $\tau_0$  denotes the first observable pulse with our apparatus.



a) Linear channel model for multipath channel.



b) Equivalent low pass channel model.

Figure 3.1 Linear channel models for multipath channel.



For a transmitted signal of the form

$$x(t) = \text{Re} \left[ p(t) e^{j2\pi f_c t} \right] \quad \text{where } p(t) \simeq \text{rect} \left[ \frac{t - 5 \times 10^{-9}}{10^{-8}} \right] \quad (3.2a)$$

the channel output is

$$\begin{aligned} y(t) &= \int_{-\infty}^{\infty} x(\zeta) h(t-\zeta) d\zeta = \text{Re} \left[ \left( \sum_k \alpha_k e^{-j2\pi f_c \tau_k} p(t-\tau_k) \right) e^{j2\pi f_c t} \right] \\ &= \text{Re} \left[ r(t) e^{j2\pi f_c t} \right] \end{aligned} \quad (3.2b)$$

where

$$r(t) = \left( \sum_k \alpha_k e^{-j2\pi f_c \tau_k} p(t-\tau_k) \right)$$

The channel may be equivalently described by the low pass impulse response  $h_b(t)$  having an output  $r(t)$  which is the complex envelope of  $y(t)$ . The low pass characterization removes the high frequency variations caused by the carrier making it analytically easier to handle. Thus, we strive to characterize the low pass equivalent channel impulse response  $h_b(t)$  which is given by

$$h_b(t) = \sum_k \alpha_k e^{-j2\pi f_c \tau_k} \delta(t-\tau_k) \quad (3.3)$$

In (3.3),  $\alpha_k$  represents a real attenuation factor,  $e^{j2\pi f_c \tau_k}$  represents a linear phase shift due to propagation, and  $\tau_k$  is the time delay of the  $k$ -th path in the channel. Figure 3.1b illustrates the equivalent low pass channel model.

By modulating an RF carrier with a 10 ns sounding probe, the output of the low pass channel closely approximates the impulse response  $h_b(t)$ . Instead of measuring the output  $r(t)$  however, we measure  $|r(t)|^2$ . Letting  $\theta_k$  represent the linear phase term in (3.3), our multipath power profile display becomes

$$|r(t)|^2 = r(t) r^*(t) = \text{Re} \left[ \sum_j \sum_k \alpha_j \alpha_k p(t-\tau_j) p(t-\tau_k) e^{-j(\theta_j - \theta_k)} \right] \quad (3.4)$$

Note that if  $|\tau_j - \tau_k| > 10$  ns for all  $j \neq k$ , then



$$|r(t)|^2 = \sum_k \alpha_k^2 p^2(t - \tau_k)$$

and the power profile measurement has a path resolution of 10 ns. For  $|\tau_j - \tau_k| < 10$  ns, there is pulse overlap and we assume there to be unresolvable sub-paths that combine to form one observable path. Although the digitizing oscilloscope provides  $\alpha_k^2$ ,  $\tau_k$  values at intervals between 1 and 5 ns, for impulse response modeling we use Turin's approach [54] in that we quantize the power profile into bins having 10 ns durations (although for calculating multipath parameters such as delay spread, all  $\alpha_k^2$ ,  $\tau_k$  values were used). Within each bin, we integrate over the  $\alpha_k^2$ 's to obtain an equivalent  $A_K^2$  at a time  $T_K$ . Thus, although our measurement is expressed by (3.4), we reduce the display as

$$|r(t)|^2 \simeq |h_b(t)|^2 = \sum_K A_K^2 p^2(t - T_K), \quad T_{K+1} - T_K = 10 \text{ ns} \quad (3.5)$$

Because we make power profile measurements at  $\lambda/4$  intervals on a  $4.3\lambda$  path, local spatial fading effects are also observed. Consequently, the measurement is not only a function of time delay but also of space. For a position  $\mathbf{x}_o$  on a given path, we measure

$$|r(t; \mathbf{x}_o)|^2 = \sum_{\mathbf{X}=\mathbf{x}_o} \sum_K A_K^2(\mathbf{X}) p^2(t - T_K(\mathbf{X})) \quad (3.6)$$

The data permits us to statistically characterize the fluctuations of path strengths and delays over local areas.

For  $5$  to  $10\lambda$  neighborhoods, other researchers have found multipath profiles to be spatially wide sense stationary (WSS) [70,71]. As is detailed in Chapters 4 and 5, this appears to hold also for the factory channel. For the WSS assumption, it is valid to approximate the measured sample records of a process by the sample average. Thus, we may average (3.6) over all local spatial locations to come up with a representative power delay profile at each measurement location.

### 3.1.2 CW Fading Model

For the CW measurements,  $p(t)$  in (3.2a) is equal to 1 for all  $t$ , and the received signal is ideally a pure sinusoid at the carrier frequency. However, motions in the channel or movement of the receiver causes fading of the signal. For this case, a suitable low pass impulse response model for the channel is [66]

$$h_b(t) = \sum_k \alpha_k(t) e^{-j2\pi f_c \tau_k(t)} \quad (3.7)$$

where it is assumed a discrete collection of phasors sum up at the receiver antenna with various path delays. For the CW case, the low pass impulse response is identically the received signal  $r(t)$  at the antenna. While it is not possible to resolve the individual  $\alpha_k$ 's or  $\tau_k$ 's of (3.7) with a CW transmission, it is possible to observe the relatively slow fading in the channel which is due to the time and spatial fluctuations of the paths comprising (3.7).

Like the multipath power profile measurements, CW envelope measurements along a short path were made while the factory was inactive. Thus, the spatial measurements dictate that the channel not be a function of time. Certain measurements performed in Factory Sites E and F, on the other hand, were conducted over the course of several minutes during normal factory activity to ascertain the time varying fading characteristics of the envelope of  $h_b(t)$ . A suitable channel model which demonstrates the dependence of the channel on both time and space is

$$r(t ; \mathbf{x}) = h_b(t ; \mathbf{x}) = \sum_k \alpha_k(t ; \mathbf{x}) e^{-j2\pi f_c \tau_k(t ; \mathbf{x})} \quad (3.8)$$

Our receiver measures  $|r(t ; \mathbf{x})|$ , the magnitude (envelope) of the low pass impulse response given above.

Disjoint statistical information regarding slow fading due to both receiver motion and ambient channel motion is readily obtained by fitting the fluctuations of the received envelope  $|r(t ; \mathbf{x})|$  to suitable probability density functions. Some indoor multipath measurements have suggested that spatial fluctuations are nearly Rayleigh [59,63]. Temporal fading has recently been shown to fit Rician distributions [77].

Envelope distributions are important for determining bit error rates in digital communications systems. With a reliable distribution model for the signal envelope, it is possible to accurately compute and predict the performance of a communication system by considering the large scale path loss and the small scale signal fluctuations about the large scale path loss [40]. These small scale signal fluctuations may occur over time (for the case of stationary terminals), over space (for the case of a mobile terminal in a temporally stationary channel) or over both time and space. As was shown in Chapter 1, a Gaussian channel assumption leads to a Rayleigh distribution of the received signal envelope. The Rayleigh distribution is given by (3.9) and is uniquely specified by the variance  $\sigma_n^2$  of the random multipath. It well describes the situation when more than a few radio paths exist between the transmitter and receiver having comparable path losses.

$$p_x(x) = \frac{x}{\sigma_n^2} e^{-x^2/2\sigma_n^2} \quad 0 \leq x < \infty \quad (3.9)$$

When a significant portion of the received signal envelope is due to a particular path, such as the LOS path, then the envelope distribution is Rician. The Rician distribution is fully specified by the ratio,  $K$ , of the dominant specular signal component to the random multipath, and is given in (3.10).

$$p_x(x) = \frac{x}{\sigma_n^2} e^{-(x^2 + A^2)/2\sigma_n^2} I_0 \left( \frac{Ax}{\sigma_n^2} \right) \quad 0 \leq x < \infty, \quad A \geq 0 \quad (3.10)$$

$$K = \frac{A^2}{2\sigma_n^2}$$

In (3.10),  $I_0(\ )$  is the modified Bessel function of the first kind and zero order. The parameter  $A$  represents the zero-peak value of the specular component, and may be set to unity to facilitate simple numerical analysis of (3.10).

Another distribution which has been found to fit some fading data is the log-normal distribution. This distribution is used to describe rain

attenuation characteristics for various earth-satellite paths [80,84]<sup>†</sup> and certain radar targets. The log-normal distribution is uniquely described by its mean  $\bar{x}$  and standard deviation  $\sigma$ . It arises in nature from the multiplication of many independent and identically distributed random variables, and has a probability density function given by (3.11) [83]. For this reason, it is difficult to postulate how the log-normal distribution would describe small scale channel fading in space or time within the factory. Although each received path is multiplied by the reflection coefficients of scattering objects in the channel, and thus is likely to have a log-normally distributed envelope at the receiver antenna, several such paths are believed to exist and add at the receiver antenna, thus suggesting a Rayleigh envelope distribution. However, if there are just a few significant multipaths that are largely and similarly affected by small receiver movement, then a log-normal distribution is plausible.

$$p_x(x) = \frac{1}{\sqrt{2\pi} \sigma x} e^{-(\log x - \bar{x})^2 / 2\sigma^2} \quad 0 \leq x < \infty \quad (3.11)$$

Data which is believed to fit a log-normal distribution is typically plotted with observations ( $x$  values) in dB about the median value. For this case, the mean is subtracted out and the observations (in dB values) are normally distributed having a median (and mean) of zero and a standard deviation of  $\sigma$  dB.

Figure 3.2 shows cumulative Rayleigh, Rician and log-normal distributions for some values of  $K$  and  $\sigma^2$ , plotted about the median. Although there are several techniques used to display distribution functions in the literature, a log-log scale such as that used in Figure 3.2 is useful because it readily indicates the likelihood of very low signal levels (deep fades) indicated by the left tails of the distributions. Deep fading is exactly the situation for which a statistical model is necessary, since it is here where bit errors occur. Indeed, the communication system performance must be considered to be conditioned on the distribution of local (or small scale) signal

<sup>†</sup>However, in these references a log normal distribution was found to hold for received signal levels given in dB. In the context here the absolute signal level (in either volts or watts) is assumed to be log-normal; i.e. normal when plotted in dB.

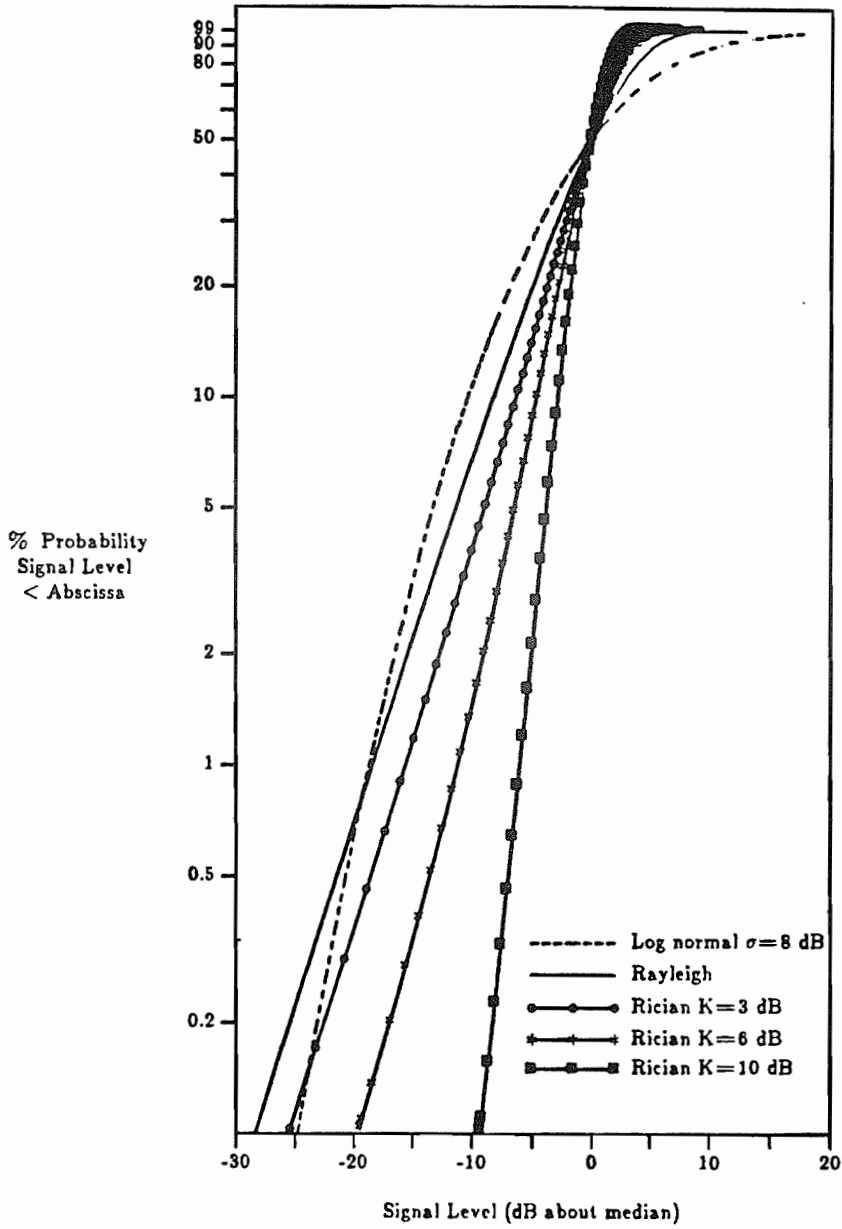


Figure 3.2 Cumulative Rayleigh, Rician and log-normal distributions.

fluctuations. An overall average system performance can be obtained by averaging the large scale path loss over these small scale fluctuations [60,61,77].

The probability of error vs. average SNR for DPSK modulation in several fading channels is shown in Figure 3.3 [77]. One immediately notes that for a given level of performance, the Rician fading channel offers substantial gain over Rayleigh fading. The figure also indicates the danger in designing a tight link budget under a Rician channel assumption. The log-normal fading channel has not been considered in [77] and is consequently not shown on Figure 3.3. Fortunately, because of the short distances and relatively low path losses involved in an indoor channel, it should be possible to design the link for adequate SNR performance regardless of the actual distribution of small scale fluctuations.

Our premise that path loss in a factory radio link is largely dependent upon factory geography and the orientation of the transmitter and receiver with respect to the factory clutter certainly stands to reason. Even after identifying distinct classes of factory geography as we have done, however, there is still randomness associated with the path loss (or "large scale") measurements since not all building structures, inventories (i.e. geographies) are identical. It is therefore useful to determine a statistical model for the large scale path loss measurements about a mean (or "typical") path loss exponent. Data from the urban mobile radio channel and propagation experiments in and around houses have revealed that received signal levels over large distances are described by a log-normal distribution (3.11) of small scale median power levels about the expected level (which is dependent upon T-R distance and the path loss exponent) [40,60,61,76].

### 3.2 Important Multipath Channel Parameters

Wide band multipath channels are grossly quantified by their mean excess delay and r.m.s. delay spread [40,53,58,70,76]. The former is the first moment of the power delay profile and is defined to be

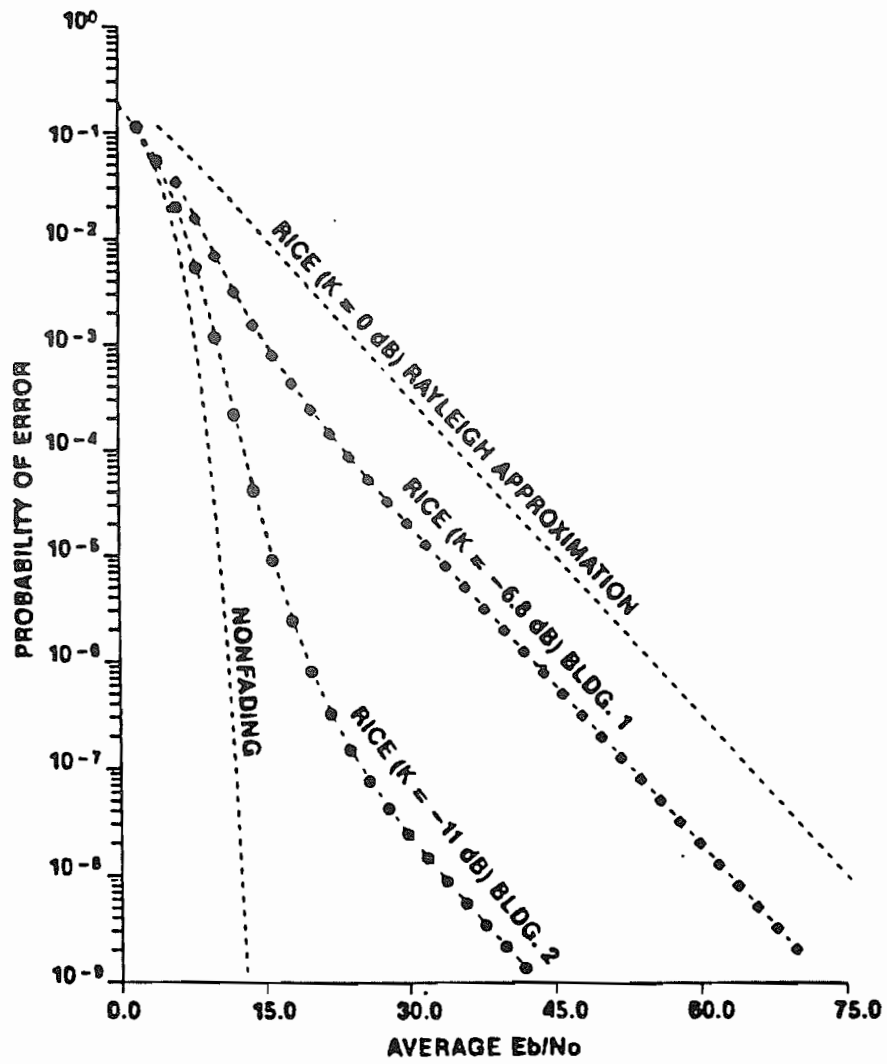


Figure 3.3 Performance curves for DPSK in fading channels. (From [77])

$$\bar{\tau} = \frac{\sum_k \alpha_k^2 \tau_k}{G_r} \quad \text{where } G_r = \sum_k \alpha_k^2 \quad (3.12)$$

The latter is the square root of the second central moment of the profile and is defined to be

$$\sigma_\tau = \sqrt{\bar{\tau^2} - (\bar{\tau})^2} \quad \text{where } \bar{\tau^2} = \frac{\sum_k \alpha_k^2 \tau_k^2}{G_r} \quad (3.13)$$

Mean excess delay is important for determining the accuracy of a CW ranging system or the extent of distortion in a narrow band FM system [81]. The r.m.s. delay spread is an important parameter in determining bandwidth capacity of a channel [40].  $G_r$ , the denominator in (3.12) and (3.13), is a measure of received power for a given profile measurement. By referencing  $G_r$  to the power received at a transmitter-receiver separation of  $10\lambda$  in free space (see Figure 2.2b) and including the factor by which the sampling time of the measurement and the reference differ, the path loss of the channel is computed. Letting PL denote path loss,  $P_t$  denote average transmitter power and  $A_t$  denote the transmitter attenuator setting for the given measurement, the path loss is given by

$$\text{PL(dB)} = P_t(\text{dBm}) - P_{10\lambda}(\text{dBm}) - A_t(\text{dB}) + A_{10\lambda}(\text{dB}) + 10 \log_{10} \left[ \frac{G_{10\lambda} \Delta\tau_{10\lambda}}{G_r \Delta\tau_r} \right] \quad (3.14)$$

where  $P_{10\lambda}$  is 13.0 dBm,  $\Delta\tau_{10\lambda}$  is the sampling interval for the  $10\lambda$  reference measurement (equal to 0.39 ns), and  $\Delta\tau_r$  is the sample interval for the profile measurement (equal to either 1.56 or 3.91 ns).

Narrow band parameters of interest include large scale path loss as a function of distance and geography. Also useful are typical and worst case fading levels as a function of time, space, and geography. The narrow band path loss is computed with reference to free space loss at a distance of  $10\lambda$ . Equation (3.15) gives the computation for path loss for a given CW measurement.

$$\text{PL(dB)} = P_t(\text{dBm}) - A_t(\text{dB}) - P_r(\text{dBm}) - \text{PL}_{10\lambda}(\text{dB}) \quad (3.15)$$

$$\text{PL}_{10\lambda} = 38.3 \text{ dB}$$



$$P_r(\text{dBm}) = 0.76V_{\text{out}} - 125.0 \quad (\text{From Figure 2.4})$$

The median  $V_{\text{out}}$  value from a given fading measurement is used in (3.15). While the measurement of path loss using both a wide band and narrow band apparatus has been claimed to yield identical results [78], it has not been previously shown what kind of experimental agreement can be achieved between the two methods.

### 3.3 Data Organization and Storage

#### 3.3.1 File Handling

The unwieldy amount of data provided by this research required that some thought be given to data management. In order to distinguish the data type contained in a file and to take advantage of the character handling capability of the UNIX-based C programming language, a filing system was employed that provided identification of the data using a very short file name.

Data collected from each measurement was assigned a file name on the HP9007 personal computer diskette which identified the type of data, the factory site, the local geography, the location in the aisle, and the relative transmitter-receiver separation. Figure 3.4 illustrates the filing protocol. It can be seen from the figure that the file "pb2cc" contains (19) multipath delay profile measurements in a LOS heavy clutter geography taken in the center of an aisle at factory site B. The measurement was made with a maximum transmitter-receiver separation. File names ending in ".d" denote diversity since those measurement were made with the antenna at the lower height. Figure 3.5 shows a listing of all data files written to diskette from factory site C.

Data files were created with the data-logging program *getdata*,<sup>†</sup> which

---

<sup>†</sup>All subsequent program names will appear in italics. Programs are documented in Appendix B.

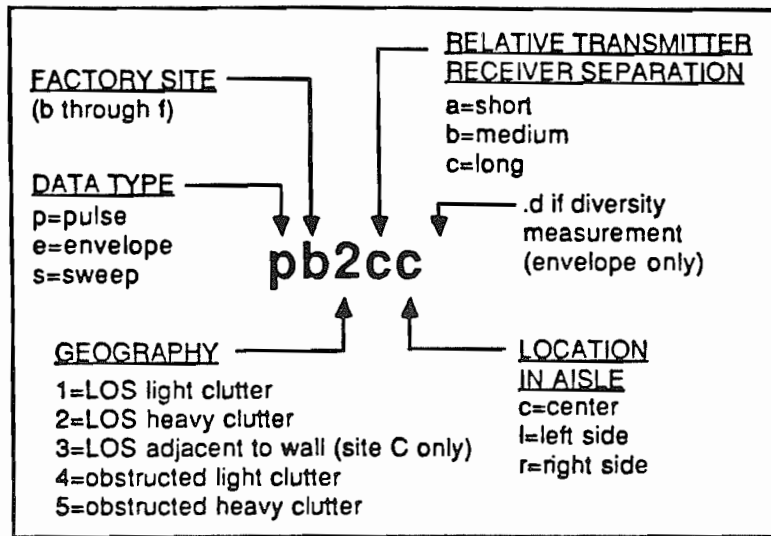


Figure 3.4 File naming system for raw data.

ec1ac	ec2ac.d	ec3ar	ec4bc	ec5bc.d	pc3ac
ec1ac.d	ec2a1	ec3bc	ec4bc.d	ec5b1	pc3bc
ec1ar	ec2bc	ec3bc.d	ec4b1	ec5cc.d	pc3cc
ec1bc	ec2bc.d	ec3b1	ec4cc	ec5c1	pc4ac
ec1bc.d	ec2br	ec3cc	ec4cc.d	pc1ac	pc4bc
ec1b1	ec2cc	ec3cc.d	ec4cr	pc1bc	pc4cc
ec1cc	ec2cc.d	ec3cr	ec5ac	pc1cc	pc5ac
ec1cc.d	ec2c1	ec4ac	ec5ac.d	pc2ac	pc5bc
ec1cr	ec3ac	ec4ac.d	ec5ar	pc2bc	pc5cc
ec2ac	ec3ac.d	ec4ar	ec5bc	pc2cc	

Figure 3.5 Listing of raw data files from Site C.

was written in BASIC for the HP9007 computer. *Getdata* was executed prior to performing each factory measurement, and provided prompts for file name, type of data to be collected, detailed description of the clutter, exact transmitter-receiver separation (in feet), transmitter power, and the transmitter attenuator setting. This information was placed line-by-line in the beginning of the newly created file. The program provided operator cues for the selected measurement, such as reminders for correct oscilloscope settings, and stored the digitized oscilloscope display data in the file. The file was then locked and stored on diskette for later transfer to the Engineering Computer Network (ECN).

Figure 3.6 shows the raw data format of a typical envelope (CW fading) measurement file produced by *getdata*. The letters "WFMPRE" and "CURVE" are generated by the Tektronix 7854 oscilloscope to designate the preamble and the display data. The scope settings are contained in the WFMPRE segment. The data following "CURVE" are the vertical coordinates for each display point starting from the far left side of the display. Pulse measurements contain 19 blocks of data, each which are formatted as shown in Figure 3.6. Single sweep measurements are formatted as shown in the figure but contain 1024 data points instead of 128.

Data collected from the factories were uploaded from the HP9007 to the ECN "ed" VAX computer via an RS-232 port. Hewlett Packard's *datacomm* software and UNIX's *umodem* program handled the file transfer. The raw data files retained their same names on ECN, and were stored in the path `/a/n9nb/Data/X`, where X denotes the name of a subdirectory ("B" through "F") corresponding to the factory site from which the data was collected. Once on the ECN VAX, a series of C, Fortran and Shell Script (a language sort of like C) programs were used to reduce the data.

### 3.3.2 Data Processing

A flow chart of the data processing steps is shown in Figure 3.7. *Striptek.auto* was the heart of a C language program used to strip the Tektronix preamble from each raw data file and place the data in a revised file with a file name appendage of ".st". *Striptek.auto* also computed the r.m.s. delay spread and power gain of each pulse measurement. The stripped output file name was simply the original file name appended with the letters

```

eb2ac
engine block mfg
heavy
much heavy clutter wash tank drilling boring machines
75
los
-3
0
WFMPRE ENCDG: ASC, NR, PT: 12B, PT, FMT: Y, XZERO: 0, XINCR: 39
. 06E-03, XUNIT: S, YZERO: 76. 37E-03, YMULT: 20E-03, YUNIT: V;
CURVE 0. 5469, 0. 5469, 0. 5957, 0. 5859, 0. 6055, 0. 6055, 0. 5762, 0. 5078, 0. 4297, 0. 3
418, 0. 1856, 0. 0586, -0. 1172, -0. 332, -0. 5273, -0. 5957, -0. 3711, -0. 0586, 0. 4004,
0. 6348, 0. 7813, 0. 8594, 0. 8691, 0. 7617, 0. 6836, 0. 5859, 0. 5371, 0. 3809, 0. 2441, 0.
0391, -0. 1563, -0. 332, -0. 4199, -0. 3809, -0. 2539, 0, 0. 1953, 0. 3516, 0. 4688, 0. 498
, 0. 5078, 0. 4688, 0. 3906, 0. 2734, 0. 1367, 0. 0781, 0. 0098, 0, 0. 0195, 0, 0. 0391, 0. 09
77, 0. 1758, 0. 3418, 0. 4492, 0. 5469, 0. 6055, 0. 6152, 0. 5567, 0. 4688, 0. 4004, 0. 3125
, 0. 2246, 0. 1172, 0, 0, 0. 0781, 0. 2344, 0. 4102, 0. 5664, 0. 7227, 0. 8203, 0. 8691, 0. 87
89, 0. 8985, 0. 8496, 0. 8008, 0. 7031, 0. 6152, 0. 5371, 0. 4688, 0. 3809, 0. 3906, 0. 3906
, 0. 3906, 0. 4395, 0. 4785, 0. 5273, 0. 5859, 0. 6446, 0. 6641, 0. 6738, 0. 625, 0. 6446, 0.
5859, 0. 5664, 0. 5176, 0. 5078, 0. 5176, 0. 4785, 0. 4395, 0. 3906, 0. 3516, 0. 2441, 0. 10
74, -0. 0781, -0. 3027, -0. 4688, -0. 6836, -0. 5469, -0. 1563, 0. 166, 0. 3516, 0. 4492, 0.
4102, 0. 2734, 0. 1172, -0. 0391, 0, 0. 2539, 0. 3906, 0. 5469, 0. 6641, 0. 6836, 0. 6934,
0. 6836, 0. 5957, 0. 4785

```

Figure 3.6 An example of raw data file format (eb2ac).

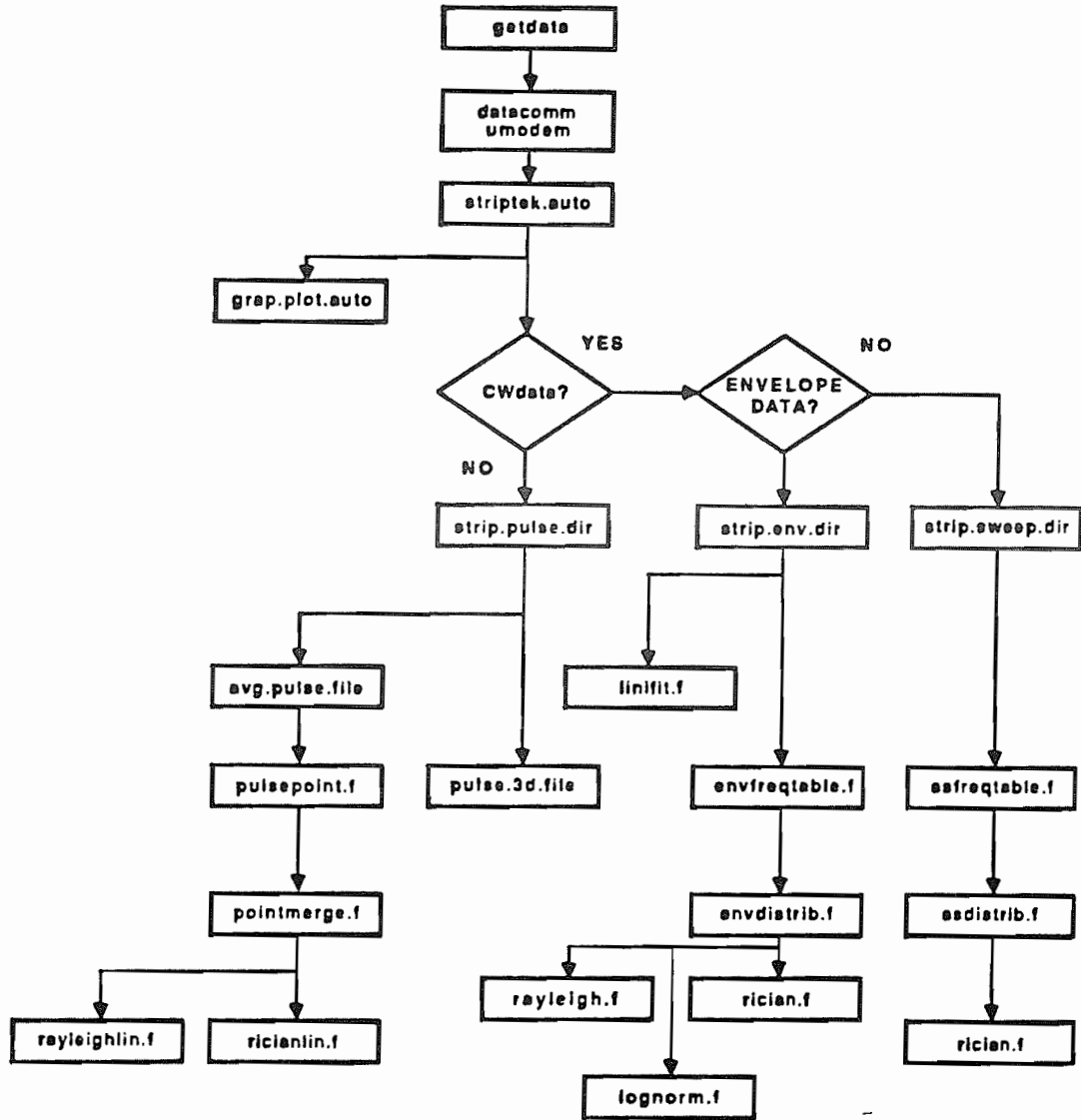


Figure 3.7 Flow chart of data processing.

".st". For pulse measurements (file names beginning with "p"), any DC bias was removed and the 19 multipath profiles were separated into files appended by the numbers 1 through 19. By providing the individual multipath profiles, rather than averaging them immediately, we were able to note multipath spatial fading characteristics and identify paths which were actually comprised of several subpaths within the 10 feet resolution. The newly created (stripped) data files were stored in new directories named "X.st". The first twelve lines of the stripped files contain, respectively, the raw data file name, the factory area, the type of clutter (heavy or light), a detailed description of significant scatterers in the area, the transmitter-receiver separation (in feet), the type of radio path (LOS or obstructed), the transmitter power (dBm), the attenuator setting (dB), the number of data points (from the 7854 oscilloscope display), the time increment between data points, the zero voltage reference on the oscilloscope display, the vertical scale (V/div.), the r.m.s. delay spread (3.13), the power gain of the data set (3.12), the mean delay (3.12), and the mean square delay (3.13). The remaining lines contain the raw data from the 7854 display. The shell script program *auto.plot.directory* was used to produce hard copies of the experimental data.

The stripped data was then processed with shell script programs *strip.env.directory*, *strip.sweep.directory* and *strip.pulse.directory* which are based on Fortran programs *stripenv.f*, *stripsweep.f* and *pulsestrip.f*. *Strip.env.directory* was used to read the envelope data files from each of the five factory X.st directories, compute the median received signal power (based on the receiver law in Figure 2.4) in each file, convert the raw data file to dB relative to the median value, compute path loss relative to  $10\lambda$  free space, calculate median received signal power (based on the receiver law in Figure 2.4), calculate distance in meters, and compute the dynamic range of received signal power over the measurement period. The modified files were placed in directories "X.st.new" having the same file name as in the "X.st" directory. Line 5 of the new data file contained the path length in meters. Line 7 contained the relative path attenuation. Lines 13 through 16 contained, respectively, the median, maximum, minimum and fade-range values of the data.

The program *strip.sweep.directory* performed operations identical to those carried out by *strip.env.directory* with the exception that it handled

1024 data points instead of 128. The new files were written to the directory "X.st.new" and kept the same file name.

The program *strip.pulse.directory* read each pulse file within a specified X.st directory and computed path loss by using the power gain (3.12, 3.14). In addition, the program scaled the data to remove any residual dc levels. The modified data files were stored in the directory "X.st.new" and kept their same file name. The program converted transmitter-receiver distance from feet to meters and wrote the value to line 5 of the new file. Line 7 contained the path loss in decibels. All other lines were similar in format used in the ".st" files.

Pulse data for each measurement location was averaged by *avg.pulse.file* and the resulting average power profile stored in Data/ALLP.avg. Averaged files were given their raw data file name appended with ".avg", and kept the identical format as the data stored in X.st.new. As was the case for each individual power delay profile measurement in X.st, multipath statistics for the overall averaged profile were available in the first several lines of the file.

Pulse data was also formatted for 3-d graphs and spatial fading analysis by concatenating the raw data file of each measurement for a given location. The program *pulse.3d.file* was used to produce a data file which contained the concatenated data of all local multipath power profiles for a given measurement location. The data was stored in Data/ALL3d; each file was given its raw data file name appended with ".3d".

The Fortran programs *sweep.freqtable.f* and *env.freqtable.f* used in conjunction with shell program *env.freqtable.directory* opened the specified file from X.st.new and computed a histogram distribution of the data. The histogram data was placed in Data/Envdist. The resulting distribution was then merged with similar files using the shell program *env.group.dist* and Fortran programs *envmerge.f* and *envdistrib.f*. The resulting CDF's were then compared to Rician and Rayleigh cumulative distribution functions using *grap.envdist*. Rayleigh and Rician distributions were numerically calculated using *rayleigh.f* and *rician.f*.

*Pulse.point* was used to normalize and transform the data files in Data/ALLP.avg into point files which had weighted delta functions at 7.8 ns increments (as suggested by eqn. (3.3)). The point files were placed in Data/PP and were merged using *pointmerge.f* to form overall averaged impulse responses for OBS and LOS geographies. *Pointmerge.f* also checked to see if each path exceeded the threshold of the receiver (17 dB down from maximum), wrote out the occurrences of path arrivals for given excess delay, and generated the data files for the path amplitude analysis. Interactive programs were used to fit the data files in Data/PP to Rayleigh, exponential and log-normal distributions on time delays. The program *lognorm.f* was eventually used to determine the best fit to the power as function of excess delay. The programs *allfreqtable.f*, *alldistrib.f* computed the CDF of all detected paths at all time delays. *Lognormlin.f*, *ricianlin.f* then computed the statistics of the path power values w.r.t. the mean square value of a particular Rician or log-normal distribution. The underlying assumption was that all paths were iid, as described by the distribution which best fit the CDF of the normalized empirical path gain data.



## CHAPTER 4 NARROW BAND MEASUREMENT RESULTS

### 4.1 Introduction

As detailed in Chapter 2, three separate CW signal strength measurement runs were made by moving the receiver with constant velocity along  $\simeq 5\lambda$  tracks at each measurement location. For each signal strength run, 128 envelope readings were taken at intervals of  $\simeq 40$  ms, which corresponded to a spatial sampling rate of 1 cm/sample. The measurements were conducted in the center of an aisle with two antenna heights (2.0 m and 1.5 m), and along the left or right side of an aisle (with 2.0 m antenna height). The antenna height adjustment simulates the use of antenna height diversity while measurements on the side of an aisle simulate the use of space diversity and indicate the type of fading likely to be experienced by an autonomous vehicle that has docked on the side of the aisle.

Previous research performed in and around buildings and in the urban mobile radio channel [40,61,76] has revealed that those channels may be modeled as a wide-sense stationary process (with small variations due to fluctuations in the phases of the paths that make up the multipath) over a short distance, coupled with a non-stationary process (due to shadowing and gross changes in the orientations of scatterers) over large distances. We believe this model to also hold well for the factory radio channel. By utilizing the median signal levels obtained at various distances within the different factories and geographies, we compute the path loss relationship as a function of distance over four ensembles of data collected in different factory geographies, and over the ensemble of all factory data. From the measurement data it is then possible to determine the shadowing effects of storage shelves and manufacturing equipment found in most factories.

These values are useful for determining transmitter power requirements and transmitter spacing as a function of factory surroundings.

#### 4.1.1 Detailed Description of Measurement Sites

The LOS light clutter path measurement in site B was made along a central (5 m wide) aisle in a dry warehouse. A preformed concrete wall was located at one end of the aisle and a steel overhead door at the other. The floor was made of concrete and was flanked by metal shelves which were sparsely filled with paper products. The LOS light clutter measurement in site C was conducted across the central aisle of a wooden floored machine shop. In site D, the LOS light clutter path was along a wide concrete aisle flanked by small stacks of metal crates, except at the largest T-R separation, where several metal extrusion tanks were stacked in 3 m piles along the aisle. Light clutter geography measurements were not made in sites E and F.

LOS heavy clutter path measurements in site B were made along a 60 m aisle in a frozen food production area which was flanked by a large conveyor belt and several freezers. Stainless steel "cook-cool" piping runs from the floor to the ceiling at one end of the aisle. In site C, the LOS heavy clutter measurements were made in a central aisle of an assembly area flanked by engine block wash tanks and large numerical control (N/C) boring machinery. The LOS heavy clutter measurements in site D were made along a secondary aisle in the finishing area of the factory. The mid-range measurement at 38 m was made in a small alley located directly behind a 2 m tall stack of aluminum piping. For this measurement, some shadowing was caused by a steel pillar that was located halfway between the transmitter and receiver. In site E, the LOS heavy clutter measurements were conducted along a major aisle that was flanked by a tool storage area and several large core blowers. The storage area consisted of several 4 m tall metal racks which were arranged perpendicular to the aisle. Floor material was wood block. The LOS heavy clutter measurements in site F were made along a major aisle flanked on both sides by automated crank shaft and connecting rod assembly lines.

Measurements were made along an aisle in site C that ran perpendicular to a reinforced concrete fire wall. Flanking the aisle on the other side was a manual assembly line area (which we would classify as light clutter). These are the only measurements made in close proximity of a wall. As is shown subsequently, observed propagation characteristics along the wall were similar to LOS heavy clutter paths.

Light clutter obstructed path measurements in site B were made in a warehouse used exclusively for storage of paper goods. Several 3 m tall stacks of cardboard boxing material and a concrete pillar blocked the LOS path. Perimeter walls of the warehouse were made of concrete block. In site C, measurements were made in an inventory storage area. A 3 m tall storage rack filled with small crank shaft and connecting rod parts obstructed the LOS path. In site D, measurements were made in the finishing area where LOS paths were blocked by small milling machines (approximately 2 m tall). Light clutter measurements were not made in sites E or F.

Heavy clutter obstructed path measurements were conducted in the main warehouse in site B. Radio path characteristics were measured between one to three metal storage racks, each 5 m tall and stocked to varying degrees with foodstuffs and paper products. The racks were over 30 m long and approximately 2.0 m deep. The farthest measurement was made with the receiver positioned behind rack storage for 40 gallon aluminum drums. site C heavy clutter obstructed path measurements were made between adjacent aisles in a crank shaft manufacturing area. LOS paths were obscured by N/C machinery such as grinders, balancers, milling and boring machines. Typical N/C machines are made of steel and are 3 - 4 m tall, 3 m deep and 4 m wide. In site D, the heavy clutter obstructed path measurements were carried out in the machine parts storage area. Measurements at transmitter-receiver separation distances of 15 m and 30 m were made with the receiver located a few meters behind a 2.5 m tall metal storage rack filled with small machine parts. The measurement at 50 m separation was shadowed by two such storage racks, each 2.5 m tall and 10 m wide. Site E obstructed path heavy clutter measurements were made between parallel aisles which surrounded core blowers and compressors, conveyor belts and a metal box storage area. In site F, the measurements were made along parallel aisles which were shadowed by a crank shaft

washer line, an RF hardening machine, metal bins stacked 3 - 4 m high, and other instrumentation.

## 4.2 Large Scale Path Loss

Figures 4.1 through 4.5 are scatter diagrams showing median path loss as a function of geography and distance at each factory site. Figure 4.2 includes data from LOS measurements made in an aisle which runs parallel to (and directly next to) a reinforced concrete fire wall. Figure 4.6 shows the path loss over all factory sites. Each point on the plot represents the median received signal strength for a CW run which has been referenced to a receiver antenna located  $10\lambda$  from the transmitter in free space. A linear least square error fit to the data<sup>†</sup>, and the variance of the fit, has been computed for each scatter plot and is useful in determining a representative exponential relationship between distance and received power. The path loss generally increases with distance ( $d$ ), as

$$PL(d) \propto d^n \quad (4.1)$$

where  $n$  is the exponential relationship we strive to find. When plotted on log-log paper, the exponential relationship between power and distance is a straight line. Figure 4.6 shows the best fit straight line to all of the factory data. Table 4.1 lists the mean path loss exponent  $\hat{n}$ , the variance of  $\hat{n}$ , the number of median values used for computation, and the correlation coefficient of the data as a function of factory site. (The correlation coefficient is computed as the square root of the product of the regression line slopes of attenuation, with distance as the independent variable, and distance, with attenuation as the independent variable [83]).

<sup>†</sup> We used the linear minimum mean square estimator  $\hat{y} = A(x+x_0)$ , where  $x_0$  forces the y-intercept value to 0 dB at the reference distance ( $x_0=10\lambda$ ) and the slope  $A$  is the estimate  $\hat{n}$  of the path loss exponent. The two parameter estimator  $\hat{y} = Ax+B$  has minimum variance but does not guarantee that  $\hat{y}$  intersect  $x_0$  for  $y = 0$ dB. For our data, the variances of the two estimators typically differ by less than 0.2 dB and the exponent values differ typically by less than 0.5.

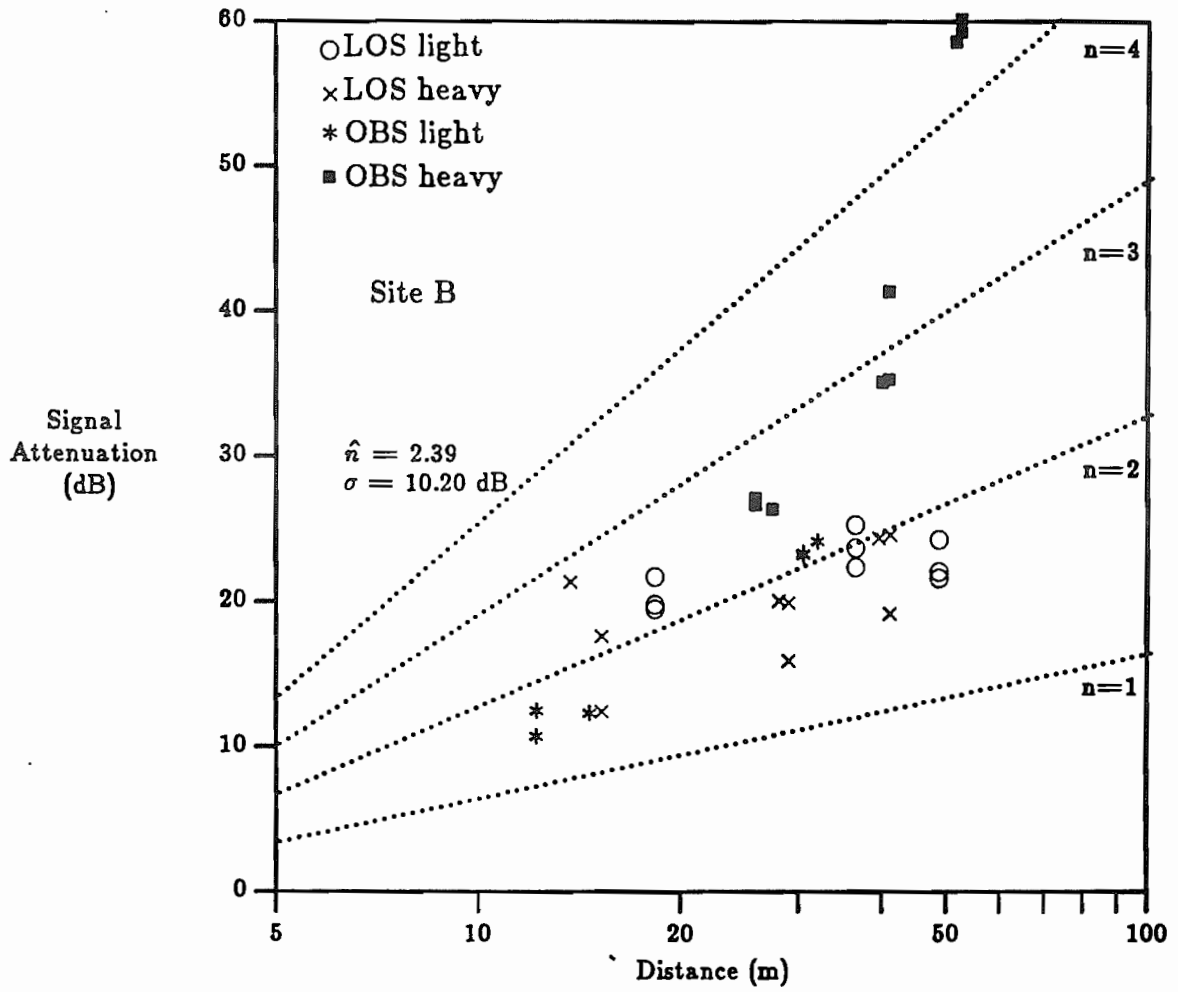


Figure 4.1 Large scale path loss at site B.

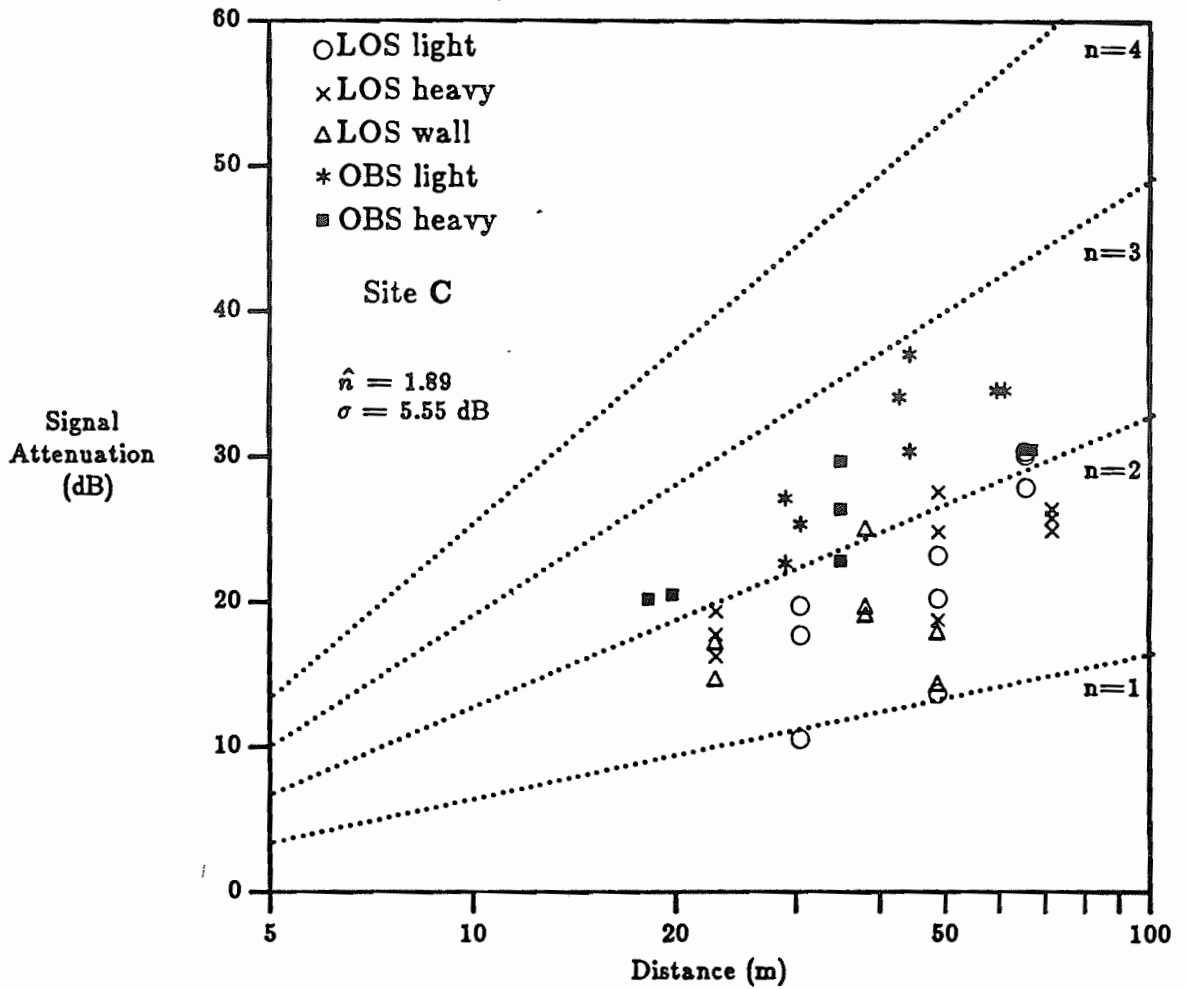


Figure 4.2 Large scale path loss at site C.

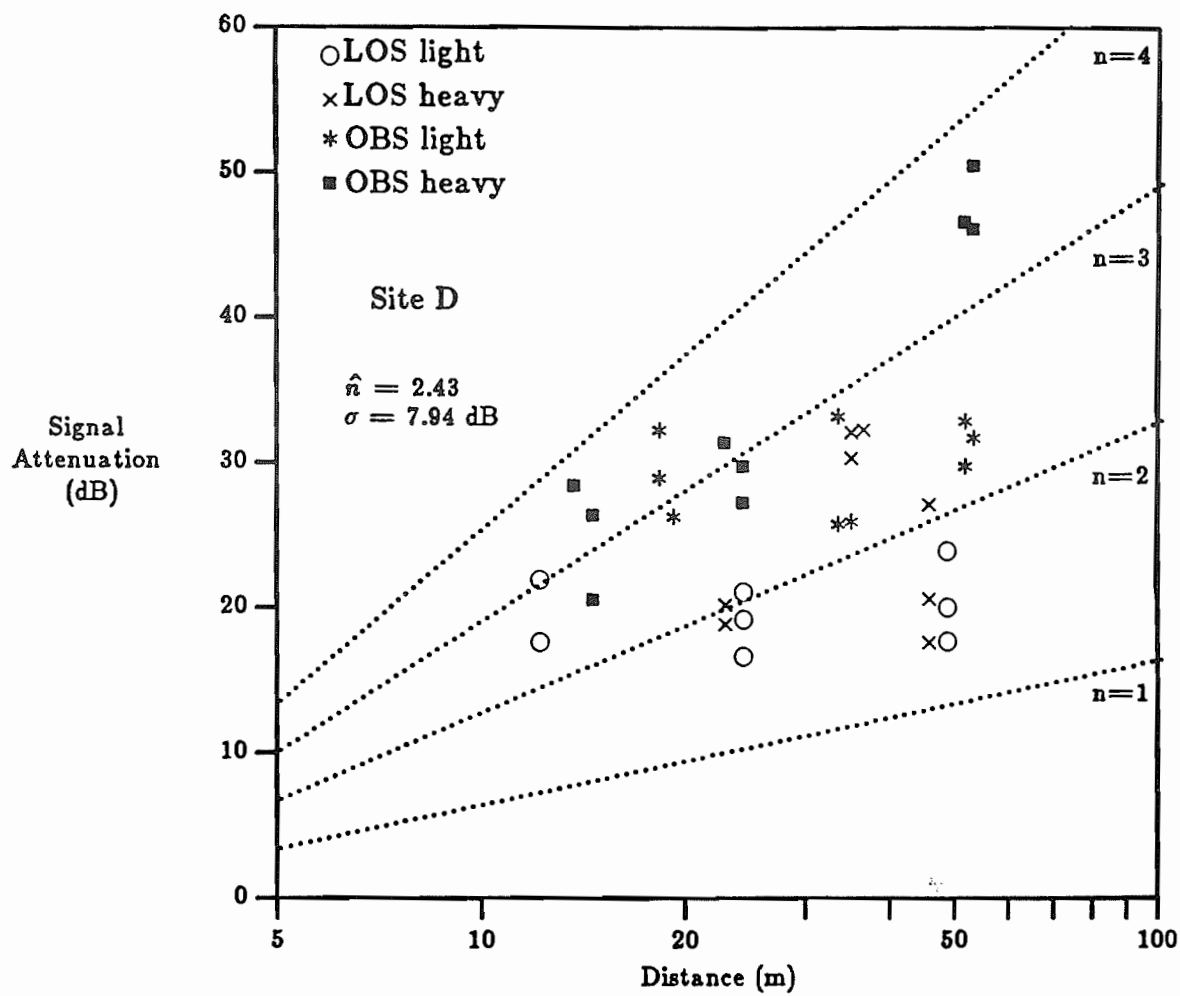


Figure 4.3 Large scale path loss at site D.

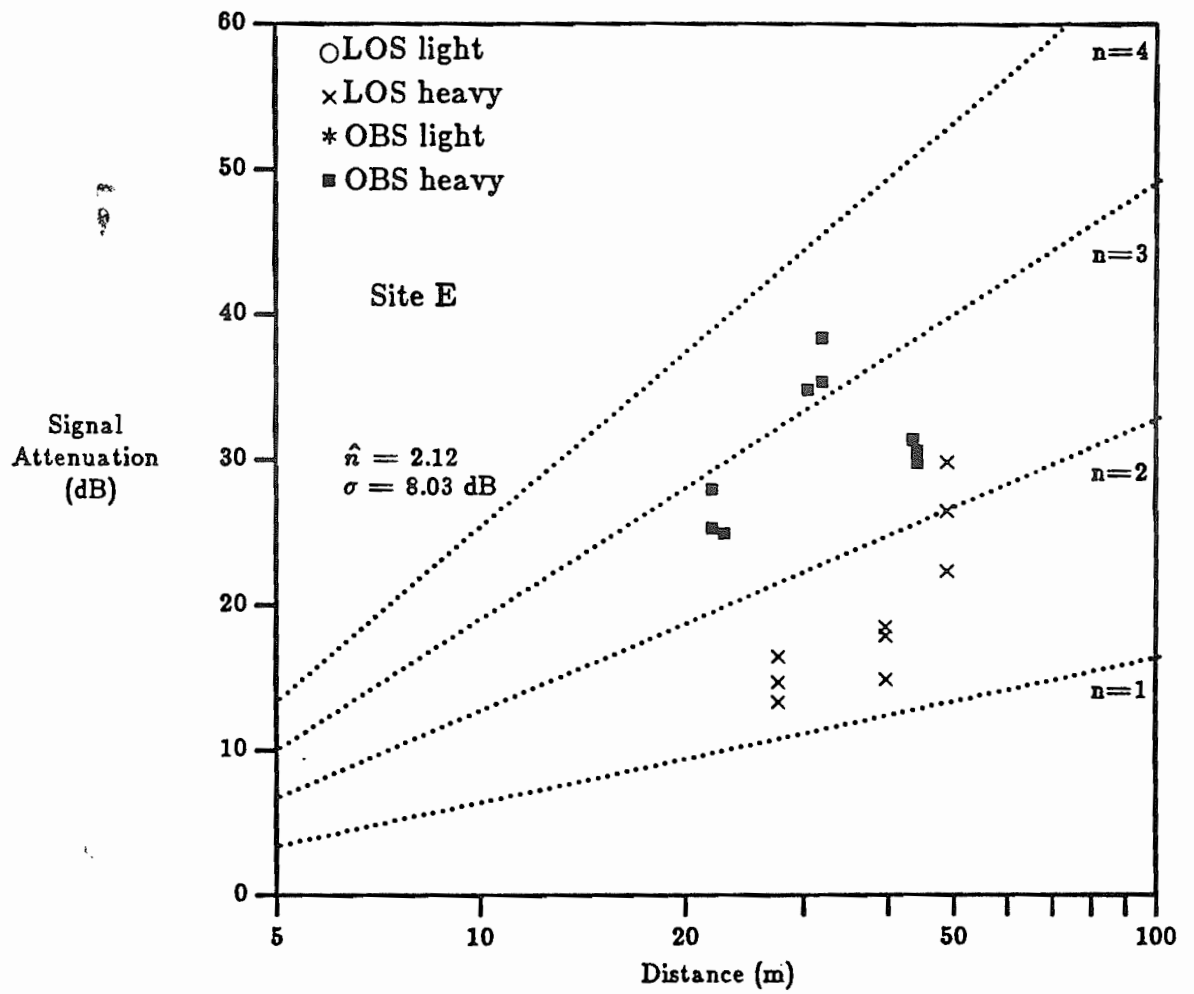


Figure 4.4 Large scale path loss at site E.



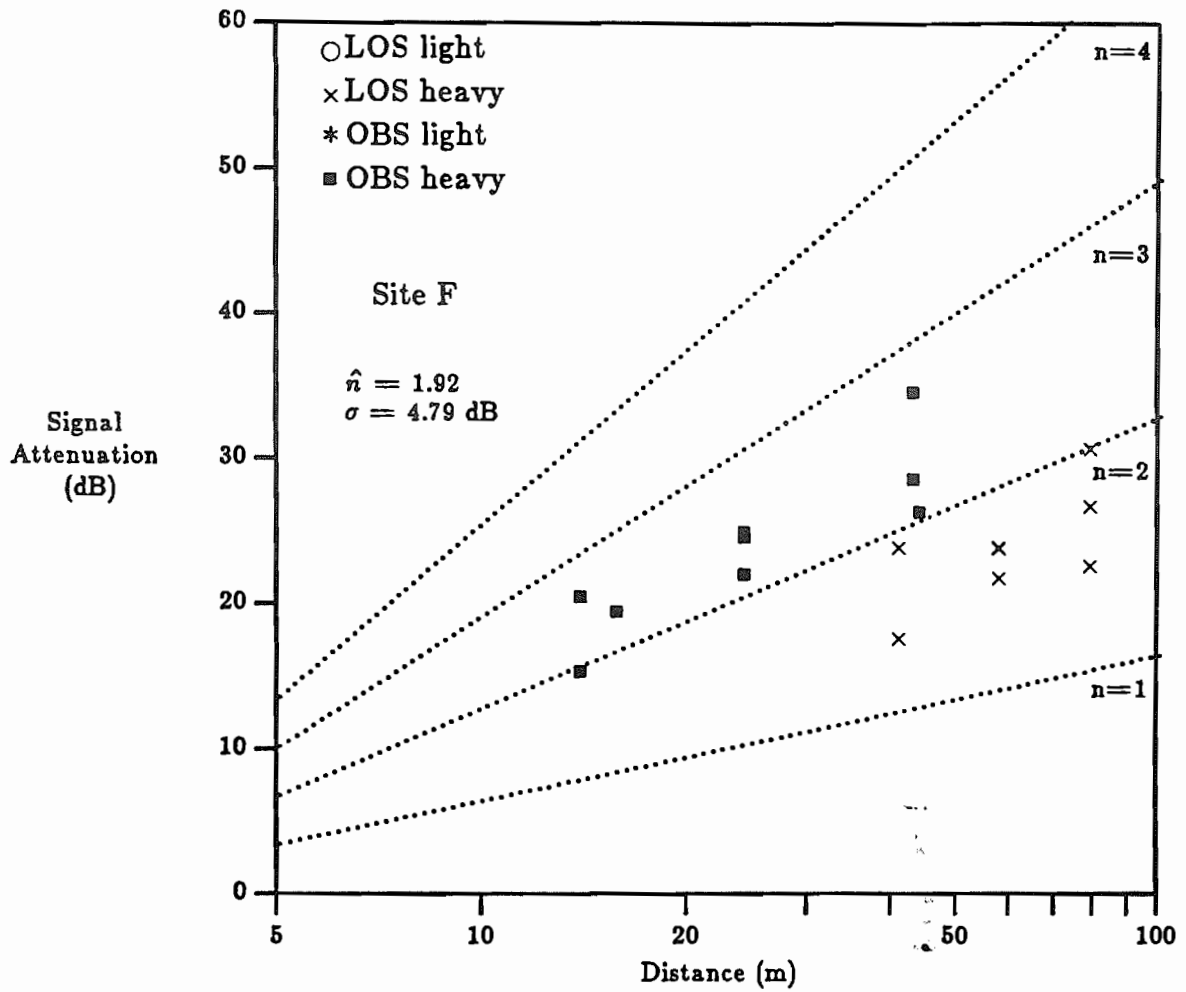


Figure 4.5 Large scale path loss at site F.

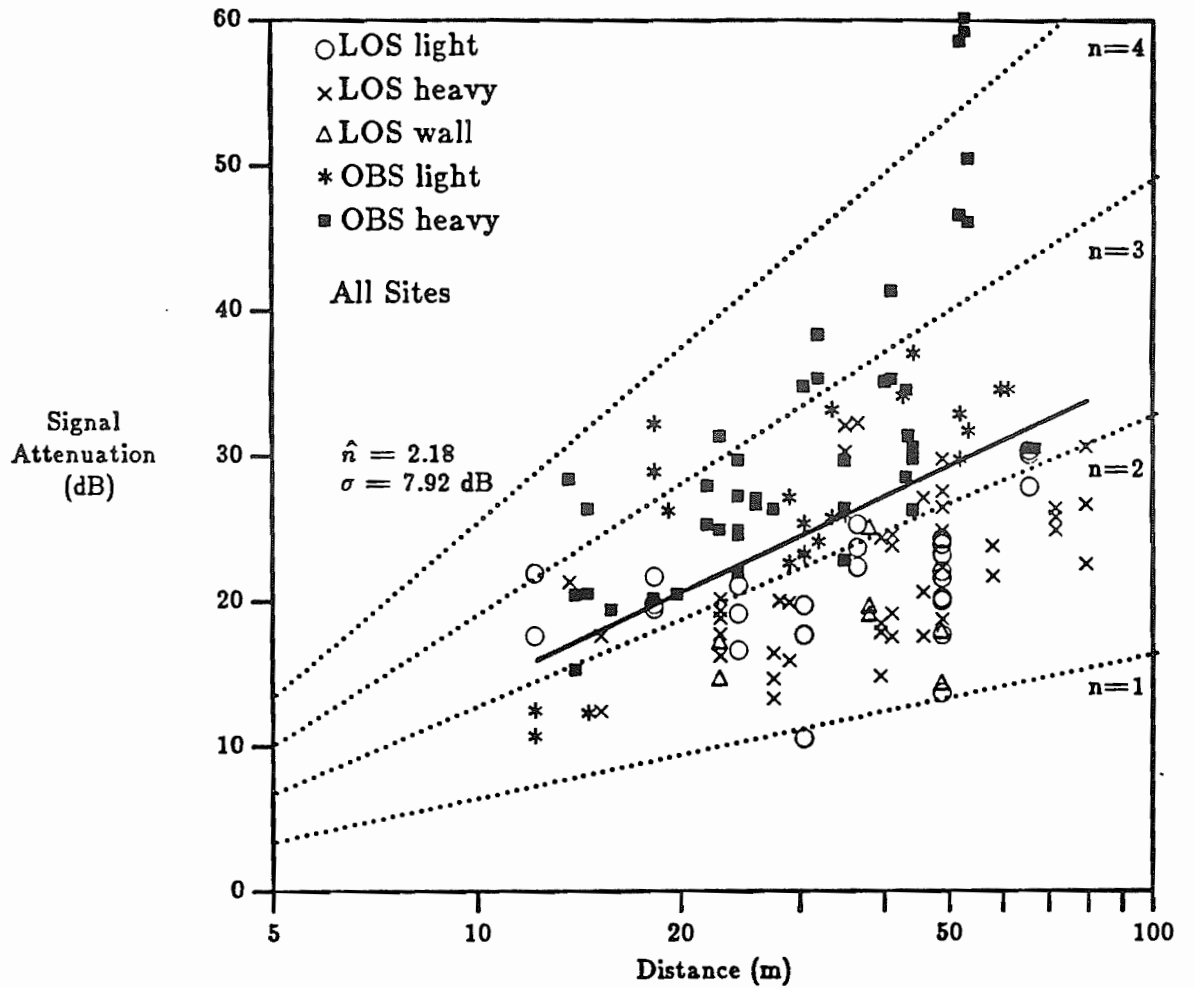


Figure 4.6 Large scale path loss at all sites.

Table 4.1 Path loss exponent as a function of factory site.

<b>Path Loss Exponents in Different Factories</b>				
Factory Site	$\hat{n}$	$\sigma$ (dB)	No. of Points	Corr. Coef.
Site B	2.39	10.20	33	.94
Site C	1.89	5.55	41	.98
Site D	2.43	7.94	34	.96
Site E	2.12	8.03	18	.96
Site F	1.92	4.79	17	.98

Table 4.2. Path loss exponent as function of geography.

<b>Path Loss Exponents in Different Factory Geographies</b>				
Factory Geography	$\hat{n}$	$\sigma$ (dB)	No. of Points	Corr. Coef.
LOS light clutter	1.79	4.55	26	.98
LOS heavy clutter	1.79	4.42	43	.98
LOS along wall	1.49	3.9	8	.98
OBS light clutter	2.38	4.67	23	.99
OBS heavy clutter	2.81	8.09	43	.97
All Geographies *	2.18	7.92	135	.96

\*LOS measurements along wall not included in computation

Figures 4.7 through 4.10 demonstrate the effects of factory geography on signal attenuation over all five factories. Not surprisingly, LOS paths are less lossy than obstructed paths. In the factory environment, LOS light clutter paths occur in "open plan" areas; spacious areas that contain very little heavy equipment which can cause shadowing. Our data suggests an exponent value of about 1.8 for factory LOS paths, while paths along walls experience attenuation as distance to the 1.5 power. Alexander performed measurements in two buildings with "open plan" layouts and reported path loss exponents of 1.2 and 2.5 [63]. The exponent value of 1.2 was obtained in an airplane hanger having metal siding and roofing. Measurements in hallways of office buildings have yielded exponents between 1.2 and 1.8 [53,72,77].

For the case of obstructed paths, the effects of shadowing determine the path loss for a given location. However, typical (average) path loss exponents, as revealed by Figures 4.9 and 4.10, are 2.4 for light clutter obstructed paths and 2.8 for obstructed paths in heavy clutter. It is clear from the scatter plots that variance of the data increases with greater transmitter-receiver (T-R) separation, and that the variance is larger for obstructed paths. This is similar to observations made by researchers in the mobile radio channel, where for metropolitan areas such as New York City, variance about the mean was found to increase. We believe the increase in variance of our data to be caused by the significant reflecting, shadowing, and waveguiding effects of large machinery found in heavy cluttered areas of the factory. Table 4.2 lists the linear regression estimate of the path loss exponent  $\hat{n}$  as a function of factory geography. The variance of  $\hat{n}$ , the number of median signal level values and the correlation coefficient of the data is also given in the table. The path loss exponent for the overall factory data was computed without 8 median values obtained near a wall at site C. Inclusion of this data lowers the exponent to 2.16 and does not significantly affect the other statistics.

Figures 4.11 through 4.13 show scatter diagrams of the data as functions of antenna height and aisle positioning over all factories and geographies. Table 4.3 summarizes the resulting best fit path loss exponents. The fact that average attenuation falls off as  $\simeq d^{2.2}$  for each of the three antenna locations further substantiates this relationship as representative for large scale path loss behavior in factories. The data also shows that

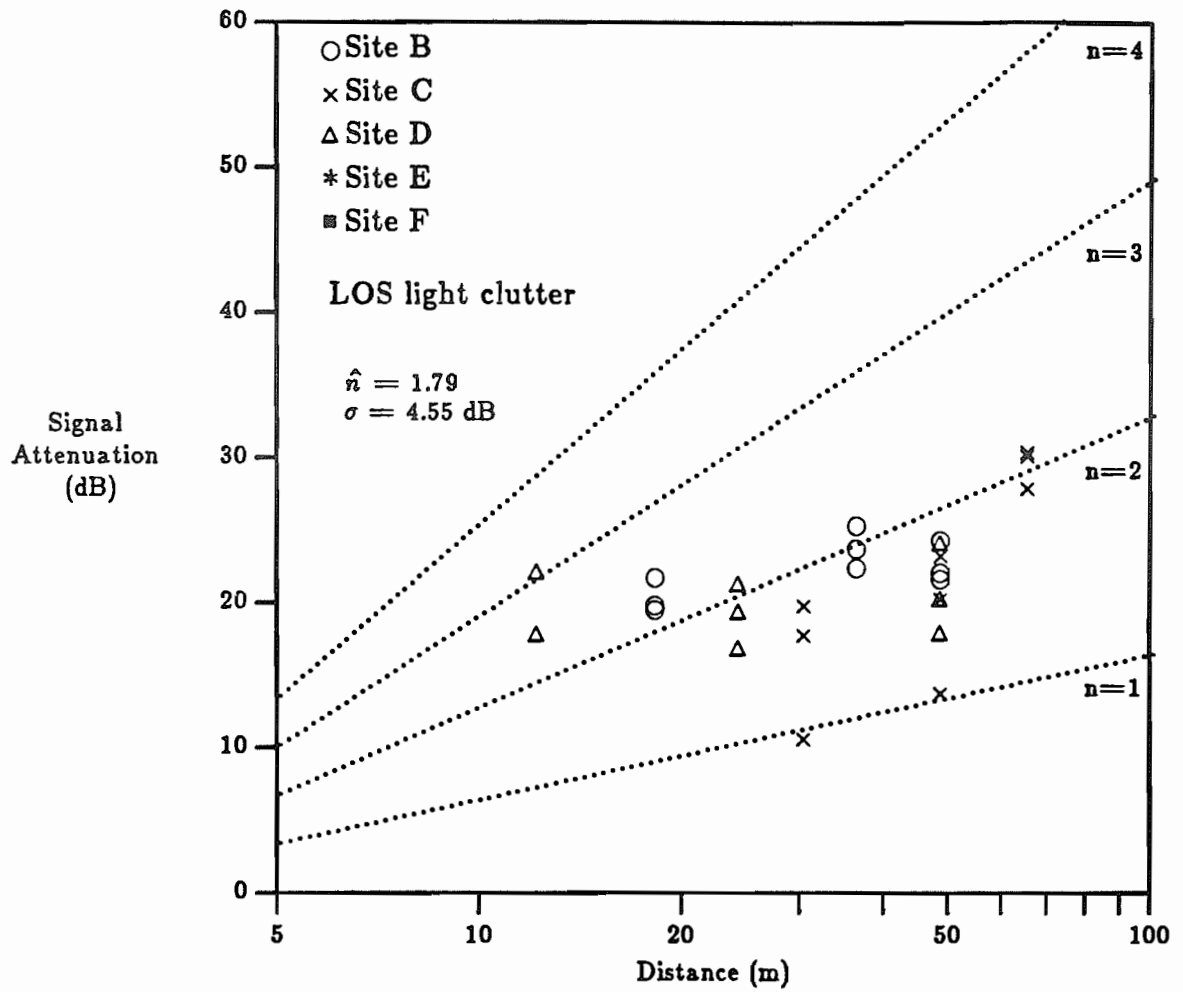


Figure 4.7 Large scale path loss in LOS light clutter paths.

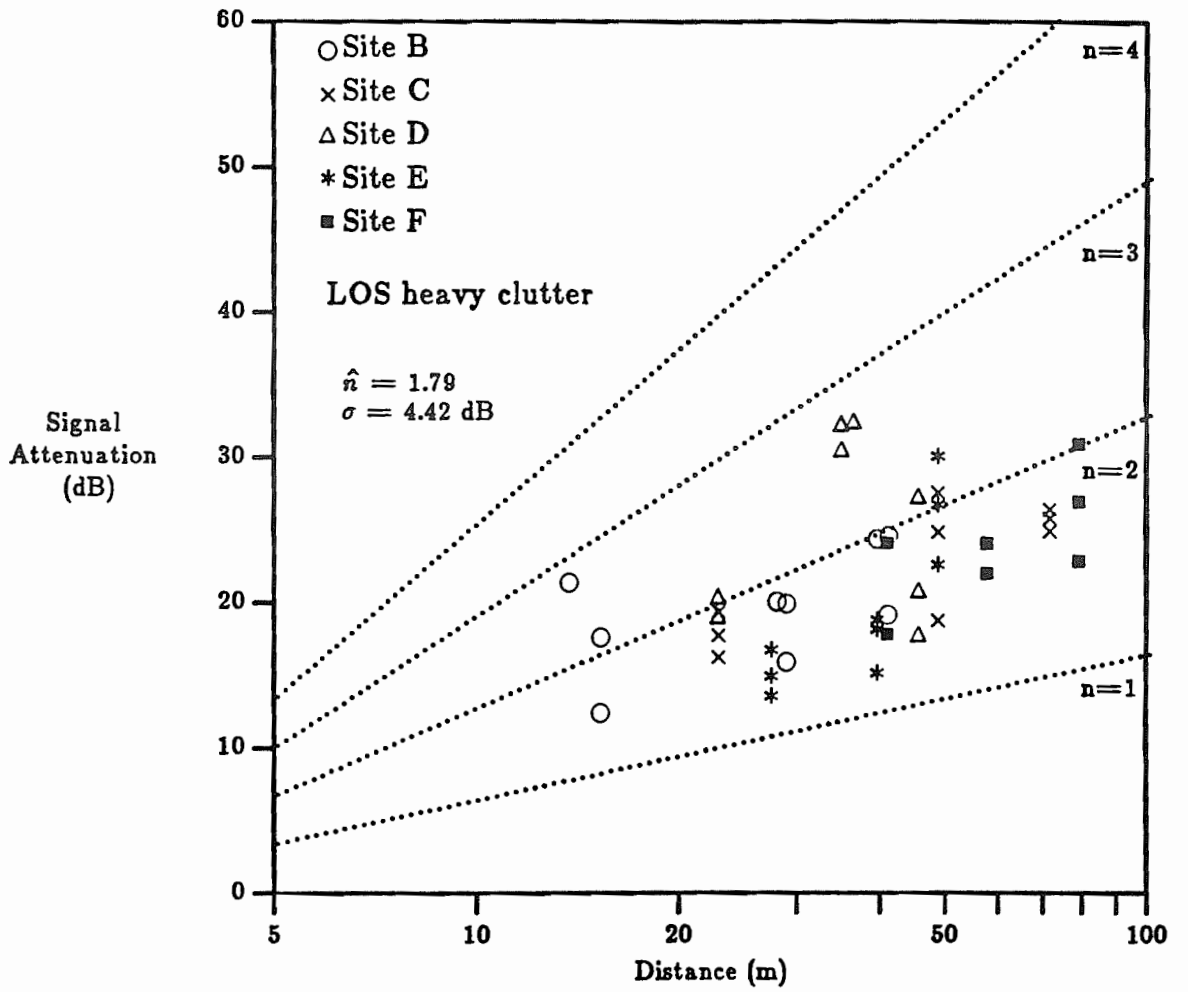


Figure 4.8 Large scale path loss in LOS heavy clutter paths.

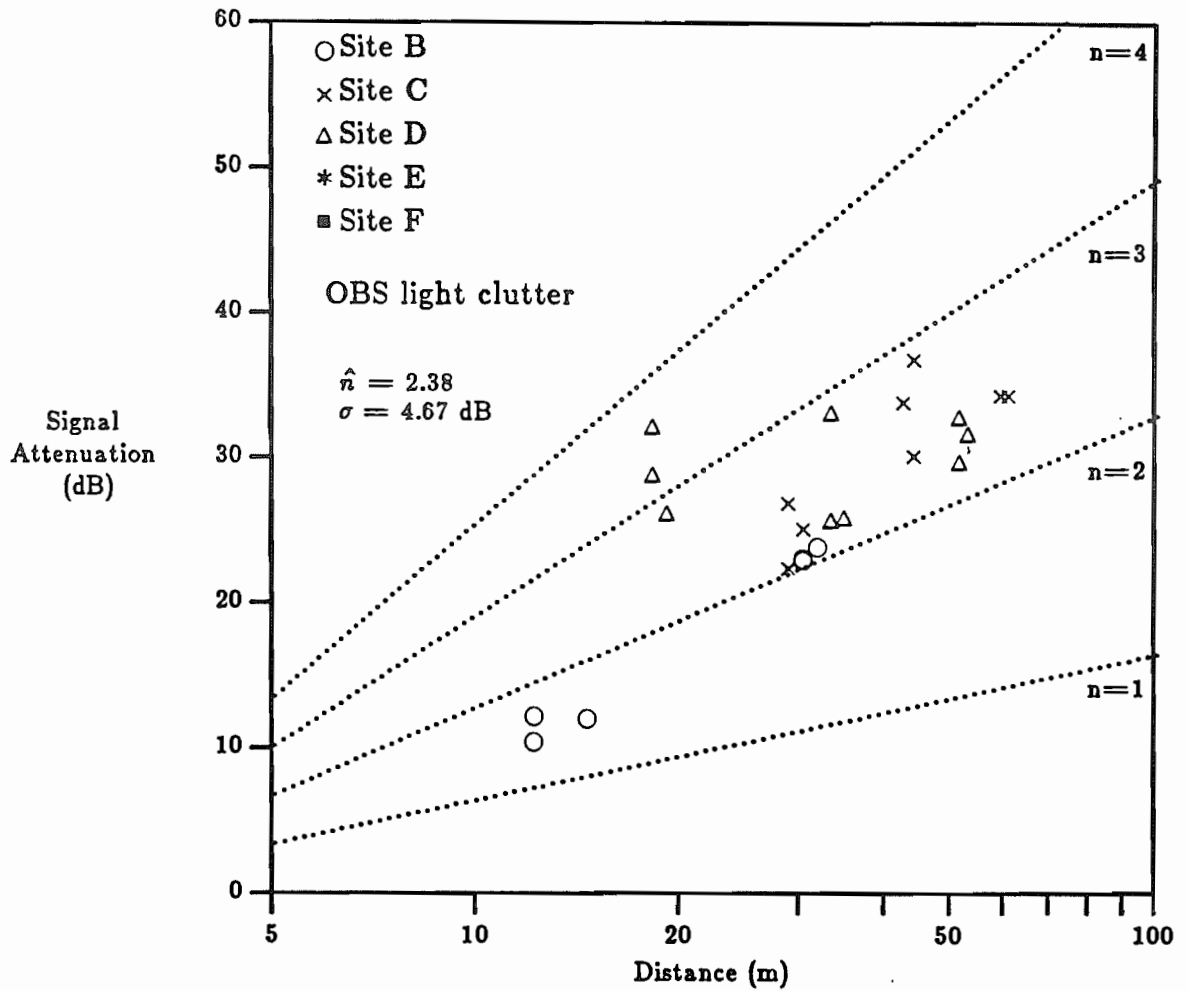


Figure 4.9 Large scale path loss in obstructed light clutter paths.

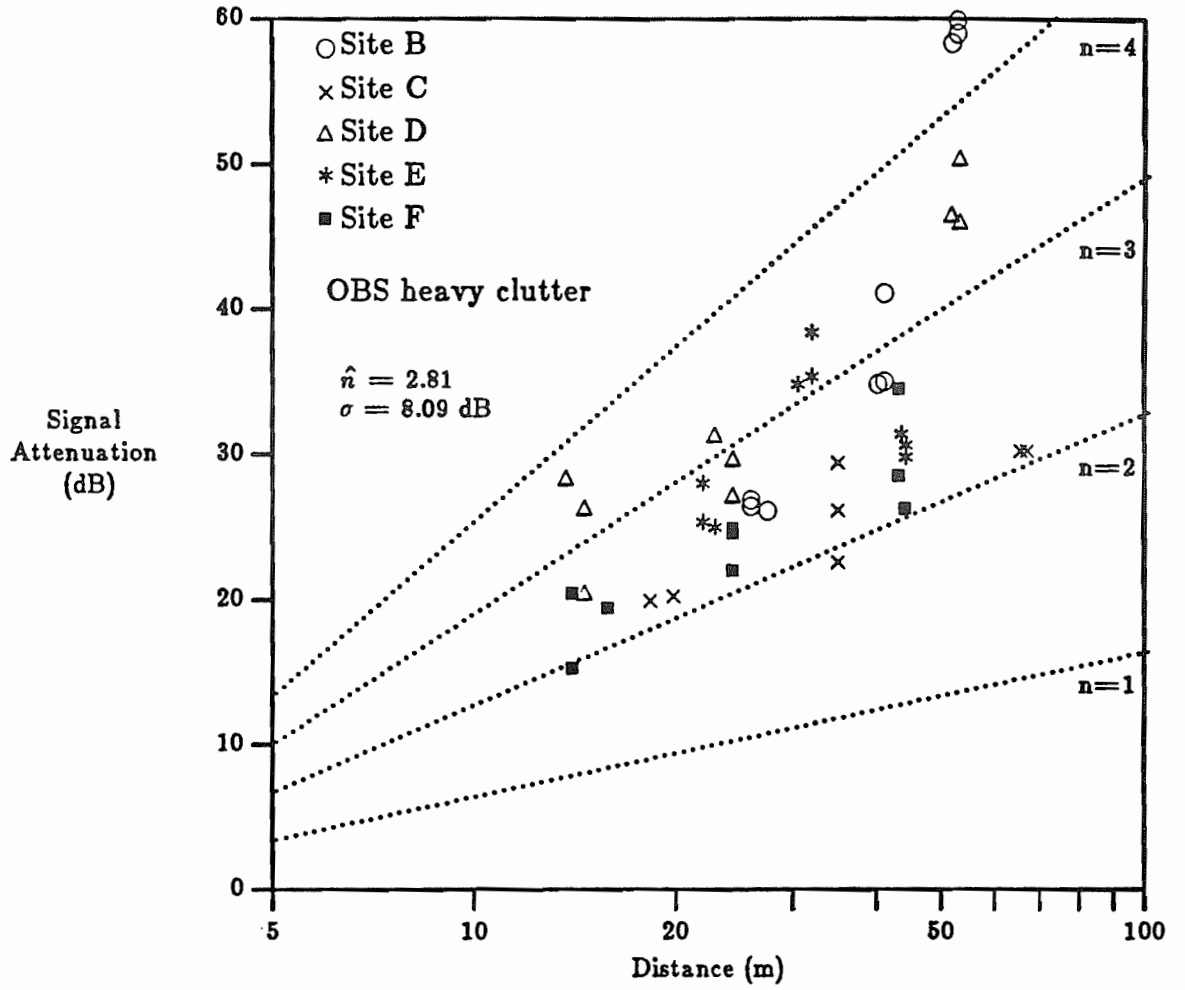


Figure 4.10 Large scale path loss in obstructed heavy clutter paths.



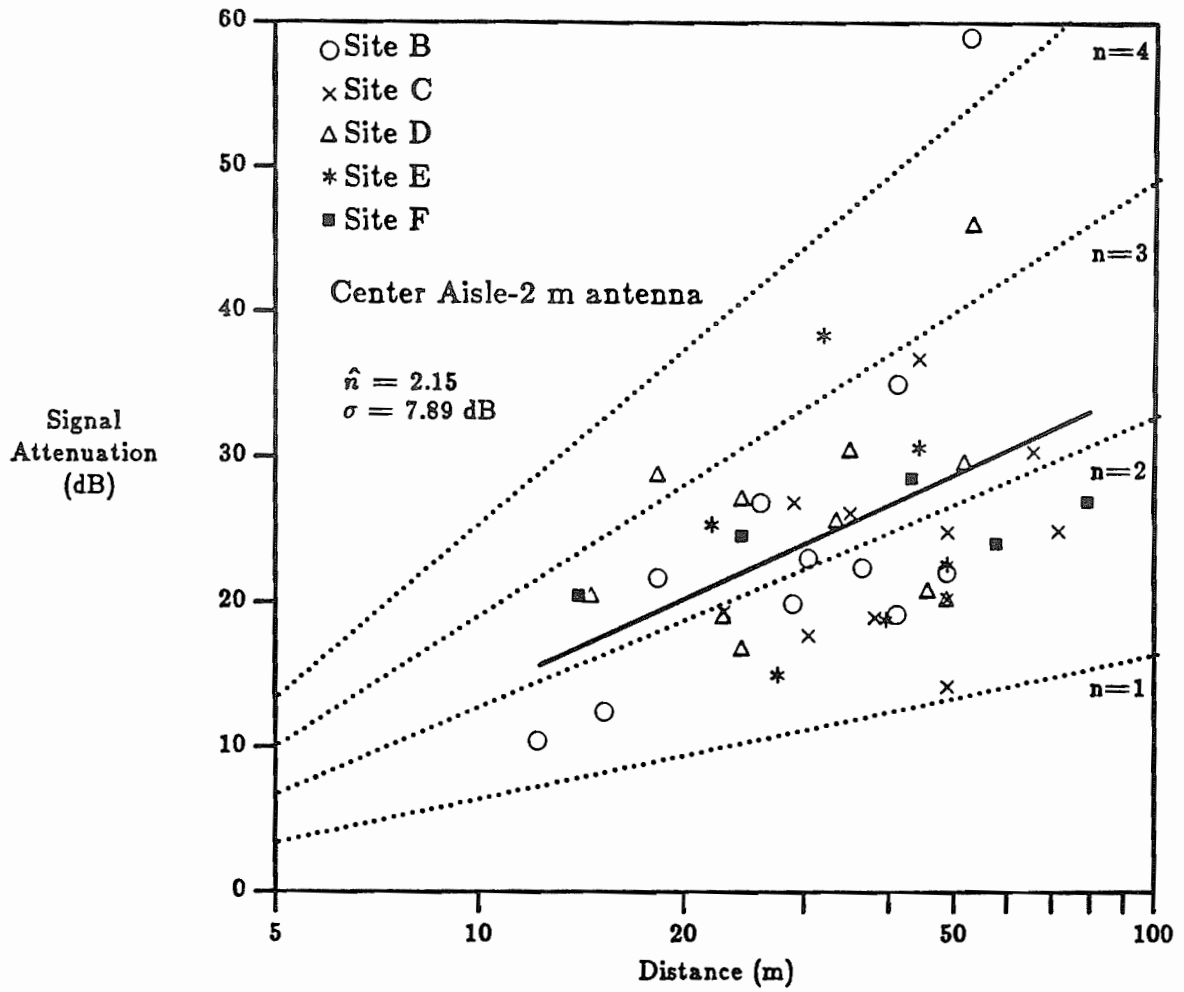


Figure 4.11 Large scale path loss with 2 m antenna in center of aisle.

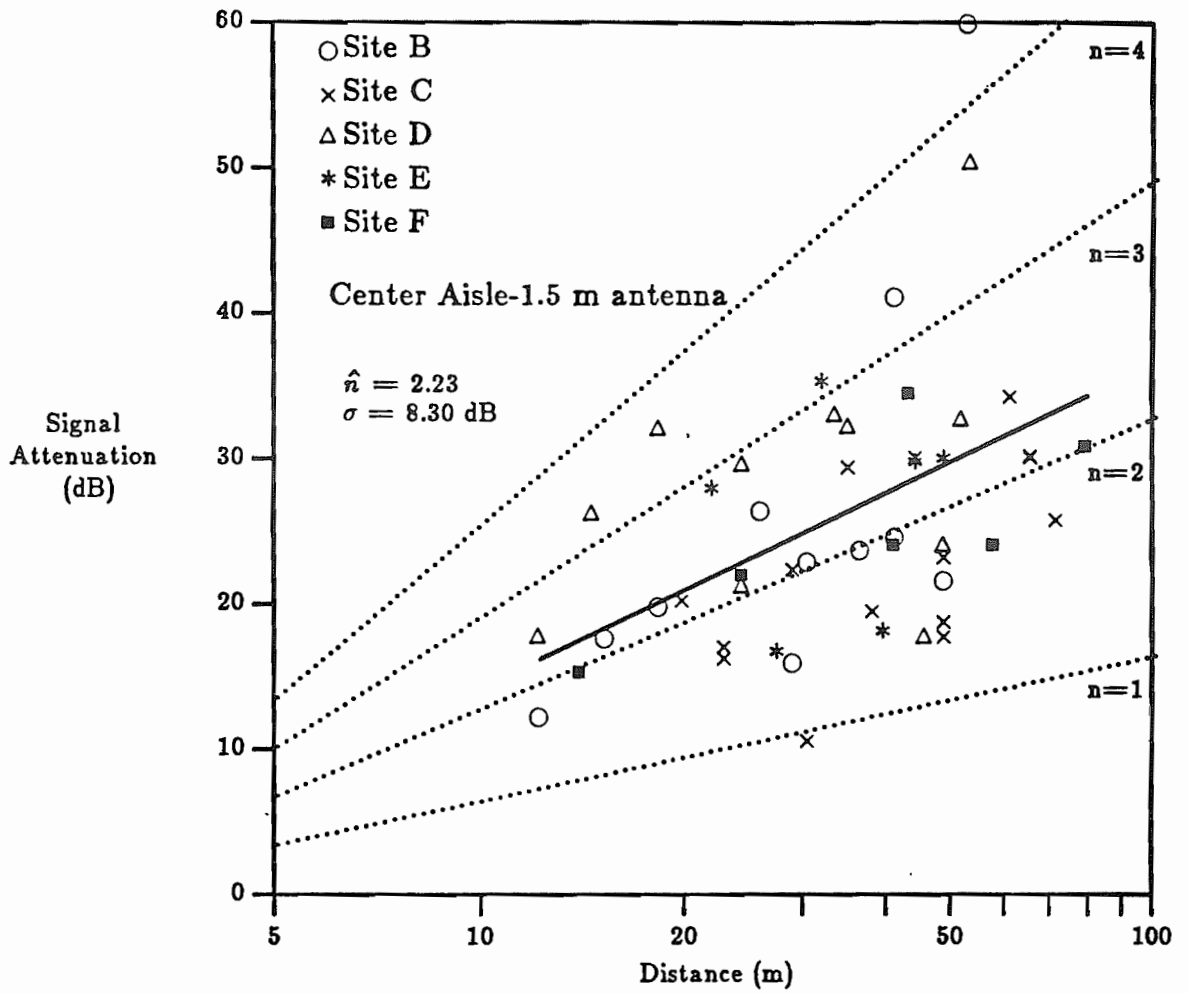


Figure 4.12 Large scale path loss with 1.5 m antenna in center of aisle.

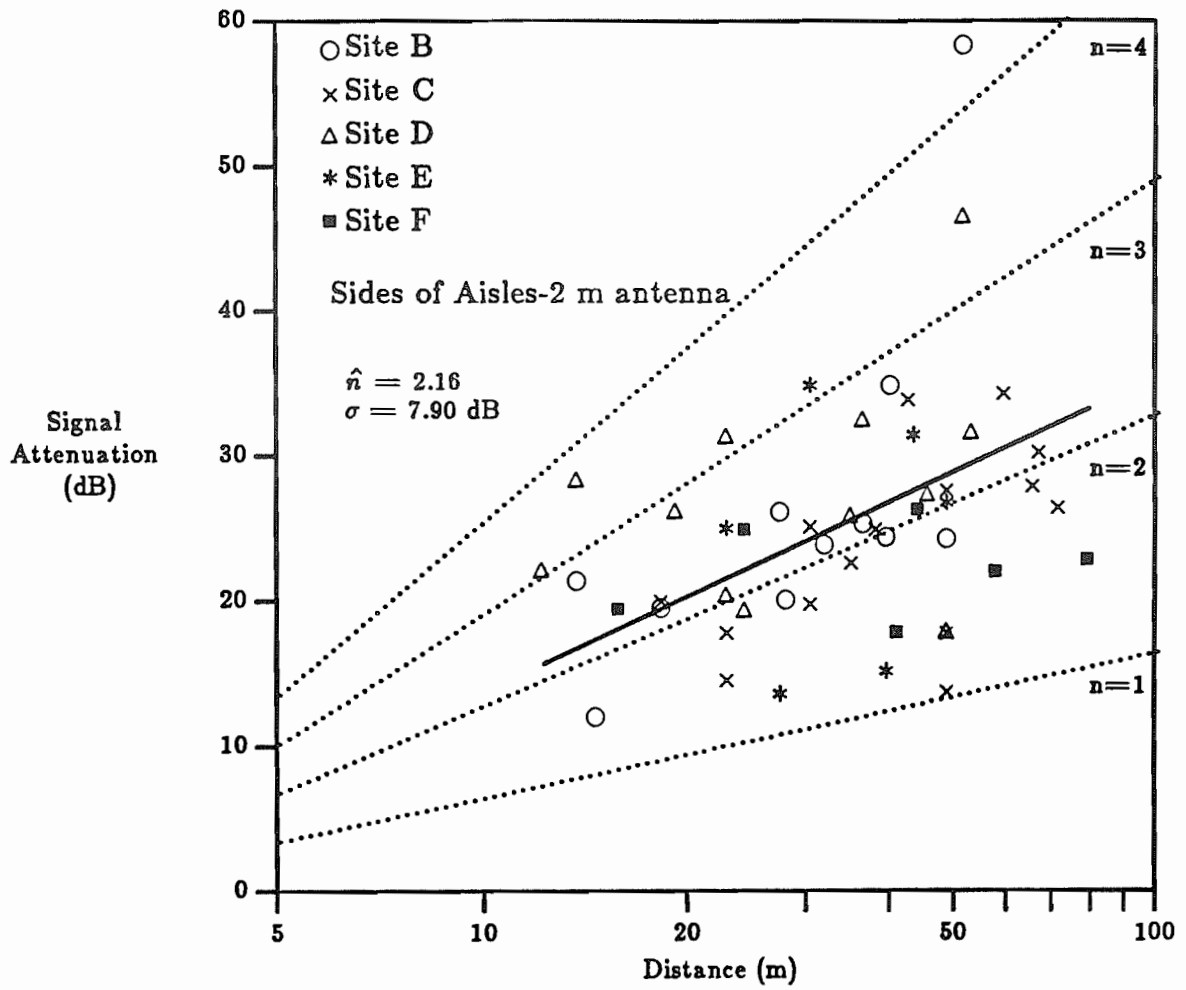


Figure 4.13 Large scale path loss with 2 m antenna on side of aisle.

average received signal strength is comparable whether a receiver is in the center or on the side of an aisle, whereas slightly poorer reception results when a shorter antenna is used. From our measurements, average gain of a 2 m tall antenna over a 1.5 m tall antenna is 1.4 dB at a T-R separation of 50 m.

Table 4.3 Path loss exponent as function of antenna position.

Path Loss Exponents as Function of Antenna Position				
Antenna Position	$\hat{n}$	$\sigma$ (dB)	No. of Points	Corr. Coef.
Center of Aisle - 2 m ht.	2.15	7.89	42	.96
Center of Aisle - 1.5 m ht.	2.23	8.30	46	.96
Side of Aisle - 2 m ht.	2.16	7.90	47	.96

Although it appears that the variance of the large scale path loss increases with distance and is a function of geography, it is useful to determine a simple yet well fitting distribution of the overall variation of signal levels about the mean (or "typical") large scale path loss. This may be readily accomplished by subtracting the mean signal level (as determined by the path loss exponent  $\hat{n}$  and the T-R distance) from the actual attenuation levels of the data and observing the resulting fluctuations. A distribution that has been found to be a good fit in other radio channels is the log-normal distribution with constant variance [40,60,61].

Using a value of  $\hat{n} = 2.18$ , the mean path loss was subtracted from all of the 135 CW measurements and the resultant CDF computed over 1 dB intervals. Figure 4.14 shows that large scale path loss is well described by a log normal distribution having a variance within 1 dB of the statistical value found using a linear least squares fit. Distributions for various geographies were also found to closely fit log normal distributions for  $\hat{n}$  and  $\sigma$  values listed in Table 4.2.

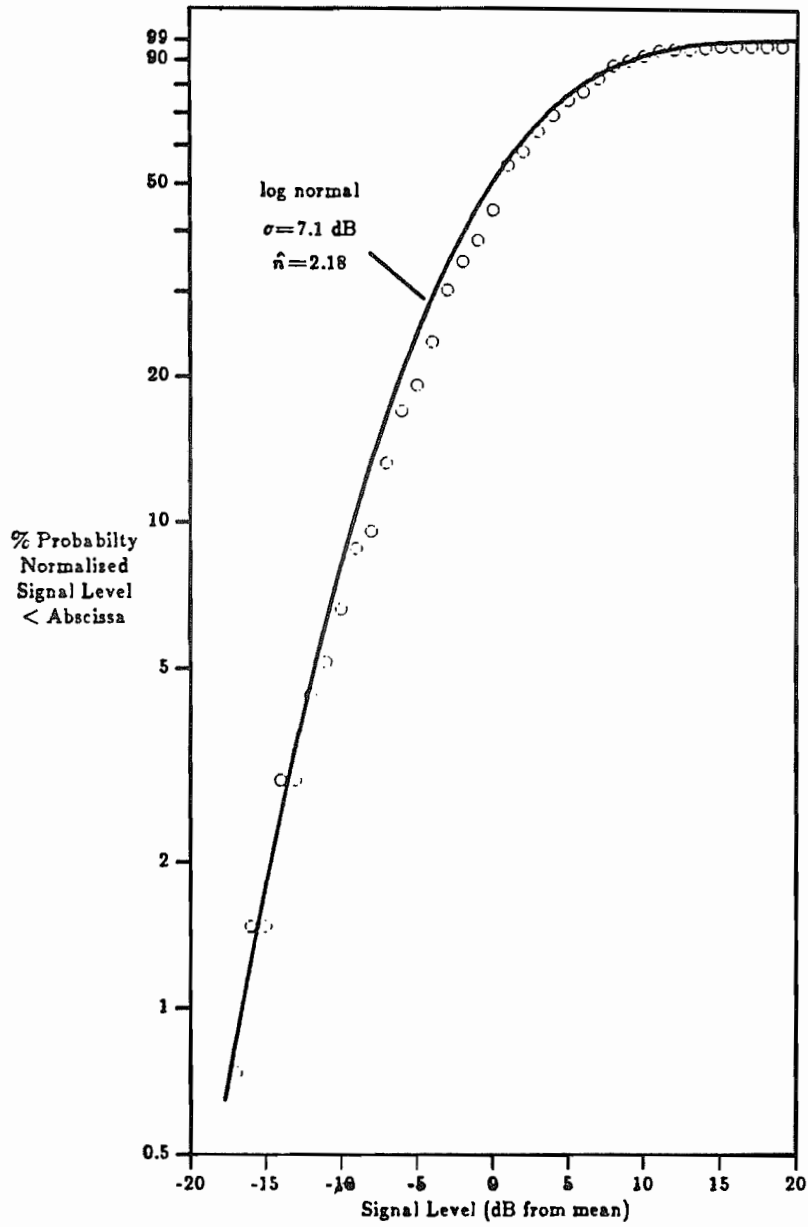


Figure 4.14 Cumulative distribution of large scale signal levels about the mean.

### 4.3 Shadowing

The increased path loss and data variance for obstructed paths as indicated by Table 4.1 suggests that shadowing caused by obstructions plays a major role in determining SNR in a heavy clutter industrial environment. Because accurate descriptions of path obstacles were kept during factory measurements, it is possible to extract from the data the RF signal loss caused by typical factory equipment.

An ideal method of measuring RF attenuation would be to first determine received power over a particular LOS path and then to place the "obstacle under test" in the way of the LOS path and observe the reduction in received signal power. An alternative method of establishing shadowing characteristics of obstructions is to observe signal levels for certain obstructions, and compare them to the average received signal level over the entire ensemble of factory measurements. While the former method is more desirable in that other propagation anomalies not directly attributable to the obstruction are calibrated out, obstructions in the factory environment (such as metal shelves stocked with inventory, large machinery, assembly lines, etc.) are generally not movable. Consequently, the latter method has been used to determine shadowing effects of common factory equipment.

Obstructed path measurements in site B are seen to be (see Figure 4.1) the most severely attenuated of all the factory data. As described in 4.1.1, these measurements were taken in a dry warehouse containing 5 m tall storage shelves. Transmitter-receiver paths were established that intersected the face of the shelves. When compared to average factory propagation ( $\hat{n}=2.18$ ), it was found that shelves loosely<sup>†</sup> filled with paper products cause about a 4 dB degradation in the received signal power. This was computed by subtracting the average value of signal attenuation for the site B heavy clutter measurement at  $d=25$  m from the expected average path loss at that distance. For a 5 m storage rack heavily packed with paper

<sup>†</sup> The terminology *loosely* and *heavily* packed refers to the size of gaps, or openings, in the obstruction. Loosely packed indicates that there are several visible openings through the obstruction having diameters much larger than a wavelength. Tightly or heavily packed infers that there are few openings in the obstruction that are no wider than a wavelength.

products, attenuation is between 5 to 7 dB as illustrated in Figure 4.1 (note that although the obstructed heavy clutter measurements at  $d=40$  m are approximately 10 dB more lossy than typical factory propagation, 4 dB is subtracted out due to shadowing of the first storage shelf.). Path loss caused by shadowing of a 5 m shelf containing tightly packed 40 gallon aluminum drums was found to be 20 dB. Attenuation due to shadowing of large machinery and stacks of metallic inventory in manufacturing areas were found to range typically from 5 to 15 dB, depending upon the local surrounding clutter and the distance of the obstruction from the receiver. For example, the semi-automated crank shaft assembly line measurements in the heavy clutter obstructed path environment at site C indicated only a 5 dB loss, where as a slightly larger assembly line measured between 7-8 dB of loss at site F. With the receiver located in an aisle immediately behind a metal box storage rack in site E, path loss was measured to be 10-12 dB.

The measurements have indicated that with the transmitter in the clear, severe attenuation ( $>10$  dB) only occurs when the receiver is situated a few meters behind a metal obstruction which is much taller than the receiver antenna. Tall obstructions located midway between transmitter and receiver generally cause less path loss ( $\approx 3-7$  dB as indicated by obstructed path measurements at sites C and D). Although this trend is predicted by knife-edge diffraction theory [40,82], received signal levels in deeply shadowed areas are consistently 5-20 dB greater than levels predicted by knife edge diffraction, while measured signal levels for paths having obstructions several meters from both transmitter and receiver are 2-5 dB greater than predicted by the diffraction model. This suggests a significant amount of received power arrives at high angles of elevation and from directions other than that of the transmitter. Some wide band measurements (see Chapter 5) indicate that a significant amount of power is received by ceiling reflections and ceiling ducting. Additional paths are believed to be from reflections and refractions from tall adjacent machinery located behind or aside the receiver, and from aisle ducting. In this vein, the factory multipath channel is similar to the urban mobile radio channel where tall buildings channel energy parallel to streets and local unshadowed obstructions illuminate the receiver by reflections [40,73,76].

The suppositions on path arrivals mentioned above are lent credence by the fact that signal attenuations on the order of 10 to 15 dB are caused

by office partitions in office buildings [59,77]. In a typical office building, ceilings and walls are made of non-metallic fiber which impede high angle radiation and inhibit propagation from directions other than the line of sight. The factory, on the other hand, typically has large ceiling expanses, wide aisles, and metal ceiling truss work which readily facilitate multiple paths.

Table 4.4 provides typical attenuation values for several factory obstructions at 1300 MHz. These results have been averaged over antenna heights of 1.5 m and 2.0 m along the center and a side of an aisle and are valid for receivers located in an aisle directly behind the obstacle (i.e. deep shadowing). The table also includes some results of measurements on walls and floors [59] that might be of interest to factory radio communication system designers. The values in Table 4.4 are conservative for receiver locations that are only lightly shadowed and in light clutter surroundings. For the latter case, knife edge diffraction modeling appears to be suitable.

Table 4.4. Shadowing effects of some common factory equipment.

Shadowing Effects of Common Factory Equipment	
Obstacle Description	Attenuation (dB)
2.5 m storage rack with small metal parts (loosely packed)	4-6
4 m metal box storage	10-12
5 m storage rack with paper products (loosely packed)	2-4
5 m storage rack with paper products (tightly packed)	6
5 m storage rack with large metal parts (tightly packed)	20
Typical N/C machine	8-10
Semi-automated Assembly Line (Large Engine)	5-7
0.6 m square reinforced concrete pillar	12-14
Stainless Steel Piping for Cook-Cool Process	15
Concrete wall [59]	8-10
Concrete floor [59]	10



#### 4.4 Small Scale Signal Fluctuations

While the previous two sections of this chapter are useful for predicting received signal levels over large distances within a factory geography (or within an entire factory), they do not discuss the local spatial fading that results when a receiver is moved about in a small region, on the order of just a few wavelengths. Since CW runs were made at different positions in an aisle and with different antenna heights at each measurement location, it is possible to determine from the data typical spatial signal fading behaviors in a local area. It is this small scale fading characteristic that in actuality degrades the performance of a portable/mobile factory radio system, since, for the case of a base transmitter, antenna placement and transmitter power is usually designed in a system link budget to maintain suitable average received power level for most factory locations.

In order to obtain an idea of the fading range over short distances in the factory channel, the weakest and strongest signal levels about the local median were extracted from the data at each measurement location. (Since the median path loss of each of the three runs was typically within  $\pm 1.5$  dB of the others, the median value of each measurement run was considered to be the same). The results are shown in Tables 4.5 through 4.7. The data indicates that the dynamic fading range is typically 30 to 35 dB over small areas and is not correlated with geography or factory site. The reader may be at first surprised that there is no fading correlation with T-R distance, either. Recall, however, that the transmitter power is adjusted for each measurement location to insure that all signal fading levels are well above the noise floor of the receiver.

The fluctuations of the received signal envelope over a particular local area may be considered to be a random variable, having a deterministic (measured) value for each spatial location (we consider the channel to be temporally invariant). By measuring values of the envelope over various paths and antenna heights within the local area, it is possible to fit the observed data to distribution functions. This approach has been used by other researchers to determine local fading characteristics inside metal buildings [61] and office buildings [59], and has been found to predict the performance of other channels well [4,40].

Table 4.5 Fading extremes from median level (10 -25 m path).

Fading Extremes from median as Function of Factory Geography (dB)					
T-R separation of 10 - 25 m					
Geography	Site B	Site C	Site D	Site E	Site F
LOS light clutter	+11.5/-21.1	+11.9/-18.4	+8.0/-11.3	-	-
LOS heavy clutter	+9.0/-22.0	+9.5/-17.7	+10.2/-16.9	+12.2/-17.9	+14.4/-21.7
LOS along wall	-	+8.0/-16.9	-	-	-
Obstructed light clutter	+6.8/-25.8	+10.1/-18.2	+10.8/-19.8	-	-
Obstructed heavy clutter	+10.0/-16.3	+11.8/-15.6	+12.8/-20.7	+14.6/-17.7	+15.2/-23.4

Table 4.6 Fading extremes from median level (25 -40 m path).

Fading Extremes from median as Function of Factory Geography (dB)					
T-R separation of 25 - 40 m					
Geography	Site B	Site C	Site D	Site E	Site F
LOS light clutter	+9.5/-13.8	+8.0/-21.7	+9.4/-22.4	-	-
LOS heavy clutter	+7.1/-21.4	+11.9/-18.7	+9.6/-23.0	+8.0/-12.6	+9.8/-17.5
LOS along wall	-	+8.6/-23.0	-	-	-
Obstructed light clutter	+8.2/-25.7	+12.5/-20.3	+11.5/-16.5	-	-
Obstructed heavy clutter	+9.2/-21.1	+12.0/-17.3	+13.2/-25.0	+10.1/-21.8	+10.1/-24.8

Table 4.7 Fading extremes from median level (40 -75 m path).

Fading Extremes from median as Function of Factory Geography (dB)					
T-R separation of 40 - 75 m					
Geography	Site B	Site C	Site D	Site E	Site F
LOS light clutter	+10.2/-20.6	+8.9/-22.6	+5.2/-13.8	-	-
LOS heavy clutter	+9.8/-25.6	+13.2/-21.7	+7.1/-17.1	+6.8/-8.9	+12.6/-17.5
LOS along wall	-	+7.1/-14.0	-	-	-
Obstructed light clutter	-	+12.2/-22.5	+14.2/-22.5	-	-
Obstructed heavy clutter	+15.1/-19.2	+10.1/-17.1	+12.4/-23.7	+10.0/-22.4	+11.6/-18.2

One may attempt to further characterize the small scale fading phenomenon by considering it to be a random process on position within a local area taken over an ensemble of various local areas (i.e. areas within particular types of factories or geographies). To measure this process, the data obtained from each local area would be viewed as a single sample function of signal envelope as a function of local position. This type of characterization is more general, and consequently more useful, than a simple statistical model based upon a few spot measurements. However, it is generally difficult to deal with such characterizations unless certain simplifying assumptions are made. For example, unless the small scale fading process is assumed to be spatially stationary (at least in the wide-sense), it is impossible to legitimately consider an average of the sample functions as representative of the process. The stationarity assumption mandates that the distribution of the random variable is unaffected by position, but it makes no statement about whether or not the distribution of each sample function (over position) is equal to the distribution down the ensemble. Such a strong condition is implied only by an ergodic random process. Either some confusion exists in the literature about the above discussion, or researchers feel the above is common knowledge and requires no comment. Another likely explanation is that the concepts of stationarity and ergodicity are disregarded for a purely probabilistic model based on the relative frequency idea of probability. In any case, some recent conclusions based on empirical channel sounding data have been made that either incorrectly or implicitly invoke the above ideas. (In [61], several local area measurements are found to closely fit a Rayleigh distribution, and a model is derived which assumes all local fading to be Rayleigh. Such an assumption is only valid if the spatial fading process is ergodic. Although the ergodic assumption is difficult to prove, no mention of the underlying assumption was made. In [59], measurements are observed by the authors to be non-stationary with regard to space, thus they claim their data may not give intrinsic statistics of the fading process. The term *wide-sense stationary* merely indicates that the mean values of the received signal are constant with regard to location and that the correlation between two received signal levels only depend upon the spatial difference between the two measurements. It says nothing about whether or not the observed measurements statistically describe the actual random process. Only with an ergodic assumption may one attempt to justify the statistical behavior of a random process through the analysis of one or a few sample functions. The spatially ergodic assumption is reasonable

for sample functions that consistently appear to be distributed in the same fashion over different local areas.).

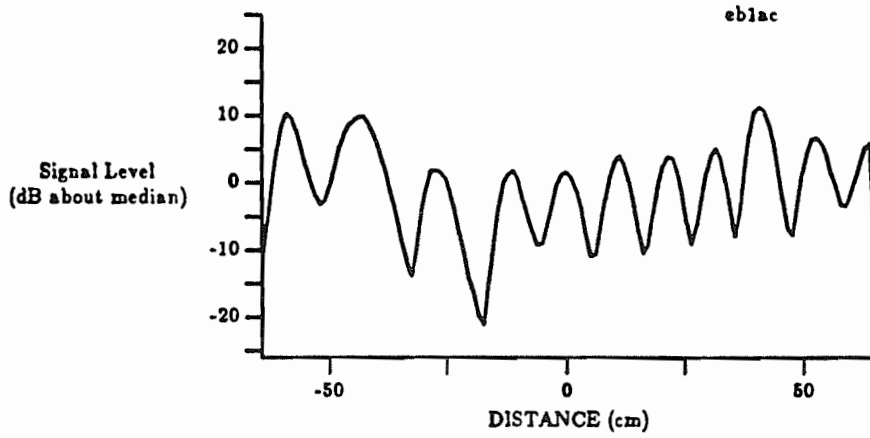
For our data, large scale median path loss values for each of the three local area records (center of aisle using 1.5 m and 2.0 m antenna heights, and along the side of an aisle), were subtracted off and the resulting data was quantized into 1dB width bins and combined to form a sample frequency distribution of receiver envelope levels for each measurement location. Additionally, the sample records (with large scale path loss removed) were concatenated to form a sample function for each of the 50 measurement locations. To ensure that the combining of the local records into a single sample function was valid, median path loss values for the records of a particular measurement location were compared and found to be within the measurement uncertainty of  $\pm 1.5$  dB from each other for almost all measurement locations. Furthermore, the CDF's of the individual records were quite similar. Such a finding indicates that the small scale fading process may be considered to be spatially ergodic (although this assumption would have to be borne out by rigorous analysis of numerous sample records from a particular location). In this thesis we describe the spatial fading in terms of signal envelope probabilities as computed in various geographies and factories. The sample functions will be used in the future to provide an in-depth analysis of the small scale spatial phenomenon.

Figure 4.15 shows three typical sample records for a measurement location (the entire raw data set is given in Appendix C). All measurements were made with the receiver cart traveling at a reasonably constant velocity between 0.25 and 0.3 m/s. (Since the cart was pushed by hand, it is impossible to know the exact velocity of the cart -- effort was made to push the cart over a 1.3 m path at uniform speed in a 5 second interval). It may be noted that fade minima are sharper than maxima, and that median level crossings occur at approximately half wavelength periods. Some of the data had positive-going zero-crossings occurring at intervals as small as  $\lambda/2$  and as large as  $3\lambda/2$ , although because of the uncertainty of vehicle velocity, these cannot be determined exactly. The sharp minima, blunt maxima, and periodic nature of Figure 4.15, which is characteristic of a significant portion of the LOS envelope spatial fading data, is characteristic of the sum of just a few sine waves of nearly equal amplitude whose phase differences are changing at a constant rate [86]. Indeed, for this measurement location,

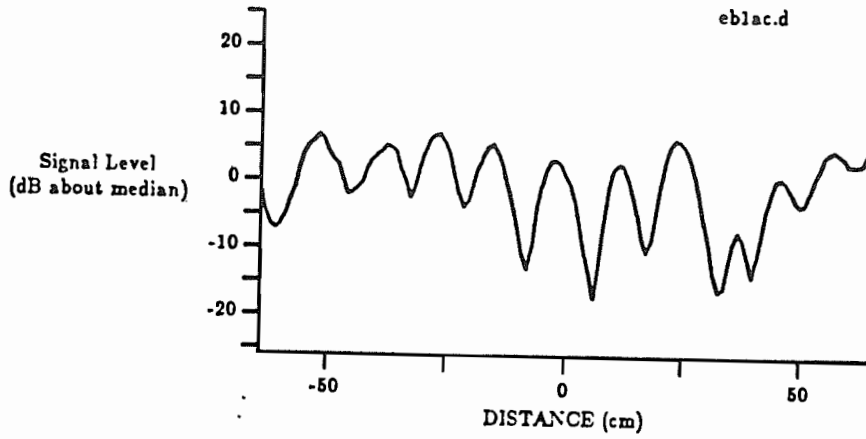
wide band measurements (see Chapter 5) show that just three main paths exist over a 250 ns spread.

Figures 4.16 and 4.17 illustrate the best case and worst case local fading measurements in terms of dynamic fading range. The data shown in Figure 4.16 were acquired on a lightly cluttered obstructed path at site B. All three records have pronounced fading which was caused by a concrete pillar located roughly one meter from the transmitter and which partially shadowed the path traversed by the receiver cart. From the figure it is clear that the median signal level is several dB greater than the mean, although all three records have large scale path loss medians within  $\pm 1.0$  dB of one another. Data in Figure 4.17 were gathered in a heavy clutter LOS environment in site C over a 50 m path and has the smallest dynamic fading range of any of the measurements. The three sample records of Figure 4.17 have large scale path loss median values within  $\pm 3.5$  dB of one another yet their CDF's agree quite well. As is discussed subsequently, the small fading range of the envelope leads to a Rician distribution, which is to be expected for LOS paths that are enhanced, or guided, by large machinery that flanks the aisle. The cumulative probability distributions (CDF's) of the typical and the two extreme fading measurements of Figures 4.15 through 4.17 are plotted on a logarithmic scale in Figure 4.18, and were computed from 384 data points (3 cw runs X 128 data points/run) at each of the three measurement locations.

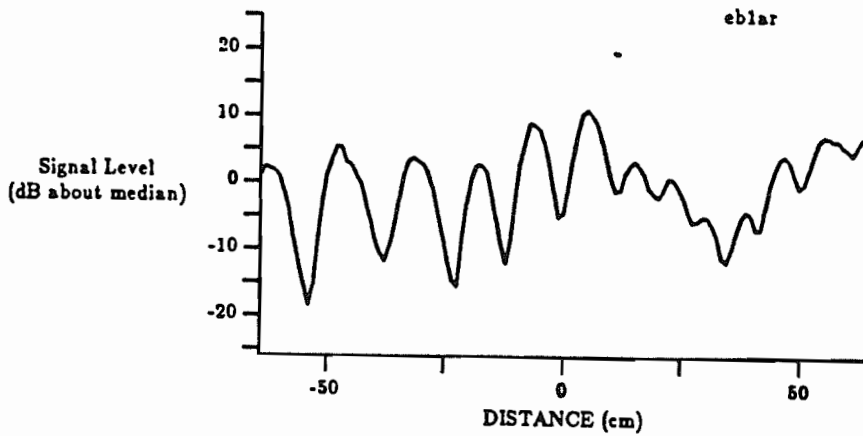
While the worst case fading measurement eb4a fits the tail of the log-normal distribution (see Figure 4.18), it is not truly log-normal because of the large percentage of signal level above the median value. This behavior is indicative of *mixture* probability distributions, where a particular trait (in this case a log-normal distribution) dominates for small signal levels and another trait (Rician) dominates the region for where signal levels are large. Suzuki briefly considered mixtures in his Ph.D. thesis [85]. Because of the shadowing caused by the concrete pillar and the lack of metal in the measurement area, it is likely that for the case when the receiver was shadowed, the signal comprised of one significant specular component that was refracted by the pillar. As the receiver moved along the path, the received signal, traveling through and around the pillar, was multiplicatively affected (attenuated) by the variation in the geometry of diffraction, thus perhaps explaining the log-normal distribution for small signal levels. Once past the



a) center of aisle - 2 m antenna height.

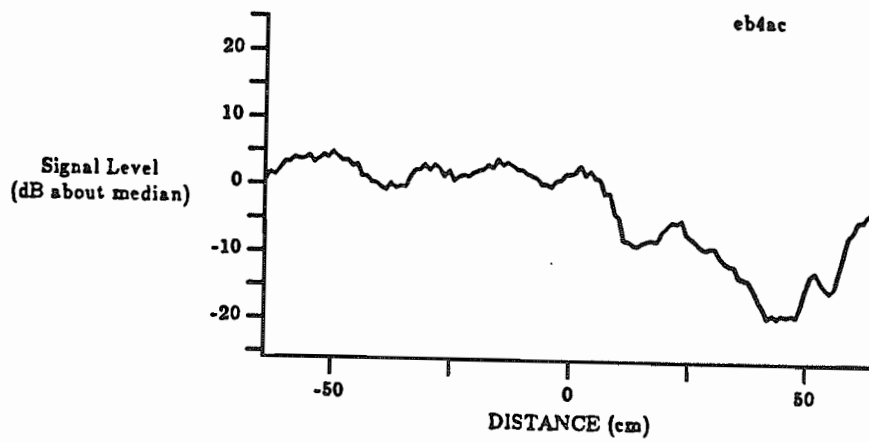


b) center of aisle - 1.5 m antenna height.

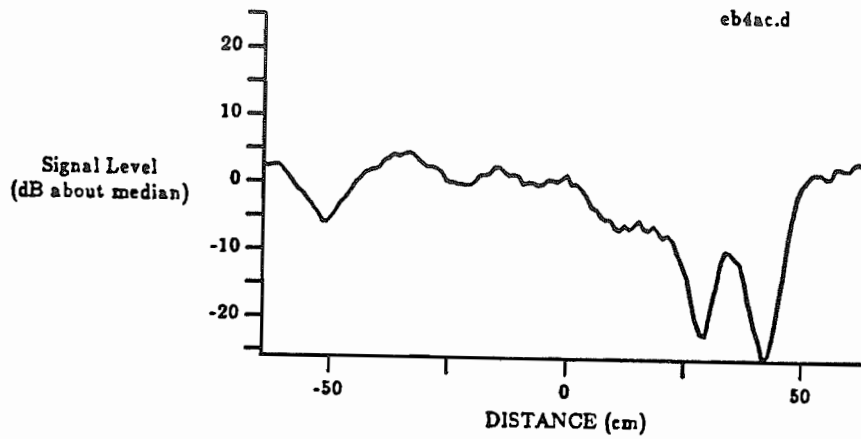


c) right side of aisle - 2 m antenna height.

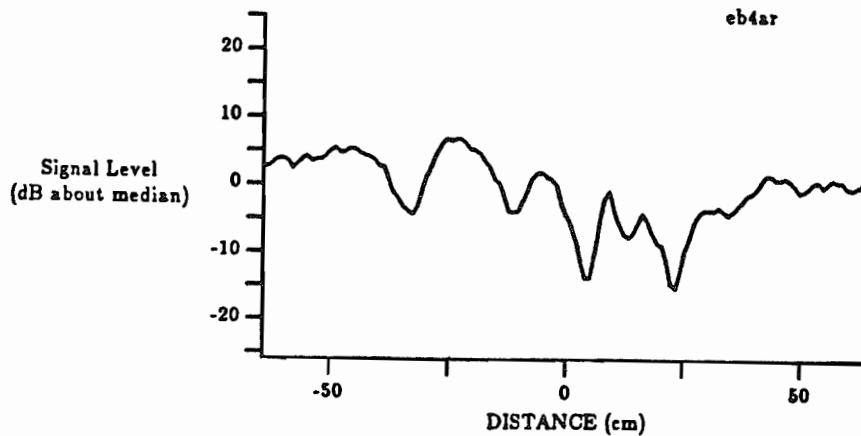
Figure 4.15 Typical small scale spatial signal fluctuations.



a) center of aisle - 2 m antenna height.

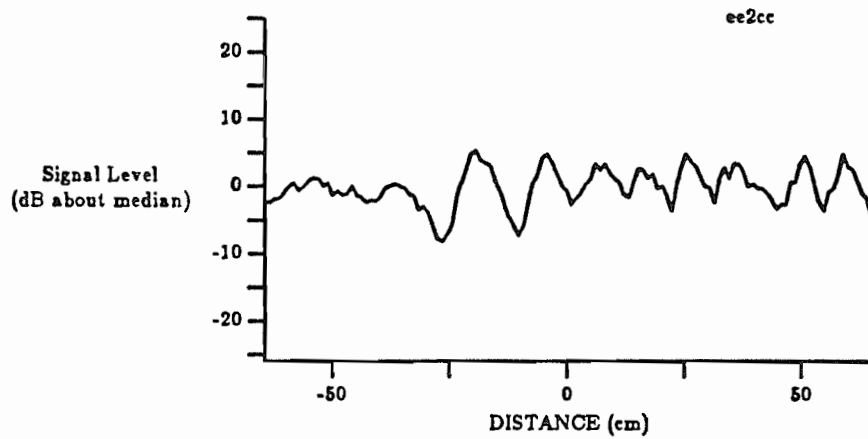


b) center of aisle - 1.5 m antenna height.

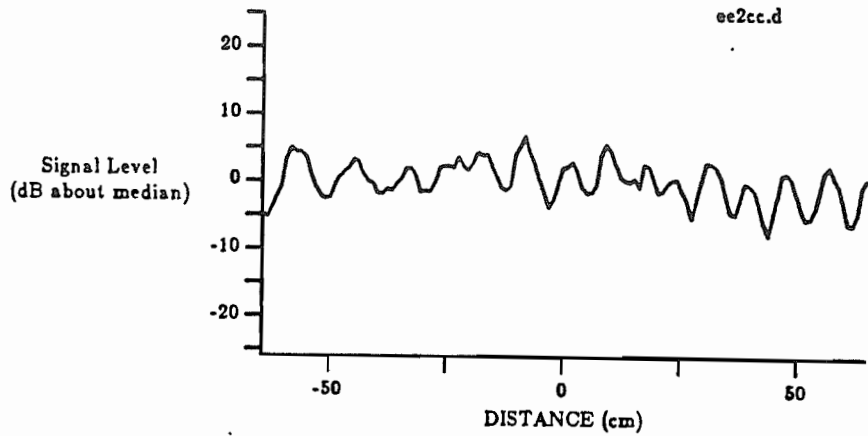


c) right side of aisle - 2 m antenna height.

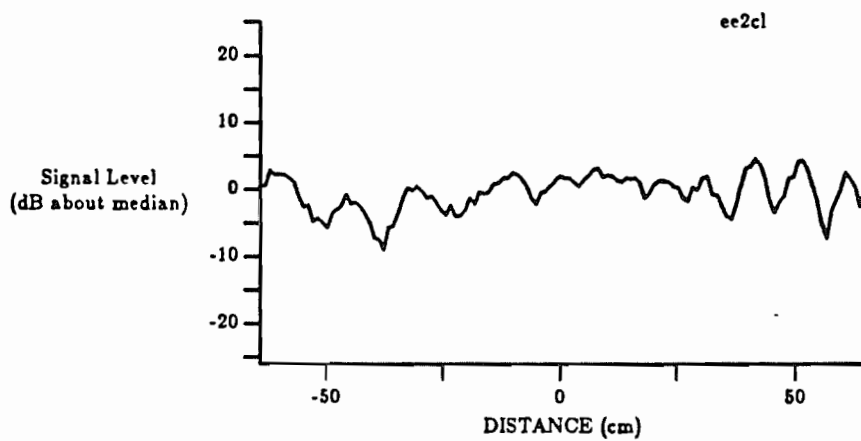
Figure 4.16 Worst case small scale spatial signal fluctuations.



a) center of aisle - 2 m antenna height.



b) center of aisle - 1.5 m antenna height.



c) left side of aisle - 2 m antenna height.

Figure 4.17 Best case small scale spatial signal fluctuations.



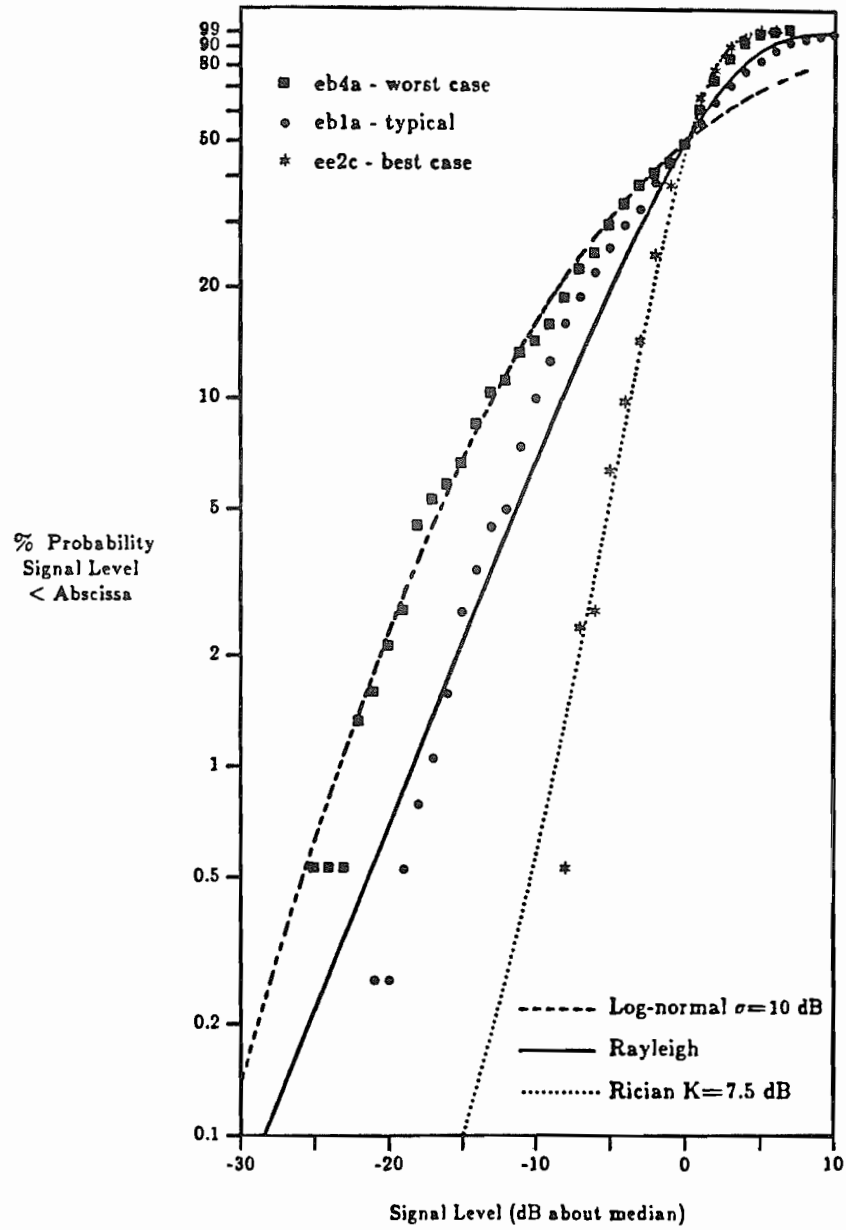


Figure 4.18 Cumulative distributions for some spatial fading measurements.

pillar, the card board box obstruction provided only slight attenuation of the main path. Interestingly, the corresponding CDF in Figure 4.18 is log-normal for all values below the median and Rician above the median. This corresponds well to the fact that during the measurement, the receiver was blocked by the pillar over approximately 50% of the path and relatively clear (with only the cardboard obstruction) for the other 50% (see Figure 4.15).

CDF curves such as shown in Figure 4.18 were made for all 50 measurement locations, and visually inspected and compared to theoretical distributions. The Rician distribution was found to fit well to 16% of the data while log-normal distributions having  $5\text{dB} \leq \sigma \leq 8\text{dB}$  fit 24% of the data well. In particular, the spatial fading data which appeared to fit the log-normal distribution had excellent agreement for values of signal level below the median, although the agreement for large signal levels was generally not good. The majority of data, 60%, had a good fit to the Rayleigh distribution. The compression of the CDF at low signal levels, typical of the log-normal distribution, was also common for much of the Rayleigh fading data below 1% ordinate values. This has been observed, but seldom commented on, by others primarily because of the lack of number of data samples available [40,60,61]. Since the transmitted power was always adjusted to ensure that fading levels never approached the noise floor of the receiver, we believe this log-normal tendency at lower signal levels to be truly a characteristic of the channel.

Analysis of the spatial fading distributions indicated that there was no correlation between T-R separation and spatial fading behavior. It is interesting to note that most lightly cluttered LOS paths exhibited nearly Rayleigh fading (a Rician distribution for  $K=2$  dB fit most of the data well) at all sites and over all T-R separations, except for the measurement ed1c which fit a Rician distribution having  $K=6$  dB. At ed1c, there was a long row of metal extrusion bins stacked in 3 m piles along the side the aisle, so the environment was actually heavy clutter. A distinct Rician distribution ( $K > 2$  dB) was evident over most LOS heavy clutter paths, regardless of the factory site. The LOS wall spatial fading measurements made at site C followed a Rician distribution having a  $K$  value of about 6 dB, except for the middle measurement which was made with the receiver located a few meters from a 0.3 m metal ceiling support beam. This

measurement was found to be closer to Rayleigh fading. Data had either a Rayleigh or a log-normal fading characteristic over obstructed paths. Figure 4.19 shows the CDF of three measurements which illustrate the typical fit of data to the aforementioned distributions.

In order to determine a suitable overall spatial fading model, the cumulative distributions of all measurement locations (about their local medians and over all T-R separations) were combined by geography and by factory. An overall CDF for the entire CW measurement data pool was also computed. For the computations, the measurement edlc was considered heavy clutter instead of light clutter.

The log-normal distribution was found to fit the combined data quite well for signal levels below the median, especially at the tail where SNR is small. The CDF's for the various factory sites are shown in Figure 4.20 and are seen to behave log-normally below the median and Rayleigh above the median. There is no apparent correlation to fading behavior and factory building. Figure 4.21 shows CDF's for the data when grouped according to geography. For the plots, a Rayleigh distribution is in all practicality a straight line for signal levels below -15 dB. Although no check for independence of the data or confidence tests have been performed to find a "best-fitting" distribution for the data and to confirm the log-normal tendency at low SNR, it is worth noting that each curve on Figures 4.20 and 4.21 represents over 2000 data points. Such a large sample size permits us to put some faith in the behavior of the sample CDF for the ordinate range given on the graphs. The CDF of all of the CW spatial fading data, computed from over 18,500 signal measurements, is shown in Figure 4.22 and emphasizes the log-normal fading for low signal levels. For the factory data, it appears that a Rayleigh fading model is a good yet conservative (safe) model for signal fluctuations for a portable terminal over short distances. A slightly more optimistic (and realistic) model would be one which assumes a different distribution that incorporates the log-normal tendency (compression) at the tail. Rician distributions having small K values (2 dB) are good models for spatial fading characteristics along lightly cluttered LOS paths, such as along secondary aisles of a factory or in manual assembly areas, whereas Rician distributions having larger K values ( $4 \text{ dB} < K < 7 \text{ dB}$ ) appear valid for LOS paths in heavy clutter areas like an automated

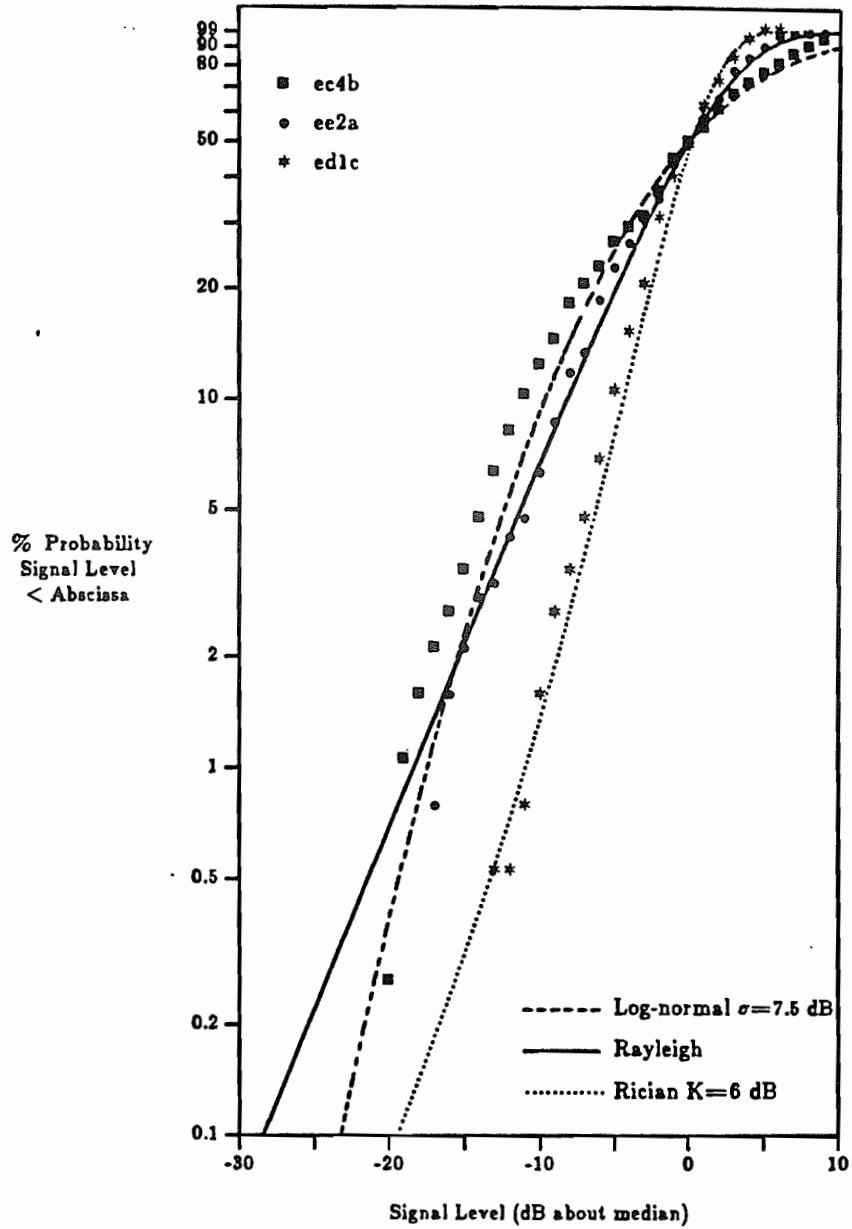


Figure 4.19 CDF's for three measurements and their fit to various distributions.

assembly line. Log-normal distributions having  $\sigma=8$  dB appear valid for some obstructed factory paths.

#### 4.5 Temporal Fading

At sites E and F, some measurements were performed to determine typical temporal fading of the received signal envelope. With the transmitter and receiver stationary, data was collected at approximately 100 ms intervals over a 100 second period in four separate locations throughout the two factories (i.e. each sample record has 1024 points). We deliberately made measurements at times having high levels of movement, such as when groups of workers were walking through the factory or during normal operation of an assembly line. Figures 4.23 through 4.26 show the fading data. Figures 4.23 and 4.24 show data taken within a fully operational gray iron foundry (site E). Figures 4.25 and 4.26 show the fading data measured in an automated engine assembly plant (site F).

The measurements shown in Figure 4.23 were made along the main aisle of the foundry core room with a T-R separation of 50 m. During the measurement, two fork lift trucks were stacking metal bins in a spacious storage area located off to the side of the aisle. Several people walked along the aisle during the measurement, as well. The large signal increase observed at 58 s occurred when a speeding fork lift truck from an adjacent aisle drove behind the transmitter. Figure 4.24 shows data taken across the core pep-set line. In this area of the foundry, people and machinery were in constant motion as employees weighed and loaded sand into machinery to form ceramic cores for engine castings. Some of the machinery in motion within the T-R path included a conveyor belt, a swinging scale and a sand packing machine. The data shown in Figure 4.25 was collected along the main aisle of a wash and assembly area with a T-R separation of 40 m. People and small vehicles frequented the area, and several pieces of equipment which flanked the aisle, such as a wash tank and drill presses, were in motion. The data in Figure 4.26 were collected with the radio path obstructed by the wash tank area. Several workers moved about a small area as they picked metal parts off of a conveyor belt, hosed them down, and placed them back on the conveyor. A 4 m ceiling-mounted fan operated directly above the area, and fork lift trucks frequented a storage

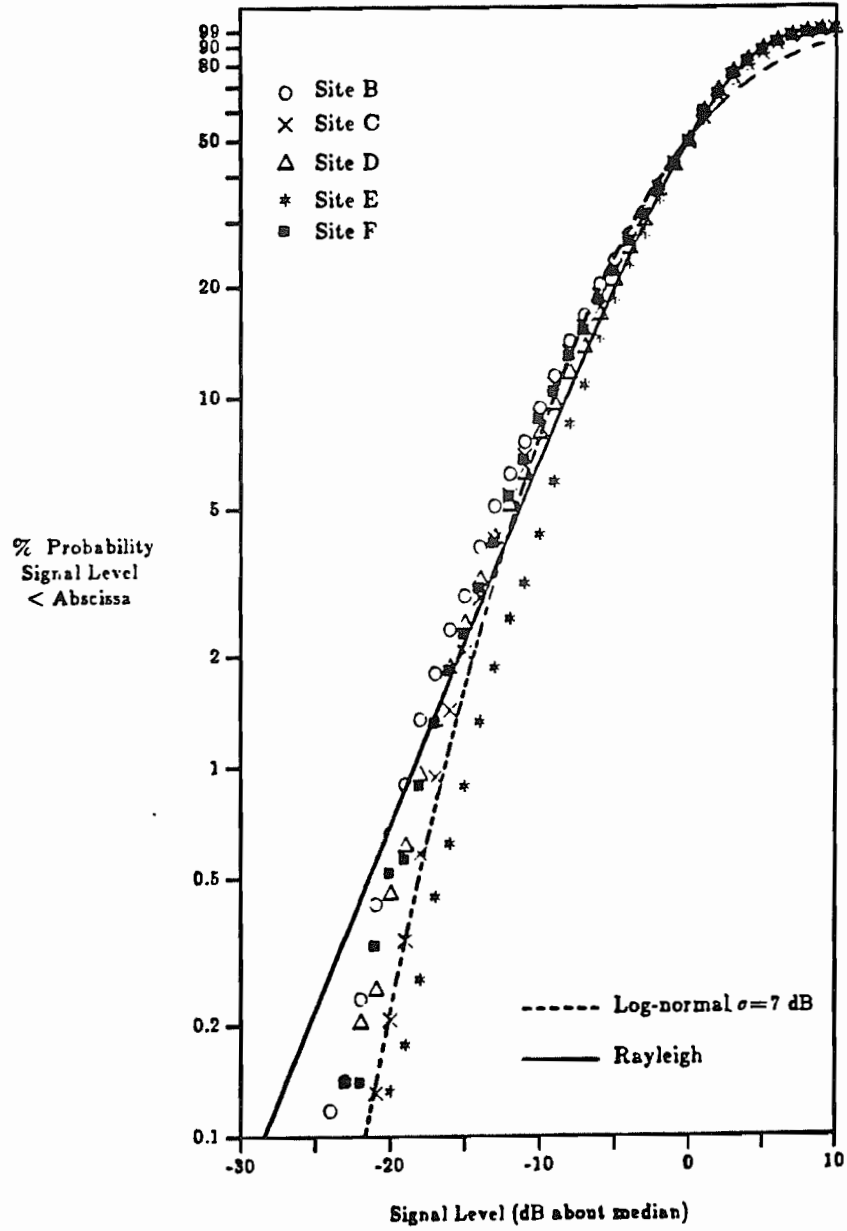


Figure 4.20 CDF of small scale spatial fading as function of factory site.

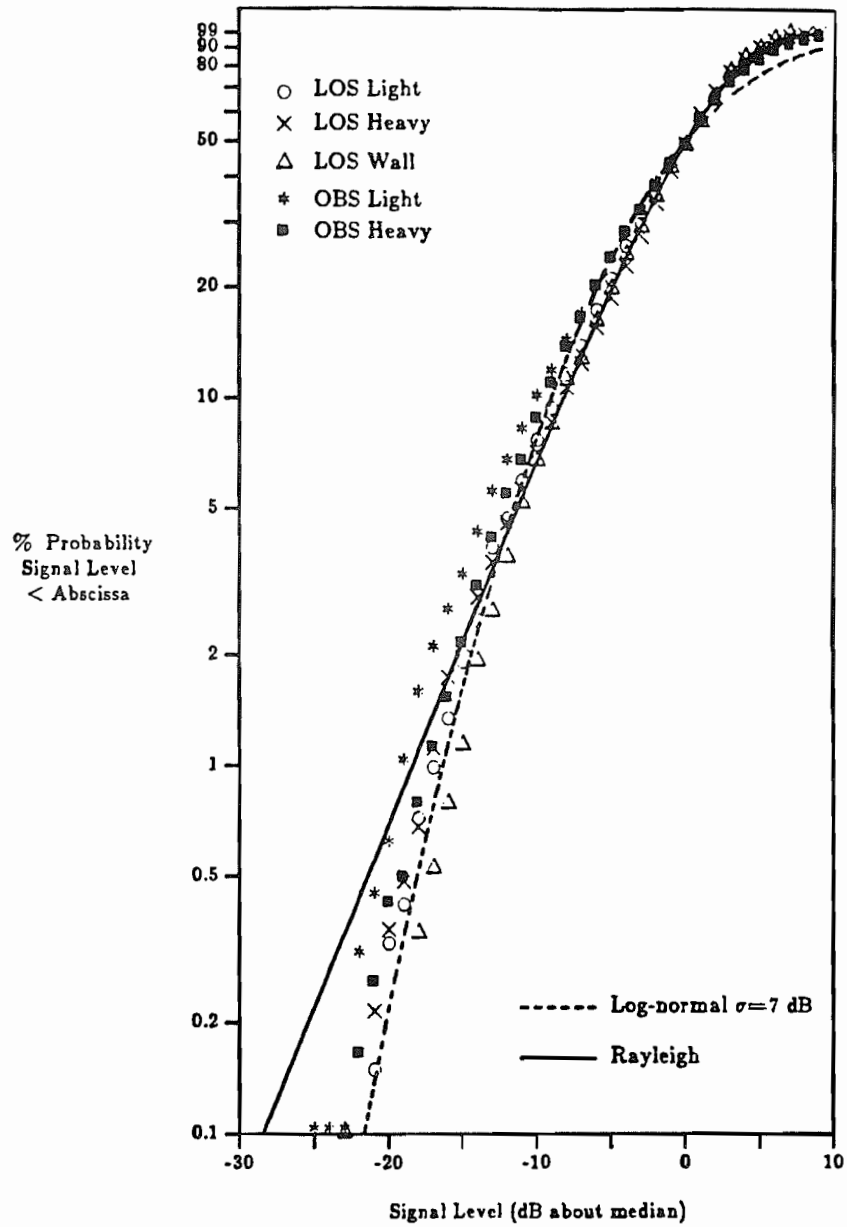


Figure 4.21 CDF of small scale spatial fading as function of geography.

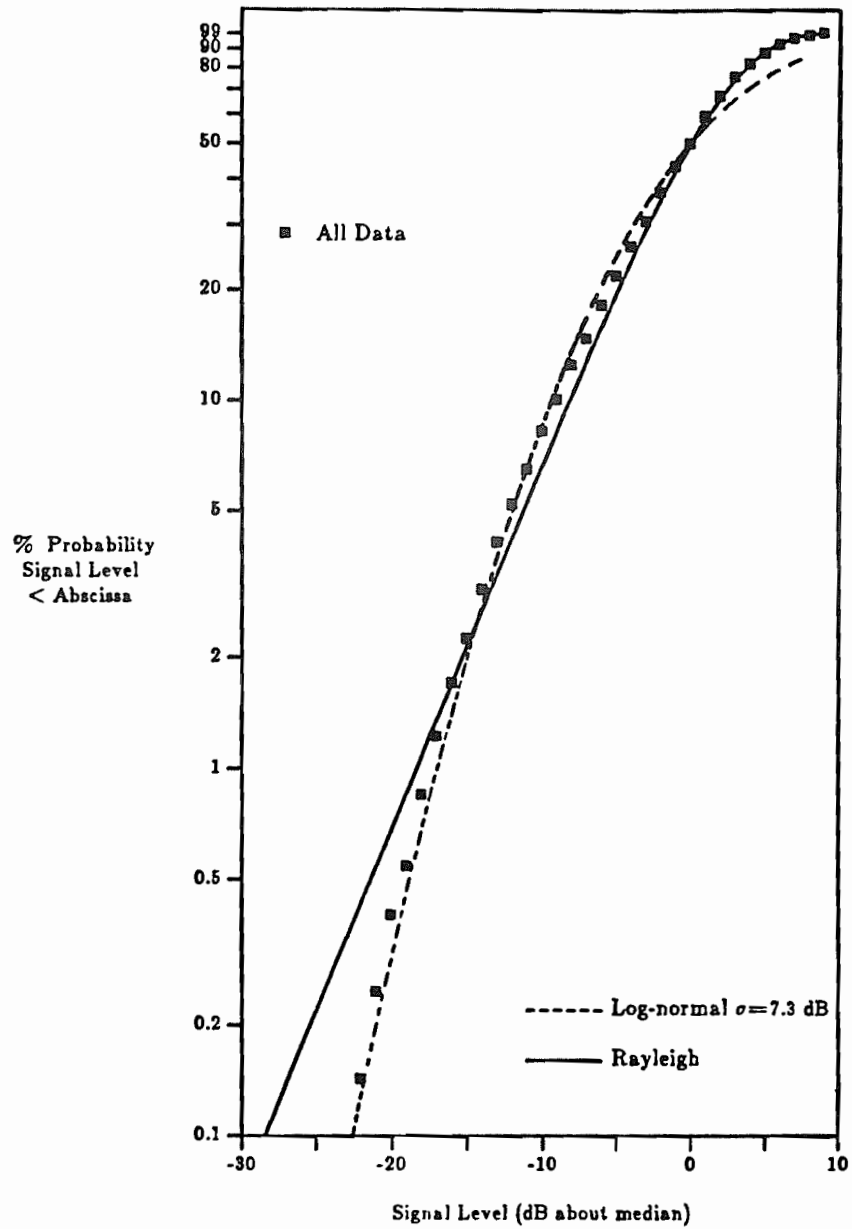


Figure 4.22 CDF of spatial fading measurements over all factories and geographies.



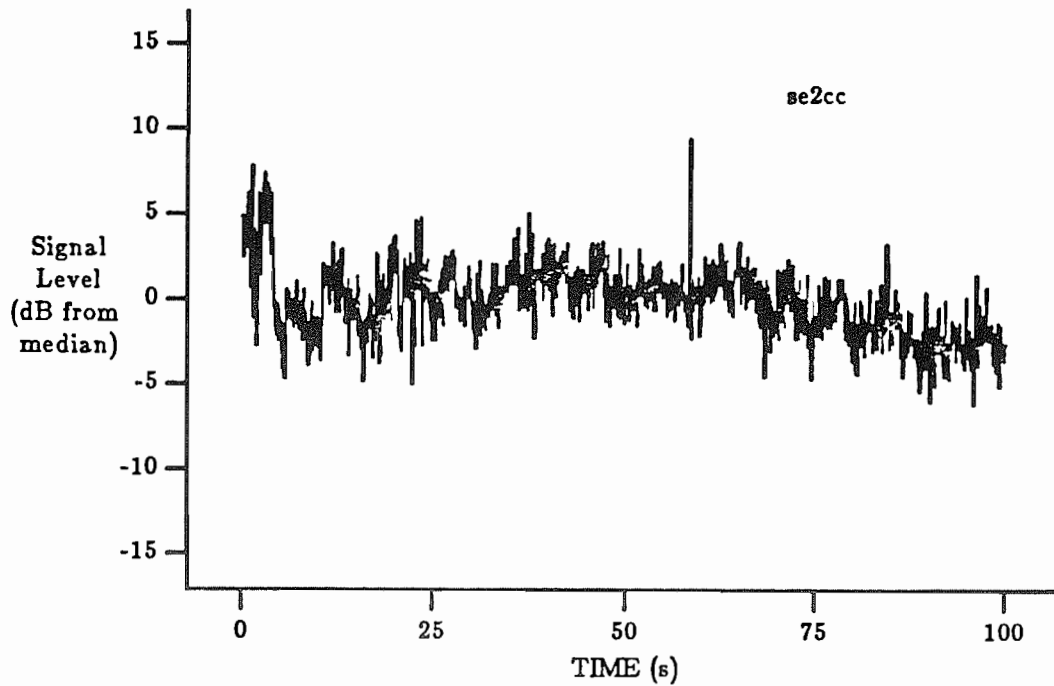


Figure 4.23 Temporal fading in core room aisle.

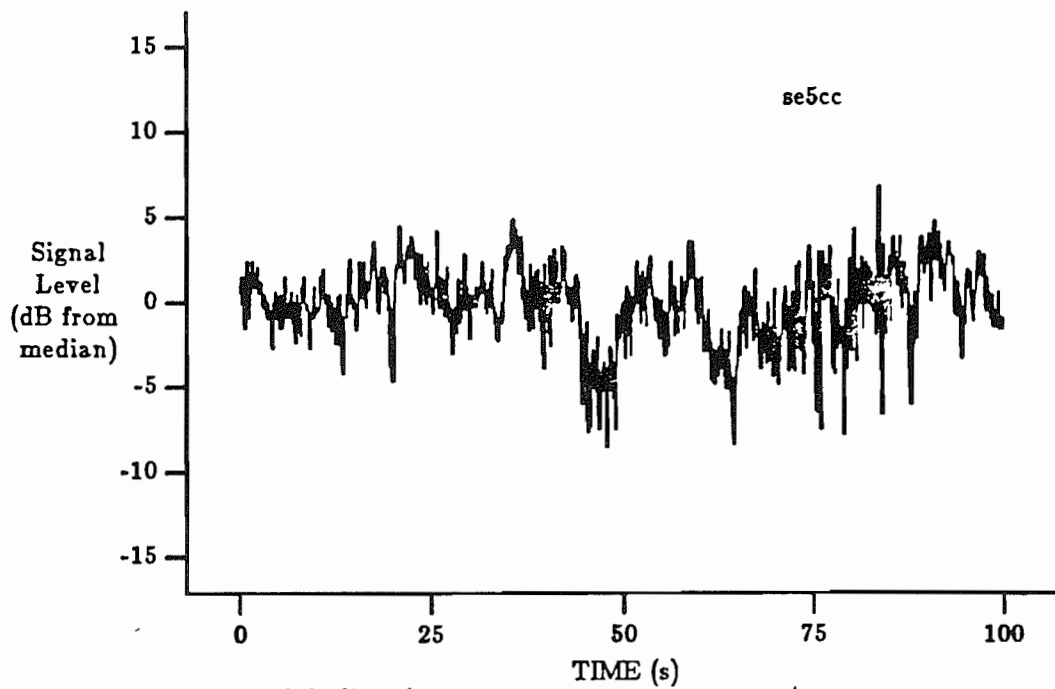


Figure 4.24 Temporal fading in core room across pep-set line.

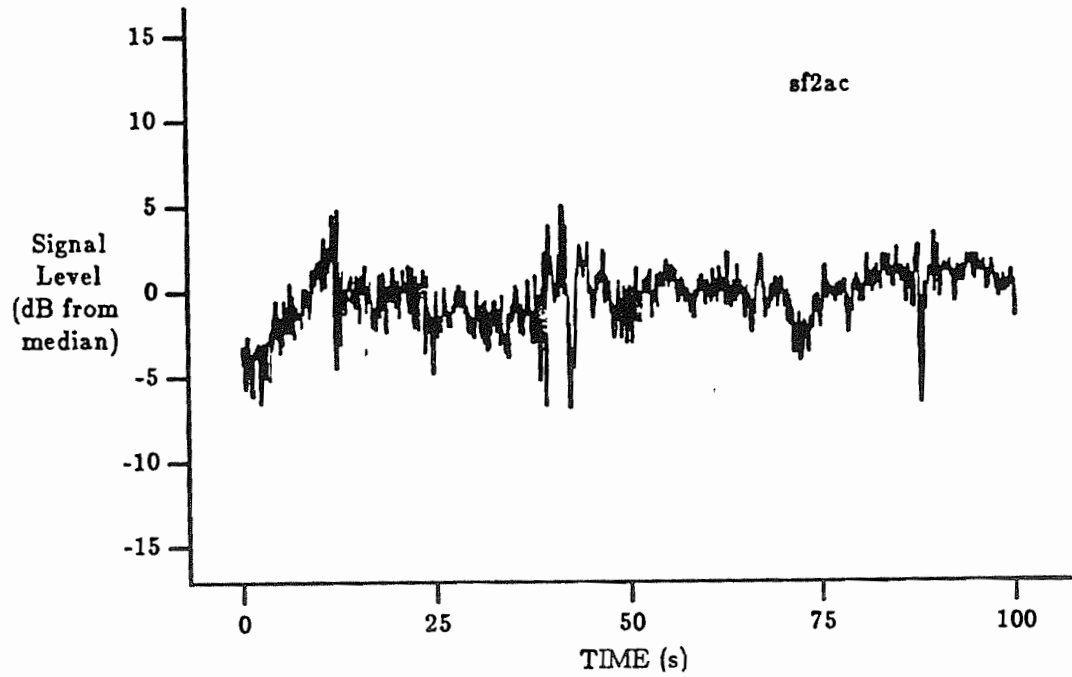


Figure 4.25 Temporal fading in engine assembly aisle.

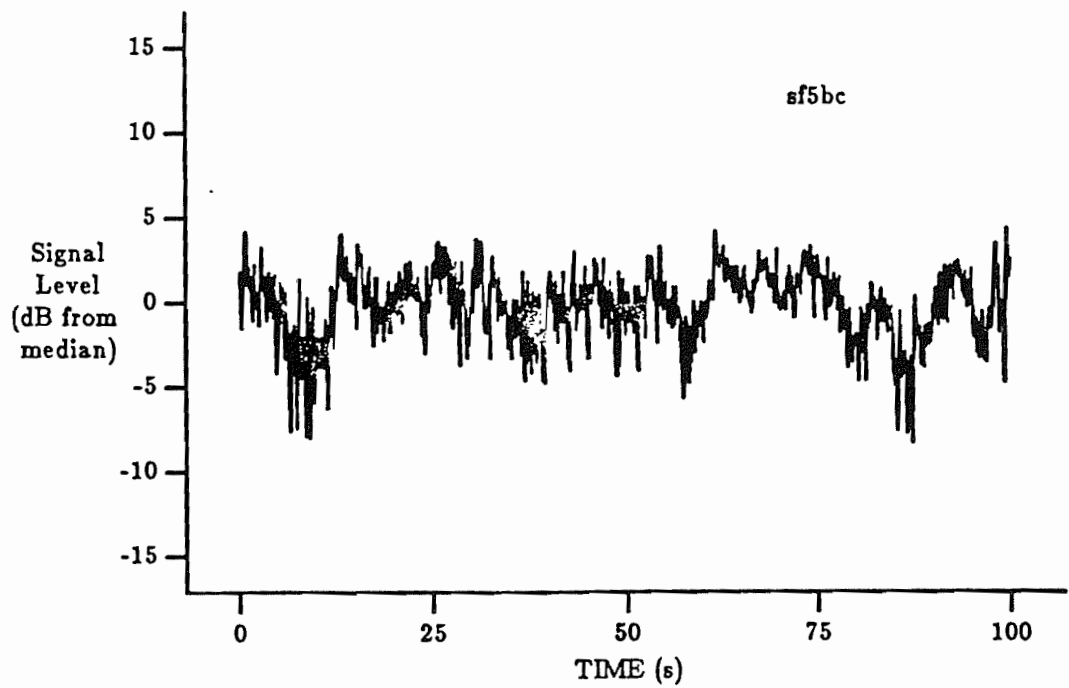


Figure 4.26 Temporal fading in engine assembly area across wash line.

rack nearby. Large storage racks and a suspended cat walk containing a massive power bay were located 20 m behind the receiver.

In order to determine confidence intervals on distributions of sample data, it is essential to have independent (random) data. Once the data is deemed independent, one may then use non-parametric methods to determine the adequacy of fit sample data has to a continuous distribution function. The sample data in the Figures 4.23 through 4.26 were checked for randomness by using the run test [41,83]. Since the data already was adjusted about the median, it was simple to compute the number of runs for each of the four measurement records using IMSL routines. The data from Figures 4.23 and 4.25 had 639 and 561 runs respectively. These numbers are too large to reasonably assume that the fading data is generated by random channel motion and indicates that a large part of the signal may be due to the constant DC level of the received signal. However, the obstructed path data from Figures 4.24 and 4.26 had 492 and 550 runs respectively. Thus, the data passed the run test at the  $\alpha=0.01$  level of significance. In fact, the data from the busy wash tank area (Figure 4.26) passes the test with an  $\alpha=0.08$  level of significance. The two measurements se5cc and sf5bc were merged and a CDF was computed using 0.25 dB bins<sup>†</sup>. Figure 4.27 shows the excellent agreement with which the temporal fading data fits a Rician distribution having  $K=10$  dB. Although no statistical analysis is performed here to determine the confidence interval on the Rician hypothesis, the true sample distribution, by inspection, has values well within the measurement uncertainty for all signal level values.

It is interesting to note that recent temporal fading measurements made by Bultitude [77] have indicated that Rician fading occurs in the office building environment, as well. In [77], temporal fading statistics gathered over obstructed paths in two different types of building structures were shown to fit Rician distributions having different  $K$  values. Although the temporal data from the se2cc and sf2ac hallway measurements are not strictly independent, it is still useful to inspect their CDF's for comparison

---

<sup>†</sup> When the two records are concatenated, the independence hypothesis on the data is further asserted by satisfying the run test at  $\alpha=0.10$ .

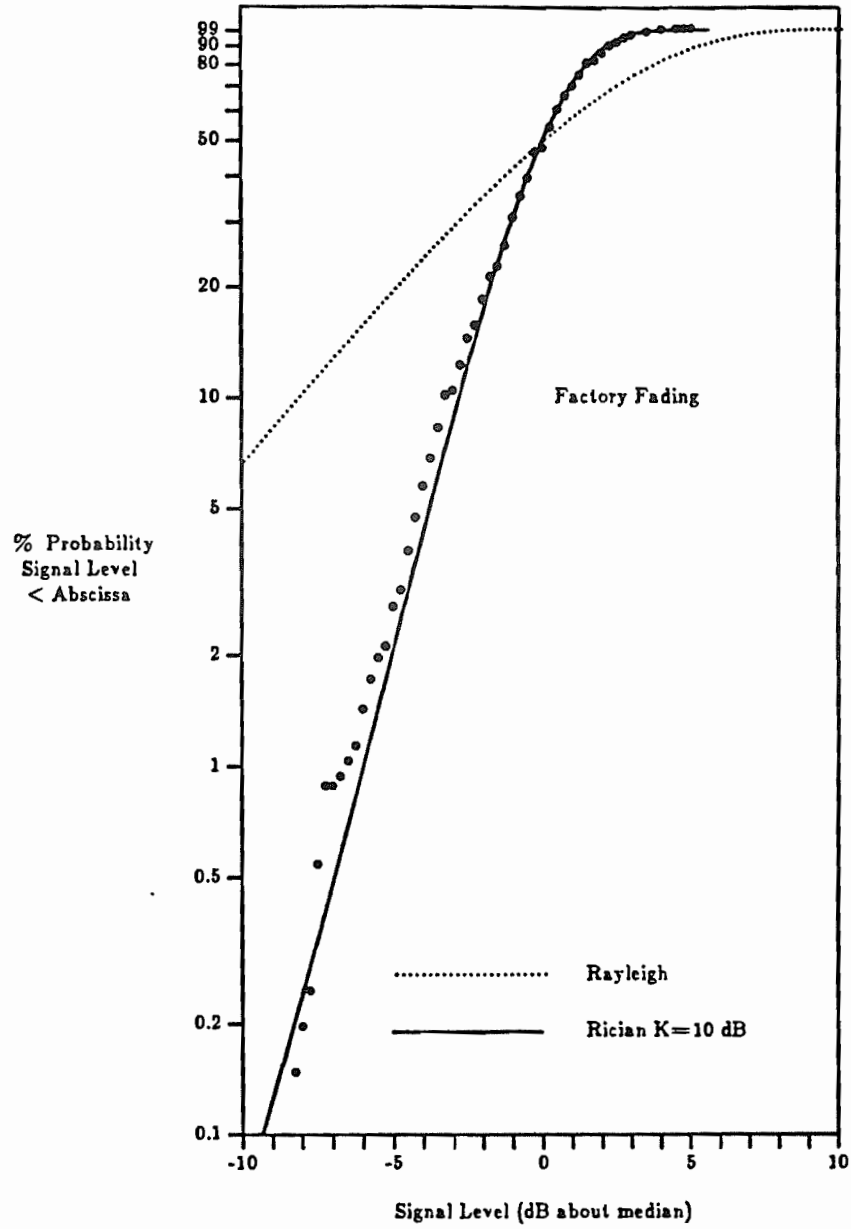


Figure 4.27 Cumulative distribution for 200 seconds of fading data.

with the obstructed paths. Figure 4.28 illustrates how for the LOS aisle paths, the Rician distribution is still a good fit, having  $K=11$  dB. It may be argued, though, that the LOS measurements were not taken during heavy fading conditions, so that the data is indicative of typical rather than worst case fading conditions.

It is interesting to note that the dynamic fading range of all the temporal fading data is less than 20 dB. This is 10 dB less than the range reported in an office building having ceramic block interior partitions [77], but on the order of fading ranges observed in a similar sized building having open plan layout and portable partitions. One plausible explanation and model for this is that in the office building, there may only be one or two main paths through over which propagation occurs (the term path here does not refer to an actual multipath, but rather to a duct or guide which is formed by the physical structure of the building, and which may contain several actual multipaths, hereby called the *supplemental paths*. An example of a main path is a hallway corridor in an office building). As objects in the channel move, they may block a main path and thus modulate the several supplemental paths. For obstructed paths in a well-partitioned building, one might expect only one or two of these main paths to exist. Such a situation explains the deep fades and the nearly Rayleigh (Rician distributions with low  $K$  values are close to Rayleigh) fading observed in the building of [77]. In the factory, however, partitions are very scarce and several major paths likely exist between transmitter and receiver due to the large metal content throughout the area. Main paths are most likely created by the illumination of large fixed scatterers located on the sides, above, and behind the receiver. Indeed, the Rayleigh spatial fading data substantiates this premise (wide band data of chapter 5 does also). Since motion in the factory is localized, confined to aisleways and production areas, but not to storage racks, ceiling trusses or large machinery, a large number of temporally stationary main paths likely exist. Thus, perturbation of the channel due to motion results in the variation of supplemental paths within only one or two main paths, but not the several others. For this case, a Rician distribution is predicted, having a  $K$  ratio dependent upon the value of the summation of stationary paths and the variance of the time varying path (or paths) at the receiver antenna. The supplemental components which make up the time varying paths are of nearly equal strength (because they are similarly altered in time, travel along the same

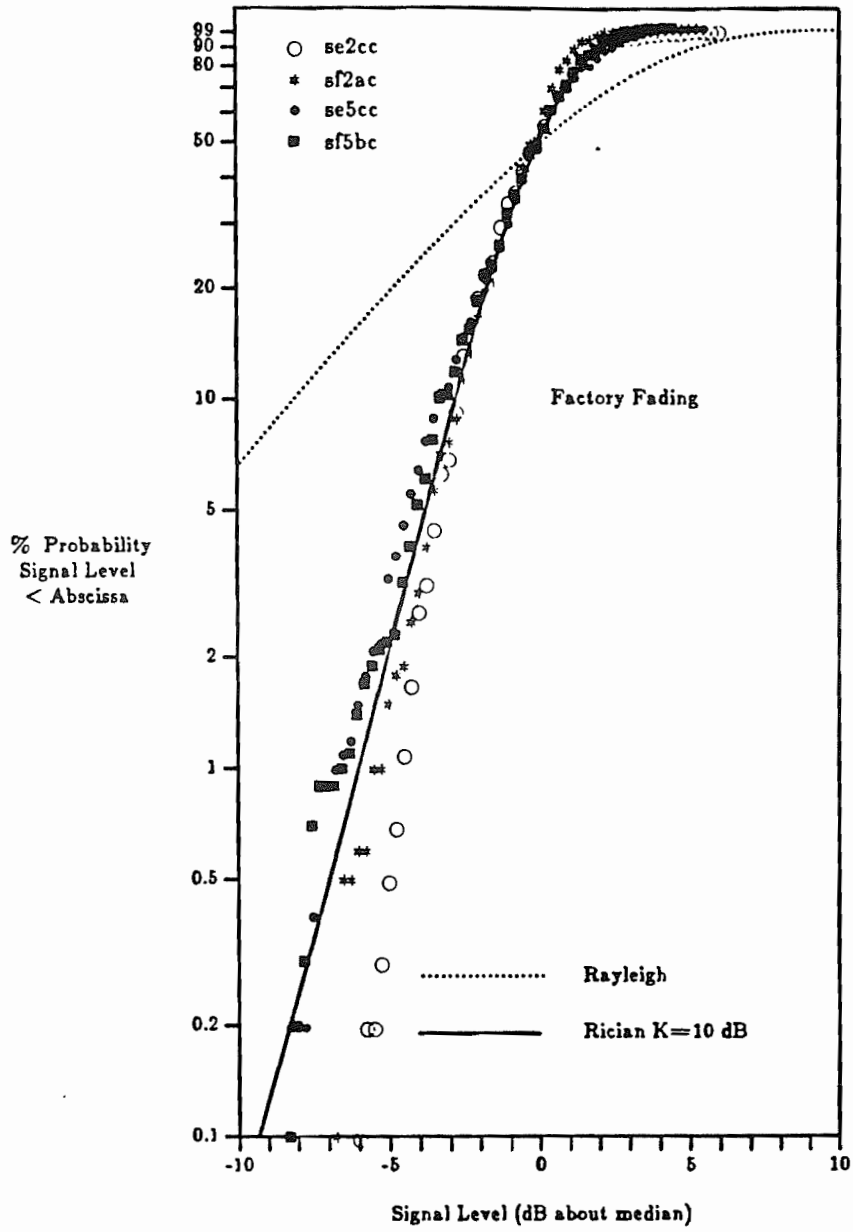


Figure 4.28 Cumulative distributions for fading data in various locations.

geography and impinge on the same scatterers) and random phase and thus are from a Gaussian process. The situation is akin to Gaussian narrow band noise adding to a steady RF carrier component, which gives rise to a Rician envelope distribution. It is also similar to a situation that arises in direct path VHF/UHF propagation. For the latter, ionospheric paths (which undergo Gaussian fading [4]) contain a strong specular path. Data supports the Rician distribution for long term temporal fading of the envelope for this case [87]. (In [87], the CDF of received signal envelope levels over month-long intervals for a 250 MHz, 189 km LOS path were nearly Gaussian, or comparable to Rician distributions having large K values). This model somewhat explains the Rician fading observations made by Bul-titude [77] in the second office building with low partitions and an open plan layout. Several main paths probably exist, but only one or two are likely perturbed by channel motion at a given instance, thus leading to his measurement of Rician fading having  $K=11$  dB [77]. In terms of temporal fading behavior, the open plan office building and the typical factory appear to be quite similar.

## CHAPTER 5 WIDE BAND MEASUREMENT RESULTS

### 5.1 Introduction

As detailed in Chapter 2, the wide band measurements were made by transmitting a repetitive probing pulse having a 10 ns duration, and by receiving and recording the dispersed version of the pulse. The measurement locations were the same as those described in Chapter 4.1, and were made along center aisle tracks that were slightly shorter than those used for the center-of-aisle CW spatial fading measurements. At each location, 19 individual multipath power profiles were recorded over a 1 m track at equal spatial increments of  $\lambda/4$ . The individual profiles are useful for determining the spatial fluctuations of multipath amplitude and delay over small distances. By assuming spatial stationarity and averaging over the collection of the 19 local profiles, a representative impulse response of the channel is obtained for a given measurement location. The local averaged impulse response is useful for making path loss measurements and for determining various multipath parameters.

#### 5.1.1 Review of the Data

Some typical wide band measurement results are shown in this section. The complete set of data may be found in the Appendices. Figure 5.1 shows some of the individual power delay profile measurements obtained at the five factories within various geographies. 19 such measurements were made along a  $4.3\lambda$  path at each of 50 different measurement locations. The complete set of 950 multipath power delay profile measurements collected during the course of the research is given in Appendix D. Figure 5.2 illustrates examples of the spatially averaged power profiles formed from 19 local area measurements. The set of 50 locally-averaged profiles obtained



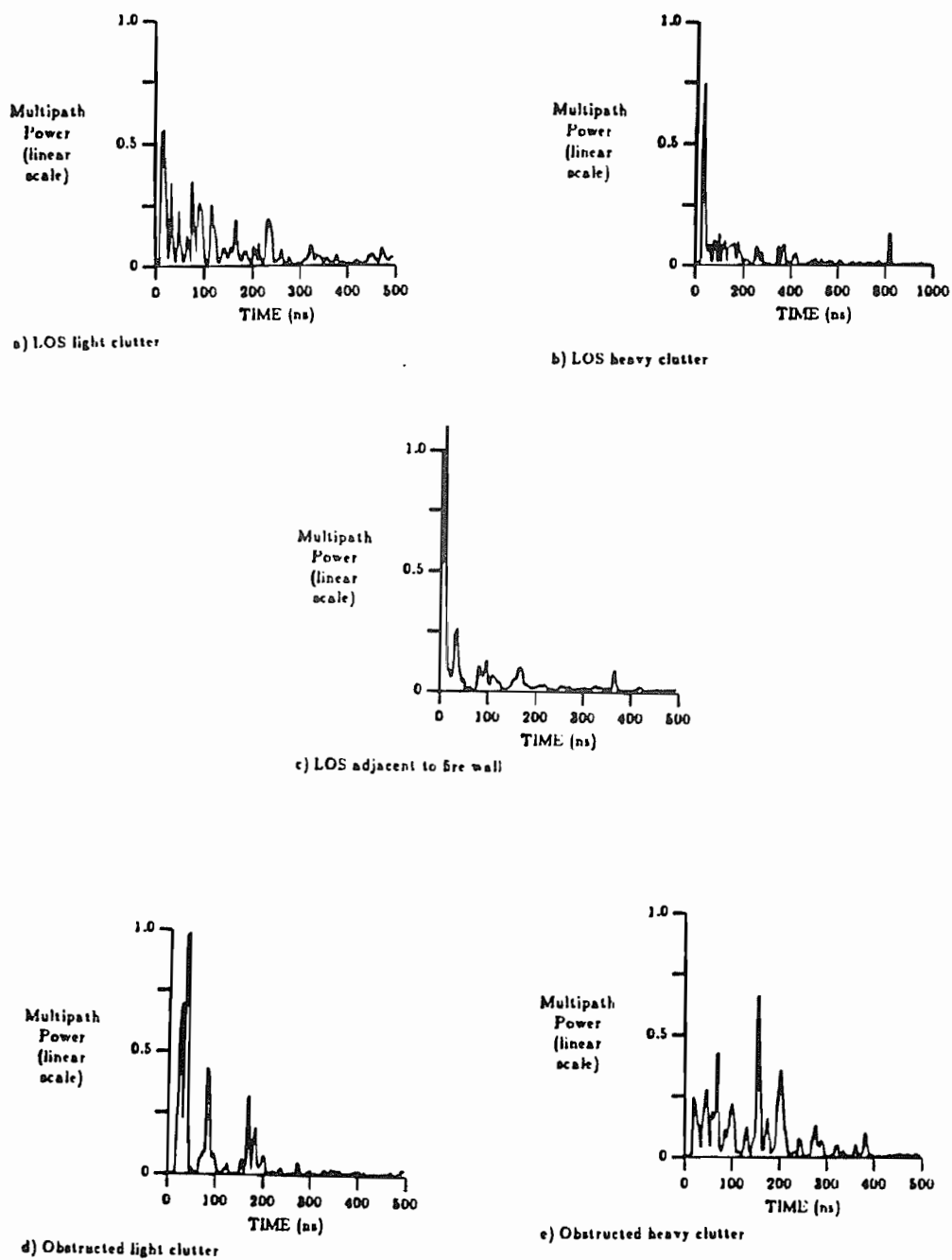


Figure 5.1 Typical individual multipath delay profiles from various geographies.

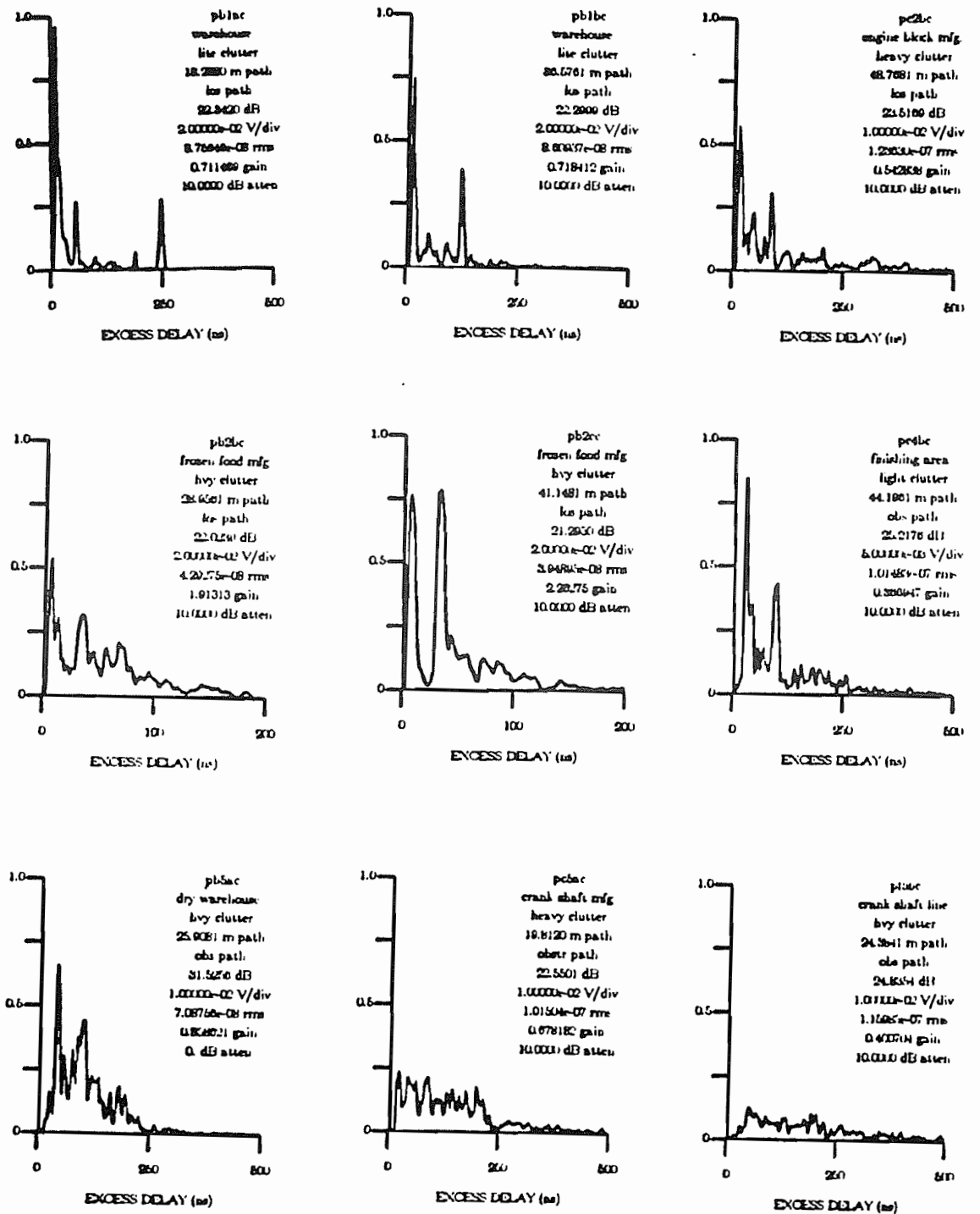


Figure 5.2 Typical spatially-averaged multipath delay profiles from various geographies.

from data collected at each measurement location are presented in Appendix E. Figures 5.3 and 5.4 illustrate typical spatial fluctuations of multipath components over a distance of a few wavelengths at measurement locations within LOS and obstructed path geographies. Spatially-varying plots of the impulse response are useful because they allow us to discern multiple paths within the 10 ns resolution of the probe. Those paths which are actually comprised of more than one sub-path will exhibit fading over space. The complete set of spatially-varying power profiles is given in Appendix F.

The shape of the delay profiles of Figure 5.1 are representative of the data. In particular, the LOS paths have large, well-defined pulses at the first observable path and a gradual smearing and decrease in power for latter paths. However, metallic walls and large pieces of machinery provide distinct specular reflections having signal levels on the order of the LOS path. A LOS heavy clutter measurement at site C (shown in Figure 5.1c) indicated the presence of a path (with amplitude only 6 dB below the LOS path) at an excess delay of 800 ns. This path was deduced to be from by a reflection off of one of the metal perimeter walls of the factory.

When a radio path is lightly obstructed, the first observable path generally has a larger amplitude as compared to latter paths. The majority of multipath power arrives within 50 to 250 ns after the first path. For the case of heavily obstructed paths, the first observable path is generally weaker than paths which arrive 25-75 ns later. In some cases, the amplitudes of all paths are within a couple dB of one another, and do not appear to decrease with time delay out to a few hundred nanoseconds. Radio paths across large obstructions result in the majority of signal power arriving within 100 to 400 ns after the first observable path.

Inspection of spatial fluctuations of the many LOS impulse responses, such as one shown in Figure 5.3, revealed that only slight fades occur for LOS paths over small distances, whereas up to 15 dB of fading occurs over local areas for strong paths which are due to reflections from the building structure and surroundings. Obstructed clutter impulse responses, such as shown in Figure 5.4, indicated that some paths, primarily those that arrive late in the profile, fade rapidly over distances on the order of a wavelength. This indicates that paths over a heavy cluttered geography are actually

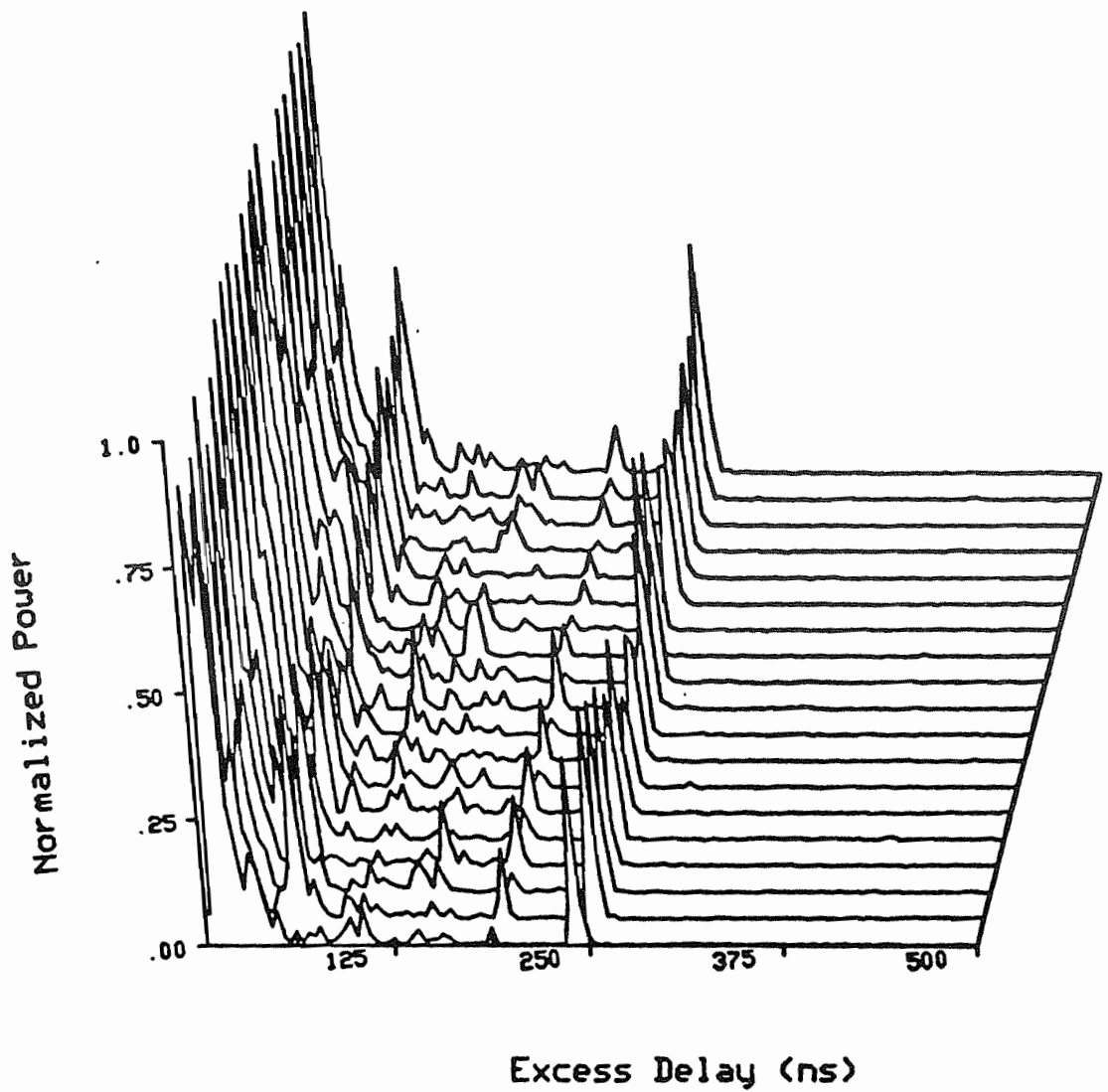


Figure 5.3 Typical spatial fluctuations of a multipath delay profile over  $4.3\lambda$  track on LOS path. (pblac)

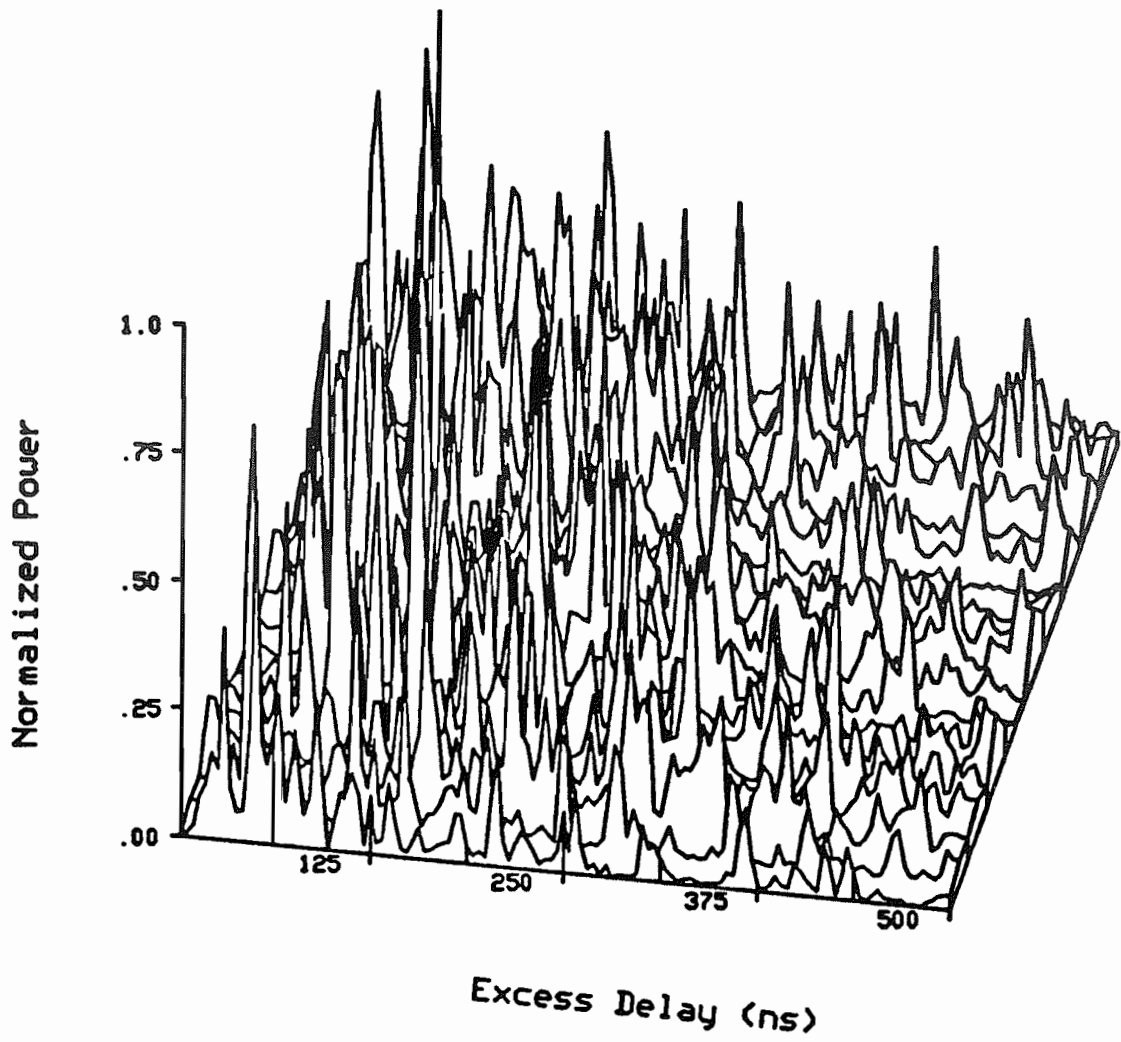


Figure 5.4 Typical spatial fluctuations of multipath delay profile over  $4.3\lambda$  track on obstructed path. (pf5bc)

comprised of many sub-paths, the relative phases of which may be altered with small movements of the receiver. It also points to the possibility of diffuse reflections from large objects (such as ribbed metal ceilings) in the channel. Both figures indicate the wide-sense spatially stationary behavior that most of the multipath delay profiles exhibit. It can be seen that although some late paths fade over small changes in distance, the predominant paths do not fade severely and the received power for a given time delay stays relatively constant (fixed mean) over the local measurements. Inspection of all the data indicates that the wide-sense stationary assumption on local multipath behavior is a good one.

## 5.2 Large Scale Signal Attenuation

Eqns. (3.12) through (3.14) were used to compute large scale signal attenuation (path loss) for each of the 50 spatially averaged multipath power delay profiles. The wide band data was collected in identical sites and along similar tracks as the CW data, except for the site B obstructed path measurement where at maximum T-R separation the received signal level was too small to be detected by the pulse receiver. We observed that for most measurement locations, the path loss varied only by  $\pm 3$  dB amongst the individual measured profiles. This confirms the well-accepted notion that small scale fading is due primarily to the fluctuations of the sum of phases of the received paths, and not variations in the path amplitudes.

The wide band path loss data from 47 measurement sites (data from the 3 LOS wall locations at site C are omitted) from all factories is shown in Figure 5.5, and has a correlation coefficient of 0.98. The bold line in the figure shows the least squares linear fit to the data, and indicates a relationship of path loss to the 2.16 power. This value drops to 2.14 with inclusion of the LOS wall data. These values compare with a path loss exponent of 2.18 for the CW measurements taken over identical paths (see Figure 4.11).

One should not take lightly the assumption commonly made that there must be good agreement between pulse path loss measurements and CW path loss measurements. This common assumption is not valid for a single measurement instance, but as will be shown subsequently, is valid for

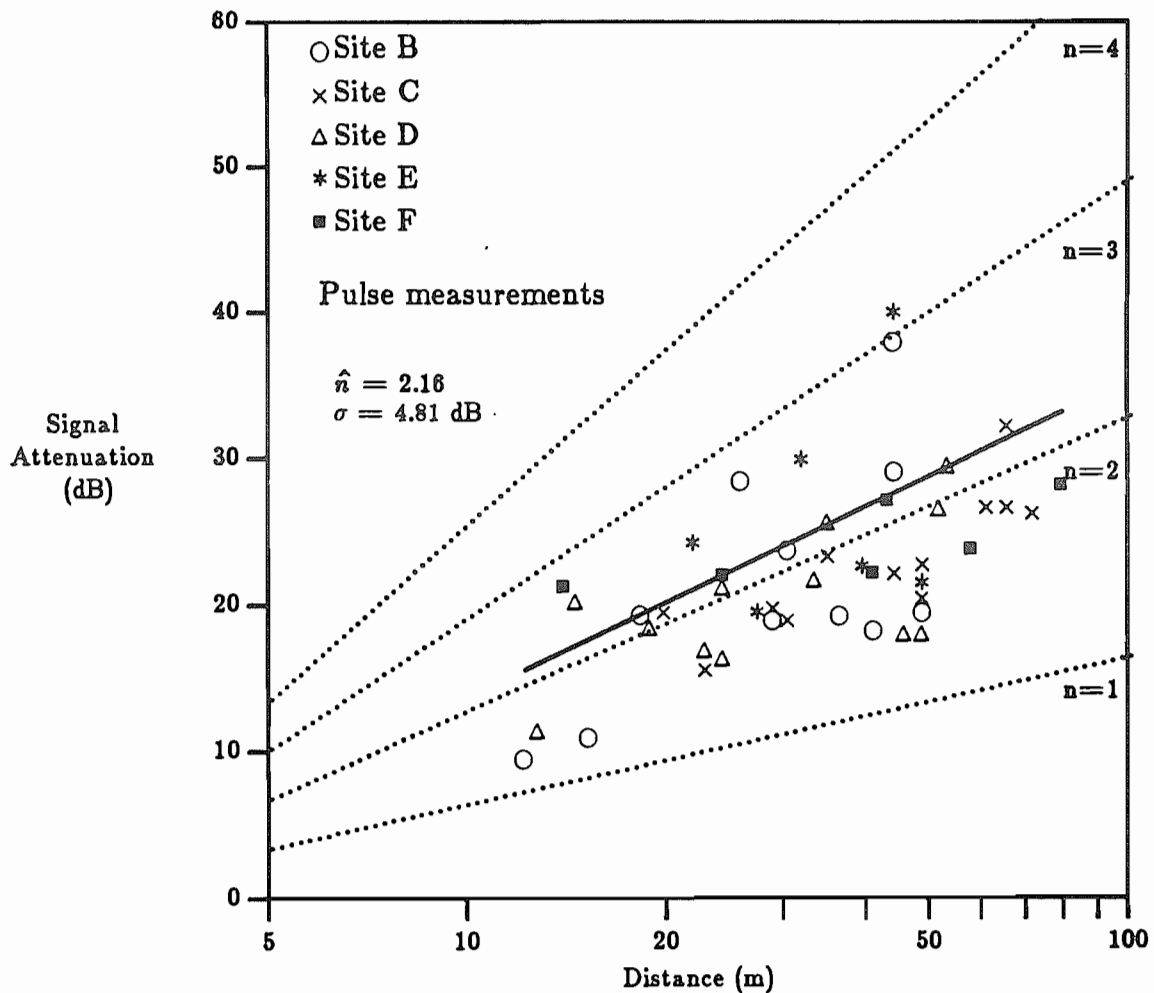


Figure 5.5 Large scale path loss over all factories using wide band measurements.

measurements averaged over a local area. To disprove the assumption for a given measurement, consider the existence of two deterministic paths: a LOS path, and a path delayed by more than the probe duration. For CW transmissions, the two paths may arrive at the receiver antenna exactly out of phase and with comparable amplitudes, thus canceling themselves out and causing a deep fade to be observed by the receiver. For a pulsed apparatus, however, these two paths will be detected and the sum of the individual path powers will be used to compute a received power level. Conversely, the paths may arrive in phase and cause the CW measurement to indicate a larger received power than the pulse measurement.

For the general multipath problem where there exist  $N$  paths, each of which is resolvable, the wide band measurement apparatus computes received power as  $P_w = \sum_i^N |\rho_i e^{j\theta_i}|^2$ . The CW receiver measures power as the square of the envelope of the sum of all signals arriving over all time, and is computed as  $P_{cw} = \left| \sum_i^N \rho_i e^{j\theta_i} \right|^2$ . To determine when wide band and narrow band path loss measurements yield equivalent results, we assume the received paths form a random process where each path has a random amplitude and phase.

Letting  $E_{\rho, \theta} [ \ ]$  denote the ensemble average over  $\rho_i$  and  $\theta_i$  and defining the path amplitude correlation coefficient  $r_{ij}$  as

$$r_{ij} = E_{\rho} \left[ \rho_i \rho_j \right] \quad (5.1)$$

we find the interesting (and perhaps well-known) result that

$$E_{\rho, \theta} \left[ P_w \right] = E_{\rho, \theta} \left[ \sum_i^N |\rho_i e^{j\theta_i}|^2 \right] = \sum_i^N \overline{\rho_i^2} \quad (5.2a)$$

$$\begin{aligned} E_{\rho, \theta} \left[ P_{cw} \right] &= E_{\rho, \theta} \left[ \left| \sum_i^N \rho_i e^{j\theta_i} \right|^2 \right] \quad (5.2b) \\ &= E_{\rho, \theta} \left[ \overline{\left( \rho_1 e^{j\theta_1} + \dots + \rho_N e^{j\theta_N} \right) \left( \rho_1 e^{-j\theta_1} + \dots + \rho_N e^{-j\theta_N} \right)} \right] \end{aligned}$$



$$= \sum_i^N \overline{\rho_i^2} + 2 \sum_i^N \sum_{j,j \neq i}^N r_{ij} \overline{\cos(\theta_i - \theta_j)}$$

Note that when  $\overline{\cos(\theta_i - \theta_j)} = 0$  or  $r_{ij} = 0$ , the CW and wide band measurements yield equivalent results. This occurs when either the path phases are identically and independently uniformly distributed or when the path amplitudes are uncorrelated. As discussed in Chapter 1, the iid uniform distribution of  $\theta_i$  is a reasonable assumption since all of the paths travel distances that are several hundred wavelengths long and are likely to arrive with arbitrary phases. If for some reason it is believed that the phases are not independent, the measurements will still be equal if the paths have uncorrelated amplitudes. However, it is likely that if the phases of the paths are dependent upon each other, then so are the amplitudes, since it is probable that the same mechanism which affects the path phases also affects the amplitudes.

In the factory, walls and large machinery are the primary causes of multipath. The building construction and shadowing confines radio propagation along aisles. Based on observations of the numerous multipath profiles, it is common for a major reflector, such as a wall, to be illuminated by several paths, each of which may have traveled different routes prior to arriving, and each of which may be delayed by tens or hundreds of nanoseconds. Such a situation dictates that several paths having uncorrelated amplitudes (because of prior reflections) and iid phases (because of the different prior paths) exists, thus suggesting that CW and wide band path loss measurements should yield identical results. By moving the measurement apparatus over a distance of several wavelengths, we effectively computed the expected value of the  $\rho_i^2$  in Eq. (5.2) and assume the  $\theta_i$  to be uniformly iid. The empirical data collected using both wide band and CW measurement equipment proves that the assumption is valid.

The agreement in path loss data between the wide band and CW measurement systems is excellent, and is perhaps a bit surprising when one considers the fact that the oscilloscope display is linear rather than logarithmic. It was feared that since weak paths (having amplitudes 17 dB below the strongest path) are difficult to discern visually, many paths which arrive beyond the chosen oscilloscope display time span may have been

missed. The data indicates otherwise, and shows that for indoor radio channels, wide band path loss measurements can be expected to give very similar results when compared with data collected using narrow band equipment<sup>†</sup>. Both narrow band and wide band path loss data indicates that received power in the factory falls off exponentially with distance, where the exponent value is about 2.2 when averaged over all factory sites and geographies. Figure 5.6 illustrates the wide band path loss data as a function of geography, and includes data from the 3 measurements made along a fire wall in site C . The results are nearly identical to those obtained using the CW measurement apparatus (see Table 4.2 and Figure 4.11) as they indicate a definite dependence on surrounding clutter.

### 5.3 R.M.S. Delay Spread ( $\sigma$ ) and Mean Excess Delay ( $\bar{\tau}$ )

The r.m.s. delay spread, denoted as  $\sigma$  and defined by eqn. (3.13), is the square root of the second central moment of the multipath power delay profile. It is used for determining data rates which a channel can support [5,56,71]. The mean excess delay, which is the first moment of the power delay profile as defined in eqn.(3.12), is useful for determining distortion in an FM signal that might be used for mobile robot navigation or ranging [81]. It has been said that the two parameters  $\sigma$  and  $\bar{\tau}$  appear to be most relevant for describing a communication channel, and in some applications are actually more useful than the shape of the channel impulse response [78],

The mean excess delay is a function of the arrival time of the first multipath. Since our measurements were not triggered by the transmitter, we can not be sure that in all cases the first observable path was a LOS path.

---

<sup>†</sup> A spread spectrum sounding apparatus, which uses 80 MHz RF bandwidth and a receiver dynamic range of about 50 dB, has provided path loss measurements that are within 2 dB of CW measurements made over identical paths ranging from 46 m to 168 m [58]. Our wide band apparatus provided agreement well within the  $\pm 1.5$  dB measurement uncertainty of the CW apparatus for most measurement sites.

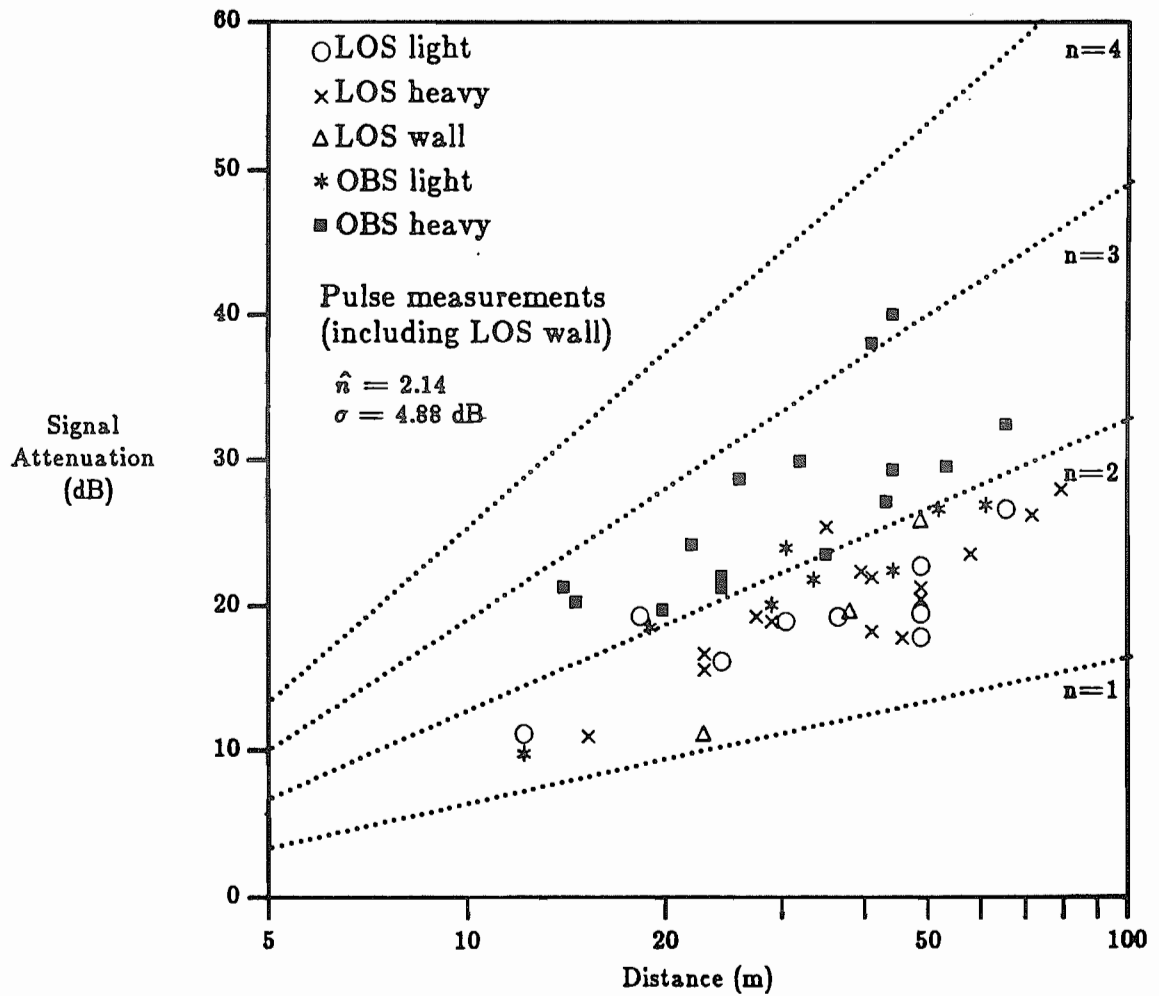


Figure 5.6 Large scale path loss over factory geographies using wide band measurements.

In fact, for obstructed paths we doubt this to have been the case. Also, since the scope trigger was manually adjusted between some measurements, it is possible that the trace trigger point varied slightly (no more than a sounding pulse width, though) between measurements. Consequently, our mean excess delay measurements may contain minor errors. Nevertheless, a reasonable estimate of mean excess delay may be obtained from the data. The r.m.s. delay spread data is independent of the arrival time of the first multipath or the initial trace position, thus this data is quite accurate.

Using the averaged power delay profiles from each of the 50 measurement locations within five factories, the r.m.s delay spread and the mean excess delay were tabulated as a function of factory site and geography. Tables 5.1 through 5.3 contain the r.m.s. delay spread data. Tables 5.4 through 5.6 contain the mean excess delay data.

It can be seen from the tables that delay spread and mean delay values are not dependent on T-R distance or geography. This observation has been made by other researchers in the mobile radio channel, and was recently observed in an office building [40,53], but disagrees with the findings made by another researcher using a more sensitive apparatus in a much larger office building [78]. The mean excess delay does, however, seem to be related to  $\sigma$ . For the case where  $\sigma = \bar{\tau}$ , ideally the multipath received power falls off exponentially over time delay since the statistics imply that the mean square value of the profile ( $\bar{\tau}^2$ ) is twice  $\bar{\tau}$  (see eq. (3.13)). This situation also corresponds to a two-path impulse response with the second path arriving at a time delay of  $2\bar{\tau}$ . For cases when  $\bar{\tau} < \sigma$ , the multipath power profile has a high concentration of received power within the first few pulse widths of the first observable pulse, and a much smaller distribution of power at later delays [78]. However, when  $\bar{\tau} > \sigma$ , a significant amount of multipath power arrives in the middle of the profile, and not in the first few paths. A scatter plot showing the relationship of  $\bar{\tau}$  vs.  $\sigma$  over various factory geographies is shown in Figure 5.7. In the figure, the data points have been obtained from the spatially averaged multipath power profiles from each of the 50 measurement sites. LOS measurements along a fire wall in site C best fit a slope of  $\frac{\bar{\tau}}{\sigma} = 0.83$ . LOS light and LOS heavy geographies were found to fit lines having slopes of  $\frac{\bar{\tau}}{\sigma} = 1.13$  and  $1.15$ , respectively. The

Table 5.1 R.M.S. delay spread data (10 -25 m path).

R.M.S. delay spread as a function of factory geography (ns)					
T-R separation of 10 - 25 m					
Geography	Site B	Site C	Site D	Site E	Site F
LOS light clutter	87.6	118.8	51.1	-	-
LOS heavy clutter	45.6	46.9	106.7	48.7	124.3
LOS along wall	-	122.4	-	-	-
Obstructed light clutter	27.7	102.6	103.2	-	-
Obstructed heavy clutter	70.9	101.5	52.0	79.3	49.6

Table 5.2 R.M.S. delay spread data ( 25 - 40 m path).

R.M.S. delay spread as a function of factory geography (ns)					
T-R separation of 25 - 40 m					
Geography	Site B	Site C	Site D	Site E	Site F
LOS light clutter	86.1	49.6	53.2	-	-
LOS heavy clutter	42.9	123.6	95.5	91.2	122.7
LOS along wall	-	100.2	-	-	-
Obstructed light clutter	37.6	101.5	101.4	-	-
Obstructed heavy clutter	55.2	112.4	101.2	93.9	116.0

Table 5.3 R.M.S. delay spread data (40 - 75 m path).

R.M.S. delay spread as a function of factory geography (ns)					
T-R separation of 40 - 75 m					
Geography	Site B	Site C	Site D	Site E	Site F
LOS light clutter	33.9	43.2	118.5	-	-
LOS heavy clutter	39.5	201.5	33.3	93.6	44.3
LOS along wall	-	92.7	-	-	-
Obstructed light clutter	-	118.5	108.9	-	-
Obstructed heavy clutter	77.2	114.7	106.8	52.5	129.6

Table 5.4 Mean excess delay data (10 -25 m path).

Mean excess delay as a function of factory geography (ns)					
T-R separation of 10 - 25 m					
Geography	Site B	Site C	Site D	Site E	Site F
LOS light clutter	76.1	150.5	46.6	-	-
LOS heavy clutter	50.4	48.1	116.4	50.5	125.6
LOS along wall	-	111.9	-	-	-
Obstructed light clutter	22.4	108.7	141.3	-	-
Obstructed heavy clutter	113.9	146.7	58.7	96.0	79.6

Table 5.5 Mean excess delay data ( 25 - 40 m path).

Mean excess delay as a function of factory geography (ns)					
T-R separation of 25 - 40 m					
Geography	Site B	Site C	Site D	Site E	Site F
LOS light clutter	92.5	50.1	53.8	-	-
LOS heavy clutter	57.0	133.5	149.2	89.4	110.0
LOS along wall	-	72.9	-	-	-
Obstructed light clutter	34.5	121.5	140.4	-	-
Obstructed heavy clutter	72.5	138.7	141.5	127.8	185.2

Table 5.6 Mean excess delay data (40 - 75 m path).

Mean excess delay as a function of factory geography (ns)					
T-R separation of 40 - 75 m					
Geography	Site B	Site C	Site D	Site E	Site F
LOS light clutter	38.5	31.9	132.1	-	-
LOS heavy clutter	47.5	203.7	34.2	86.5	33.2
LOS along wall	-	71.4	-	-	-
Obstructed light clutter	-	142.1	132.8	-	-
Obstructed heavy clutter	109.8	188.0	147.8	58.4	139.9

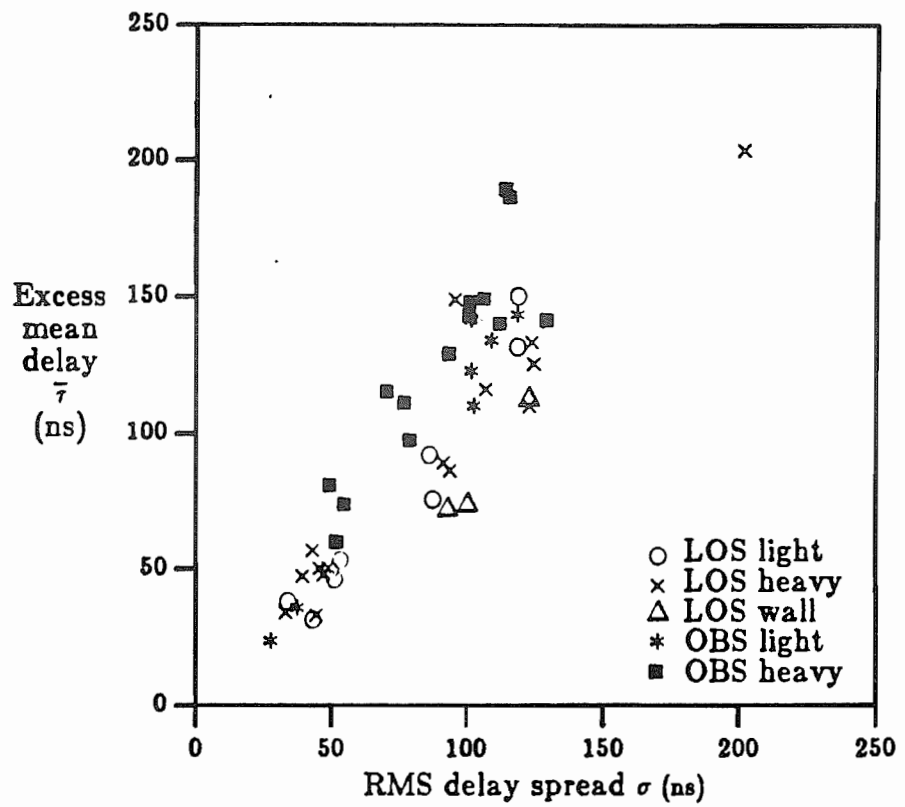


Figure 5.7 Scatter plot of excess mean delay vs. r.m.s. delay spread as a function of factory geography.

obstructed light clutter paths fit a slope of 1.25, whereas heavy clutter obstructed paths have  $\frac{\bar{\tau}}{\sigma} = 1.57$ . The data confirms the observations made in Chapter 5.1; namely, that obstructed paths tend to have the majority of received power arrive at longer time delays, whereas LOS paths receive most of the signal early in the profile.

Cumulative distributions of  $\sigma$  for the various factories and geographies were plotted. In order to simplify the data synthesis, delay spread data for LOS paths in light and heavy geographies (including LOS wall) were classified simply as LOS. Similarly, data from both light and heavily obstructed clutter geographies were classified as obstructed (OBS) paths. Plots showing the CDF's of  $\sigma$  in LOS paths as a function of factory site are shown in Figures 5.8 through 5.12. The CDF's of  $\sigma$  in obstructed paths as a function of factory site are given in Figures 5.13 through 5.17. Figures 5.18 and 5.19 show the CDF of  $\sigma$  for the LOS and obstructed path data from all factory sites. Figure 5.20 gives the CDF of  $\sigma$  over the entire data pool of wide band measurements. All CDF's have been computed using individual multipath power delay profiles (not local averages) and 1 ns increments of delay spread.

It is interesting to note the effects which building age and inventory have upon  $\sigma$ . Site B, which produces dry and frozen food stuffs, has considerably less metal inventory and more paper inventory than do the other sites. The building is also different in that it does not follow the typical open plan layout of other sites since there are concrete block walls used to separate the various factory areas. The large amount of shelved paper products, such as cardboard boxing material and dry food products, is believed to cause the low median value of  $\sigma$  as shown in Figures 5.8 and 5.13. The site B obstructed path measurements were taken in a main (100 m X 60 m) warehouse and a smaller warehouse (80 m X 50 m), and have median r.m.s. delay spread values of 56 ns. The LOS measurements were made within the main warehouse and a frozen food production area, and have a median  $\sigma$  value of 49 ns. From Figures 5.18 and 5.19, median  $\sigma$  values for all LOS and obstructed paths are 96 ns and 109 ns, respectively. Thus, site B has median r.m.s. delay spreads consistently half that found over all of the factories. Given the size of the warehouses in which much of the data was collected, the decreased delay spread is believed to be caused primarily by the



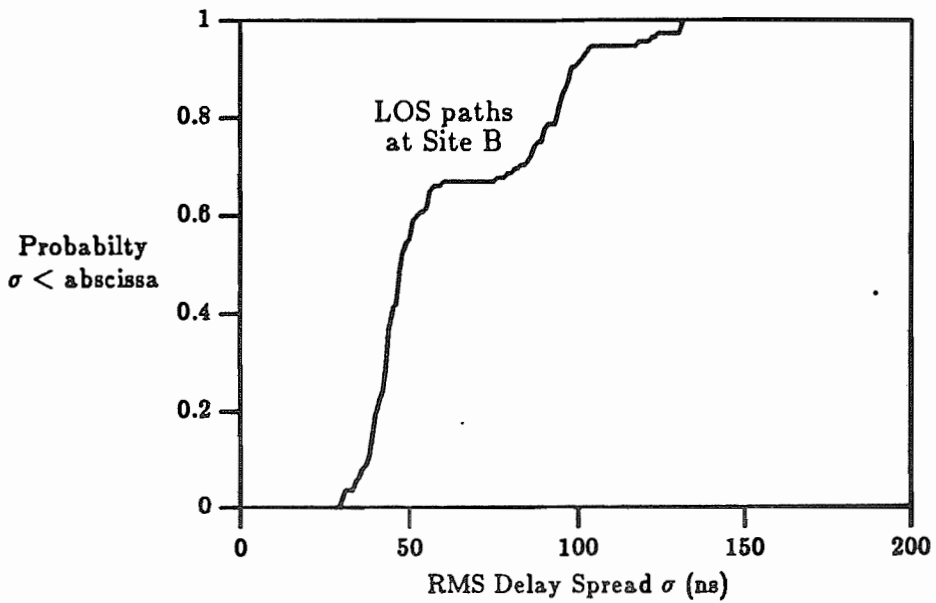


Figure 5.8 CDF of  $\sigma$  for site B LOS paths.

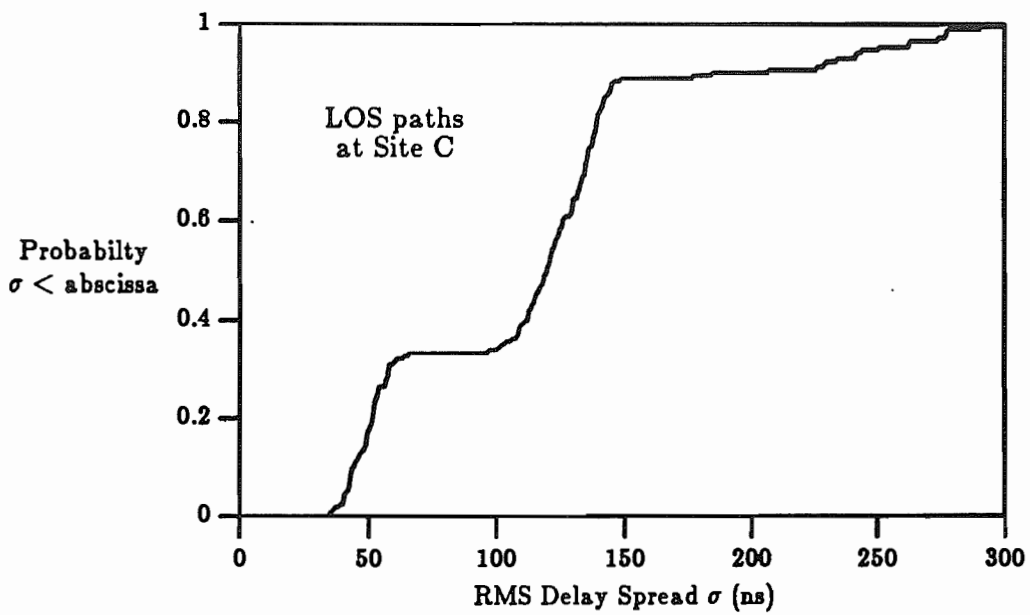


Figure 5.9 CDF of  $\sigma$  for site C LOS paths.

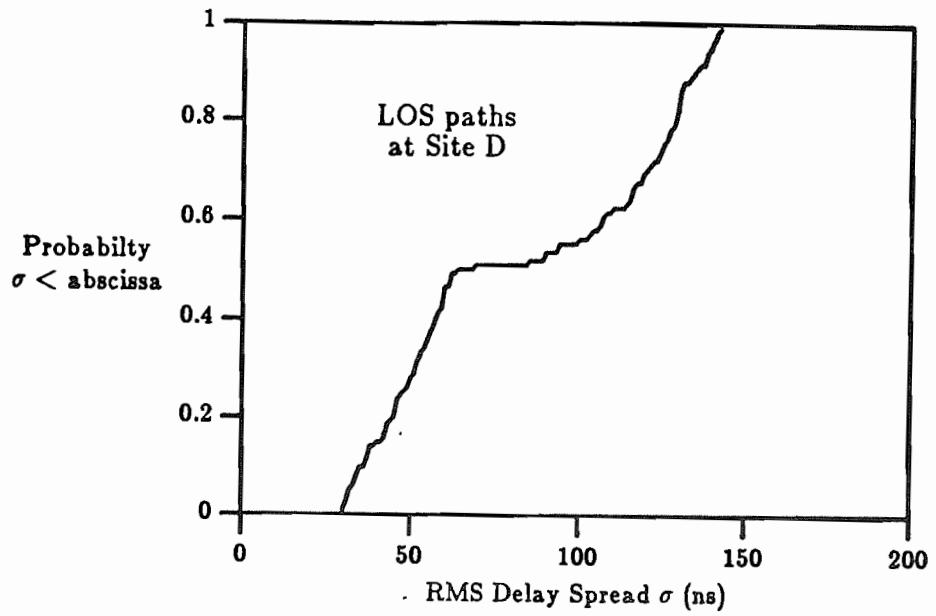


Figure 5.10 CDF of  $\sigma$  for site D LOS paths.

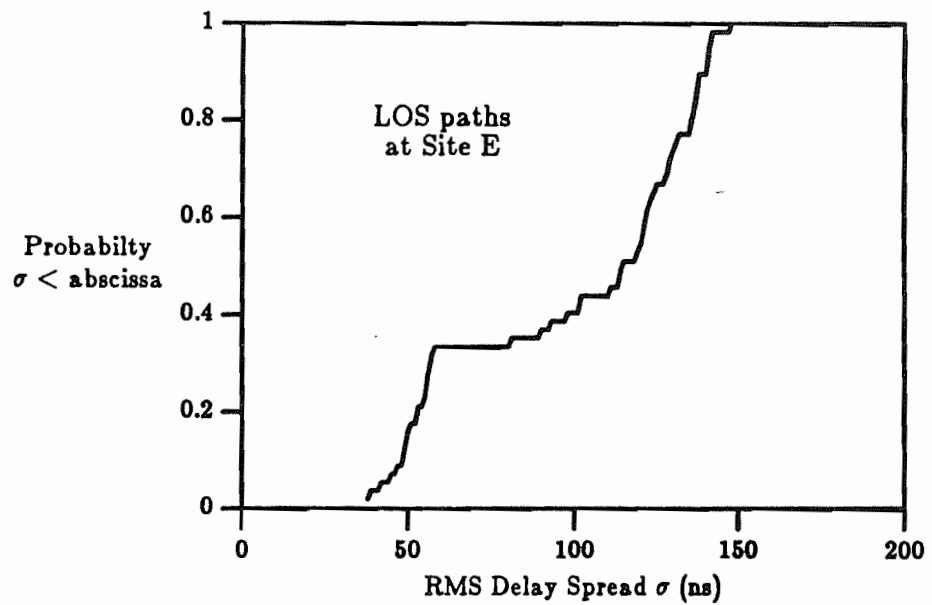


Figure 5.11 CDF of  $\sigma$  for site E LOS paths.

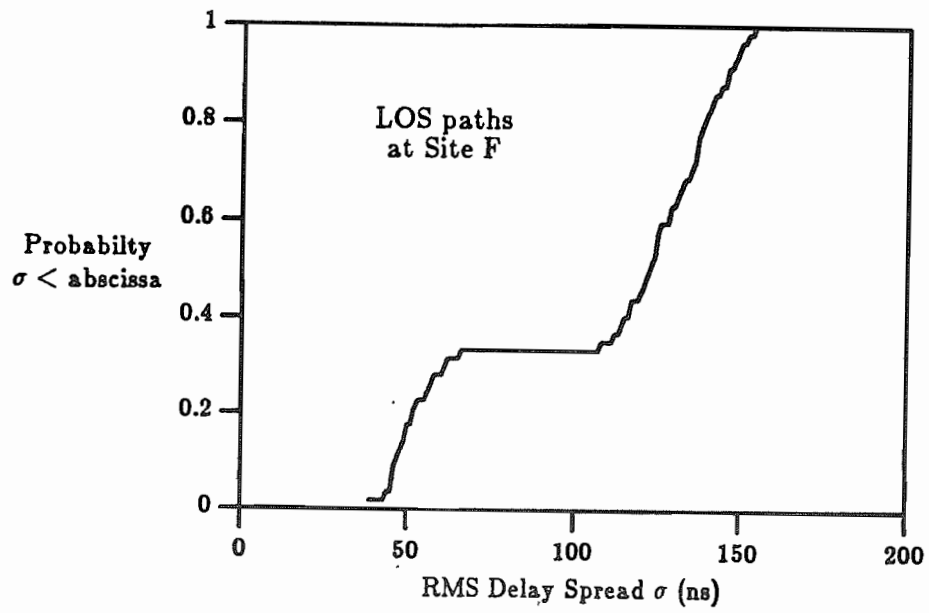


Figure 5.12 CDF of  $\sigma$  for site F LOS paths.

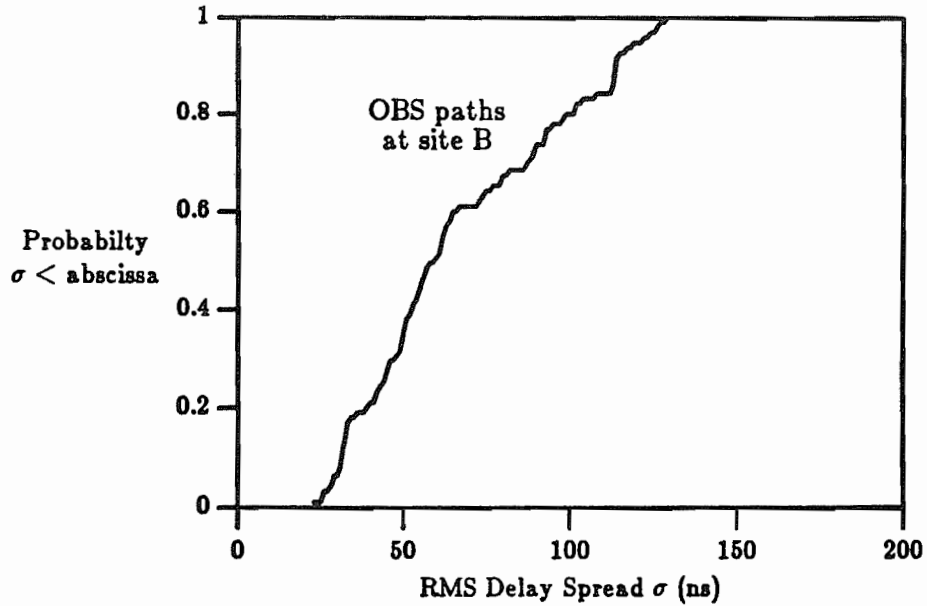


Figure 5.13 CDF of  $\sigma$  for site B obstructed paths.

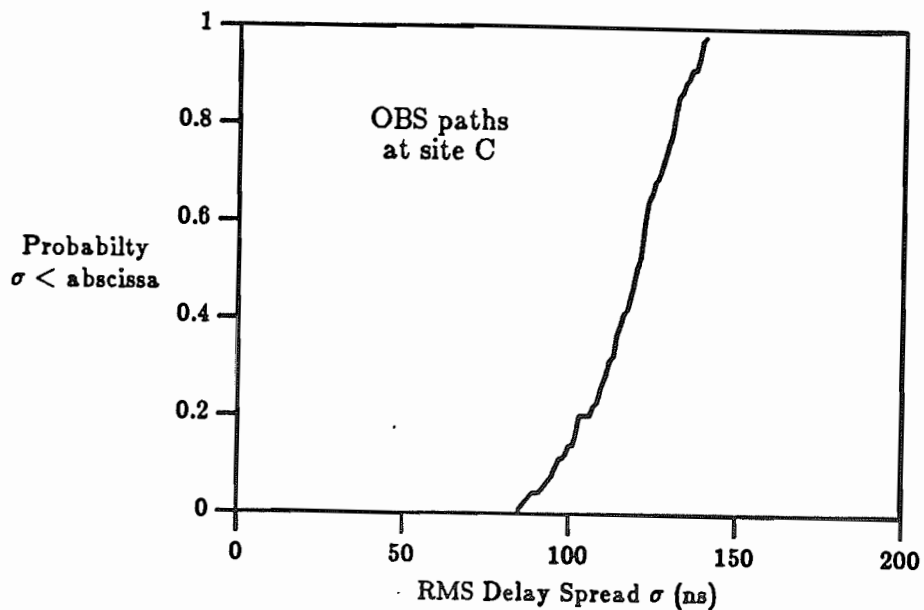


Figure 5.14 CDF of  $\sigma$  for site C obstructed paths.

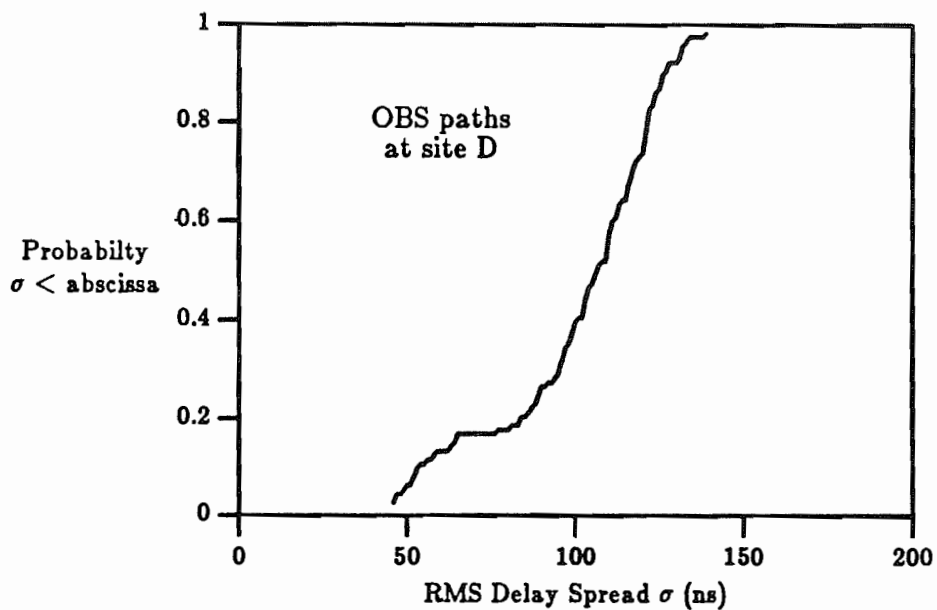


Figure 5.15 CDF of  $\sigma$  for site D obstructed paths.

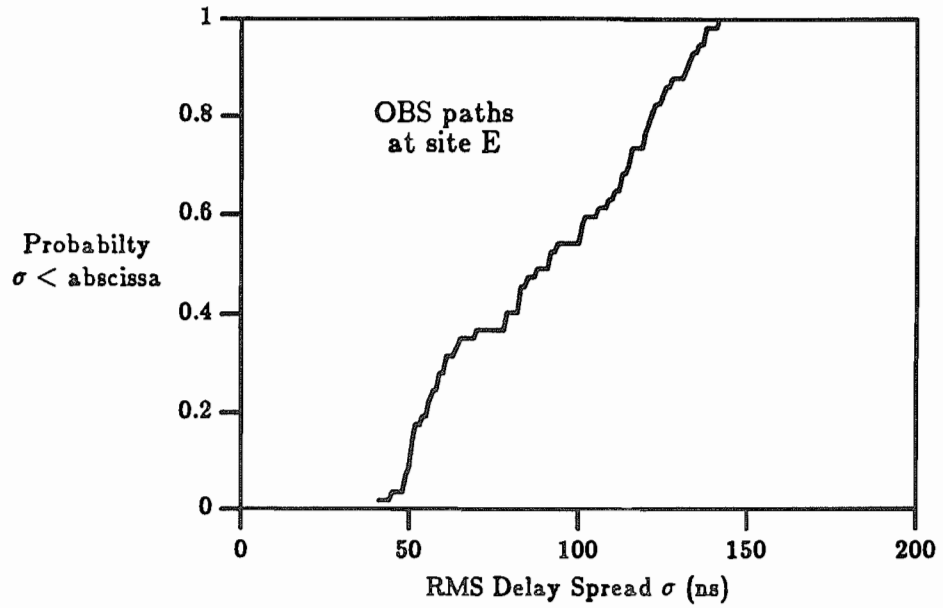


Figure 5.16 CDF of  $\sigma$  for site E obstructed paths.

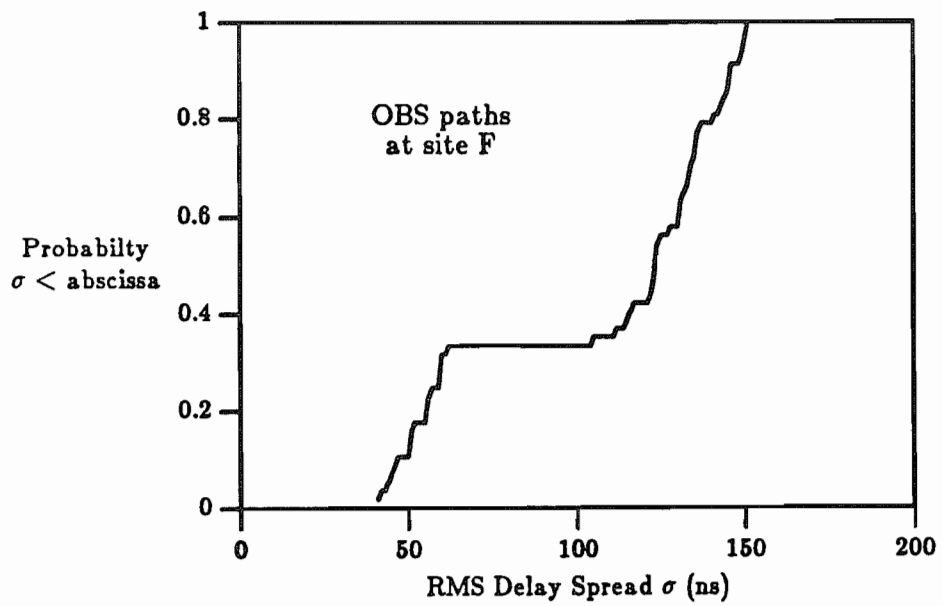


Figure 5.17 CDF of  $\sigma$  for site F obstructed paths.

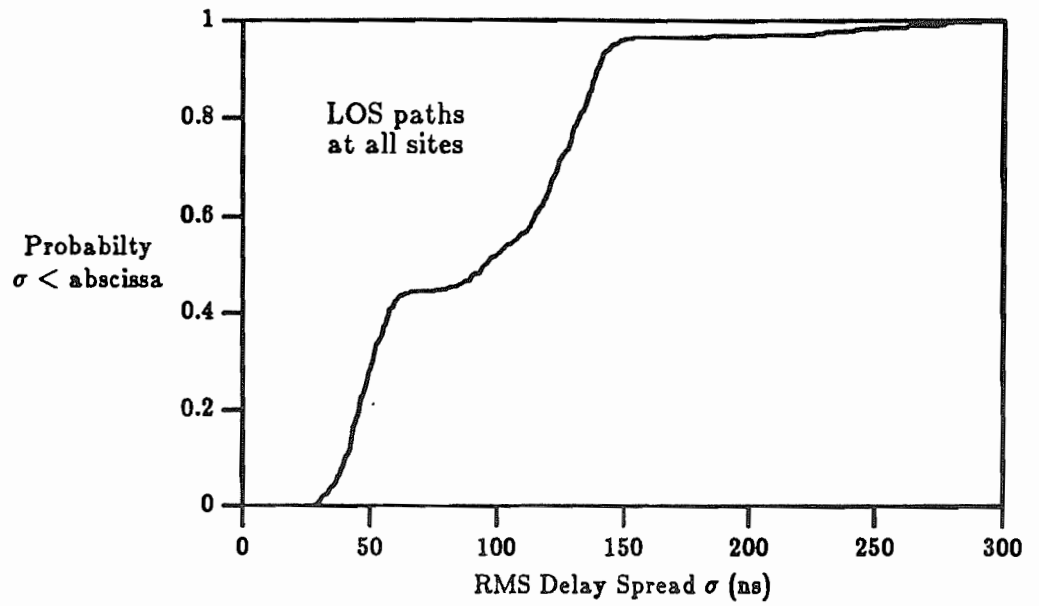


Figure 5.18 CDF of  $\sigma$  for LOS paths at all sites.

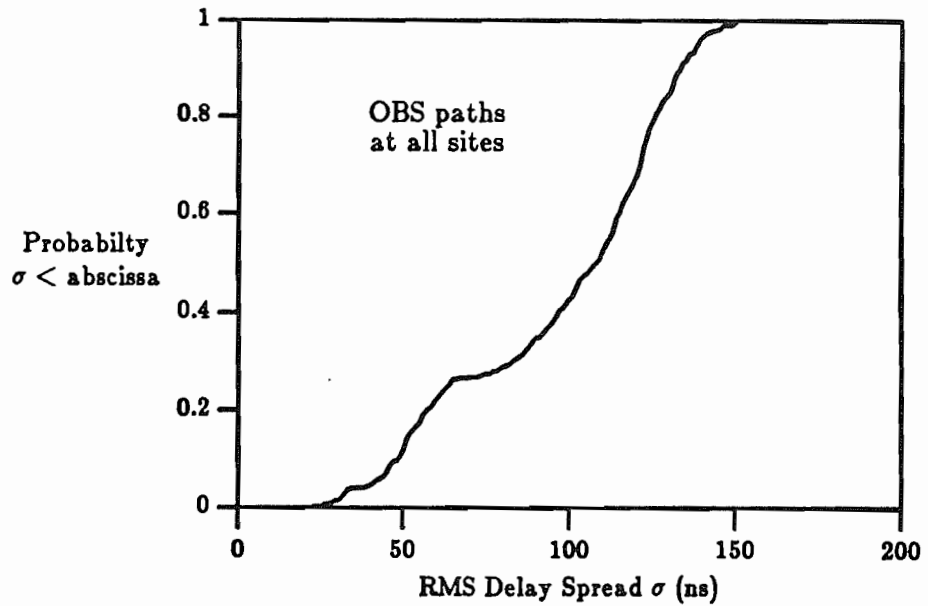


Figure 5.19 CDF of  $\sigma$  for obstructed paths at all sites.

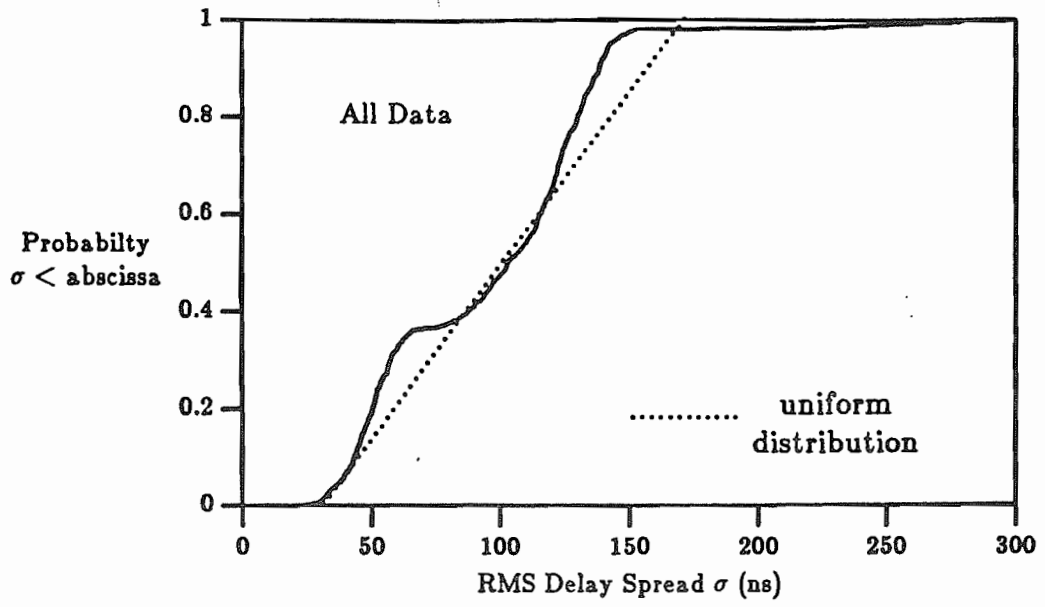


Figure 5.20 CDF of  $\sigma$  for all wide band factory data.

non-conducting inventory, and not the cement block walls. This premise is supported, too, by the r.m.s. delay spread results for LOS paths at site D (Figure 5.10). The LOS light clutter measurements in site D were made in the boxing/shipping area of the open plan style factory. It is precisely these measurements, which were made in an aisle flanked by stacks of cardboard, which contributed the small values of  $\sigma$  shown in Figure 5.10.

The distribution functions also illustrate the effect which building age has upon multipath propagation. Sites C and F, which both manufacture engine products, were the most modern factory sites visited and contained huge state-of-the-art automated machining lines. The building structure also incorporates noticeably more metal than the other sites. As an example of the modern construction, in both of the modern factories all of the perimeter walls were made of preformed insulated steel, whereas at other sites, perimeter walls were made of cement, brick, or wood. Ceiling truss work was obviously more complex at the modern sites and used many large steel reinforcing members. Some of the construction differences in factories reflect the drop in the cost of metal construction products and the relative rise in the cost of wood and brick over the last few decades. The data shows that in the modern factories, r.m.s. delay spreads were consistently larger than those found in older sites which manufacture similar products (for example, sites D and E). This is found by observing that the median r.m.s. delay spread values for sites C and F on LOS paths (120 ns and 123 ns) are the largest measured from all of the factories. Similarly, the obstructed path median  $\sigma$  values for the modern factories (119 ns and 126 ns) are the largest values found across the obstructed path data from five factories.

LOS paths from all sites exhibit distinct flat regions on the CDF plots, indicating that no measurements had certain  $\sigma$  values. Obstructed path data from all sites except site F, where only 6 measurement locations were used, have much smoother distributions of  $\sigma$ . Because we cannot expect to fully characterize the UHF factory radio channel with only a handful of measurements, conclusions we draw from the data must be taken with a grain of salt until more empirical data is collected from the factory channel. Given the data at hand, however, it appears that the factory geography has a definite effect on the r.m.s. delay spread distribution. Figures 5.18 and 5.19 illustrate that obstructed paths have a nearly uniform distribution of  $\sigma$



with a median value of 109 ns, whereas LOS paths have a median value of 90 ns and possess a bi-modal tendency which indicates definite delay spread dead zones. Such an observation indicates that multipaths along LOS aisle paths in a factory are caused primarily by reflections off of objects or walls at the ends of the aisles or floor and ceiling bounce within the aisle, and not paths which arrive from many different directions and time delays. Indeed, measurements performed in site A confirmed this to be the case for propagation in building corridors. The discrete nature of wall reflections in LOS geographies is also shown in Figures 5.1 and 5.2.

We speculate that the consistency of the r.m.s. delay spread dead zones between 50 and 80 ns is due to the measurement locations which were chosen within each factory. Effort was made to ensure that all measurements were taken across very comparable and typical geographies at all of the sites. Effects due to wall reflections were mitigated by locating both the transmitter and the receiver in as central a location as possible for all measurements. It is possible, and in fact quite likely, that had different transmitter or receiver locations been selected, the observed  $\sigma$  statistics would be different. We speculate from the repeated discrete distributions of  $\sigma$  over all of the LOS paths, however, that for a fixed transmitter-receiver orientation in LOS paths, the discrete distribution on  $\sigma$  would still be present, but the values of the modes would be different since they depend on the location of transmitter and receiver from the ends of the aisles. Thus, for a distribution of  $\sigma$  accumulated over an entire aisleway, we surmise that the gaps in the distribution would be filled.

The more continuous and nearly uniform distribution of  $\sigma$  for obstructed paths is explained by the fact that propagation is not largely confined to an aisleway. Rather, the multipath arrives by several paths which may include refraction around an obstruction, and by illumination of the ceiling and large objects in the aisle of the receiver. This is consistent with the continuous distribution of the multipath arrival as shown in Figures 5.1 and 5.2, and accounts for the increase in the median value of delay spread as compared to LOS paths.

Measured  $\sigma$  values for all of the individual profiles were found to range between 30 and 300 ns, with median values for factories ranging from 49 ns to 126 ns. Path distances ranged from 12 to 82 m, and measured path loss

ranged between 10 and 42 dB below that received by a  $10\lambda$  reference in free space. The entire pool of data indicates that for the average factory channel, the r.m.s. delay spread is slightly greater than 100 ns, and has an approximately uniform distribution between 30 to 170 ns as shown on Figure 5.20. The fact that the distributions of  $\sigma$  are similarly shaped over such a diverse collection of building structures and industries suggests that the measurements are indeed indicative of typical r.m.s. delay spread values that would be encountered in any factory. Furthermore, one would intuitively expect non-metallic inventory to attenuate signals and diminish the amount of multipath in site B, and would expect metallic inventory and walls to induce greater multipath spreads in sites C and F. The r.m.s. delay spread data clearly supports the intuition.

Scatter plots using  $\sigma$  values computed from the spatially-averaged power delay profiles were made to ascertain the dependence of r.m.s. delay spread on path loss or T-R separation. Figures 5.21 and 5.22 show scatter diagrams of r.m.s. delay spread vs. T-R separation as functions of factory site and geography. Figures 5.23 and 5.24 show scatter diagrams of r.m.s. delay spread vs. path loss as functions of factory site and geography. The path loss values are referenced to a free space path of  $10\lambda$ .

Figures 5.21 and 5.22 indicate that  $\sigma$  is uncorrelated with T-R separation over all factories and geographies. Figure 5.22 also demonstrates the uniform distribution of  $\sigma$  over heavy cluttered obstructed paths, whereas LOS paths (and obstructed light clutter paths) are seen to have a distinctive bi-modal distribution about 45 ns and 105 ns.

Figures 5.23 and 5.24 indicate that  $\sigma$  is also uncorrelated with path loss over all factories and geographies. Such a finding is similar to that observed by Turin in the urban mobile radio channel [11], and similar to that made by Saleh and Valenzuela [53] in a medium size office building using an apparatus like ours. Our factory data, unlike Devasirvatham's which has been collected from several office buildings, does not suggest that delay spread increases for larger path loss values. Our data does agree with Devasirvatham's in that  $\sigma$  decreases over LOS paths; however, the improve-

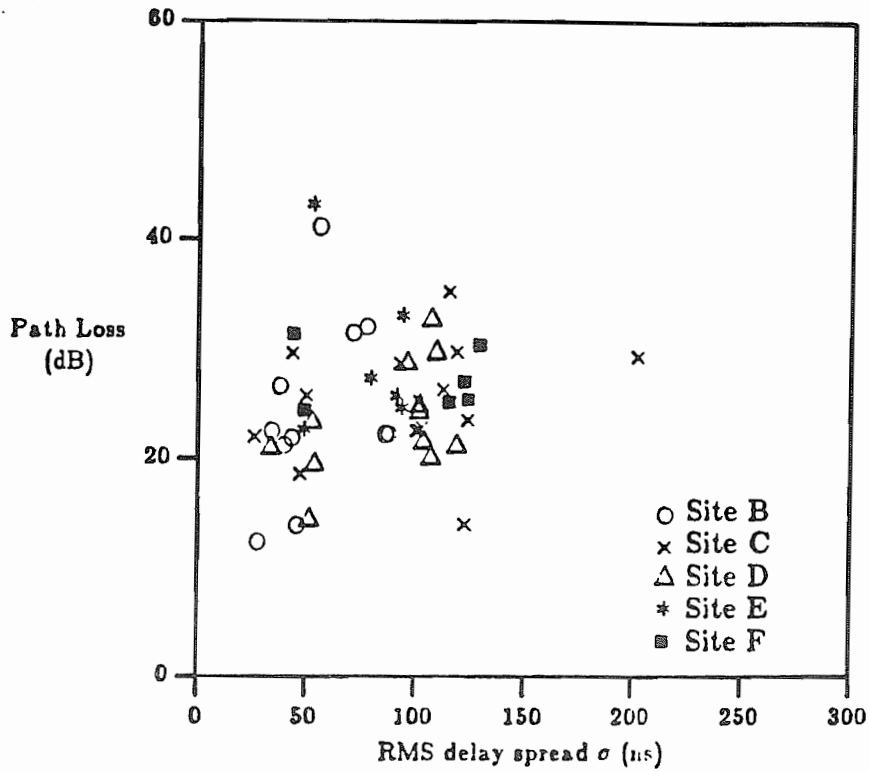


Figure 5.21 Scatter plot of R.M.S. delay spread vs. received power as a function of factory site.

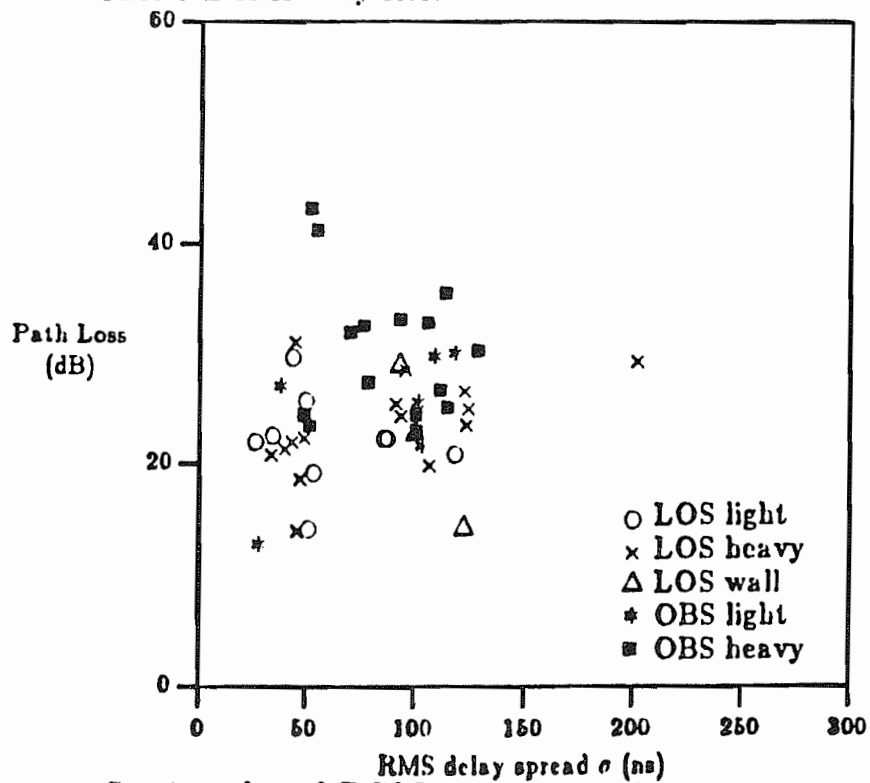


Figure 5.22 Scatter plot of R.M.S. delay spread vs. received power as a function of geography.

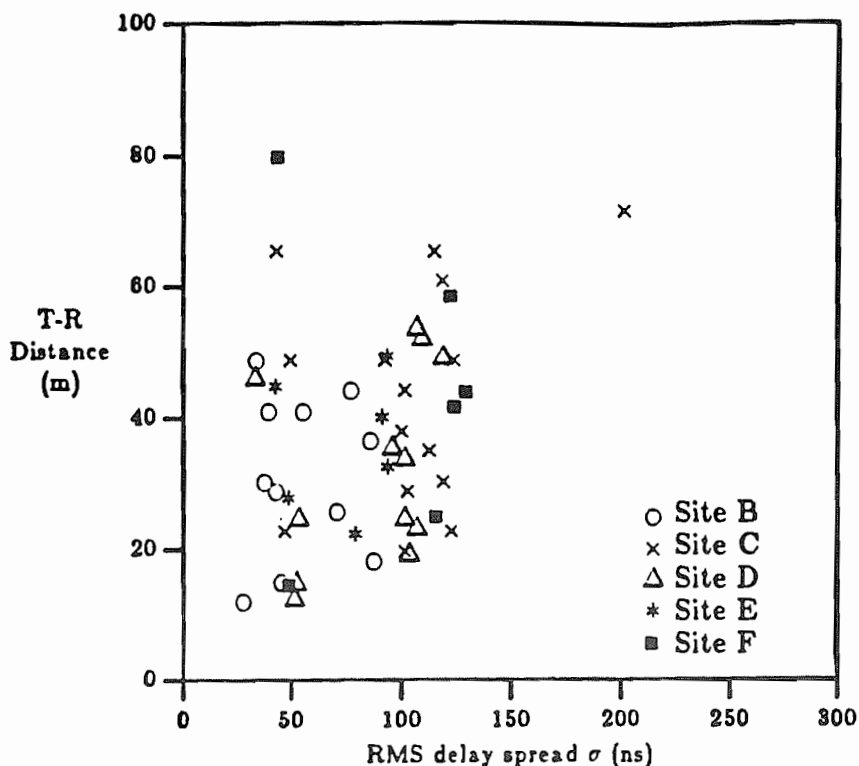


Figure 5.23 Scatter plot of R.M.S. delay spread vs. T-R separation as a function of factory site.

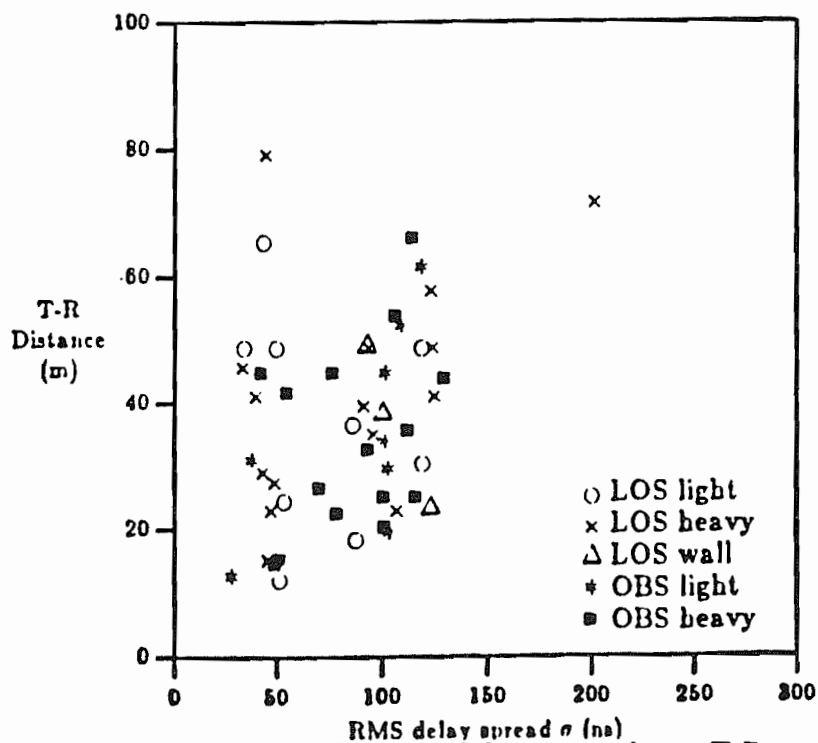


Figure 5.24 Scatter plot of R.M.S. delay spread vs. T-R separation as a function of geography.

ment is not nearly as significant in the factory channel as it is in the office building environment. This is undoubtedly due to the open plan layout of factories and the abundance of reflecting material along and at the ends of the aiseways.

#### 5.4 Impulse Response Statistical Model

While the parameters presented in the previous sections of Chapter 5 are useful and necessary for an accurate description and prediction of performance of radios in the factory multipath channel, they do not statistically describe the likelihood of path arrivals or the fading effects of the individual received paths within a factory. By fitting the path amplitudes and delays to distribution functions, we can develop a statistical channel model that may be used for analysis and simulation of factory communication systems.

The numerous multipath profiles, some of which are shown in Figure 5.1, indicate that for the resolution of our equipment, the factory is a discrete multipath channel. We reach this conclusion based on the almost insignificant fading which most paths undergo over a local area. Thus we assume that the (voltage) impulse response is a series of delta functions spaced in time delay at intervals no less than the duration of our sounding pulse. This model is given in eq. (3.3). Since the r.m.s. delay spreads and shapes of the spatially averaged profiles seem not to be dependent on path loss, but rather on the surrounding geography, we remove the effect of path loss from all profiles by normalizing each of the spatially averaged profiles with respect to the amplitude of its largest path. Thus, for responses in similar geographies, the averaged impulse response will equally weight the paths within the individual profiles. Based on inspection of our data, this appears to be an accurate model, as the first path arriving in a LOS geography is nearly always the largest, and for obstructed paths, the largest paths arrive within 25 - 70 ns after the first detected path. We assume the paths

to be resolvable down to the r.m.s. duration of our probing pulse, which is approximately 7.8 ns<sup>†</sup>. We then convert the spatially averaged power profiles into discretized power impulse responses. Figure 5.25 shows two such responses formed from spatially averaged multipath power delay profiles taken in LOS and obstructed path environments. All responses are truncated to 500 ns excess delay time since only one of the measurements was found to have significant multipath arriving after such a time. Because the time delay spreads are much larger than the duration of the sounding pulse, no effort was made to deconvolve the probe from the received profiles. In the impulse response formulation, however, the time delay axes of all measured data have been shifted to the right by 10 ns so that a measured LOS path is represented as an impulse at an excess delay time of 0 ns.

Since the multipath parameters of the factory channel indicate distinct differences in LOS and obstructed paths, and because differences between light and heavy clutter measurements are not so pronounced, we restrict our attention to two general factory impulse response models: one for LOS paths and another for obstructed paths. Statistics from the spatially averaged power profiles out to 250 ns excess delay (32 impulses) at 27 measurements sites are used to develop the LOS multipath model. Statistics from the spatially averaged power profiles out to 250 ns excess delay (32 impulses) at 23 measurement sites are used to develop the OBS multipath model.

Figures 5.25 and 5.26 indicate that multipath powers decrease as a function of time delay. This is expected given the exponential relationship of power vs. distance. We can describe the received paths, the  $\alpha_k$ 's, as random variables having a variance that is dependent upon the arrival time of the k-th path. Such a conjecture has been used in other models [53] and appears to be a good one for the factory channel, too. For both obstructed and LOS paths, an overall power impulse response was formed from all of the spatially averaged power profiles in the corresponding geography. The

---

<sup>†</sup> By assuming a path resolution of 7.8125 ns instead of 10 ns, it is simple to compute the points of the discretized impulse responses by merely integrating over an integer number of raw data points from the spatially averaged profile. This is because all of the measured data was sampled at intervals which are integers of 1.5625 ns. The value 7.8125 ns is exactly five times the smallest sampling interval.

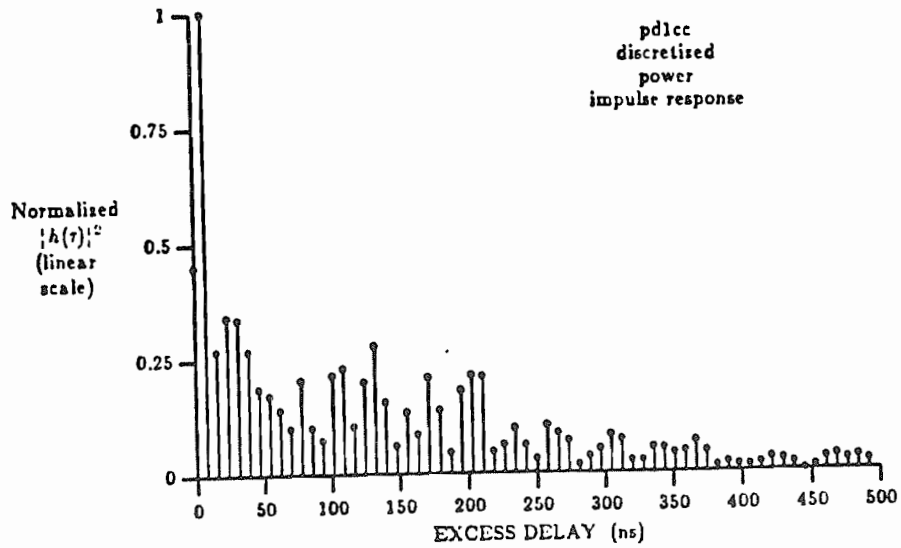


Figure 5.25 Discretized power impulse response formed from spatially averaged profile in LOS path. (pd1cc)

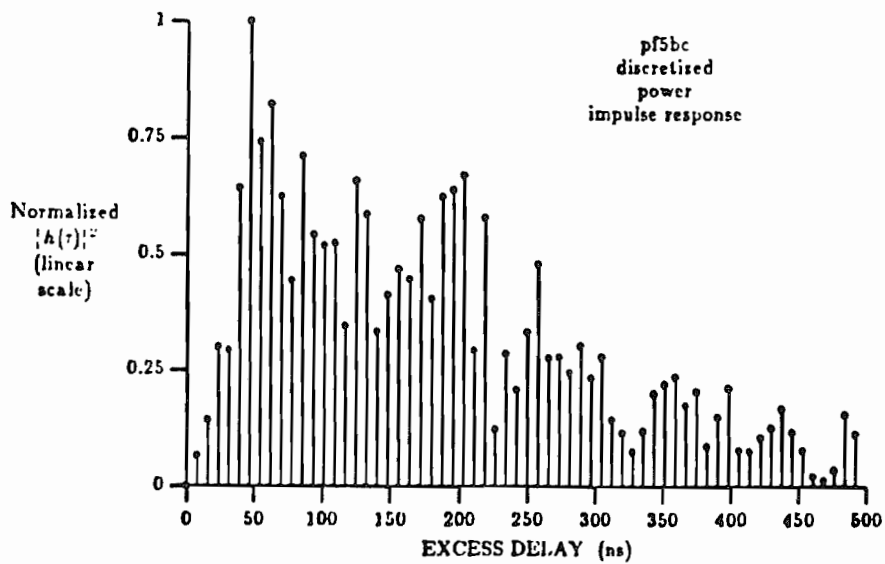


Figure 5.26 Discretized power impulse response formed from spatially averaged profile in obstructed path. (pf5bc)

averaged power profiles for both LOS and obstructed paths, and the variances about the average power levels, are shown in Figures 5.27 and 5.28. The shapes of the averaged profiles are somewhat different during the first 120 ns of excess delay; after this delay, both profiles have an exponential power decay.

We also were interested in observing, for fixed values of  $\tau_k$ , how many of the profiles which comprised the average actually had discernible paths. By determining the likelihood of path arrivals, it is possible to condition the distribution of path amplitudes on the likelihood of a path actually existing [11]. Since our pulse measurement apparatus had a linear and digitized display, the best dynamic range possible was on the order of 25 dB, although paths less than 17 dB below full scale deflection were very difficult to discern visually. The noise floor, as dictated by our data, was consistently on the order of 20 dB below the full scale deflection value. By assuming a path existed for power levels larger than 17 dB down from the strongest path within each normalized spatially averaged power profile, we computed a histogram of the path arrivals as a function of excess delay. The results are shown in Figures 5.29 and 5.30

#### 5.4.1 Assumptions

In order to simplify the model, we make the assumption that the distribution of the path voltage gains and phases are not dependent upon the likelihood of path arrival for a given excess delay time. This assumption is similar to Turin's in his first efforts to characterize multipath channels [55], and was made recently for another indoor channel model [53]. We also assume that the distributions on path amplitudes are independent of one another. This hypothesis simplifies the use of the model, and has been shown to be effective for other indoor channel models [53]. As in [53], we do insist that the variances of the distributions on the paths eventually decrease as a function of excess delay. However, as shown by Figure 5.28 and by much of the data, the variances of obstructed paths do not monotonically decrease with excess delay, but rather reach a rather flat peak somewhere between 25 and 70 ns. We believe this peak is due to ceiling bounce, as the times of arrival of such signals are consistently in agreement with those predicted by a one-hop path off of the ceiling for our various T-R separations. We furthermore assume that paths at all of the excess time



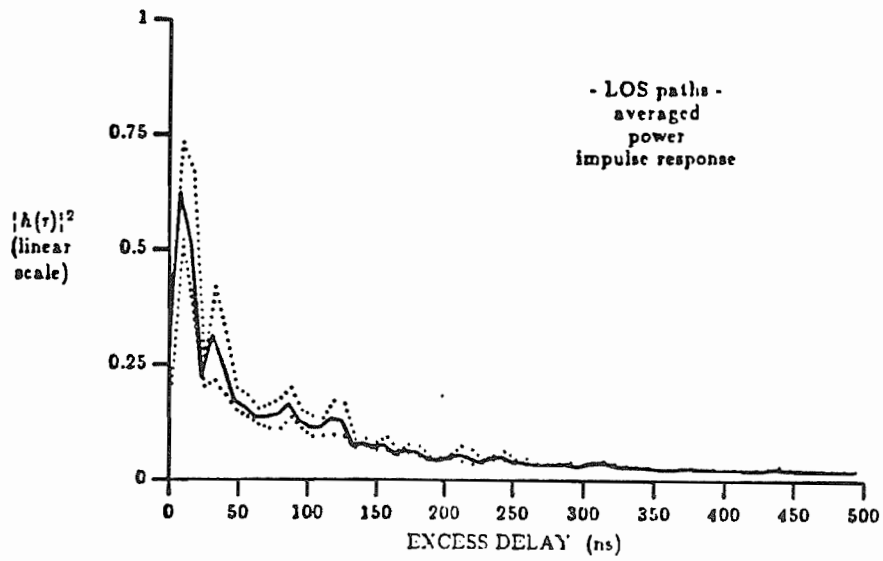


Figure 5.27 Averaged power delay profile for all LOS paths.

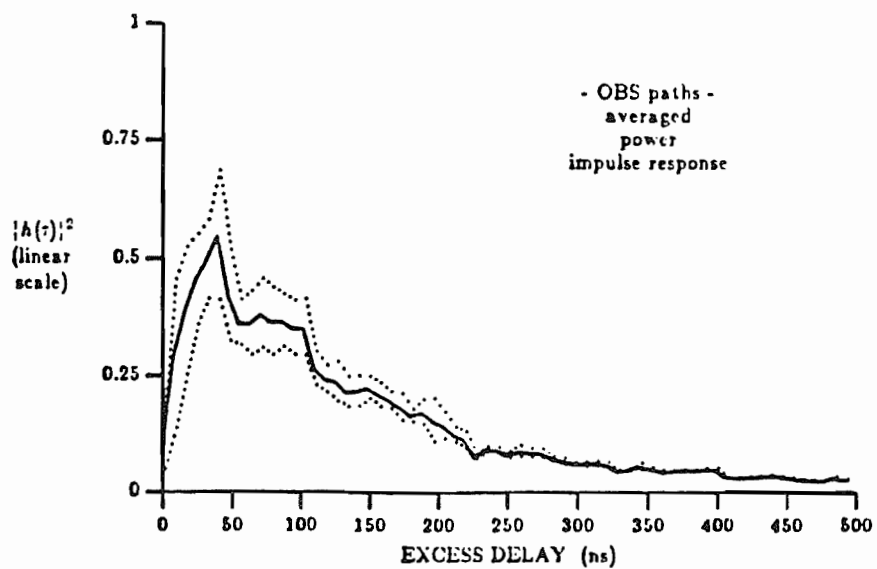


Figure 5.28 Averaged power delay profile for all obstructed paths.

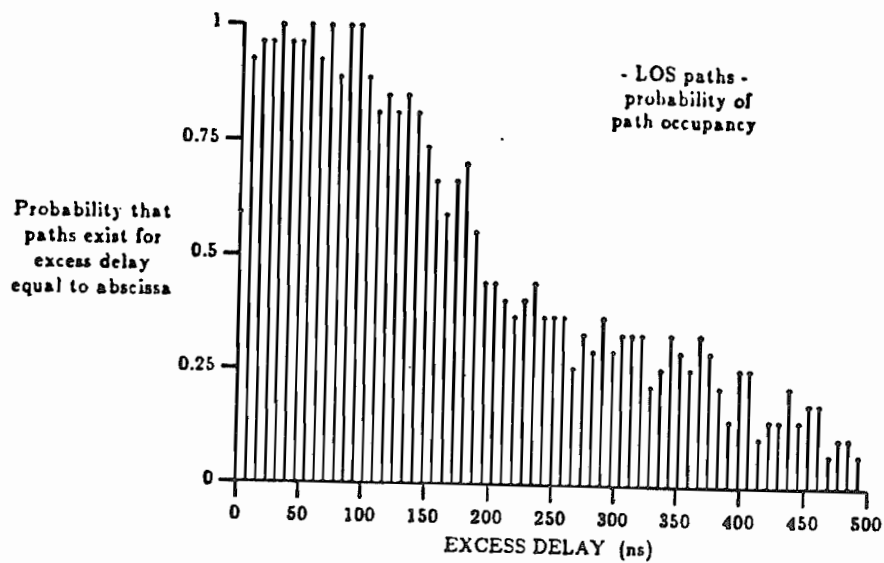


Figure 5.29 Probability of path arrival (from 27 locations) at a particular excess time delay in LOS geographies.

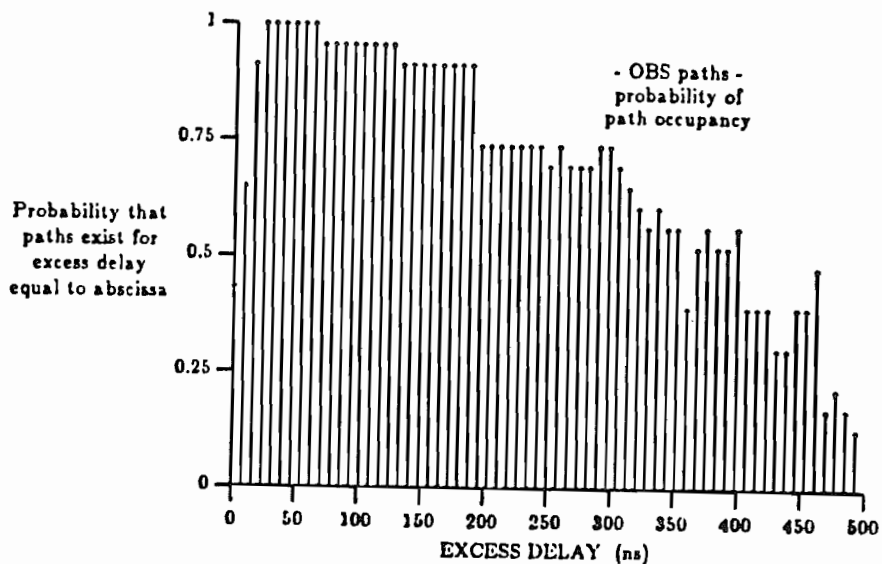


Figure 5.30 Probability of path arrival (from 23 locations) at a particular excess time delay in obstructed geographies.

delay values exist. Thus, in this report we do not attempt to describe the arrival times of the multipath statistically, but rather assume the paths to exist deterministically at all excess delays which are integer multiples of the sounding probe duration. Our assumption that all paths exist at any time is a conservative description of the factory multipath environment but is one which nevertheless should be useful. For the obstructed environment, however, Figure 5.30 shows this assumption is not far from the truth, as consecutive paths exist out to 400 ns. for well over half of our measurements. One may note, however, that the path occupancy probability data shown in Figure 5.29 indicates that, at least for LOS geographies, the arrival times of the multipath might fit an exponential conditional path arrival probability of the form

$$p(\tau_k | \tau_{k-1}) = \lambda e^{-\lambda(\tau_k - \tau_{k-1})} \quad (5.3)$$

where  $1/\lambda$  is the mean time interval between successive path arrivals. Determination of the distribution of the path interarrival times would be a useful refinement of the channel model presented here.

#### 5.4.2 Mean Square Value of Path Amplitudes

We now strive to determine a function that adequately describes the mean square value of the distribution on the  $\alpha_k$ 's, where the mean square value is estimated by the average power profiles of all the data in the specific geography. From Figures 5.26 and 5.27, we would expect an exponential decay of the power over time delay to be a good fit to the LOS data, whereas a skewed function should fit the obstructed path data well.

Rayleigh, exponential, and log-normal distribution functions were used with interactive programs to determine a good functional description of the dependence of received path power as a function of excess time delay. The averaged LOS and obstructed path power impulse responses were both found to be described best by log-normal functions. The log-normal function, as given in (3.11), is generally specified by two parameters-  $\sigma$  and  $\bar{\tau}$ ; thus, it gives more modeling flexibility than the exponential and Rayleigh functions, which are both characterized by just a single parameter. (The use of  $\sigma$  here is just as a parameter--it should not be confused with r.m.s. delay spread of the preceding section). Additional modeling parameters may be considered to be a time scaling constant  $\alpha$  which shifts the function

about the excess delay axis, and a gain constant  $K$ . We let  $\overline{\alpha_{k,G}^2}$  denote the average power (mean square value) of the  $k$ -th path in the geography contained in the set  $G$  of possible geographies. For our model,  $G$  is the two element set of LOS path and OBS path geographies. Although the LOS averaged power profile is fairly well fit by an exponential function of the form

$$\overline{\alpha_{k,G}^2} |_{G=\text{LOS paths}} = Ke^{(-\alpha\tau_k)}, \quad (5.4)$$

a much better fit was found using the log-normal function

$$\overline{\alpha_{k,G}^2} |_{G=\text{LOS paths}} = \frac{1}{\sqrt{2\pi\sigma}10^7[\tau_k-\alpha]} e^{\left[\frac{-1}{2\sigma^2}(\log_e(10^7[\tau_k+\alpha]) - 10^7\bar{\tau})^2\right]} \quad (5.5a)$$

where  $\bar{\tau}=5$  ns,  $\alpha=20$  ns, and  $\sigma=2$ . This fit was found directly by scaling and time shifting the standardized log-normal distribution with  $\bar{x}=0.05$  and  $\sigma=2$ . The fit between the empirical data and eqn. (5.5a) is shown in Figure 5.31.

The obstructed path power vs. excess delay relationship was best described by the log-normal function

$$\overline{\alpha_{k,G}^2} |_{G=\text{OBS paths}} = \frac{1}{\sqrt{2\pi\sigma}10^7[\tau_k-\alpha]} e^{\left[\frac{-1}{2\sigma^2}(\log_e(10^7[\tau_k+\alpha]) - 10^7\bar{\tau})^2\right]} \quad (5.5b)$$

where  $\bar{\tau}=25$  ns,  $\alpha=5$ ns, and  $\sigma=1.1$ . The function was adjusted to match the broad peaks between 25 and 75 ns caused by ceiling bounce and refraction. The comparison between eqn. (5.5b) and the empirical data is shown in Figure 5.32.

The average power profiles were also computed using just the paths from each individual profile that exceeded the threshold (17 dB of our pulse power receiver). This may be looked upon as a weighted, or biased, average, since for each discrete  $\tau_k$  we sum up the power of the detected paths, and divide only by the number of detected paths (not the total number of profiles as was done in Figures 5.27 and 5.28). The number of paths above the threshold as a function of  $\tau$  may be found easily from Figures 5.29 and 5.30. The weighted impulse responses for both geographies are shown in Figures 5.33 and 5.34. Notice that for the LOS paths, those paths which were detected had a constant average power level from 150 to 400 ns. A few paths were found to exist having significant signal strengths at excess

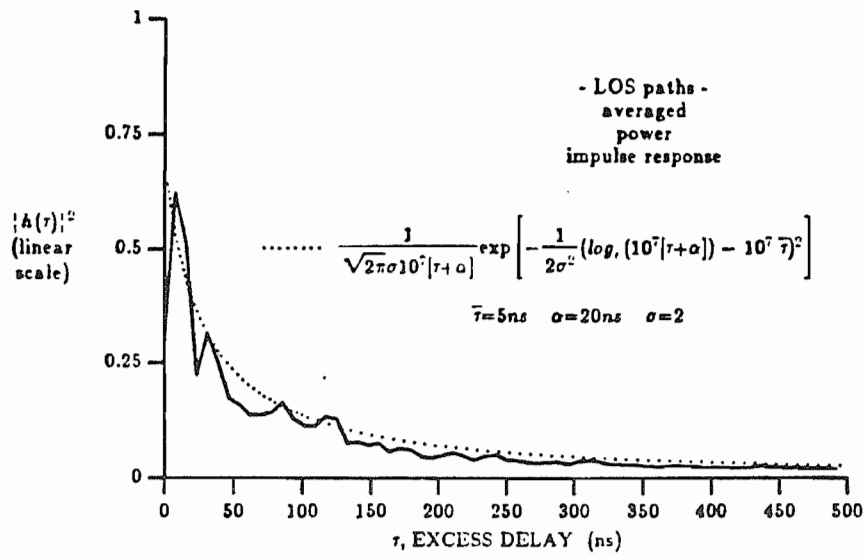


Figure 5.31 Log-normal fit to LOS multipath power behavior as a function of excess delay.

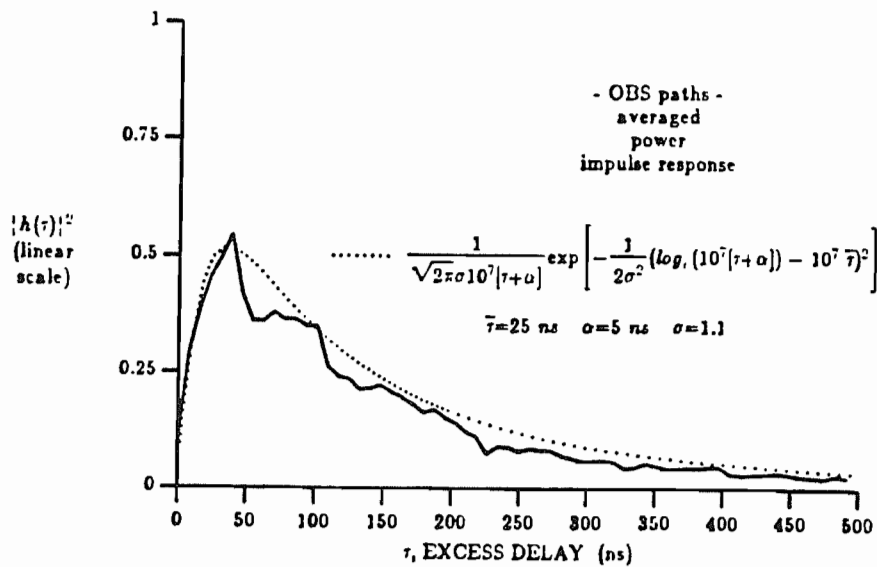


Figure 5.32 Log-normal fit to OBS multipath power behavior as a function of excess delay.

delays of 400 - 500 ns. The OBS paths follow the fitted curve more closely, which indicates that a large number of paths with significant strength arrive with excess delays of several hundred nanoseconds and are included in the overall average of Figure 5.32. These paths which occur later in the profile were determined to be from sites C and F, and are the cause of the larger r.m.s. delay spreads observed there. For our model, we assume that the log-normal functions described above are adequate, especially since we assume that all paths exist and therefore must be included in the estimate of  $\overline{\alpha_{k,G}^2}$ .

#### 5.4.3 Distribution of Path Voltage Gains ( $\alpha_k$ 's)

An attractive supposition made by Saleh and Valenzuela [53] is that all of the paths are identically distributed. Cox, in the mobile radio channel, did show that at a few excess time delays the received paths undergo Rayleigh fading. In [53], the authors pooled all resolved paths into a homogeneous data pool where each arrived path was normalized to its mean square value. Here, we try to fit the same model, which is quite elegant in its simplicity, to the factory multipath channel.

It is simple to show that a Rayleigh distributed random variable, when passed through a square law device, becomes exponentially distributed. This is shown in [53] and can be performed for any r.v. as shown in [86]. We were interested in determining statistics for the paths  $\alpha_k$ 's, but have measured the  $\overline{\alpha_k^2}$ 's instead. By collecting all of the observed  $\alpha_k^2$  and normalizing by the  $\overline{\alpha_k^2}$  as specified by eqn. (5.5), we may then hope to characterize all fading paths by a single distribution. We know [86] that for any r.v. having strictly nonnegative values and a density  $f_x(x)$ , the r.v.  $y$ , given by

$$y = a x^2 \quad \text{where } a > 0 \quad (5.6)$$

may be derived directly from  $f_x(x)$  using the relationship

$$f_y(y) = \frac{1}{2\sqrt{ay}} \left[ f_x \left( \sqrt{\frac{y}{a}} \right) \right] \quad (5.7)$$

Normalized path power data was collected for all detected paths out to 250 ns excess delay within each normalized spatially averaged profile by dividing received path power by  $\overline{\alpha_{k,G}^2}$ . Because of the deviation of our mean

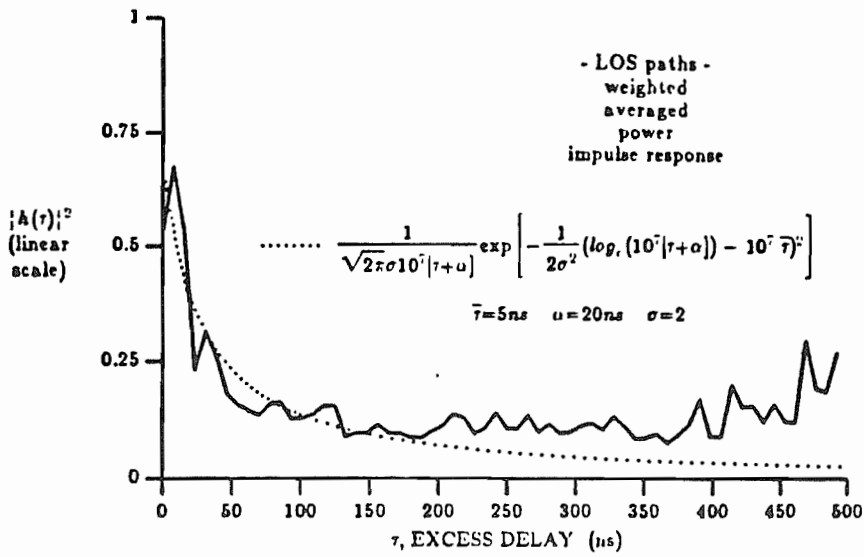


Figure 5.33 Weighted average power profile in LOS paths using detected paths only.

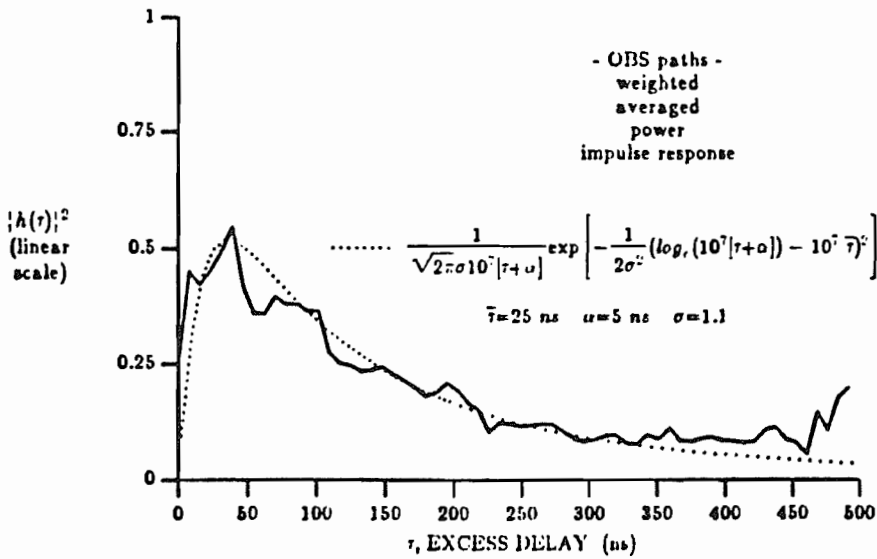


Figure 5.34 Weighted average power profile in OBS paths using detected paths only.

square models from the data at excess delay values larger than 250 ns, the latter received pulses were not used. Using (5.7), Rayleigh and Rician distributions on  $\alpha_k$  (the subscript may be dropped since all paths are normalized and assumed iid) were transformed to distributions on the variable  $\frac{\alpha^2}{\bar{\alpha}^2}$ . The data, which consisted of over 850 distinguishable LOS paths and 750 obstructed paths, was used to plot cumulative distributions (CDF's) of the normalized received path powers.

The resulting CDF's for both geographies are shown in Figure 5.35, and are plotted on a log-linear scale. On the figure, a straight line indicates an exponential distribution of the  $\frac{\alpha^2}{\bar{\alpha}^2}$  which implies a Rayleigh distribution on the  $\alpha_k$ . The OBS paths fit a Rayleigh distribution very well for ordinate values greater than 0.1. The LOS paths follow a linear slope, but are well off the Rayleigh line. This appears to be due to a majority of paths having powers on the order of  $0.5\bar{\alpha}^2$ . Also notice the slight hitch in both curves at a normalized power gain of about 2.0. At this point the strong LOS paths are accounted for, undoubtedly due to the strong first path arrival. The LOS path gain behavior suggests that the iid model with deterministic path arrival times is not good for LOS channels in buildings, and that the first few paths may actually be Rician. This is further suggested by the fact that signals arriving via strong paths early in the profile consistently underwent only slight fading over local areas. Also, we observed from the data that in LOS light clutter paths, there were seldom more than a few significant paths within the profile. Another explanation of the large number of weaker paths in LOS geographies is that since spatially averaged data, and not individual profiles, were used in this path gain analysis, it stands to reason that occasional strong LOS paths would be de-emphasized in the average.

From the data, it appears that a Rayleigh amplitude distribution for obstructed factory paths is a good model, with the profile power being a function of the height of obstructions, the T-R distance, and the ceiling height. For LOS paths, it is not clear what model to use, but Rayleigh iid paths are simple to use in analysis and likely can be made to hold by modifying the averaged power profile. This may be accomplished by scaling or adding an offset to the mean square  $\alpha_{k,G}^2$  function given in (5.5). The fact



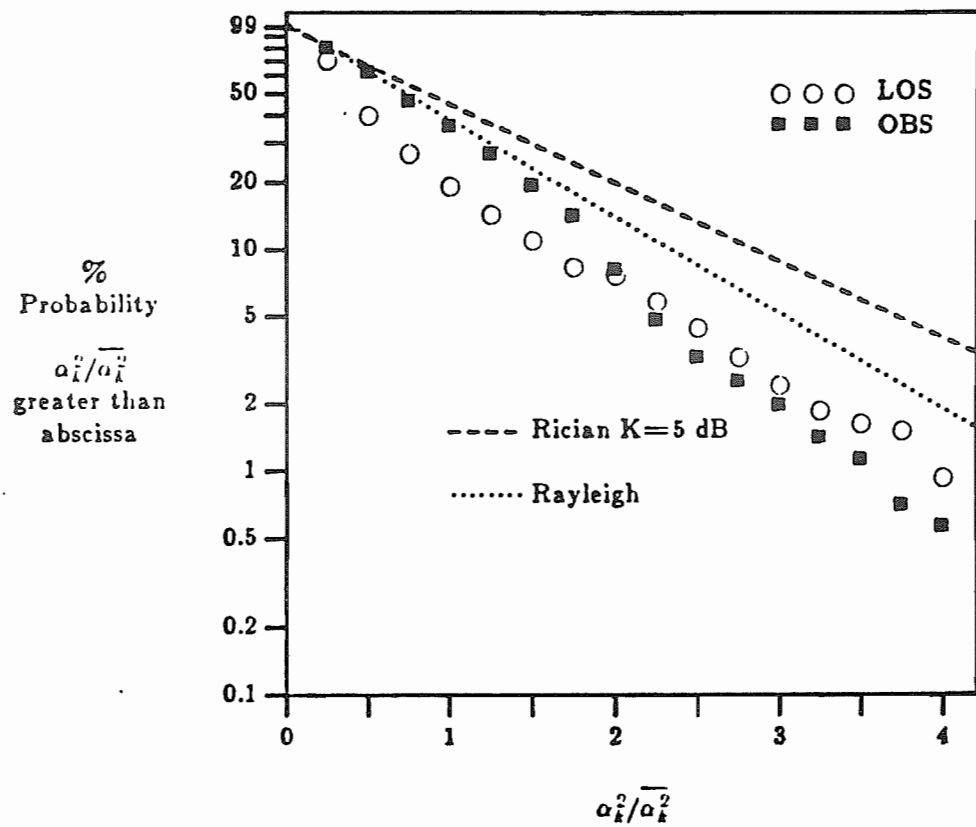


Figure 5.35 CDF of normalized path gains over all spatially averaged profiles.

that obstructed paths fit well to the Rayleigh fading curve indicates the iid assumption on path amplitudes is a good one, and should hold in other indoor obstructed path scenarios such as hospitals and warehouses.

#### 5.4.4 Using the Model

CW and wide band path loss measurements agree well, and provide average exponential relationships between T-R separation and receiver power. We noted that r.m.s. delay spreads and the average shapes of our multipath profiles did not seem strongly related to T-R separation or path loss. We observed that all but one of the spatially averaged profiles had no energy arrive beyond 500 ns excess delay. Our model may be used independently of T-R distance, then, to predict delay spreads and relative path strengths within a given geography. To include the effects of path loss, which is a function of distance, one merely needs to scale the mean square function  $\alpha_{k,G}^2$  given in (5.5).

A normalized baseband received multipath profile is described with our model by the equation

$$h_b(\tau, G) = \sum_k^N \alpha_{k,G} \delta(\tau - N\Delta\tau) e^{-j\theta_k} \quad (5.8)$$

where  $N$  is 64,  $\Delta\tau$  is on the order of 8 ns, the  $\theta_k$  are iid uniform, and the  $\alpha_{k,G}$  are assumed to be iid Rayleigh distributed having a mean square value which is dependent solely upon path arrival time and geography.

To consider path loss effects, we scale the mean square value of all paths by the average attenuation due to distance with respect to a reference level. This is the identical procedure followed by Saleh and Valenzuela [53]. Recall from Chapter 2, the power over a  $10\lambda$  path is known to have free space path loss. By defining  $\alpha_{k,G}^2$  of eqn. (5.5) to be the reference profile at a T-R separation of  $10\lambda$ , the total power  $P_{o,G}$  received at the reference may be represented as

$$P_{o,G} = \sum_k^N \overline{\alpha_{k,G}^2}$$

Let  $\overline{\mu_{k,G}^2}$  denote the mean square value of each  $\alpha_{k,G}$  in eqn. (5.8) at a specified T-R distance  $R$ . Then, the paths have mean square values given

by

$$\overline{\mu_{k,G}^2} = \overline{\alpha_{k,G}^2} P_{o,G} R^{-x} \quad (5.9)$$

The exponential factor  $x$  is 1.8 for LOS paths (1.5 for paths along walls) and 2.8 for OBS paths. The variable  $R$  in (5.10) denotes the line of sight distance between the receiver and the transmitter in meters.

The channel model is used by specifying a particular T-R separation and geography. The path amplitudes are then generated from a Rayleigh distribution which has a mean square value found from eqns. (5.5 and 5.9) and the phases are generated from a uniform distribution on  $[0, 2\pi]$ . Thus, the form of the impulse response model is identical to (5.8), where the mean square values of the paths are dependent upon the T-R separation.

## CHAPTER 6 CONCLUSION

### 6.1 Summary

This report has dealt with the problem of characterizing the UHF factory multipath channel. Measurements were made in five factories which made up a diverse collection of industries and building structures. Propagation measurements in such an environment have not been reported previously in the literature.

Our goal was to collect data essential for the design and development of a factory portable radio communication system. We envisage such a system as an integral part of the factory of the future. The results of numerous measurements made in the 1200-1400 MHz band have been presented here, and indicate that although the factory is similar in many respects to other indoor channels, the unique building structure and metallic content provide varied types of propagation not found in a typical office or residential building.

We found that most factories are similarly arranged. Aisleways are straight and uncluttered, and are generally flanked with machinery or inventory. There are very few walls, although large equipment and inventory can serve as RF partitions. Certain factory areas are dedicated to heavy machining, assembly line production, or bulk storage. These areas have been found in all factories and provide obstructed paths for portable or mobile radios in the area. Other areas, such as manual assembly lines, small parts storage, and main aisleways, are lightly cluttered and do not have many tall obstructions.

There is a significant amount of metal used in ceiling truss construction. At all sites, we observed multipath arriving at excess delays which

correlated well to ceiling bounce propagation over obstructed paths. Line of sight propagation exhibited several large paths due primarily to reflections from within and at the end of an aisleway.

By combining factory data from the five representative industries and building structures, gross channel characterizations showed that: path loss is a function of distance to the 2.2 power; multipaths have maximum delay spreads ranging from 40 ns to 800 ns; r.m.s. delay spreads range from 30 ns to 300 ns.; temporal fading is typically Rician with  $K=10$  dB; small scale fluctuations are usually Rayleigh but are sometimes well described by Rician or log-normal distributions; and that typical factory machinery can cause as much as 20 dB of attenuation due to shadowing.

We discovered that path loss in lightly cluttered LOS paths offer improvement over free space loss, having power/distance relationships of between  $d^{-1.5}$  to  $d^{-1.8}$ . Obstructed paths offer power/distance relationships of between  $d^{-2.4}$  to  $d^{-2.8}$ . Deviations about the mean path loss values were shown to fit a log-normal distribution having  $\sigma=7$  dB.

Shadowing effects of common factory equipment were measured, and compared to knife edge diffraction theory. We found that for obstructions located several meters from either transmitter or receiver, diffraction theory is a good estimate of path loss due to shadowing. For deep shadowing, however, our empirical data indicates a 10 to 15 dB improvement over what is predicted by diffraction theory. We suspect this is caused by illumination of local objects in the vicinity of the receiver. In this report, results of deep shadowing attenuation measurements for some typical manufacturing equipment are presented.

CW fading measurements were made in 50 local areas within the factories to determine fading statistics. We observed a 30 - 35 dB dynamic fading range over various antenna heights and positions. We found that average path loss is unaffected by lateral position in an aisleway, but 1 dB average gain is achieved at a distance of 50 m by using a 2 m antenna as opposed to a 1.5 m antenna. Data has been collected for diversity performance analysis, although none has been carried out in this thesis. A cursory inspection of some of the local fading data indicates that between 3-10

dB of gain may be achieved by instantaneously selecting the largest of two received signals from antennas separated in height by  $2\lambda$ . Local area fading was found to be Rayleigh over 50% of the time, and in some LOS paths the fading was Rician. Obstructed paths occasionally fit well to log-normal distributions. Statistics compiled from nearly 20,000 CW measurements indicate that the Rayleigh fading model fits the data well for most signal levels; however, at low SNR, the data tends towards a log-normal distribution.

Temporal fading statistics were compiled from 200 seconds of data acquired over a path which traversed an operational assembly line. The data was found to fit excellently to a Rician distribution having  $K=10$  dB. A preliminary temporal fading model was presented.

Wide band measurements, conducted with a sounding probe having an 8 ns r.m.s. duration, were used to measure path loss, r.m.s. delay spreads, and excess mean delays for various factories and geographies. Path loss measurements agreed well with CW measurements conducted at identical locations. Excess delays were found to exceed r.m.s. delay spread values over obstructed paths, while the opposite was true for LOS paths. Surprisingly, there was no apparent correlation between r.m.s. delay spread and path loss. Site B, a food manufacturer with predominantly non-metallic inventory, exhibited the lowest value of  $\sigma$ , having a median value of 50 ns over all geographies. Sites C and F, the most modern factories, exhibited median  $\sigma$  values of  $\approx 125$  ns over all geographies. LOS paths in all factories typically consisted of a few main paths and several smaller ones, whereas obstructed paths generally were characterized by many paths having comparable amplitudes, with the strongest paths arriving 25 - 75 ns after the first observable path.

A simple impulse response model, based on the attractive features of a recent indoor channel model [53], was formulated using the averaged multipath delay profiles in LOS and obstructed path geographies. Formulation of the model is based on the assumption that the paths arrive deterministically in time over a 500 ns delay window, and have Rayleigh amplitudes that are independent and which have mean square values determined by the shape of the averaged power profile and the T-R separation. The model is very simple and should be useful for preliminary performance evaluations

of various factory communication systems. Refinement of the model is planned by the author in the near future.

## 6.2 Possible Extensions of This Work

As no other research has appeared in the open literature describing the vagaries of the factory radio environment, the data collected in this report may be used to further the understanding of this unique channel. Data has been collected for height and space diversity analysis, but has not been examined in detail. A useful extension of this work would be to determine the improvement offered by such diversity techniques.

A path arrival model has not yet been formulated for the channel, although the data exists for a confident determination of such a model. The data presented in Chapter 5 indicates that although obstructed paths seem to arrive deterministically over several hundred nanoseconds, the LOS paths clearly should be described by an interarrival distribution on the paths. Enhancing the channel model presented here with a probabilistic description of the path arrival time would be a useful extension of the results discovered here.

Using a channel model based on the data presented here, it is possible to analyze the performances of various types of modulation and coding schemes. This is an obvious next step in the development of a futuristic portable/mobile factory multiple access communication system.

Additionally, the data presented here may serve as a useful data base for the development of a generic building propagation model which takes into account the physical dimensions of the structure and the surroundings. A propagation model based on the geometry of the factory layout and inventory storage would be an interesting extension of this work. The data contained here would be of value since proposed models could be compared with the empirical results herein.

Finally, the findings of this report will be of use to indoor communications researchers in that, as further empirical and analytical work is done

to characterize radio communication in buildings, our data will always be available to test the applicability of new propagation discoveries and models for the unique environment of the factory.



1

**LIST OF REFERENCES**



## LIST OF REFERENCES

- [1] E. Skomal, A. Smith, *Measuring the Radio Frequency Environment*, Van Nostrand Reinhold, c. 1985.
- [2] J. Parsons, T. Reyhan, "Prediction of bit error rate in the presence of impulsive noise: a numerical approach using measured noise data," *IEE Proceedings*, Vol. 132, Part F, No. 5, August 1985, p. 335.
- [3] C. Loo, "A statistical model for a land mobile satellite link," *IEEE Trans. Veh. Tech.*, Vol. VT-34, No. 3, August, 1985, p. 123.
- [4] H. Shaver, B. Tupper, J. Lomax, "Evaluation of a Gaussian HF channel model," *IEEE Trans. Comm. Tech*, February 1967, p. 79.
- [5] L. Greenstein, "A multipath fading channel model for terrestrial digital radio systems," *IEEE Trans. Comm.*, Vol. COM-26, No. 8, August, 1978, p. 1247.
- [6] P. Engels, "A channel simulator for L-band satellite-mobile communications," *AGARD Conference Proc. #299*, 23/1-9, 1979.
- [7] R. Iyer, et.al., "Effects of spaced diversity reception on multipath induced distortions in terrestrial microwave channels," *IEEE International Communication Conference-1982*, 3b.5.1.
- [8] R. Schweikert, J. Hagenauer, "Channel modeling and multipath compensation with forward error correction for small satellite ship earth stations," *IEEE 6th International Conference On Digital Satellite Communications-1983*, XII-32.
- [9] D. Cox, "Universal portable radio communications," *IEEE Trans. Veh. Tech.*, Vol. VT-34, No. 3, August 1985, p. 117.

- [10] D. Cox, et.al., "Cross polarization coupling measured for 800 MHz radio transmission in and around houses and large buildings," *IEEE Trans. Ant. Prop.*, Vol. AP-34, No. 1, January 1986, p. 83.
- [11] G. L. Turin, "Introduction to spread-spectrum antimultipath techniques and their application to urban digital radio," *Proceedings of the IEEE*, Vol. 68, No. 3, March 1980, p. 328.
- [12] B. Davis, R. Bogner, "Propagation at 500 MHz for mobile radio," *IEE Proceedings*, Vol. 132, Part F, No. 5, August 1985, p. 307.
- [13] A. Clark, "Digital modems for land mobile radio," *IEE Proceedings*, Vol. 132, Part F, No. 5, August 1985, p. 348.
- [14] A. Bajwa, "UHF wideband statistical model and simulation of mobile radio multipath propagation effects," *IEE Proceedings*, Vol. 132, Part F, No. 5, August 1985, p. 327.
- [15] L. Ladell, "Multipath characteristics at UHF in rural irregular terrain," *AGARD Conference Proceeding #244*, 18/1-12, 1979.
- [16] P. Bello, "Wideband line-of-sight channel simulation system," *AGARD Conference Proceeding #244*, 12/1-14, 1979.
- [17] A. Rustako, Jr., et.al., "A laboratory simulation facility for multipath fading microwave radio channels," *AT&T Tech. J.*, Vol. 64, No. 10, December 1985, p. 2281.
- [18] H. Suzuki, "A statistical model for urban radio propagation," *IEEE Trans. Comm.*, Vol. COM-25, No. 7, July 1977, p. 673.
- [19] H. Hashemi, "Simulation of the urban radio propagation channel," *IEEE Trans. Veh. Tech.*, Vol. VT-28, No. 3, August 1979, p. 213.
- [20] —, "Simulation of the urban radio propagation channel," *National Telecommunications Conference*, -1977, 38:1-1.
- [21] W. Rummler, "A new selective fading model: application to propagation data," *BSTJ*, Vol. 58, No. 5, May-June 1979, p. 1037.

- [22] ---, "More on the multipath fading channel model," *IEEE Trans. Comm.*, Vol. COM-29, No. 3, March 1981, p. 346.
- [23] ---, "A statistical model of multipath fading on a space diversity radio channel," *IEEE International Communication Conference-1982*, 3b.4.1.
- [24] S. Smith, J. Cormack, "Measurement and characterization of a multipath fading channel for application to digital radio links," *IEEE International Communication Conference-1982*, 7b.4.1.
- [25] M. Liniger, "Sweep measurements of the transfer function of an RF channel and their representation by polynomials," *IEEE International Communication Conference-1982*, 7b.3.1.
- [26] W. Rummier, "Extensions of the multipath fading channel model," *IEEE International Communication Conference-1979*, 32.3.1
- [27] ---, "A multipath channel model for line-of-sight digital radio systems," *IEEE International Communication Conference-1978*, 47.5.1.
- [28] L. Greenstein, "A statistical model for multipath fading channel responses," *IEEE International Communication Conference-1979*.
- [29] W. Jakes, Jr., "An approximate method to estimate an upper bound on the effect of multipath delay distortion on digital transmission," *IEEE International Communication Conference-1978*, 47.1.1.
- [30] K. Gladstone, "Computer simulation of multipath fading in the land mobile radio environment," *IEE Proceedings*, Vol. 127, Part G, No. 6, December 1980, p. 323.
- [31] Multipath detection in stationary VHF FM Channels," *Electronics Letters*, 15 March 1984, Vol. 20, No. 6.
- [32] D. Reudink, "Mobile radio propagation in tunnels," *IEEE Vehicular Technology Group Conference*, December 1968, San Francisco, CA.
- [33] J. Solberg, Research for CIDMAC (Computer Integrated Design Manufacturing Automation Center), Purdue University, 1982.

- [34] C. McGillem, J. Solberg, et.al., Proposal for Engineering Research Center, Purdue University, 1985.
- [35] E. Kent, M. Shneier, "Eyes for Automation," *IEEE Spectrum*, March 1986, p. 37.
- [36] J. Voelcker, "Helping computers communicate," *IEEE Spectrum*, March 1986, p. 61.
- [37] M. Kaminski, Jr., "Protocols for communicating in the factory," *IEEE Spectrum*, April 1986, p. 56.
- [38] P. Accampo, "MAP Pilots: promises and pitfalls," *CIM Technology*, Spring 1986.
- [39] R. Kennedy, *Fading Dispersive Communication Channels*, Wiley-Interscience, c. 1969.
- [40] W. Jakes, Jr., *Microwave Mobile Communications*, Wiley-Interscience, c. 1974.
- [41] J. Bendat, A. Piersol, *Random Data: Analysis and Measurement Procedures*, Wiley-Interscience, c. 1971.
- [42] S. Rice, "Mathematical analysis of random noise," *BSTJ*, 23, July 1944, p. 282.
- [43] C. McGillem, G. Cooper, *Modern Communications and Spread Spectrum*, McGraw Hill, c. 1986.
- [44] P. Bello, "Characterization of randomly time-variant linear channels," *IEEE Trans. Comm. Sys.*, December 1963, p. 360.
- [45] H. Raemer, "Modeling of propagation aspects of digital communication systems," *AGARD Conference Proceedings #239*, 10/1-11, 1979.
- [46] S. Yoshida, F. Ikegami, "A comparison of multipath distortion characteristics among digital modulation techniques," *IEEE Trans. Veh. Tech.*, Vol. VT-34, No. 3, August 1985, p. 128.

- [47] R. Lerez, H.-J. Gelbrich, "Bit error distribution in digital mobile radio communication- comparison between field measurements and fading simulation," *IEE Proceedings*, Vol. 132, Part F, No. 5, August 1985, p. 343.
- [48] K. Metzger, R. Valentin, "An analysis of the sensitivity of digital modulation techniques to frequency-selective fading," *IEEE Trans. Comm.*, Vol. COM-33, No. 9, September 1985, p. 986.
- [49] M. Kavehrad, "Performance of nondiversity receivers for spread spectrum in indoor wireless communications," *AT&T Tech. J.*, Vol. 64, No. 6, July-August 1985, p. 1181.
- [50] M. Kavehrad, P. J. McLane, "Performance of low-complexity channel coding and diversity for spread spectrum in indoor, wireless communication," *AT&T Tech. J.*, Vol. 64, No. 8, October 1985, p. 1927.
- [51] P. Bello, B. Nelin, "The influence of binary fading spectrum on the binary error probabilities of incoherent and differentially coherent matched filter receivers," *IRE Trans. Comm. Sys.*, June 1962, p. 160.
- [52] S. J. Patsiokas, B. Johnson, J. Dailing, "Propagation of radio signals inside buildings at 150, 450 and 800 MHz," *IEEE Vehicular Technology Conference*.
- [53] A. A. M. Saleh, R. A. Valenzuela, "A Statistical Model for Indoor Multipath Propagation," *IEEE Journal on Selected Areas in Communications*, Vol. SAC-5, No. 2, February 1987, p. 138.
- [54] G. L. Turin, et. al., "A statistical model of urban multipath propagation," *IEEE Trans. Vehl. Tech.*, Vol. VT-21, No. 1, February 1972, p. 1.
- [55] G.L. Turin, "Communication through noisy, random-multipath channels," *1956 IRE National Convention Record*.
- [56] D.C. Cox, "Time and frequency-domain characterizations of multipath propagation at 910 MHz in a suburban mobile-radio environment," *Radio Science*, Vol. 7, No. 12, December 1972 pp. 1069-1077.

- [57] J. Van Rees, "Measurements of impulse response of a wideband radio channel at 910 MHz from a moving vehicle," *Electronics Letters*, 27 Feb. 1986, Vol. 22, No. 5, pp. 246-7.
- [58] D. M. J. Devasirvatham, "Time delay spread and signal level measurements of 850 MHz radio waves in building environments," *IEEE Trans. Ant. Prop.*, Vol. AP-34, November 1986, pp. 1300-08.
- [59] J. Horikoshi, et. al, "1.2 GHz band wave propagation measurements in concrete building for indoor radio communications," *IEEE Trans. Veh. Tech.*, November 1986, pp. 146-152.
- [60] D.C.Cox, R.R. Murray, and A. W. Norris, "800 MHz attenuation measured in and around suburban houses," *AT&T Tech. J.*, Vol. 63, No. 6, pp. 921-954, July 1984.
- [61] D.C. Cox, R.R. Murray, and A.W. Norris, "Measurements of 800 MHz radio transmission into buildings with metallic wall," *BSTJ*, Vol. 62, No. 9, pp. 2695-2717, Nov. 1983.
- [62] H. H. Hoffman and D.C. Cox, "Attenuation of 900 MHz radio waves propagating into a metal building," *IEEE Trans. Ant. Prop.*, July 1982, pp. 808-811.
- [63] S. E. Alexander, "Radio propagation within buildings at 900 MHz," *Electronics Letters*, Vol. 19, No. 20, pp. 860, September 1983.
- [64] D.C. Cox, "Antenna diversity performance in mitigating the effects of portable radiotelephone orientation and multipath propagation," *IEEE Trans. Comm.*, Vol. COM-31, pp. 620-628 May 1983.
- [65] R. Kalman, et. al., *Aspects of Network & System Theory*, "Models for Signal-Distorting Media", book chapter by E.J. Baghdady, Holt, Rhinehart & Winston, c. 1971.
- [66] J. G. Proakis, *Digital Communications*, Chapter 7, McGraw-Hill, c. 1983.
- [67] G. R. Cooper, C. D. McGillem, "Random Signal Radar," Purdue University Final Technical Report TR-EE67-11, June 30, 1967.



- [68] A. Vigants, "Space-diversity engineering," *BSTJ*, January 1975, pp. 103-142.
- [69] B. Glance, L.J. Greenstein, "Frequency-Selective Fading Effects in Digital Mobile Radio with Diversity Combining," *IEEE Trans. Comm.*, Vol. COM-31, No. 9, September 1983, p. 1086.
- [70] D. C. Cox, "Delay Doppler Characteristics of Multipath Propagation at 910 MHz in a Suburban Mobile Radio Environment," *IEEE Trans. Ant. Prop.*, Vol. AP-20, No. 5, September 1972, p. 625.
- [71] D. Devasirvatham, "A Comparison of Time Delay Spread Measurements within Two Dissimilar Office Buildings," *1986 Intl. Conference on Communications Record*, Vol. 2, June 1986, p. 852.
- [72] R. R. Murray, et. al., "815 MHz Radio Attenuation Measured within a Commercial Building," *Digest 1986 IEEE International Symposium on Ant. and Prop.*, Vol. 1, June 1986, p. 209.
- [73] J. van Rees, "Measurements of the Wide-Band Radio Channel Characteristics for Rural, Residential, and Suburban Areas," *IEEE Trans. Veh. Tech.*, February 1987, p. 2.
- [74] A. Bruckstein, T. Shan, T. Kailath, "The Resolution of Overlapping Echos," *IEEE Trans. Acoustics, Speech, Sig. Proc.*, Vol. ASSP-33, No. 6, December 1985, p. 1357.
- [75] T.S. Rappaport, "Discone Design Using Simple N-connector Feed," *1987 Antenna Applications Symposium*, Allerton Park, Illinois, 23 September 1987.
- [76] D.C. Cox, "910 MHz Urban Mobile Radio Propagation: Multipath Characteristics in New York City," *IEEE Trans. Comm.*, Vol. COM-21, Nov. 1973, pp. 1187-94.
- [77] R.J.C. Bultitude, "Measurement, Characterization and Modeling of Indoor 800/900 MHz Radio Channels for Digital Communications," *IEEE Communications Magazine*, Vol. 25, No.6, June 1987, pp. 5-12.

- [78] D.M.J. Devasirvatham, "Multipath Time Delay Spread in the Digital Portable Radio Environment," *IEEE Communications Magazine*, Vol. 25, No.6, June 1987, pp. 13-21.
- [79] E.S.K Chien, et. al., "Cellular Access Digital Network (CADN): Wireless Access to Networks of the Future," *IEEE Communications Magazine*, Vol. 25, No.6, June 1987, pp. 22-31.
- [80] J. Goldhirsh, W. J. Vogel, "Roadside Tree Attenuation Measurements at UHF for Land Mobile Satellite Systems," *IEEE Trans. Ant. and Prop.*, Vol. AP-35, No. 5, May 1987, pp. 589-596.
- [81] J.S. Engel, "Effects of Multipath Transmission on the Measured Propagation Delay of an FM Signal," *IEEE Trans. Veh. Tech.*, Vol. VT-18, May 1969, pp. 44-52.
- [82] Browne, Sharpe, Hughes and Post, Lines, Waves and Antennas, J.W.Wiley, Second Edition, c. 1973, p. 400.
- [83] W. Dixon, F. Massey, Jr., Introduction Statistical Analysis, McGraw-Hill, Fourth Edition, c. 1983, p. 221.
- [84] S. Lin, J. Goldhirsh, "Statistical Behavior of Rain Attenuation for Earth-Satellite Paths at 800 MHz," *BSTJ*, Vol. 52, No. 4, April 1981, p. 557-581.
- [85] H. Suzuki, "A Statistical Model for Urban Radio Propagation," *Ph.D. Thesis*, University of California, Berkeley, June 1975.
- [86] K. Davies, Ionospheric Radio Propagation, Dover Publications, 1966, p. 244.
- [87] F. Carassa and P. Quarta, "Propagation Tests at 250, 500, 1000, 2000 Mc/s on a 189 Km Path," Electromagnetic Wave Propagation, (International Conference Sponsored by the Postal and Telecommunications Group of the Brussels Universal Exhibition) edited by M. Desirant and J.L. Michiels, Academic Press, 1960, pp.471-478.

[88] A.Papoulis, "Probability, Random Variables and Stochastic Processes", McGraw Hill, c. 1965, p. 129.

[89] I. Olkin, L. Gleser, C. Derman, "Probability Models and Applications", Macmillan, c. 1978.



**APPENDICES**

**Appendix A**  
**Discone Design Using Simple N-Connector Feed**

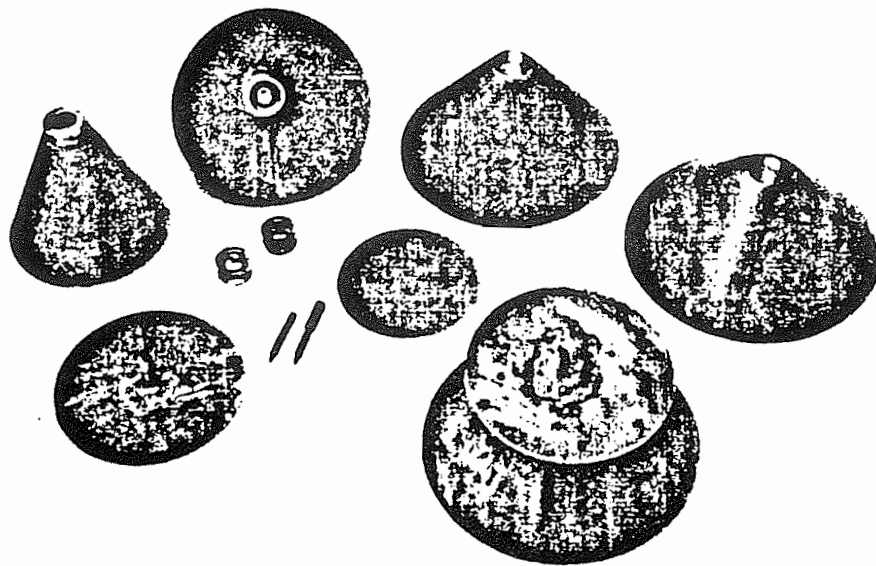


Figure A1.1 Photograph of several discone antennas developed by the author. These antennas were designed for the factory multipath measurement apparatus detailed in Chapter 2.

The following paper was presented by the author at the 1987 Antenna Applications Symposium, held at Allerton Park, IL on September 24, 1987.

## Discone Design Using Simple N-connector Feed

Theodore S. Rappaport

Engineering Research Center for Intelligent Manufacturing Systems

Electrical Engineering Department

Purdue University

West Lafayette, IN 47907

### Abstract

As part of an indoor multipath measurement system, discone antennas featuring simple N-connector feed systems have been fabricated for the 1.0 to 2.0 GHz band. Experimentation reveals that excellent performance ( $VSWR < 1.5 :1$  across the band) can be obtained with a simple "snap-on" feed/mount method, and that VSWR is most sensitive to the diameter of the disc feed conductor. Performance data from over 70 discone antennas having a variety of flare angles, disc-to-cone spacings and feed conductor diameters are summarized here. Results show that for N-connector mounts, best flare angles range between  $45^\circ$  and  $75^\circ$ , and that the disc feed conductor should be 0.33 times the diameter of the cone top. The empirical data reveals that the antennas may be tuned for even better match by using a simple clamp nut tuning scheme. Design equations, which differ from Nail's<sup>2</sup> because of the large minimum cone diameter, are presented.

### Introduction

The discone antenna is well documented in the literature and has been used extensively<sup>1-6</sup>. The discone's main virtue is that it provides low VSWR over a bandwidth of several octaves<sup>1,2</sup>. As part of an

experimental wideband indoor multipath measurement system<sup>7</sup>, several disccone antennas for the 1.0 to 2.0 GHz band have been developed. Each antenna uses a standard male N-connector as both an RF feed and mechanical support. This technique affords quick and inexpensive antenna construction and deployment. It is shown here that antenna performance is not compromised despite the large ( $\lambda/12$  at high pass cutoff) diameter of the feed connector. Design equations, which differ slightly from Nail's<sup>2</sup> because of the large minimum cone diameter, are presented.

#### Antenna Construction

As shown in Figure 1, the disccone may be characterized by the dimensions  $D$ ,  $L$ ,  $M$ ,  $\theta$ ,  $m$ ,  $s$  and  $w$ , where  $m$  is the minimum cone diameter,  $w$  is the diameter of the disc feed conductor and  $s$  is the disc-to-cone spacing. In the literature (e.g. refs. 2 and 5) it is usually assumed that  $s \ll D$ , and  $w$  is not considered. In fact, we have not seen previous data discussing the effects  $w$  and  $s$  have upon antenna loading when  $m$  is large with respect to the high pass cutoff frequency of the antenna (as is the case here). Nail found that useful design formulas (for  $m \cong \lambda/75$  at high pass cutoff) are

$$s = 0.3m \quad ; \quad D = 0.7M \quad (1)$$

regardless of  $\theta$ , where  $L$  is slightly larger than  $\lambda/4$  at cutoff<sup>2</sup>. For the case here,  $m = \lambda/12$  at high pass cutoff and Nail's design formulas were found to be helpful but incomplete.



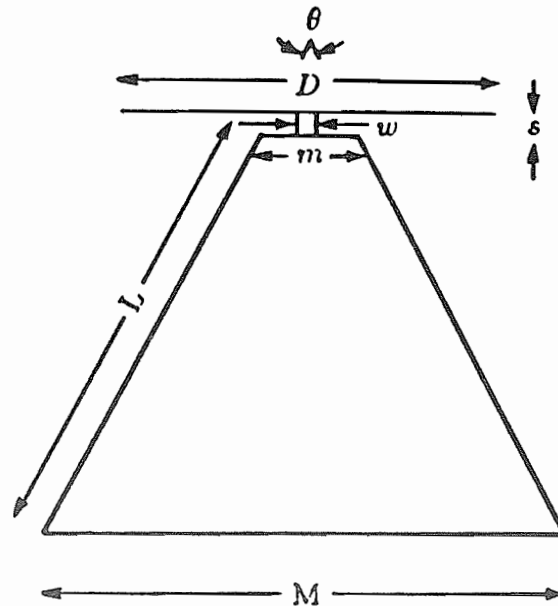


Figure A1.2. The discone antenna.

Table A1.1 Antenna cone dimensions.

Parameters	Ant. 1	Ant. 2	Ant. 3	Ant. 4
$\theta$	45°	60°	75°	90°
M	74.2 mm (3")	95.2 mm (3 3/4")	108 mm (4 1/4")	120.6 mm (4 3/4")
m	19.1 mm (3/4")	19.1 mm (3/4")	19.1 mm (3/4")	19.1 mm (3/4")
L	73 mm (2 7/8")	73 mm (2 7/8")	73 mm (2 7/8")	73 mm (2 7/8")

Four cones made of pliable copper sheet were built with flare angles ( $\theta$ ) of 45°, 60°, 75° and 90°. The four cone dimensions are given in Table 1. Slant lengths of all four cones were cut for  $\lambda/4$  at 1000 MHz. Each cone was soldered to the body of a UG-21D/U connector, giving each antenna a minimum cone diameter ( $m$ ) of 19.0 mm (3/4"). The connector was positioned and soldered completely within the cone. The rear end of the connector was made flush with the (small) top of the cone. Care was taken so that solder did not flow into the clamp nut threads on

the rear of the connector. It was discovered through experimentation that the clamp nut is useful for tuning the antenna. Discs of varying diameters were centered and soldered on copper rods that were beveled and soldered to the removable center pins of the N-connectors. A disccone antenna was formed by plugging a particular disc into a cone-mounted connector. Antenna feed was accomplished by simply mating the disccone with 50  $\Omega$  coaxial cable having a female N-connector termination.

## Experiments

### Set-up

Reflection coefficient measurements were made by placing the antenna under test in a large clear area surrounded by electromagnetic absorption material. The measurement set-up consisted of a UHF signal generator, a dual directional coupler and a dual channel power meter that was programmed to read return loss ( $= -20 \log |\Gamma|$ , where  $\Gamma$  is the reflection coefficient) referenced to a 50 ohm load. The system was calibrated across the band to remove the loss of the antenna feed cable as well as the frequency dependent variations of the equipment. Antenna return loss measurements were made at 50 MHz intervals across the 1000-2000 MHz band. Care was taken to insure power levels were sufficient to provide reliable measurements. Antenna performances were evaluated by the average value of the reflection coefficient across the 1.20 to 2.0 GHz band.

## Results

Equation (1) was first used to develop four discones described in Table 1. Of particular importance, the antennas had parameters  $s = 0.33$  m and  $w = 0.16$  m. Clamp nuts were not installed on the connectors, and a value of  $D = 0.7M$  was used for each antenna. The antenna loading characteristics of all four discones were disappointing, and are shown in Figure 2.

The disc separation,  $s$ , was then varied in increments of 0.082 m over the range  $[0m, .66m]$  for each of the four antennas to obtain lowest average VSWR over the band. For antenna 1, optimum separation was found to be 0.41 m (8.0 mm, 5/16"). Antennas 2, 3 and 4 were optimized when  $s = 0.5$  m (9.6 mm, 3/8"). These values are 50% larger than the values suggested by (1). Even with optimum disc-to-cone spacing, the loading characteristics of all four antennas were still poor. For each antenna, the VSWR averaged about 2.0:1 throughout the band. Thus, the data indicates that for large  $m$  ( $m \cong \lambda/10$ ), the common discone design equations (e.g. found in refs. 2 or 5) are lacking.

With  $s$  optimized, the disc diameter  $D$  was varied in 0.05  $M$  increments over the range  $[0.55M, 0.75M]$ . The loading characteristics of each antenna was slightly affected, most noticeably at the low frequency end and at the first harmonic of the cutoff frequency. A value of  $D = 0.70 M$  provided the best broadband response for antennas 2 and 3, whereas antennas 1 and 2 performed slightly better with  $D = 0.75 M$ . All subsequent measurements were made with disc values of  $D = 0.75M$ . This is in close agreement with Nail<sup>2</sup>.

Changing the diameter of the disc feed conductor dramatically affected the loading performances of the antennas. Values used for  $w$  ranged from 0.082 m to 0.41 m in 0.082 m increments. For each value of  $w$ , the disc-to-cone spacing ( $s$ ) on each antenna was readjusted for lowest VSWR. It was found that best matching for nearly all antennas occurred for values  $w = 0.33$  m,  $s = 0.5$  m. Figure 3 illustrates the effect of variations in  $w$  upon the loading characteristics of antenna 3 with  $s = 0.5$  m and all other antenna parameters fixed. The other three antennas demonstrated very similar behavior, although the 90° antenna provided a consistently poor match over the lower part of the band. Figure 4 displays the loading characteristics of the four optimized disccone antennas, each having parameters  $w = 0.33$  m,  $s = 0.5$  m,  $D = 0.75$  M and cone dimensions given in Table 1.

From the data it appears that a large disc feed conductor diameter mitigates a substantial impedance mismatch within the connector. Due to the structure of the UG-21D/U connector, the disc feed conductor travels a non-negligible distance ( $\cong \lambda/10$ ) within the throat of the connector before reaching the connector end. Hence, a simple coaxial transmission line model of the feed conductor within the connector seems applicable. The impedance of an air-dielectric coaxial transmission line is well known to decrease with increasing center wire diameter<sup>8</sup> and is solely a function of the ratio ( $m/w$ ). Thus the results shown in Figure 3 are not surprising. For  $w = 0.33$  m, the characteristic impedance offered by the feed conductor/connector transmission line segment is 66.5  $\Omega$ , very close to a 50  $\Omega$  match.

The experimental results justify the modification of Nail's original design equations to include relationships for  $w$  and  $s$  when  $m$  is large, on

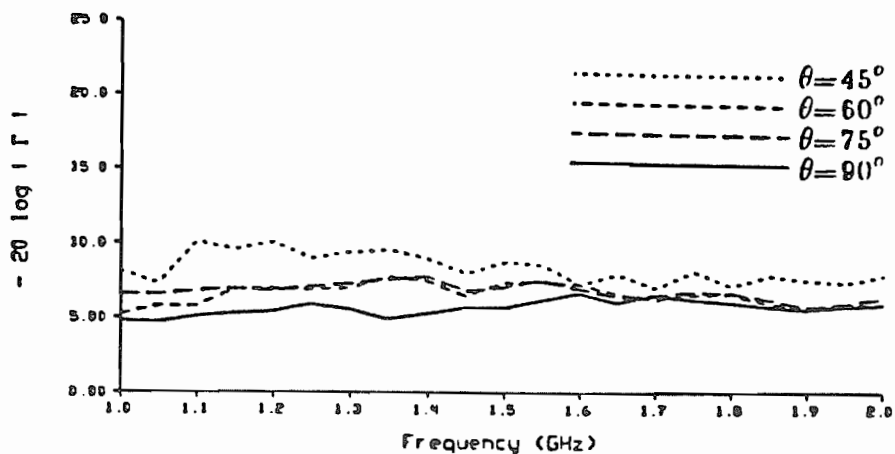


Figure A1.3. Loading characteristics of disccone antennas. (using (1))

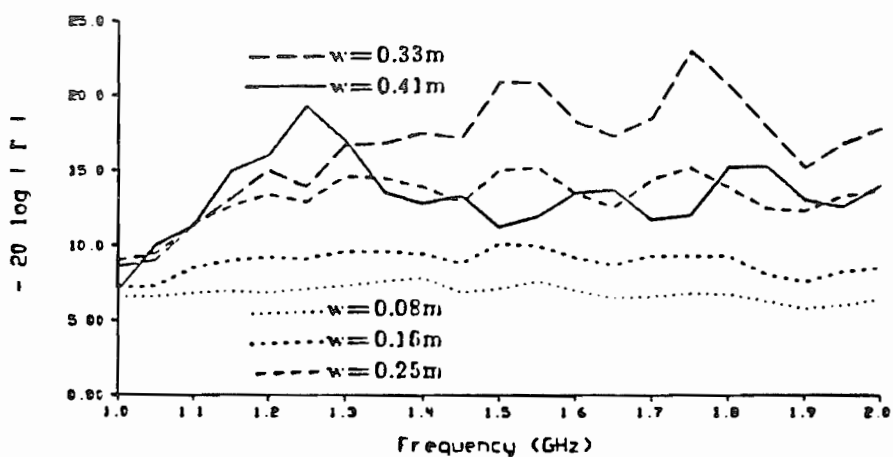
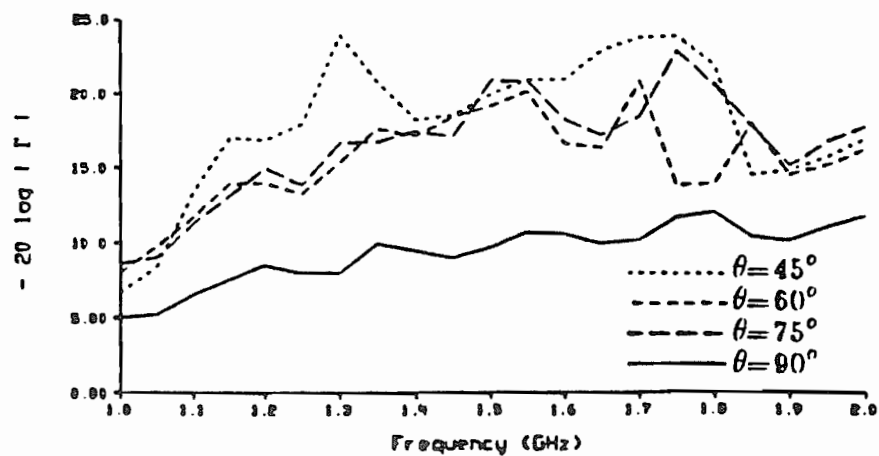
Figure A1.4. Loading characteristics as function of disc feed diameter. ( $\theta=75^\circ$ )

Figure A1.5. Loading characteristics of disccone antennas. (using(2))

the order of  $\lambda/10$  at high pass cutoff. Our data suggests the following:

$$\text{For } m \cong \lambda/10, s = 0.5m ; w = 0.33m ; D = 0.75M \quad (2)$$

Because the impedance relationship within the feed housing is not a function of just  $m$  alone, (2) should hold for any discone coaxial feed system with large  $m$ .

A second independent set of four discone antennas was fabricated using eqn. (2) to test the reliability of the design formula. Measurements performed on the second set of antennas yielded results within  $\pm 2.0$  dB of those shown in Figure 4 for most frequency points.

#### Clamp nut tuning

Further experiments were conducted to see how inserting the clamp nut into the connector would affect antenna loading characteristics. In particular, we strived to improve the match of the  $90^\circ$  discone.

An immediate benefit of the clamp nut is  $s$  can easily be adjusted. In addition, the clamp nut serves to further reduce the impedance mismatch created within the connector, and may be thought of as a low impedance transmission line segment in a tapered line.

By fastening the clamp nut into the connector, improvement in VSWR performance for three of the four antennas was accomplished. The  $45^\circ$  discone performance deteriorated substantially, however, with the clamp nut installed (when  $D=0.75M$ ).

An optimum  $w$  value of  $0.25 m$  (4.8 mm,  $3/16''$ ) was found to hold for each of the three discs. Disc-to-cone spacing was kept at  $0.5 m$

(0.6 mm, 3/8"); however, with the clamp nut inserted,  $s_{eff}$  (the effective value of  $s$ ) was decreased by 3.2 mm (1/8") due to the protrusion of the clamp nut from the cone top. Clamp nut penetration into the connector was measured to be 7.9 mm (5/16"). All other parameters remained the same. Figure 5 illustrates the loading behaviors of the three discone antennas with clamp nuts securely fastened on the top of the cones.

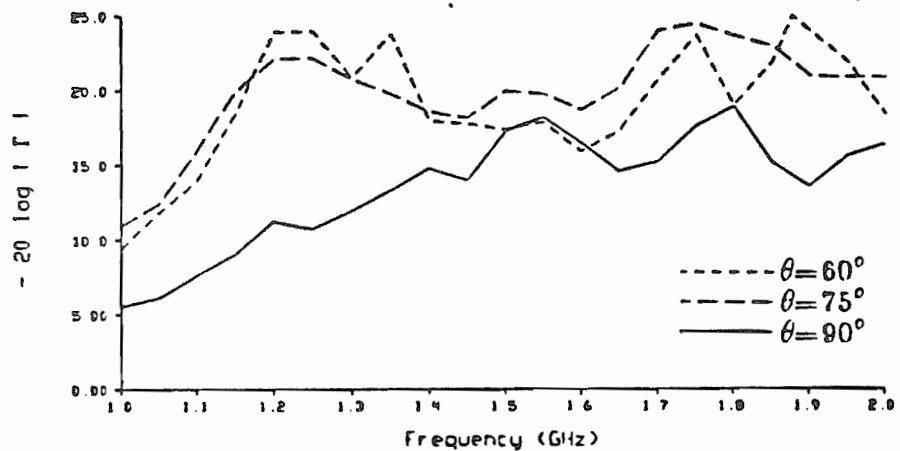


Figure A1.6. Loading characteristics of discone antennas (w/clamp nut).

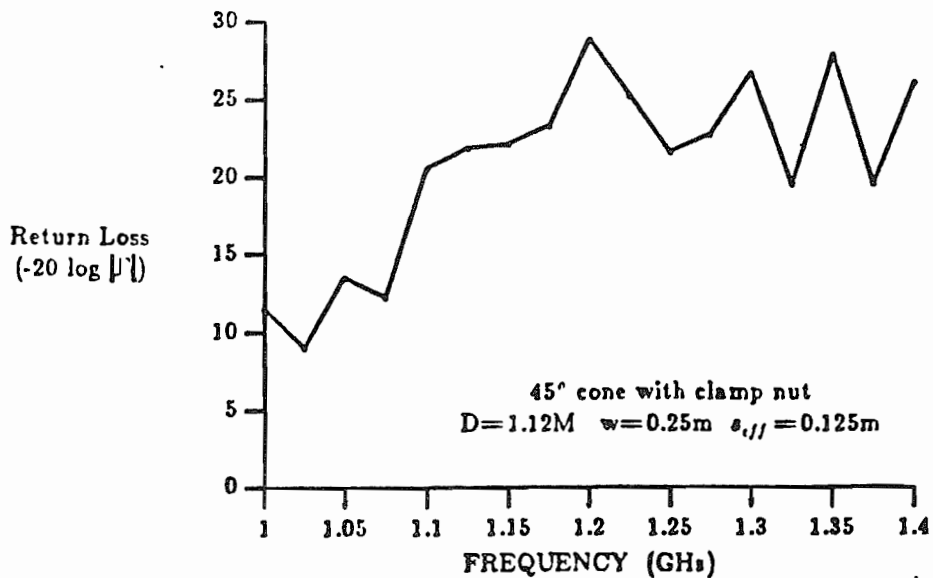


Figure A1.7. 45° discone loading optimized for 1.1 - 1.4 GHz.

For other disc feed conductor diameters, clamp nut tuning improved the reflection coefficient (i.e. those shown in Figure 3) by 5 dB on the average throughout the band.

For the 45° discone, additional experiments were conducted to determine the effects of disc diameter upon loading when clamp nut tuning is used. In particular, we strived to lower the high pass cut off frequency without changing the cone dimensions. Figure 6 shows the matching characteristics of an optimized 45° discone at 25 MHz increments across the 1.0 -1.4 GHz band. The data illustrates that with clamp nut tuning, better low frequency response may be obtained by simply increasing the disc diameter. The results also suggest that for large minimum cone diameters (on the order of  $\lambda/10$  at high pass cutoff), antenna loading anomalies due to disc feed conductor diameter,  $w$ , and disc-to-cone spacings,  $s$ , can be neutralized by a cable clamp nut (a standard part supplied with all coaxial connectors).

### Conclusion

Discone antennas are quickly and easily constructed as appendages to coaxial connectors. Such antennas are easily deployable and are suitable for use in UHF/microwave wideband indoor communications systems. In this paper, extensive experimental data were analyzed to determine design equations for discone antennas mounted on N-connectors. Such a mounting forces the minimum cone diameter  $m$  to be on the order of  $\lambda/10$  at high pass cutoff. For this case, the data illustrates the significance of antenna parameters  $s$  and  $w$  upon antenna loading. For discone antenna design using coaxial connector feeds, Nail's equations<sup>2</sup> must be modified to include the effect of the diameter of the disc feed



conductor. By selecting the disc feed conductor diameter to be about  $0.33 \lambda$ , the experiments reveal that a VSWR below 1.3 :1 is easily achievable across an octave and further suggest that cone flare angles between  $45^\circ$  and  $75^\circ$  yield best results. Eqn. (2) is a suitable modification of the well-accepted discone design equation and should hold for any discone coaxial feed system when  $m$  is large. By using a simple clamp nut adjustment and slightly decreasing the diameter of the disc feed conductor ( $w$ ), it is possible to optimize VSWR characteristics of a discone antenna mounted on a coaxial connector. When used in conjunction with clamp nut tuning, lowering the operating frequency of the antenna may be accomplished by increasing the disc diameter. The construction, design and tuning techniques described here should be valid for discones designed to operate at much higher frequencies, although this must be borne out by experimentation.

#### Acknowledgement

The author wishes to express his gratitude to Professors Walter L. Weeks and Clare D. McGillem who encouraged this work, and to the Engineering Research Center for Intelligent Manufacturing Systems at Purdue University for permission to publish these results. This work was sponsored in part by a GTE Graduate Fellowship in Electrical Engineering and by National Science Foundation Engineering Research Center Grant CDR8500022.

#### References

1. A.G. Kandoian (1946) Three New Antenna Types and Their

Applications, *Proc. IRE*, vol. 34, p. 70W - 75W, February 1946.

2. J. J. Nail (1953) Designing Discone Antennas, *Electronics*, pp. 167 - 169, August 1953.

3. K. F. Woodman (1977) Dielectric-Clad Discone, *Electronics Letters*, vol. 13(9), pp. 264 - 265, April 28, 1977.

4. A. Z. Fradin (1961) *Microwave Antennas*, Pergamon Press, 1961, pp. 7, 214 - 215.

5. W. L. Stutzman and G. A. Thiele (1981) *Antenna Theory and Design*, Wiley, 1981, ch. 6.

6. A. A. M. Saleh, R. A. Valenzuela (1987) A Statistical Model for Indoor Multipath Propagation, *IEEE Journal on Selected Areas in Communications*, vol. SAC-5 (2), pp. 128 - 137, February 1987.

7. T. S. Rappaport (1987) Characterizing the UHF Factory Multipath Channel, *Electronics Letters*, to be published.

8. S. Ramo, J. Whinnery, T. Van Duzer (1984) *Fields and Waves in Communication Electronics*, Wiley, 1984, p. 252.

## Appendix B Computer Programs

The following are programs which were used to process the multipath data. All programs are commented. Many Fortran programs were run using subroutines from the imsl subroutine package. Computation was done on the Engineering Computer Network at Purdue University with the *ed* VAX 11/780 computer.

avg.pulse.file SHELL SCRIPT program

```
#!/bin/sh
# This shell script prgm allows 19 pulse files to be averaged
# into one single file, and that average file is placed in ALLP.avg.

echo -n "Enter Directory under Data containing fileset (include .st.new): "
read path
echo -n "Now input the file series within $path for averaging: "
read file
echo -n "~Data/$path/$file ($file.st.* ) is to be averaged , Press n to cancel:
read input
if [ $input -eq "n" ]
then
    echo "strip not performed"
    exit 0
fi
    cd /a/n9nb/Data/$path
# / NOW IN THE CHOSEN STRIPPED DATA DIRECTORY and file batch
#f77. ../Programs/pulseavginit.f
#mv a.out ../Programs/a0.out
#f77. ../Programs/pulseavg.f
#mv a.out ../Programs/a1.out
#f77. ../Programs/pulseavgfinal.f
#mv a.out ../Programs/a2.out
# / LET M be the counter...use initialization when m=1 only
    m=0

# / NOW crunch on the 19 filenames.st
for i in $file*.st.*
do
# / a.out file is located in Data/Programs directory from "pulseavg.ex"
# / The pulseavg.X.f contains output target filename
    m= expr $m + 1

    if [ $m -eq "1" ]
    then
        echo $i | ../Programs/pulscavginit.ex
    else
        echo $i | ../Programs/pulseavg.ex
    fi
done
    echo $file.avg | ../Programs/pulseavgfinal.ex
    mv $file.avg ../ALLP.avg
exit 0
env.group.dist SHELL SCRIPT program
#!/bin/sh
# This shell script prgm allows an group of files to be merged
# into a frequency table of 1 dB bins (-30/+20)

echo "This to be used for combining the envelope freq tables in Data/Endist"
echo "into cummlative PDF's for each measurement location"
echo "(the original frequency tables generated are removed)"
echo
echo -n "Enter file prefix for the grouping: "
read prefix
    cat /dev/null>/tmp/n9nb/fnames.merge
    echo $prefix >>/tmp/n9nb/fnames.merge
for i in ${prefix}*.ifreq
do
    echo "Glomming data $i..."
    echo $i >>/tmp/n9nb/fnames.merge
done
    echo "xxxxxxxxxxxxxxxxxxxxxx">>/tmp/n9nb/fnames.merge
    echo " ">>/tmp/n9nb/fnames.merge
```

```

/a/n9nb/Data/Programs/envmerge.ex < /tmp/n9nb/fnames.merge
# now remove the individual files *.freq to clean directory
for i in /a/n9nb/Data/Envdist/${prefix}*.freq
do
    rm $i
done
# NOW compute cumulative distribution for prefix file
echo $prefix | /a/n9nb/Data/Programs/envdist.ex

exit 0
envdistrib.f
c This program is used to break the 50 or so bins having
c frequency bins of 1 dB width into cumulative probability
c data for local distributions of envelope fading. The program
c assumes dynamic range of 50 dB (+20/- 30dB) about the median value

real binpercent
integer i,atten,npts,k
real bincnt
character lilname*15,actname*17
character actoutfile*22,liloutfile*20

write(*,*)"Enter cumulative file that is to be integrated"
read (*,'(a17)') actname
write(*,*)"We read in the character string:",actname

c if actname has all 17 nonblank, then lilset=0
lilset=0
if ( actname(16:) .eq. ' ' ) then
    lilset=1
    lilname= actname(1:15)
    write(*,*)"The lilname file is stored as",lilname
endif

c PROGRAM TO BE EXECUTED IN ENVDIST DIRECTORY...integrates file
c CONTAINING A FREQTABLE
c TO GET cumulative percent probability
npts=0
k=0
c npts is total # of data points in input file
c actname is 17 character file name (i.e. eclac.d.st.1)
c lilname is 15 character file name (i.e. eblac.st.1)

if (lilset .eq. 0) then
open(unit=7,file=actname)
do 2 i=1,50
read(7,*)atten,bincnt
npts=npts+bincnt
2 continue
rewind(7)
close(7)
open(unit=7,file=actname)
else
open(unit=7,file=lilname)
do 3 j=1,50
read(7,*)atten,bincnt
npts=npts+bincnt
3 continue
rewind(7)
close(7)
open(unit=7,file=lilname)
endif

c npts has the total # of data pts

```

```

        write(*,*)"input file has",npts,"datapoints"
c      now read in the values of atten and the count
c      use a 50 db dynamic fading range (conservative)

c open the destination.hist file in Data/Envdist

        if (lilset .eq. 0) then
        actoutfile='prob.'//actname
        open(unit=8,file=actoutfile)
        else
        liloutfile='prob.'//lilname
        open(unit=8,file=liloutfile)
        endif

c now open the output file
c bincnt is 0 at first, keep aggregate % of distribution in binpercent
        binpercent=0.
        bincnt=0
        atten=0
        do 12 i=1,50
            read(7,*)atten,bincnt
            binpercent=(1./npts)*bincnt+binpercent
            if (k .eq. 1) then
                goto 89
            endif
            if (binpercent .ge. 0.000001) then
                write(8,*)atten,binpercent
            endif
89        if (binpercent .ge. 0.999999) then
            k=1
        endif

12        continue
        rewind (7)
        close (7)
        rewind (8)
        close (8)
        end
envfreqtable.f.
c      This program is used to break the 128 (or 1024 SS) data
c      points into bins of 1 dB width for the purpose of analyzing
c      the local distributions of envelope fading. The program
c      assumes a dynamic range of +15/- 25dB about the median value

        character tjunk,ljunk*70
        real median,rjunk,data(128)
        integer i,j,k,bincnt
        character lilname*10,actname*12
        character actoutfile*28,liloutfile*26

        write(*,*)
        write(*,*)"Enter envelope filename that is to be freq tabled"
        read (*,'(a12)') actname
        write(*,*)"We read in the character string:",actname

c      if actname has all 12 nonblank, then lilset=0
        lilset=0
        if ( actname(11:) .eq. ' ' ) then
            lilset=1
            lilname= actname(1:10)
            write(*,*)"The lilname file is stored as",lilname
        endif

```

```

c PROGRAM TO BE EXECUTED IN DATA FILE DIRECTORY...MOVES HISTOGRAM
c TO THE DIRECTORY ../Envdist...with file name.freq
c   actname is 12 character file name (i.e. eclac.d.st.1)
c   lilname is 10 character file name (i.e. eblac.st.1)

      if (lilset .eq. 0) then
        open(unit=7,file=actname)
      else
        open(unit=7,file=lilname)
      endif

      do 5 i=1,3
        read (7,*)tjunk
5      continue
c line 4 is a weird one in raw data file
      read (7,'(A70)',iostat=k)ljunk
c if error in reading character, than must be a digit in line 4
c   read (7,*)rjunk
      read (7,*)rjunk
      read (7,*)tjunk
      do 6 i=7,13
        read (7,*)rjunk
6      continue

c get the median power from the ".st.new" envelope file line 14
      read (7,*)median
c get rid of last 2 preamble line
      read (7,*)rjunk
      read (7,*)rjunk
      do 15 i=1,128
        read(7,*)data(i)
15      continue
      close(7)

c open the destination.freq file in Data/Envdist

      if (lilset .eq. 0) then
        actoutfile='../Envdist/'//actname//'.freq'
        open(unit=8,file=actoutfile)
      else
        liloutfile='../Envdist/'//lilname//'.freq'
        open(unit=8,file=liloutfile)
      endif

c now scan the data looking for points in the 1dB bins

c now open the output file
c bincnt is 0 at first, keep frequency of distribution
      do 12 i=-30,20
        bincnt=0.
        do 13 j=1,128
c          we have the data in array
          if ((data(j) .lt. i) .and. (data(j) .ge. i-1)) then
            bincnt=bincnt+1
          endif
13        continue
          write(8,*)i,bincnt
12      continue
      rewind (8)
      close (8)
      end

c this program merges the freq distribution data of several input
c files into one large file that has the cumulative distribution
c in 1 dB intervals

```

```

integer atten(50),bin(50),tot(50)
integer i,ifile
character target*10
character fname*17

ifile=1
do 1 i=1,50
  atten(i)=0
  bin(i)=0
  tot(i)=0
1  continue

write(*,*)"Enter the target file containing merged data(10 letters)"
read(*,*)target
5 write(*,*)"Enter ",ifile,"file to be merged- or x's to stop"
read(*,*)fname
if (fname .ne. 'xxxxxxxxxxxxxxxxxxxx') then
  call merge(atten,bin,tot,fname)
  ifile=ifile+1
10 goto 5
endif
open(unit=8,file=target)
do 13 i=1,50
  write(8,*)atten(i),tot(i)
13 continue
rewind(8)
close(8)
end
C *****
subroutine merge(a,b,t,fn)
character fn*17
integer a(50),b(50),t(50)
open(unit=7,file=fn)
do 60 k=1,50
  read(7,*)a(k),b(k)
  t(k)=t(k)+b(k)
60 continue
rewind(7)
close(7)
end
envmerge.f
c this program merges the freq distribution data of several input
c files into one target file that has the cumulative distribution
c in 1 dB intervals

integer atten(50),bin(50),tot(50)
integer i,ifile
character target*10
character fname*17

ifile=1
do 1 i=1,50
  atten(i)=0
  bin(i)=0
  tot(i)=0
1  continue

write(*,*)"Enter the target file containing merged data(10 letters)"
read(*,*)target
5 write(*,*)"Enter ",ifile,"file to be merged- or x's to stop"
read(*,*)fname
if (fname .ne. 'xxxxxxxxxxxxxxxxxxxx') then
  call merge(atten,bin,tot,fname)
  ifile=ifile+1
. 10 goto 5

```



```

endif
open(unit=8,file=target)
do 13 i=1,50
13 write(8,*)atten(i),tot(i)
continue
rewind(8)
close(8)
end
c *****
subroutine merge(a,b,t,fn)
character fn*17
integer a(50),b(50),t(50)
open(unit=7,file=fn)
do 60 k=1,50
read(7,*)a(k),b(k)
60 t(k)=t(k)+b(k)
continue
rewind(7)
close(7)
end
envstrip.f
c This is envstrip.f

c Use -limslsp after f77. fname for the IMSL library
c This program used for massaging some of the early data
c
c Use this program with strip.env.directory....
c
c This program is used for computing mean signal level of envelope
c data. The data is scanned for filename, path distance,pwr,atten
c and max and min fading level. The exponential loss factor, the
c avg signal received signal and max and min fading levels is returned.
c The program uses the receiver law-- Pr(dbm) = Vif * 760dB/V - 125 db
c The final output
c is written into the directory C.st.new/FILENAME
c
character*5 actname*12,lname*7,sname,clutpath,path,descrip*60,area*25
character lilname*10,actoutfile*26,liloutfile*24
real dist,pwr,atten,xincr,ymult,vzr,d(128),dsort(128)
real rmsdelay,pwrgain,avgt1,avgt2,min,max,minrcvpwr,maxrcvpwr
real rcvpwrmedian
integer i,npts,lilset

c actname is 12 character file name (i.e. eclac.d.st.1)
c lilname is 10 character file name (i.e. eblac.st.1)
c lname is first line in file with seven letters (i.e. eclac.d)
c sname (short) is first line in file with five letters (i.e. eblac)
c min=1.0
c max=0.
c The data is in mV and never is greater than 200 mV
write(*,*)"Enter envelope filename that is to be processed"
read (*,'(a12)') actname
write(*,*)"We read in the character string:",actname

c if actname has all 12 nonblank, then lilset=0
lilset=0
if ( actname(11:) .eq. ' ' ) then
lilset=1
lilname= actname(1:10)
write(*,*)"The lilname file is stored as",lilname
endif

if (lilset .eq. 0) then
open(unit=7,file=actname)
else

```

```

open(unit=7,file=lilname)
endif

read(7,*)lname
if ( lname(7:) .eq. ' ') then
    inset=1
    sname= lname(1:5)
    write(*,*)"The short name in file is",lname
endif
read(7,'(A25)')area
read(7,*)clutpath
read(7,'(A60)')descrip
read(7,*) dist
read(7,*)path
read(7,*)pwr
read(7,*)atten
read(7,*)npts
read(7,*)xincr
read(7,*)vzr
read(7,*)ymult
read(7,*)rmsdelay
read(7,*)pwr gain
read(7,*)avgt1
read(7,*)avgt2

c Now read in the 128 lines of raw data, and obtain minimum value in set
do 10 i=1,npts
read(7,*)d(i)
    dsort(i)=d(i)
    if (d(i) .lt. min) then
        min=d(i)
    endif
    if (d(i) .gt. max) then
        max=d(i)
    endif
10 continue

c Now compute the average rcv sig, pwr gain and the decay exponent
rcvpwr=0.
loss=0.
c Now pwr gain put into dBm readings of the received pwr
do 45 i=1,npts
rcvpwr= rcvpwr +d(i)*760. - 125.
45 continue
avgrcvpwr=rcvpwr/npts
maxrcvpwr=max*760. - 125.
minrcvpwr=min*760. - 125.
call vsrta(dsort,npts)
rcvpwrmedian=dsort(64)*760. -125.
write(*,*) "the avg db received value=",avgrcvpwr
write(*,*) "The median db value is", rcvpwrmedian
write(*,*)"Signal has dynamic range of (dB)",maxrcvpwr-minrcvpwr
c Now compute path loss, exponential decay relative to 10 wavelengt

relpwratten=pwr-atten-rcvpwrmedian-38.3
write(*,*) "The path loss is (dB) ",relpwratten
dist=dist*12./39.37
write(*,*)"Over path having distance (m) ",dist
c relpwratten is now in

if (lilset .eq. 1) then
liloutfile='../B.st.new/'//lilname
open (unit=8,file=liloutfile)

```

```

else
actoutfile='../B.st.new/'//actname
open (unit=8,file=actoutfile)
endif

c      Output file contains distance (m) on line 5
c      pathloss on line 7, median rcv pwr on line 13
c      min and max levels on lines 14,15, dynamic fading range on 16
c      The output data is given in dB relative to median

if (inset .eq. 1) then
write(8,'(A5)') sname
else
write(8,'(A7)') lname
endif

write(8,'(A25)')area
write(8,'(A5)')clutpath
write(8,'(A80)')descrip
write(8,*) dist
write(8,'(A5)')path
write(8,*)relpwratten
write(8,*)atten
write(8,*)npts
write(8,*)xincr
write(8,*)vzr
write(8,*)ymult
write(8,*)rcvpwrmedian
write(8,*)minrcvpwr
write(8,*)maxrcvpwr
write(8,*)maxrcvpwr-minrcvpwr

c      the received data samples normalized to median signal
do 50 i=1,npts
write(8,*)d(i)*760. -125. -rcvpwrmedian
50 continue

close (8)
close (7)
end

freqtable.env.directory SHELL SCRIPT program

#!/bin/sh
# This shell script prgm allows entire directory of files to be operated
# upon with the envfreqtable.f for later computation of signal distirbtn
# This program computes envelope table of each e* file and PLACES IT
# into the Data/Envdlist dir (through the use of envfreqtable.ex)

echo -n "Enter Directory in Data with envdata (include .st.new): "
read dir
echo -n "~Data/$dir (e*) is to be freq tabled , Press n to cancel: "
read input
if [ $input -eq "n" ]
then
echo "freq table operation not performed"
exit 0
fi
echo -n "envfreqtable.f contains target directory Data/Envdlist"
cd /a/n9nb/Data/$dir
#!/ NOW IN THE CHOSEN STRIPPED DATA DIRECTORY
cp /a/n9nb/Data/Programs/envfreqtable.ex envfreqtable.ex
for i in e*.st.*
do
#!/ The a.out file from envfreqtable.f contains the output target directory
echo $i | envfreqtable.ex
done

```

```

rm envfreqtable*
exit 0
getdata HP9007 BASIC program
1 REM Ted Rappaport, May 27, 1985...Basic Program for Datalogging
2 REM with HP Integral Personal Computer 9007 and Tektronix 7854.
3 REM Program written in a hurry ...so pardon the sloppy code.
4 REM An I/O problem with the HP computer prevented direct handshaking,
5 REM so data is logged through the "Enter" key on HP computer.
10 DIM setting$(80),descrip$(80),filename$(18)
20 DIM area$(40),clutter$(18),path$(18)
30 REM THIS PROGRAM IS USED WITH HP9007 COMPUTER AND TEK 7854 SCOPE TO ACQUIRE
40 REM PULSED, ENVELOPE, AND SINGLE SWEEP MEASUREMENTS IN FACTORY ENVIRONMENTS.
50 REM ...EACH SCOPE PROFILE IS STORED ON DISK AS IT IS TAKEN, A RUN CONSISTS
60 REM OF 19 CONSECUTIVE PROFILES TAKEN ALONG A 3 FOOT TRACK.
70 REM FIRST LOAD THIS PROGRAM INTO COMPUTER RAM, THEN ENTER DATA DISK TO STORE
80 REM THE FACTORY DATA
90 DISP
100 DIM indata$(8200),predata$(200)
110 REM assume that srqs handled...will set clear 8
120 ASSIGN 8 TO "hpib"
130 CLEAR 8
140 CONTROL 8,7 ; 1 !change to ready for data hold-off mode
150 DISP "Welcome to waveform data logging program..currently establishing comli
160 DISP @ DISP @ DISP " ENTER FLEXIBLE DISK FOR DATA STORAGE"
170 BEEP @ BEEP @ BEEP @ BEEP @ BEEP @ BEEP @ BEEP @ BEEP @ BEEP @ BEEP @
180 DISP @ DISP
190 OUTPUT 810 ; "1 2 8 >p/w"
200 DISP @ DISP @ DISP "DATA COLLECTION DISK SHOULD BE INSTALLED IN DRIVE..."
210 DISP "PRESS P for Pulse measurement, E for envelope measurement, S for SS {e
220 INPUT a$
230 IF a$="p" OR a$="P" THEN 280
240 IF a$="e" OR a$="E" THEN 650
250 IF a$="s" OR a$="S" THEN 1120
260 IF m=0 THEN GOTO 210 @ DISP @ DISP @ DISP
270 REM begin pulse acquisition software
280 DISP "ENTER file name to contain this run of 19 snapshots"
290 INPUT filename$
295 ASSIGN 11 TO filename$
300 DISP "Enter factory work area" @ INPUT area$ @ IF area$="" OR area$=" " THE
310 ASSIGN 11 TO filename$
320 REM
330 DISP "Enter local clutter condition(hvy or lite)" @ INPUT clutter$ @ IF clu
340 DISP "Enter clutter details,inventory, obstructions, etc." @ INPUT descrip$
350 DISP "Enter path distance in feet" @ INPUT d @ IF d=0 THEN 350
360 DISP "Enter path characteristics (LOS or obstructed)" @ INPUT path$
370 IF path$="" OR path$=" " THEN 360
380 DISP "ENTER TRANSMITTER POWER LEVEL DBM" @ INPUT pwr @ IF pwr=0 THEN 380
390 DISP "Enter xmtr attenuator setting in dB" @ INPUT atten
400 OUTPUT 11 USING "K,/,K,/,K,/,K,/,K,/,K,/,K,/,K,/,K" ; filename$,area$,clutter$,
401 DISP " " @ DISP @ DISP @ DISP "GROUND THE SCOPE!!!! GROUND THE SCOPE!!!
402 OUTPUT 810 ; "1 2 8 >p/w"
410 FOR i=1 TO 19 @ DISP @ DISP
420 DISP "Snapshot";i;"Enter setting or description {x to abort/save run}"
430 INPUT setting$
440 IF setting$="x" THEN GOTO 590
450 DISP @ DISP @ DISP "Press Enter for logging of snapshot";i
460 INPUT a$ @ IF a$<>" " THEN 450
470 OUTPUT 810 ; "stored 1 5 avg 0 wfm sendx" !get waveform from scope
480 DISP "press enter when data is logged and want to load"
490 INPUT a$
500 IF a$<>" " THEN 480
510 REM
520 ENTER 810 ; predata$
530 ENTER 810 ; indata$
540 OUTPUT 11 ; setting$
550 OUTPUT 11 ; predata$

```

```

c xbar,ybar are sample averages
c ssx,ssy are sum of squares of residuals
c sxy is sum of products of x,y residuals
c b is sxy/ssx
c N is the number of samples
c sse is ssy-b**2ssx
c the varian (unblased estimate) is sse/N-2
  xbar=0
  logxbar=0
  ybar=0
  xsum=0
  ysum=0
  xysum=0
  x2sum=0
  y2sum=0
  ssx=0
  ssy=0
  sxy=0
  a=0
  b=0
write(*,*) "Enter file having xdata (distance in m), ydata (atten dB) pa
read(*, '(a10)')filename
write(*,*) " Program assumes xo = 2.3...in dB=", 10*log10(2.3)
xo=10*log10(2.3)

open (unit=7, file=filename)
write(*,*) "Enter number of data points for linfit calc:"
read(*,*)n

do 10 i=1,n
read(7,*)x(i), y(i)
x(i)=10*log10(x(i))
c NOW x is logarithmic (dB) AFTER THIS POINT X IS DB
xbar=xbar+x(i)
logxbar=logxbar + x(i)
ybar=ybar+y(i)
xsum=xsum+(x(i))
ysum=ysum+y(i)
x2sum=x2sum+x(i)**2
y2sum=y2sum+y(i)**2
xysum=xysum+x(i)*y(i)
10 continue

c ALL x in dB
xbar=xbar/n
ybar=ybar/n
logxbar=logxbar/n

write(*,*) "x sample average =",xbar,"dB ",10**(xbar/10.)
write(*,*) "y sample average =",ybar
c GREAT TO HERE! sample avgs ok

ssx=x2sum - ( xsum**2 / n )
ssy=y2sum - ( ysum**2 / n )
sxy=xysum - (xsum*ysum/n)

a=ybar
b=sxy/ssx
sse=ssy-ssx*b**2
var=sse/(n-2)
write(*,*) "npts=",n,"A=(dB)",a,"B=(slope)",b,"SIGMA=(dB)",sqrt(var)
write(*,*) "for x=2.3m, y=",a+b*(10*log10(2.3)-xbar)
write(*,*) "for x=12.3m,y=",a+b*(10*log10(12.3)-xbar)
write(*,*) "for x=80.0m,y=",a+b*(10*log10(80.) - xar)

```

```

c Now use the best mmse estimator fixing B=-10log(2.3)A
  xoy=0
  xxo2=0
  do 55 i=1,n
  xy=xy + x(i)*y(i)
  xoy=xoy+ xo*y(i)
  xxo2=xxo2 + (x(i) - xo )**2
55  continue
  a=( xy - xoy )/ xxo2
  var=0
  do 56 i=1,n
  var= (y(i)- a*(x(i)-xo) )**2+var
56  continue
  var=var/(n-2)
  write(*,*)
  write(*,*)"MMSE LIN FIT", "A=(slope)", a, "SIGMA=(dB)", sqrt(var)
  write(*,*)"Y(dB) =", a, "[X(dB) -", xo, "(dB)]"
  write(*,*) "for x=2.3m, y=", a*(10*log10(2.3) -xo)
  write(*,*) "for x= 12.3m, y=", a*(10*log10(12.3) -xo)
  write(*,*) "for x= 80.0m, y=", a*(10*log10(80.) -xo)

c Now perform F test
  k=5
c use 8 bins for frequency table
  do 100 i=1,k
  kbin(i)=0
  ybinbar(i)=0
  xbinbar(i)=0
  ssybin(i)=0
  yyxi(i)=0
  f=0
  sptot2=0
  totssy=0
100  continue
  do 101 i=1,n
c generate frequency table having k bins (k=8)
c *****
  if ( (x(i) .lt. 10*log10(20.)) .and. (x(i) .ge. 10*log10(10.)) ) then
  q=1
  kbin(q)=kbin(q)+1
  xbinbar(q)=xbinbar(q)+x(i)
  ybinbar(q)=ybinbar(q)+y(i)
  endif
  if ( (x(i) .lt. 10*log10(30.)) .and. (x(i) .ge. 10*log10(20.)) ) then
  q=2
  kbin(q)=kbin(q)+1
  xbinbar(q)=xbinbar(q)+x(i)
  ybinbar(q)=ybinbar(q)+y(i)
  endif
  if ( (x(i) .lt. 10*log10(40.)) .and. (x(i) .ge. 10*log10(30.)) ) then
  q=3
  kbin(q)=kbin(q)+1
  xbinbar(q)=xbinbar(q)+x(i)
  ybinbar(q)=ybinbar(q)+y(i)
  endif
  if ( (x(i) .lt. 10*log10(50.)) .and. (x(i) .ge. 10*log10(40.)) ) then
  q=4
  kbin(q)=kbin(q)+1
  xbinbar(q)=xbinbar(q)+x(i)
  ybinbar(q)=ybinbar(q)+y(i)
  endif
  if ( (x(i) .lt. 10*log10(70.)) .and. (x(i) .ge. 10*log10(50.)) ) then
  q=5
  kbin(q)=kbin(q)+1
  xbinbar(q)=xbinbar(q)+x(i)
  ybinbar(q)=ybinbar(q)+y(i)

```

```

560 OUTPUT 11 ; indata$
570 OUTPUT 810 ; "scope"
580 NEXT i
590 DISP "Measurement run terminates with";i-1;"snapshots"
600 ASSIGN 11 TO "*"
610 CLEAR 8
620 DISP @ DISP "DATA FILE ";filename$;" IS CLOSED, PRESS ENTER TO TAKE NEW DATA
630 INPUT a$ @ IF a$="" THEN GOTO 180
640 END
650 REM ENVELOPE DATA RECORDING PROGRAM
660 CLEAR
670 DISP "Enter filename for following envelope run"
680 INPUT filename$
690 ASSIGN 11 TO filename$
700 DISP "Enter factory work area" @ INPUT area$ @ IF area$="" OR area$=" " THE
710 DISP "Enter local clutter condition(hvy or lite)" @ INPUT clutter$ @ IF clu
715 DISP "Enter clutter details,inventory, obstructions, etc." @ INPUT descrip$
720 DISP "Enter path distance in feet" @ INPUT d @ IF d=0 THEN 720
730 DISP "Enter path characteristics (LOS or obstructed)" @ INPUT path$
740 IF path$="" OR path$=" " THEN 730
750 DISP "ENTER TRANSMITTER POWER LEVEL DBM" @ INPUT pwr @ IF pwr=0 THEN 750
760 DISP "Enter xmtr attenuator setting in dB" @ INPUT atten
770 OUTPUT 11 USING "K,/,K,/,K,/,K,/,K,/,K,/,K,/,K,/,K,/" ; filename$,area$,clutter$,
780 DISP "Be sure the scope GND reference is at 0 USE LEFT, AUTO TRIGGER"
785 DISP @ DISP @ DISP @ DISP " GROUND THE SCOPE !!! GROUND THE SCOPE!!!"
790 DISP @ DISP @ DISP "SET THE SCOPE TO 500 uS display for Sweep --insure trigg
800 WAIT 3000
810 REM ENVELOPE DATA ACQUISITION
814 OUTPUT 810 ; "1 2 8 >p/w"
820 REM
830 BEEP 1500,20
840 DISP " scope should be triggering on dc signal with S meter between 2 and 9"
850 DISP "Now locate yourself for a 2 second pre-walk before the 5 second data"
860 REM the samples are made at roughly 40 mS each
870 DISP @ DISP
880 BEEP 500,50
890 DISP " DO MAKE SURE THESE ARE SET..... 500 uS, /1000,LEFT, AUTO, GND!!!"
900 REM
910 DISP "START WALKING! and press STORED and F AQS on scope"
920 REM
930 WAIT 10000
940 DISP "PRESS ENTER WHEN ENVELOPE MEASUREMENT COMPLETE"
950 INPUT a$ @ IF a$<>"" THEN 940
960 OUTPUT 810 ; "0 wfm send:"
970 DISP "Waveform send command sent, PRESS ENTER TO LOG THE DATA"
980 INPUT a$ @ IF a$<>"" THEN 970
990 REM
1000 REM
1010 REM
1020 ENTER 810 ; predata$
1030 ENTER 810 ; indata$
1040 OUTPUT 11 ; predata$
1050 OUTPUT 11 ; indata$
1060 REM
1070 ASSIGN 11 TO "*"
1080 CLEAR 8
1090 DISP @ DISP "DATA FILE ";filename$;" IS CLOSED),PRESS ENTER TO TAKE NEW DATA
1100 INPUT a$ @ IF a$="" THEN GOTO 180
1110 END
1120 REM SINGLE SWEEP ACQUISITION @ clear
1130 DISP "SINGLE SWEEP MEASUREMENT--100 seconds of data/ 80ms sample"
1140 DISP ""
1150 DISP @ DISP @ DISP @ DISP
1160 DISP "First...Acquire good display using LINE TRIGGER, AUTO TRIGGER MODE "
1170 DISP "Also...place time base on /1000 and 10mS/div display"
1180 DISP @ DISP @ DISP "ENTER file name to contain this SINGLE SWEEP Measuremen

```

```

1190 INPUT filename$
1200 ASSIGN 11 TO filename$
1210 DISP "Enter factory work area" @ INPUT area$ @ IF area$="" OR area$=" " THE
1220 DISP "Enter local clutter condition(hvy or lite)" @ INPUT clutter$ @ IF clu
1225 DISP "Enter clutter details,inventory, obstructions, etc." @ INPUT descrip$
1230 DISP "Enter path distance in feet" @ INPUT d @ IF d=0 THEN 1230
1240 DISP "Enter path characteristics (LOS or obstructed)" @ INPUT path$
1250 IF path$="" OR path$=" " THEN 1240
1260 DISP "ENTER TRANSMITTER POWER LEVEL DBM" @ INPUT pwr @ IF pwr=0 THEN 1260
1270 DISP "Enter xmtr attenuator setting in dB" @ INPUT atten
1275 OUTPUT 810 ; "1 0 2 4 >p/w"
1280 OUTPUT 11 USING "K,/,K,/,K,/,K,/,K,/,K,/,K" ; filename$,area$,clutter$,
1290 CLEAR @ DISP @ DISP @ DISP @ DISP
1292 DISP @ DISP @ DISP "GROUND THE SCOPE!! GROUND THE SCOPE!!"
1300 DISP "MAKE SURE THAT TIME BASE ON /1000 and DISPLAY is on 10ms/div!"
1310 DISP
1320 DISP "FOR SINGLE SWEEP, press STORED and F AQS on scope,then press ENTER"
1330 INPUT a$ @ IF a$<>" " THEN 1290
1340 FOR i=1 TO 10 @ WAIT 10000 @ CLEAR @ DISP @ DISP @ DISP @ DISP @ DISP
1350 DISP "PLEASE WAIT WHILE SINGLE SWEEP DATA IS RECORDED"
1360 BEEP 800,50
1370 NEXT i
1380 DISP " SINGLE SWEEP DATA OBTAINED, WAVEFORM BEING STORED ON DISK"
1390 OUTPUT 810 ; "0 wfm sendx"
1400 LET a=SPOLL(810)
1410 IF a=210 THEN 1440
1420 LET a=SPOLL(810)
1430 IF a<>210 THEN 1400
1440 ENTER 810 ; predata$
1450 ENTER 810 ; indata$
1460 REM
1470 REM
1480 OUTPUT 11 ; predata$
1490 OUTPUT 11 ; indata$
1500 REM
1510 OUTPUT 810 ; "scope"
1520 DISP @ DISP @ DISP "RESET THE TIME BASE TO EXT/AQR!!! AND THE TRIGGER TO SO
1530 BEEP 800,100
1540 ASSIGN 11 TO "*"
1550 CLEAR 8
1560 DISP @ DISP "DATA FILE ";filename$;" IS CLOSED, PRESS ENTER TO TAKE NEW DAT
1570 INPUT a$ @ IF a$="" THEN GOTO 180
1580 END
1590 DISP "Enter factory work area" @ INPUT area$ @ IF area$="" OR area$=" " THE
1600 DISP "Enter local clutter condition(hvy or lite)" @ INPUT clutter$ @ IF clu
1610 DISP "Enter path distance in feet" @ INPUT d @ IF d=0 THEN 1610
1620 DISP "Enter path characteristics (LOS or obstructed)" @ INPUT path$
1630 IF path$="" OR path$=" " THEN 1620
1640 DISP "ENTER TRANSMITTER POWER LEVEL DBM" @ INPUT pwr @ IF pwr=0 THEN 1640
1650 DISP "Enter xmtr attenuator setting in dB" @ INPUT atten
1660 OUTPUT 11 USING "K,/,K,/,K,/,K,/,K,/,K,/,K" ; filename$,area$,clutter$,d,pa
linearfit.f

```

c This program uses linear estimator to establish exponential  
c path loss for factory data (modified Chapter 11 of Dixon/Massey)

```

c x is dist y is atten
  real xbar,ybar,ssx,sse,ssy,sxy,a,b,var,x(150),y(150)
  real xsum,ysum,x2sum,y2sum,xysum
  real xo,xy,xxo2,xoy
  real loqxbar
  integer i,n
  character filename*12
  real ssybin(8),totssy,sptot2,yyxi(8),f,ybinbar(8),xbinbar(8)
  integer k,q,kbin(8)

```



```

endif
c *****
101 continue

write(*,*)
write(*,*)"The bins have the following numbers in them"
do 102 i=1,k
c adjust the bin x,y averages by diving by #pts/bin
if (kbin(i) .ge. 1) then
ybinbar(i)=ybinbar(i)/kbin(i)
xbinbar(i)=xbinbar(i)/kbin(i)
endif
102 continue

c now generate the mean square error in each bin
do 103 i=1,n
c *****
if ( (x(i) .lt. 10*log10(20.)) .and. (x(i) .ge. 10*log10(10.)) ) then
q=1
ssybin(q)=ssybin(q)+ ( y(i) - ybinbar(q) )**2
endif
if ( (x(i) .lt. 10*log10(30.)) .and. (x(i) .ge. 10*log10(20.)) ) then
q=2
ssybin(q)=ssybin(q)+ ( y(i) - ybinbar(q) )**2
endif
if ( (x(i) .lt. 10*log10(40.)) .and. (x(i) .ge. 10*log10(30.)) ) then
q=3
ssybin(q)=ssybin(q)+ ( y(i) - ybinbar(q) )**2
endif
if ( (x(i) .lt. 10*log10(50.)) .and. (x(i) .ge. 10*log10(40.)) ) then
q=4
ssybin(q)=ssybin(q)+ ( y(i) - ybinbar(q) )**2
endif
if ( (x(i) .lt. 10*log10(70.)) .and. (x(i) .ge. 10*log10(50.)) ) then
q=5
ssybin(q)=ssybin(q)+ ( y(i) - ybinbar(q) )**2
endif

c *****
103 continue
write(*,*)"i kbin(i) ybinbar xbinbar(dB) ssybin yyxi f"
do 104 i=1,k
totssy=totssy+ssybin(i)
yyxi(i)= ybinbar(i)- ( a*(xbinbar(i) - xo) )
f= f+ ( kbin(i)*yyxi(i)**2 )
write(*,*) i,kbin(i),ybinbar(i),xbinbar(i),ssybin(i),yyxi(i),f
104 continue
sptot2=totssy/(n-k)
write(*,*)"sptot2, f=",sptot2, f
f= ( f/(k-2) )/sptot2
write(*,*)"Value for F =",f," k=",k," N=",n

c now compute correlation coefficient using inverse

aprime= (xy - xoy)/y2sum
write(*,*)"a=",a,"aprime=",aprime," correl. coef =",sqrt(a*aprime)

end
c *****
lognorm.f
c Log-normal numerical integration program-used for lognormal plot.
c This program allows user to specify the std dev (in dB)
c For gaussian we assume mean =0dB, specify just the standard deviation sigma
c and the program numerically integrates a gaussian density function.
c and the median level (i.e. the value of x for 50% below) is also

```

c written to screen.....This is standard riemann numerical integration

```

character filename*12
real x,rect,cdf,kdb,k,delt
integer i
write(*,*)"Log-Gaussian CDF program, Enter sigma (dB value):"
read(*,*)kdb
x=-5.0*kdb
delt=10*kdb/1000
cdf=0
rect=0
k=kdb
write(*,*)"The value for std dev k (dB) is",k
do 1 i=1,1000
x=(-5.0*kdb)+i*delt
call evaluate(x,k,rect,delt)
rect=rect*delt
cdf=cdf + rect
if (cdf .ge. 0.022 .and. cdf .le. 0.024) then
write(*,*)x,cdf
endif
if (cdf .ge. 0.099 .and. cdf .le. .102) then
write(*,*)x,cdf
endif
if (cdf .ge. 0.195 .and. cdf .le. 0.205) then
write(*,*)x,cdf
endif
if (cdf .ge. 0.295 .and. cdf .le. 0.305) then
write(*,*)x,cdf
endif
if (cdf .ge. 0.495 .and. cdf .le. 0.505) then
write(*,*)"MEDIAN VALUE FOR K=",kdb," IS X=",x
endif
if (cdf .ge. 0.695 .and. cdf .le. 0.705) then
write(*,*)x,cdf
endif
if (cdf .ge. 0.795 .and. cdf .le. 0.805) then
write(*,*)x,cdf
endif
if (cdf .ge. 0.895 .and. cdf .le. 0.905) then
write(*,*)x,cdf
endif
if (cdf .ge. .976 .and. cdf .le. 0.978) then
write(*,*)x,cdf
endif
1 continue
c now write results to file in largedist
write(*,*)"Now write this data for lognormal plotting"
write(*,*)"recall stddev=",k, "Enter filename for dist"
read(*,*)filename
open (unit=8,file=filename)
delt=10*kdb/1000
cdf=0
rect=0
k=kdb
do 13 i=1,2000
x=(-5.0*kdb)+i*delt
call evaluate(x,k,rect,delt)
rect=rect*delt
cdf=cdf + rect
if (cdf .ge. 0.005 .and. cdf .le. 0.9999) then

if (1 .eq. mod(i,10) .and. x .ge. -20.0 .and. x .le. 20.0) then
write(8,*)x,cdf*100.
endif
endif

```

```

13      continue
        end

c *****
      subroutine evaluate (xval,kval,riemann,delta)
      real xval,kval,arg,riemann,delta
c this subroutine evaluates riemann rectangle of rician distributin
c having K dB ratio of random power to specular power
      arg=1./(kval * sqrt(2*3.14159265) )

      riemann=arg*2.7182818**((-1*xval**2)/(2*kval**2) )

      end
normalize.3d.f
c This program takes a raw data input file
c and converts it to normalized values....
c This useful for the 3d plots normalization zaxis

c the raw data file name is requested by this program
c and that file is opened, the data read in, the max
c value found, and all measurements adjusted relative
c to the max (max value =1 )

      real d(2432),max
      integer i
      character filename*8

      write(*,*)"Enter raw datafile to be normalized to max:"
      read(*,*)filename
      write(*,*)"Filename",filename, "to be normalized"

      open(unit=7,file=filename)
      max=0

      do 10 i=1,2432
      read(7,*)d(i)
      if (d(i) .gt. max) then
          max=d(i)
      endif
10      continue
      rewind(7)
      close(7)

      open(unit=7,file=filename)
      do 11 i=1,2432
      d(i)= d(i)/max
      write(7,*)d(i)
11      continue
      rewind(7)
      close(7)
      end

pulse.3d.file.las SHELL SCRIPT PRINTER program

#!/bin/sh
# This shell script prgm allows 19 pulse datafiles to be concatenated
# on one single file , and that file is displayed on plot3d
# on the laser printer...use plot3d.las from /a/n9nb/bin

echo -n "Enter Directory under Data containing fileset (include .st.new): "
read path
echo -n "Now input the file series within $path for 3d-concatenation: "
read file
echo -n "Enter the full scale (ns) range of x axis (200,500,1000)":
read scale

```

```

echo -n "Data/$path/$file.st.* to be concatenated, Press n to cancel "
read input
if [ $input -eq "n" ]
then
    echo "strip not performed"
    exit 0
fi
    cd /a/n9nb/Data/$path

# Zero out temp buffer ($file3dsmall) and concatenation file ($file.3d)
    mkdir /tmp/n9nb

for i in $file*.st.*
do
# / a.out file is located in Data/Programs directory "normalize.3d.ex"
# / The pulseavg.X.f contains output target filename
    cat $i > /tmp/n9nb/$i
    sed -e "1,16d" /tmp/n9nb/$i >> /tmp/n9nb/$file.3d
done
# MOVE the concatenated data file into ALL3d directory
    mv /tmp/n9nb/$file.3d /a/n9nb/Data/ALL3d
# NOW SCALE THE DATA USING NORMALIZATION
    cd /a/n9nb/Data/ALL3d
    echo $file.3d | /a/n9nb/Data/Programs/normalize.3d.ex

#plot3d.las is located in /a/n9nb/bin...contains formatting for plot3d
# USE THE SCALE TO PLOT THE XAXIS IN NS (LOCATED in /a/n9nb/bin)
case $scale
in
0) plot3d.las /a/n9nb/Data/ALL3d/$file.3d > /tmp/n9nb/tesd.plt;;
200) plot3d.las /a/n9nb/Data/ALL3d/$file.3d /a/n9nb/bin/200 > /tmp/n9nb/tesd.plt;
500) plot3d.las /a/n9nb/Data/ALL3d/$file.3d /a/n9nb/bin/500 > /tmp/n9nb/tesd.plt;
1000) plot3d.las /a/n9nb/Data/ALL3d/$file.3d /a/n9nb/bin/1000 > /tmp/n9nb/tesd.plt;
esac
# NOW CENTER THE PLOT AND INDENT...can also add text
echo '.sv 1.5i' > /tmp/n9nb/tesd.pic
echo '.in 0.80i' >>/tmp/n9nb/tesd.pic
echo '.PS 5.9' >>/tmp/n9nb/tesd.pic
cat /tmp/n9nb/tesd.plt | plot -Tpic > /tmp/n9nb/tesd.plotout
#EDIT /tmp/n9nb/plotout for .PS 5i
sed -e "1d" /tmp/n9nb/tesd.plotout >> /tmp/n9nb/tesd.pic
echo '.sp .25i'>>/tmp/n9nb/tesd.pic
echo '.in 3.2i'>>/tmp/n9nb/tesd.pic
echo '.B'>>/tmp/n9nb/tesd.pic
echo '.ps 18'>>/tmp/n9nb/tesd.pic
echo '$file'>>/tmp/n9nb/tesd.pic
echo '.R'>>/tmp/n9nb/tesd.pic

# standard lasout mst. -Ti300 -p -t -e /tmp/tesd.pic | lpr -Pei3 -n
# for prerasterization,use:
nmt. -Ti300 -p /tmp/n9nb/tesd.pic | ns ee -S /usr/dwb/di300 -t |
    (echo -n "@document(prerasterization on)";cat -) |
    lpr -Pei3 -l

rm /tmp/n9nb/tesd.*
rm /tmp/n9nb/$file.*
exit 0

pulseavg.f
c      This is pulseavg.f

c This program is used for averaging the 19 multipath data.

```

```

c Specifically, Use this program (Pulseavg.X.f) to compute
c the delay spread and average of the 19 local multipath measurements
c
c Use this program to produce the a.out for use in avg.pulse.directory
c shell script routine
c
c The output is placed in Directory X.st
c   The voltage level is adjusted for all data
c   so that zero is true minimum envelope...The rms delay spread and
c   the power gain is computed for all files....final output
c   is written into the directory X.st.new/FILENAME
c   where X is either A,B,C,D,E or F
c
c
character*5 actname*11,lname*7,clutpath,path,descrip*60
character lilname*10,avgfile*9
character*5 area*25,lnameold*7,clutpathold,pathold
character descripold*60
character areaold*25

real dist,pwr,atten,xincr,ymult,vzr,d(128)
real pwrgain,avgt1,avgt2
real rmsdelayold,pwrgainold,avgt1old,avgt2old
real distold,pwroid,attenold,xincroid,ymultold,vzroid,dold(128)

integer i,npts,lilset

write(*,*)"Enter pulse fname that is to be added to avg "
read (*,'(all)') actname
write(*,*)"We read in the character string:",actname

c   if actname has all 11 nonblank, then lilset=0
c   used to differentiate between 11 and 10 chars in filename

lilset=0
if ( actname(11:) .eq. ' ' ) then
    lilset=1
    lilname= actname(1:10)
endif

if (lilset .eq. 0) then
open(unit=7,file=actname)
else
open(unit=7,file=lilname)
endif

c   NOW the desired data file is opened and ready to be read

read(7,*)lname
read(7,'(A25)')area
read(7,*)clutpath
read(7,'(A60)')descrip
read(7,*)dist
read(7,*)path
read(7,*)pwr
read(7,*)atten
read(7,*)npts
read(7,*)xincr
read(7,*)vzr
read(7,*)ymult
read(7,*)rmsdelay
read(7,*)pwrgain
read(7,*)avgt1
read(7,*)avgt2

c Now read in the 128 lines of data from the new file to be avgd in

```

```

        do 10 i=1,npts
        read(7,*)d(i)
10      continue

c Now open and check the running average file (..old)
      avgfile=actname(1:5)//'.avg'
      open(unit=8,file=avgfile)

      read(8,*)lnameold
      read(8,'(A25)')areaold
      read(8,'(A5)')clutpathold
      read(8,'(A80)')descripold
      read(8,*)distold
      read(8,'(A5)')pathold
      read(8,*)pwrold
      read(8,*)attenold
      read(8,*)nptsold
      read(8,*)xincrold
      read(8,*)vzrold
      read(8,*)ymultold
      read(8,*)rmsdelayold
      read(8,*)pwrgainold
      read(8,*)avgt1old
      read(8,*)avgt2old

c Now check to see that new data file and running sum
c have the same units (xincr) value
      if( (distold .eq. dist) .and. (xincrold .eq. xincr) .and.
/ (nptsold .eq. npts) .and. (attenold .eq. atten) ) then
      else
        write (*,*)"ERROR...mismatch heading data"
        write (8,*)"ERROR...mismatch heading data"
      close(8)
      goto 99
      endif

c Now increment running sum counter
      avgt2old=avgt2old+1.0

c Now read in the sum data
      do 22 i=1,npts
        read(8,*)dold(i)
        dold(i)=dold(i)+d(i)
22      continue

c Now erase the former fname.avg file since we now havee data
      rewind(8)
c Now store the new running sum in the fname.avg file
      open(unit=8,file=avgfile)

      write(8,*)lnameold
      write(8,'(A25)')areaold
      write(8,'(A5)')clutpathold
      write(8,'(A80)')descripold
      write(8,*)distold
      write(8,'(A5)')pathold
      write(8,*)pwrold
      write(8,*)attenold
      write(8,*)nptsold
      write(8,*)xincrold
      write(8,*)vzrold

```

```

write(8,*)ymultold
write(8,*)rmsdelayold
write(8,*)pwrgainold
write(8,*)avgt1old
write(8,*)avgt2old

do 33 i=1,npts
33 write(8,*)dold(i)
   continue

   close(8)
99 end
pulseavgfinal.f
c   This is pulseavgfinal.f

c This program is used for averaging the 19 mpth data.
c Specifically, Use this program (Pulseavgfinal.X.f) to compute
c the delay spread and path loss of the avg pulse measurements
c
c Use this program to produce the a.out for use in avg.strip.directory
c shell script routine
c
c The output is placed in Directory X.st
c The voltage level is adjusted for all data
c so that zero is true minimum envelope...The rms delay spread and
c the power gain is computed for all files....final output
c is written into the directory X.st.new/FILENAME
c where X is either A,B,C,D,E or F
c
c
character*5 actname*11,lname*7,sname,clutpath,path,descrip*60,area*25
character lilname*10,actoutfile*25,liloutfile*24
real dist,pwr,atten,xincr,ymult,vzr,d(128)
real divisor
real rmsdelay,pwrgain,avgt1,avgt2,min,relpwratten
integer i,j,npts,lilset

min=1.0
write(*,*)"Enter pulse fname that is to have massaged amplitude"
read(*,'(all)') actname
write(*,*)"We read in the character string:",actname

c   if actname has all 11 nonblank, then lilset=0
   lilset=0
   if ( actname(11:).eq. ' ' ) then
       lilset=1
       lilname= actname(1:10)
   endif

   if (lilset .eq. 0) then
       open(unit=7,file=actname)
   else
       open(unit=7,file=lilname)
   endif

   read(7,*)lname
   if ( lname(7:).eq. ' ' ) then
       inset=1
       sname= lname(1:5)
   endif
   read(7,'(A25)')area
   read(7,*)clutpath
   read(7,'(A60)')descrip
   read(7,*)dist
   read(7,*)path

```

```

read(7,*)pwr
read(7,*)atten
read(7,*)npts
read(7,*)xincr
read(7,*)vzr
read(7,*)ymult
read(7,*)rmsdelay
read(7,*)pwrgain
read(7,*)avgt1
read(7,*)avgt2
c avgt2 is the divisor for the summed data...take the avg
divisor=avgt2

c Now read in the 128 lines of data, and obtain minimum value in set
do 10 i=1,npts
read(7,*)d(i)
c TAKE THE AVERAGE PASSED BY pulseavg.f
d(i)=d(i)/divisor
if (d(i) .lt. min) then
min=d(i)
endif
10 continue
write(*,*)"In pulseavgfinal.f, divisor=",divisor

c close up unit 7 the fname.avg file
close(7)
rewind(7)
c Adjust the data for absolute zero (with slight offset for dB work)
c ACTUALLY, no need to adjust for absolute zero in avg...since all
c were adjusted individually! But, to remove noise floor we do it.
do 61 i=1,npts
d(i)=d(i)-min+0.001*ymult
61 continue

c Now compute the gain and the rmsdelay spread
avgt1=0.
avgt2=0.
pwrgain=0.
rmsdelay=0.
do 45 i=1,npts
avgt1=i*xincr*d(i) + avgt1
avgt2=(i*xincr)**2 * d(i) + avgt2
pwrgain=d(i)+pwrgain
45 continue
avgt1=avgt1/pwrgain
avgt2=avgt2/pwrgain
rmsdelay= sqrt(avgt2 - (avgt1)**2)
c The distance already in meters from X.st.new data
relpwrtatten=13.-atten-10*log10(pwrgain*xincr)-(13.-40.-10*log10(1.22
x *0.0000000003906 ) )

if (lilset .eq. 1) then
liloutfile=lilname
open (unit=8,file=liloutfile)
else
actoutfile=actname
open (unit=8,file=actoutfile)
endif

write(*,*)"Loss is (dB)",relpwrtatten," for path length (m) ",dist
c line 5 has distance in meters, line 7 has path loss (dB)
c relative to 10 wavelength reference
c line 13 has rmsdelayspread, line 14 has pwrgain
c line 15 has the mean excess delay, line 16 has m.s.delay

```



```

if (inset .eq. 1) then
    write(8,'(A5)') sname
else
    write(8,'(A7)') lname
endif

write(8,'(A25)')area
write(8,'(A5)')clutpath
write(8,'(A80)')descrip
write(8,*)dist
write(8,'(A5)')path
write(8,*)relpwratten
write(8,*)atten
write(8,*)npts
write(8,*)xincr
write(8,*)vzr
write(8,*)ymult
write(8,*)rmsdelay
write(8,*)pwrgain
write(8,*)avgt1
write(8,*)avgt2

do 50 i=1,npts
write(8,*)d(i)
50 continue

end
pulseavginit.f
c This is pulseavginit.f
c THIS IS TH
c This program is used for averaging the 19 multipath data.
c Specifically, Use this program (Pulseavginit.X.f) to compute
c the delay spread and average of the 19 local multipath measurements
c
c Use this program to produce the a.out for use in avg.pulse.directory
c shell script routine
c
c The output is placed in Directory X.st
c The voltage level is adjusted for all data
c so that zero is true minimum envelope...The rms delay spread and
c the power gain is computed for all files...final output
c is written into the directory X.st.new/FILENAME
c where X is either A,B,C,D,E or F
c
c
character*5 actname*11,lname*7,sname,clutpath,path,descrip*60,area*25
character lilname*10,avgfile*9
real dist,pwr,atten,xincr,ymult,vzr,d(128)
real rmsdelay,pwrgain,avgt1,avgt2,min
integer i,npts,lilset

min=1.0
write(*,*)"Enter pulse fname that initializes running average "
read (*,'(all)') actname
write(*,*)"We read in the character string:",actname

c if actname has all 11 nonblank, then lilset=0
c used to differentiate between 11 and 10 chars in filename

lilset=0
if ( actname(11:) .eq. ' ' ) then
    lilset=1
    lilname= actname(1:10)
endif

```

```

if (lilset .eq. 0) then
open(unit=7,file=actname)
else
open(unit=7,file=lilname)
endif

c NOW the desired data file is opened and ready to be read

read(7,*)lname
if ( lname(7:) .eq. ' ') then
inset=1
sname= lname(1:5)
endif

read(7,'(A25)')area
read(7,*)clutpath
read(7,'(A60)')descrip
read(7,*)dist
read(7,*)path
read(7,*)pwr
read(7,*)atten
read(7,*)npts
read(7,*)xincr
read(7,*)vzr
read(7,*)ymult
read(7,*)rmsdelay
read(7,*)pwrgain
read(7,*)avgt1
read(7,*)avgt2

c Let avgt2 be the increment for averaging
avgt2=1.0

c Now read in the 128 lines of data from the new file to be avgd in

do 10 i=1,npts
read(7,*)d(i)
10 continue
close(7)
rewind(7)

c Now open and write the running average file
avgfile=actname(1:5)//'.avg'
open(unit=8,file=avgfile)

if (inset .eq. 1) then
write(8,*)sname
else
write(8,*)lname
endif

write(8,'(A25)')area
write(8,'(A5)')clutpath
write(8,'(A80)')descrip
write(8,*)dist
write(8,'(A5)')path
write(8,*)pwr
write(8,*)atten
write(8,*)npts
write(8,*)xincr
write(8,*)vzr
write(8,*)ymult
write(8,*)rmsdelay
write(8,*)pwrgain
write(8,*)avgt1

```

```

        write(8,*)avgt2

        do 50 i=1,npts
        write(8,*)d(i)
50      continue

        end
pulsepoint.f
c      This is pulsepoint.f

c This program is used for integrating all of the averaged
c multipath delay profiles
c Specifically, Use this program (pulsepoint.ex) to compute
c a point impulse response with a spacing of 7.8125 ns between impulses.
c This was selected becuz it is the rms duration of our sounding pulse
c and also because it divides evenly into the deltat values for all of
c the data (i.e. 200,500,1000ns full scale at 128 points per scale)
c we place the first impulse at ndelt/2 (or at 3.9 ns)
c Use this program to produce files with the word ".point" appended
c to the filename of data from ALLP.avg directory. Use program in PP direc.

c The output is placed in PP directory (here)
c
c
        character*5 actname*10,lname*7,sname,clutpath,path,descrip*60,area*25
        character lilname*9,actoutfile*25,liloutfile*24
        real dist,pwr,atten,delt,ymult,vzr,d(128)
        real sumbin
        integer i,j,npts,lilset,n,halt

        min=1.0
        write(*,*)"Enter pulse.avg fname that is to be integrated into point dat
        read (*,'(a10)') actname
        write(*,*)"We read in the character string:",actname

c      if actname has all 11 nonblank, then lilset=0
        lilset=0
        if ( actname(10:) .eq. ' ' ) then
                lilset=1
                lilname= actname(1:9)
        endif

        if (lilset .eq. 0) then
        open(unit=7,file=actname)
        else
        open(unit=7,file=lilname)
        endif

        read(7,*)lname
        if ( lname(7:) .eq. ' ' ) then
                inset=1
                sname= lname(1:5)
        endif
        read(7,'(A25)')area
        read(7,*)clutpath
        read(7,'(A60)')descrip
        read(7,*)dist
        read(7,*)path
        read(7,*)pwr
c      This is actual transmitter from old X.st directory...
        read(7,*)atten
        read(7,*)npts
c xincr is a key!
        read(7,*)delt

```

```

        write(*,*)"read in delt=",delt
        read(7,*)vzr
        read(7,*)ymult
c scale data with ymult, thus all data has equal profile
        read(7,*)rmsdelay
        read(7,*)pwrgain
        read(7,*)avgt1
        read(7,*)avgt2

        if (lilset .eq. 1) then
        liloutfile='../PP/'//lilname//'.point'
        open (unit=8,file=liloutfile)
        else
        actoutfile='../PP/'//actname//'.point'
        open (unit=8,file=actoutfile)
        endif

c get the data from the .avg file
        do 6 i=1,128
        read(7,*) d(i)
        d(i)=d(i)/(ymult)
6 continue
        n=nint(0.000001000/(128*delt) )
        write(*,*)"getting value of n=",n
        do 10 i=1,128
            if (halt .ne. 10) then
                sumbin=0
                do 15 j=1,n
                    sumbin=sumbin+( d(j+n*(i-1)) )
15 continue
            else
                sumbin=0
                goto 12
            endif
            if((n*i +1) .ge. 128 ) then
                halt=10
            else
12 write(8,*) n*i*delt-(n*delt/2.), sumbin/n
                write (*,*)n*i*delt-(n*delt/2.), sumbin/n
            endif
10 continue

            rewind(8)
            close(8)

        end
pulsestrip.f
c This is pulsestrip.f

c This program is used for massaging some of the early data.
c Specifically, Use this program (Pulsestrip.X.f) to compute
c the delay spread and set the noise floor of the pulse measurements
c
c Use this program to produce the a.out for use in strip.pulse.directory
c shell script routine
c store a.out as pulsestrip.ex

c The output is placed in Directory X.st
c The voltage level is adjusted for all data
c so that zero is true minimum envelope...The rms delay spread and
c the power gain is computed for all files....final output
c is written into the directory X.st.new/FILENAME
c where X is either A,B,C,D,E or F
c
c
c

```

```

character*5 actname*11,lname*7,sname,clutpath,path,descrip*60,area*25
character lilname*10,actoutfile*25,liloutfile*24
real prefincr,dist,pwr,atten,xincr,ymult,vzr,d(128)
real rmsdelay,pwrgain,avgt1,avgt2,min,relpwritten
integer i,j,npts,lilset

min=1.0
c write(*,*)"Enter pulse fname that is to have massaged amplitude"
read (*,'(all)') actname
c write(*,*)"We read in the character string:",actname

c if actname has all 11 nonblank, then lilset=0
lilset=0
if ( actname(11:) .eq. ' ' ) then
    lilset=1
    lilname= actname(1:10)
endif

if (lilset .eq. 0) then
open(unit=7,file=actname)
else
open(unit=7,file=lilname)
endif

read(7,*)lname
if ( lname(7:) .eq. ' ' ) then
    inset=1
    sname= lname(1:5)
endif
read(7,'(A25)')area
read(7,*)clutpath
read(7,'(A60)')descrip
read(7,*)dist
read(7,*)path
read(7,*)pwr
c This is actual transmitter from old X.st directory...
read(7,*)atten
read(7,*)npts
read(7,*)xincr
read(7,*)vzr
read(7,*)ymult
read(7,*)rmsdelay
read(7,*)pwrgain
read(7,*)avgt1
read(7,*)avgt2

c Now read in the 128 lines of data, and obtain minimum value in set
do 10 i=1,npts
read(7,*)d(i)
if (d(i) .lt. min) then
min=d(i)
endif
10 continue

c Adjust the data for absolute zero (with slight offset for dB work)
do 20 j=1,npts
d(j)=d(j)-min + .001*ymult
20 continue

c Now compute the gain and the rmsdelay spread
avgt1=0.
avgt2=0.
pwrgain=0.

```

```

rmsdelay=0.
do 45 i=1,npts
  avgt1=i*xincr*d(i) + avgt1
  avgt2=(i*xincr)**2 * d(i) + avgt2
  pwrgain= d(i)*pwrgain
45  continue
  avgt1=avgt1/pwrgain
  avgt2=avgt2/pwrgain
  rmsdelay= sqrt(avgt2 - (avgt1)**2)
  dist=dist*12./39.37
  prefincr=0.000000003906
  relpwratten=pwr-atten-10*log10(pwrgain*xincr)-(13.-40.-10*log10(
x 1.22*prefincr) )

  if (lilset .eq. 1) then
    liloutfile='../F.st.new/'//lilname
    open (unit=8,file=liloutfile)
    else
    actoutfile='../F.st.new/'//actname
    open (unit=8,file=actoutfile)
    endif

c   write(*,*)"Loss is (dB)",relpwratten," for path length (m) ",dist
c   line 5 has distance in meters, line 7 has path loss (dB)
c   relative to 10 wavelength reference
c   line 13 has rmsdelayspread, line 14 has pwrgain
c   line 15 has the mean excess delay, line 16 has m.s.delay

  if (inset .eq. 1) then
    write(8,'(A5)') sname
  else
    write(8,'(A7)') lname
  endif

  write(8,'(A25)')area
  write(8,'(A5)')clutpath
  write(8,'(A80)')descrip
  write(8,*)dist
  write(8,'(A5)')path
c The output (into X.st.new) now has path loss in place of xmit pwr
  write(8,*)relpwratten
  write(8,*)atten
  write(8,*)npts
  write(8,*)xincr
  write(8,*)vzr
  write(8,*)ymult
  write(8,*)rmsdelay
  write(8,*)pwrgain
  write(8,*)avgt1
  write(8,*)avgt2

  do 50 i=1,npts
    write(8,*)d(i)
50  continue

  end
pulsezero.f

c This program is used for massaging some of the early data.
c The data is scanned and adjusted to move the first received
c multipath to the zero time axis. The zeros are then appended
c to the end of the data.
c THIS IS to be USED INTERACTIVELY WITHIN DATA DIRECTORY
c Also, the zero is adjusted for all data

```

```

character*5 actname*11,lname*7,sname,clutpath,path,descrip*80,area*25
character lilname*10,actoutfile*11,liloutfile*10
real dist,pwr,atten,xincr,ymult,vzr,d(128)
real rmsdelay,pwrgain,avgt1,avgt2,min
integer i,j,npts,lilset,latency

min=1.0
write(*,*)"Enter pulse filename that is to be time-zeroed"
read(*,'(all)') actname
write(*,*)"We read in the character string:",actname

c   if actname has all 11 nonblank, then lilset=0
    lilset=0
    if ( actname(11:) .eq. ' ' ) then
        lilset=1
        lilname= actname(1:10)
        write(*,*)"The lilname file is stored as",lilname
    endif
c   DELCAR LATENCY
    latency=7

    if (lilset .eq. 0) then
        open(unit=7,file=actname)
    else
        open(unit=7,file=lilname)
    endif

    read(7,*)lname
    if ( lname(7:) .eq. ' ' ) then
        inset=1
        sname= lname(1:5)
        write(*,*)"The short name in file is",lname
    endif
    read(7,'(A25)')area
    read(7,*)clutpath
    read(7,'(A80)')descrip
    read(7,*)dist
    read(7,*)path
    read(7,*)pwr
    read(7,*)atten
    read(7,*)npts
    read(7,*)xincr
    read(7,*)vzr
    read(7,*)ymult
    read(7,*)rmsdelay
    read(7,*)pwrgain
    read(7,*)avgt1
    read(7,*)avgt2

c   Now read in the 128 lines of data, and obtain minimum value in set
    do 10 i=1,npts
        read(7,*)d(i)
        if (d(i) .lt. min) then
            min=d(i)
        endif
10   continue
    write(*,*)"input has minimum of",min

c   ZERO ADJUST..remove dc bias
    do 20 j=1,npts
        d(j)=d(j)-min + .001*ymult
20   continue

```

```

c Now adjust the latency...shift plot over to left by "latency" points
do 30 j=1,npts-latency
  d(j)=d(j+latency)
30  continue

  do 40 j=1,latency
  d(j+npts-latency)=.001*ymult
40  continue

c Now compute the gain and the rmsdelay spread
  avgt1=0.
  avgt2=0.
  pwrgain=0.
  rmsdelay=0.
  do 45 i=1,npts
  avgt1=i*xincr*d(i) + avgt1
  avgt2=(i*xincr)**2 * d(i) + avgt2
  pwrgain=d(i)+pwrgain
45  continue
  avgt1=avgt1/pwrgain
  avgt2=avgt2/pwrgain
  rmsdelay= sqrt(avgt2 - (avgt1)**2)

  rewind(7)
  close(7)

  if (lilset .eq. 1) then
  liloutfile=lilname
  open (unit=8,file=liloutfile)
  else
  actoutfile=actname
  open (unit=8,file=actoutfile)
  endif

  if (insct .eq. 1) then
  write(8,'(A5)') sname
  else
  write(8,'(A7)') lname
  endif

  write(8,'(A25)')area
  write(8,'(A5)')clutpath
  write(8,'(A80)')descrip
  write(8,')dist
  write(8,'(A5)')path
  write(8,')pwr
  write(8,')atten
  write(8,')npts
  write(8,')xincr
  write(8,')vzr
  write(8,')ymult
  write(8,')rmsdelay
  write(8,')pwrgain
  write(8,')avgt1
  write(8,')avgt2

  do 50 i=1,npts
  write(8,')d(i)
  write(*,*)d(i),"is the ",i,"th Data value"
50  continue

  end
rawstrip.directory SHELL SCRIPT program
#!/bin/sh

```



```

# This shell script prgm allows an entire directory to be stripped
# and then placed in new directory

echo -n "Enter Directory under Data containing raw data: "
read dir
echo -n "~Data/ $dir is to be stripped for printing, Press n to cancel: "
read input
if [ $input -eq "n" ]
then
    echo "Strip not performed"
    exit 0
fi
    cd $dir
#/ NOW IN THE CHOSEN RAW DATA DIRECTORY
for i in *
do
    echo "Stripping data $i..."
    striptek.auto $i
    mv $i.st.* ../$dir.st
done
    cd ..
    exit 0
rayleigh.f
c Rayleigh numerical integration program
c This program allows user to specify the K ratio (in dB)
c For rayleigh, this is just the standard deviation sigma**2
c and the program numerically integrates a rician density function.
c This is similar to Mcgillem's in that A=1, k=sigman**2/A**2.
c K=kdb= is = 10 log10(k)..... The output data is written to the screen
c and the median level (i.e. the value of x for 50% below) is also
c written to screen.....This is standard riemann numerical integration

real x,rect,cdf,kdb,k,delt
integer i
write(*,*)"Rician CDF program, Enter K (minus dB value):"
read (*,*)kdb
x=0
delt=0.01
cdf=0
rect=0
k=sqrt(10.**(kdb/10.) )
write(*,*)"The value for k (voltage) is",k
do 1 i=1,1000
x=i*delt
call evaluate(x,k,rect,delt)
rect=rect*delt
cdf=cdf + rect
if (cdf .ge. 0.099 .and. cdf .le. .102) then
write(*,*)x,cdf
endif
if (cdf .ge. 0.195 .and. cdf .le. 0.205) then
write(*,*)x,cdf
endif
if (cdf .ge. 0.295 .and. cdf .le. 0.305) then
write(*,*)x,cdf
endif
if (cdf .ge. 0.495 .and. cdf .le. 0.505) then
write(*,*)"MEDIAN VALUE FOR K=",kdb," IS X=",x
endif
if (cdf .ge. 0.695 .and. cdf .le. 0.705) then
write(*,*)x,cdf
endif
if (cdf .ge. 0.795 .and. cdf .le. 0.805) then
write(*,*)x,cdf
endif
if (cdf .ge. 0.895 .and. cdf .le. 0.905) then

```

```

write(*,*)x,cdf
endif
if (cdf .ge. .99 .and. cdf .le. 0.995) then
write(*,*)x,cdf
endif
1
continue
end
c *****
c subroutine evaluate (xval,kval,riemann,delta)
c real xval,kval,arg,riemann,delta,first,exponent,bessel
c this subroutine evaluates riemann rectangle of rician distributin
c having K dB ratio of random power to specular power
c arg=xval/((kval**2))

c first=xval/((kval**2)/2.)
c exponent=2.7182818**(-1.*(xval**2. + 1.)/(2*kval**2.))
c bessel= 1.- ((arg**2)/4.)+ ((arg**4.)/64.) - ((arg**6)/2304.)
c x + ((arg**8)/147456.)
c riemann=first*exponent*bessel
c used 4 terms of zero order bessel function of the first kind
c riemann=arg*2.7182818**((-1*xval**2)/(2*kval**2))

end
rayleighdistrib.f
c This program allows interactive fitting of rayleigh
c distribution...allows one to pick the value sigma
c for the rayleigh distribution
c real sigma, mid,min,max

write(*,*) "Input value for sigma, the std deviation of Rayleigh density"
read(*,*)sigma

c Consider 30 dB dynamic range (+/-15 db)
c Median in Rayleigh distribution is 1.1774sigma
xmed=1.1774*sigma

mid=1 - exp( - (1.*xmed)**2 /(2.*sigma**2) )
min=1 - exp( - (.17782794*xmed)**2 /(2.*sigma**2) )
max=1 - exp( - (2.*xmed)**2 /(2.*sigma**2) )

open (unit=6, file="temprayleigh")
write (6,*)"15.", min
write (6,*)"0.", mid
write (6,*)"6.", max
pointmerge.f
c this program merges the point impulse response data of several input
c files into one large file that has the overall average
c in 7.8125 ns bins...starting at 3.906 ns and out to 500 ns
c THIS PROGRAM PRODUCES MANY DATTA FILES, from the collection
c of the entire geography set....
c
c produces patharrival.target: contains # out of ifile
c times that path > 0.02
c meanabs.target: contains mean value of path
c sdev+abs,sdev-abs.target:contains variance abt mean
c normraypwrlos,normraypwrabs:all values of path pwr
c can adjust line 107 for ifile (all paths) or sdevifile (i) ONLYI

real meansqlos(64), meansqobs(64), normraypwrlos(64,50)
real normraypwrabs(64,50)
real s,so,s1,offo,offl
real time(64),bin(64),tot(64),median(64)
real qplotout(3200),meanabs(64),x1abs(64),x2abs(64)
real x2(64),x1(64),sdev(64),sdevabs(64)
real densitypt(64,50),max,timebin(50),x1abssdev(64),x2absd(64)

```

```

integer i,ifile,sdevifile(64)
character target*10
character fname*17

open(unit=13, file="combinedlos")
open(unit=14, file="combinedobs")

do 32 i=1,64
do 33 j=1,50
densitypt(i,j)=0
33 continue
32 continue

do 1 i=1,64
sdevifile(i)=1
time(i)=0
meanabs(i)=0
bin(i)=0
tot(i)=0
x2abs(i)=0
xlabs(i)=0
1 continue

max=0
ifile=1

write(*,*)"Enter the TARGET file containing merged data(10 letters)"
read(*,*)target
5 write(*,*)"Enter ",ifile,"file to be merged- or xxxxxxxx's to stop"
read(*,*)fname
if (fname .ne. 'xxxxxxxxxxxxxxxxxxx') then
call merge(time,bin,tot,fname,ifile,densitypt,sdevifile)
ifile=ifile+1
10 goto 5
c NOW LOOP BACK IF NOT XXXXXXXX
endif
c HERE SPECIFY BEST FITTING POWER CURVE
c s1 is los stddev, so is obs stddev, off1 is los offset, off0 obs offst
s1=2.
so=1.1
off1=0.00000002
off0=0.000000005
s=10000000.
do 200 i=1,64
meansqobs(i)=(1/(so*2.50663))*(1/(s*(time(i)+off0)))*2.7182818**
c ( -0.5*(1/(so**2))*(alog(s*(time(i)+off0)) -0.25 ) **2 )
meansqlos(i)=(1/(s1*2.50663))*(1/(s*(time(i)+off1)))*2.718
c 2818**(-1/(2*(s1)**2))*( alog(s*(time(i)+off1))-0.05 )**2 )
c write(*,*)meansqobs(i),meansqlos(i)
200 continue
c now subtract off one from the count for correct # of profiles
do 999 i=1,64
sdevifile(i)=sdevifile(i)-1
c write(*,*)"sdevifile(",i,")=",sdevifile(i)
999 continue
ifile=ifile-1
open(unit=11, file="patharrival."//target)
do 1000 i=1,64
c now write out the number of path arrivals for Ti
write(11,*) time(i),sdevifile(i)
1000 continue

close (11)
c ok now we have totally captured all points in densitypt(64,ifi)
c now accumulate the sum at particular time interval
do 1376 i=1,64

```

```

        do 1400 j=1,ifile
            xlabs(i)=xlabs(i)+densitypt(i,j)
            x2abs(i)=x2abs(i)+densitypt(i,j)**2
c         write(*,*)xlabs(i),x2abs(i),"at j=",j
1400        continue
1376        continue

c OK TO HERE
c NOW COMPUTE AVG, variance of the power data and write to files
        open(unit=8,file="meanabs."//target)
        open(unit=9,file="sdev+abs."//target)
        open(unit=10,file="sdev-abs."//target)
        do 1111 i=1,64
            if(sdevifile(i) .le. 2)then
                sdevifile(i)=2
            endif
c         HERE USE sdevifile(i) to compute DETECTED PATHS ONLY
c         OR USE IFILE to AVERAGE OVER ALL paths
            meanabs(i)=xlabs(i)/ifile
            write(8,*) time(i), meanabs(i)
            sdevabs(i)= (x2abs(i)-((xlabs(i)**2) / ( ifile ) ))/( ifile -1)
            write(9,*) time(i),meanabs(i)+sdevabs(i)
            write(10,*) time(i),meanabs(i)-sdevabs(i)
1111        continue
            close(8)
            close(9)
            close(10)

c largest value - will be 1 for all data normalized to 1 on input
        do 100 j=1,ifile
            do 98 i=1,64
                if (densitypt(i,j) .ge. max) then
                    max=densitypt(i,j)
                endif
98            continue
100        continue
            write(*,*)"WE HAVE MAX=",max
c now put all of the data in dB
c and write out to combinedobs,combinedlos
            do 279 j=1,ifile
c 25 for 200ns LOS, 40 for 300ns OBS
                do 289 i=1,25
c now just keep the detected rays out to 250 ns!
                    if(densitypt(i,j) .ge. 0.021) then
                        normraypwrlos(i,j)= densitypt(i,j)/meansqobs(i)
                        normraypwrlos(i,j)=densitypt(i,j)/meansqlos(i)
                        write(13,*)normraypwrlos(i,j)
                        write(14,*) normraypwrlos(i,j)
                    endif
289                continue
279            continue

                    close(13)
                    close(14)

                end
c *****
                subroutine merge(a,b,t,fn,ifi,dens,sdevifi)
c this subroutine gets the impulses over time from each file
c a is the time, on input
                character fn*17
                real a(64),b(64),t(64),dens(64,50)
                integer ifi,sdevifi(64)
                open(unit=7,file=fn)
                do 60 k=1,64
                    read(7,*)a(k),b(k)

```

```

        if (b(k) .le. 0.02) then
            b(k)=0.02
            sdevifi(k)=sdevifi(k)
        else
            sdevifi(k)=sdevifi(k)+1
        endif
        t(k)=t(k)+b(k)
        dens(k,ifi)=b(k)
c       write(*,*)"density(",k,ifi,")=",dens(k,ifi)
60      continue
        rewind(7)
        close(7)
        end
pulsepoint.f
c       This is pulsepoint.f

c This program is used for integrating all of the averaged
c multipath delay profiles
c Specifically, Use this program (pulsepoint.ex) to compute
c a point impulse response with a spacing of 7.8125 ns between impulses.
c This was selected becuz it is the rms duration of our sounding pulse
c and also because it divides evenly into the deltat values for all of
c the data (i.e. 200,500,1000ns full scale at 128 points per scale)
c we place the first impulse at ndelt/2 (or at 3.9 ns)
c Use this program to produce files with the word ".point" appended
c to the filename of data from ALLP.avg directory. Use program in PP direc.

c The output is placed in PP directory (here)
c
c
        character*5 actname*10,lname*7,sname,clutpath,path,descrip*60,area*25
        character lilname*9,actoutfile*25,liloutfile*24
        real dist,pwr,atten,delt,ymult,vzr,d(128)
        real sumbin
        integer i,j,npts,lilset,n,halt

        min=1.0
        write(*,*)"Enter pulse.avg fname that is to be integrated into point dat
        read (*,'(a10)') actname
        write(*,*)"We read in the character string:",actname

c       if actname has all 11 nonblank, then lilset=0
        lilset=0
        if ( actname(10:) .eq. ' ' ) then
            lilset=1
            lilname= actname(1:9)
        endif

        if (lilset .eq. 0) then
            open(unit=7,file=actname)
        else
            open(unit=7,file=lilname)
        endif

        read(7,*)lname
        if ( lname(7:) .eq. ' ' ) then
            inset=1
            sname= lname(1:5)
        endif
        read(7,'(A25)')area
        read(7,*)clutpath
        read(7,'(A60)')descrip
        read(7,*)dist
        read(7,*)path

```

```

        read(7,*)pwr
c This is actual transmitter from old X.st directory...
        read(7,*)atten
        read(7,*)npts
c xincr is a key!
        read(7,*)delt
        write(*,*)"read in delt=",delt
        read(7,*)vzr
        read(7,*)ymult
c scale data with ymult, thus all data has equal profile
        read(7,*)rmsdelay
        read(7,*)pwrgain
        read(7,*)avgt1
        read(7,*)avgt2

        if (lilset .eq. 1) then
        liloutfile='../PP/'//lilname//'.point'
        open (unit=8,file=liloutfile)
        else
        actoutfile='../PP/'//actname//'.point'
        open (unit=8,file=actoutfile)
        endif

c get the data from the .avg file
do 6 i=1,128
read(7,*) d(i)
d(i)=d(i)/(ymult)
6 continue
n=nint(0.000001000/(128*delt) )
write(*,*)"getting value of n=",n
do 10 i=1,128
    if (halt .ne. 10) then
        sumbin=0
        do 15 j=1,n
            sumbin=sumbin+( d(j+n*(i-1)) )
15 continue
        else
        sumbin=0
        goto 12
        endif
        if((n*i +1) .ge. 128 ) then
            halt=10
        else
12 write(8,*) n*i*delt-(n*delt/2.), sumbin/n
            write (*,*)n*i*delt-(n*delt/2.), sumbin/n
        endif
10 continue

        rewind(8)
        close(8)

        end
ricianlin.f
c This program allows user to specify the K ratio (in dB)
c and the program numerically integrates a rician density function.
c This is similar to Bultitude's in that  $A=1$ ,  $k=2\sigma^2/A^2$ .
c  $K=kdb/10$  is  $= 10 \log_{10}(k)$ 
c This is standard riemann numerical integration
c USED FOR LOOKING AT PULSE AMPLITUDES
        character dbplotname*10
        real meansq
        real rice2
        real x,rect,cdf,kdb,k2,delt ,medianval,v
        integer i
        write(*,*)"Rician CDF program, Enter K (minus dB value):"
        read (*,*)kdb

```

```

x=0
delt=0.0025
cdf=0
rect=0
k2=(10.**(kdh/10.) )
write(*,*)"The value for k2 (power)= 2sigma**2/A**2 is",k2
do 1 i=1,1000
x=i*delt
c evaluate mean square value at K value gien
call evaluatems(x,k2,rect,delt)
rect=rect*delt
cdf=cdf + rect
1
continue
meansq=cdf
write(*,*)"The mean square value for K=",k,meansq

c write the cdf value
write(*,*)"Recall value for K (power)= 2sigma**2/A**2 is",k2
write(*,*)"Please enter filename for saving db/cdf data for plot"
read(*,*)dbplotname
open(unit=7,file=dbplotname)
x=0
delt=0.0025
cdf=0
rect=0
do 2 i=1,2500
x=i*delt
call evaluate(x,k2,rice2,delt,meansq)
rect=rice2
c the rect output is the prob density of ak**2/ms
rect=rect*delt
cdf=cdf + rect
c multiply cdf by 100 for the grap.envdist plot routine
if (cdf .ge. 0.001 .and. cdf .le. 0.99999 ) then
if (mod(i,100) .eq. 1) then
c write out the prob ak2/ms > abscissa
write(7,*) x,-cdf*100. + 100.
write(*,*)x,100-cdf*100
endif
endif

2
continue
close(7)
end
c *****
subroutine evaluatems (xval,kval2,ricesq,delta)
real xval,mnbsi0,kval2,arg,riemann,delta,first,exponent,bessel
real ricesq
integer ier
c this subroutine evaluates riemann rectangle of rician distributin
c that is multiplied by x**2.....will be integrated to get msvalue
c forg K dB ratio of random power to specular power
c kval2 = 2sigma**2/A**2

ier=0
arg=xval/(kval2/2.)
first=arg
exponent=2.71828183**(-1.*((1.+xval**2)/(kval2)))
bessel=mnbsi0(1,arg,ier)
riemann=first*exponent*bessel
ricesq=riemann*xval**2
end
c *****
subroutine evaluate (xval,kval2,ricesq,delta,ms)
real xval,mnbsi0,kval2,arg,riemann,delta,first,exponent,bessel

```

```

        real ricesq,ms
        integer ier
c this subroutine evaluates riemann rectangle of rician distributin
c that is passed thru sq law detector
c having K dB ratio of random power to specular power
c kval2 = 2sigma**2/A**2
c perform transform  $y = (1/2 ms \sqrt{y}) f(\sqrt{y}/a)$ 

        ier=0
        xval=sqrt(xval/ms)
c so now xval is really sqrt of passed variable
        arg=xval/(kval2/2.)
        first=arg
        exponent=2.71828183**(-1.*((1.+xval**2)/(kval2)))
        bessel=mmbsi0(1,arg,ier)
        riemann=first*exponent*bessel
c now the returned value of riemann is 1/(2 sqrt(y)) fx(sqrt(y))
c so square again the value of xval to get original y
c use the pl29 papoulis... a=ms
        ricesq=riemann*(1/(2*xval*ms))
        xval=ms*xval**2
        end
c *****
pulseampfreqtable.f
c This program is used to break the 128 (or 1024 -1024 SS) data
c points into bins of 1/5 width for the purpose of analyzing
c the distributions of pulse power. The program
c assumes a  $ak^2/akmsval2$  of 0 to 5

character tjunk,ljunk*70
real median,rjunk,data(1024),binval
integer i,j,k,bincnt,npts
character lilname*10,actname*12
character actoutfile*28,liloutfile*26

write(*,*)
write(*,*)"Enter ALLPWR filename that is to be freq tabled"
read(*,'(a12)') actname
write(*,*)"We read in the character string:",actname
write(*,*)"Enter npts"
read(*,*)npts

c if actname has all 12 nonblank, then lilset=0
lilset=0
if (actname(11:).eq.' ') then
        lilset=1
        lilname=actname(1:10)
        write(*,*)"The lilname file is stored as",lilname
endif

c PROGRAM TO BE EXECUTED IN SSdist FILE DIRECTORY...MOVES HISTOGRAM
c TO THE DIRECTORY ../SSdist...with file name.freq
c actname is 12 character file name (i.e. eclac.d.st.1)
c lilname is 10 character file name (i.e. eblac.st.1)

if (lilset .eq. 0) then
open(unit=7,file=actname)
else
open(unit=7,file=lilname)
endif

do 999 i=1,npts
read(7,*)data(i)
999 continue

```



```

c open the destination.freq file in PP

    if (lilset .eq. 0) then
    actoutfile='D.'//actname//'.freq'
    open(unit=8,file=actoutfile)
    else
    liloutfile='D.'//lilname//'.freq'
    open(unit=8,file=liloutfile)
    endif

c now scan the data looking for points in the 1/4dB bins

c now open the output file
c bincnt is 0 at first, keep frequency of distribution
    do 12 i=1,17
    bincnt=0.
    binval=i/4.
    do 13 j=1,npts
c      we have the data in array
        if (j .eq. 633) then
    write(*,*)"at j=633, data,binval=",data(j),binval
        endif
        if ((data(j) .lt. binval) .and. (data(j) .ge. binval-0.25)) then
            bincnt=bincnt+1
        endif
    13      continue
    write(8,*)binval,bincnt
    12      continue
    rewind (8)
    close (8)
    end
pulseampdistrib.f
c This program is used to break the 17 or so bins having
c frequency bins of 1/4 width into cumulative probability
c data for the iid distributions of pulse amps. The program
c assumes dynamic range of 0 to 5 of ak2/ak2msval

    real atten,binpercent
    integer i,npts,k
    real bincnt
    character lilname*15,actname*17
    character actoutfile*22,liloutfile*20

    write(*,*)"Enter cumulative file that is to be integrated"
    read (*,'(a17)') actname
    write(*,*)"We read in the character string:",actname

c    if actname has all 17 nonblank, then lilset=0
    lilset=0
    if ( actname(16:) .eq. ' ' ) then
        lilset=1
        lilname= actname(1:15)
        write(*,*)"The lilname file is stored as",lilname
    endif

c PROGRAM TO BE EXECUTED IN PP DIRECTORY...integrates file
c CONTAINING A FREQTABLE
c TO GET cumulative percent probability
    npts=0
    k=0
c npts is total # of data points in input file
c actname is 17 character file name (i.e. eclac.d.st.1)

```

```

c      lilname is 15 character file name (i.e. eblac.st.1)

      if (lilset .eq. 0) then
      open(unit=7,file=actname)
      do 2 i=1,17
      read(7,*)atten,bincnt
      npts=npts+bincnt
2      continue
      rewind(7)
      close(7)
      open(unit=7,file=actname)
      else
      open(unit=7,file=lilname)
      do 3 i=1,17
      read(7,*)atten,bincnt
      npts=npts+bincnt
3      continue
      rewind(7)
      close(7)
      open(unit=7,file=lilname)
      endif

c npts has the total # of data pts
      write(*,*)"input file has",npts,"datapoints"
c      now read in the values of atten and the count
c      use a 5 to 1 ratio

c open the destination.hist file in DIST.actname.freq

      if (lilset .eq. 0) then
      actoutfile='PROB.'//actname
      open(unit=8,file=actoutfile)
      else
      liloutfile='PROB.'//lilname
      open(unit=8,file=liloutfile)
      endif

c now open the output file
c bincnt is 0 at first, keep aggregate % of distribution in binpercent
      binpercent=0.
      bincnt=0
      atten=0
      do 12 i=1,17
      read(7,*)atten,bincnt
      binpercent=(1./npts)*bincnt+binpercent
      if (k .eq. 1) then
      goto 89
      endif
      if (binpercent .ge. 0.000001) then
      write(8,*)atten,1-binpercent
      endif
89      if (binpercent .ge. 0.999999) then
      k=1
      endif

12      continue
      rewind (7)
      close (7)
      rewind (8)
      close (8)
      end

rician.f
c This program allows user to specify the K ratio (in dB)
c and the program numerically integrates a rician density function.

```

```

c This is similar to Bultitude's in that  $A=1$ ,  $k=2\sigma^2/A^2$ .
c  $K=kdb$  is  $= 10 \log_{10}(k)$ .... The output data is written to the screen
c and the median level (i.e. the value of  $x$  for 50% below) is also
c written to screen....This is standard riemann numerical integration
c Then, the data is scaled about the median value, and the  $x$  (db) vs  $y$  (cdf)
c is written to output file for plotting with rap

```

```

character dbplotname*10
real x,rect,cdf,kdb,k2,delt ,medianval,v
integer i
write(*,*)"Rician CDF program, Enter K (minus dB value):"
read (*,*)kdb
x=0
delt=0.0025
cdf=0
rect=0
k2=(10.**(kdb/10.) )
write(*,*)"The value for k2 (power)=  $2\sigma^2/A^2$  is",k2
do 1 i=1,1000
x=i*delt
call evaluate(x,k2,rect,delt)
rect=rect*delt
cdf=cdf + rect
if (cdf .ge. 0.0975 .and. cdf .le. .103) then
write(*,*)x,cdf
endif
if (cdf .ge. 0.198 .and. cdf .le. 0.201) then
write(*,*)x,cdf
endif
if (cdf .ge. 0.299 .and. cdf .le. 0.302) then
write(*,*)x,cdf
endif
if (cdf .ge. 0.495 .and. cdf .le. 0.502) then
write(*,*)"MEDIAN VALUE FOR K=",kdb," IS X=",x
medianval=x
endif
if (cdf .ge. 0.698 .and. cdf .le. 0.701) then
write(*,*)x,cdf
endif
if (cdf .ge. 0.795 .and. cdf .le. 0.803) then
write(*,*)x,cdf
endif
if (cdf .ge. 0.899 .and. cdf .le. 0.902) then
write(*,*)x,cdf
endif
if (cdf .ge. 0.99 .and. cdf .le. 0.991) then
write(*,*)x,cdf
endif
if (cdf .ge. 0.999 .and. cdf .le. 0.9991) then
write(*,*)x,cdf
endif
endif
1 continue

c Now the median is in the value medianval
c now rescale the data so that the x(db) val is written with
c the cdf value
if (medianval .ne. 0) then
write(*,*)
write(*,*)"Recall value for K (power)=  $2\sigma^2/A^2$  is",k2
write(*,*)"Please enter filename for saving db/cdf data for plot"
read(*,*)dbplotname
open(unit=7,file=dbplotname)
x=0
delt=0.0025
cdf=0
rect=0

```

```

do 2 i=1,2000
  x=i*delt
  call evaluate(x,k2,rect,delt)
  rect=rect*delt
  cdf=cdf + rect
  v=20*log10(x/medianval)
c multiply cdf by 100 for the grap.envdist plot routine
  if (cdf .le. .0011 .and. cdf .ge. .00099) then
    write(7,*)v,cdf*100.
  endif
  if (cdf .ge. 0.001 .and. cdf .le. 0.99999 .and. v .ge. -30.) then
    if (mod(i,10) .eq. 1) then
      write(7,*)v,cdf*100.
    endif
  endif
  endif
2 continue
endif
close(7)
end
c *****
subroutine evaluate (xval,kval2,riemann,delta)
  real xval,mmbisi0,kval2,arg,riemann,delta,first,exponent,bessel
  integer ier
c this subroutine evaluates riemann rectangle of rician distributin
c having K dB ratio of random power to specular power
c kval2 = 2sigma**2/A**2

  ier=0
  arg=xval/(kval2/2.)
  first=arg
  exponent=2.71828183*( -1.* ( (1.+xval**2)/(kval2) ) )
c  bessel= 1.+ ((arg**2)/4.)+ ((arg**4.)/64.) + ((arg**6)/2304.)
c  x + ((arg**8)/147456.) + ((arg**10)/(1024.*120.))
  bessel=mmbisi0(1,arg,ier)
  riemann=first*exponent*bessel
c used 4 terms of zero order bessel function of the first kind

  end
c *****
ssdistrib.f
c This program is used to break the 80 or so bins having
c frequency bins of 1/4 dB width into cumulative probability
c data for local distributions of envelope fading. The program
c assumes dynamic range of 20 dB (+10/- 10dB) about the median value

  real binpercent
  integer i,atten,npts,k
  real bincnt
  character lilname*15,actname*17
  character actoutfile*22,liloutfile*20

  write(*,*)"Enter cumulative file that is to be integrated"
  read (*,'(a17)') actname
  write(*,*)"We read in the character string:",actname

c  if actname has all 17 nonblank, then lilset=0
  lilset=0
  if ( actname(16:) .eq. ' ' ) then
    lilset=1
    lilname= actname(1:15)
    write(*,*)"The lilname file is stored as",lilname
  endif

c PROGRAM TO BE EXECUTED IN SSDIST DIRECTORY...integrates file

```

```

c CONTAINING A FREQTABLE
c TO GET cumulative percent probability
  npts=0
  k=0
c npts is total # of data points in input file
c actname is 17 character file name (i.e. eclac.d.st.1)
c lilname is 15 character file name (i.e. eblac.st.1)

  if (lilset .eq. 0) then
    open(unit=7,file=actname)
    do 2 i=-40,40
      read(7,*)atten,bincnt
      npts=npts+bincnt
2    continue
    rewind(7)
    close(7)
    open(unit=7,file=actname)
  else
    open(unit=7,file=lilname)
    do 3 i=-40,40
      read(7,*)atten,bincnt
      npts=npts+bincnt
3    continue
    rewind(7)
    close(7)
    open(unit=7,file=lilname)
  endif

c npts has the total # of data pts
  write(*,*)"input file has",npts,"datapoints"
c now read in the values of atten and the count
c use a 20 db dynamic fading range (conservative)

c open the destination.hist file in Data/SSdist

  if (lilset .eq. 0) then
    actoutfile='prob.'//actname
    open(unit=8,file=actoutfile)
  else
    liloutfile='prob.'//lilname
    open(unit=8,file=liloutfile)
  endif

c now open the output file
c bincnt is 0 at first, keep aggregate % of distribution in binpercent
  binpercent=0.
  bincnt=0
  atten=0
  do 12 i=-40,40
    read(7,*)atten,bincnt
    binpercent=(1./npts)*bincnt+binpercent
    if (k .eq. 1) then
      goto 89
    endif
    if (binpercent .ge. 0.000001) then
      write(8,*)atten,binpercent
    endif
89  if (binpercent .ge. 0.999999) then
    k=1
  endif

12  continue
    rewind (7)
    close (7)

```

```

        rewind (8)
        close (8)
    end
ssfrequable.f
c   This program is used to break the 128 (or 1024 -2048 SS) data
c   points into bins of 1/4 dB width for the purpose of analyzing
c   the local distributions of envelope fading. The program
c   assumes a dynamic range of +10/- 10dB about the median value

character tjunk,ljunk*70
real median,rjunk,data(2048),binval
integer i,j,k,bincnt
character lilname*10,actname*12
character actoutfile*28,liloutfile*26

write(*,*)
write(*,*)"Enter envelope filename that is to be freq tabled"
read (*,'(a12)') actname
write(*,*)"We read in the character string:",actname

c   if actname has all 12 nonblank, then lilset=0
    lilset=0
    if ( actname(11:) .eq. ' ' ) then
        lilset=1
        lilname= actname(1:10)
        write(*,*)"The lilname file is stored as",lilname
    endif

c PROGRAM TO BE EXECUTED IN SSdist FILE DIRECTORY...MOVES HISTOGRAM
c TO THE DIRECTORY ../SSdist...with file name.freq
c   actname is 12 character file name (i.e. eclac.d.st.1)
c   lilname is 10 character file name (i.e. eblac.st.1)

    if (lilset .eq. 0) then
        open(unit=7,file=actname)
    else
        open(unit=7,file=lilname)
    endif

    do 999 i=1,2048
999   read(7,*)data(i)
        continue

c open the destination.freq file in Data/Envdist

    if (lilset .eq. 0) then
        actoutfile='../SSdist/'//actname//'.freq'
        open(unit=8,file=actoutfile)
    else
        liloutfile='../SSdist/'//lilname//'.freq'
        open(unit=8,file=liloutfile)
    endif

c now scan the data looking for points in the 1/4dB bins

c now open the output file
c bincnt is 0 at first, keep frequency of distribution
    do 12 i=-40,40
        bincnt=0.
        binval=i/4.
        do 13 j=1,2048
c   we have the data in array
            if ((data(j) .lt. binval) .and. (data(j) .ge. binval-0.25)) then

```

```

                bincnt=bincnt+1
            endif
13         continue
            write(8,*)binval,bincnt
12         continue
            rewind (8)
            close (8)
            end
strip.directory

#!/bin/sh
# This shell script prgm allows files to be printed
# and then plotted on line printer for inspection

echo -n "Enter Directory under Data containing data (include .st): "
read dir
echo -n "~Data/$dir is to be stripped , Press n to cancel: "
read input
if [ $input -eq "n" ]
then
    echo "strip not performed"
    exit 0
fi
    cd $dir
#!/ NOW IN THE CHOSEN STRIPPED DATA DIRECTORY
for i in p*
do
    echo $i | ../a.out
done
exit 0
strip.env.directory

#!/bin/sh
# This shell script prgm allows entire directory of files to be operated
# upon with the envstrip.f program for coputation of median,mean signal

echo -n "Enter Directory under Data containing data (include .st): "
read dir
echo -n "~Data/$dir (e*) is to be stripped , Press n to cancel: "
read input
if [ $input -eq "n" ]
then
    echo "strip not performed"
    exit 0
fi
echo -n "The file envstrip.f contains output target directory"
    cd /a/n9nb/Data/$dir
#!/ NOW IN THE CHOSEN STRIPPED DATA DIRECTORY
f77. ../Programs/envstrip.f -limslsp
mv a.out ../Programs
for i in e*
do
#!/ The a.out file from envstrip.f contains the output target directory
    echo $i | ../Programs/a.out
done
exit 0
strip.pulse.directory

#!/bin/sh
# This shell script prgm allows pulse files to be stripped
# for noise floor and path loss calculation

echo -n "Enter Directory under Data containing data (include .st): "
read dir
echo -n "~Data/$dir (p* ) is to be stripped , Press n to cancel: "
read input

```

```

if [ $input -eq "n" ]
then
    echo "strip not performed"
    exit 0
fi
    cd /a/n9nb/Data/$dir
#/ NOW IN THE CHOSEN STRIPPED DATA DIRECTORY
# f77. ../Programs/pulstrip.f
# mv a.out ../Programs
for i in p*
do
#/ a.out file is located in Data/Programs directory from "pulstrip.X.f"
#/ The pulstrip.X.f contains output target directory
    echo $i | ../Programs/pulstrip.ex
done
echo -n "Be sure now to go back and fix destination of pulstrip.f"
exit 0
strip.sweep.directory

#!/bin/sh
# This shell script prgm allows entire directory of files to be operated
# upon with the sweepstrip.f program for coputation of median,mean signal

echo -n "Enter Directory under Data containing data (include .st): "
read dir
echo -n "~Data/$dir (s*) is to be stripped , Press n to cancel: "
read input
if [ $input -eq "n" ]
then
    echo "strip not performed"
    exit 0
fi
echo -n "The file sweepstrip.f contains output target directory"
    cd /a/n9nb/Data/$dir
#/ NOW IN THE CHOSEN STRIPPED DATA DIRECTORY
f77. ../Programs/sweepstrip.f -limslsp
mv a.out ../Programs
for i in s*
do
#/ The a.out file from sweepstrip.f contains the output target directory
    echo $i | ../Programs/a.out
done
exit 0
sweepstrip.f
c      This is      sweepstrip.f

c Use -limslsp after f77. fname for the IMSL library
c This program used for processing some of the early data
c not used often except for the singlesweep 1024 pt measurements
c over long intervals (100 seconds)
c Use this program with strip.sweep.directory.....
c
c This program is used for computing mean signal level of envelope
c data. The data is scanned for filename, path distance,pwr,atten
c and max and min fading level. The exponential loss factor, the
c avg signal received signal and max and min fading levels is returned.
c The programuses the receiver law-- Pr(dbm) = Vif * 760dB/V - 125 db
c      The final output
c      is written into the directory B.st.new/FILENAME
c
c
c
character*5 actname*12,lname*7,sname,clutpath,path,descrip*60,area*25
character lilname*10,actoutfile*26,liloutfile*24
real dist,pwr,atten,xincr,ymult,vzr,d(1024),dsort(1024)
real rmsdelay,pwrgain,avgt1,avgt2,min,max,minrcvpwr,maxrcvpwr
real rcvpwrmedian

```



```

integer i,npts,lilset

c  actname is 12 character file name (i.e. eclac.d.st.1)
c  lilname is 10 character file name (i.e. eblac.st.1)
c  lname is first line in file with seven letters (i.e. eclac.d)
c  sname (short) is first line in file with five letters (i.e eblac)
   min=1.0
   max=0.
c The data is in mV and never is greater than 200 mV
   write(*,*)"Enter envelope filename that is to be processed"
   read (*,'(a12)') actname
   write(*,*)"We read in the character string:",actname

c   if actname has all 12 nonblank, then lilset=0
   lilset=0
   if ( actname(11:) .eq. ' ' ) then
       lilset=1
       lilname= actname(1:10)
       write(*,*)"The lilname file is stored as",lilname
   endif

   if (lilset .eq. 0) then
       open(unit=7,file=actname)
   else
       open(unit=7,file=lilname)
   endif

   read(7,*)lname
   if ( lname(7:) .eq. ' ' ) then
       inset=1
       sname= lname(1:5)
       write(*,*)"The short name in file is",lname
   endif
   read(7,'(A25)')area
   read(7,*)clutpath
   read(7,'(A60)')descrip
   read(7,*) dist
   read(7,*)path
   read(7,*)pwr
   read(7,*)atten
   read(7,*)npts
   read(7,*)xincr
   read(7,*)vzr
   read(7,*)ymult
   read(7,*)rmsdelay
   read(7,*)pwrgain
   read(7,*)avgt1
   read(7,*)avgt2

c Now read in the 1024 lines of raw data, and obtain minimum value in set
   do 10 i=1,npts
       read(7,*)d(i)
       dsort(i)=d(i)
       if (d(i) .lt. min) then
           min=d(i)
       endif
       if (d(i) .gt. max) then
           max=d(i)
       endif
10  continue

c Now compute the average rcv sig, pwr gain and the decay exponent
   rcvpwr=0.
   loss=0.

```

```

c Now pwr gain put into dBm readings of the received pwr
do 45 i=1,npts
  rcvpwr= rcvpwr +d(i)*760. - 125.
45 continue
  avgrcvpwr=rcvpwr/npts
  maxrcvpwr=max*760. - 125.
  minrcvpwr=min*760. - 125.
  call vsrta(dsort,npts)
  rcvpwrmedian=dsort(npts/2)*760. -125.
  write(*,*) "the avg db received value=",avgrcvpwr
  write(*,*) "The median db value is", rcvpwrmedian
  write(*,*)"Signal has dynamic range of (dB)",maxrcvpwr-minrcvpwr
c Now compute path loss, exponential decay relative to 10 wavelenght

  relpwrtten=pwr-atten-rcvpwrmedian-38.3
  write(*,*) "The path loss is (dB) ",relpwrtten
  dist=dist*12./39.37
  write(*,*)"Over path having distance (m) ",dist
c relpwrtten is now in

  if (lilset .eq. 1) then
    liloutfile='../B.st.new/'//lilname
    open (unit=8,file=liloutfile)
  else
    actoutfile='../B.st.new/'//actname
    open (unit=8,file=actoutfile)
  endif

c Output file contains distance (m) on line 5
c pathloss on line 7, median rcv pwr on line 13
c min and max levels on lines 14,15, dynamic fading range on 16
c The output data is given in dB relative to median

  if (inset .eq. 1) then
    write(8,'(A5)') sname
  else
    write(8,'(A7)') lname
  endif

  write(8,'(A25)')area
  write(8,'(A5)')clutpath
  write(8,'(A80)')descrip
  write(8,*) dist
  write(8,'(A5)')path
  write(8,*)relpwrtten
  write(8,*)atten
  write(8,*)npts
  write(8,*)xincr
  write(8,*)vzr
  write(8,*)ymult
  write(8,*)rcvpwrmedian
  write(8,*)minrcvpwr
  write(8,*) maxrcvpwr
  write(8,*)maxrcvpwr-minrcvpwr

c the received data samples normalized to median signal
do 50 i=1,npts
  write(8,*)d(i)*760. -125. -rcvpwrmedian
50 continue

  close (8)
  close (7)
end

```

STRIPTEK C LANG PROGRAM.. USED TO FORMAT RAW DATA INTO ASCII FILES ON ED  
Raja Kadiyala's Makefile program

```

AWK= /bin/awk
TOUCH= touch -cf
DESTDIR=
DESTMACH=
PROFILE=
CFLAGS= -O
LDFLAGS= -O
CTAGS= /usr/ucb/ctags -w
LIBS= -lm
OBJECTS=strip_auto.o find.o getword.o search.o getw.o itoa.o reverse.o

```

```

striptek.auto: $(OBJECTS)
        cc $(LDFLAGS) -o striptek.auto $(OBJECTS) $(LIBS)

```

```

find.o: getword.c

```

```

getword.o:

```

```

itoa.o: reverse.c

```

```

search.o: getw.c

```

```

Raja's find.c routine

```

```

/* routine to find a string (str) in a file (fp) */
/* returns 0 if the word has been found */

```

```

#include <strings.h>; /* include string lib */
#include <stdio.h>; /* include i/o lib */
#define MAXWORD 384 /* Maximum word length */

```

```

find(fp, str)
char str[MAXWORD];
FILE *fp;
{

```

```

    char tmp[MAXWORD];

```

```

    getword(fp, tmp);
    return(strcmp(str, tmp));
}

```

```

Raja's getw.c routine

```

```

/* searches for next word in the stream fp and returns the */
/* strcmp of st and the next word */

```

```

#include <strings.h>; /* include string lib */
#include <stdio.h>; /* include i/o lib */
#define EOLN '\n' /* End of line character */
#define TAB '\t' /* Tab character */
#define MAXWORD 384 /* Maximum word length */

```

```

getw(fp, st)

```

```

    FILE *fp;
    char st[MAXWORD];

```

```

{
    int c=0, i=0;
    char tmp[MAXWORD];

```

```

    while (((c=getc(fp))!=EOF) && ((c==TAB) || (c==EOLN) || (c==' ') || (c==',')) |
        ; /* Get rid of white space */

```

```

    if (c == EOF)
        return(c);

```

```

    tmp[i++] = c;
    while (((c=getc(fp))!=EOF) && !((c==TAB) || (c==EOLN) || (c==' ') || (c==','))
        tmp[i++] = c;

```

```

    tmp[i] = '\0';

```

```

    if (c == EOF)

```

```

    return(c);

    strcpy(st,tmp);
    return(l);
}
Raja's getword.c routine
/* same as getw.c put does not exit if at EOF */

#include <strings.h>;          /* include string lib */
#include <stdio.h>;           /* include i/o lib */
#define EOLN '\n'             /* End of line character */
#define TAB '\t'              /* Tab character */
#define MAXWORD 384           /* Maximum word length */

getword(fp,st)
FILE *fp;
char st[MAXWORD];
{
    int c=0,i=0;
    char tmp[MAXWORD];

    while (((c=getc(fp))!=EOF) && ((c==TAB) || (c==EOLN) || (c==' ') || (c==',')))
        ; /* Get rid of white space */

    if (c == EOF)
    {
        printf("Bad input data -- quit \n\n");
        exit(3);
    }

    tmp[i++] = c;
    while (((c=getc(fp))!=EOF) && !((c==TAB) || (c==EOLN) || (c==' ') || (c==',')))
        tmp[i++] = c;

    tmp[i] = '\0';
    if (c == EOF)
    {
        printf("Bad input data -- quit \n\n");
        exit(3);
    }

    strcpy(st,tmp);
    return(l);
}
Raja's itoa.c routine
/* converts integer s to the string n */

#include <strings.h>;          /* include string lib */
#include <stdio.h>;           /* include i/o lib */

itoa(n,s)
int n;
char s[];
{
    int i=0,sign;

    if ((sign = n) < 0)
        n = -n;

    do {
        s[i++] = n % 10 + '0';
    } while ((n /= 10) > 0);

    if (sign < 0)
        s[i++] = '-';
    s[i] = '\0';
}

```



```

char
    flnm[MAXLEN],          /* input filename          */
    oflnm[MAXLEN],        /* output filename         */
    tmps[MAXLEN],         /* temporary string space  */
    tmps2[MAXLEN],        /* temporary string space  */
    header[800];          /* header information      */

double
    tmpfl,                /* temporary float         */
    xincr,                /* XINCR                  */
    yzero,                /* YZERO                  */
    ymult,                /* YMULT                  */
    data[MAXPTS],         /* data points            */
    pwrq,                 /* power gain             */
    rmsd,                 /* rms delay              */
    avg1,                 /* AVGT1                  */
    avg2,                 /* AVGT2                  */
    fabs();               /* absolute value for floats */

FILE
    *fp1,                 /* file pointer for input file */
    *fp2,                 /* file pointer for output file */
    *fp3;                 /* file pointer to scan input */

if (argc != 2)           /* check to see if number of
    {                       /* command line arguments is
        if (argc >= 3)     /* correct
            printf("Too many input files named\n");
        else
            printf("No input file given\n");

        printf("Usage -- %s infile \n",argv[0]);
        exit(1);
    }

    if ((fp1 = fopen(argv[1],"r")) == NULL) /* open input
        {                                     /* file
            printf("%s: can't open %s\n",argv[0],argv[1]);
            exit(2);
        }

    strcpy(flnm,argv[1]); /* copy input filename
                          /* into string

    fscanf(fp1,"%s",oflnm); /* create output
    strcpy(header,oflnm); /* file & store in header
    strcat(header,"\n");

    strcat(oflnm,".st"); /* tack on ".st"

    while ((c = getc(fp1)) != EOLN) /* trash rest of line
        ;

    for (i=0;i<7;i++) /* get rest of header info
        {
            fscanf(fp1,"%[^\\n]",tmps);
            strcat(header,tmps);
            strcat(header,"\n");
            c = getc(fp1);
        }

    if ((fp3 = fopen(argv[1],"r")) == NULL) /* open input
        {                                     /* for scan

```

```

        printf("%s: can't open %s\n",argv[0],argv[1]);
        exit(2);
    }

    numb = search(fp3,"CURVE");          /* scan for search      */
    fclose(fp3);

    if (!(numb))
    {
        printf("\nNo blocks of data within %s -- quit\n",flnm);
        exit(1);
    }
    else
    if (!(numb-1))
    {
        printf("\n%d block of data within \"%s\"\n",numb,flnm);
        printf("Creating individual file %s.l\n\n",oflnm);
    }
    else
    {
        printf("\n%d blocks of data within \"%s\"\n",numb,flnm);
        printf("Creating individual files %s.l through %s.%d\n\n",oflnm,oflnm,numb);
    }

    for (i=0;i<numb;i++)                /* loop to process info    */
    {
        strcpy(tmps,oflnm);              /* create output filename  */
        itoa(i+1,tmps2);
        strcat(tmps,".");
        strcat(tmps,tmps2);

        if ((fp2=fopen(tmps,"w")) == NULL) /* open output            */
        {
            printf("Can not open %s\n",tmps);
            exit(-1);
        }
        fprintf(fp2,"%s",header);         /* tack on header         */

        while (find(fp1,"NR.PT"))         /* get NR.PT              */
        {
            fscanf(fp1,"%e",&tmp1);
            nr = tmp1;
            fprintf(fp2,"%d\n",nr);
        }

        while (find(fp1,"XINCR"))         /* get XINCR              */
        {
            fscanf(fp1,"%f",&xincr);
            fprintf(fp2,"%e\n",xincr);
        }

        while (find(fp1,"YZERO"))         /* get YZERO              */
        {
            fscanf(fp1,"%f",&yzero);
        }

        while (find(fp1,"YMULT"))         /* get YMULT              */
        {
            fscanf(fp1,"%f",&ymult);
        }

        /* check to see if 0              */
        if (((fabs(1.0*yzero)) < 1e-06) && (!(i)))
        {
            printf("%s: Warning YZERO is zero\n",argv[0]);
            printf("Enter value to multiply YMULT with, for new YZERO: ");
            scanf("%e",&tmp1);
            c = getchar();
            printf("\n");
        }
    }

```

```

    ]

    if ((fabs(1.0*yzero)) < 1e-06) /* adjust */
        yzero = tmp1*ymult;

    fprintf(fp2,"%f\n",yzero);
    fprintf(fp2,"%e\n",ymult);

    while (find(fp1,"CURVE")) /* search for curve data*/
        ;

    pwrq = 0.0;
    rmsd = 0.0;
    avq1 = 0.0;
    avq2 = 0.0;

    for (j=0;j<nr;j++) /* get and process data */
    {
        fscanf(fp1,"%f",&data[j]);
        c =getc(fp1);
        data[j] = data[j]*ymult + yzero;
        avq1 = (j+1)*xincr*data[j] + avq1;
        avq2 = (j+1)*(j+1)*xincr*xincr*data[j] + avq2;
        pwrq = data[j] + pwrq;
    }
    avq1 = avq1/pwrq;
    avq2 = avq2/pwrq;
    rmsd = (avq2 - avq1*avq1);

    if (rmsd < 0.0)
    {
        printf("%s: AVGT2 - AVGT1^2 is less than zero\n",argv[0]);
        printf("Starting execution over\n\n");
        fclose(fp1);
        fclose(fp2);
        strcpy(tmps,argv[0]);
        strcat(tmps,argv[1]);
        system(tmps);
        exit(0);
    }

    rmsd = sqrt(rmsd);

    fprintf(fp2,"%e\n",rmsd);
    fprintf(fp2,"%e\n",pwrq);
    fprintf(fp2,"%e\n",avq1);
    fprintf(fp2,"%e\n",avq2);

    for (j=0;j<nr;j++) /* output data */
        fprintf(fp2,"%e\n",data[j]);

    fclose(fp2);
}

fclose(fp1);
fclose(fp2);
} /* end main */

Raja's strip_auto.c routine
#include <stdio.h> /* standard i/o lib */
#include <strings.h> /* strings lib */
#include <math.h> /* math lib */
#define MAXLEN 80 /* Maximum string length*/
#define MAXPTS 2048 /* Maximum number of */
/* data pts per block */
#define EOLN '\n' /* End Of Line char */

```



```

main(argc,argv)
int argc;                /* number of command */
                          /* arguements */
char *argv[];           /* string of command */
                          /* arguements */

{
    /* begin main */

int
    i=0,                 /* counter variable */
    c,                  /* character variable */
    j,                  /* counter variable */
    ptest,              /* Pulse test - scope gnd ref */
    numb,               /* number of blocks in file */
    nr;                 /* number of pts in data block */

char
    flnm[MAXLEN],       /* input filename */
    oflnm[MAXLEN],     /* output filename */
    tmps[MAXLEN],       /* temporary string space */
    tmps2[MAXLEN],     /* temporary string space */
    header[800];       /* header information */

double
    tmp1,               /* temporary float */
    xincr,              /* XINCR */
    yzero,              /* YZERO */
    ymult,              /* YMULT */
    data[MAXPTS],      /* data points */
    pwr,                /* power gain */
    rmsd,               /* rms delay */
    av1,                /* AVGT1 */
    av2,                /* AVGT2 */
    fabs();             /* absolute value for floats */

FILE
    *fp1,               /* file pointer for input file */
    *fp2,               /* file pointer for output file */
    *fp3;               /* file pointer to scan input */
                          /* file */

    if (argc != 2)      /* check to see if number of */
    {                   /* command line arguements is */
        if (argc >= 3) /* correct */
            printf("Too many input files named\n");
        else
            printf("No input file given\n");

        printf("Usage -- %s infile \n",argv[0]);
        exit(1);
    }

    if ((fp1 = fopen(argv[1],"r")) == NULL) /* open input */
        /* file */
    {
        printf("%s: can't open %s\n",argv[0],argv[1]);
        exit(2);
    }

    strcpy(flnm,argv[1]); /* copy input filename */
                          /* into string */

    tmps[0] = flnm[0];
    tmps[1] = '\0';

```

```

ptest = strcmp(tmps,"p");

fscanf(fp1,"%s",oflnm);          /* create output */
strcpy(header,oflnm);          /* file & store in header */
strcat(header,"\n");

strcat(oflnm,".st");           /* tack on ".st" */

while ((c = getc(fp1)) != EOLN) /* trash rest of line */
;

for (i=0;i<7;i++)             /* get rest of header info */
{
    fscanf(fp1,"%[\n]",tmps);
    strcat(header,tmps);
    strcat(header,"\n");
    c = getc(fp1);
}

if ((fp3 = fopen(argv[1],"r")) == NULL) /* open input */
{                                       /* for scan */
    printf("%s: can't open %s\n",argv[0],argv[1]);
    exit(2);
}

numb = search(fp3,"CURVE");          /* scan for search */
fclose(fp3);

if (!(numb))
{
    printf("\nNo blocks of data within %s -- quit\n",flnm);
    exit(1);
}
else
if (!(numb-1))
{
    printf("\nid block of data within \"%s\"\n",numb,flnm);
    printf("Creating individual file %s.1\n\n",oflnm);
}
else
{
    printf("\nid blocks of data within \"%s\"\n",numb,flnm);
    printf("Creating individual files %s.1 through %s.%d\n\n",oflnm,oflnm,numb)
}

for (i=0;i<numb;i++)             /* loop to process info */
{
    strcpy(tmps,oflnm);          /* create output filename */
    itoa(i+1,tmps2);
    strcat(tmps,".");
    strcat(tmps,tmps2);

    if ((fp2=fopen(tmps,"w")) == NULL) /* open output */
    {
        printf("Can not open %s\n",tmps);
        exit(-1);
    }
    fprintf(fp2,"%s",header);     /* tack on header */

    while (find(fp1,"NR.PT"))     /* get NR.PT */
    ;
    fscanf(fp1,"%e",&tmp1);
    nr = tmp1;
    fprintf(fp2,"%d\n",nr);
}

```

```

while (find(fp1,"XINCR"))          /* get XINCR          */
    i
    fscanf(fp1,"%f",&xincr);
    fprintf(fp2,"%e\n",xincr);

while (find(fp1,"YZERO"))          /* get YZERO          */
    i
    fscanf(fp1,"%f",&yzero);

while (find(fp1,"YMULT"))          /* get YMULT          */
    i
    fscanf(fp1,"%f",&ymult);

/* check to see if 0          */
if ((fabs(1.0*yzero)) < 1e-06)     /* adjust          */
    {
        if (ptest)
            yzero = 3.85*ymult;     /* ptest = 1 env or ss */
        else
            yzero = 3.85*ymult;     /* ptest = 0 pulse     */
    }

fprintf(fp2,"%f\n",yzero);
fprintf(fp2,"%e\n",ymult);

while (find(fp1,"CURVE"))          /* search for curve data*/
    i

pwrq = 0.0;
rmsd = 0.0;
avg1 = 0.0;
avg2 = 0.0;

for (j=0;j<nr;j++)                /* get and process data */
    {
        fscanf(fp1,"%f",&data[j]);
        c =getc(fp1);
        data[j] = data[j]*ymult + yzero;
        avg1 = (j+1)*xincr*data[j] + avg1;
        avg2 = (j+1)*(j+1)*xincr*xincr*data[j] + avg2;
        pwrq = data[j] + pwrq;
    }
avg1 = avg1/pwrq;
avg2 = avg2/pwrq;
rmsd = (avg2 - avg1*avg1);

if (rmsd < 0.0)
    {
        printf("%s: AVGT2 - AVCT1^2 is less then zero\n",argv[0]);
        printf("Setting RMS Delay to zero\n\n");
        rmsd = 0.0;
    }

rmsd = sqrt(rmsd);

fprintf(fp2,"%e\n",rmsd);
fprintf(fp2,"%e\n",pwrq);
fprintf(fp2,"%e\n",avg1);
fprintf(fp2,"%e\n",avg2);

for (j=0;j<nr;j++)                /* output data          */
    fprintf(fp2,"%e\n",data[j]);

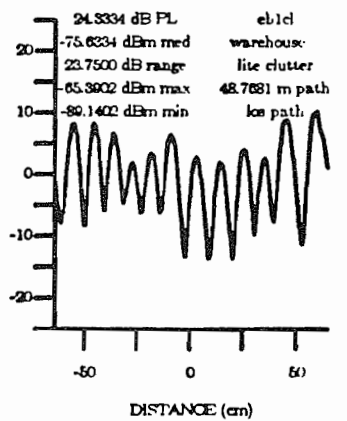
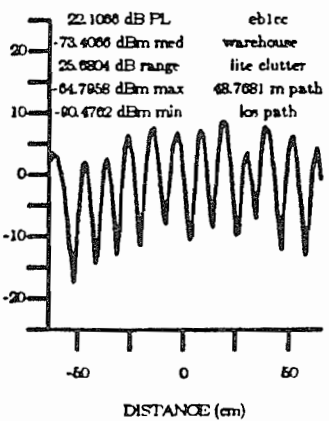
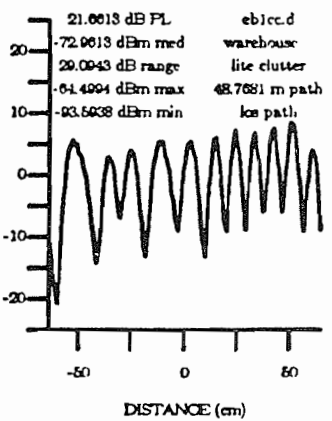
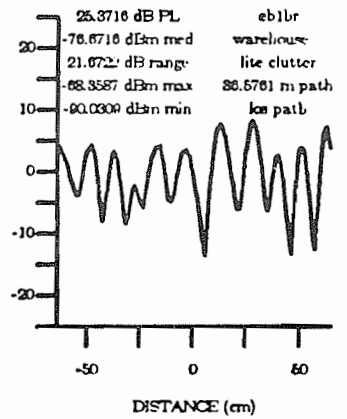
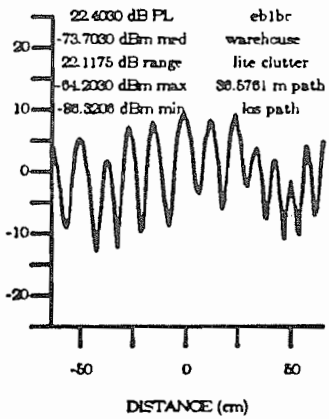
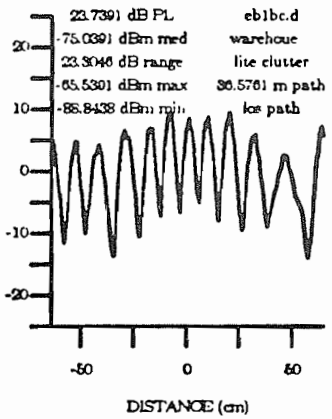
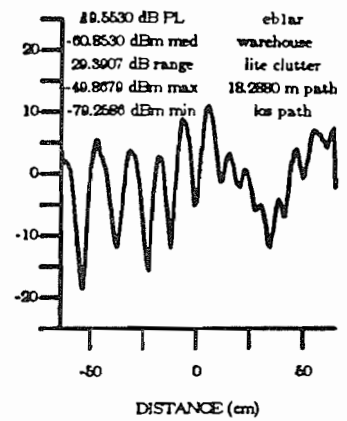
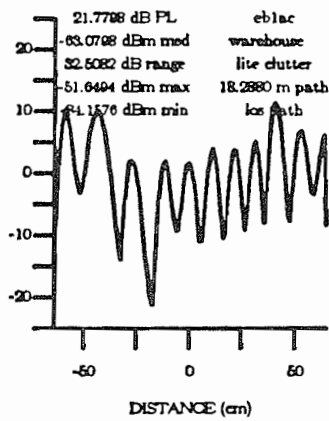
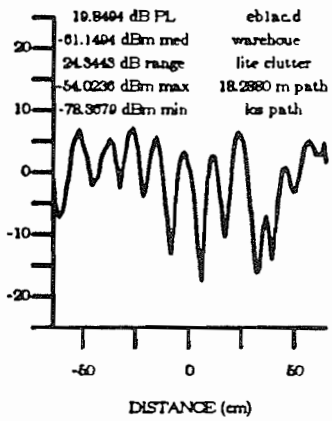
```

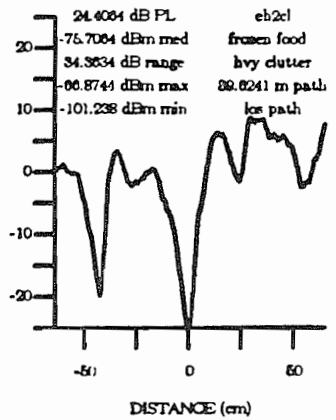
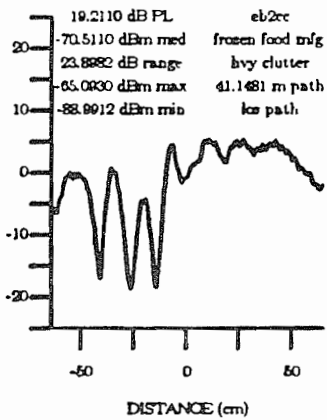
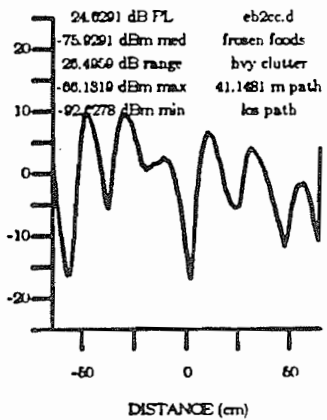
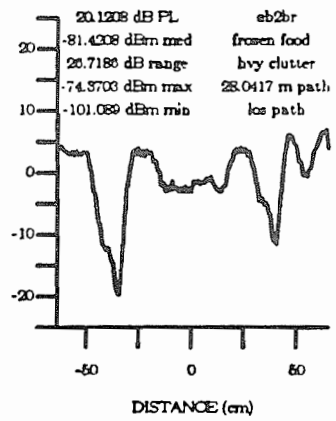
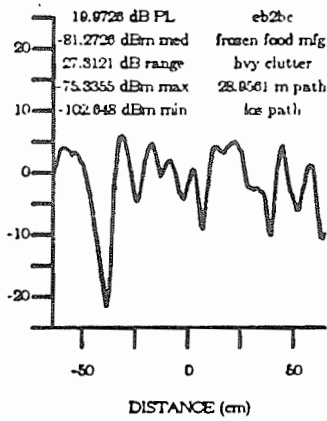
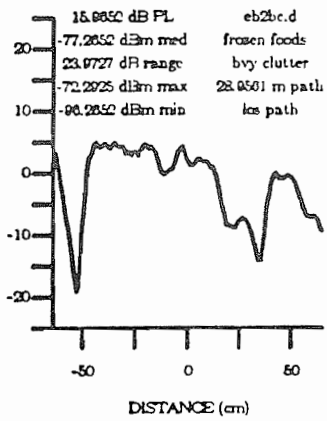
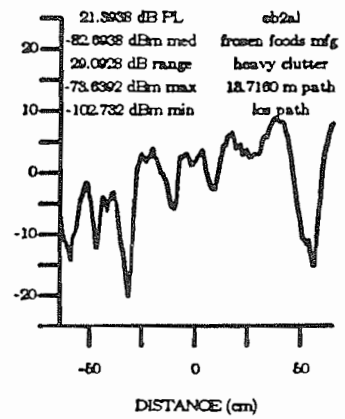
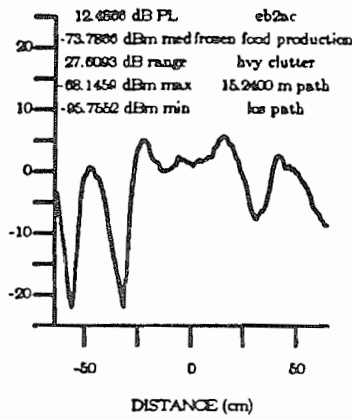
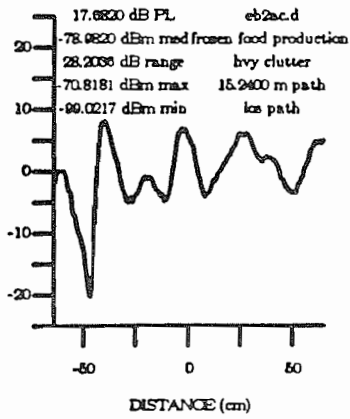
```
        fclose(fp2);
    }
    fclose(fp1);
    fclose(fp2);
}
.fi                                     /* end main */
```

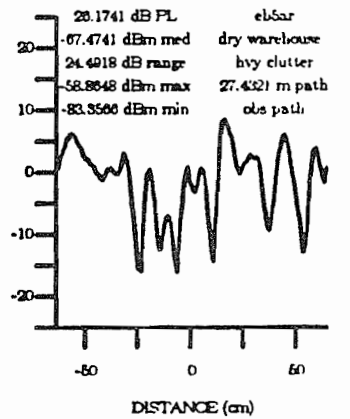
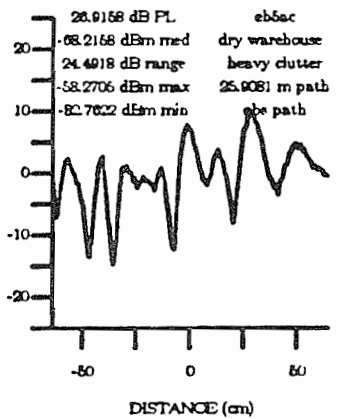
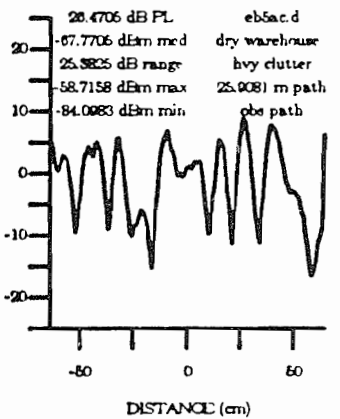
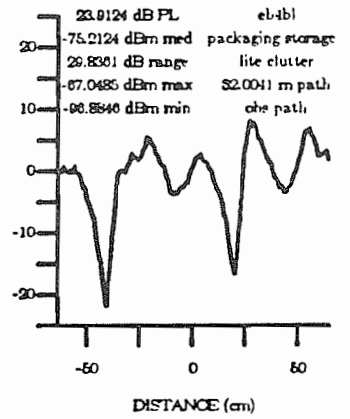
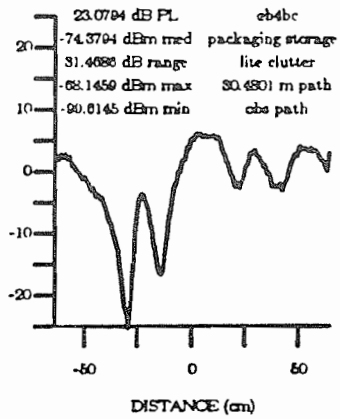
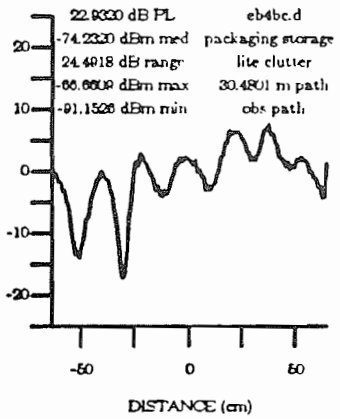
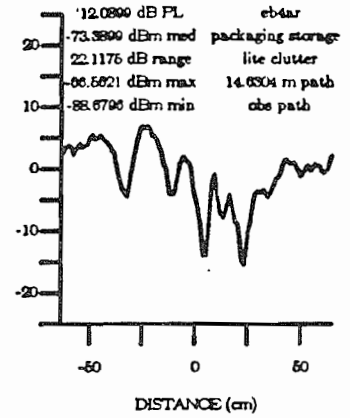
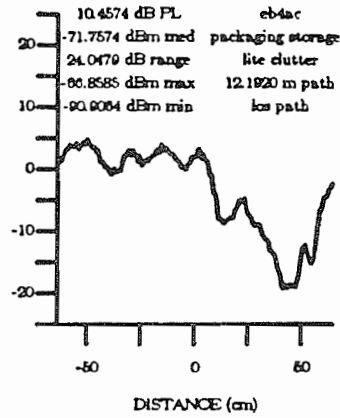
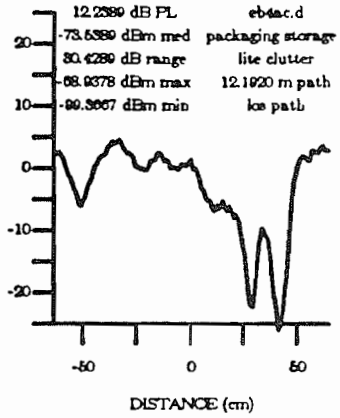
## Appendix C

### CW Envelope Measurements

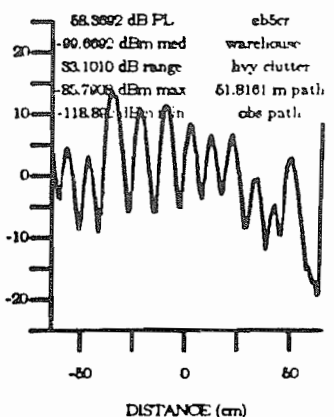
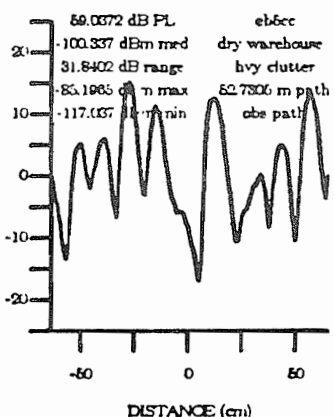
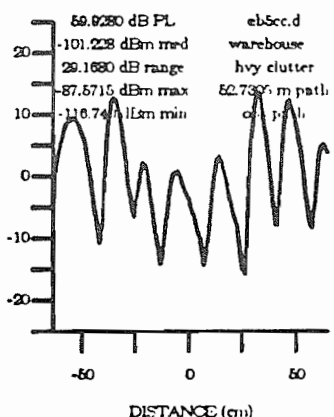
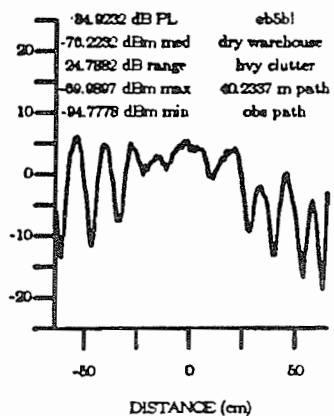
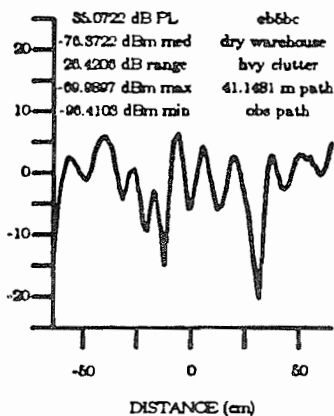
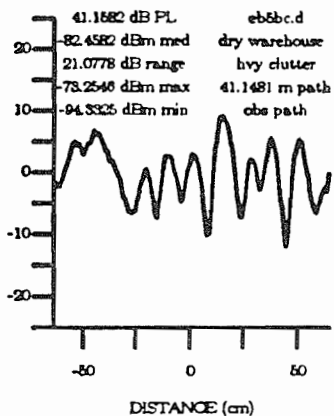
The following are raw data plots of all the CW envelope measurements made in 5 factories. The filename located in the upper right hand corner identifies the measurement location (see Figure 3.4). In the left corner of each plot, the following data is given from top to bottom: path loss, median value, dynamic fading range, maximum value, minimum value. In the upper right corner of each plot, the following data is given from top to bottom: filename, factory area, clutter conditions, T-R separation, LOS or obstructed path.

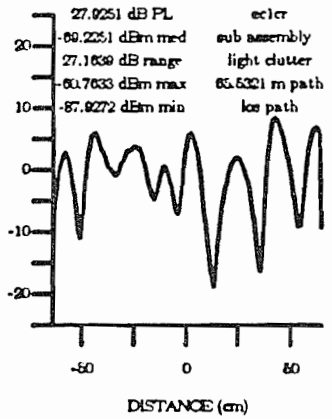
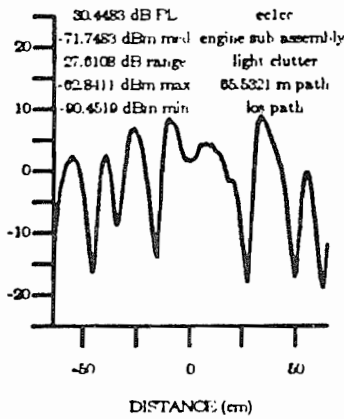
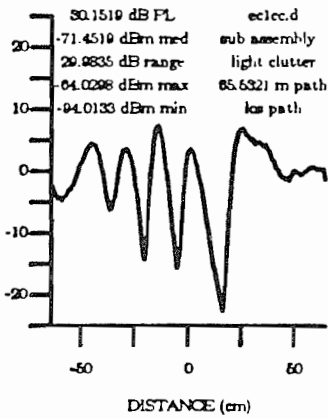
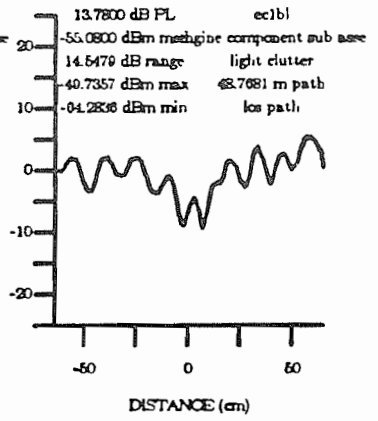
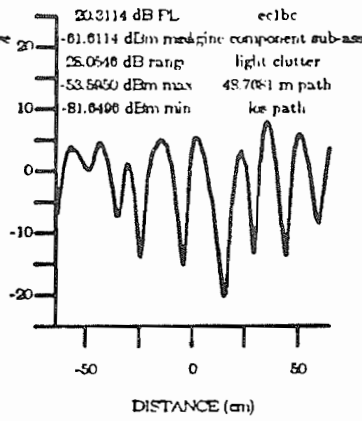
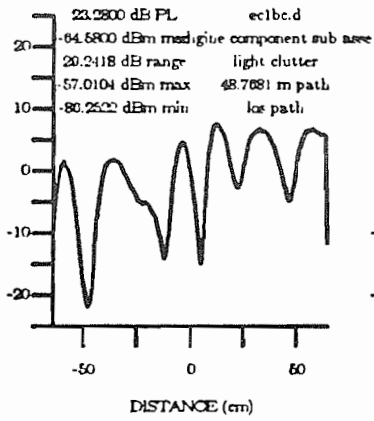
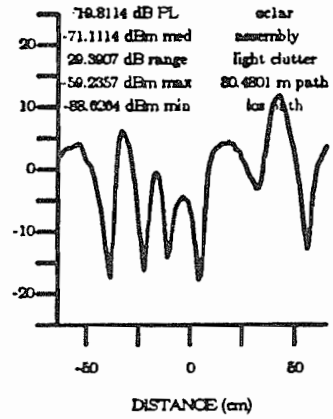
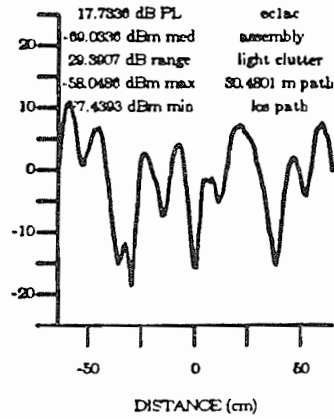
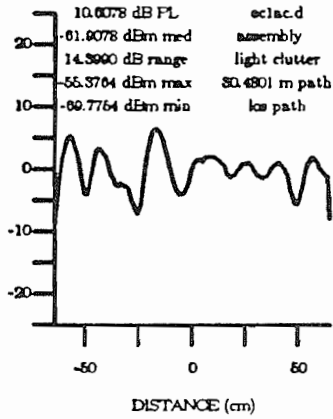


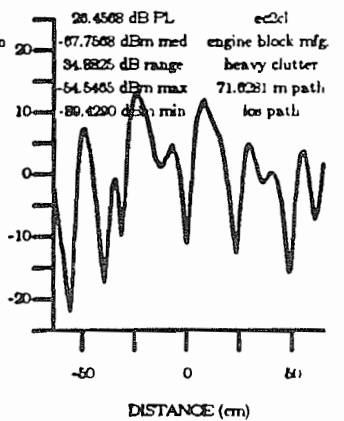
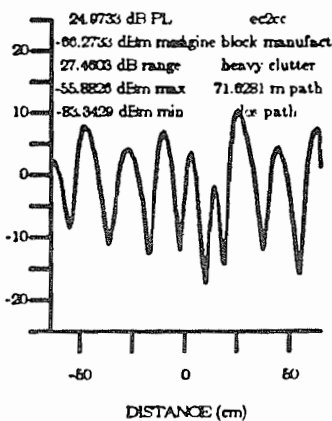
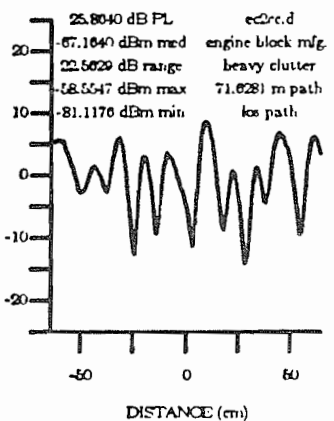
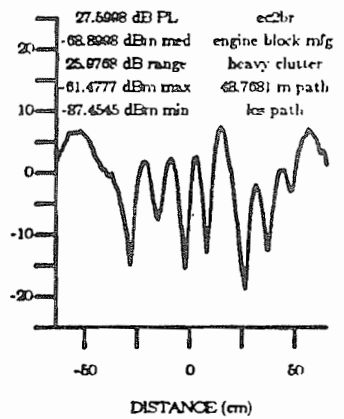
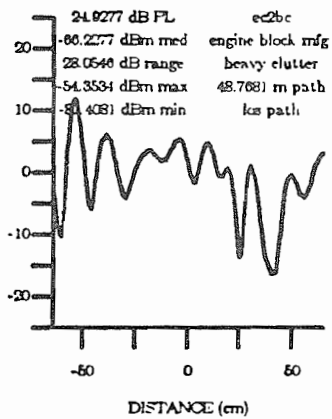
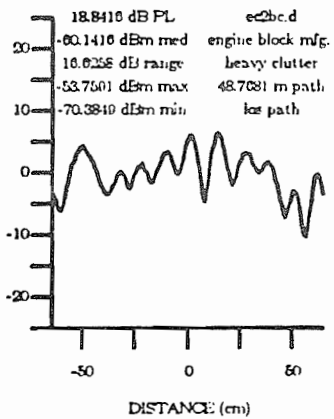
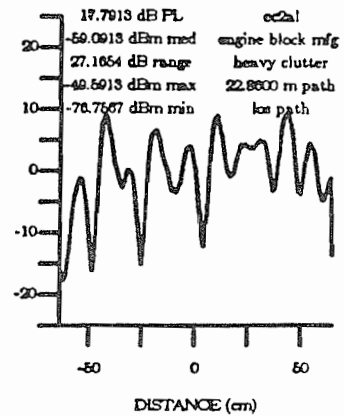
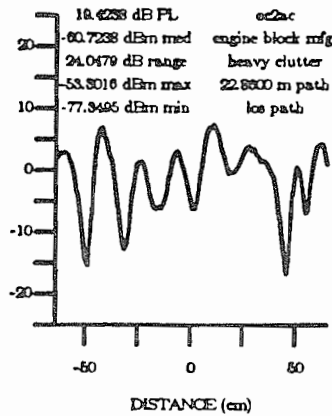
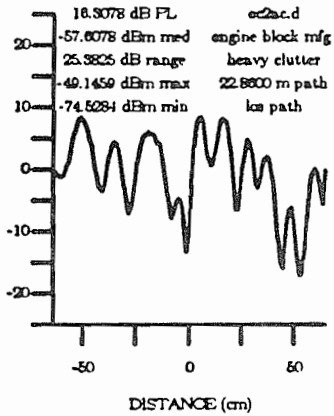


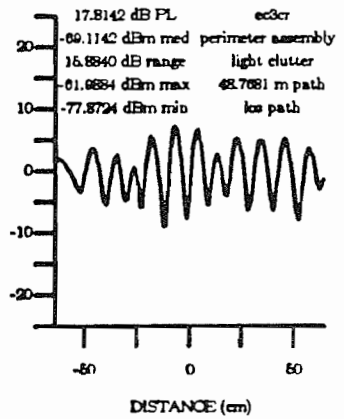
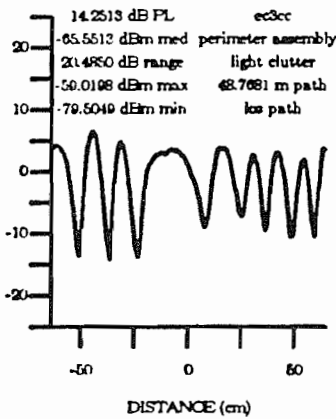
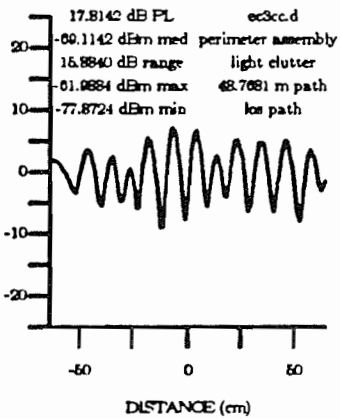
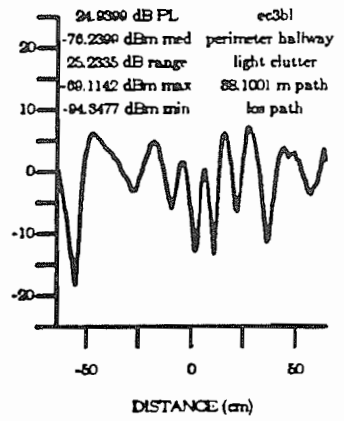
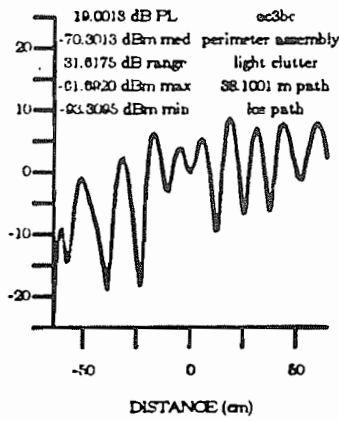
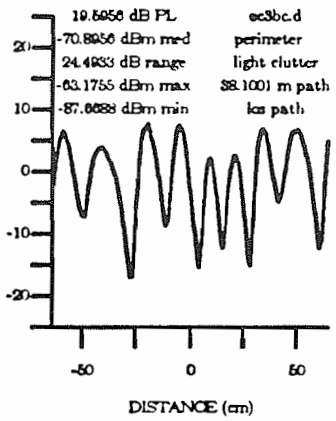
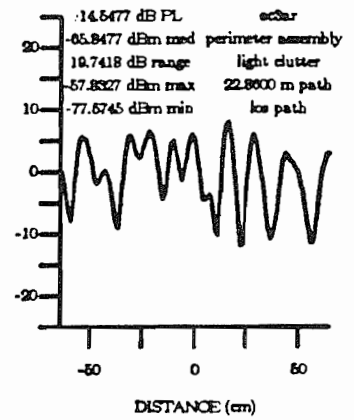
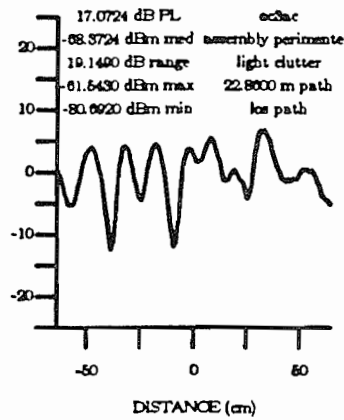
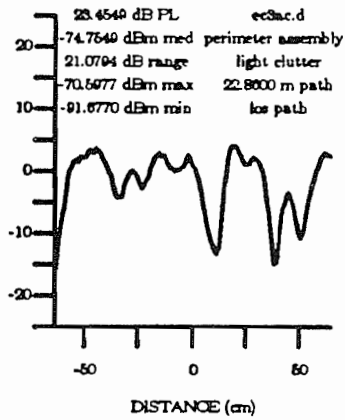


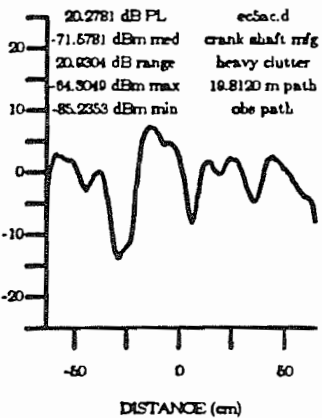
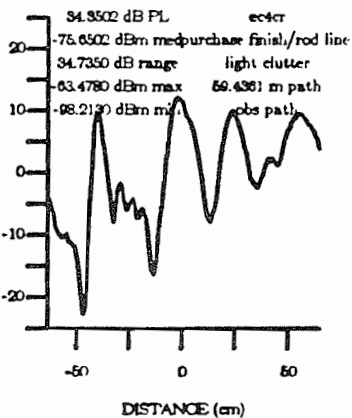
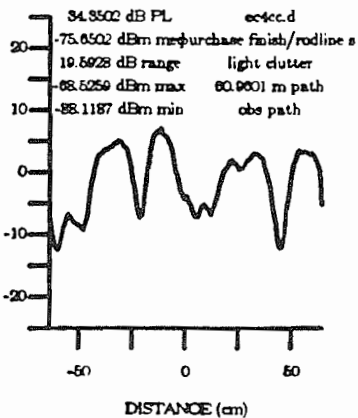
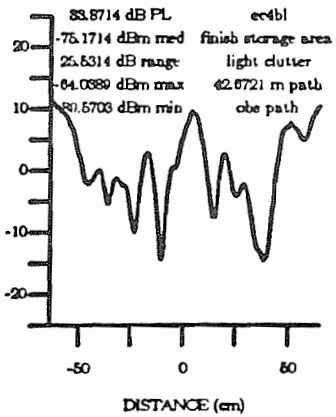
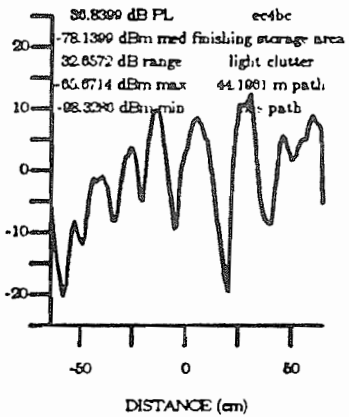
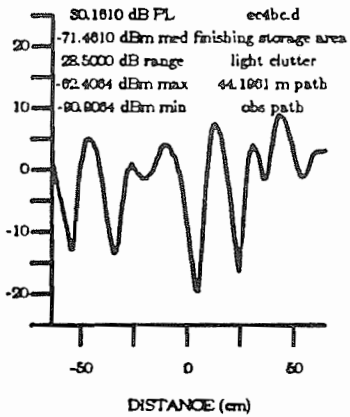
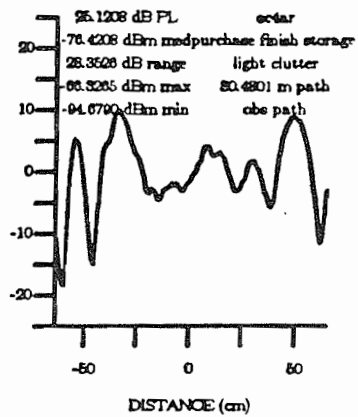
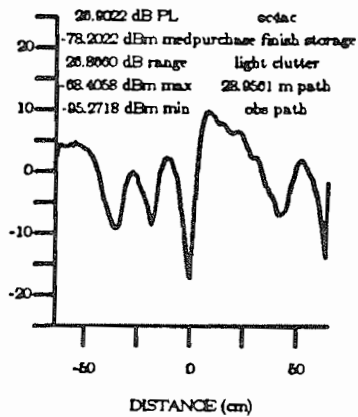
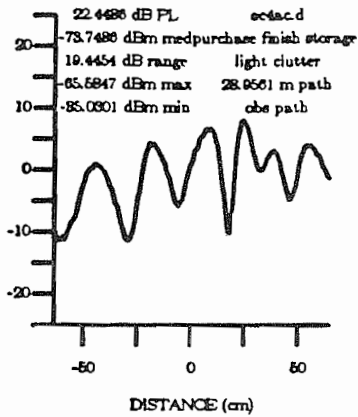


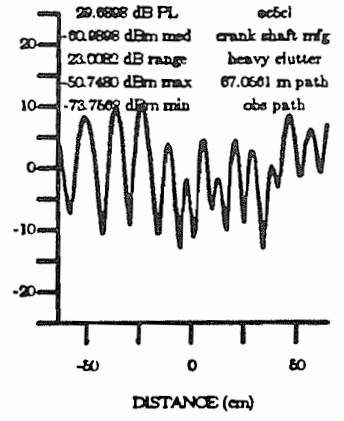
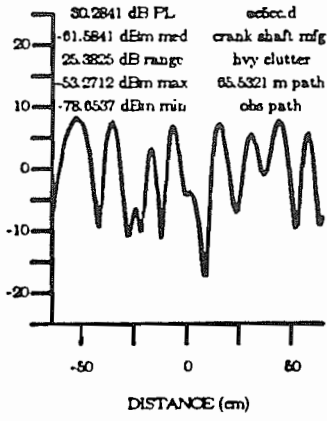
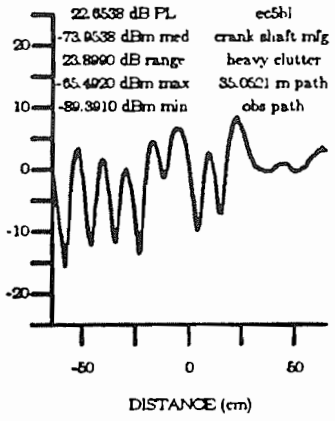
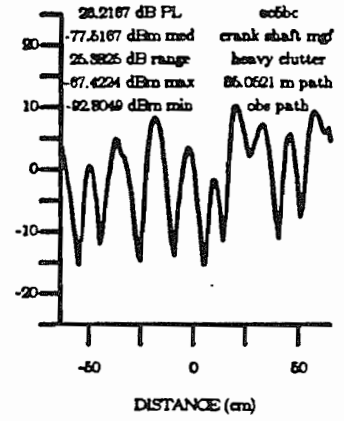
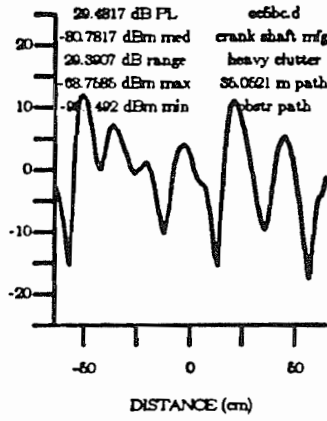
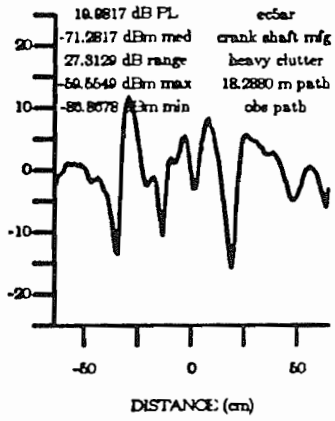


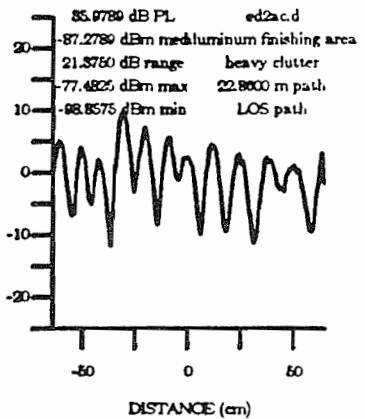
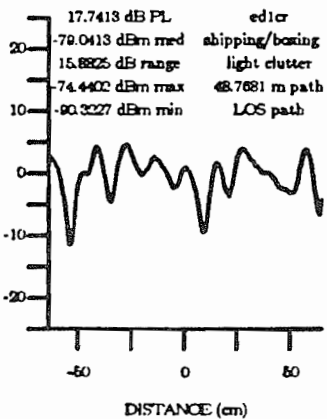
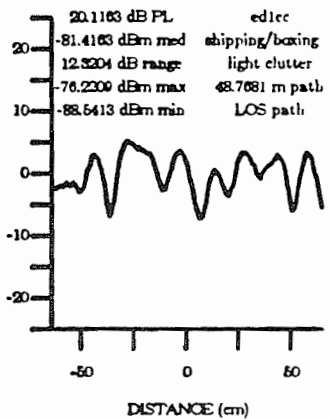
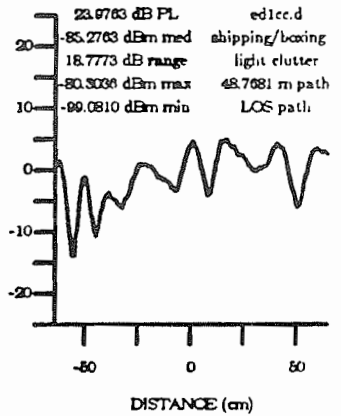
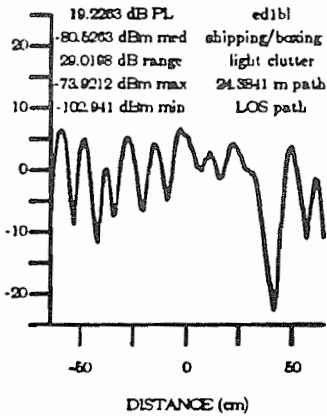
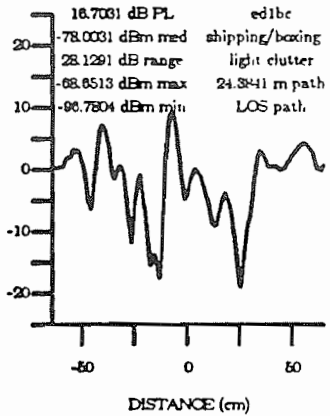
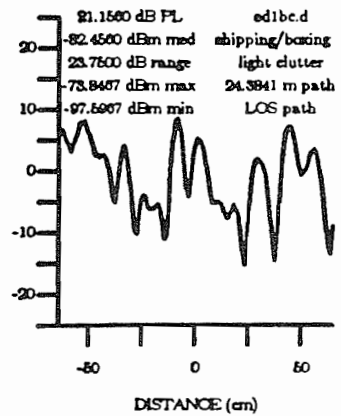
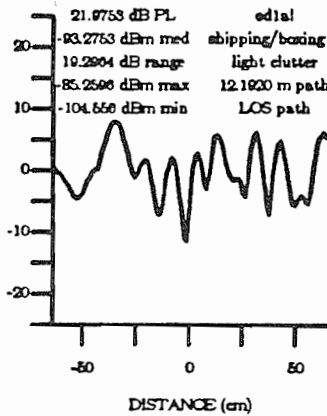
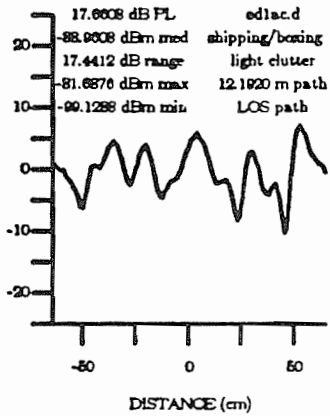


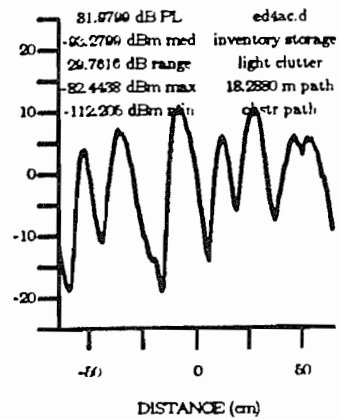
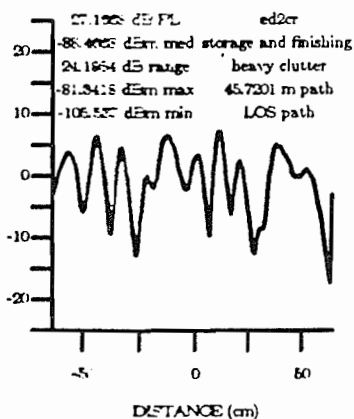
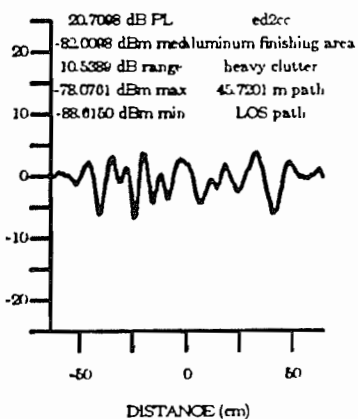
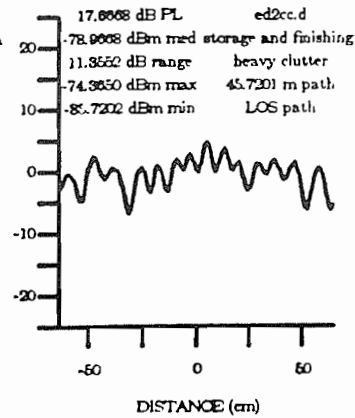
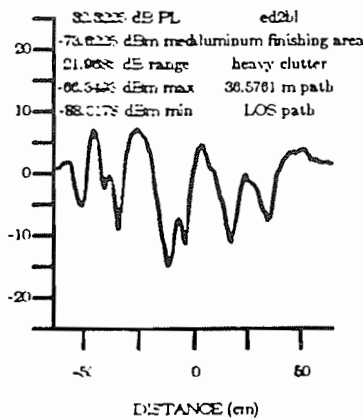
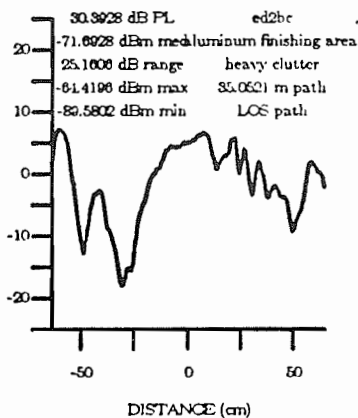
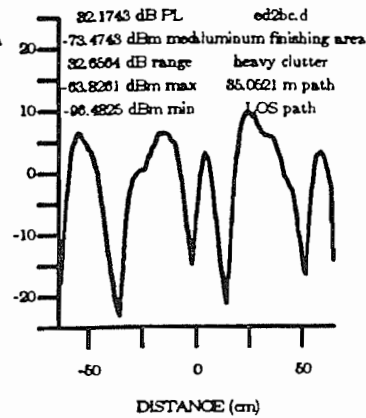
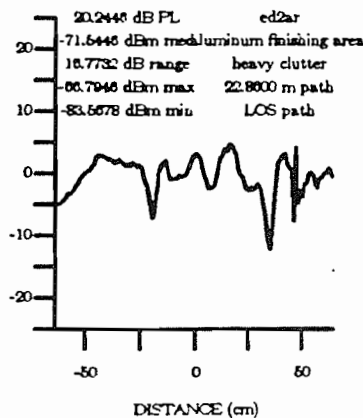
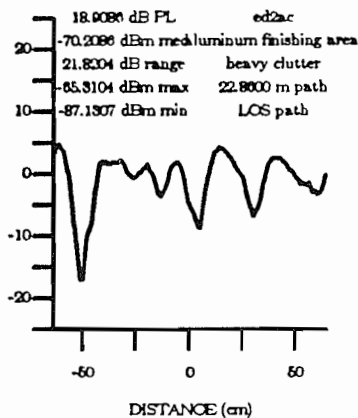




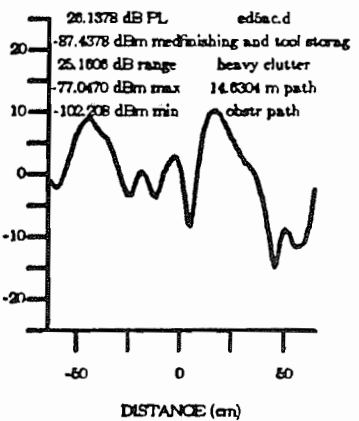
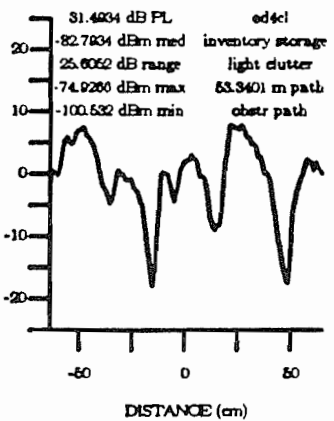
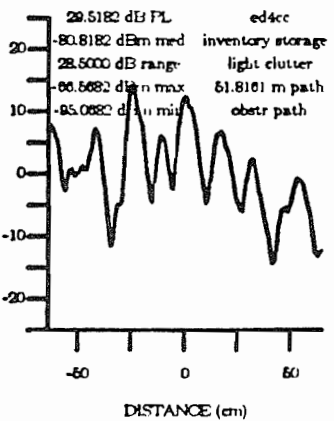
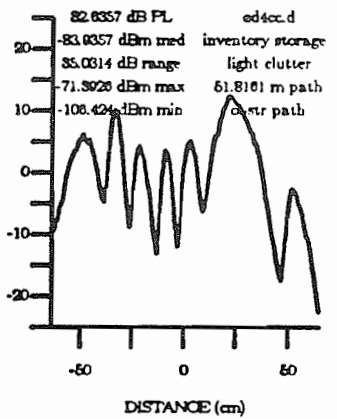
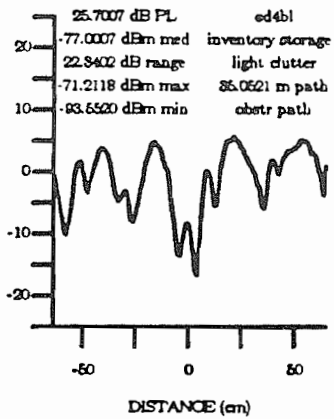
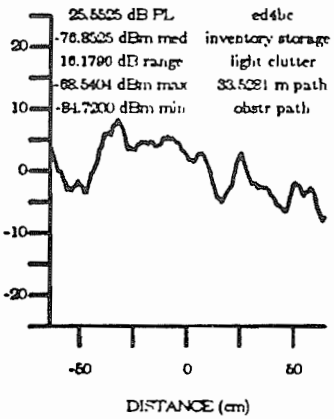
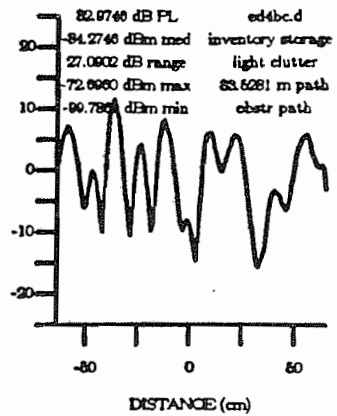
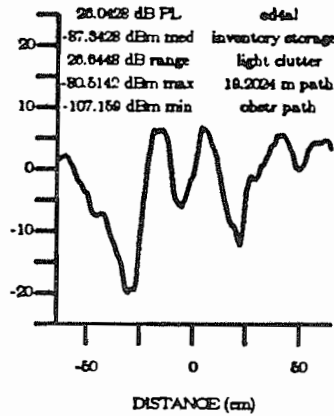
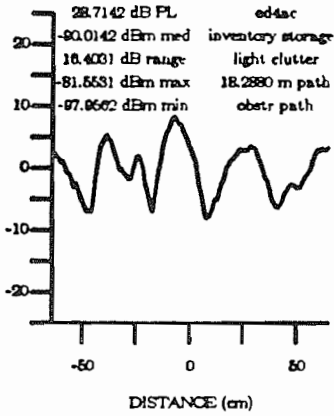


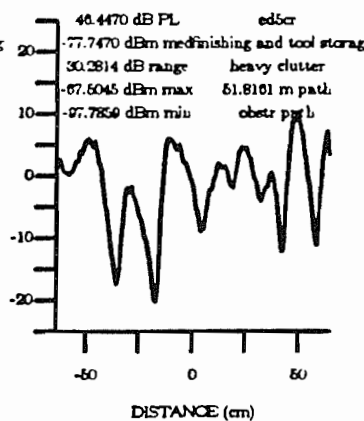
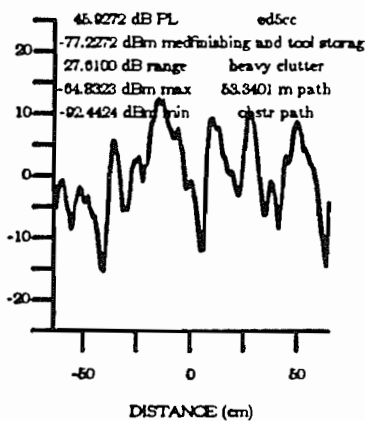
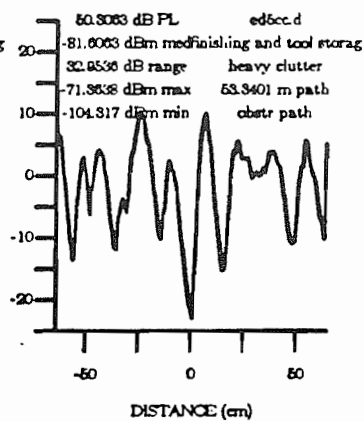
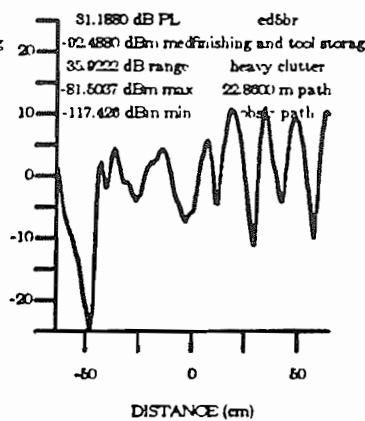
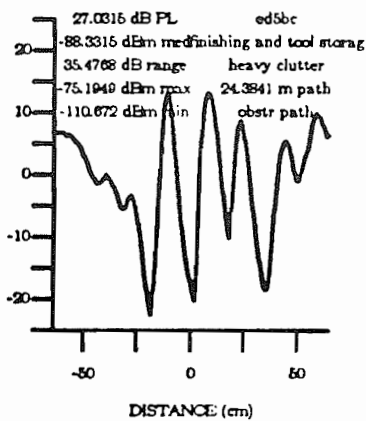
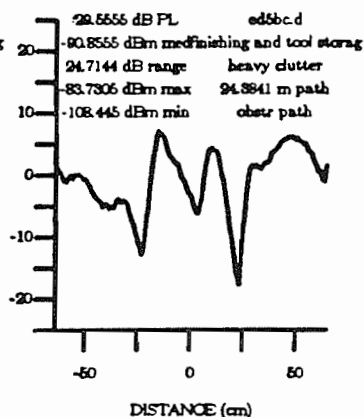
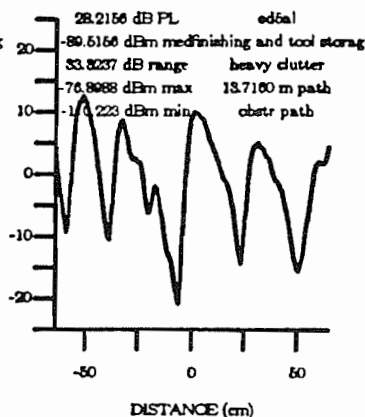
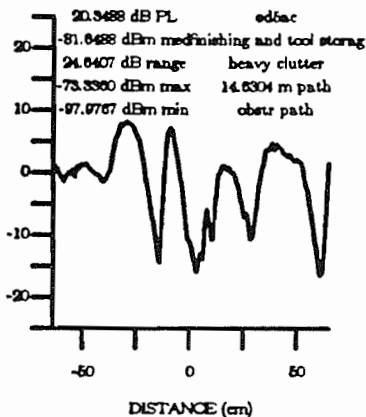


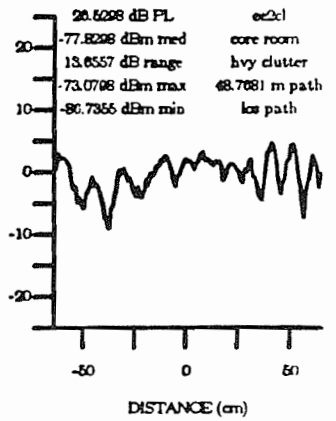
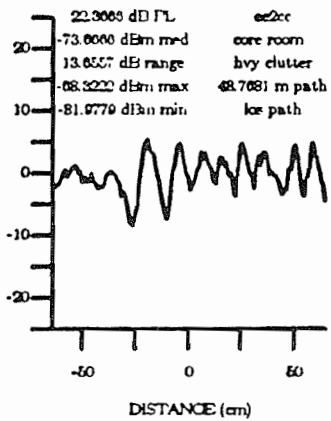
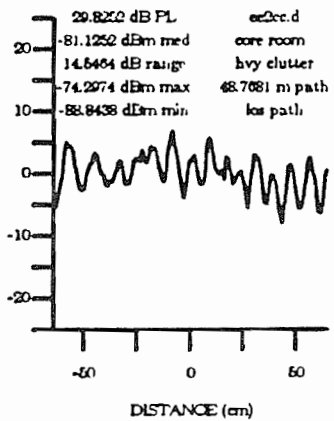
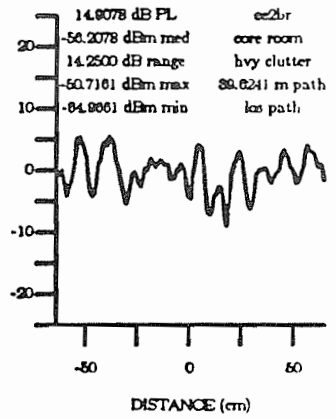
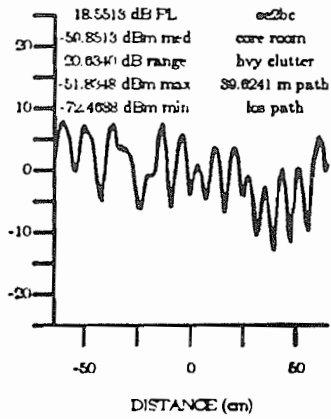
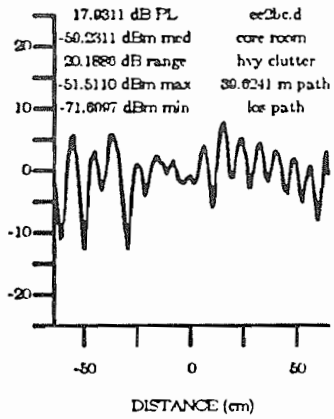
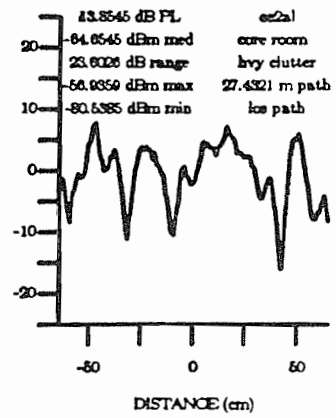
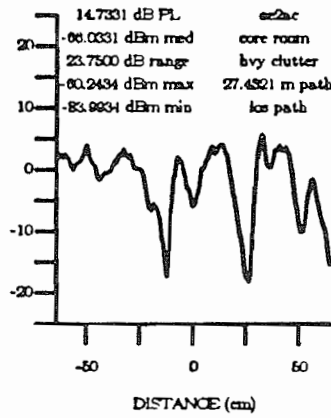
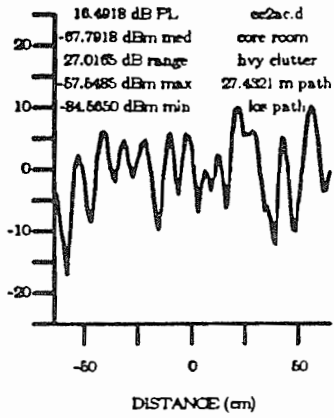


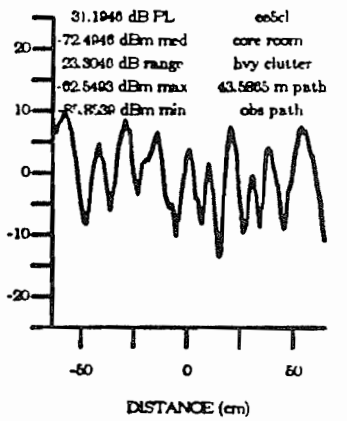
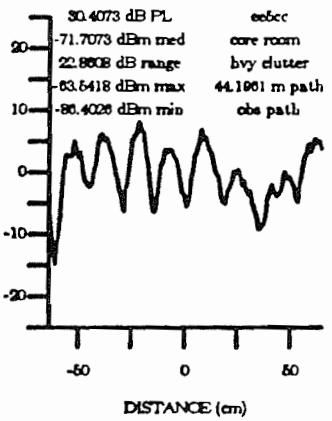
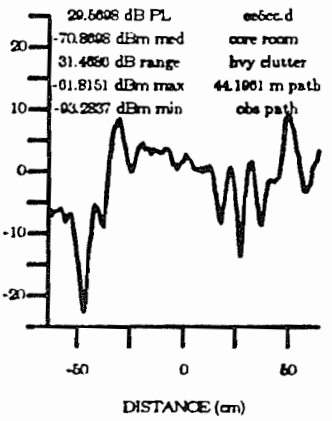
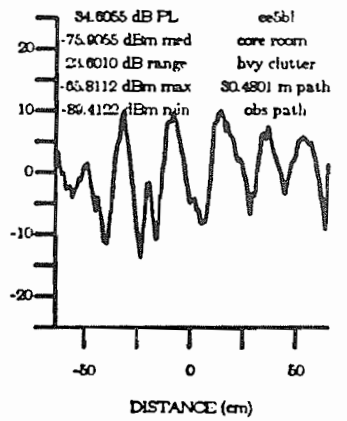
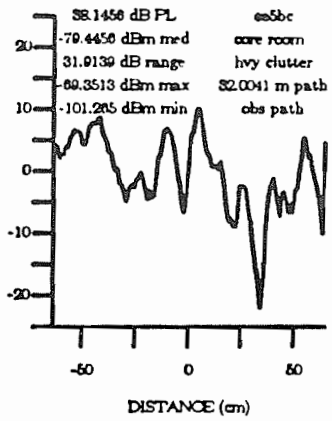
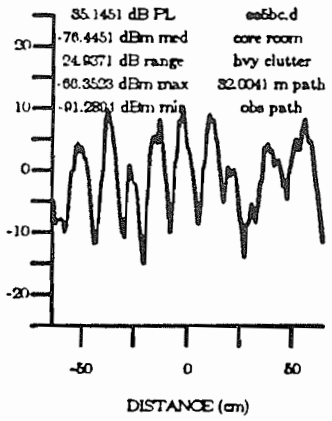
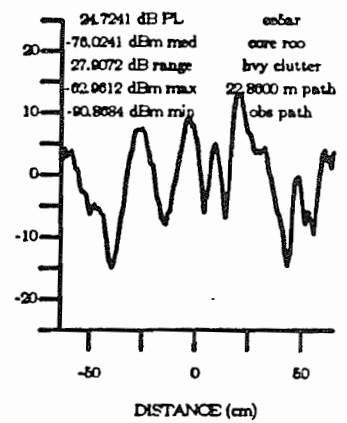
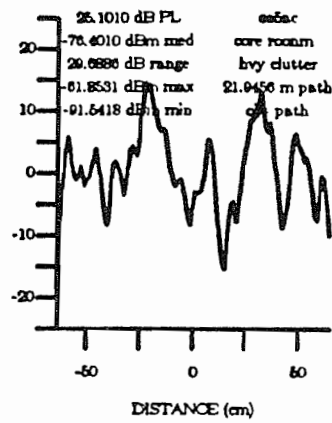
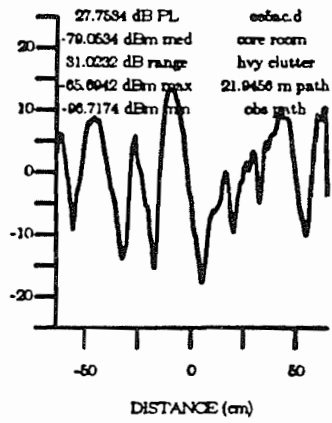


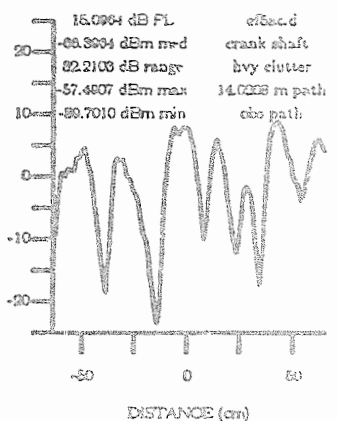
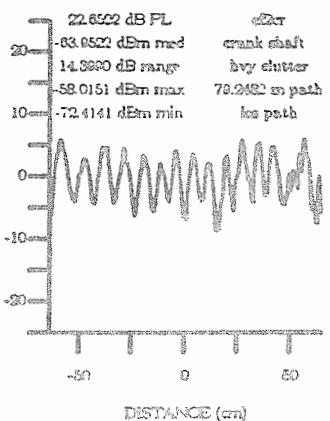
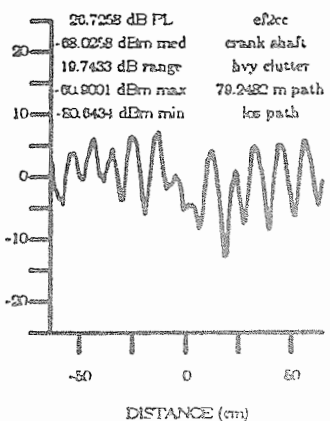
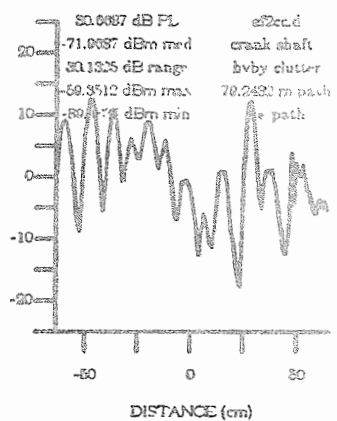
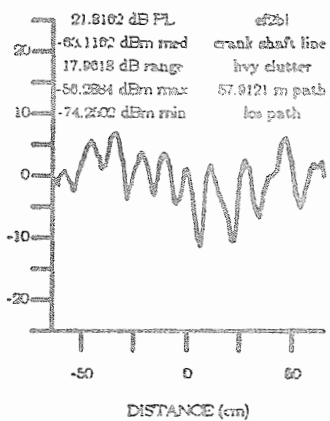
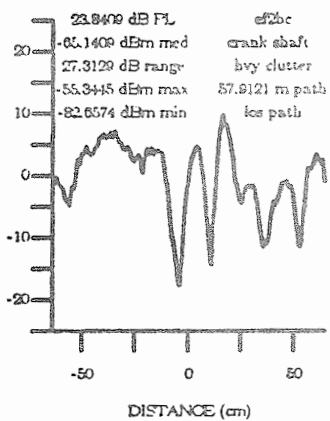
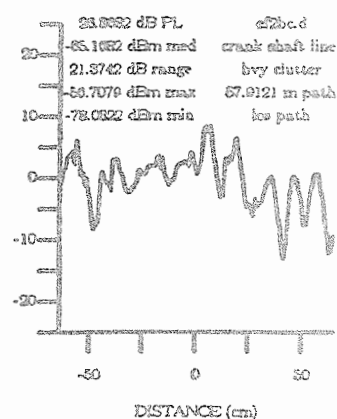
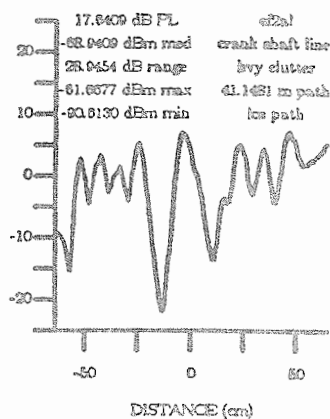
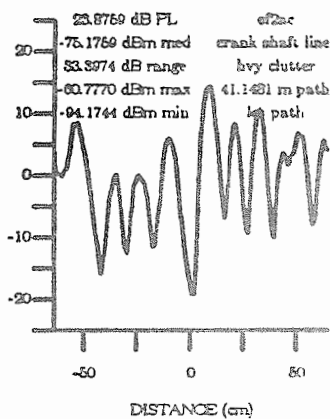


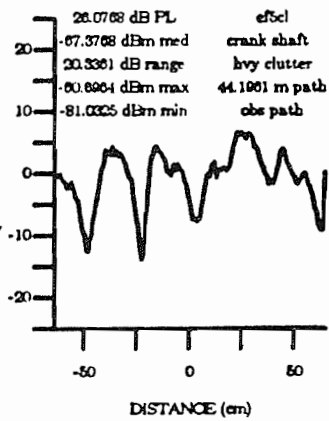
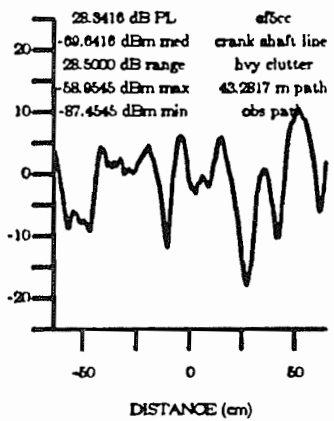
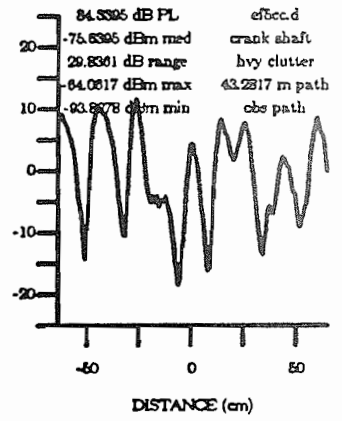
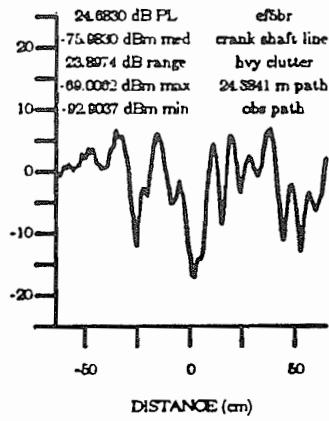
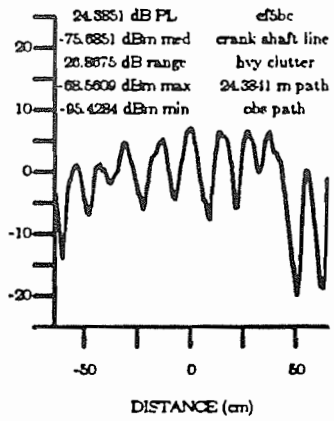
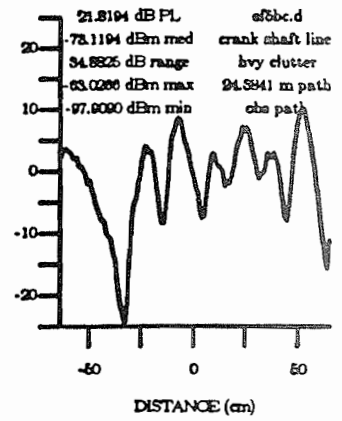
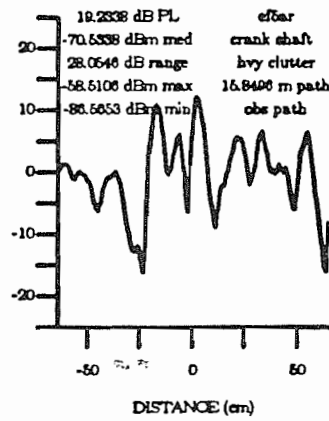
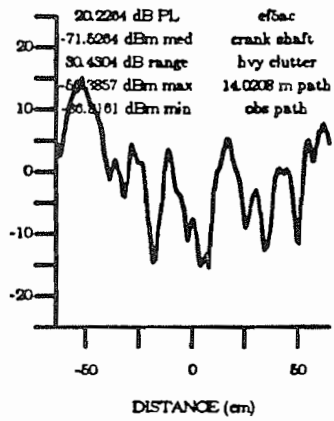








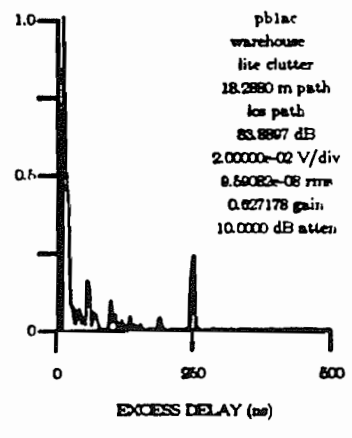
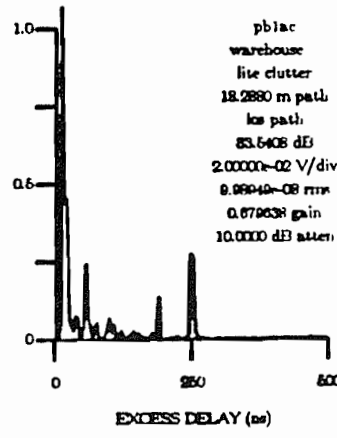
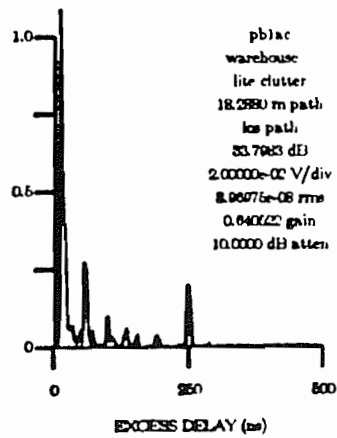
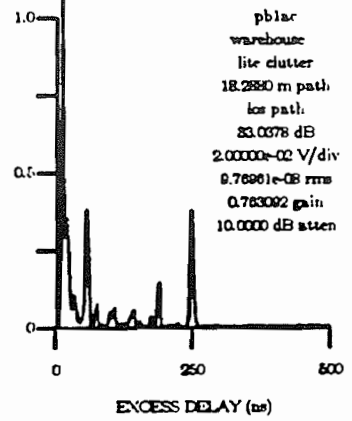
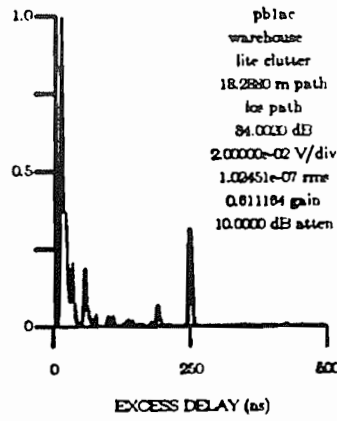
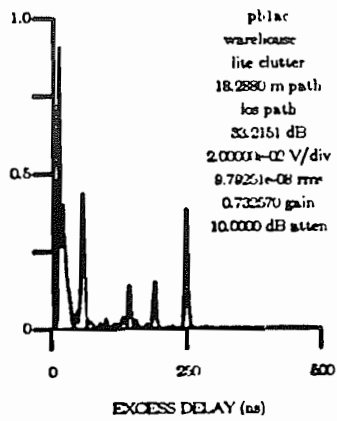
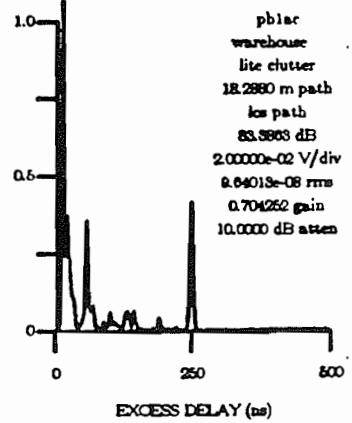
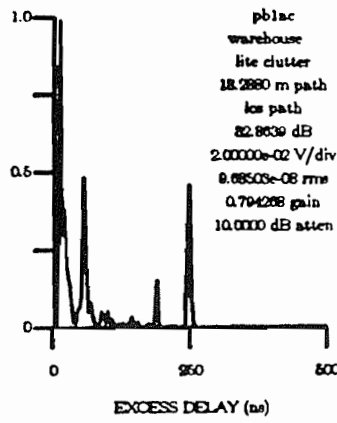
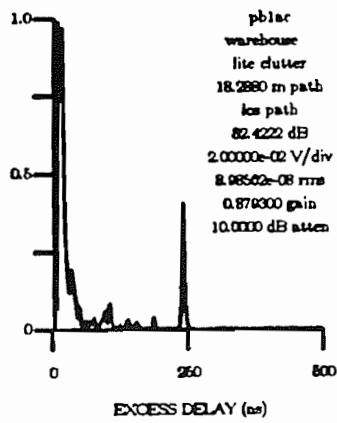




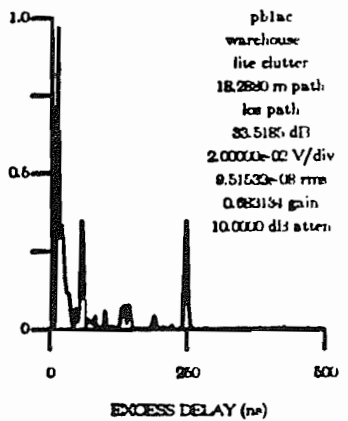
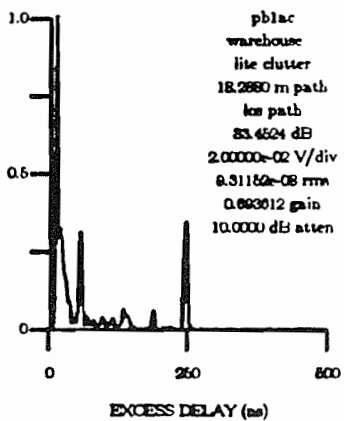
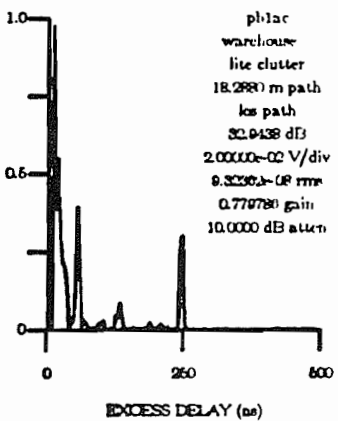
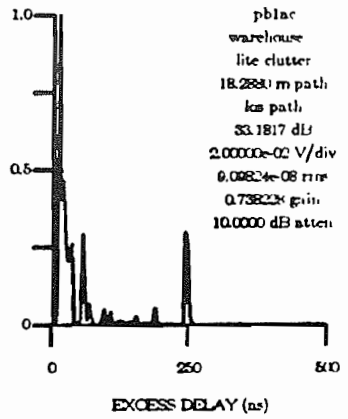
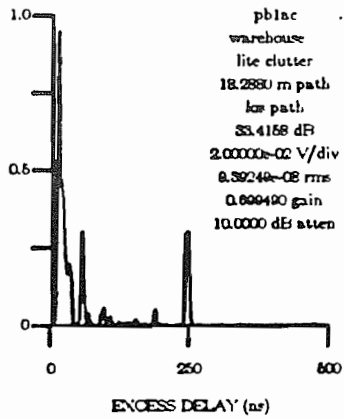
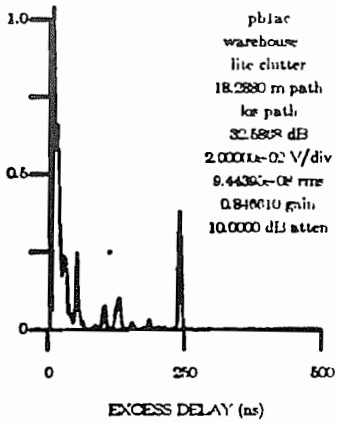
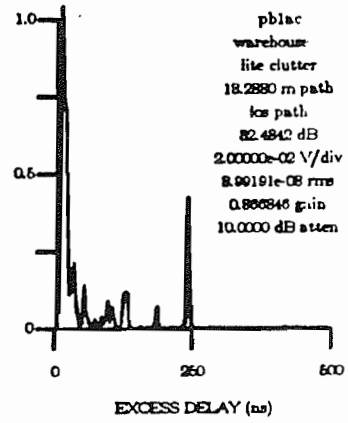
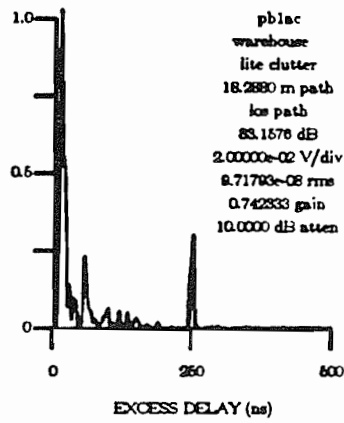
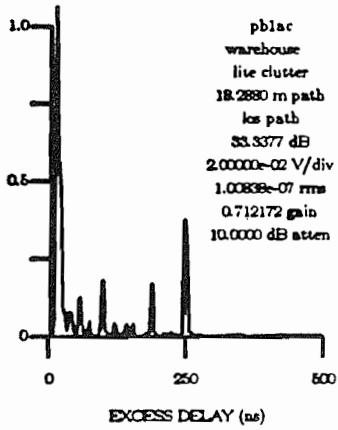
## Appendix D

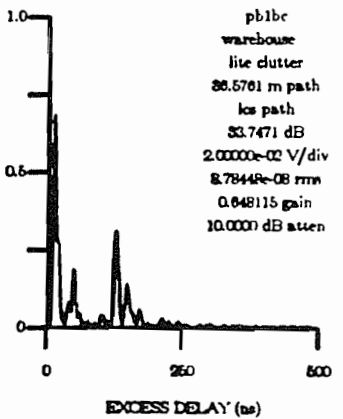
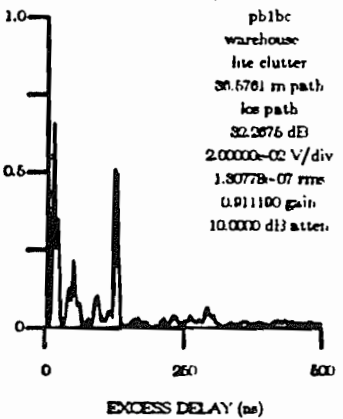
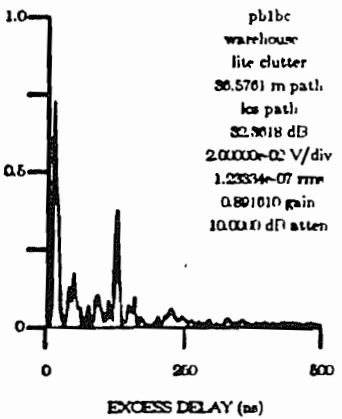
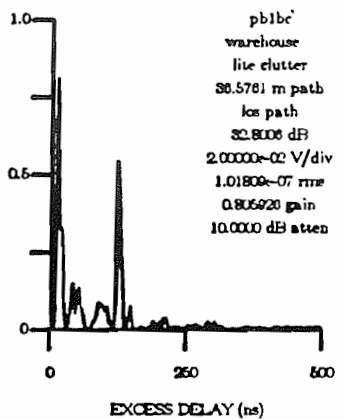
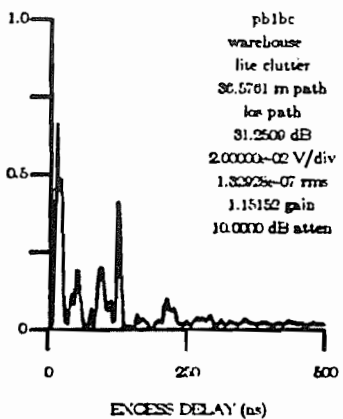
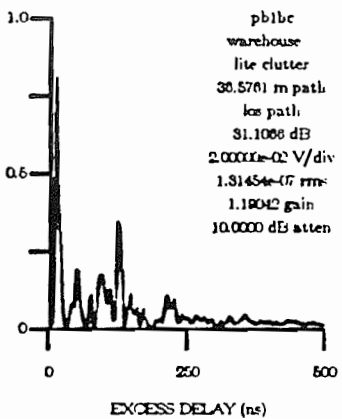
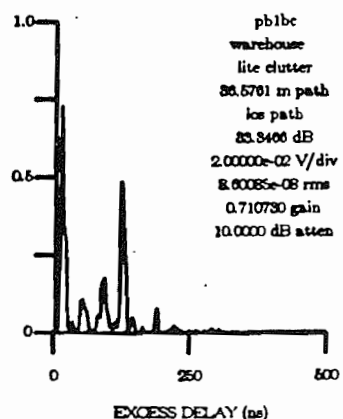
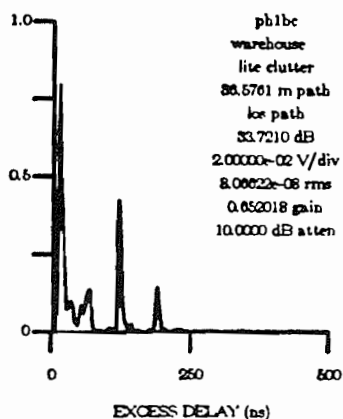
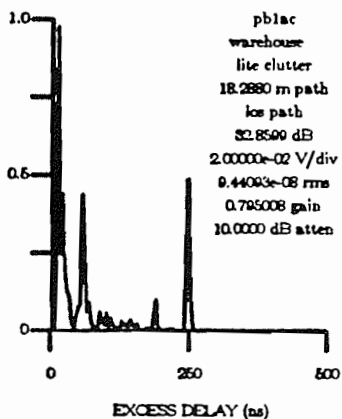
### Pulse Measurements - Raw Data

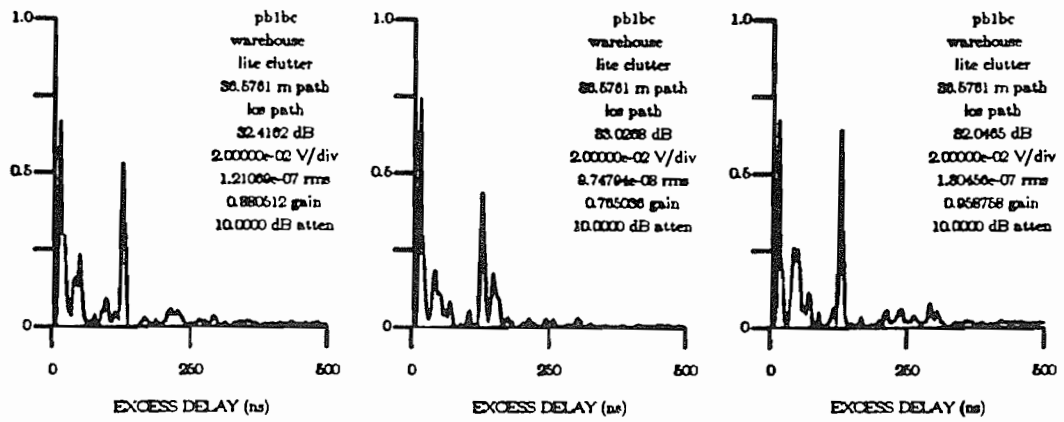
The following are raw data plots of all the individual multipath power delay profiles collected in 5 factories. The filename is located in the upper right hand corner of each plot and indicates the measurement location (see Figure 3.4). The following data is given from top to bottom on each profile plot: filename, factory area, clutter conditions, T-R separation, LOS or obstructed path, relative path loss, vertical scale setting of oscilloscope, r.m.s. delay spread, relative path gain, transmitter attenuator setting. Actual path loss (in dB) relative to a  $10\lambda$  free space path may be found for each profile by subtracting the quantity  $10\log_{10}(T_{\max}/50)$  from the value displayed on the 6th line, where  $T_{\max}$  is the largest displayed excess delay value in ns (200 or 500 for most measurements).

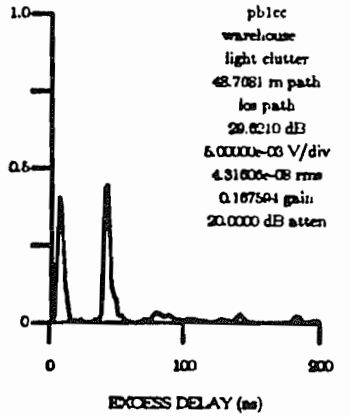
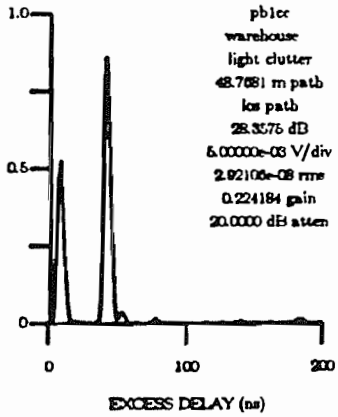
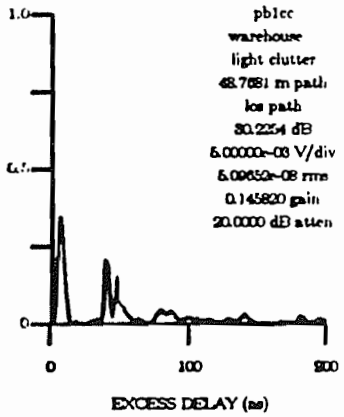
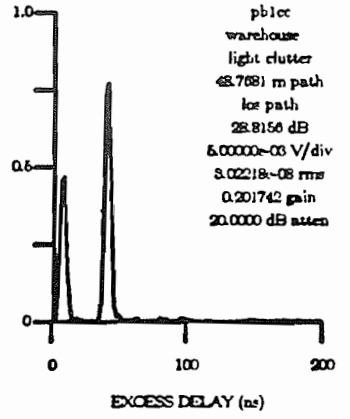
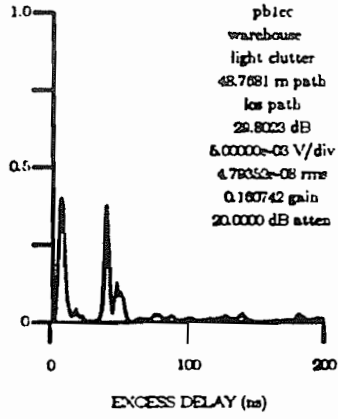
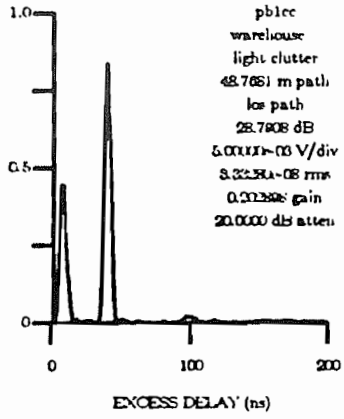
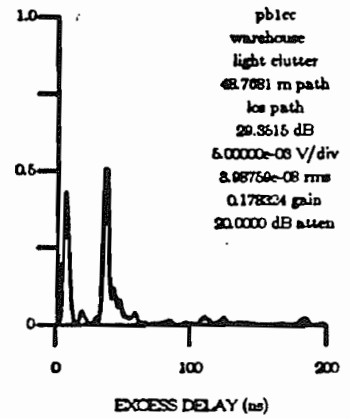
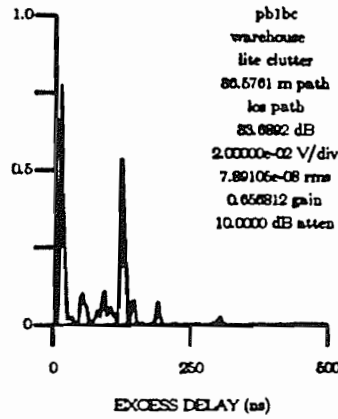
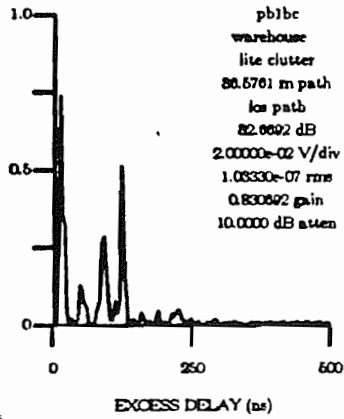


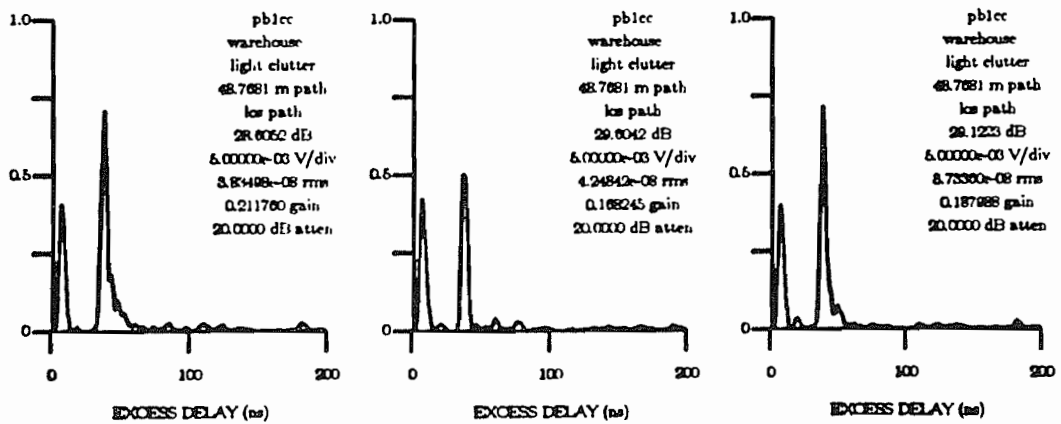
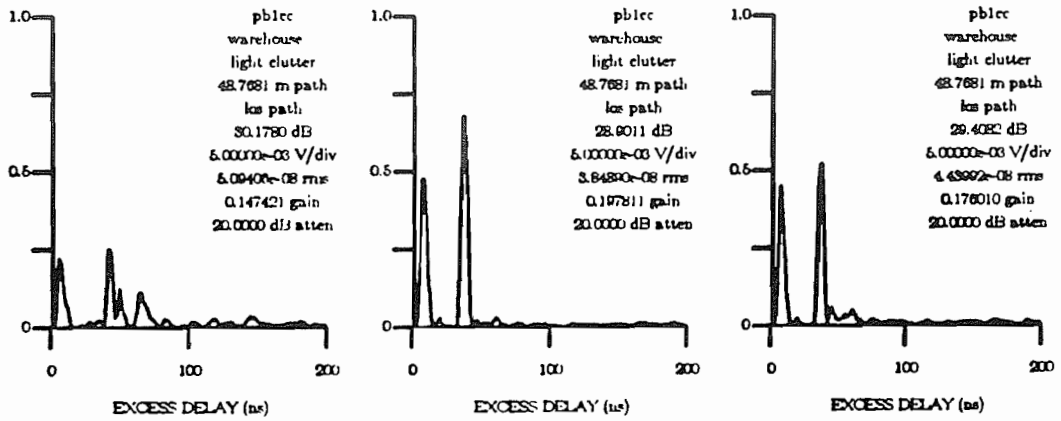
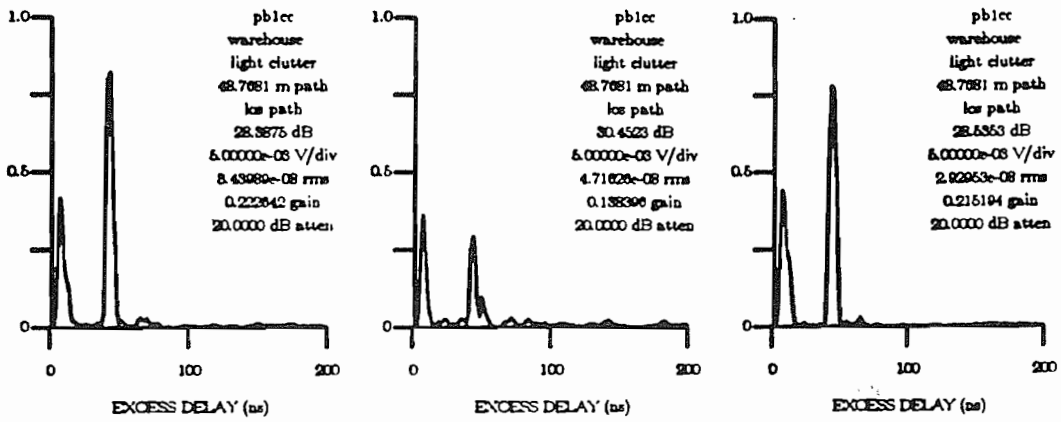


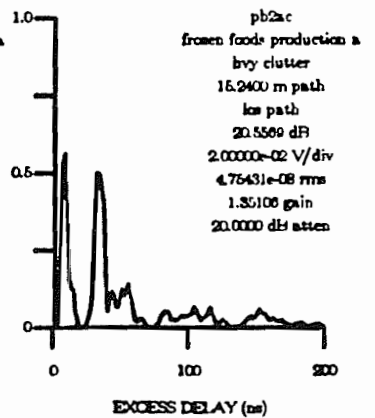
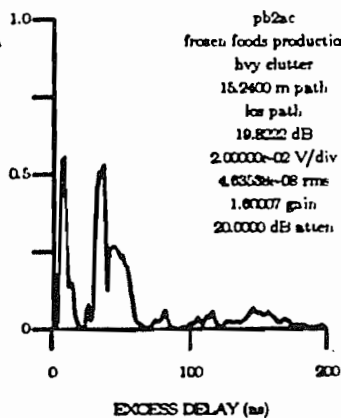
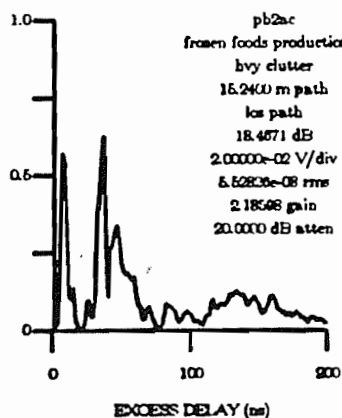
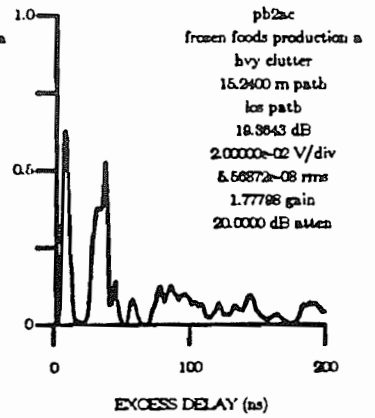
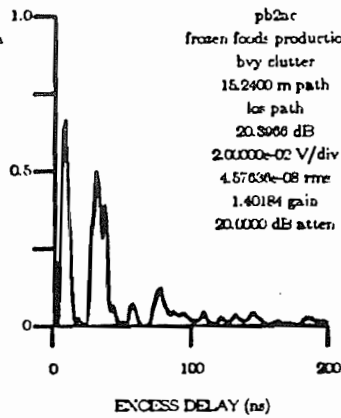
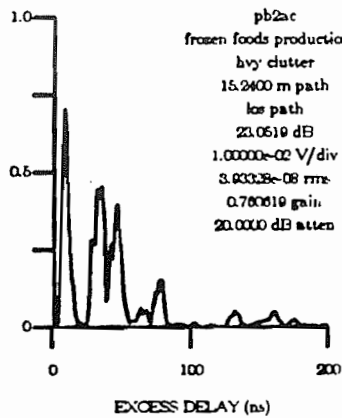
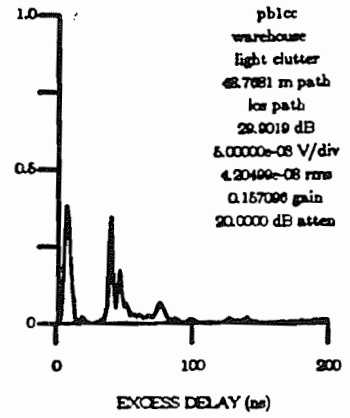
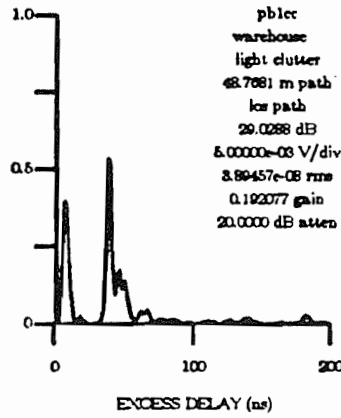
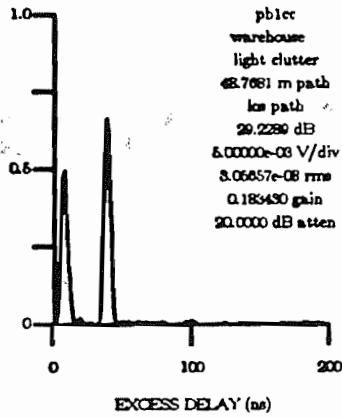


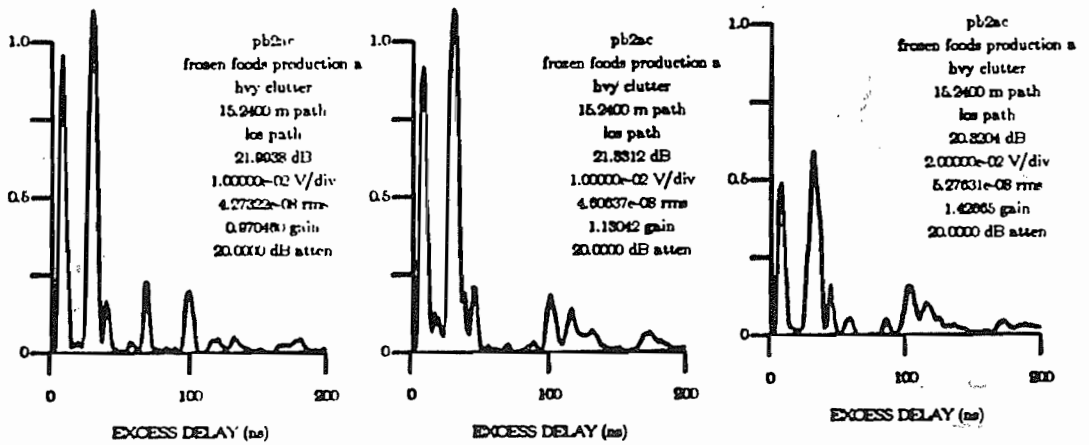
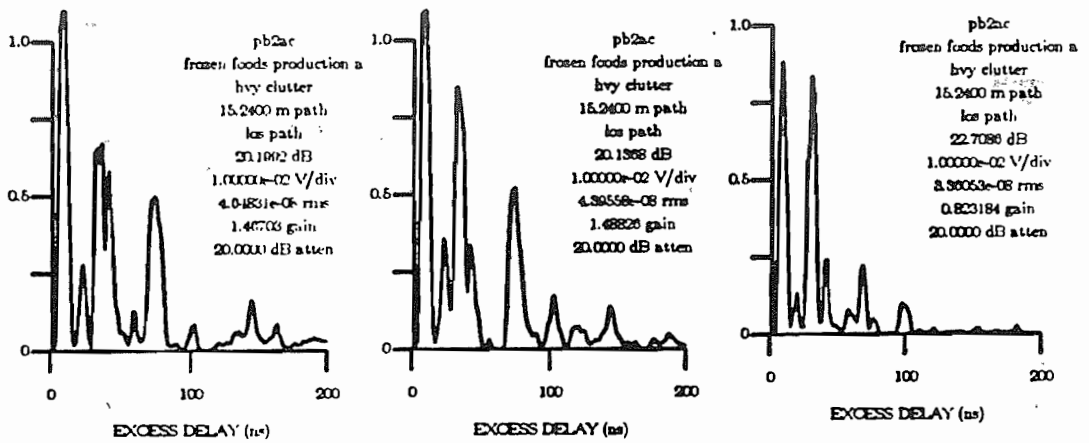
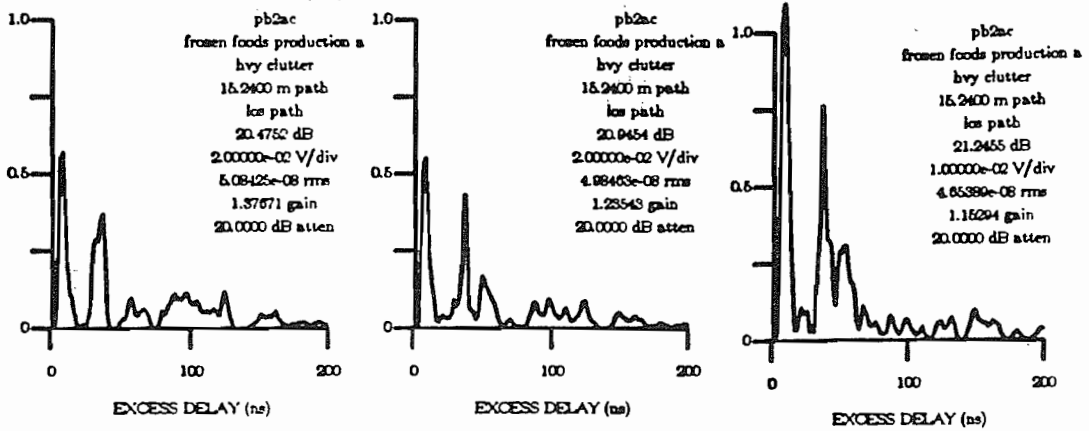


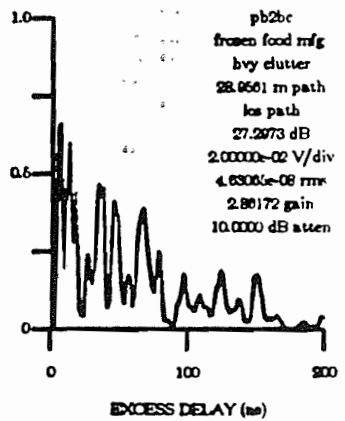
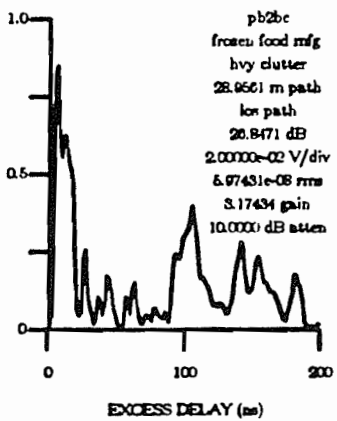
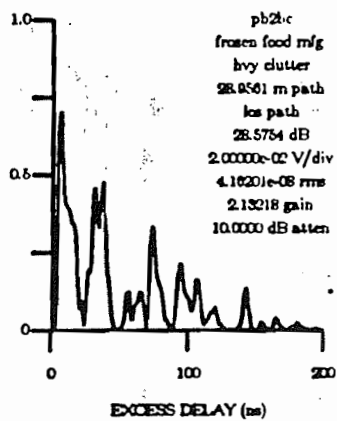
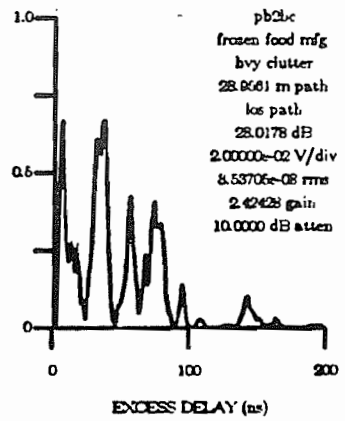
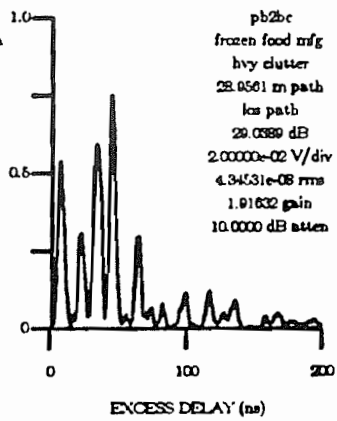
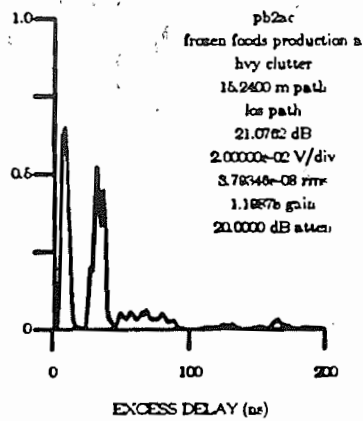
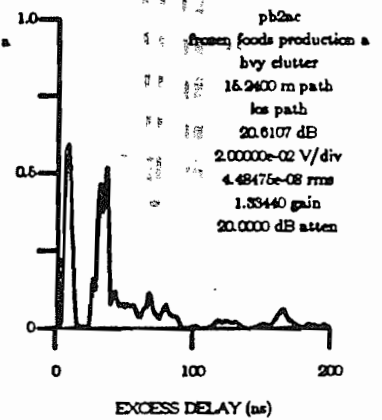
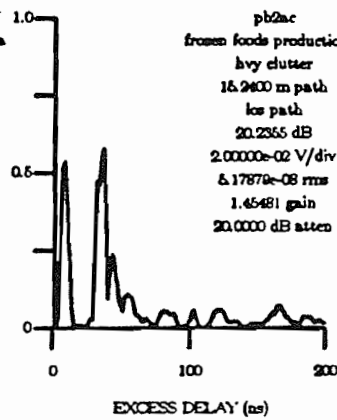
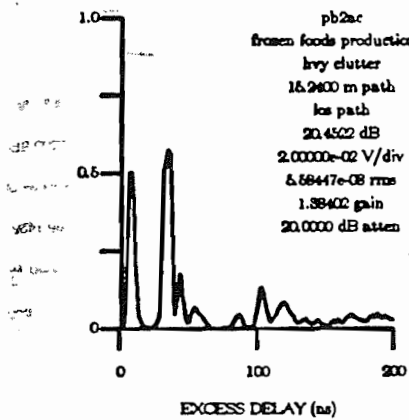




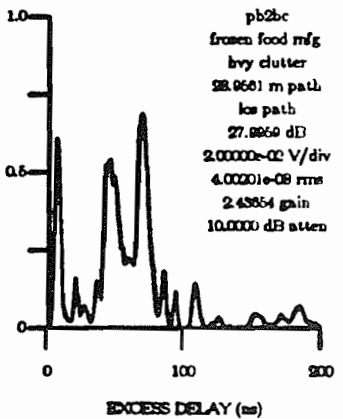
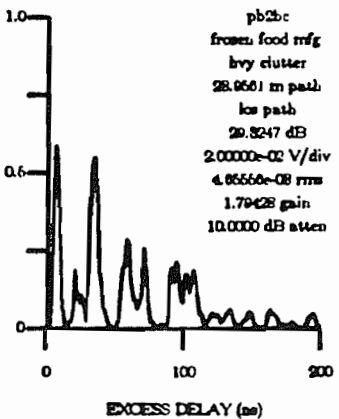
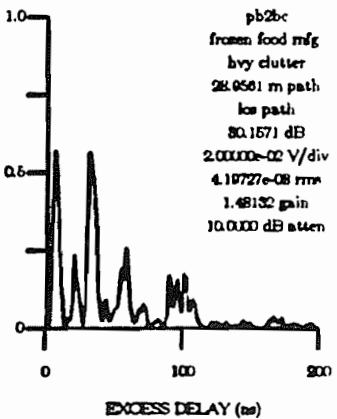
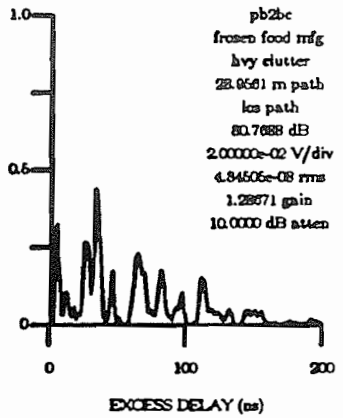
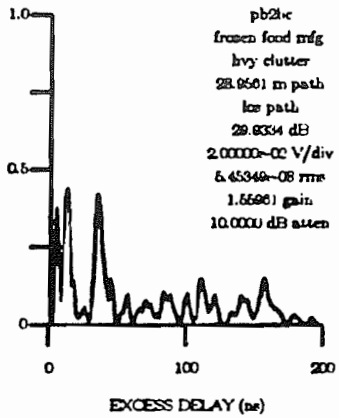
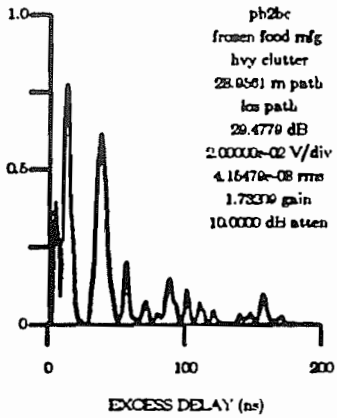
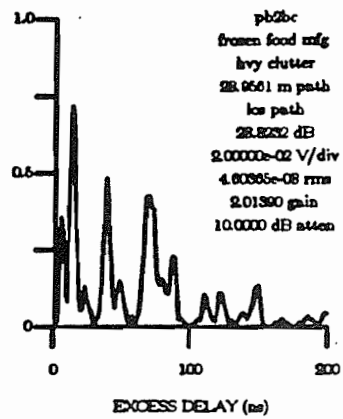
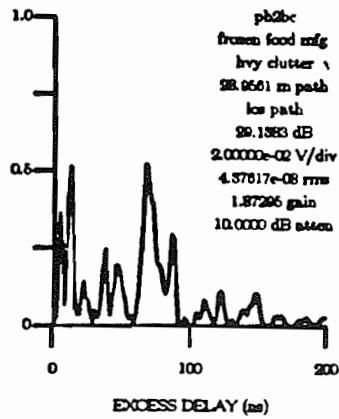
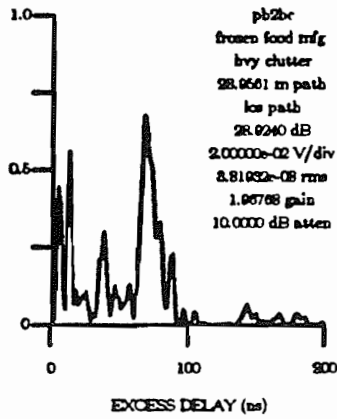


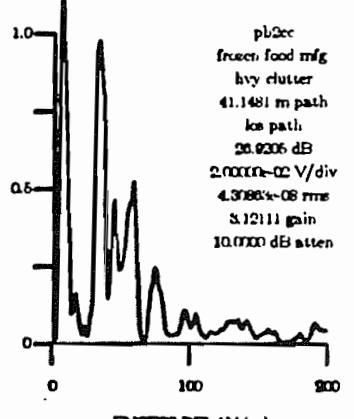
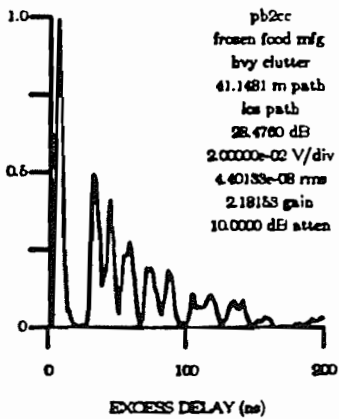
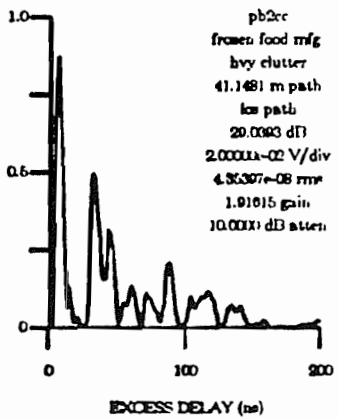
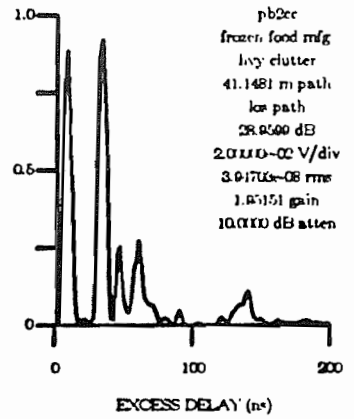
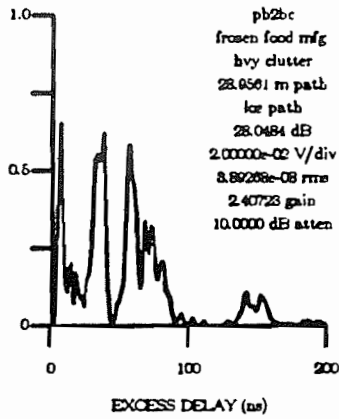
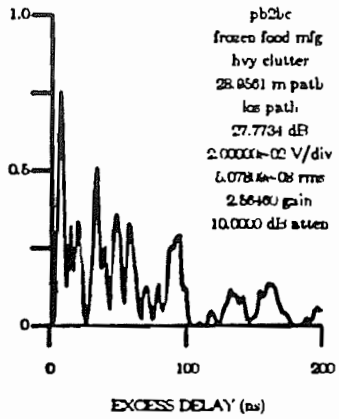
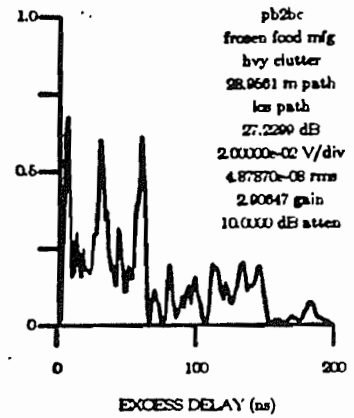
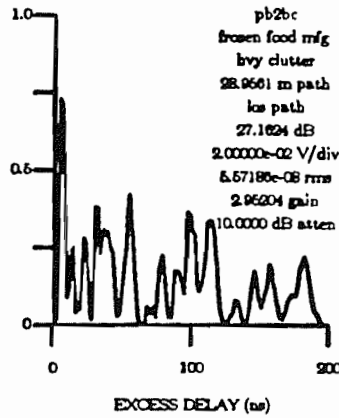
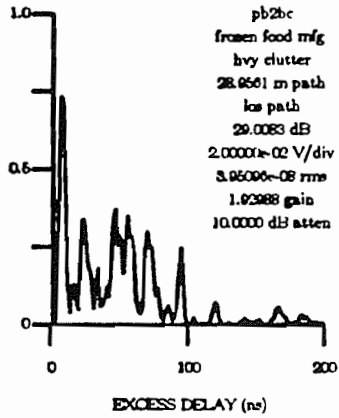


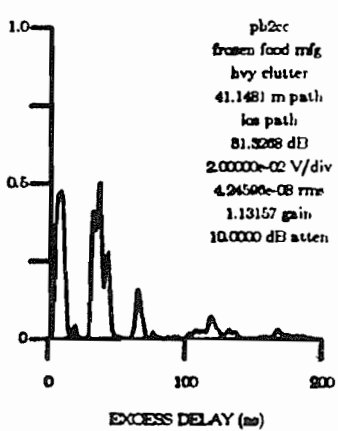
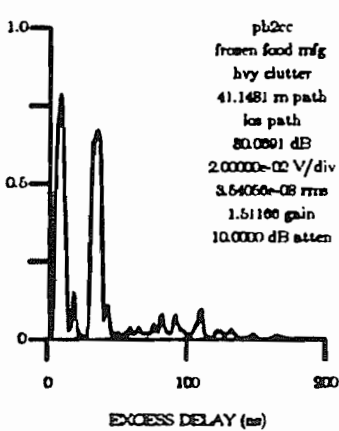
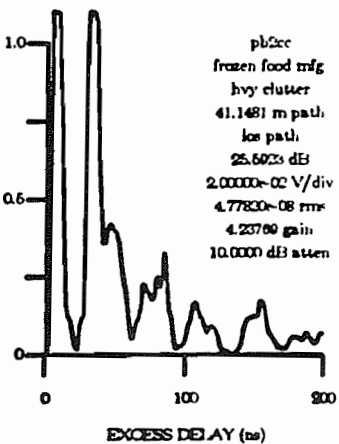
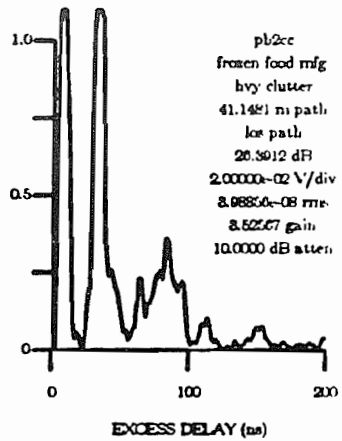
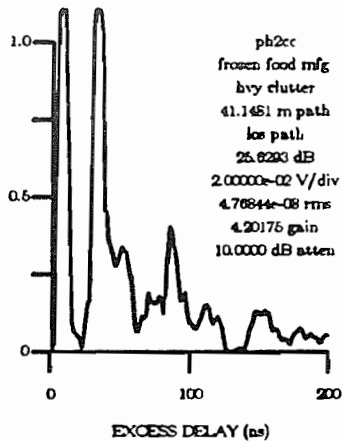
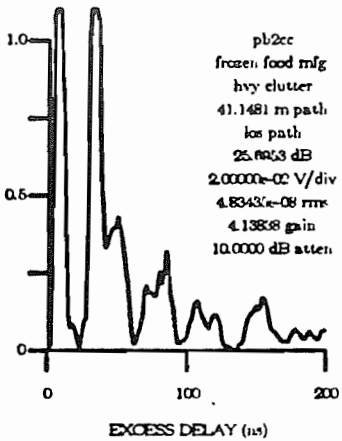
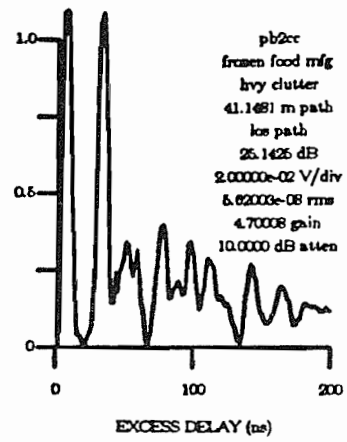
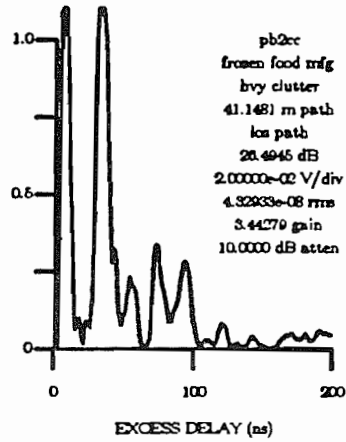
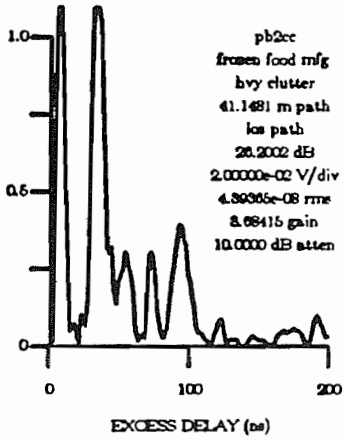


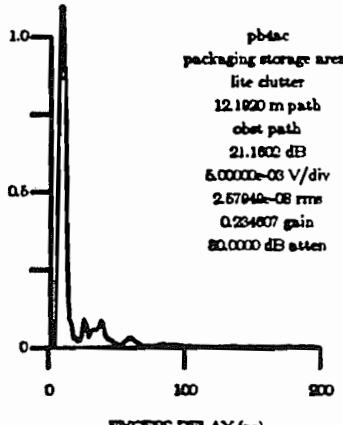
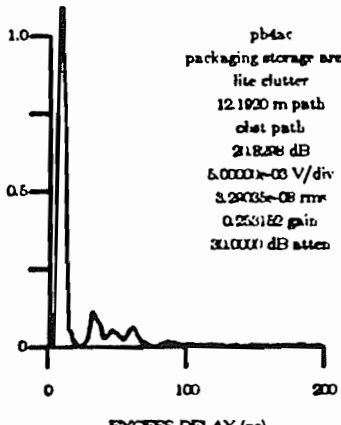
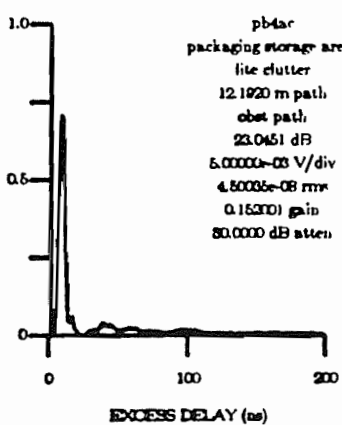
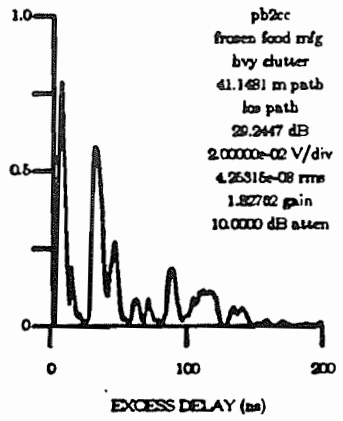
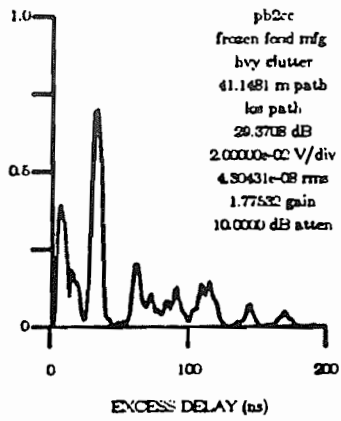
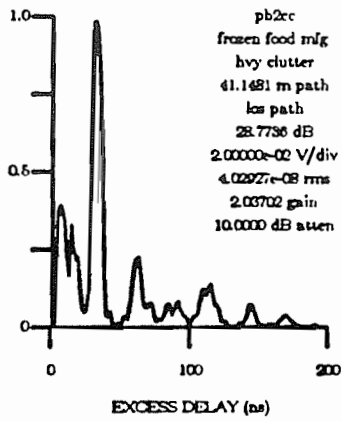
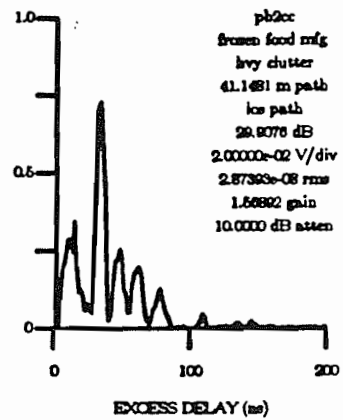
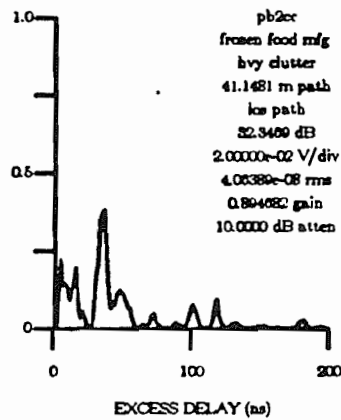
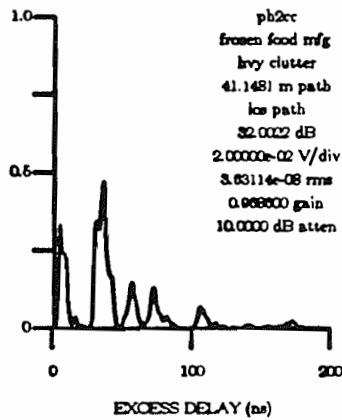


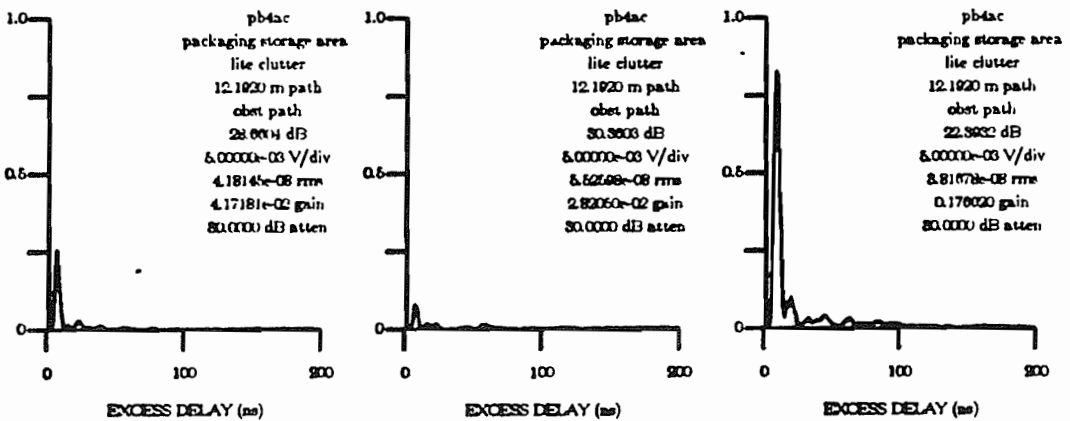
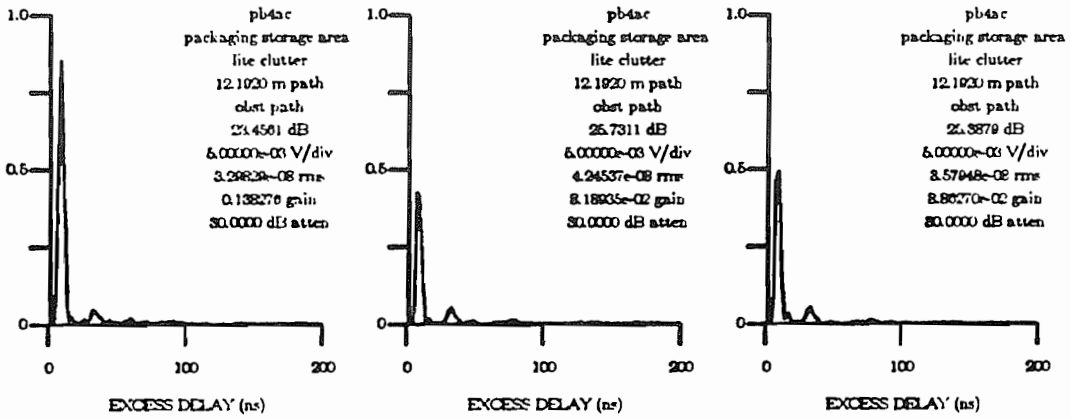
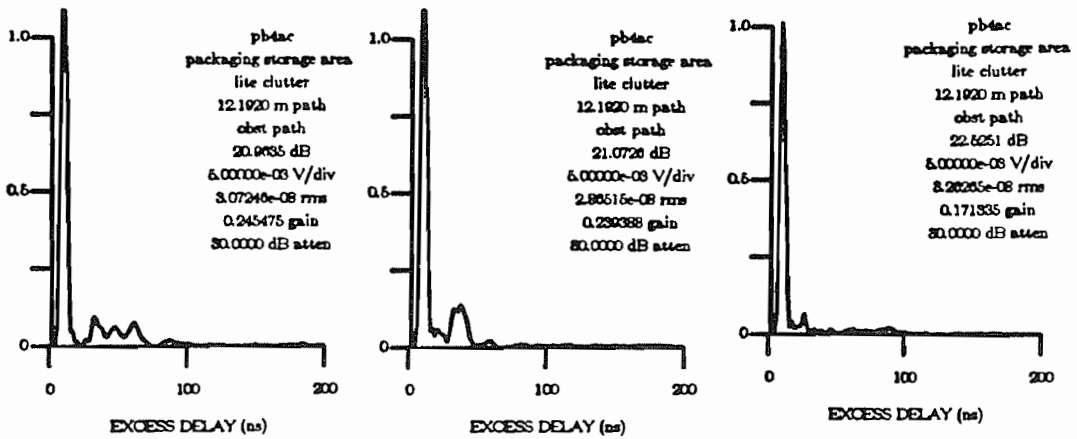


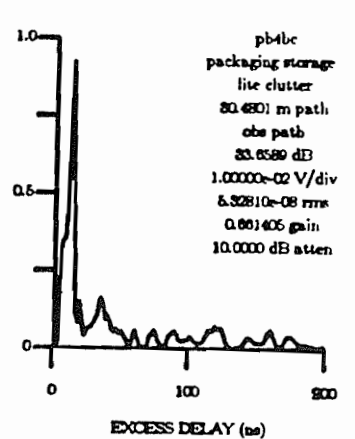
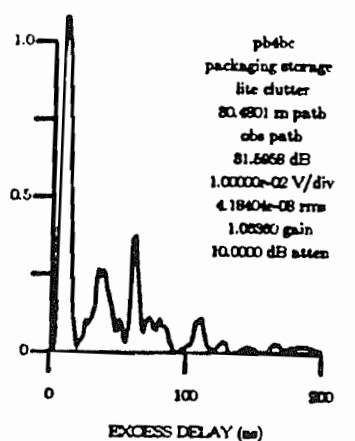
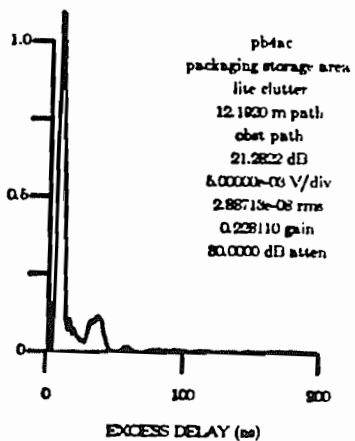
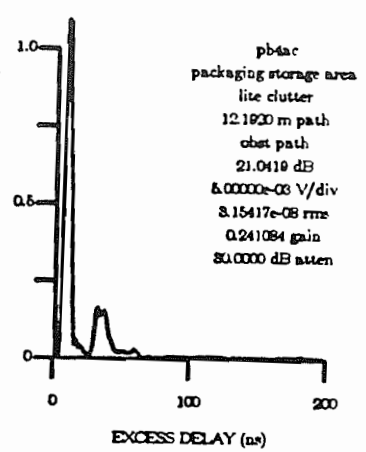
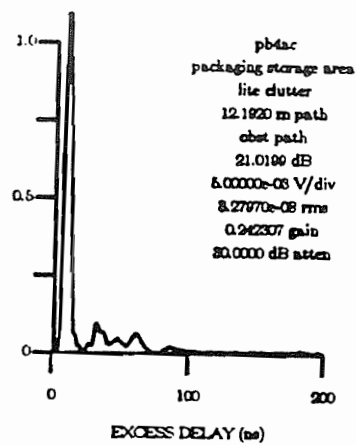
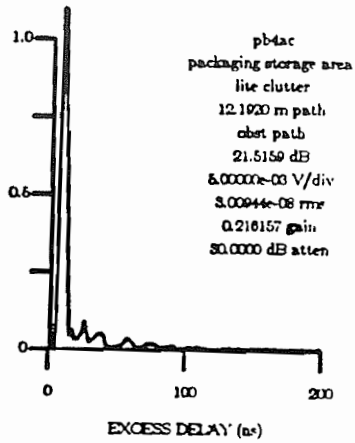
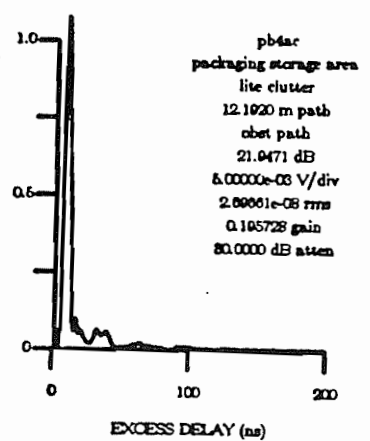
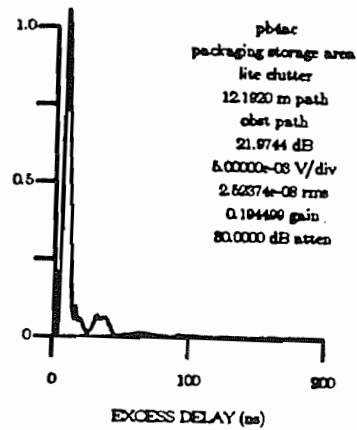
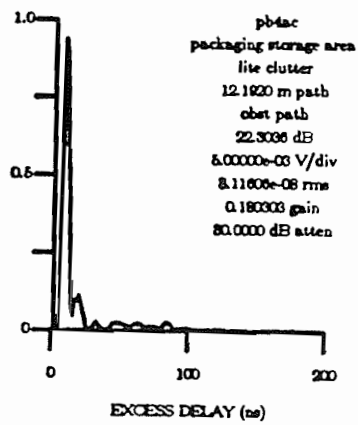


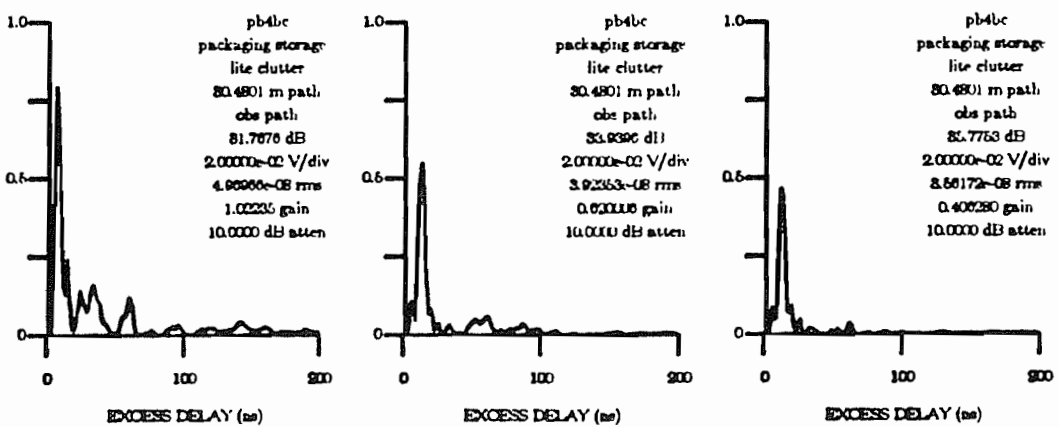
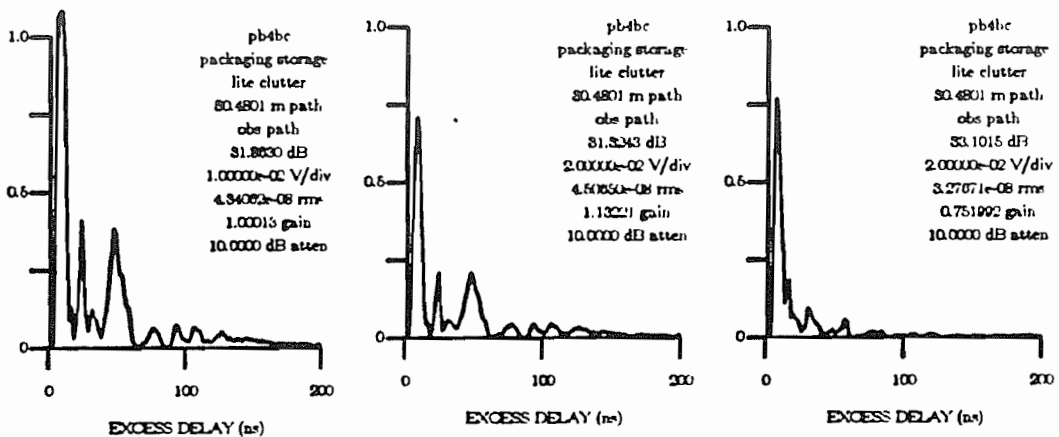
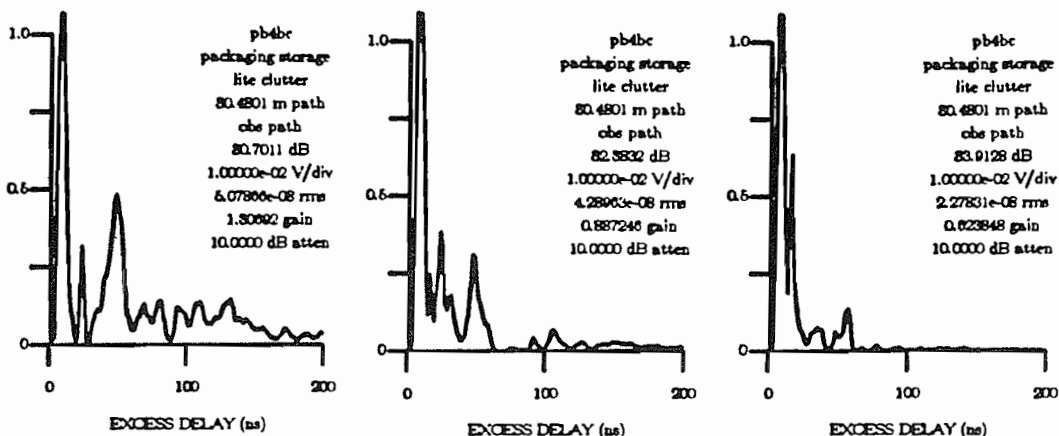


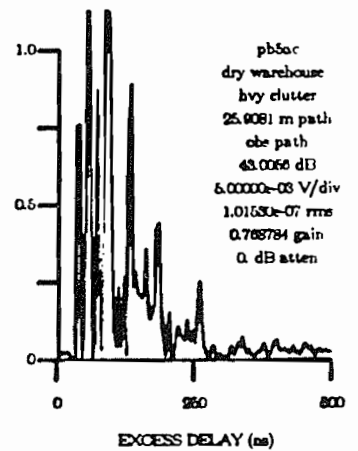
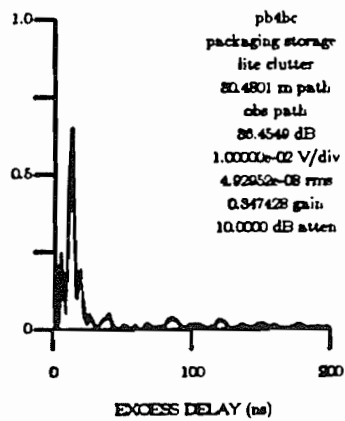
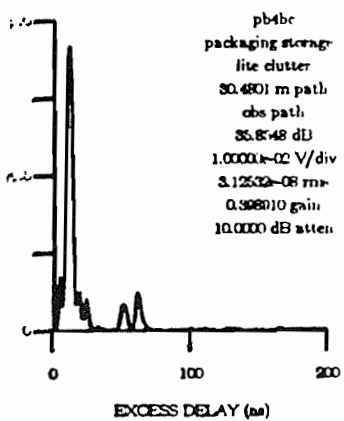
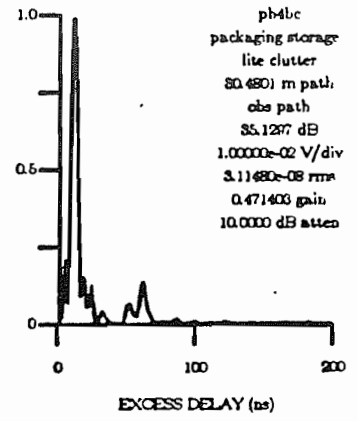
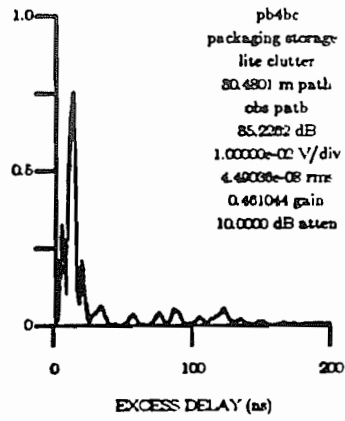
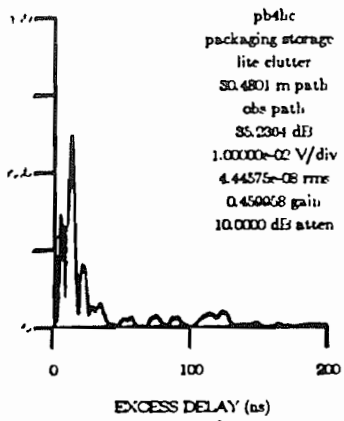
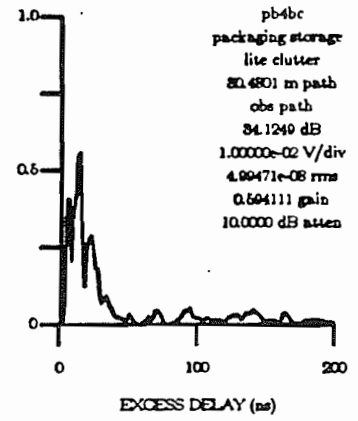
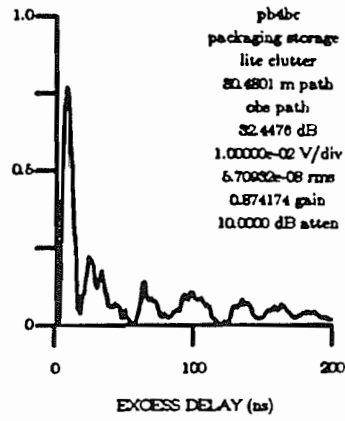
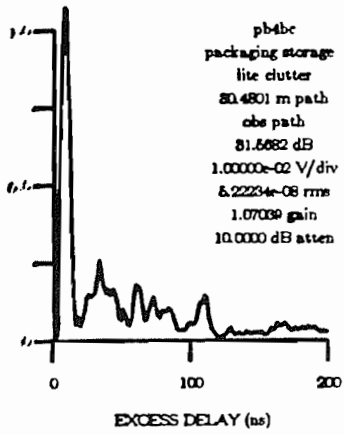




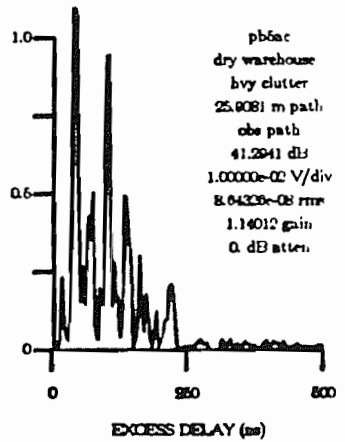
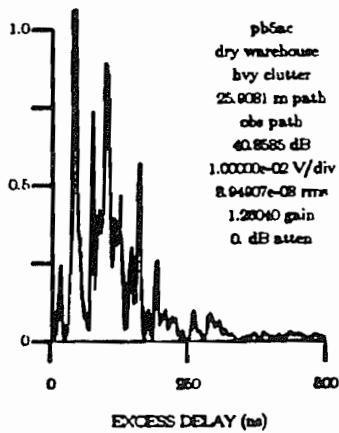
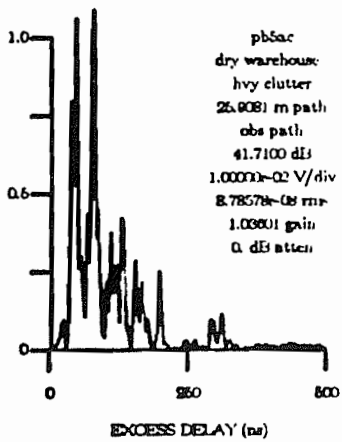
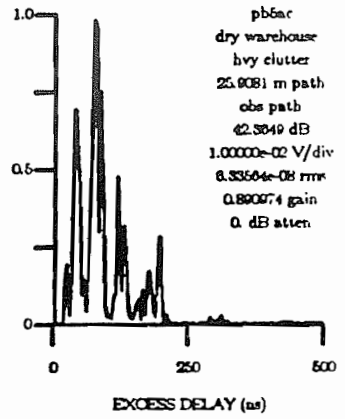
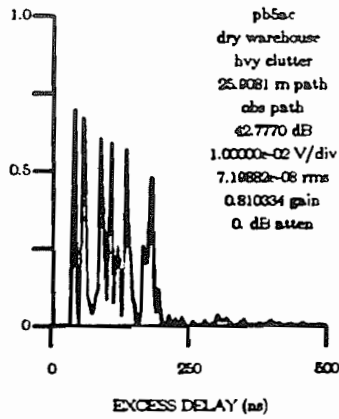
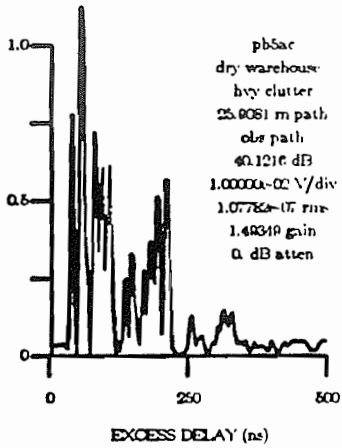
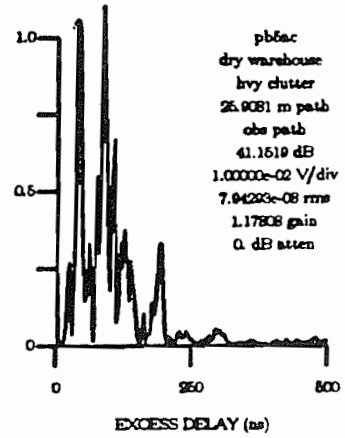
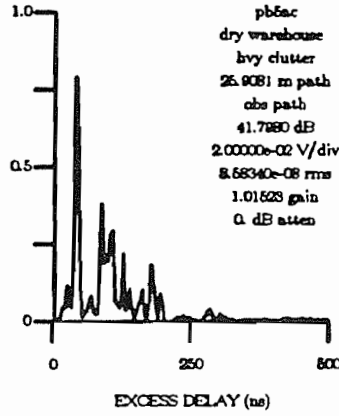
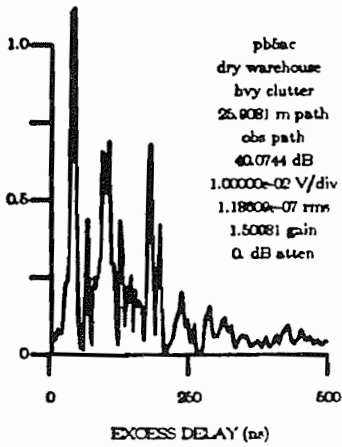


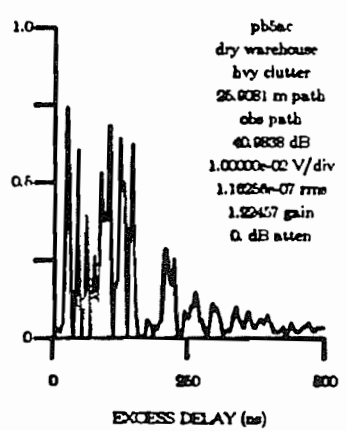
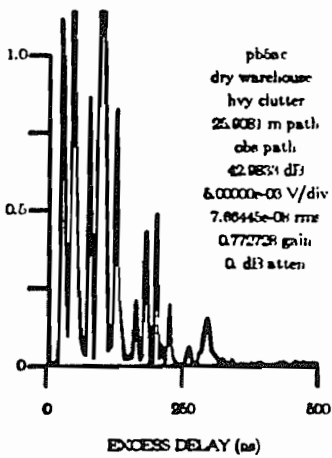
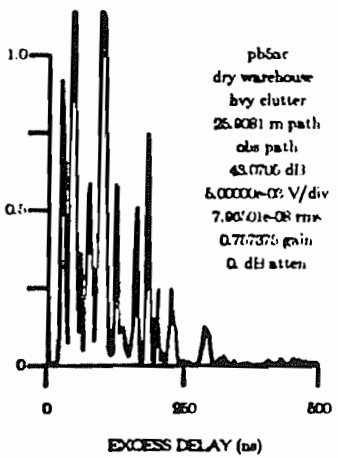
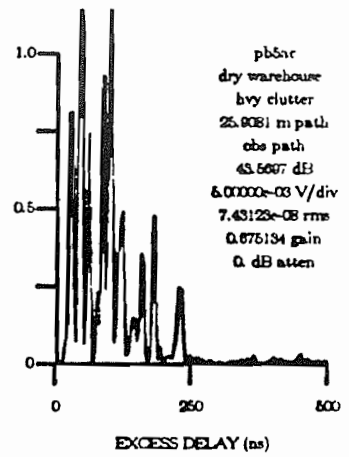
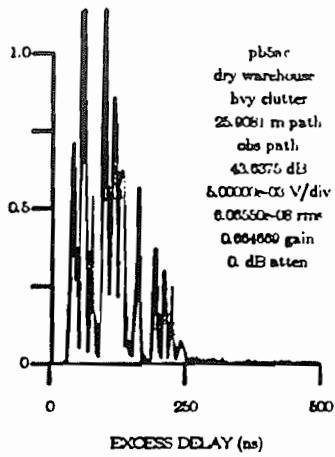
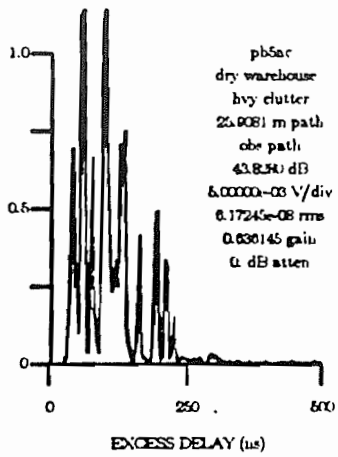
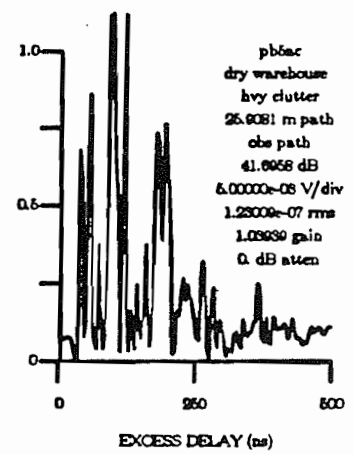
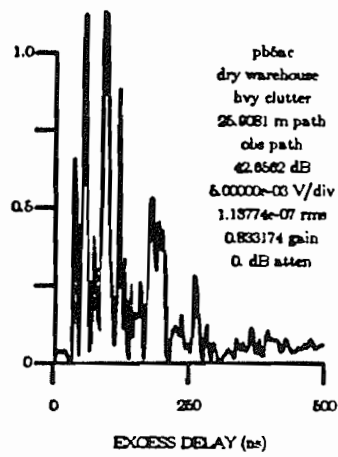
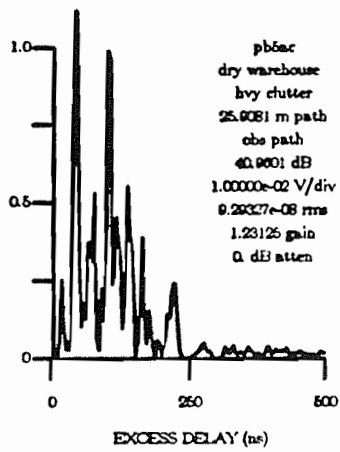


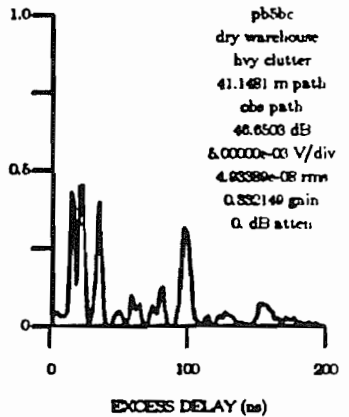
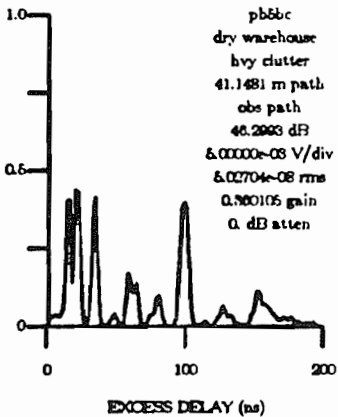
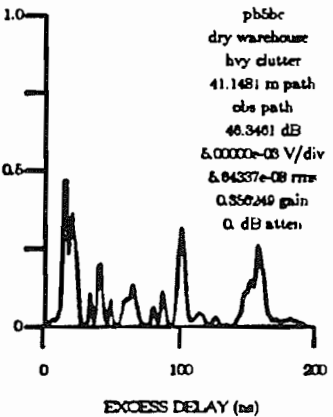
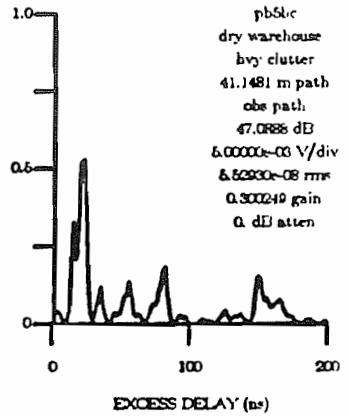
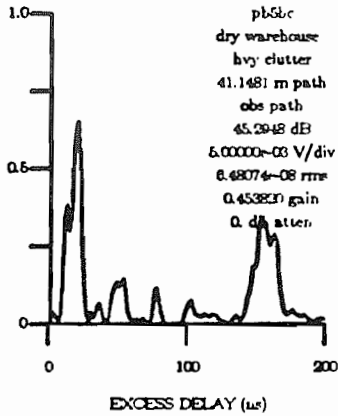
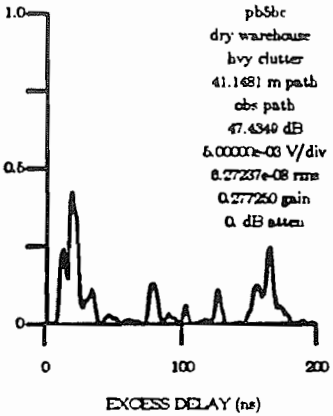
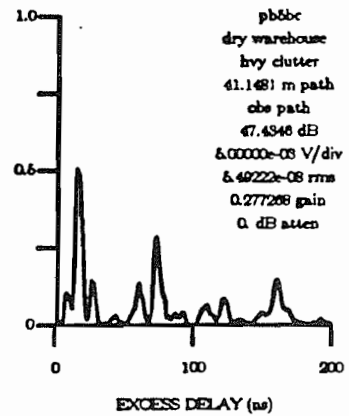
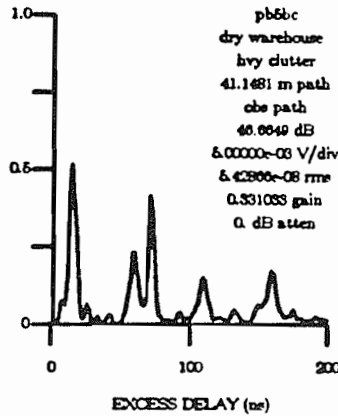
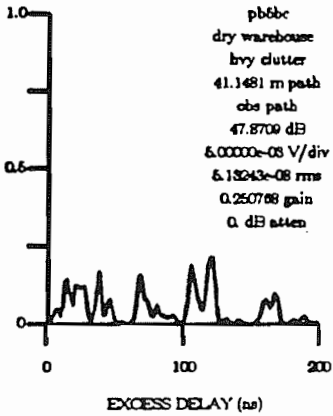


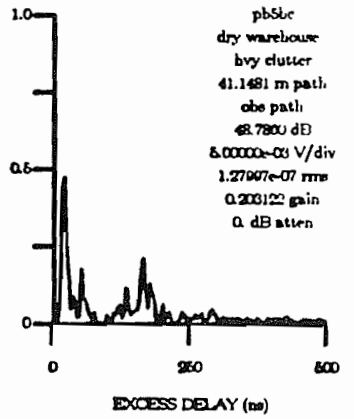
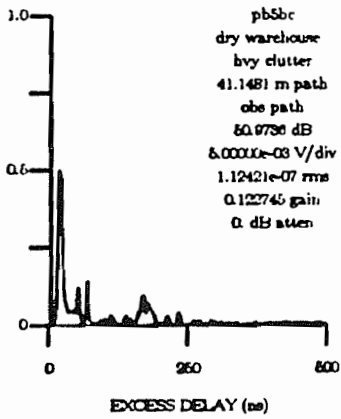
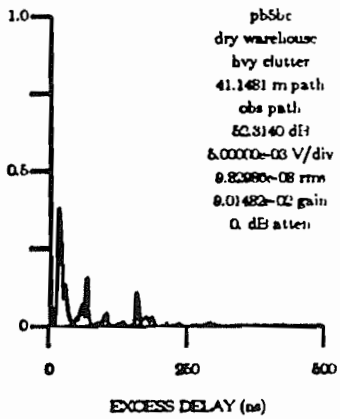
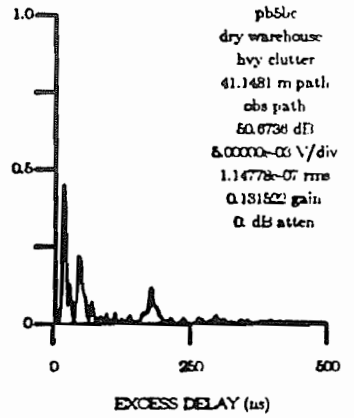
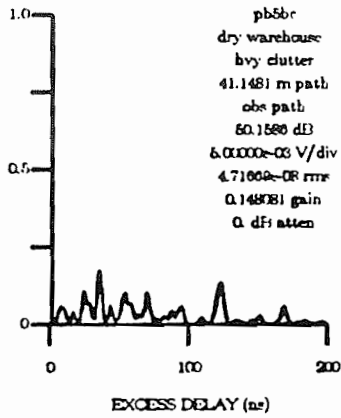
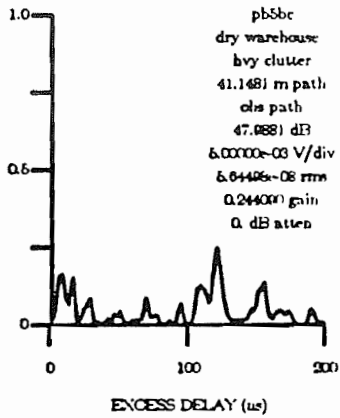
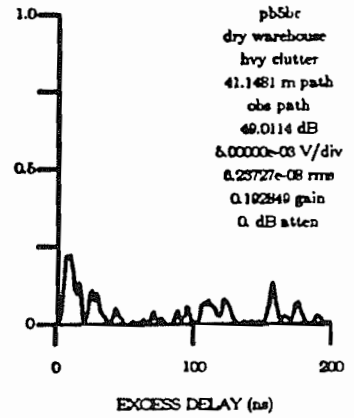
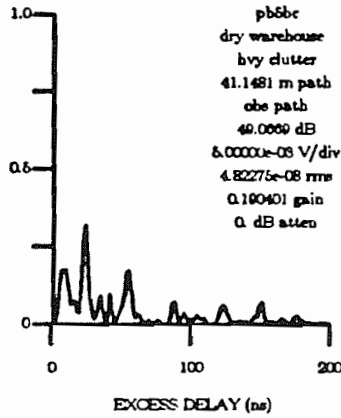
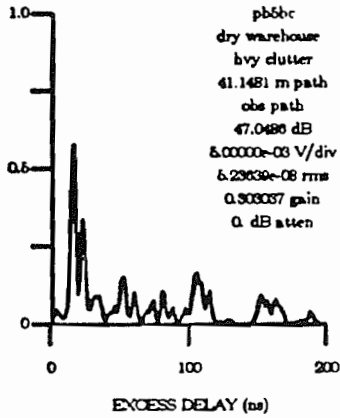


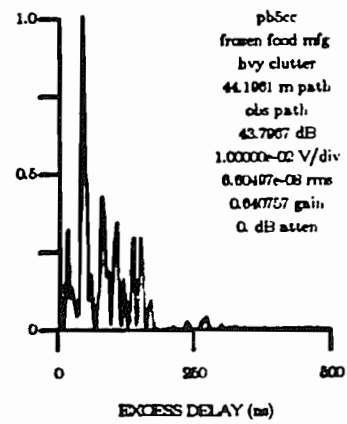
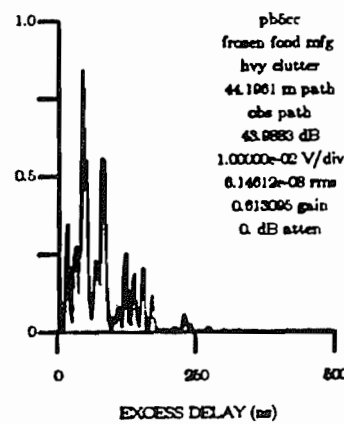
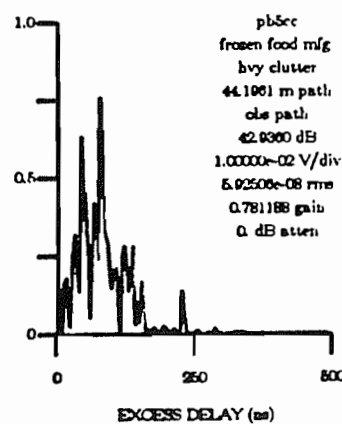
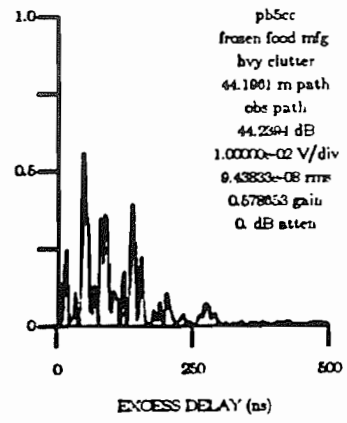
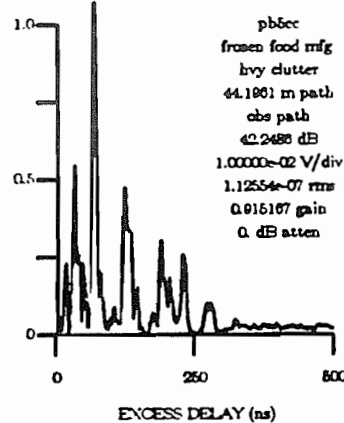
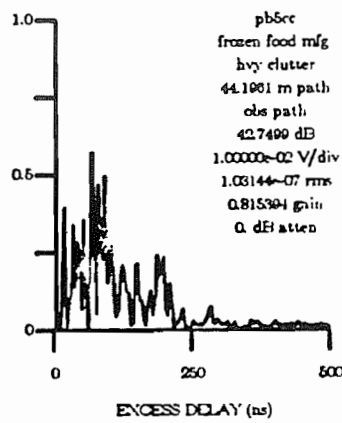
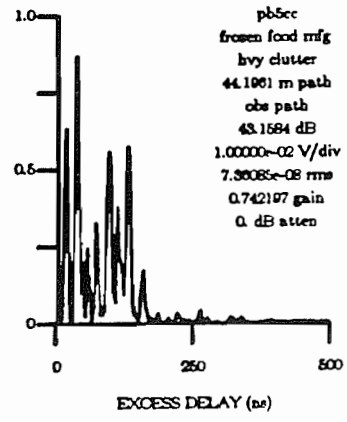
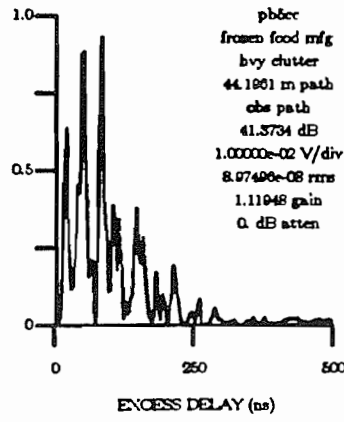
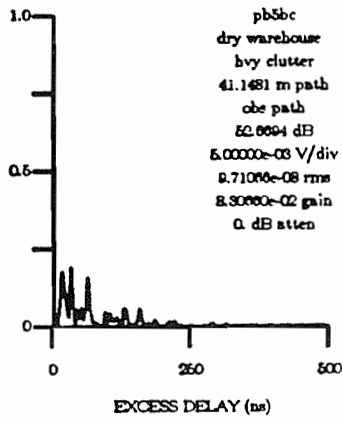


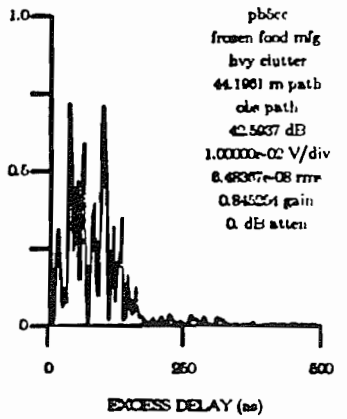
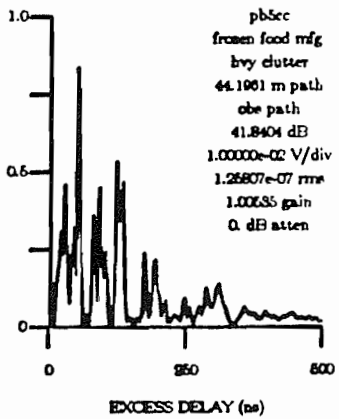
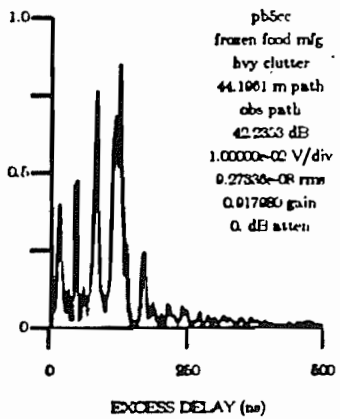
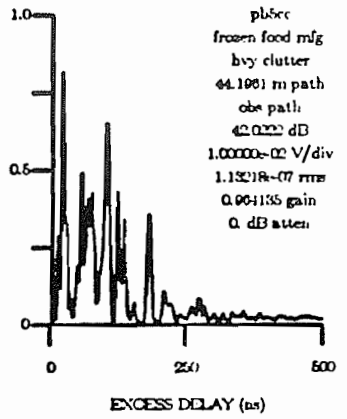
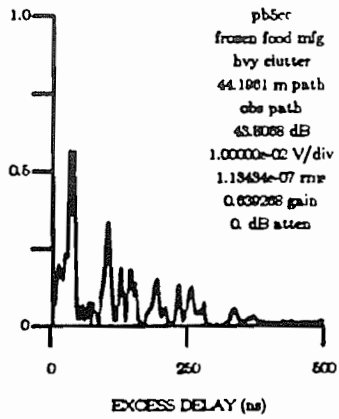
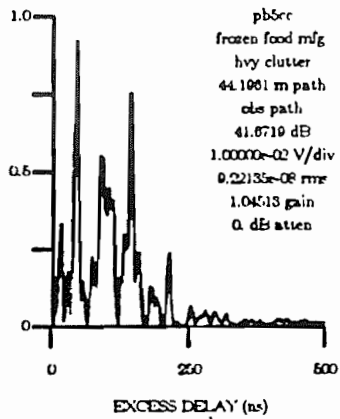
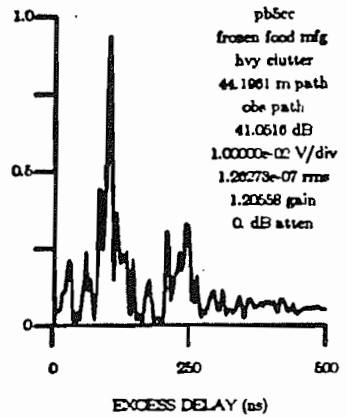
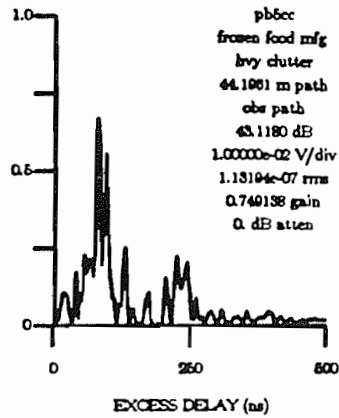
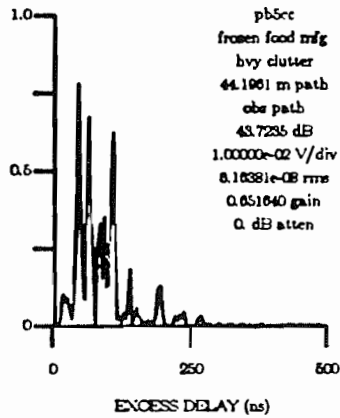


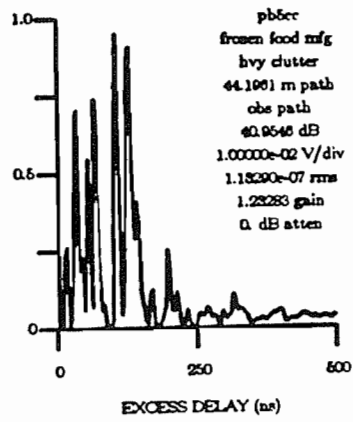
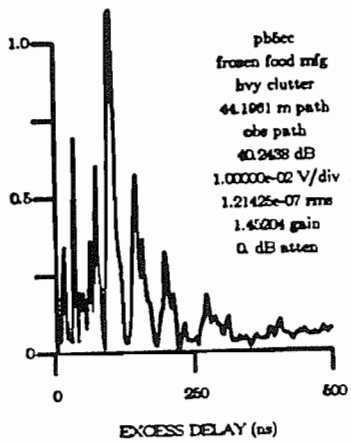


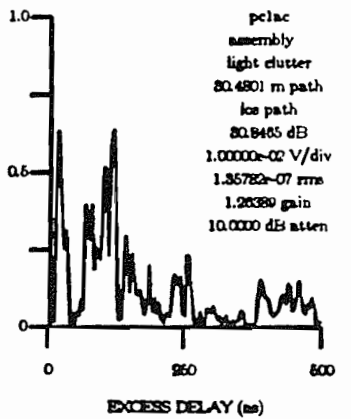
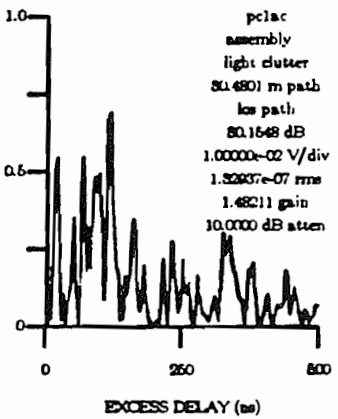
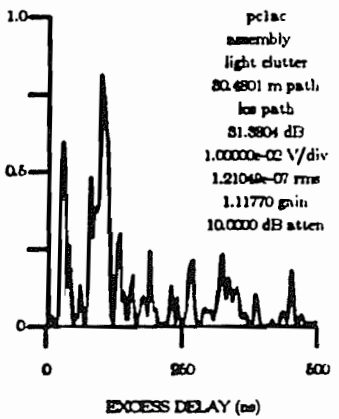
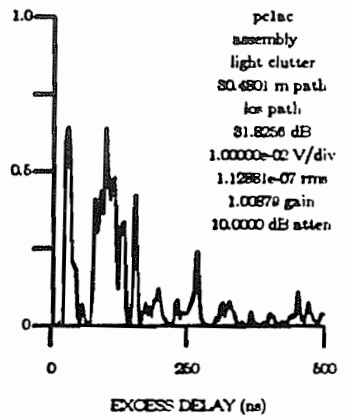
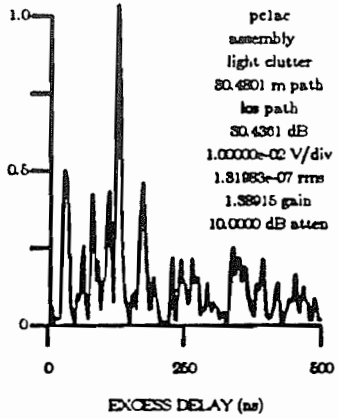
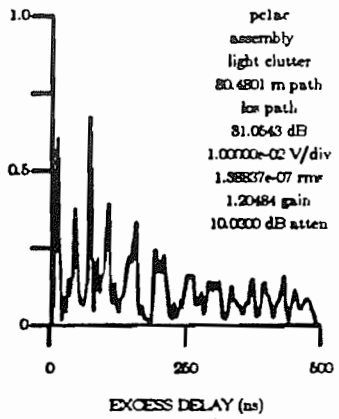
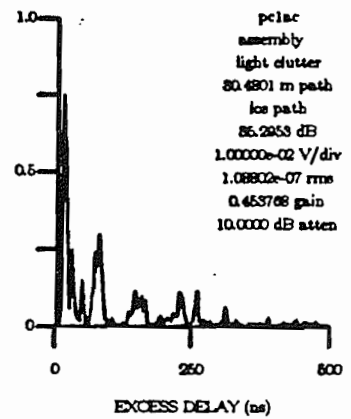
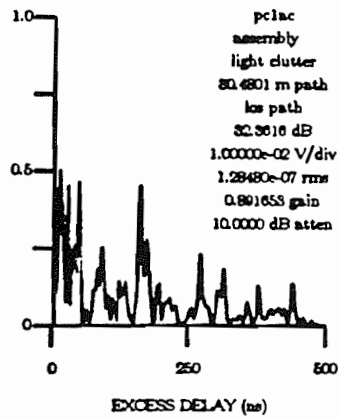
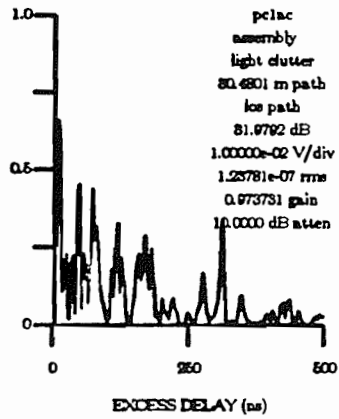




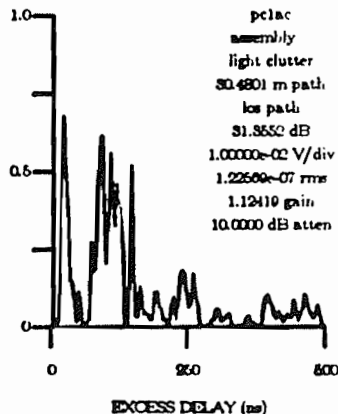
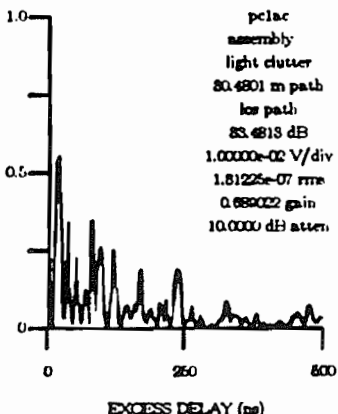
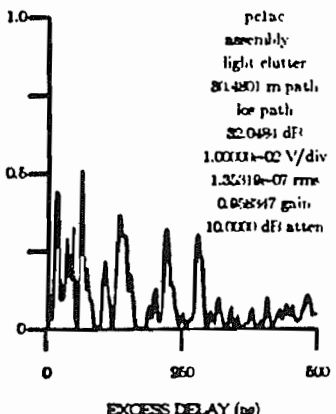
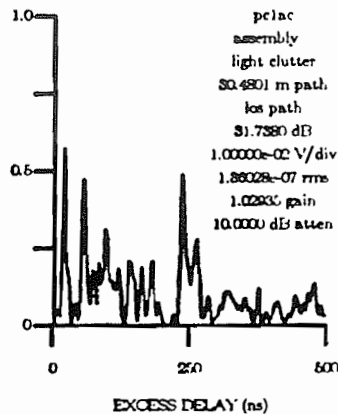
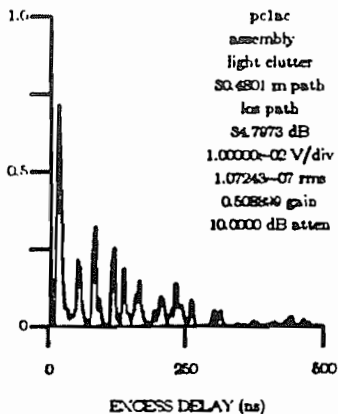
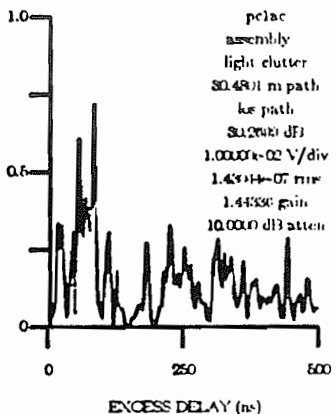
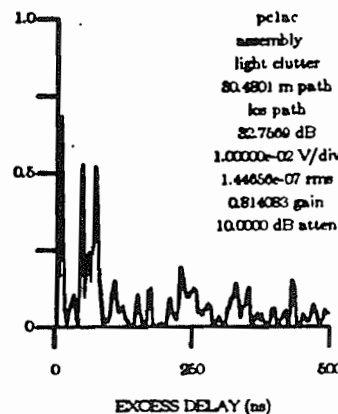
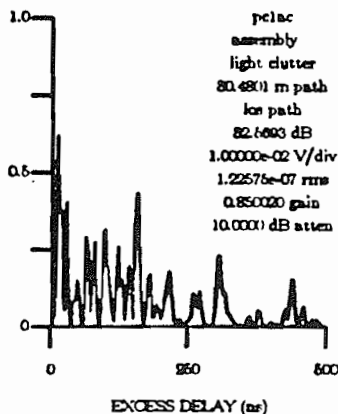
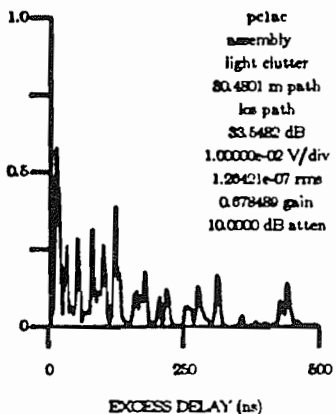


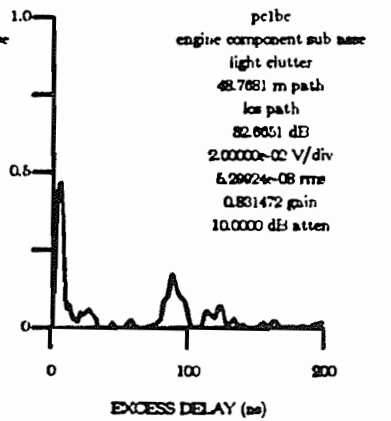
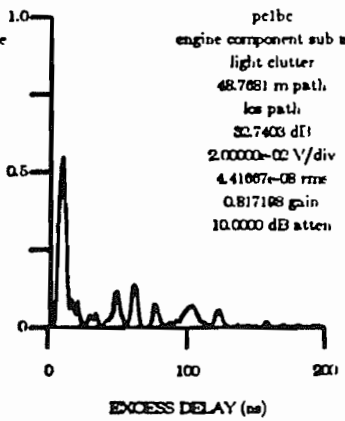
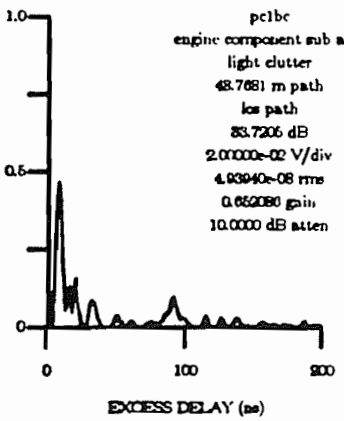
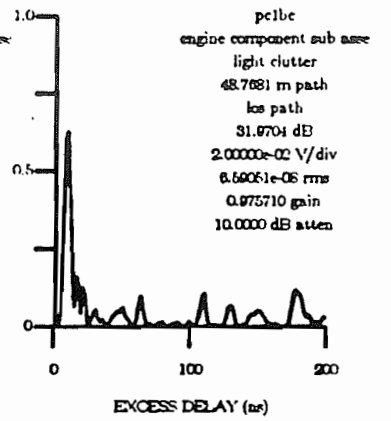
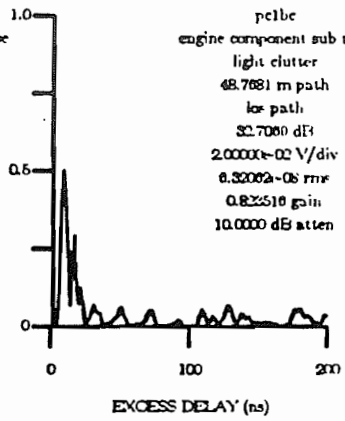
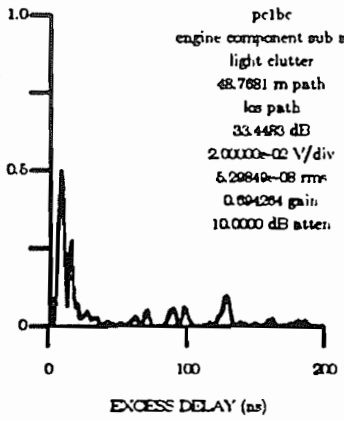
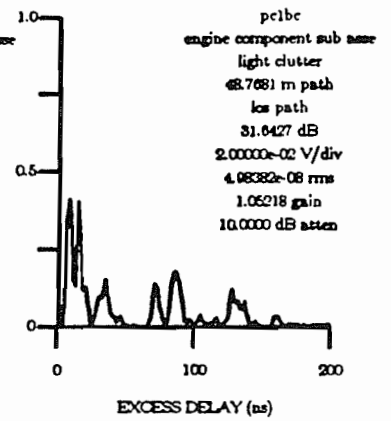
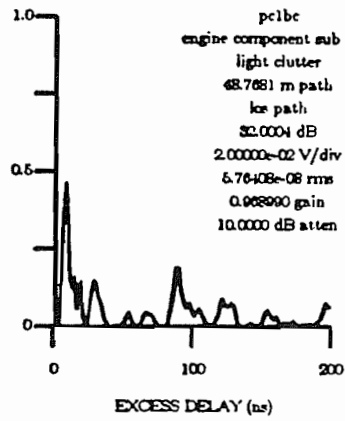
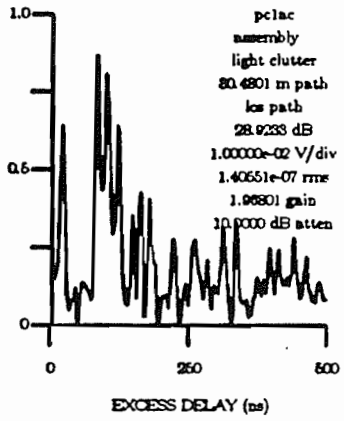


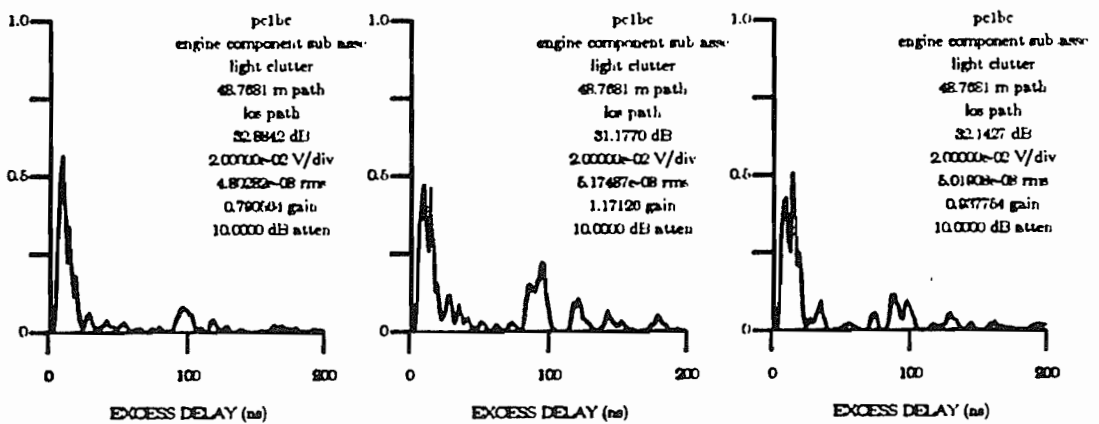
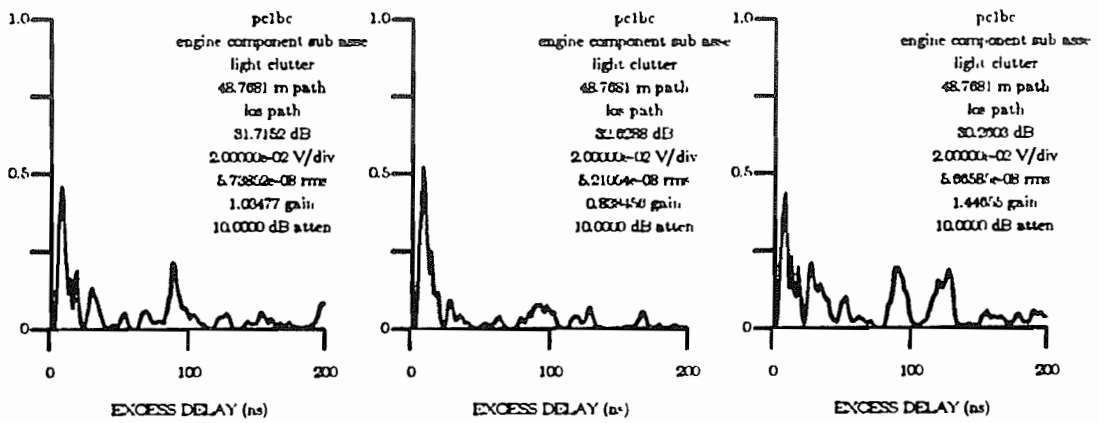
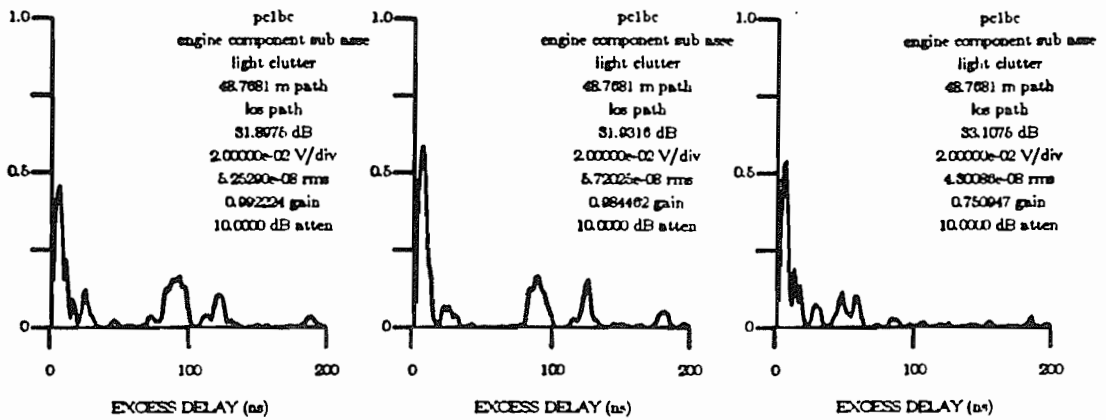


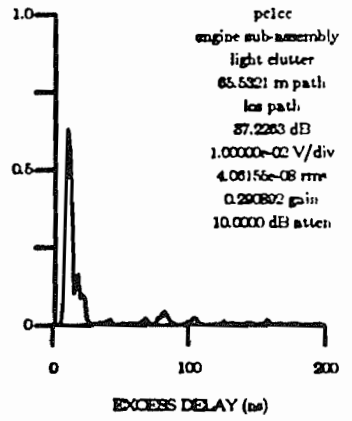
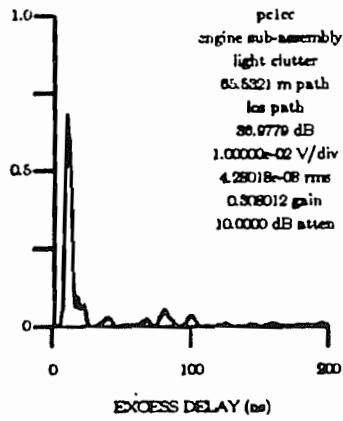
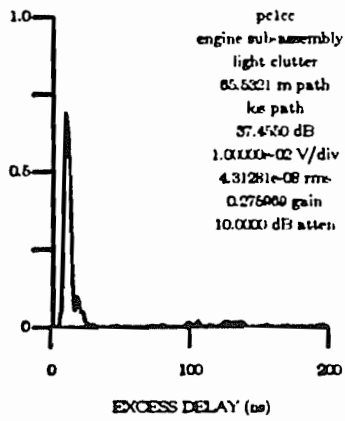
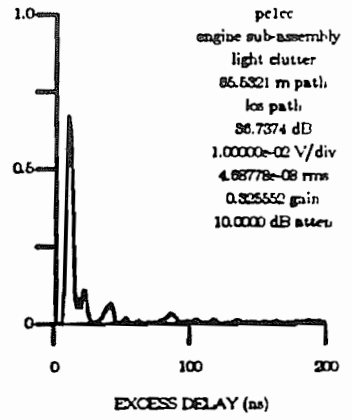
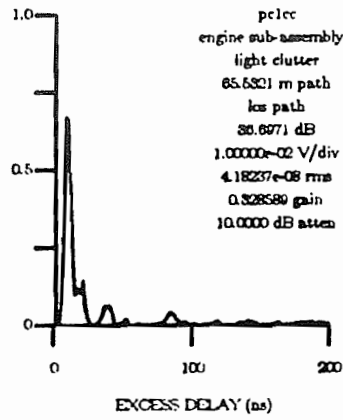
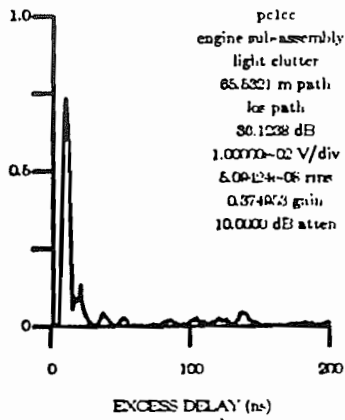
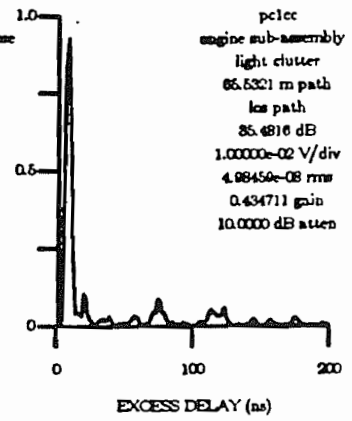
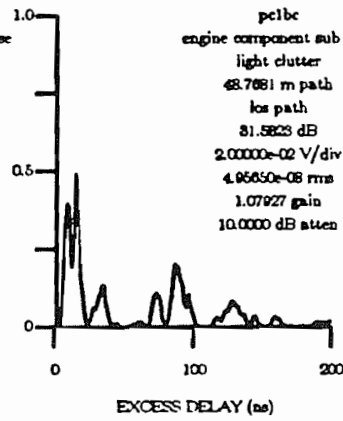
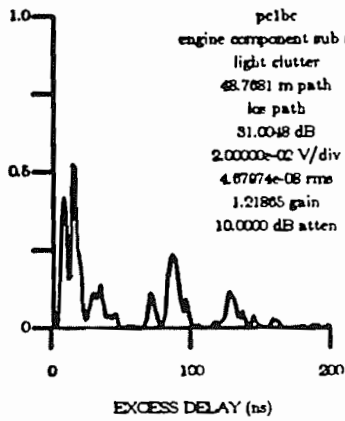


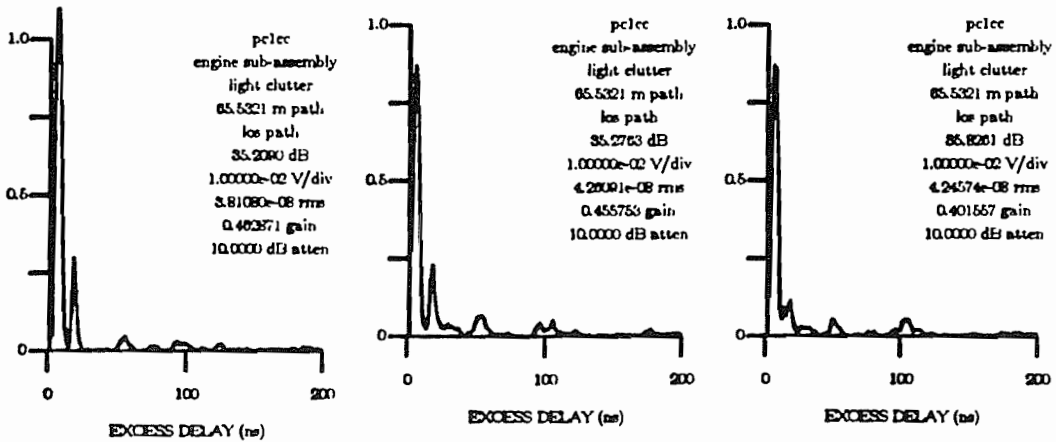
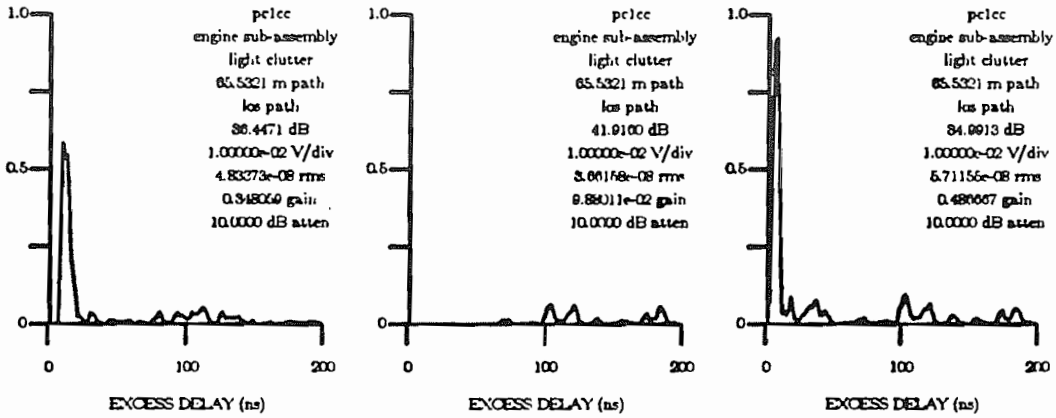
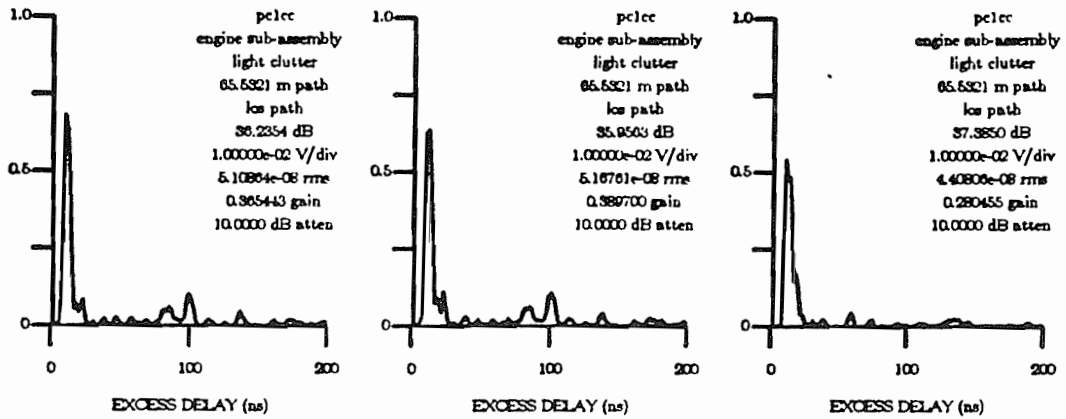


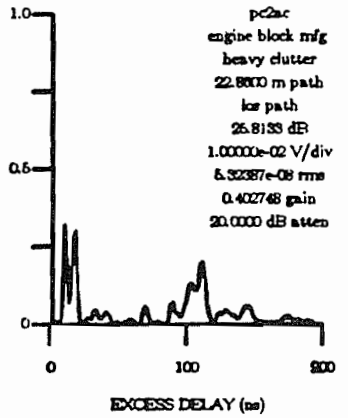
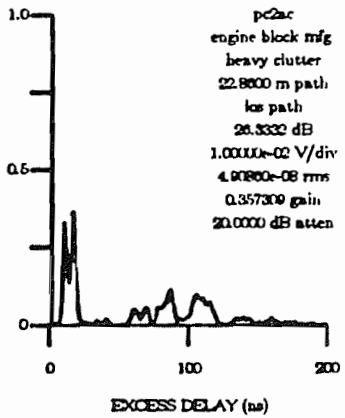
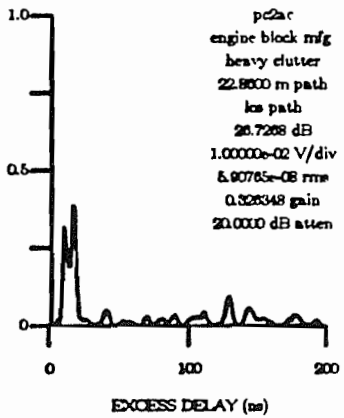
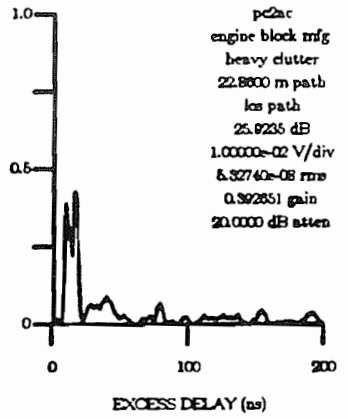
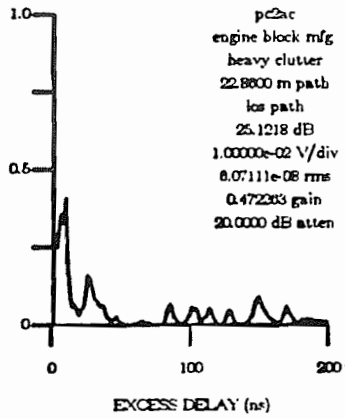
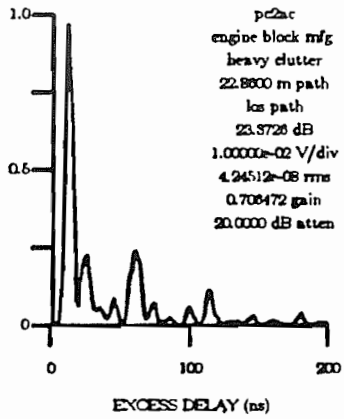
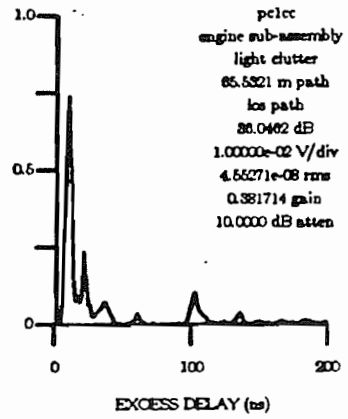
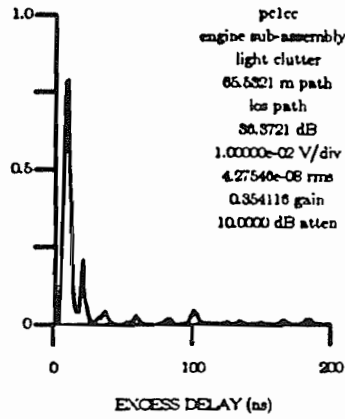
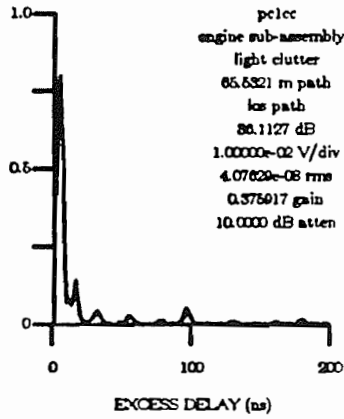


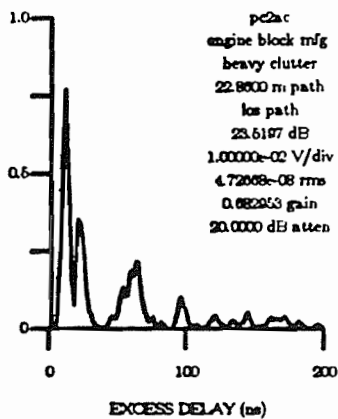
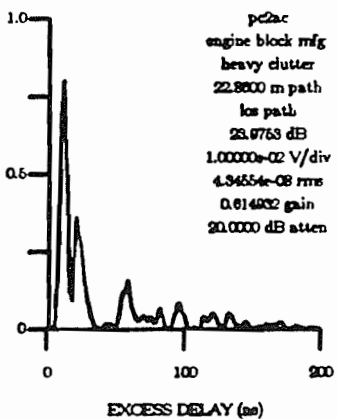
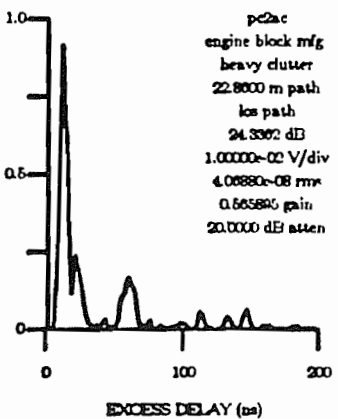
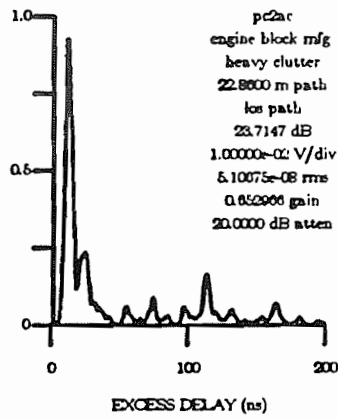
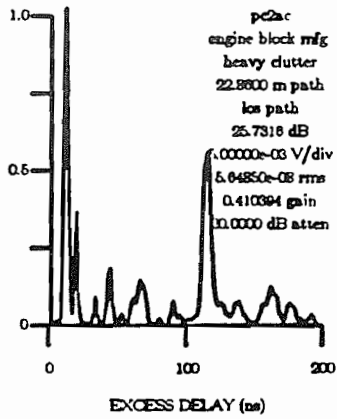
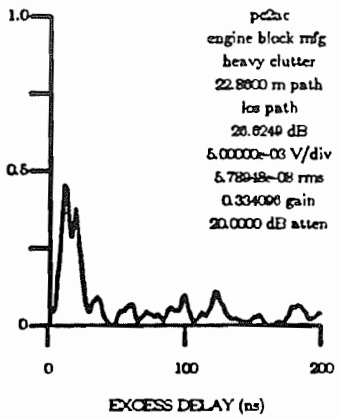
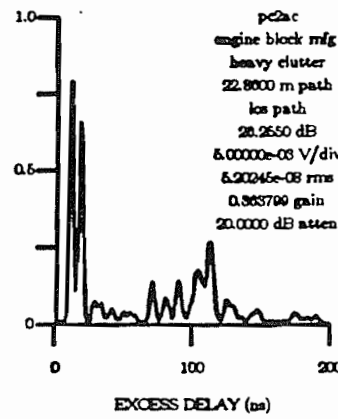
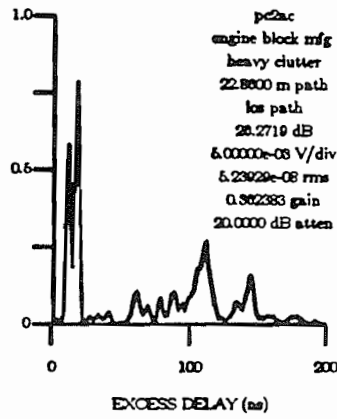
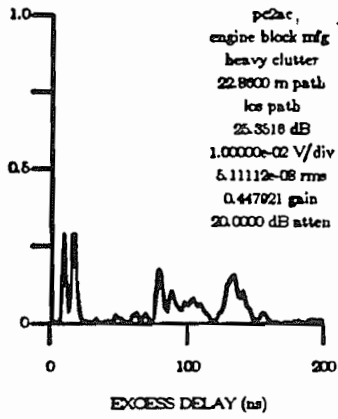


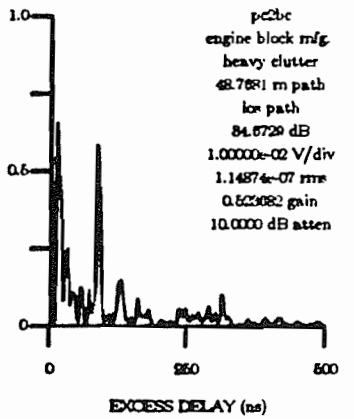
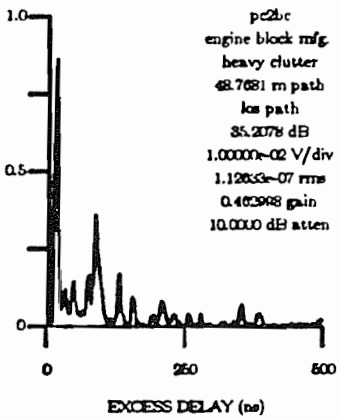
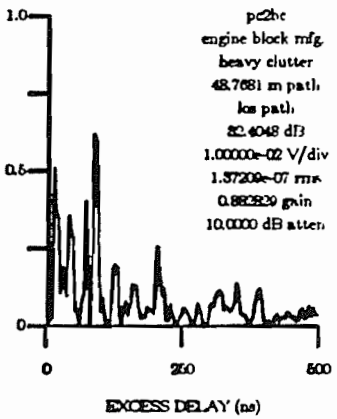
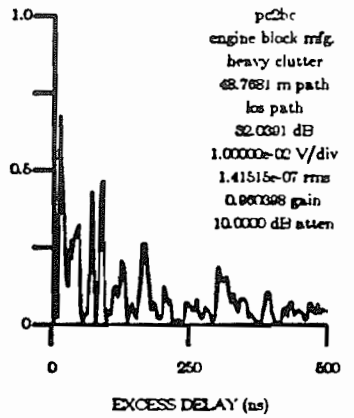
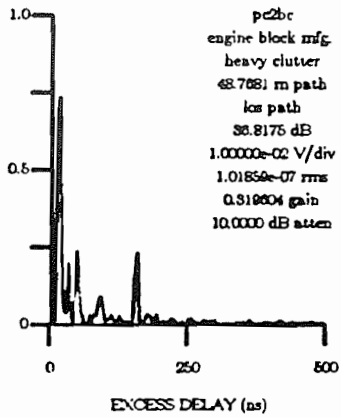
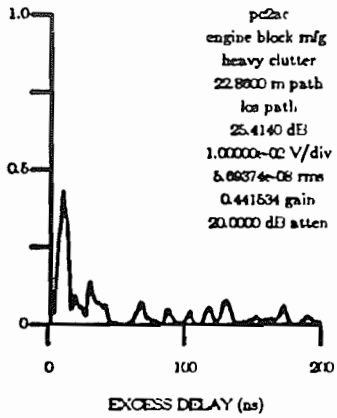
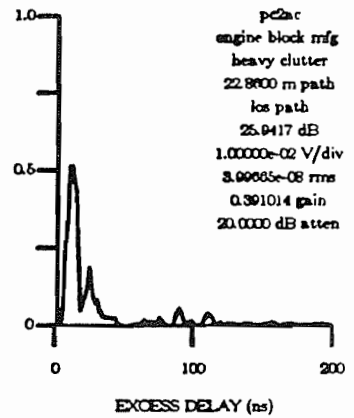
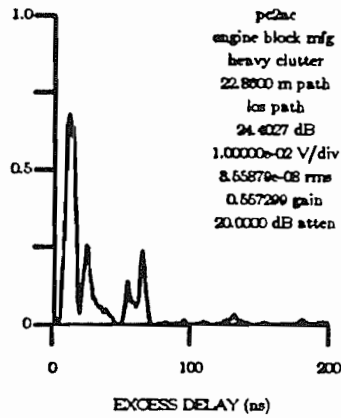
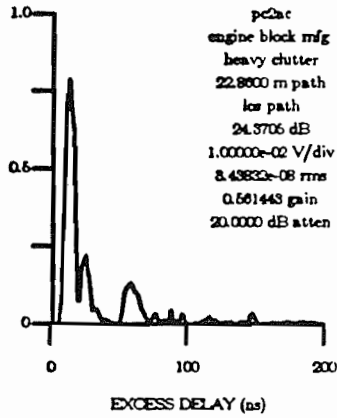




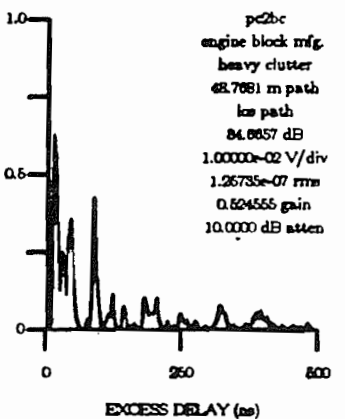
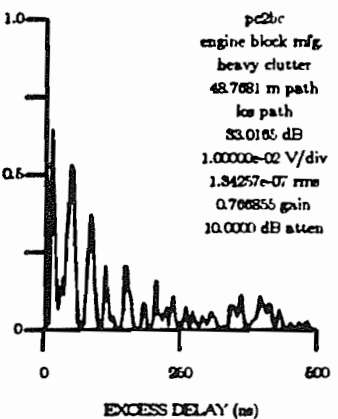
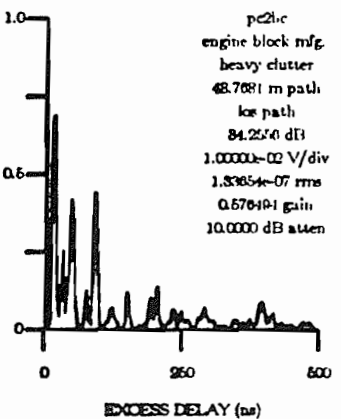
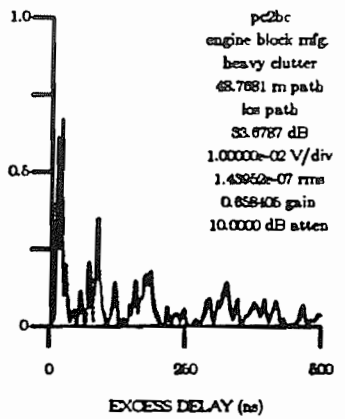
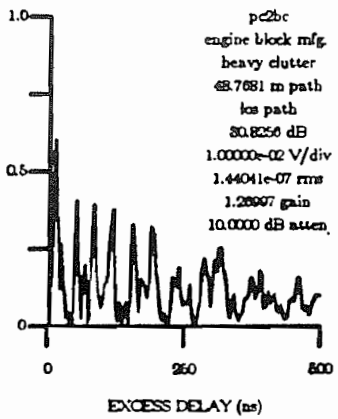
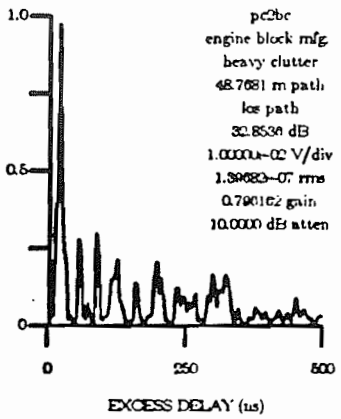
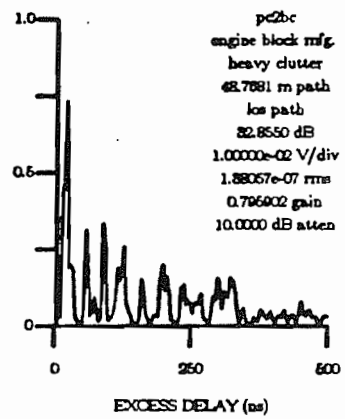
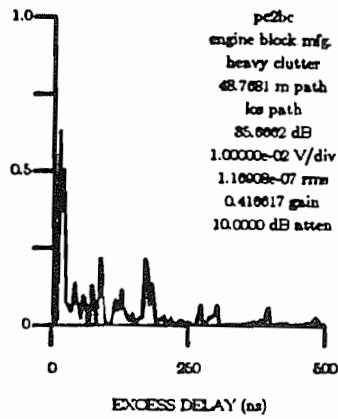
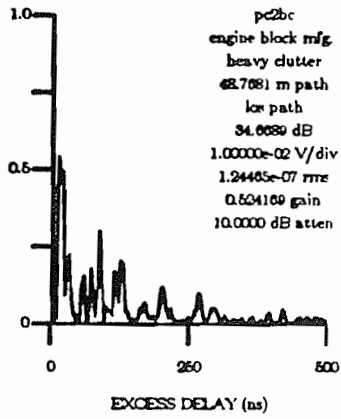


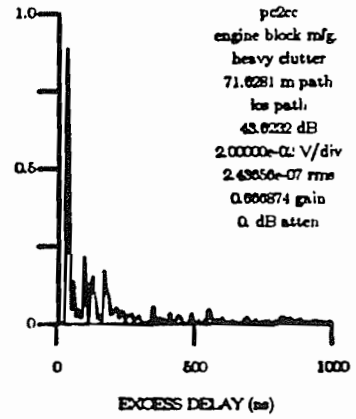
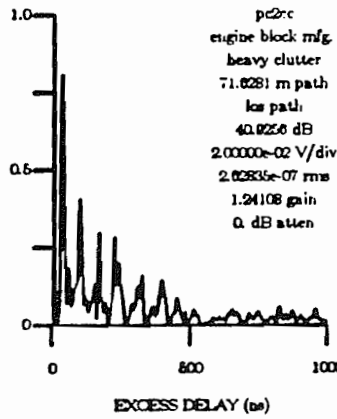
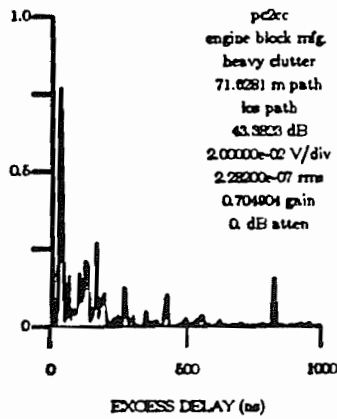
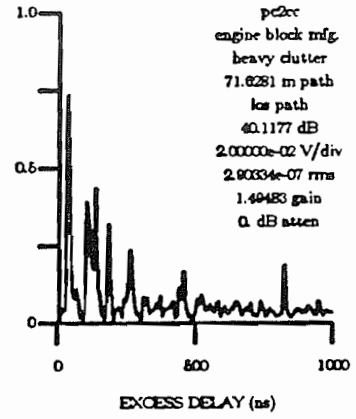
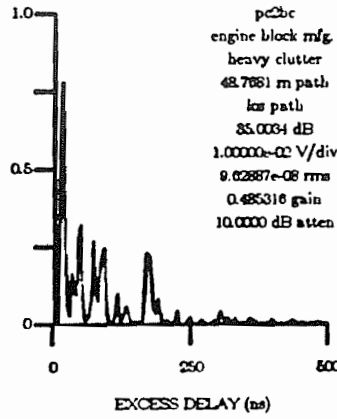
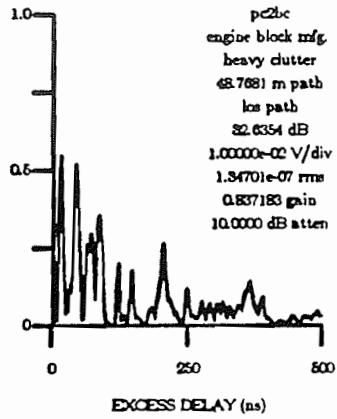
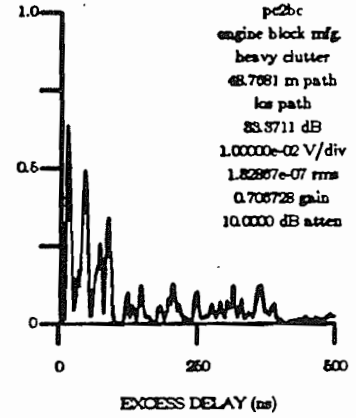
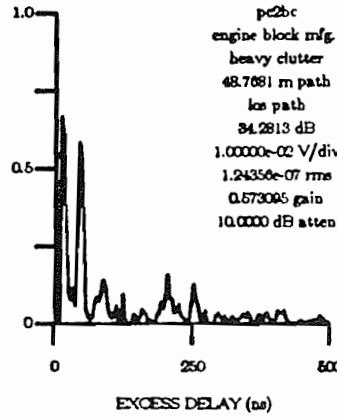
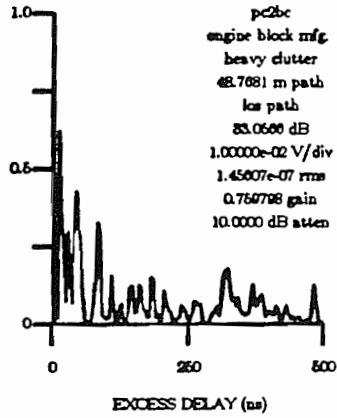


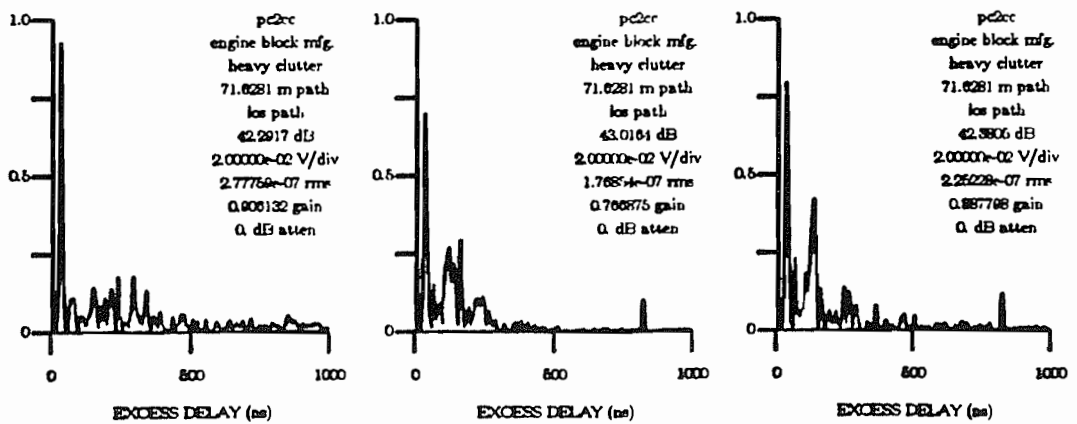
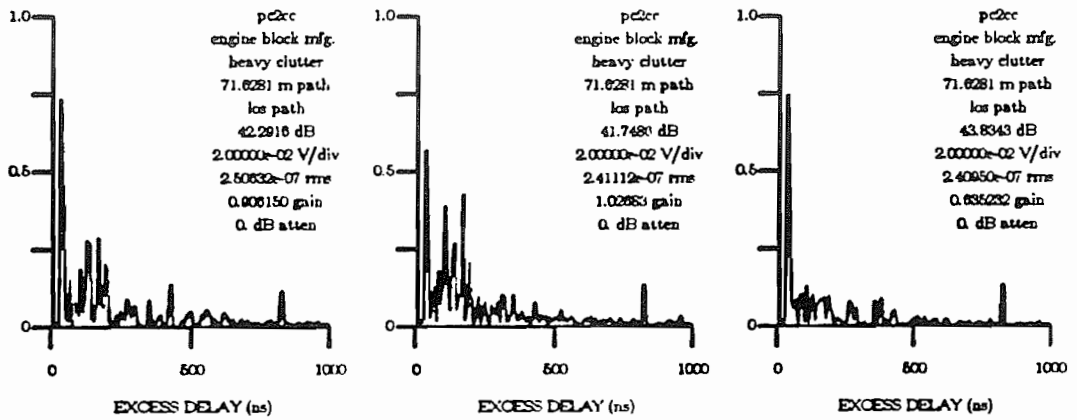
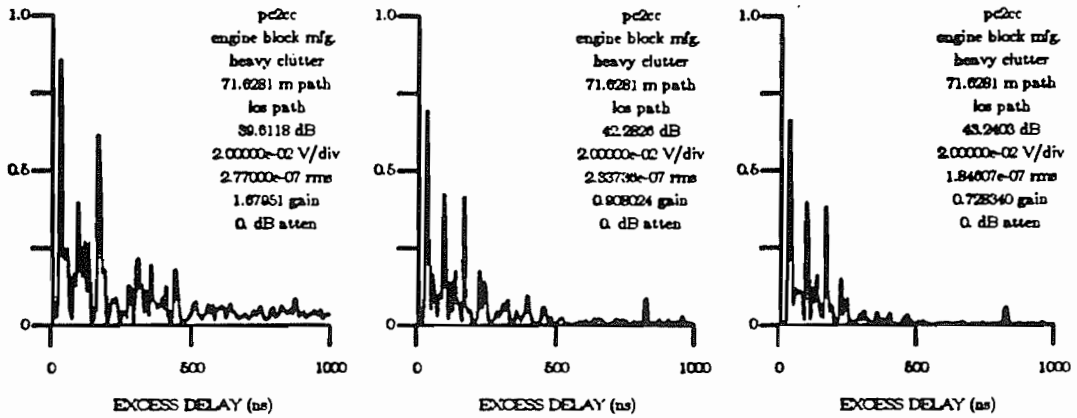


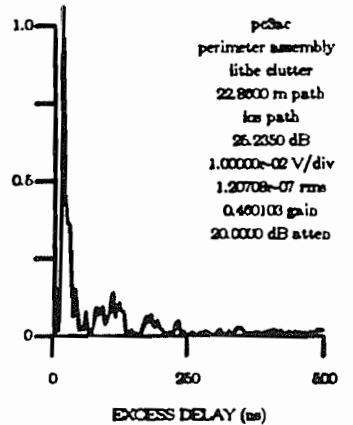
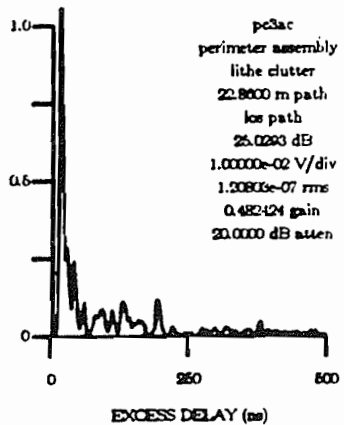
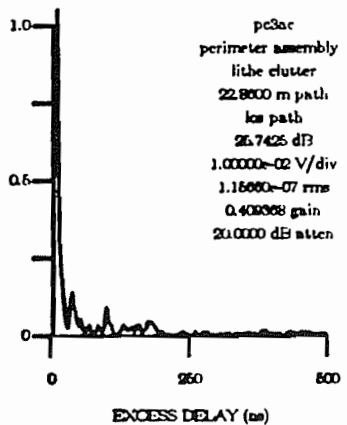
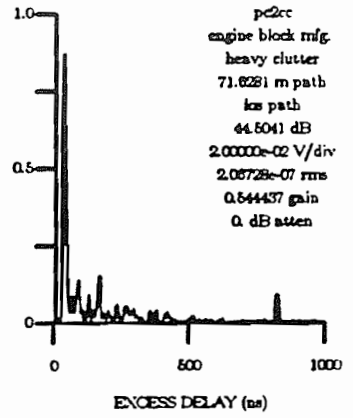
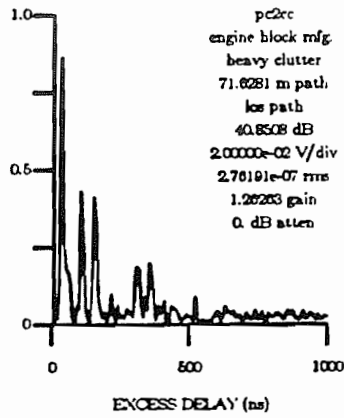
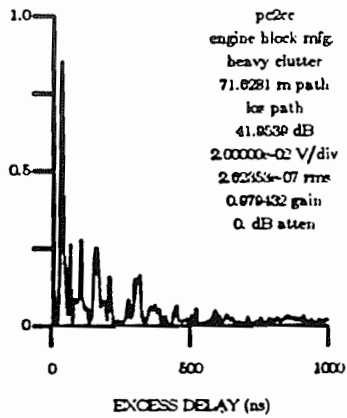
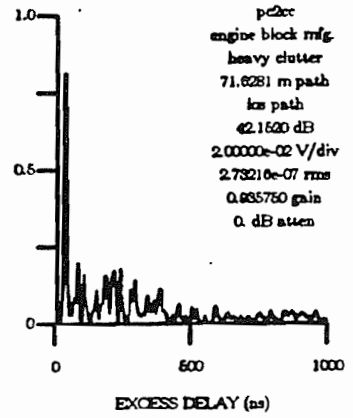
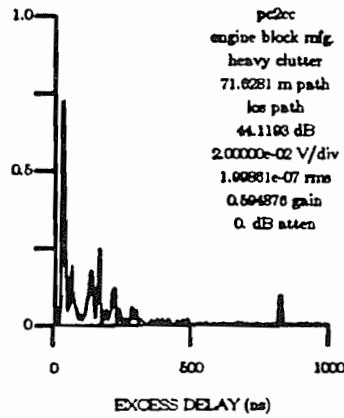
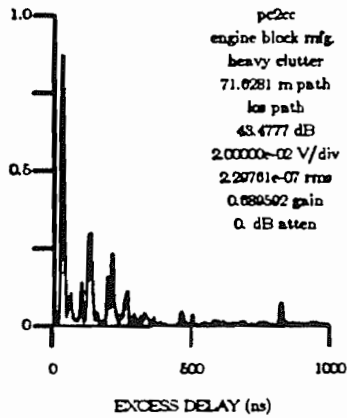


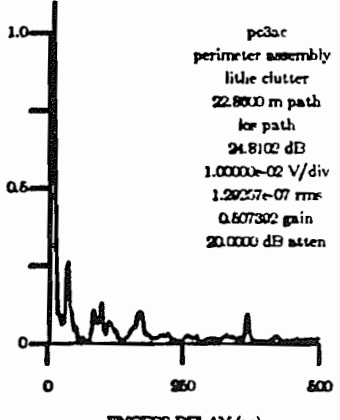
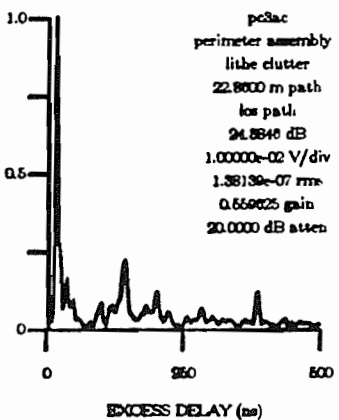
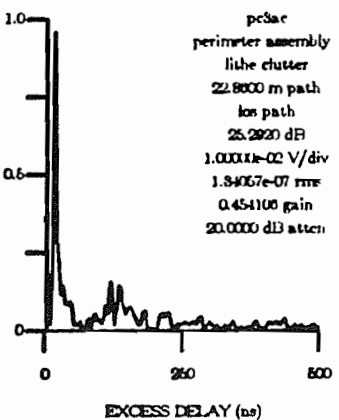
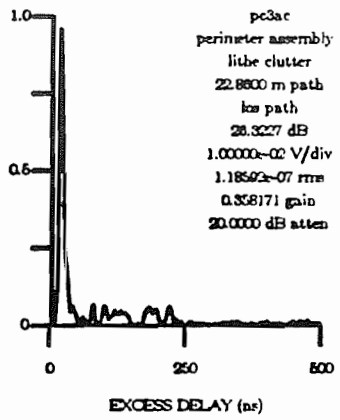
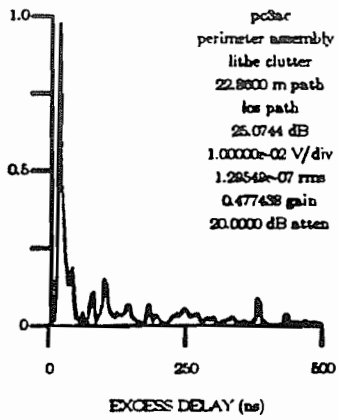
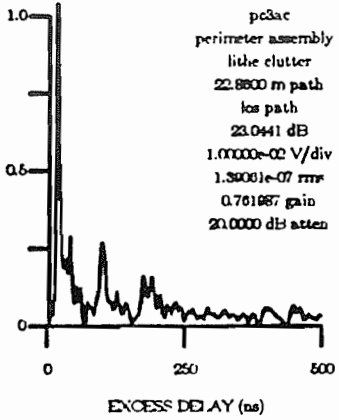
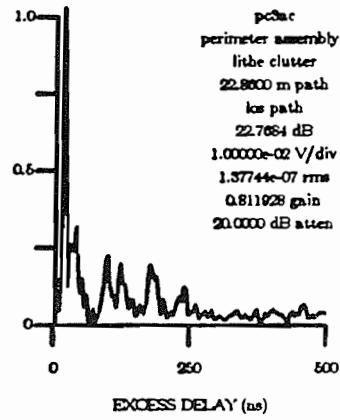
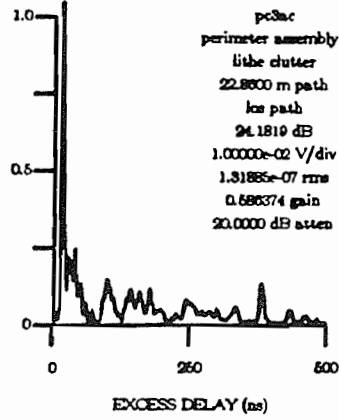
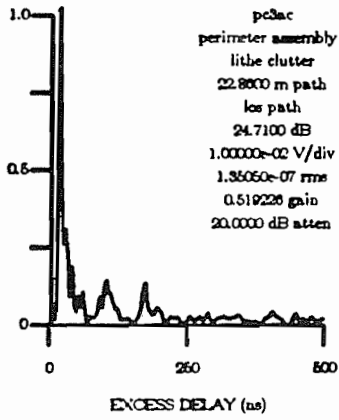


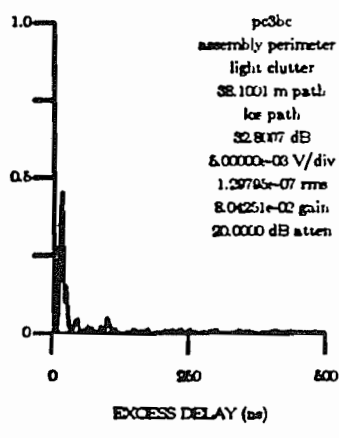
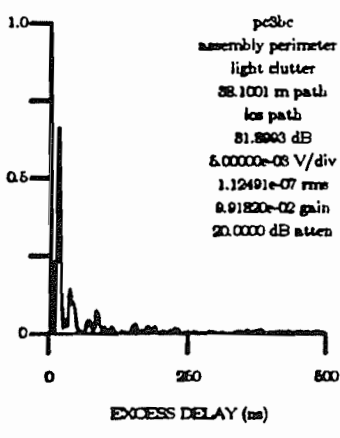
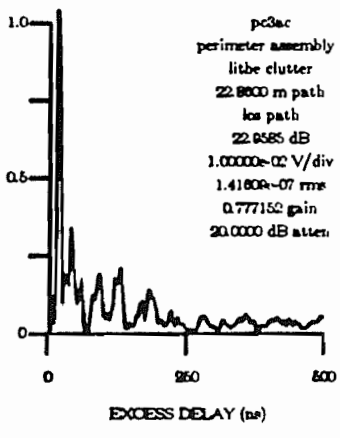
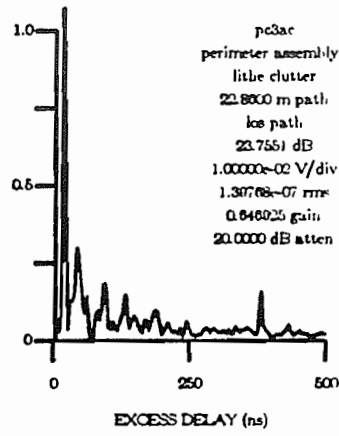
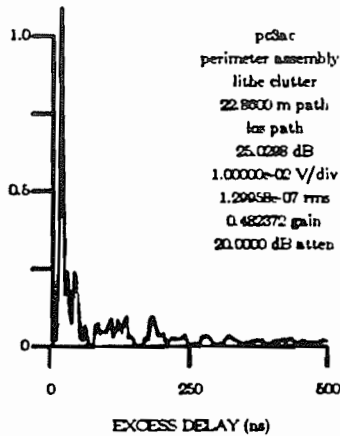
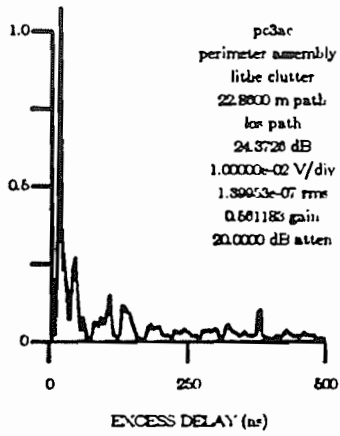
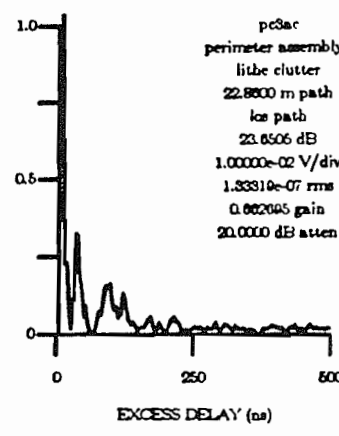
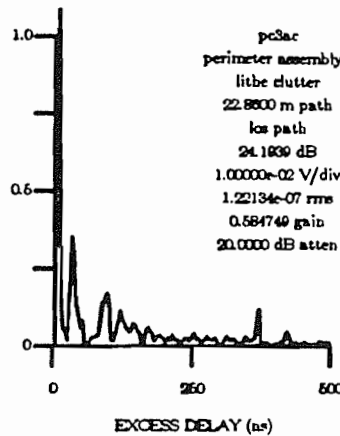
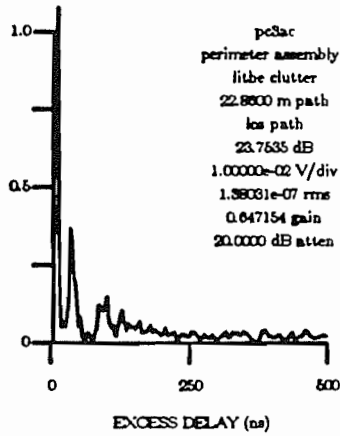


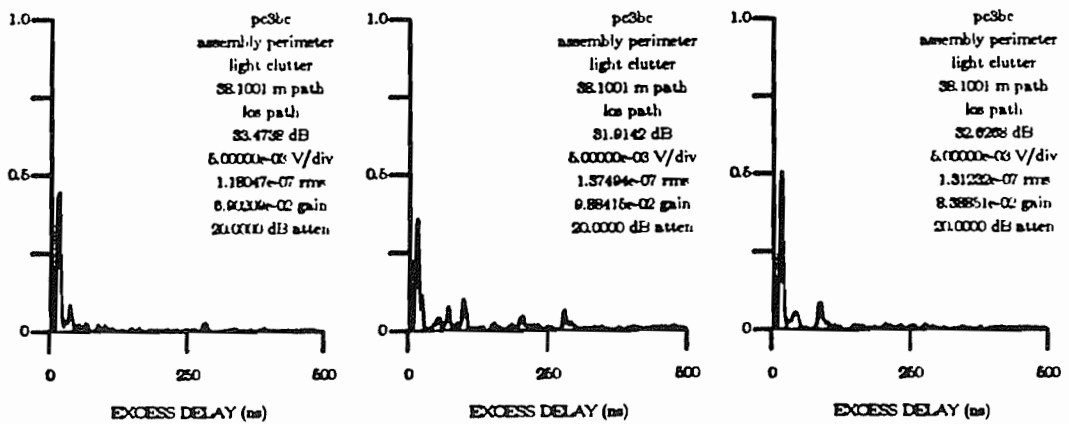
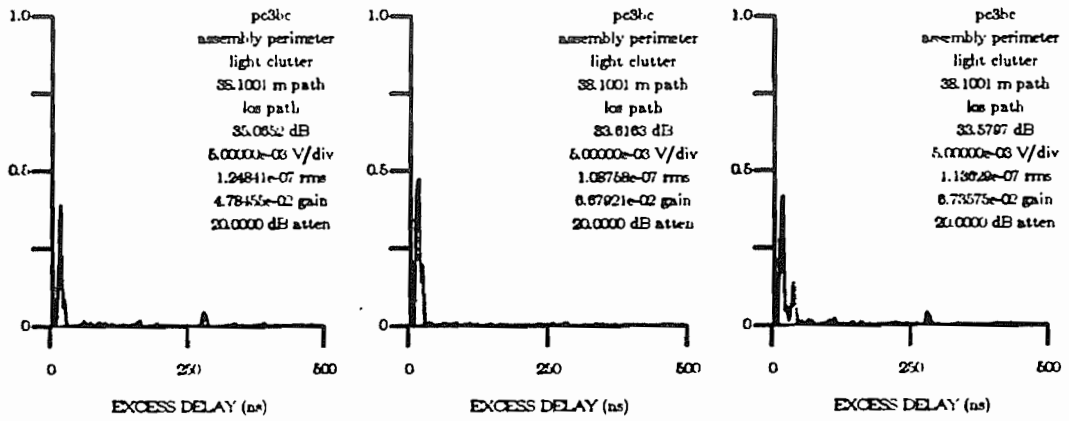
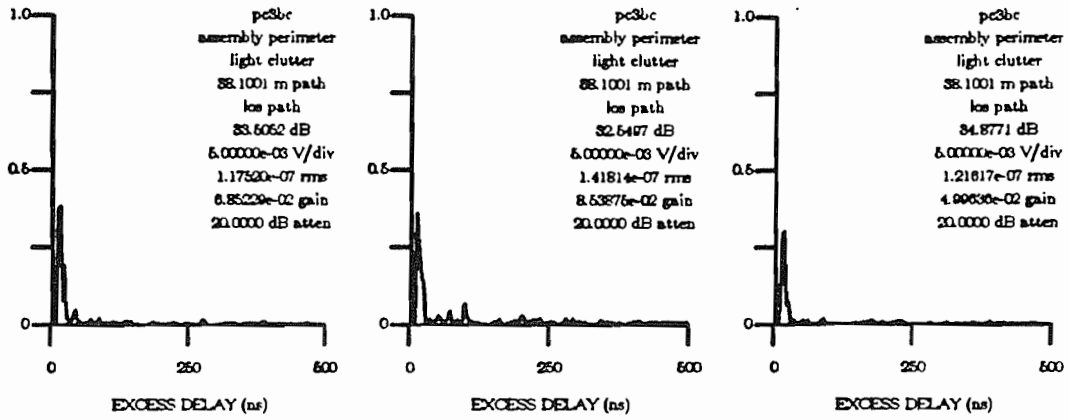


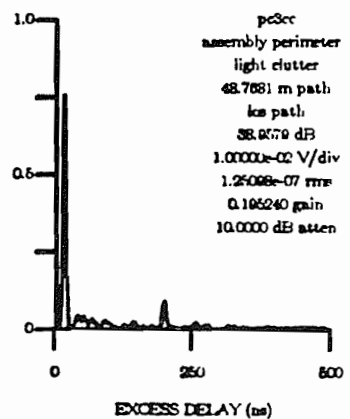
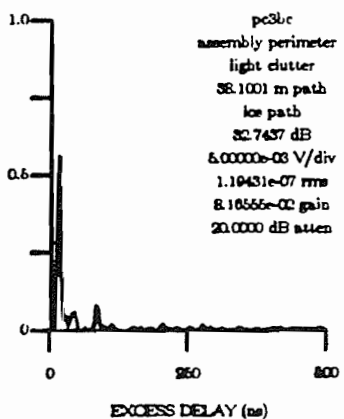
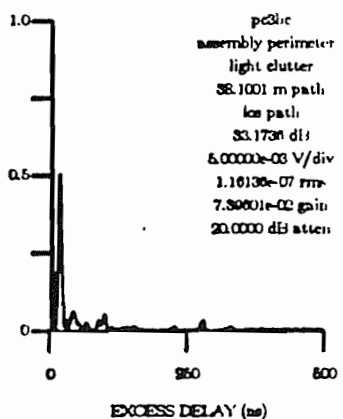
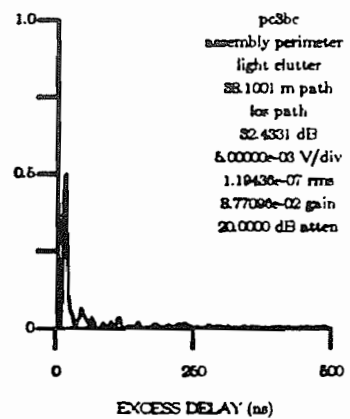
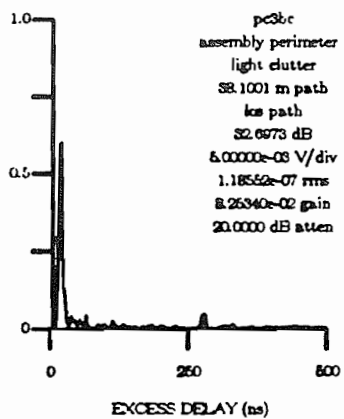
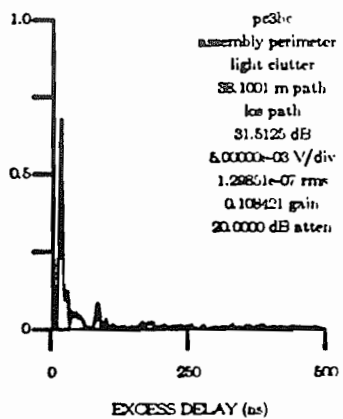
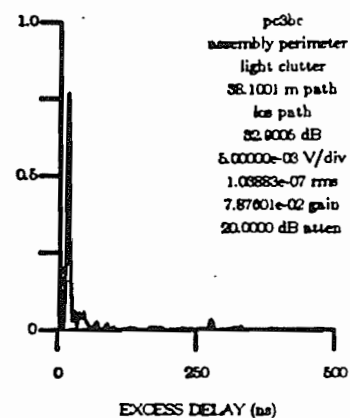
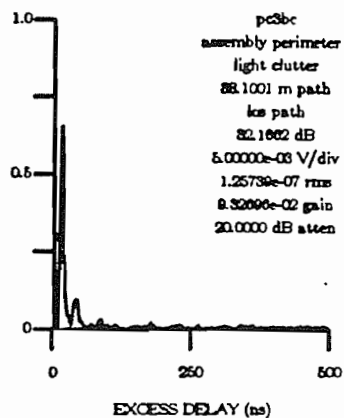
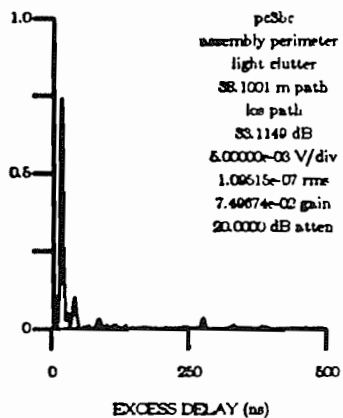




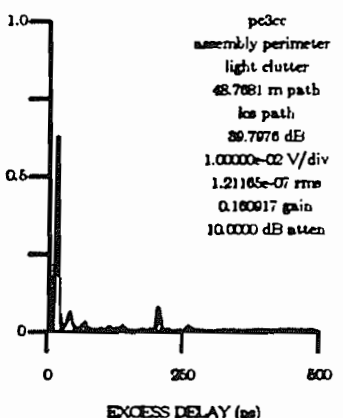
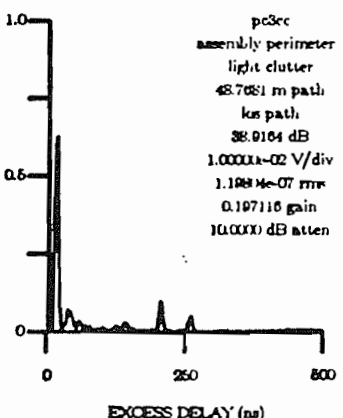
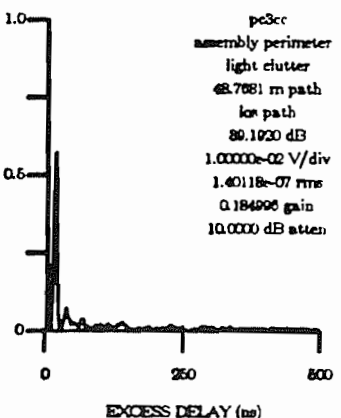
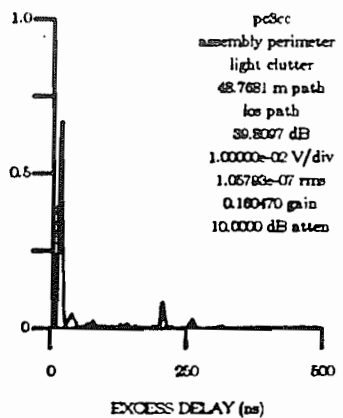
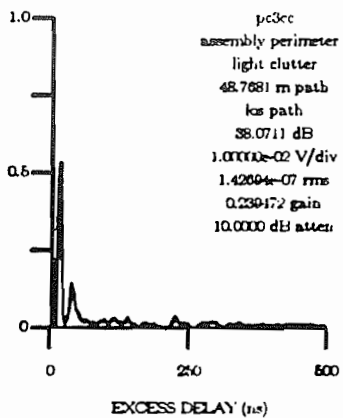
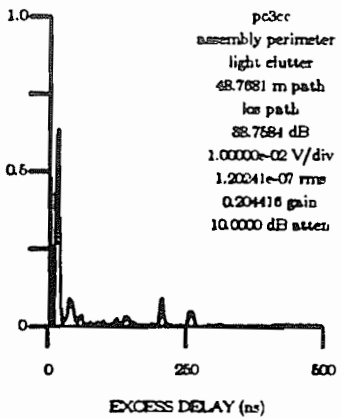
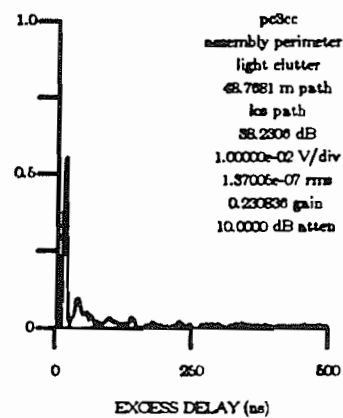
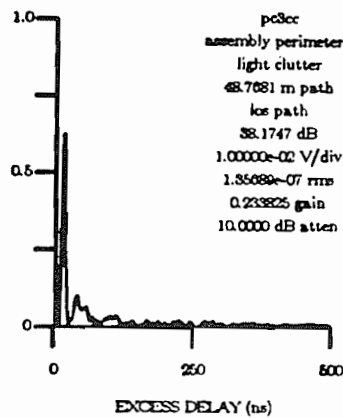
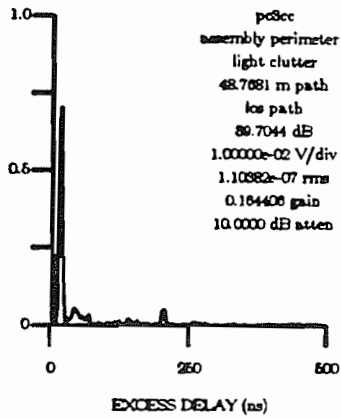


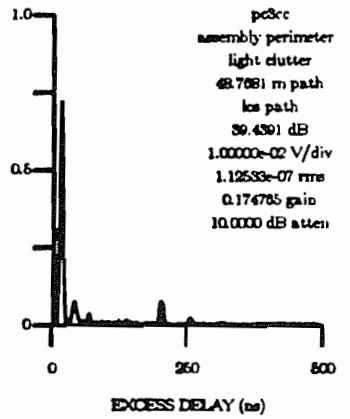
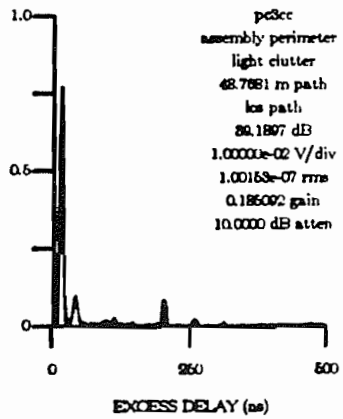
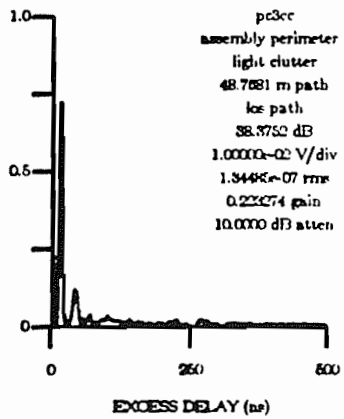
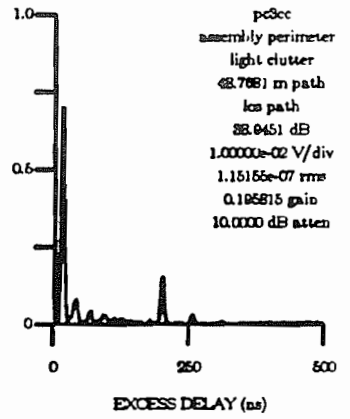
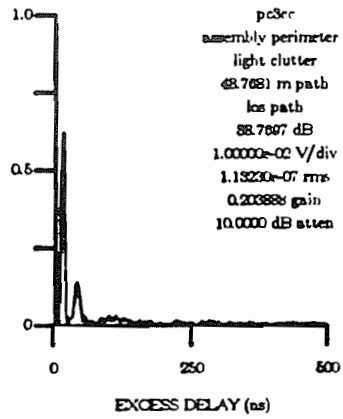
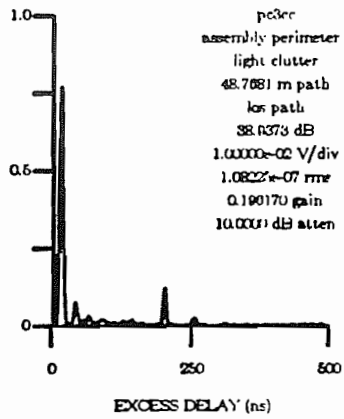
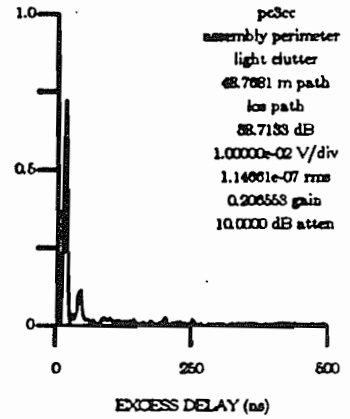
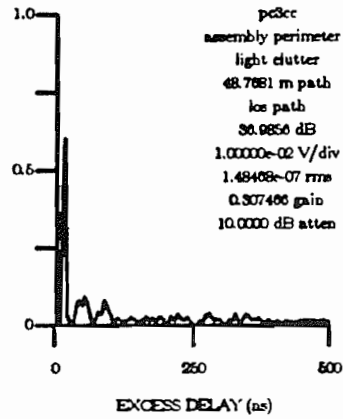
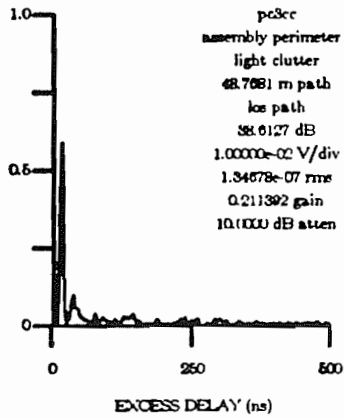


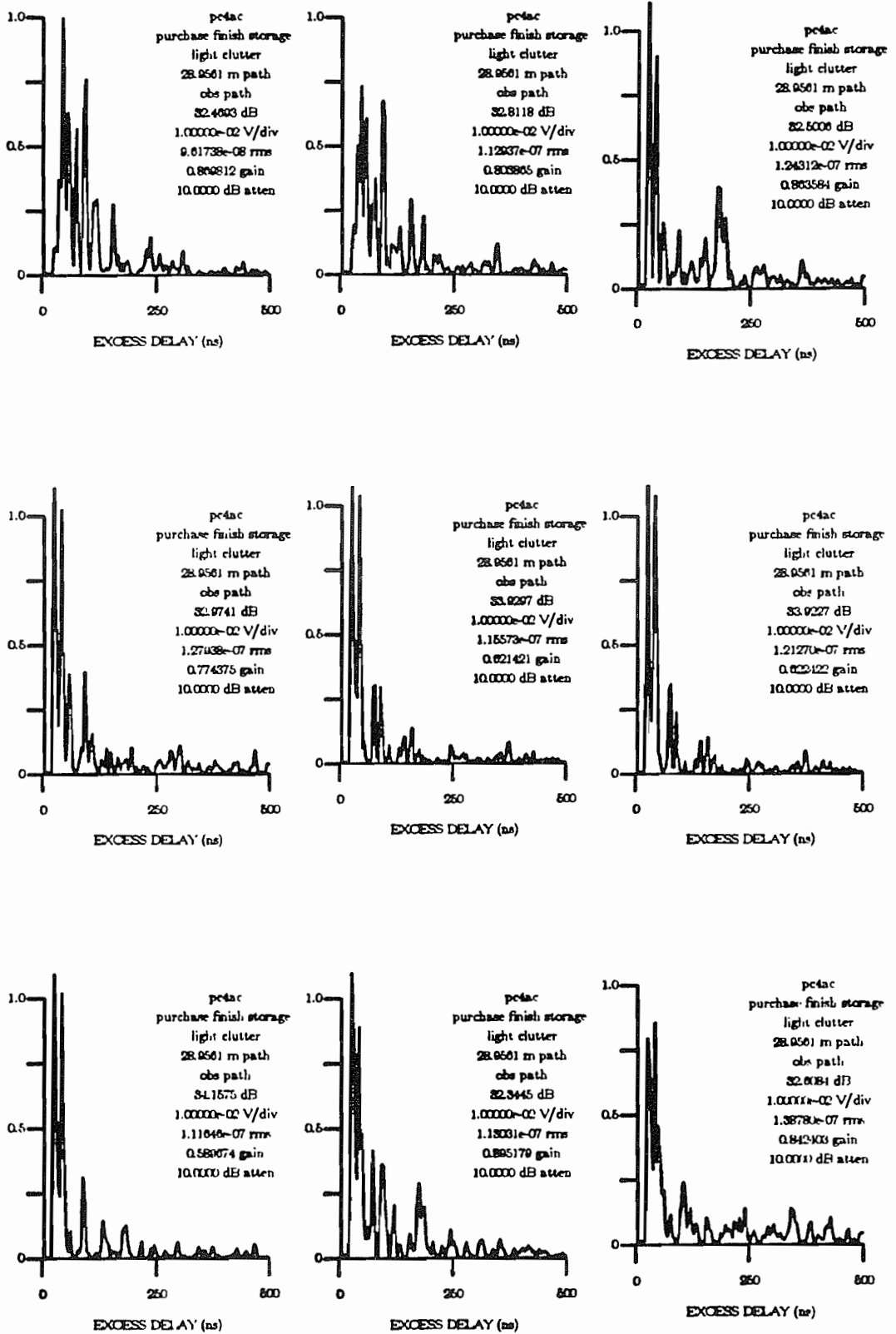


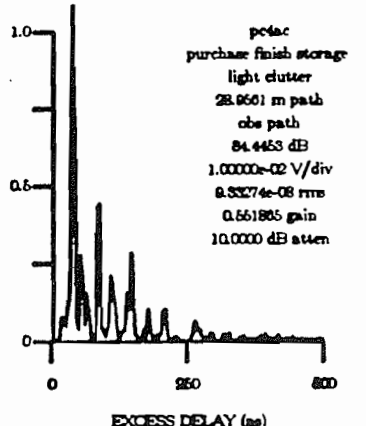
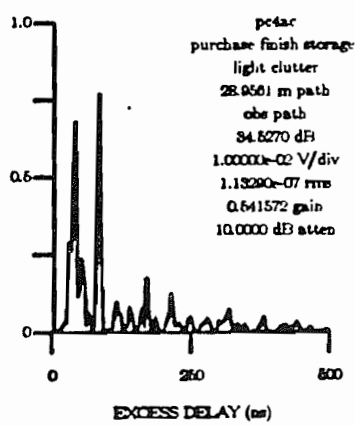
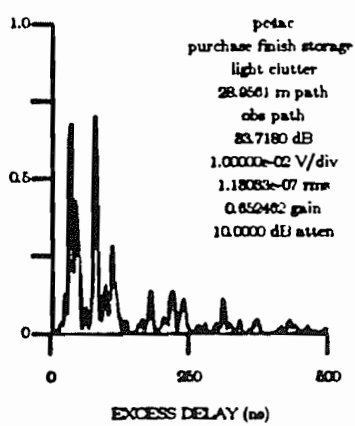
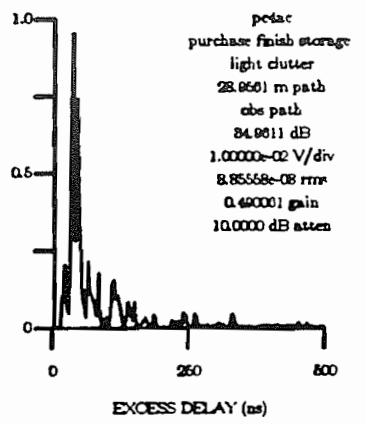
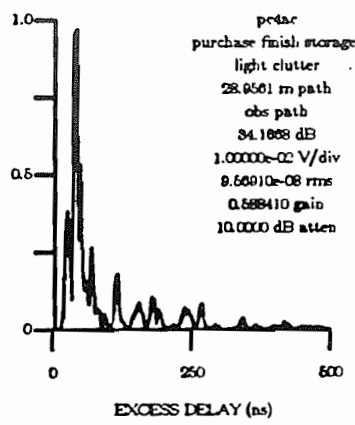
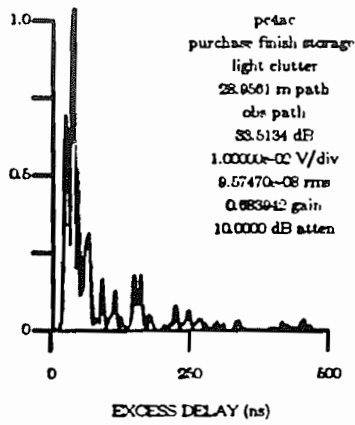
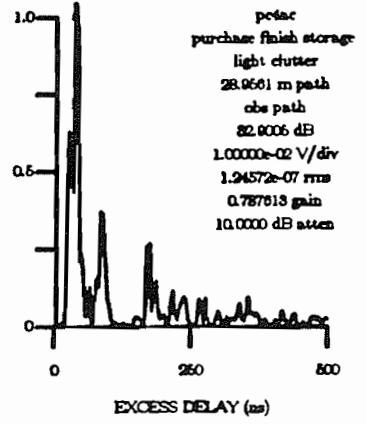
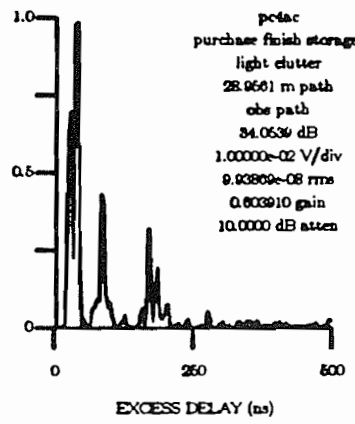
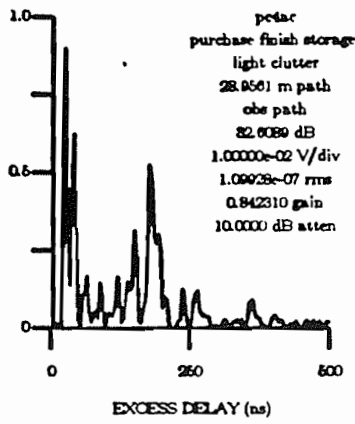


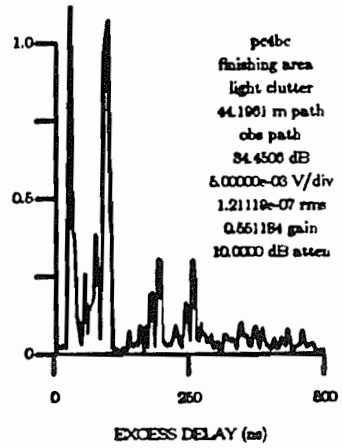
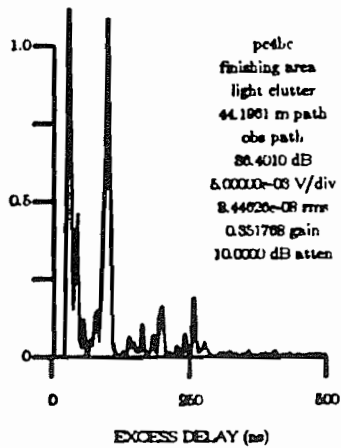
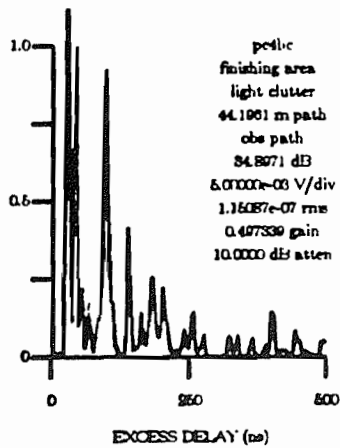
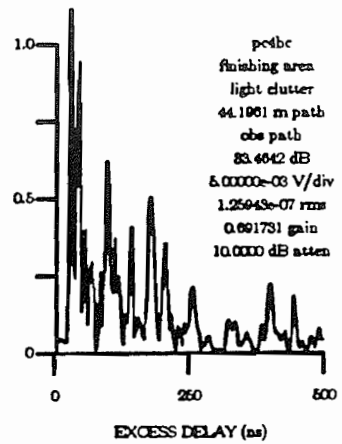
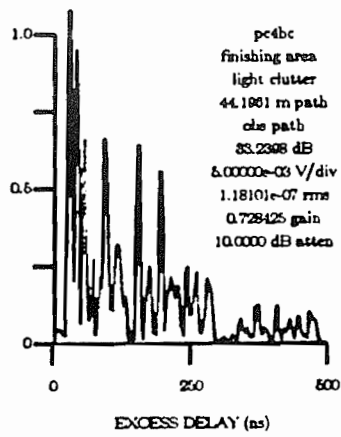
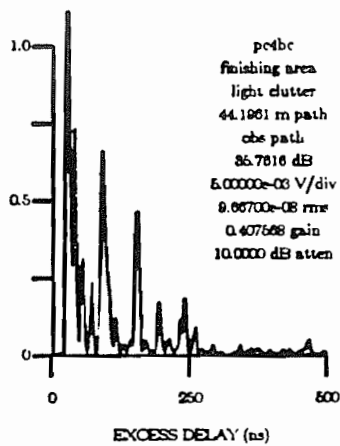
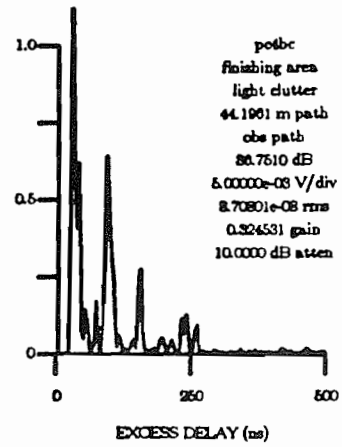
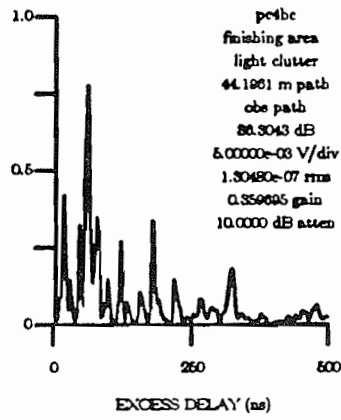
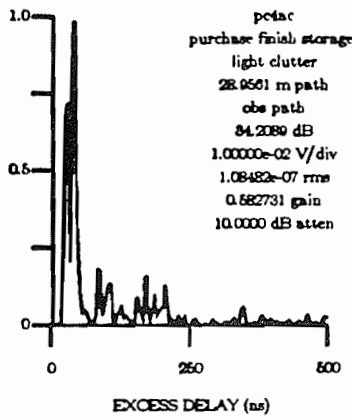


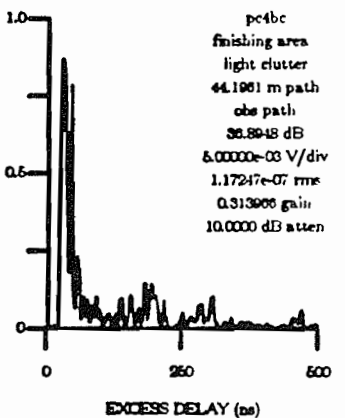
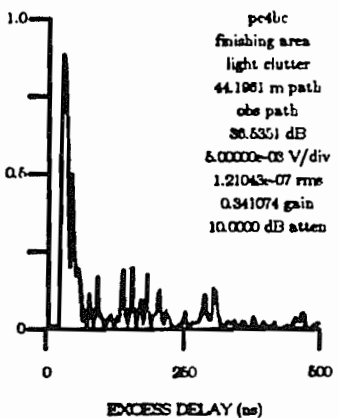
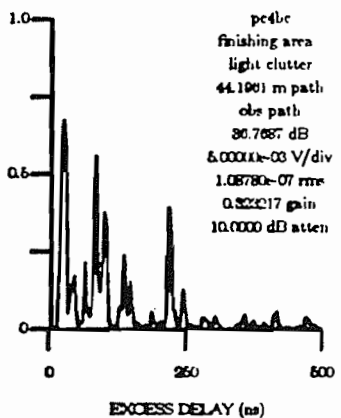
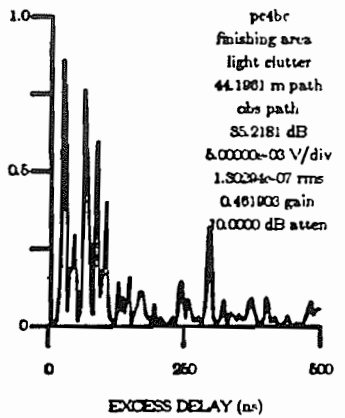
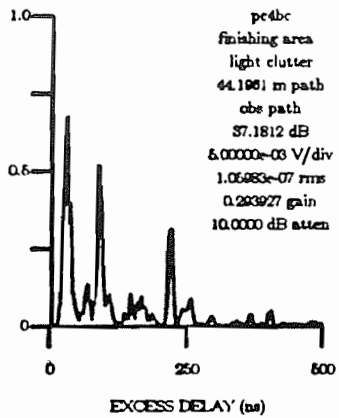
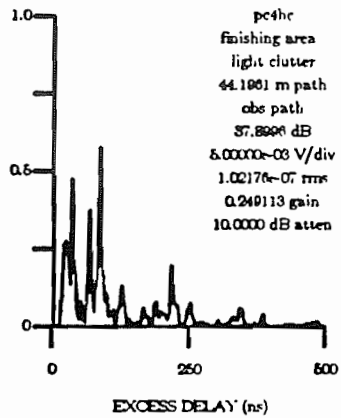
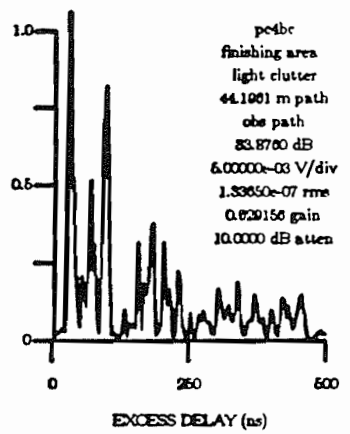
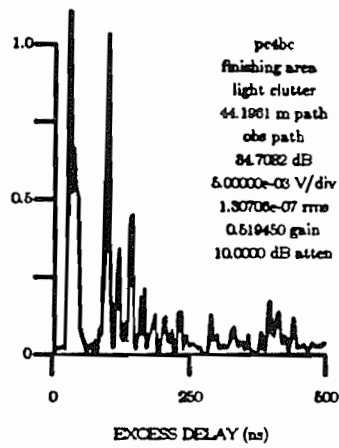
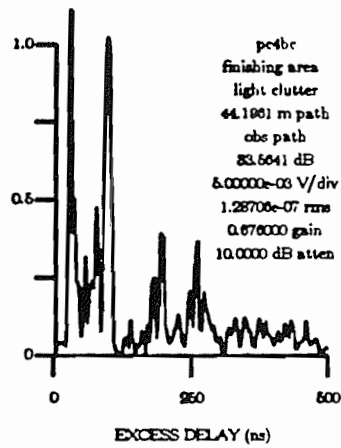


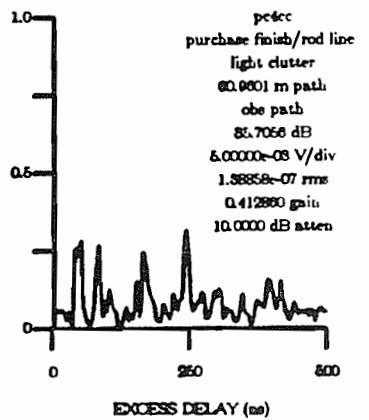
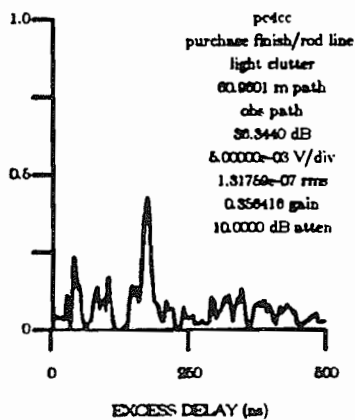
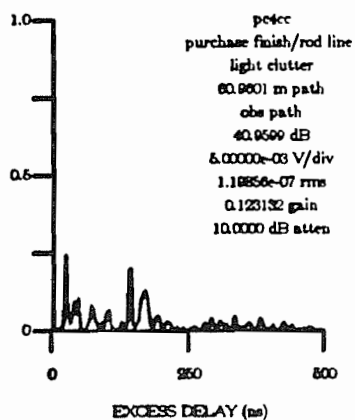
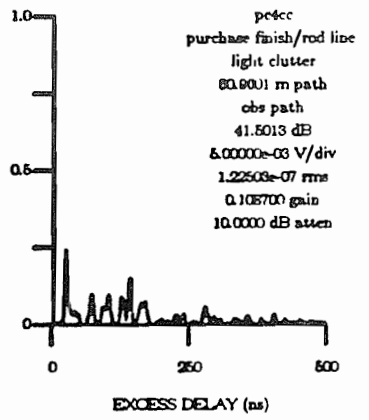
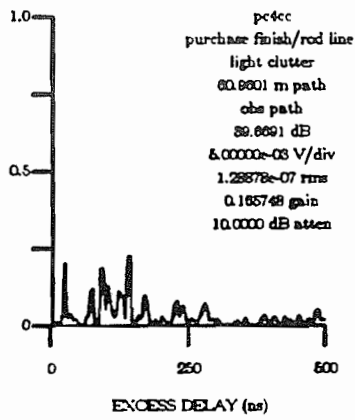
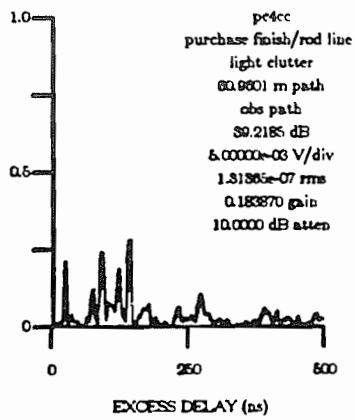
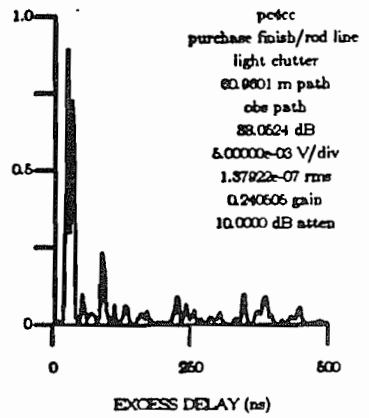
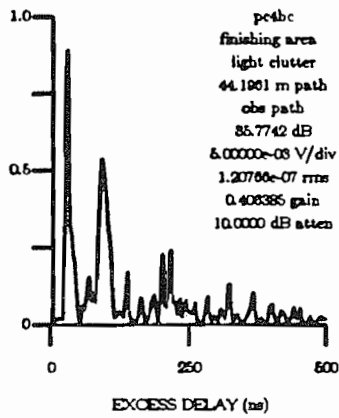
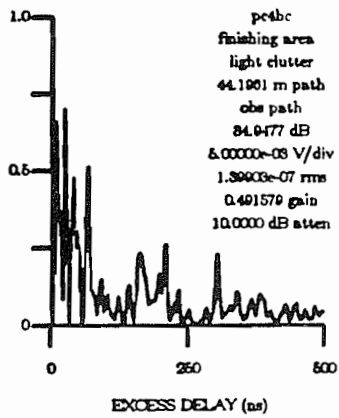


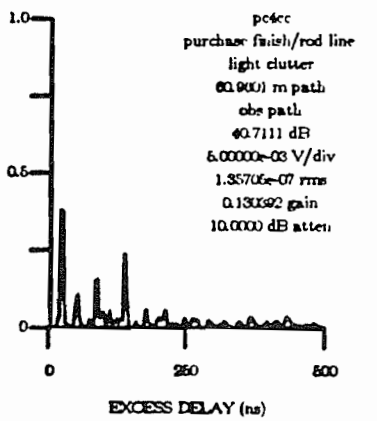
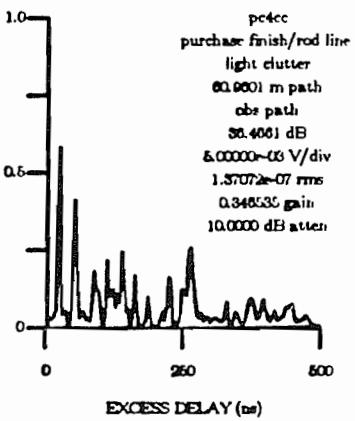
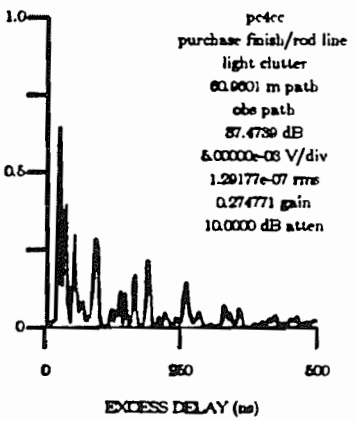
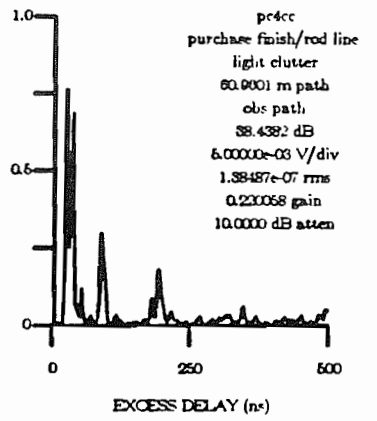
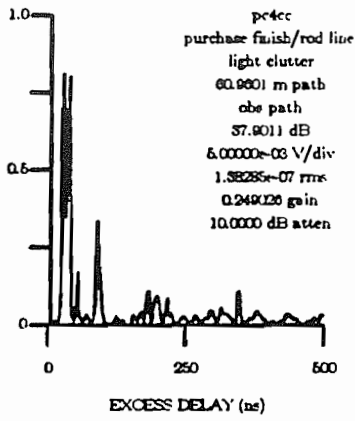
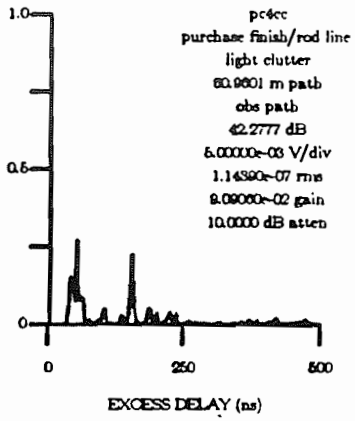
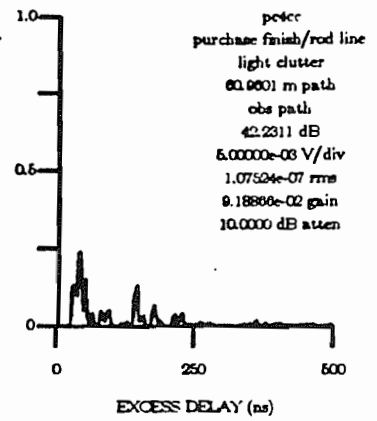
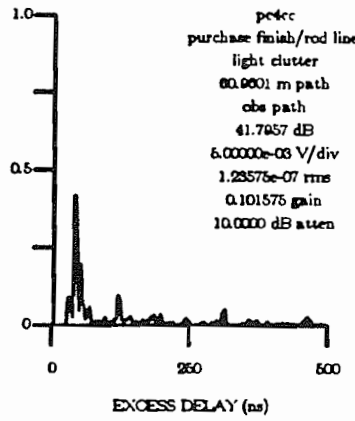
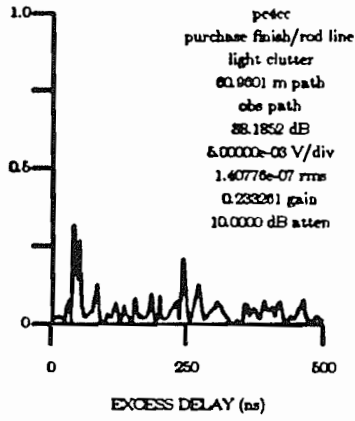




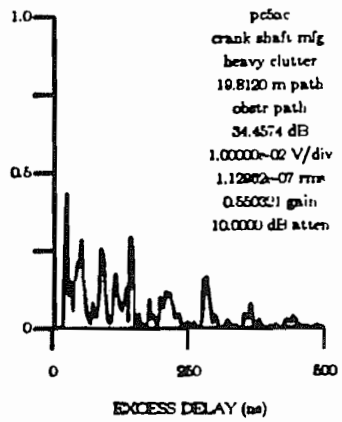
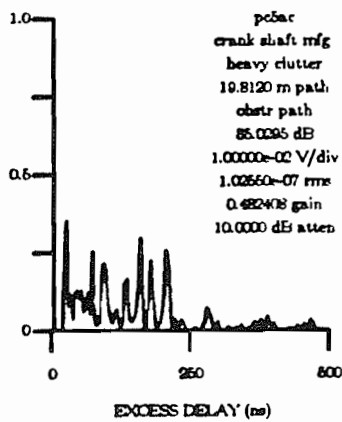
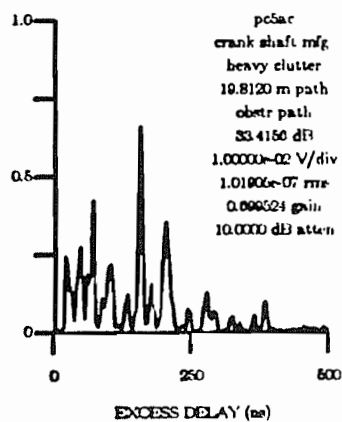
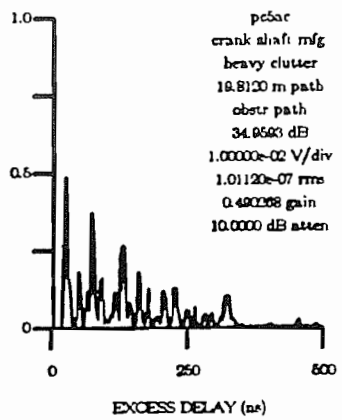
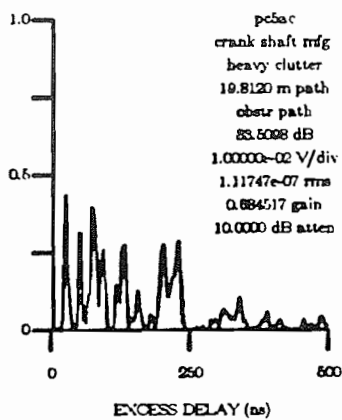
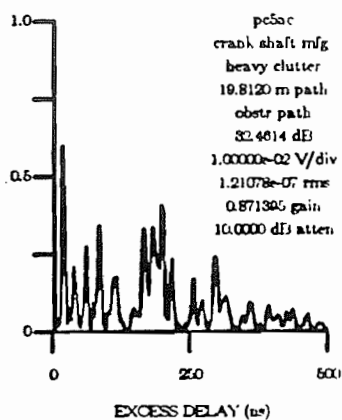
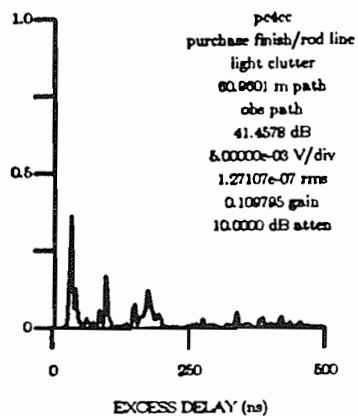
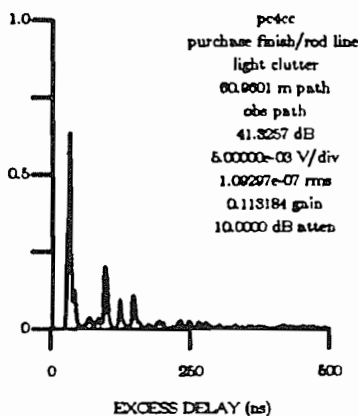
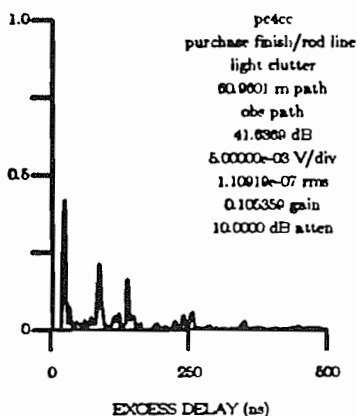


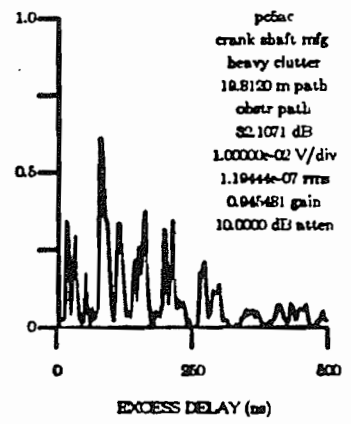
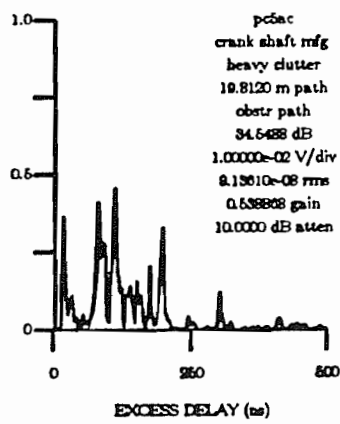
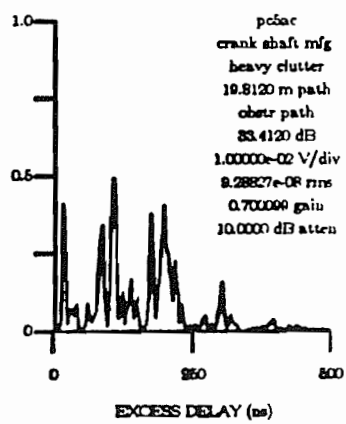
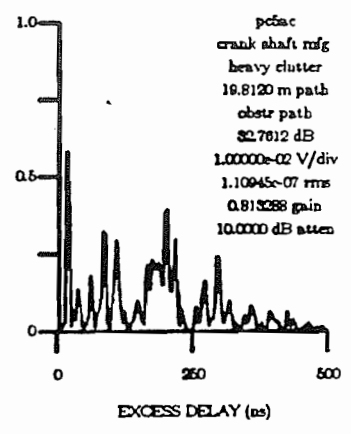
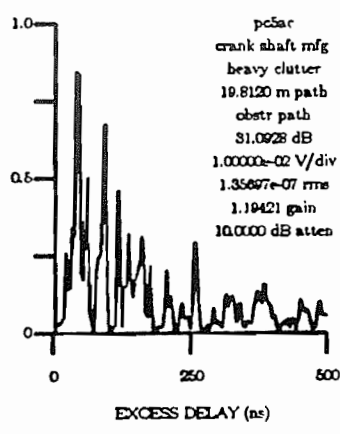
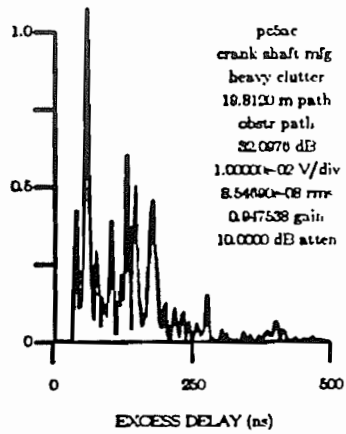
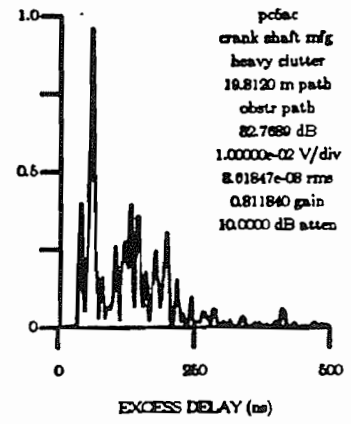
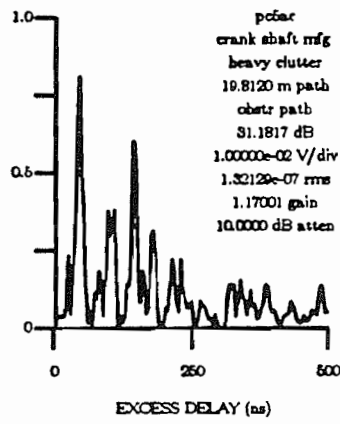
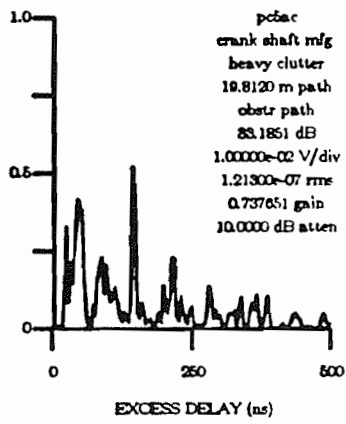


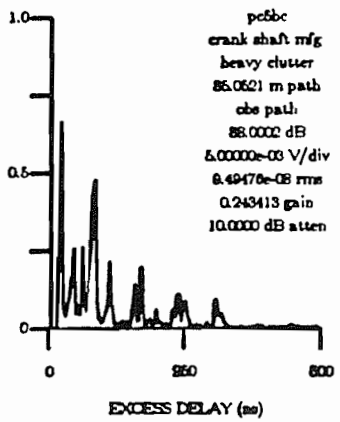
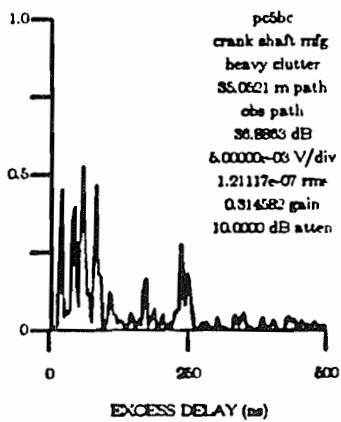
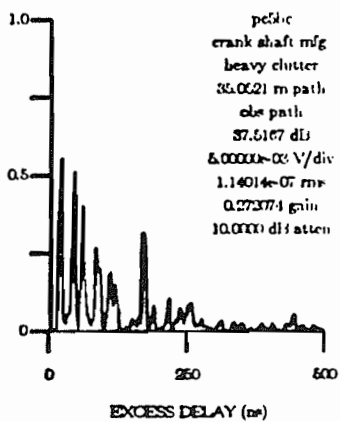
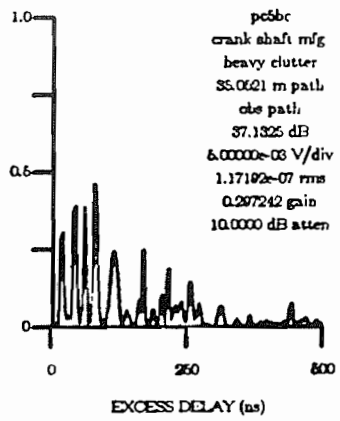
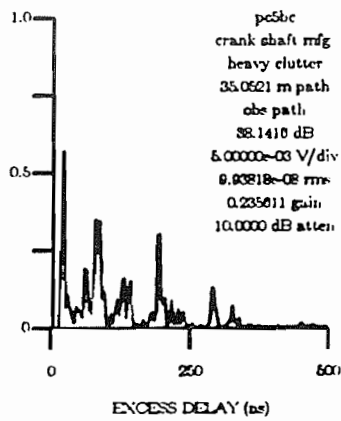
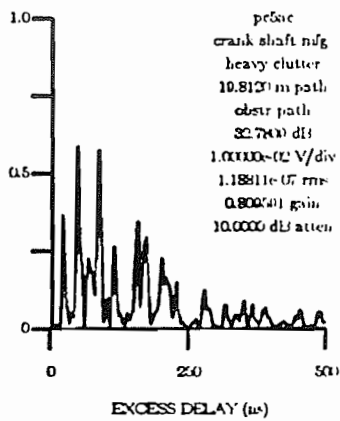
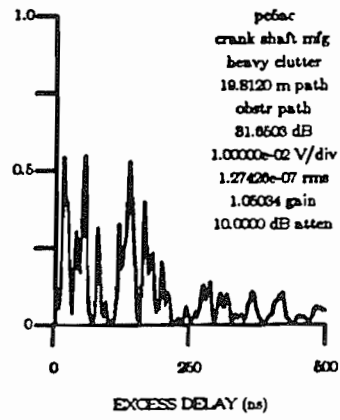
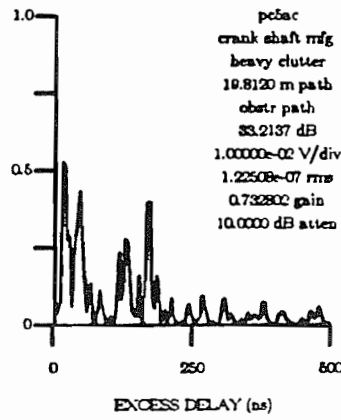
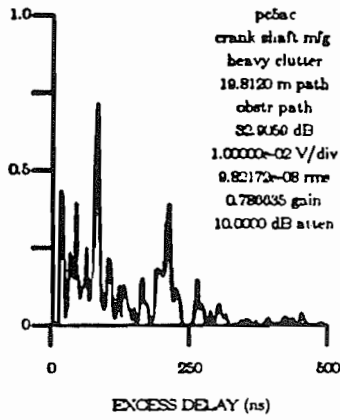


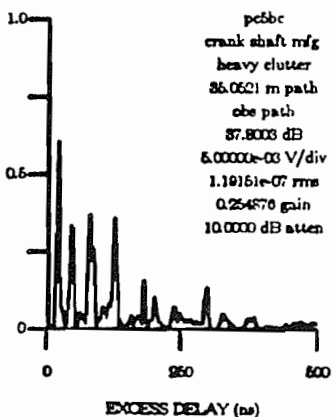
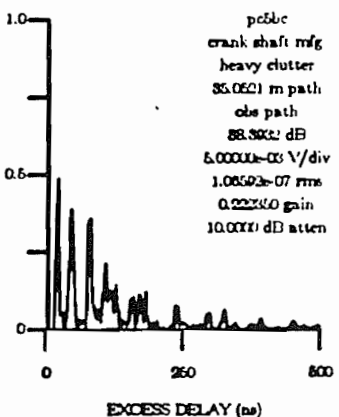
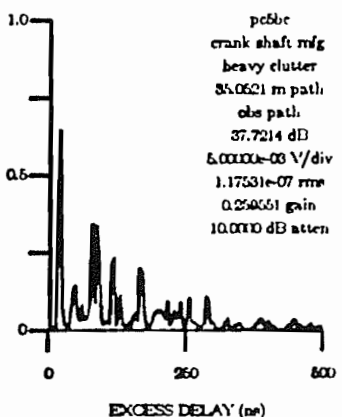
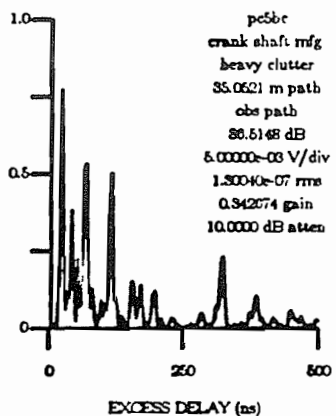
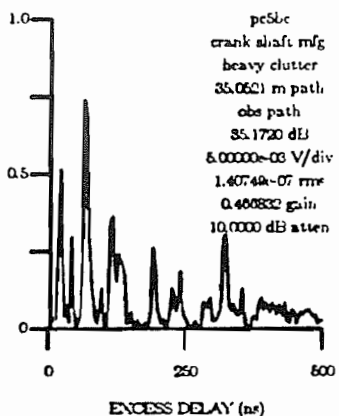
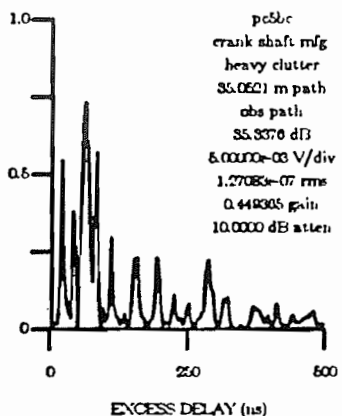
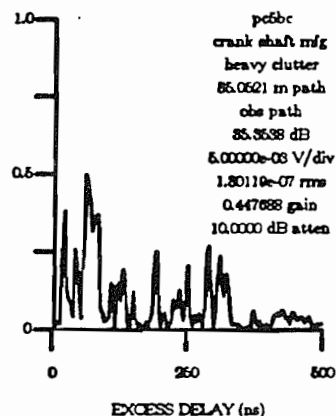
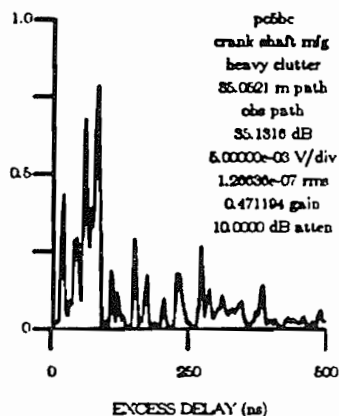
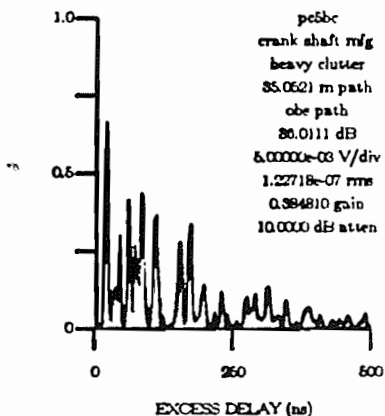


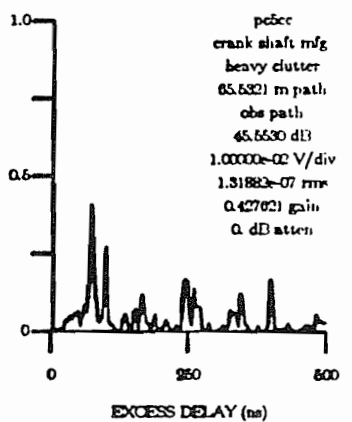
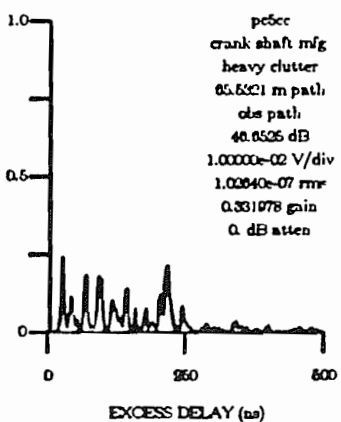
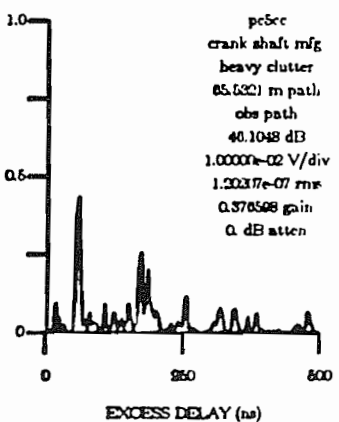
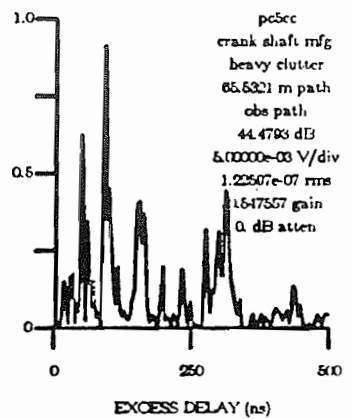
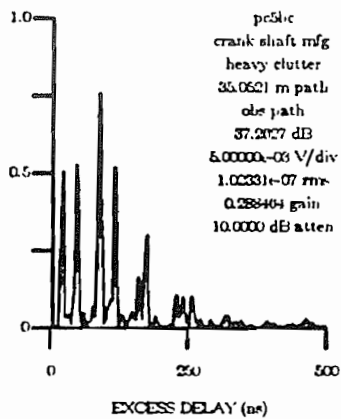
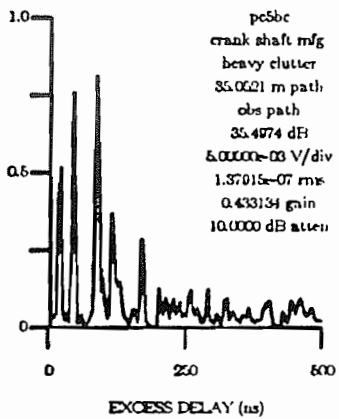
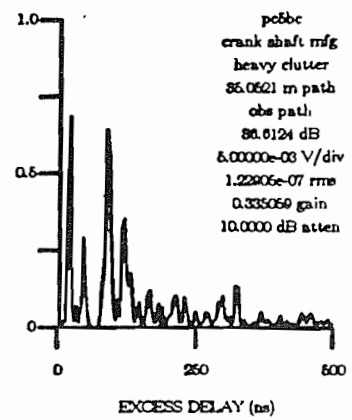
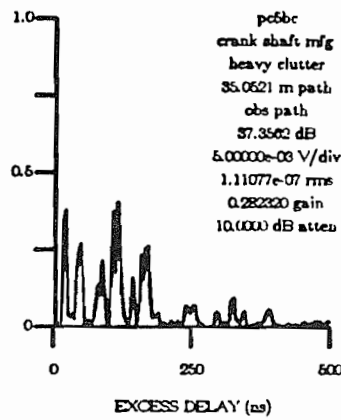
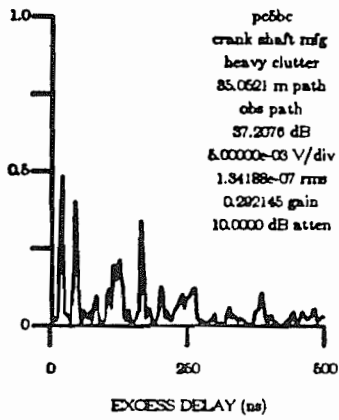


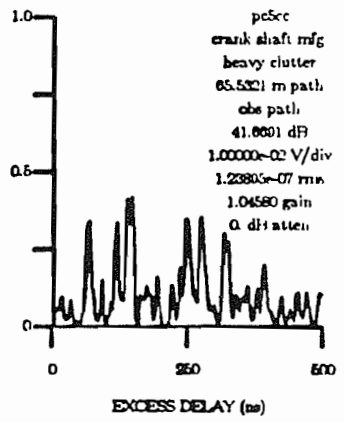
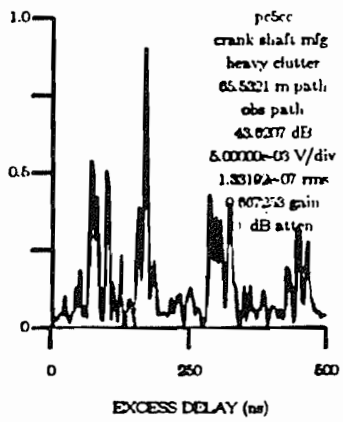
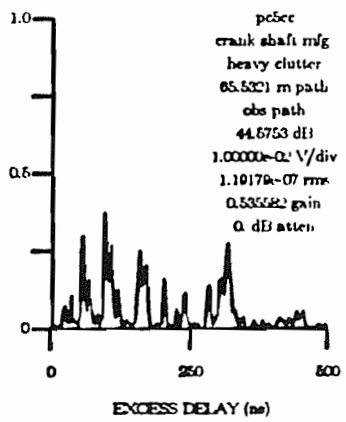
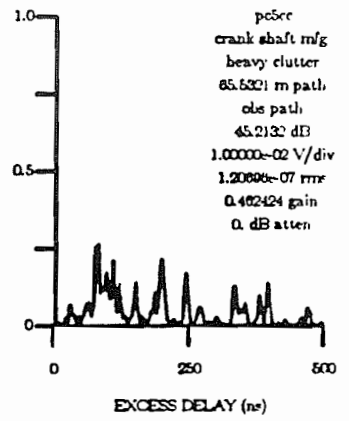
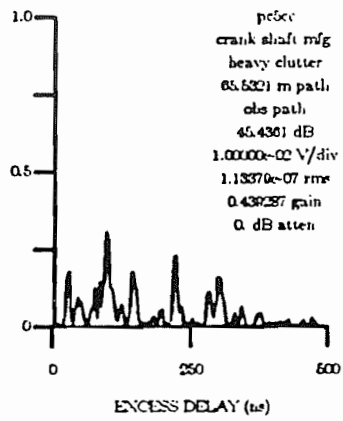
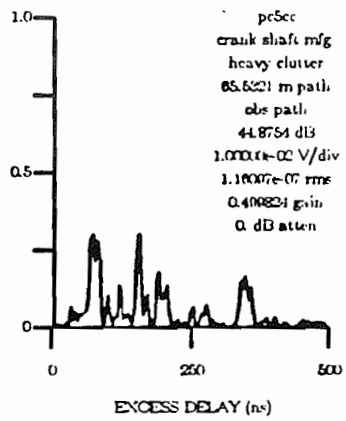
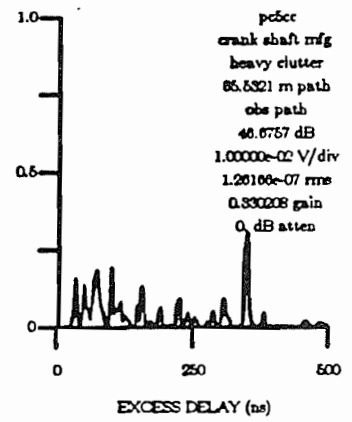
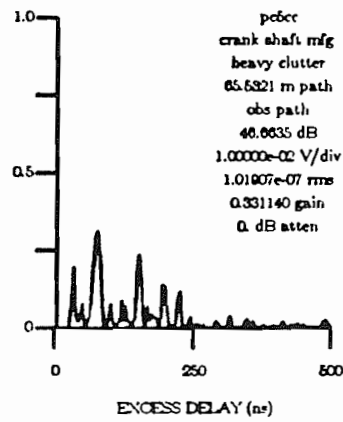
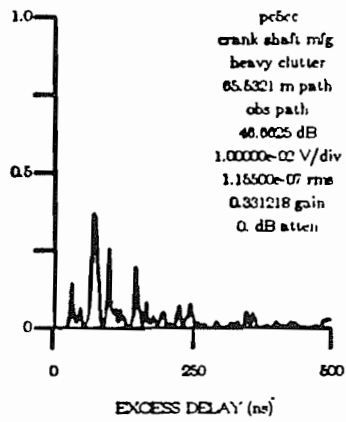


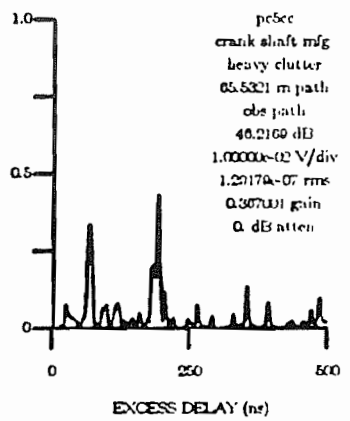
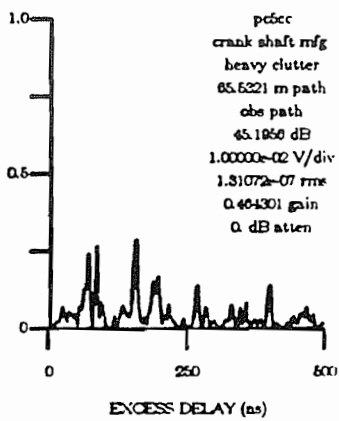
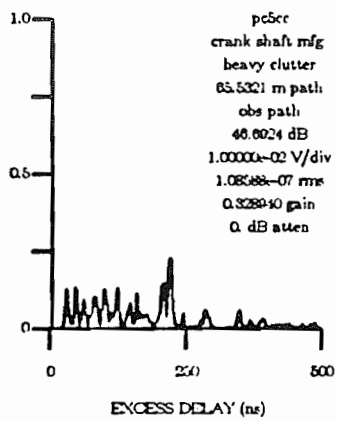
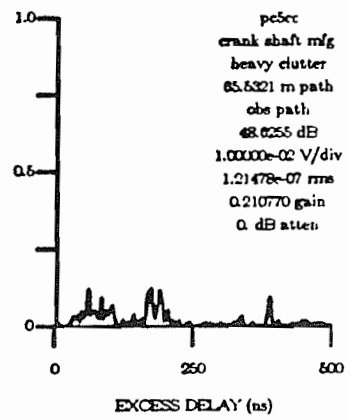
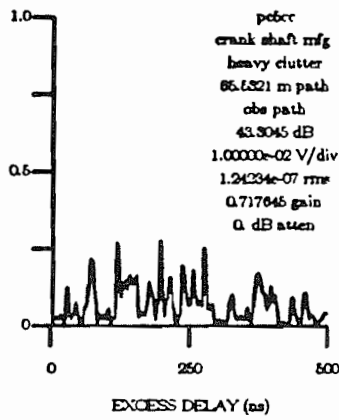
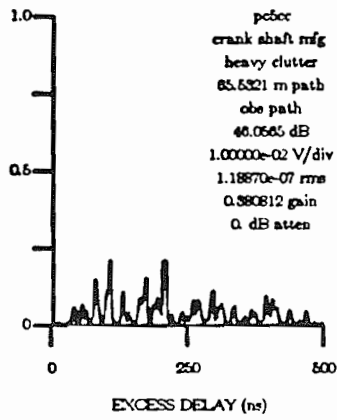


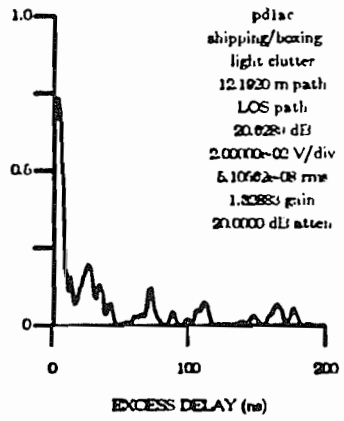
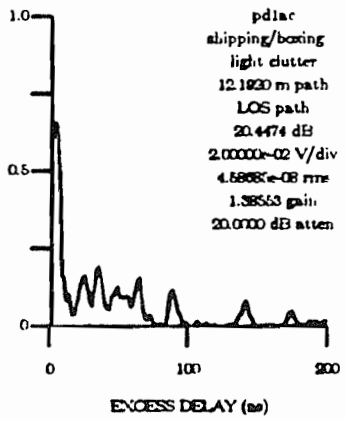
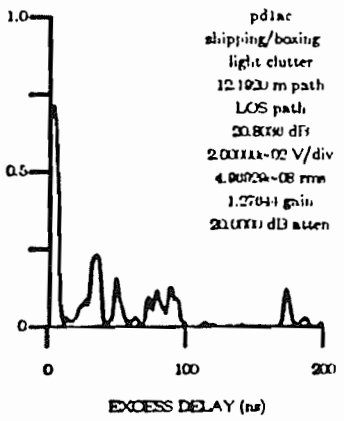
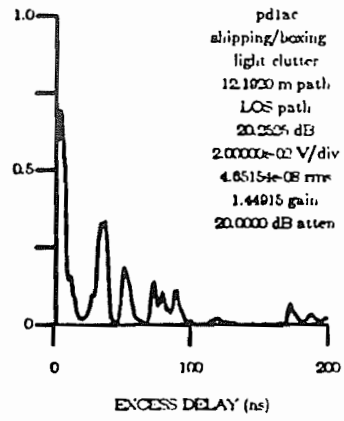
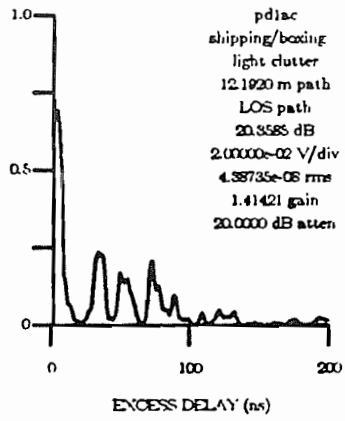
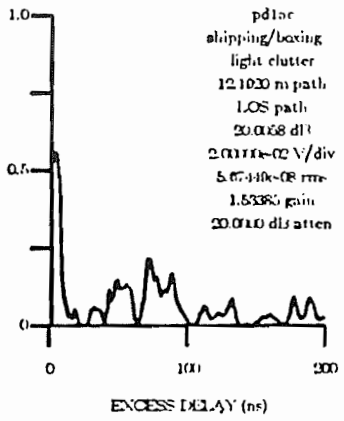
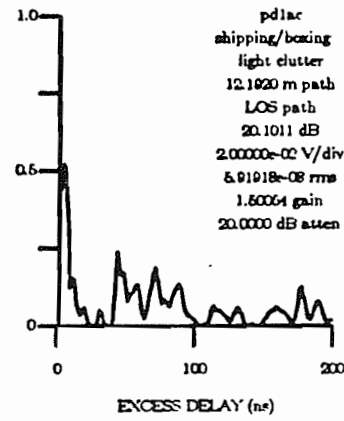
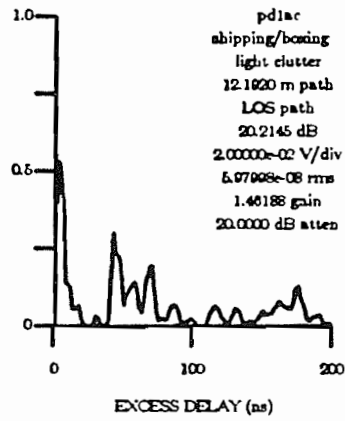
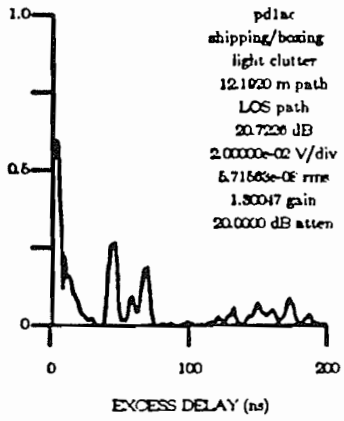




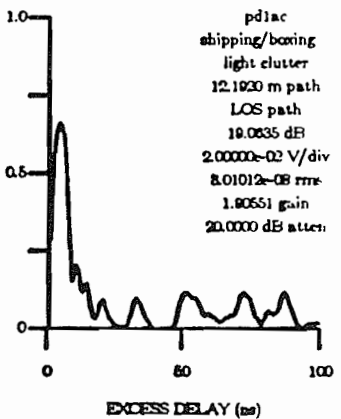
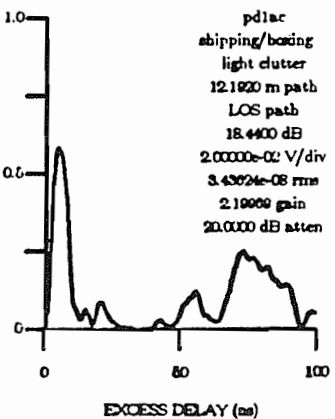
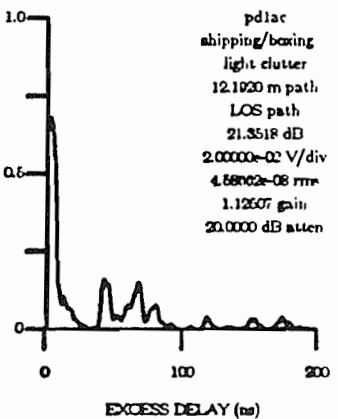
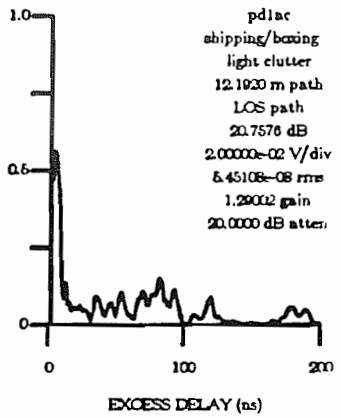
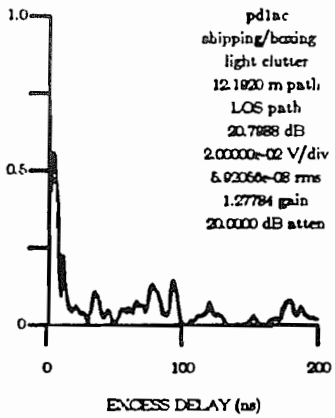
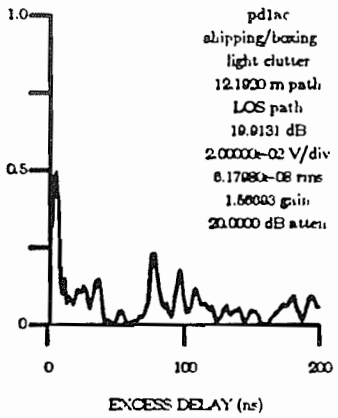
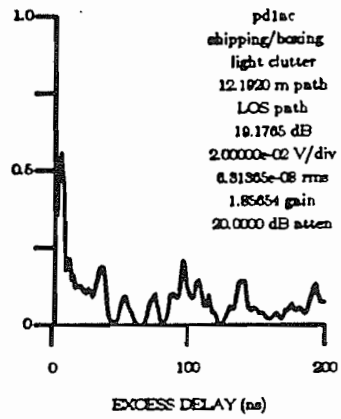
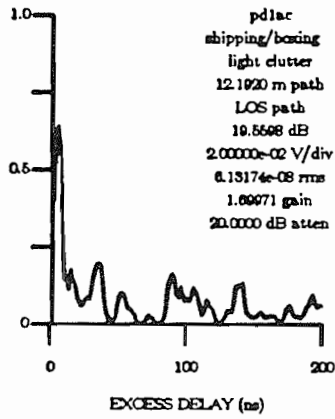
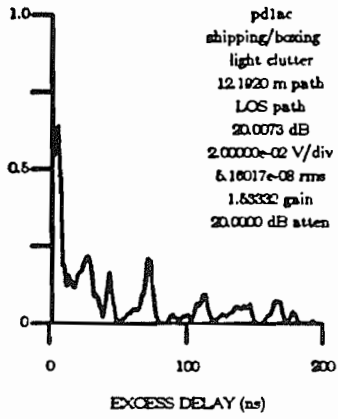


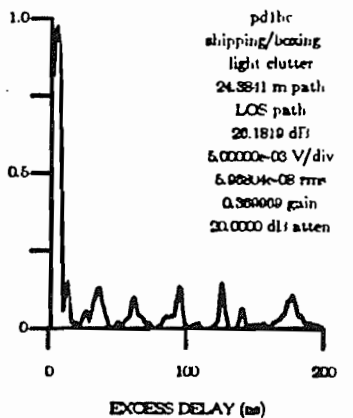
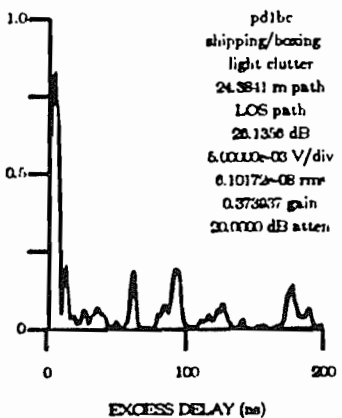
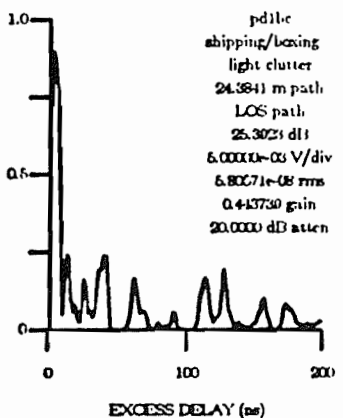
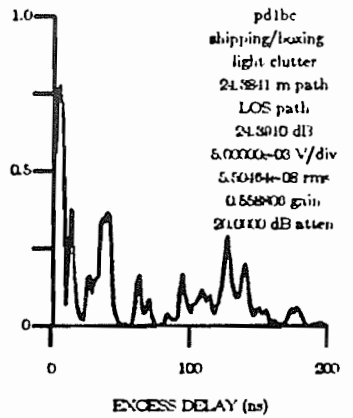
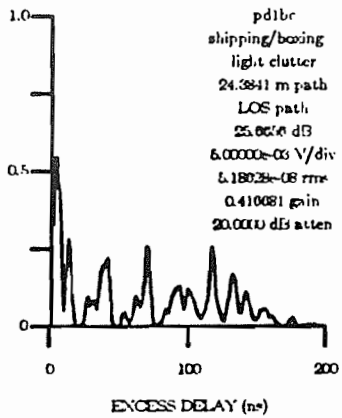
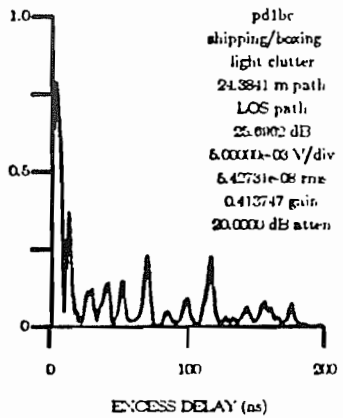
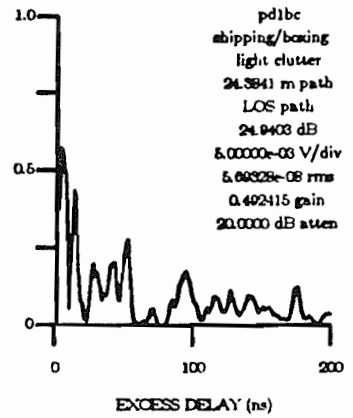
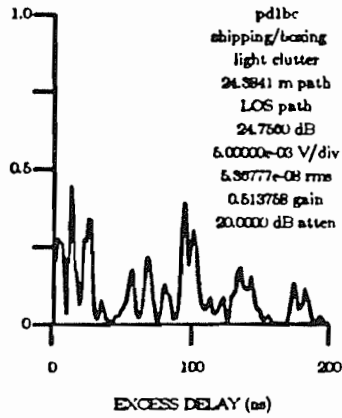
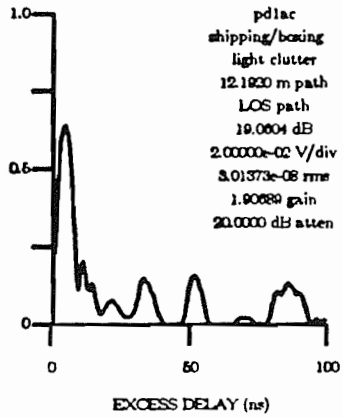


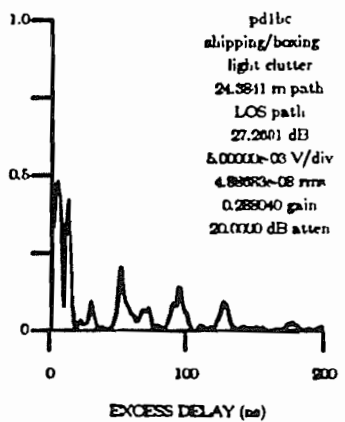
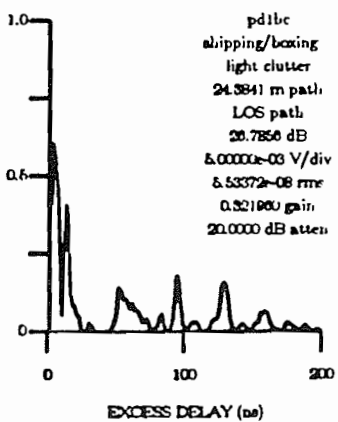
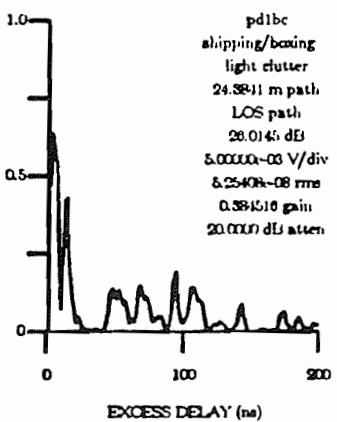
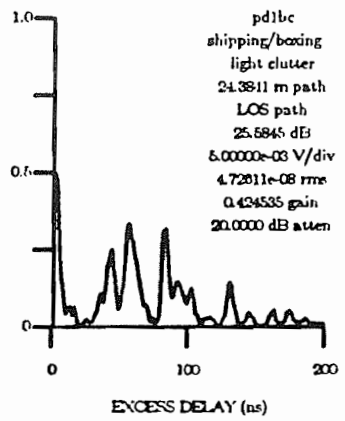
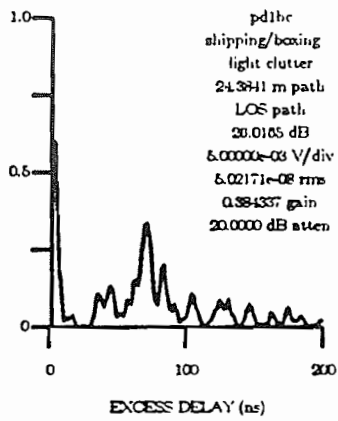
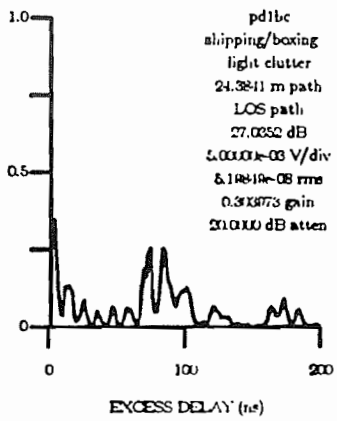
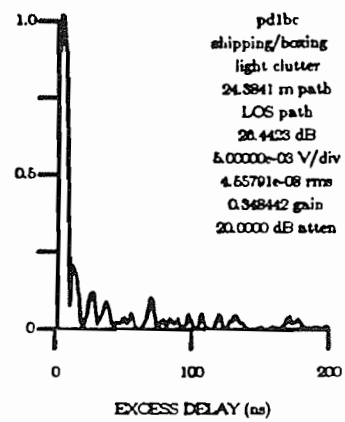
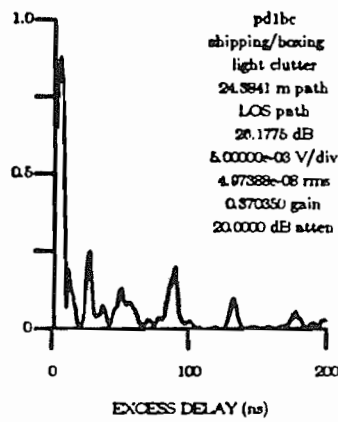
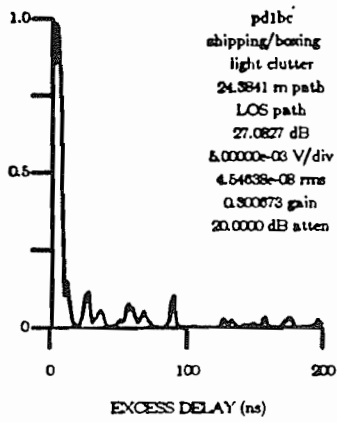


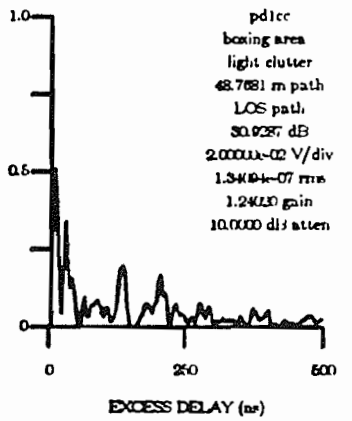
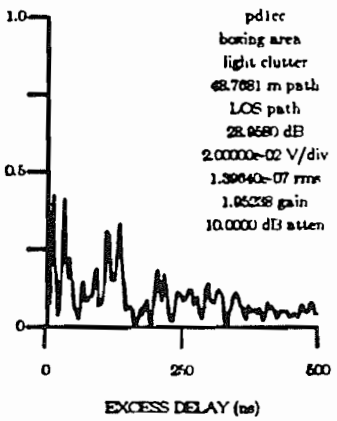
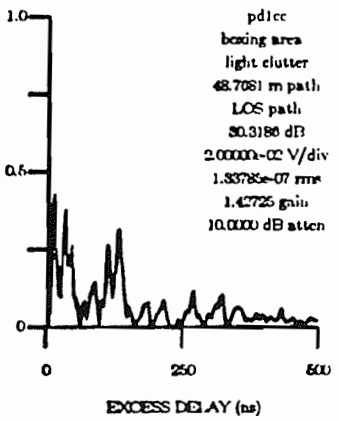
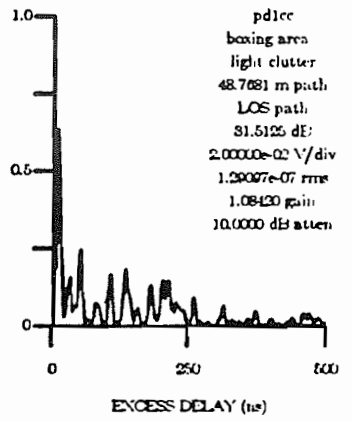
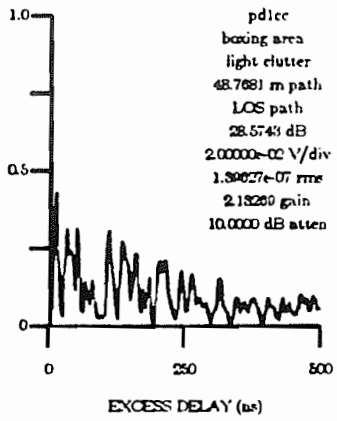
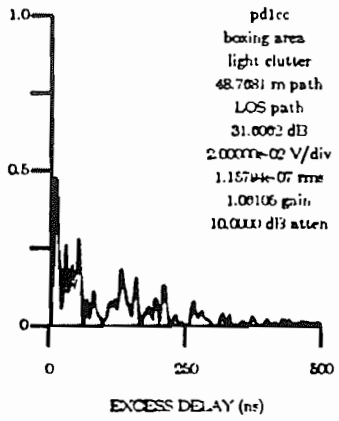
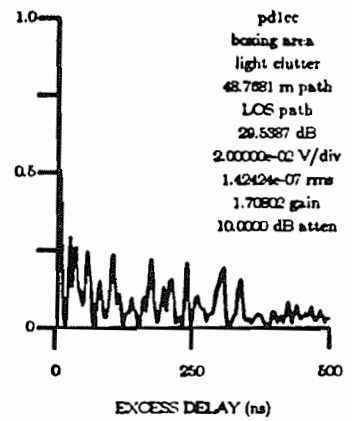
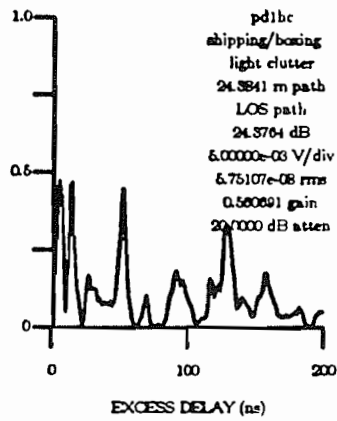
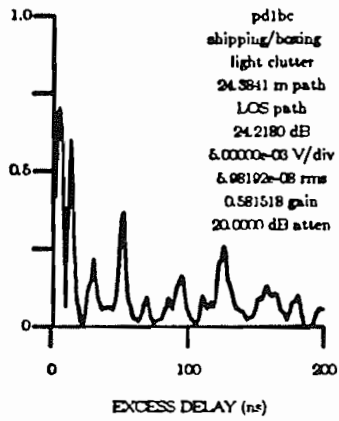


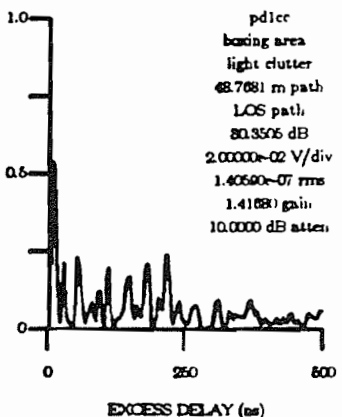
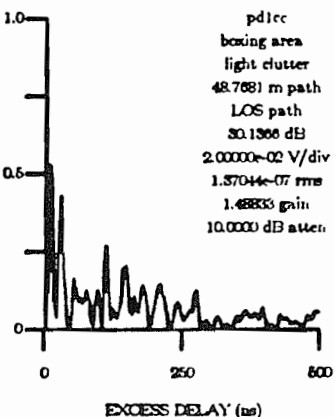
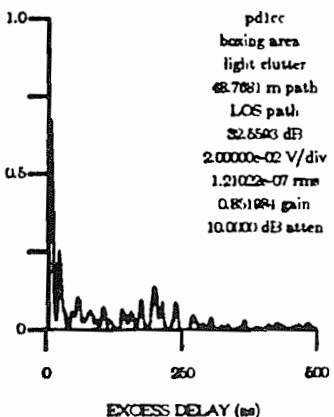
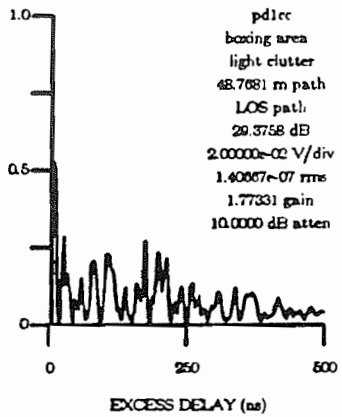
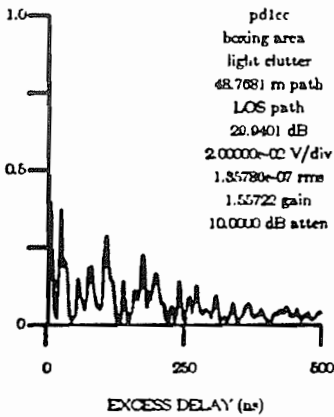
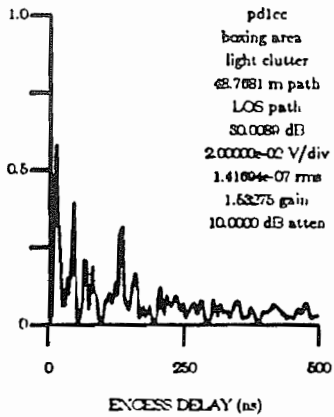
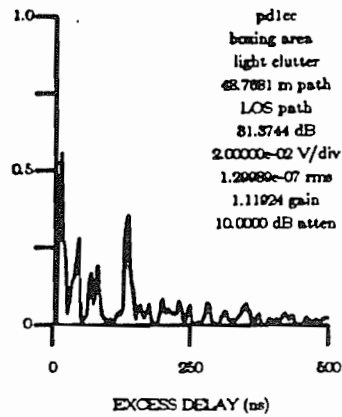
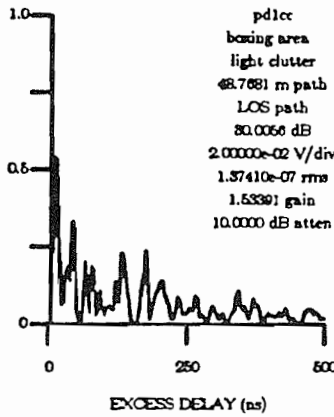
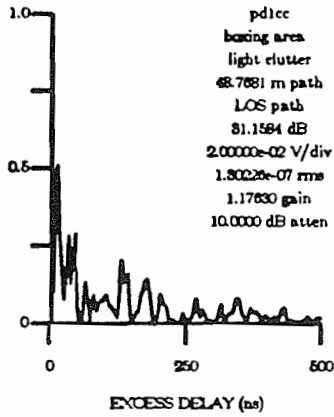


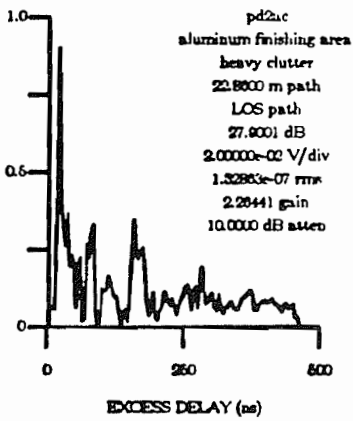
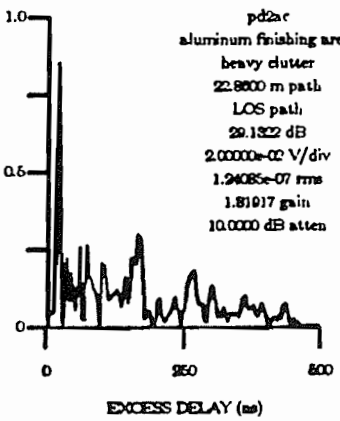
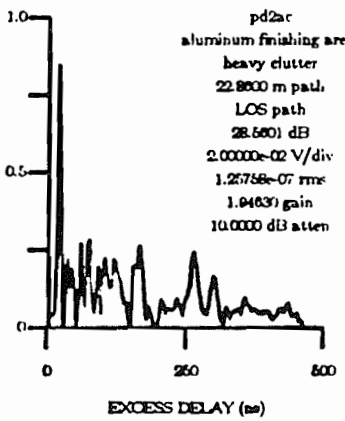
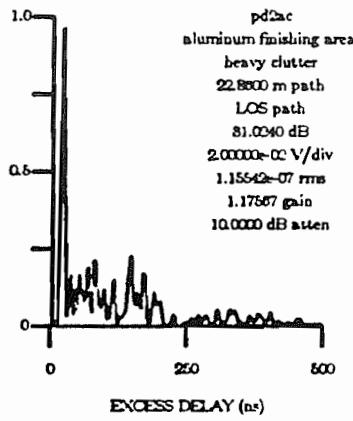
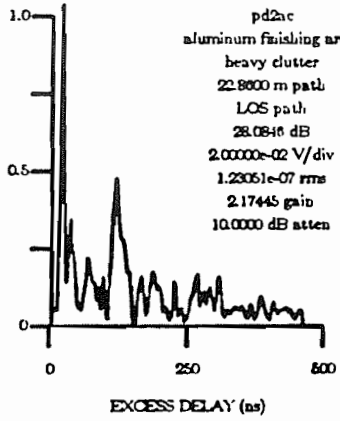
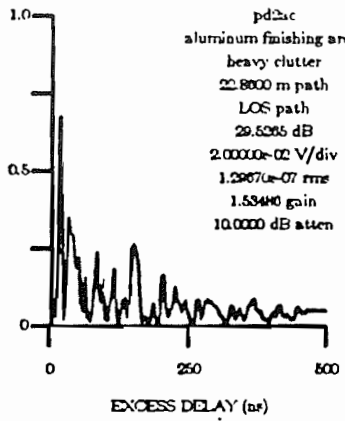
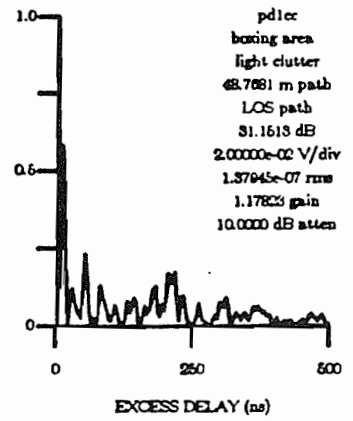
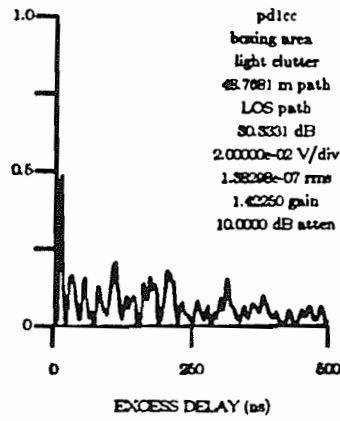
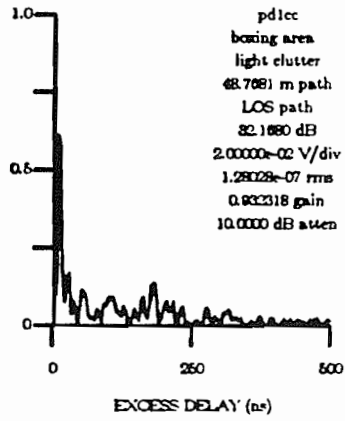


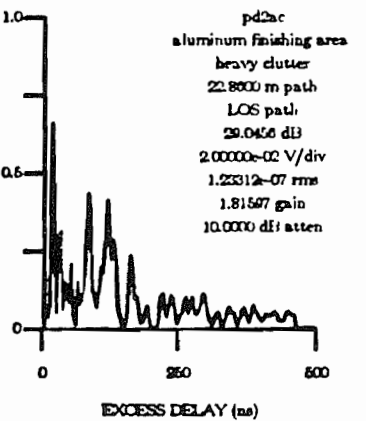
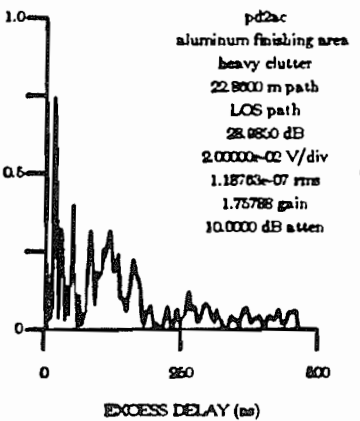
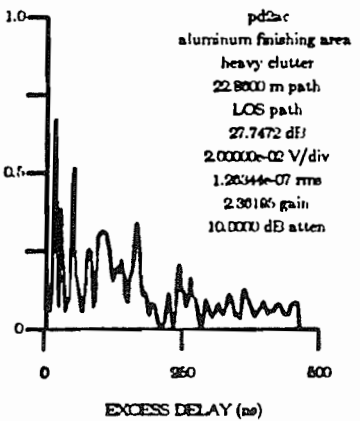
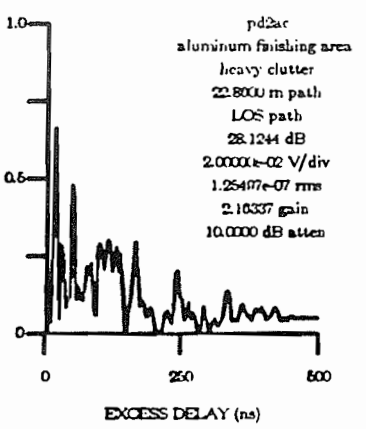
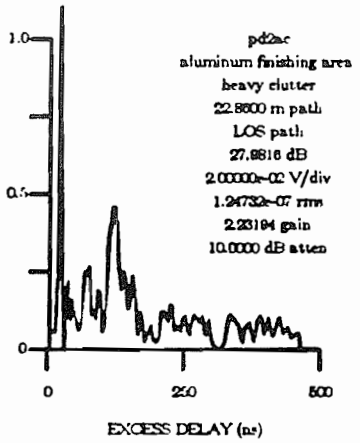
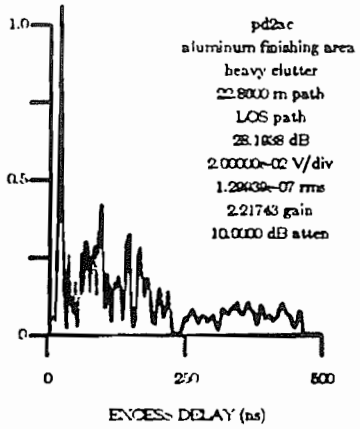
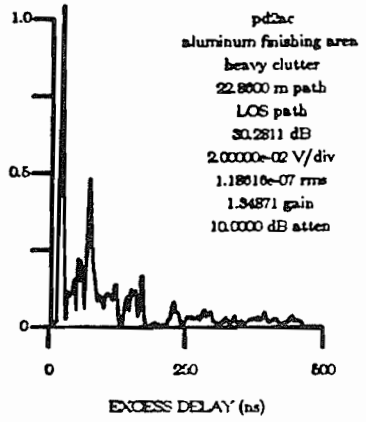
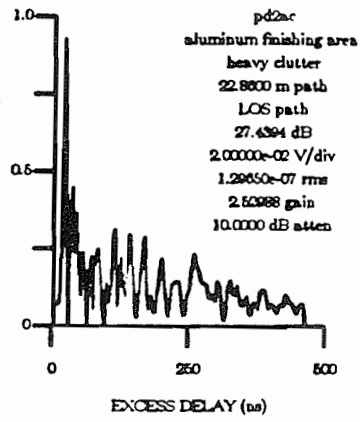
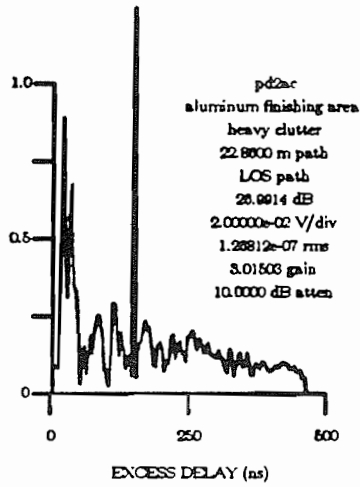


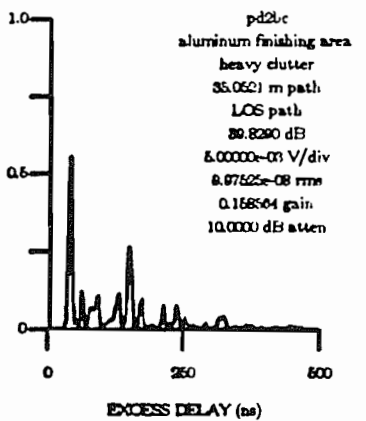
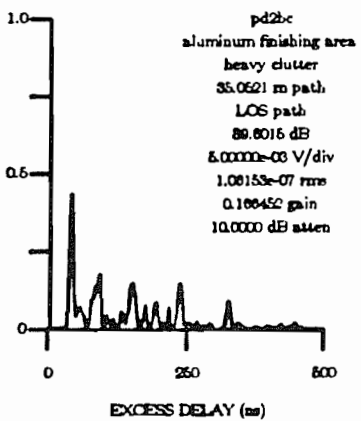
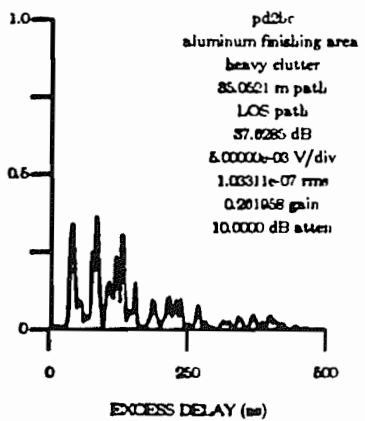
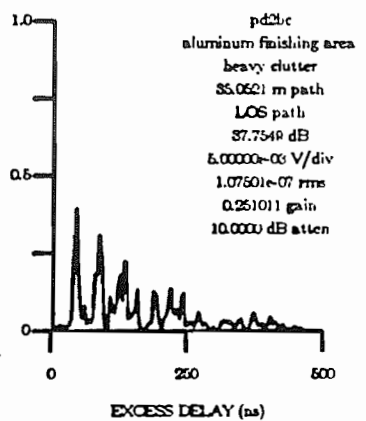
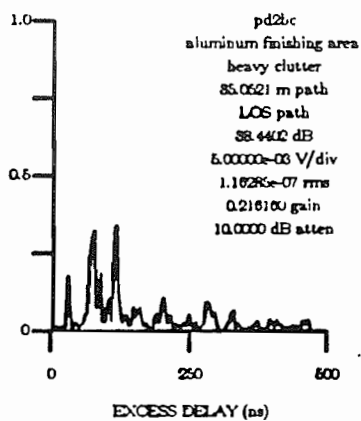
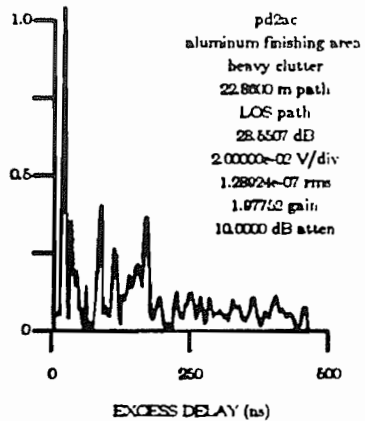
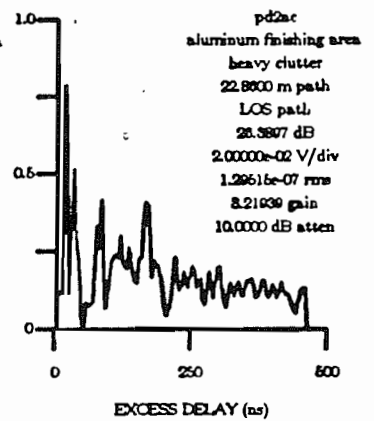
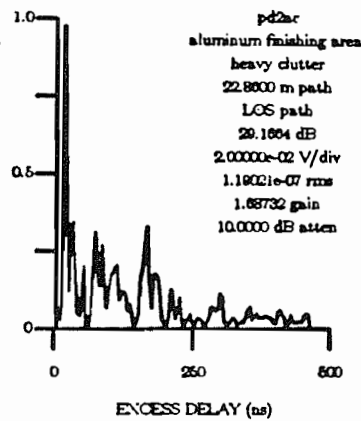
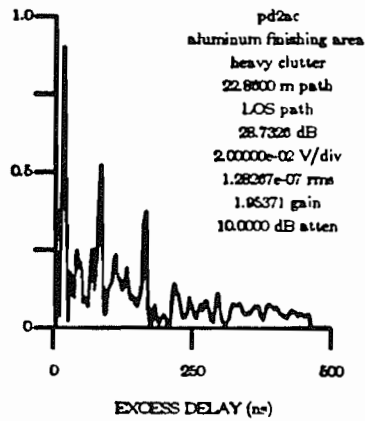




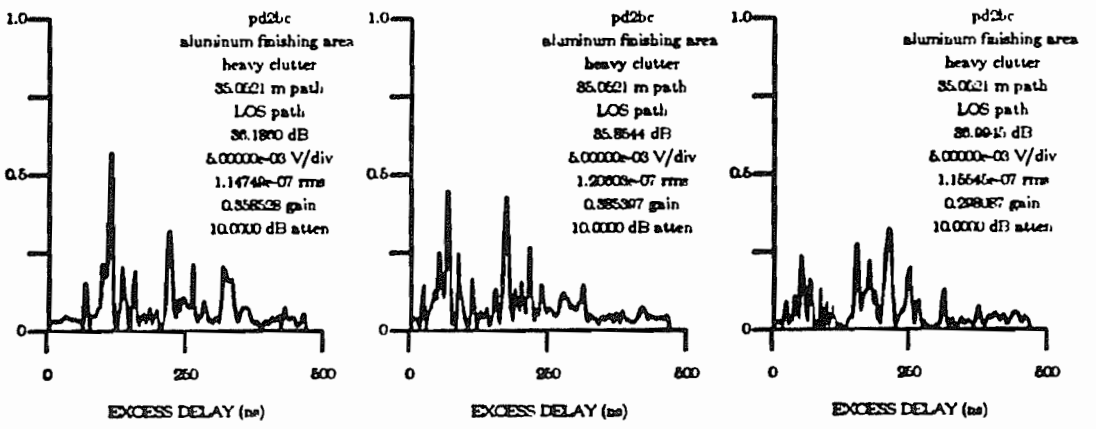
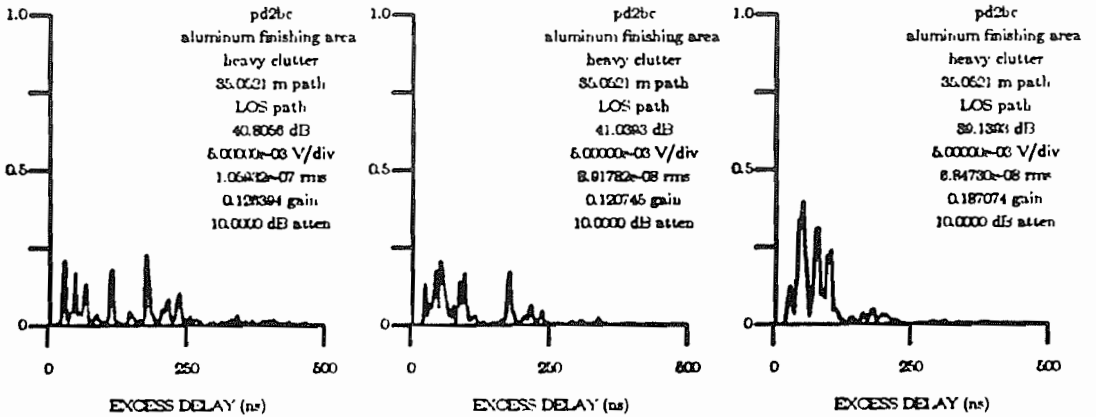
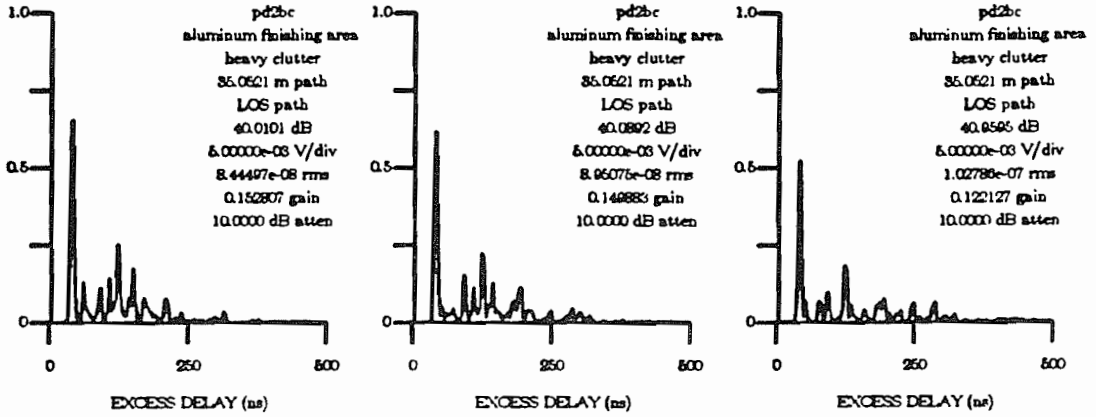


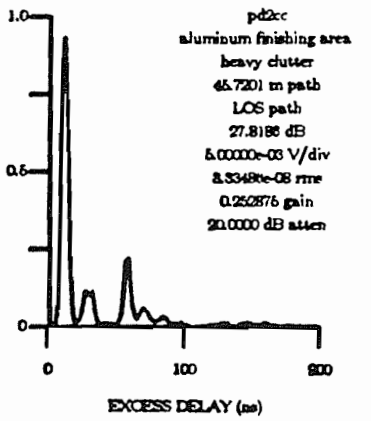
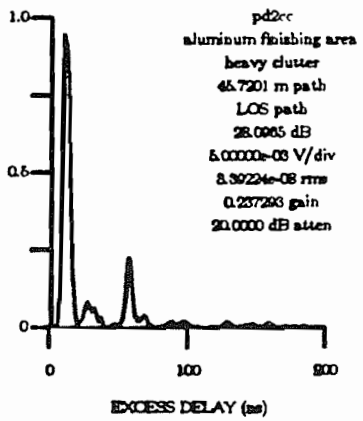
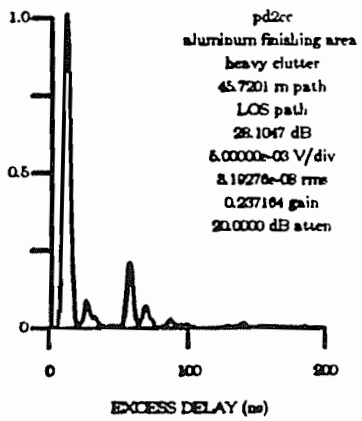
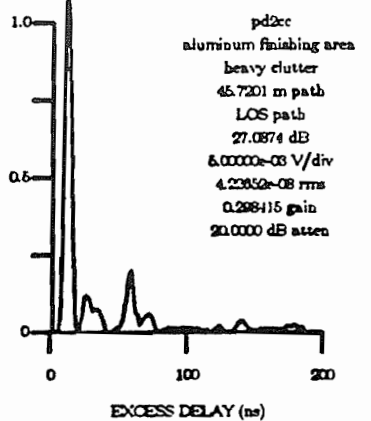
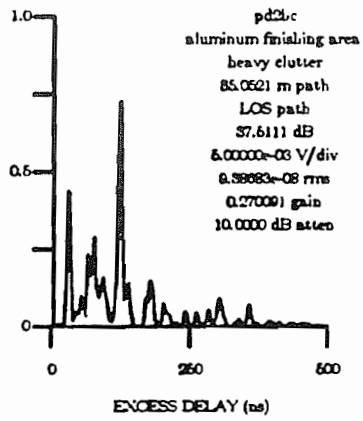
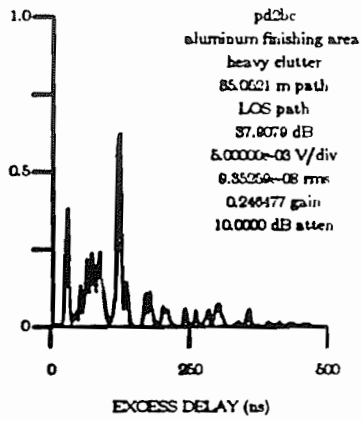
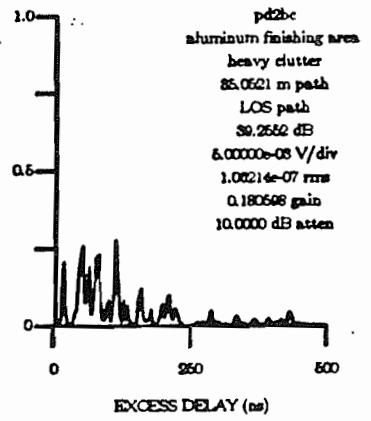
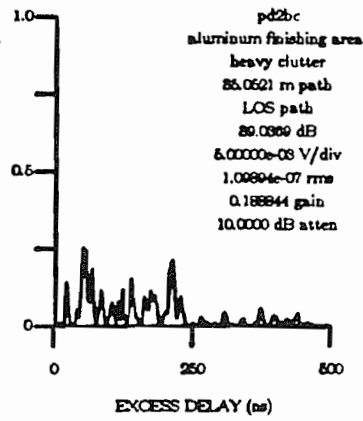
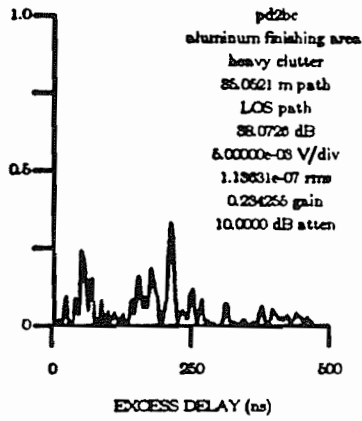


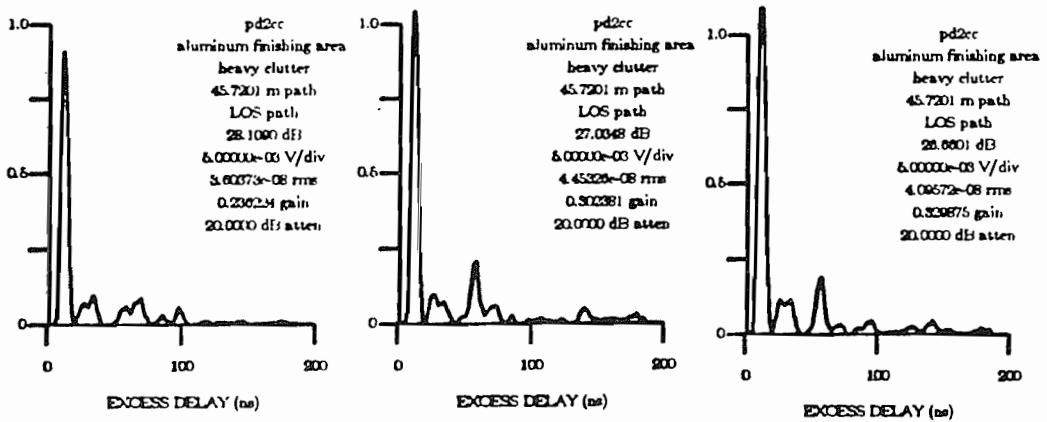
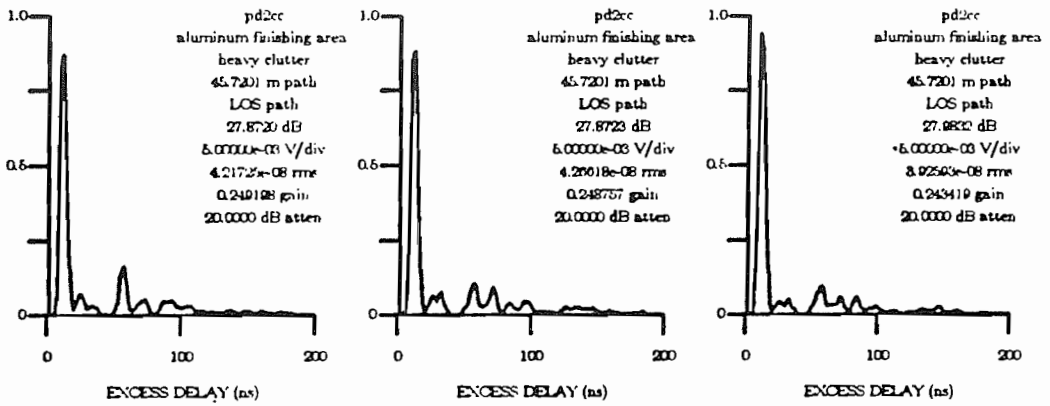
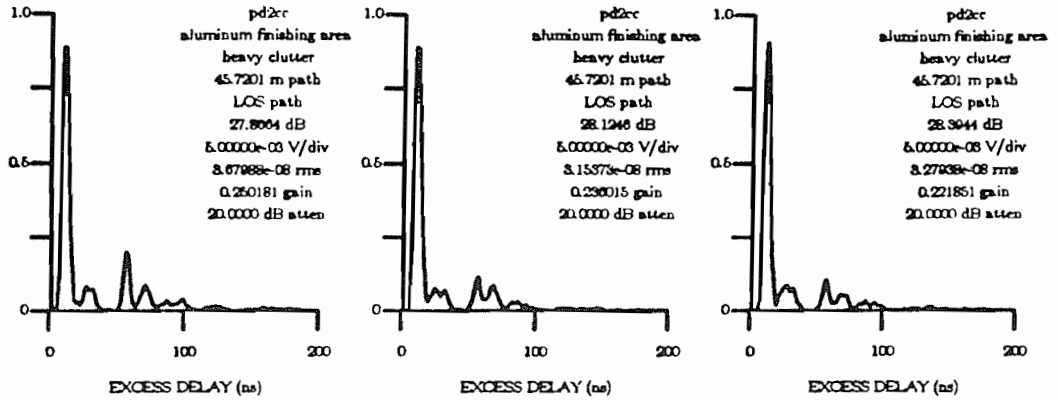


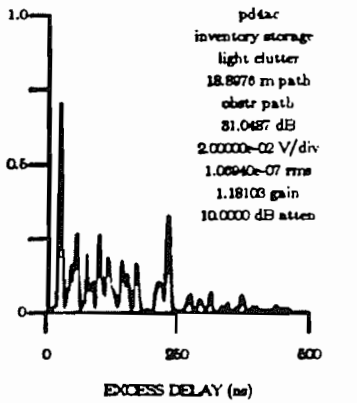
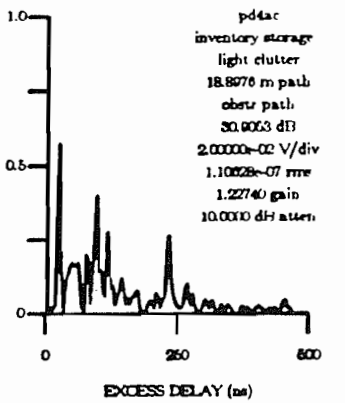
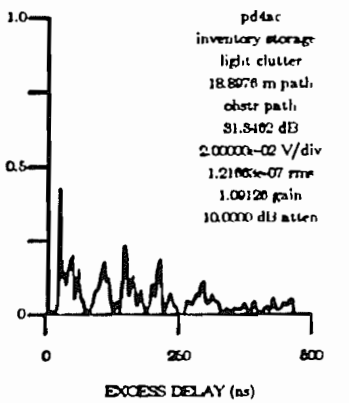
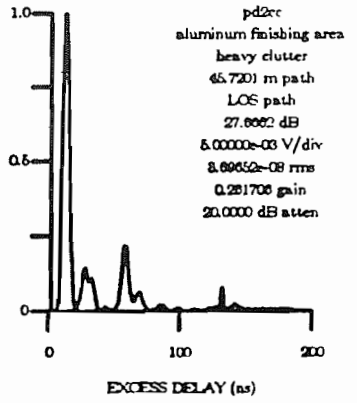
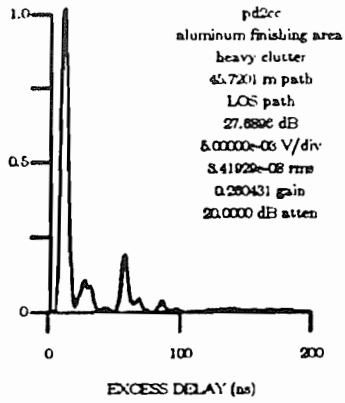
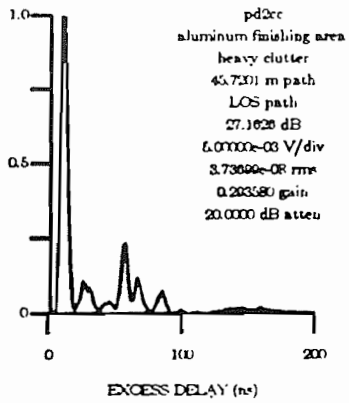
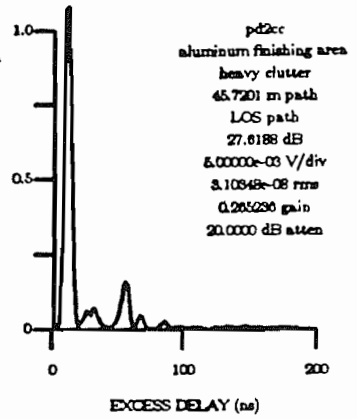
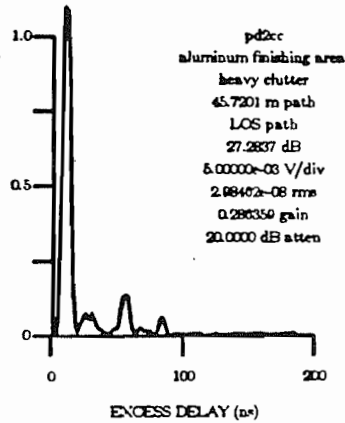
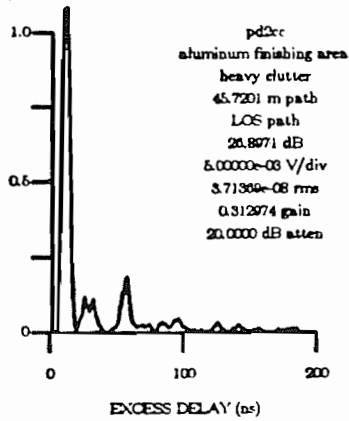


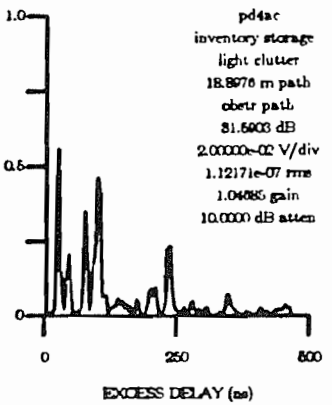
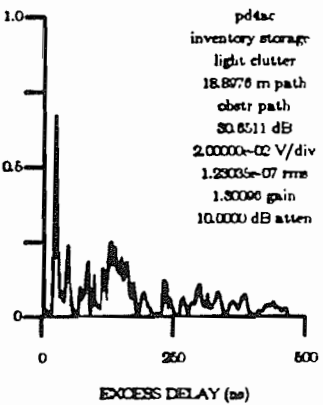
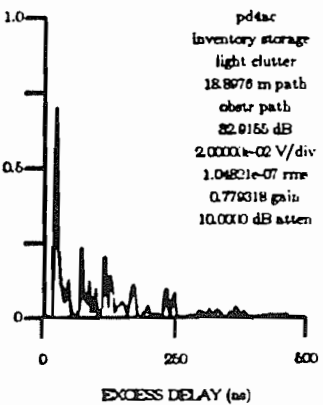
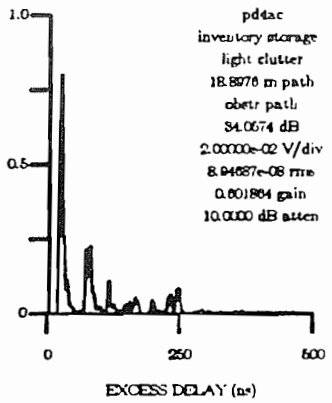
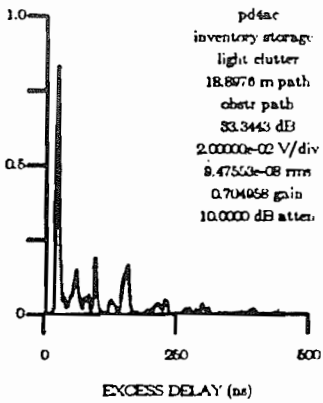
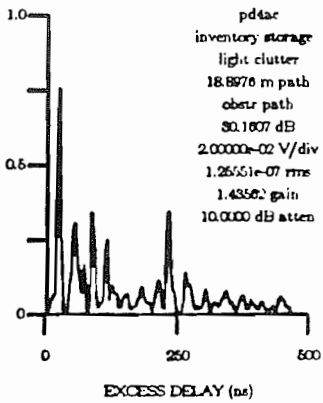
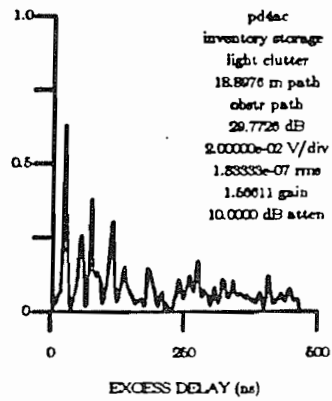
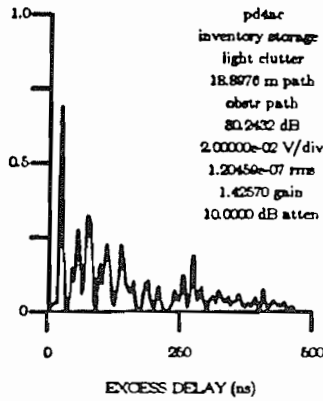
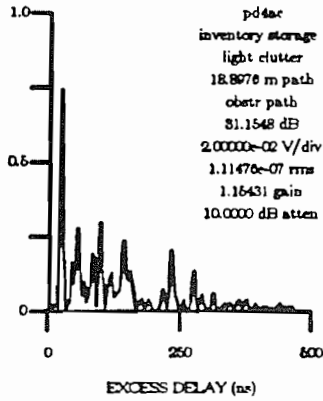


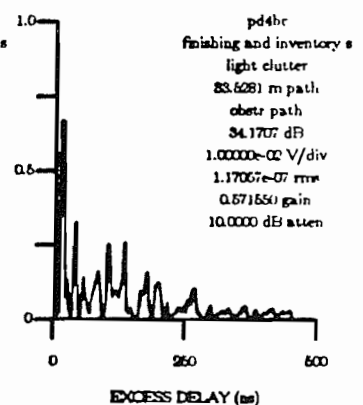
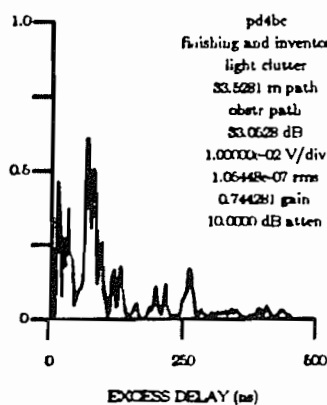
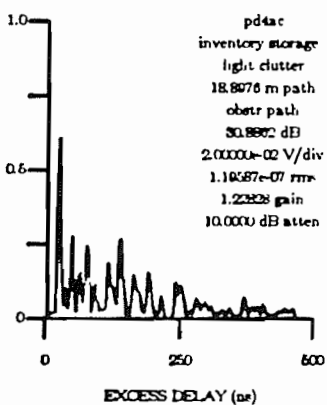
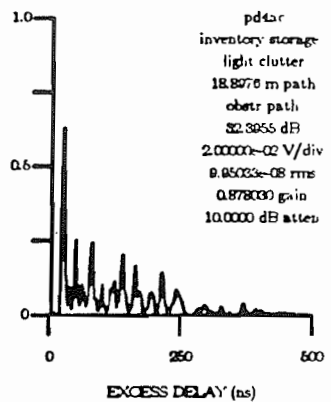
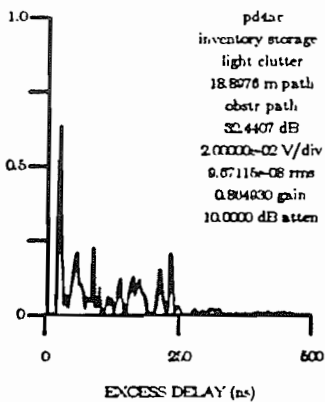
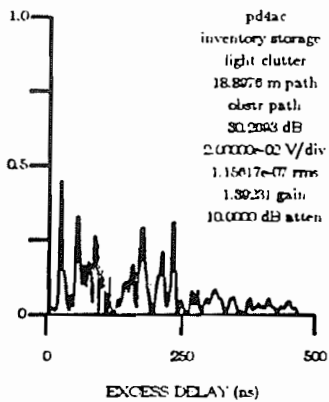
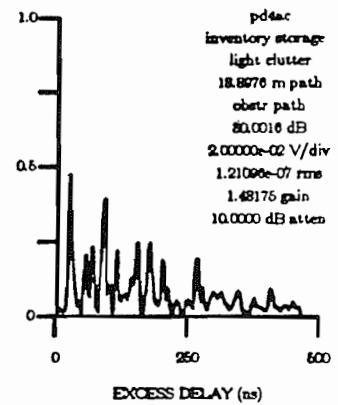
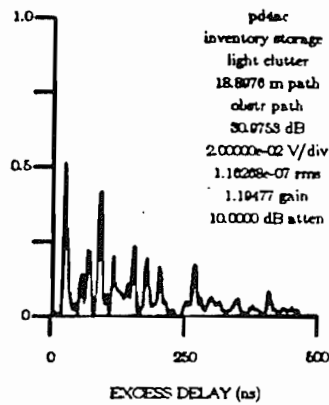
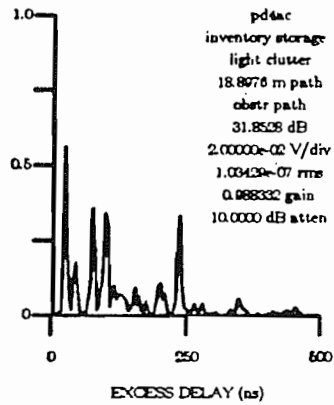


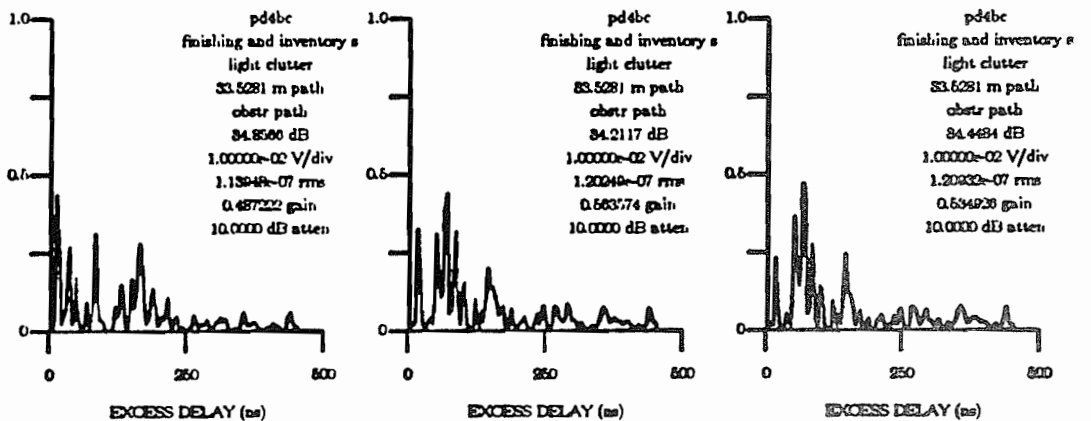
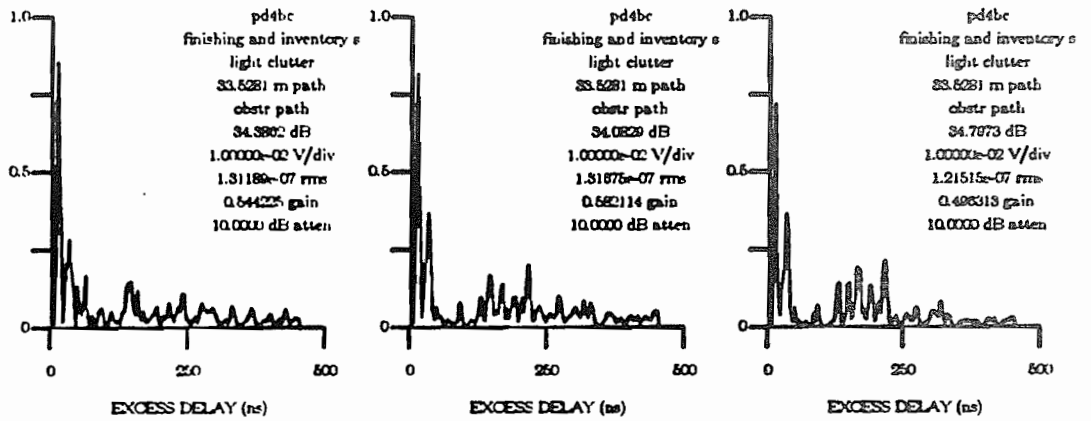
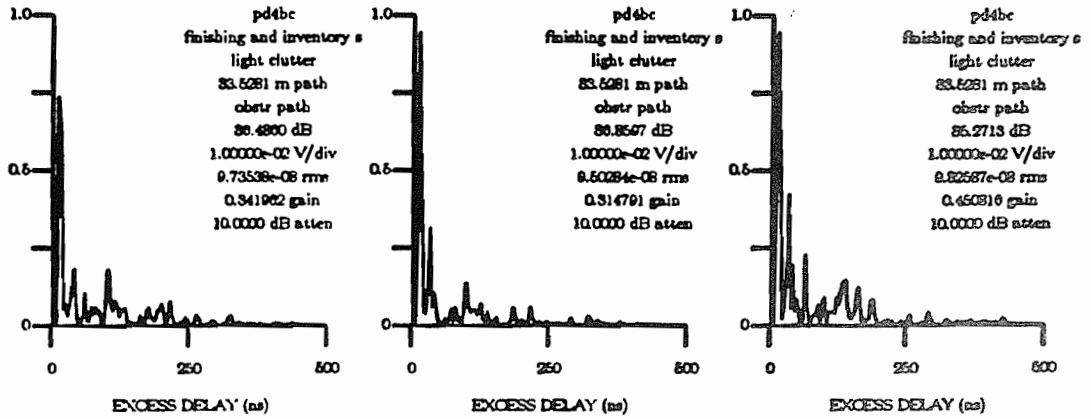


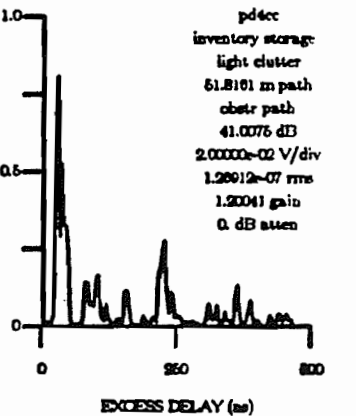
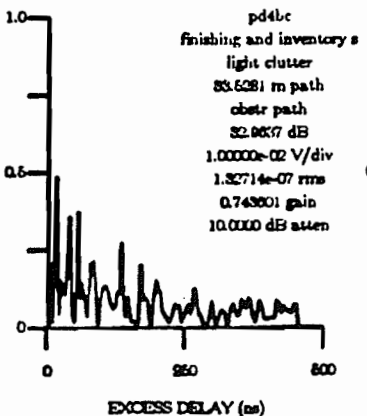
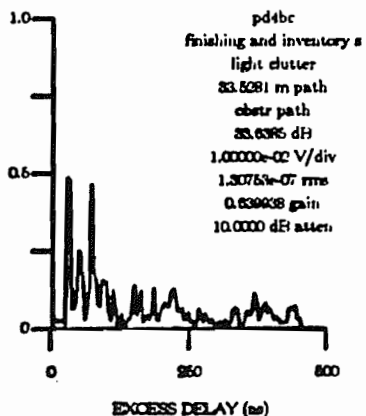
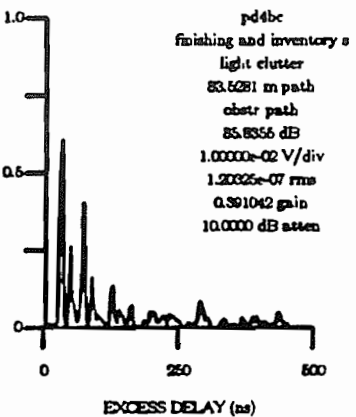
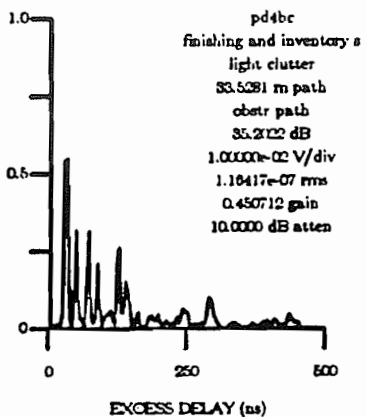
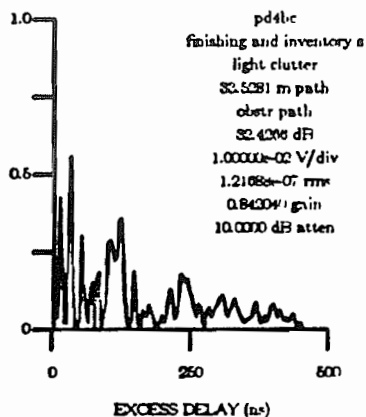
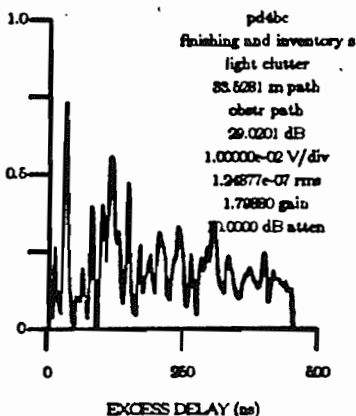
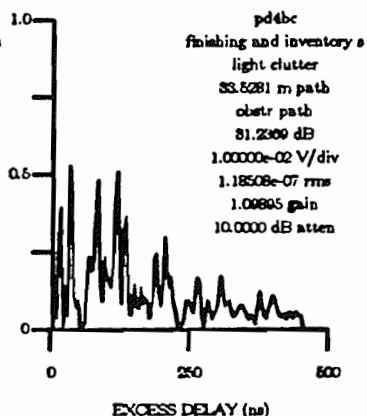
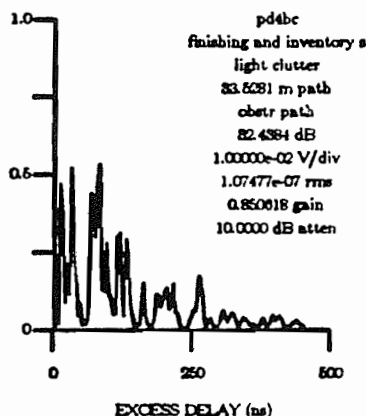




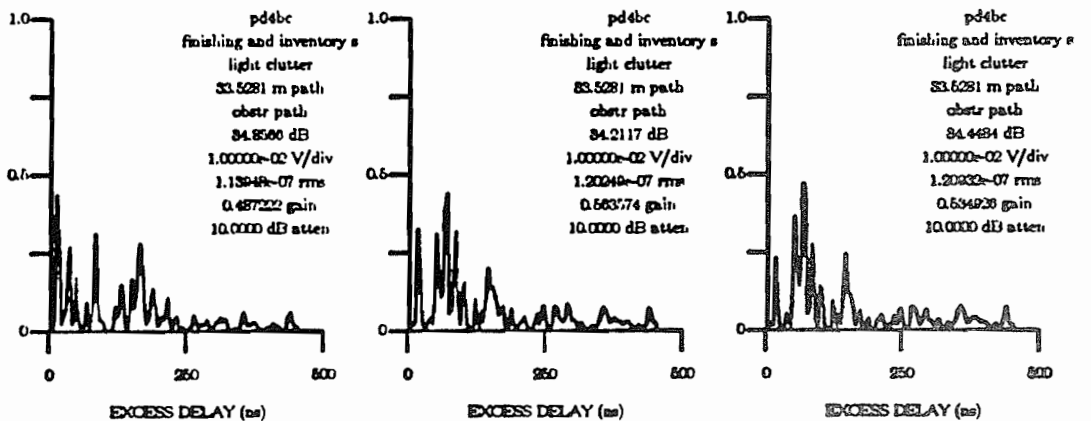
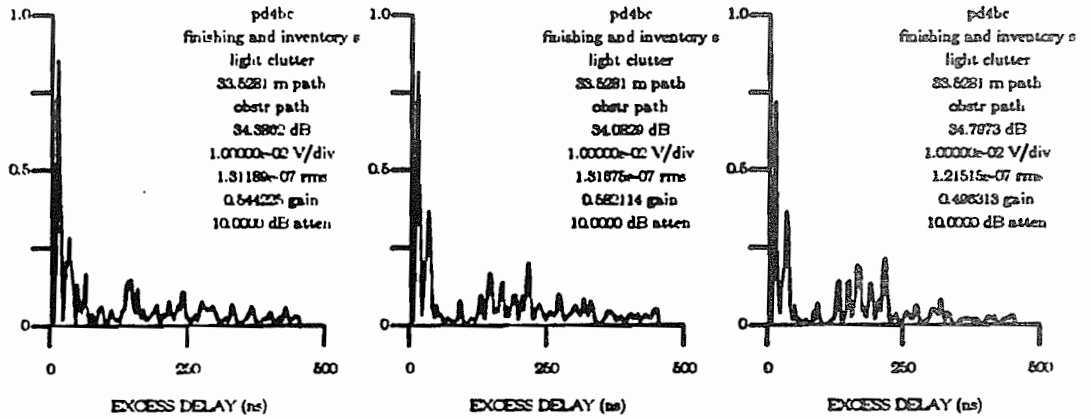
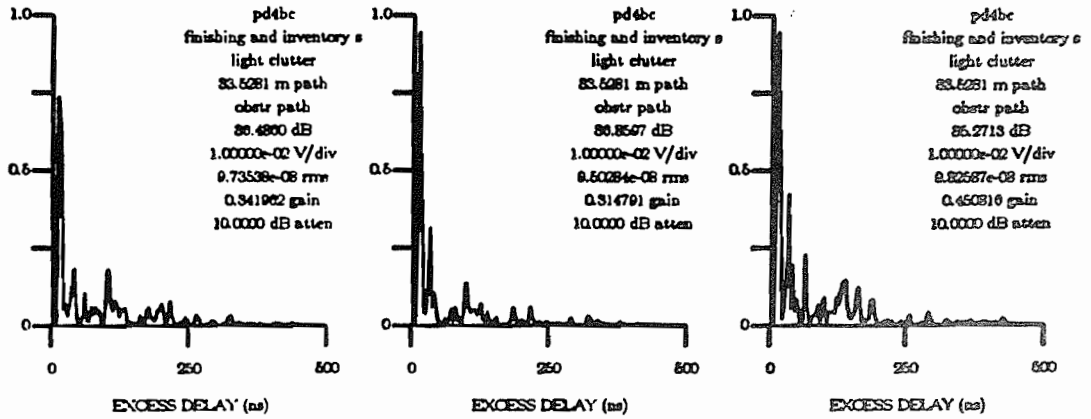


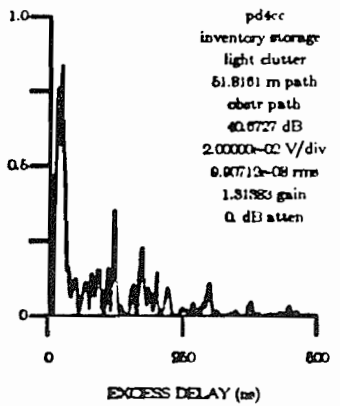
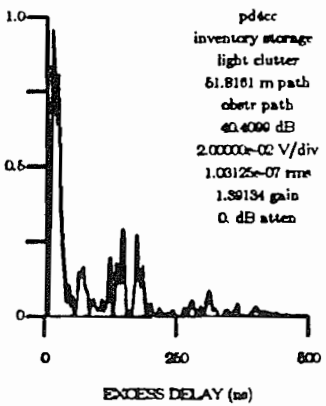
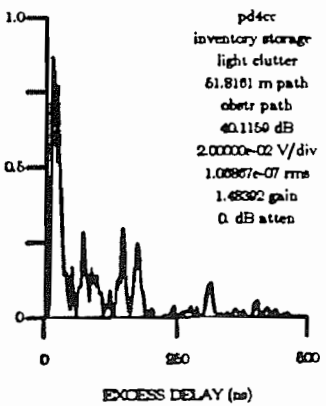
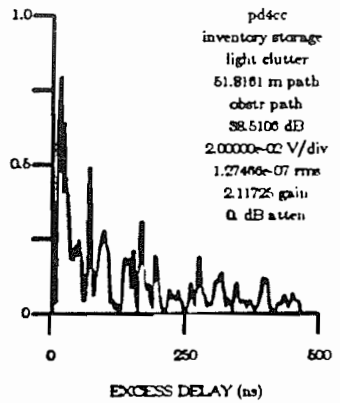
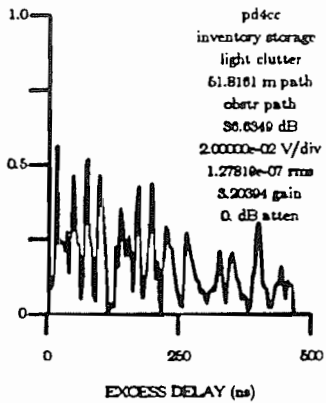
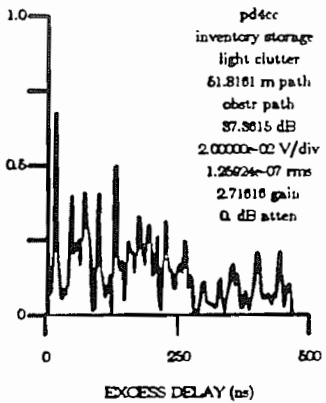
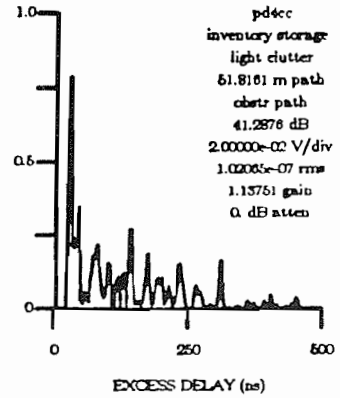
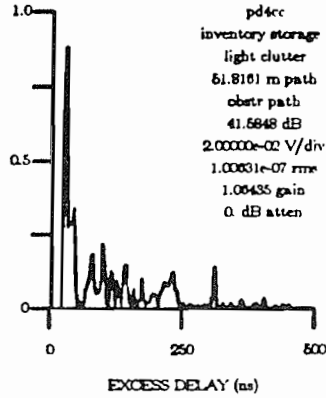
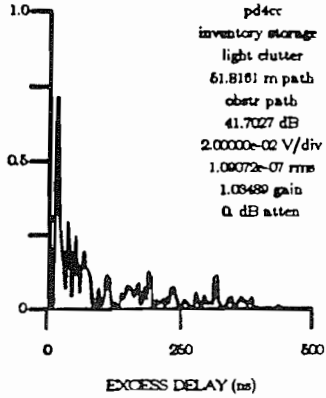


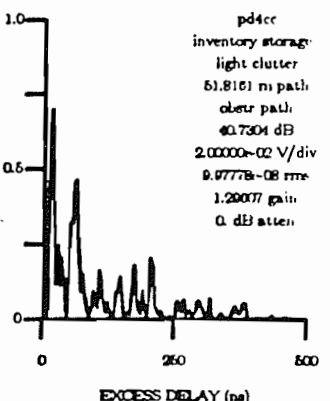
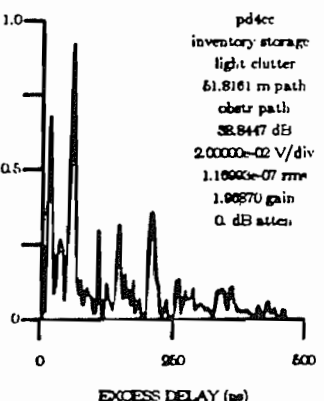
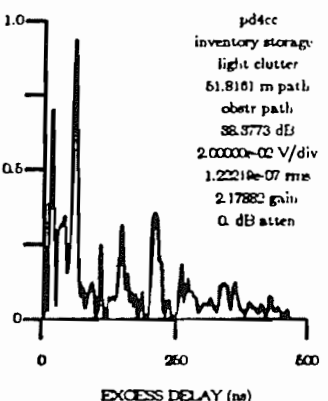
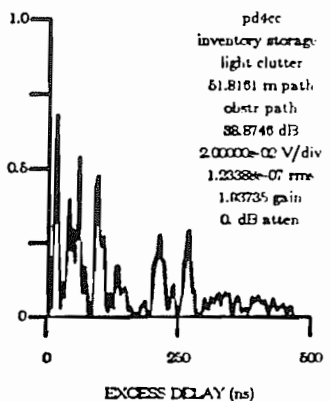
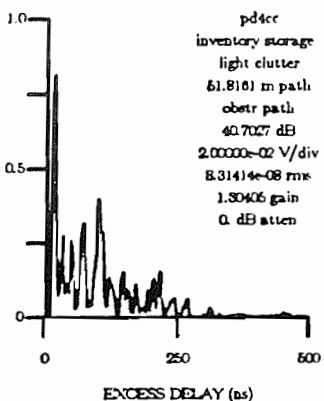
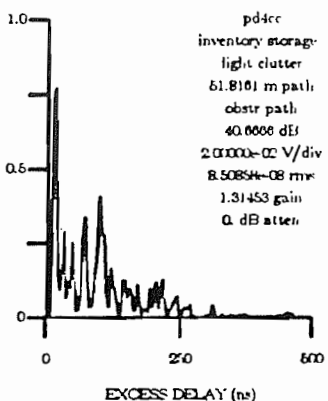
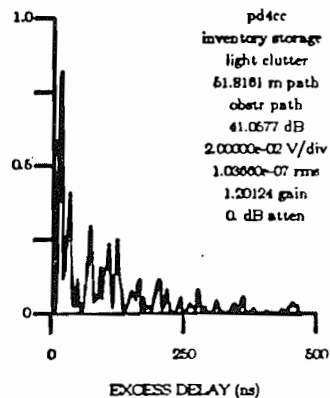
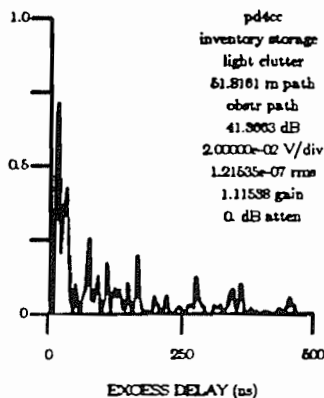
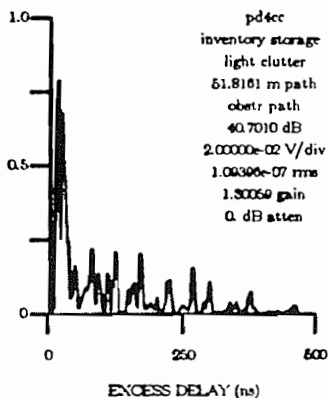


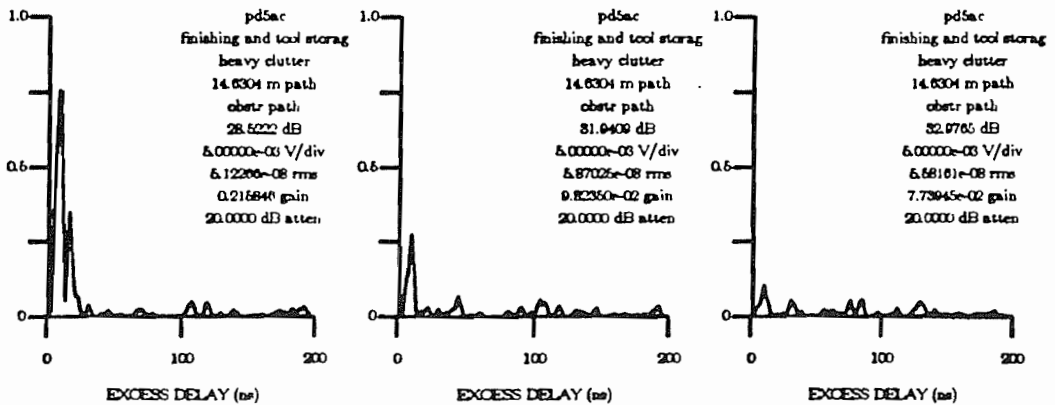
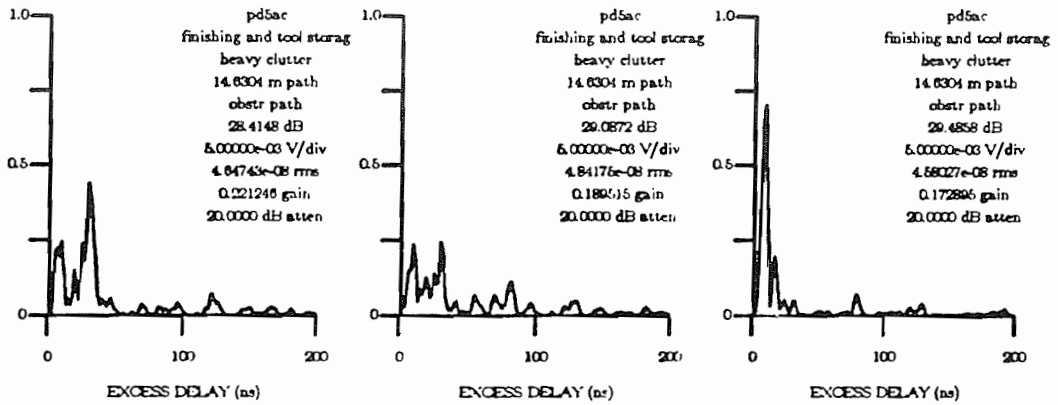
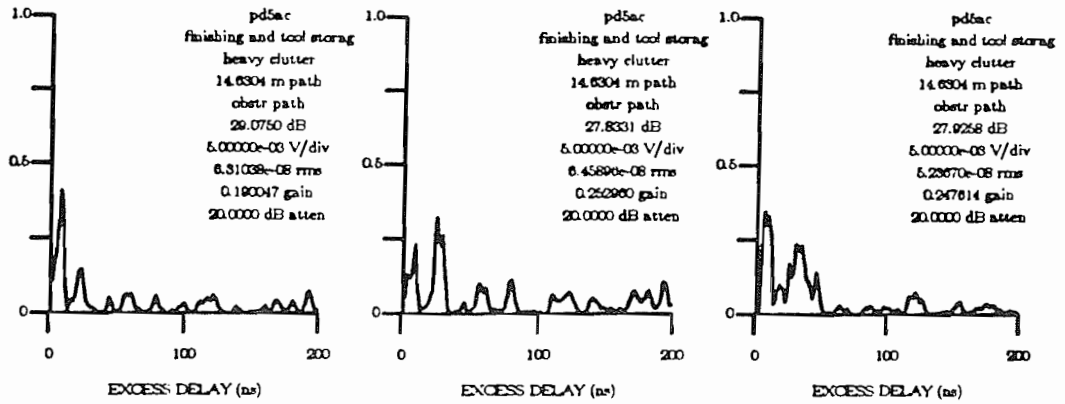


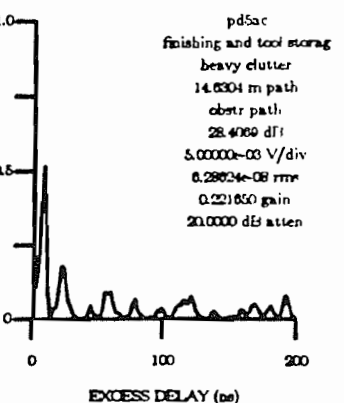
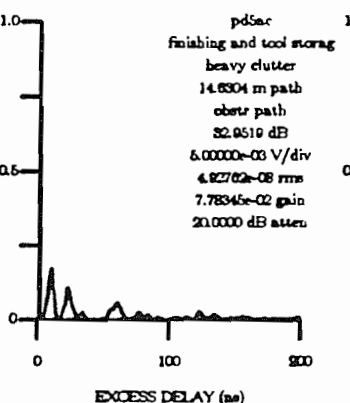
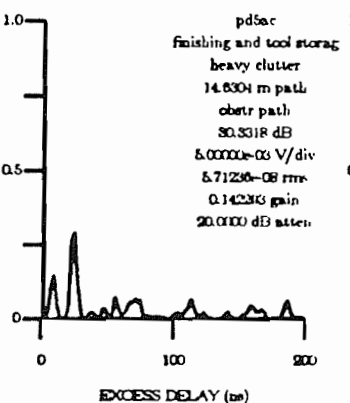
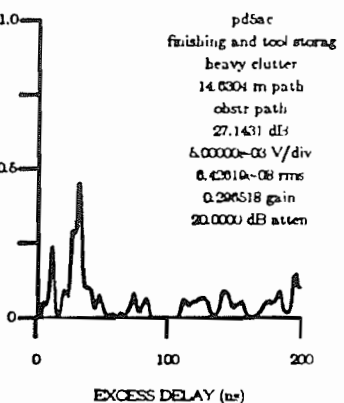
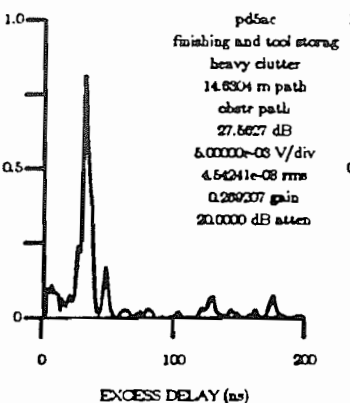
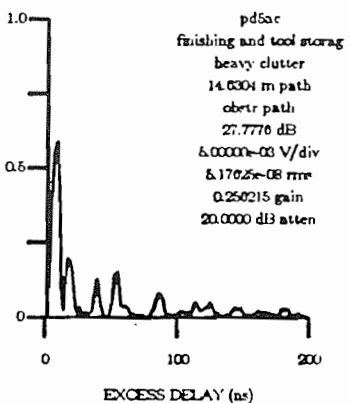
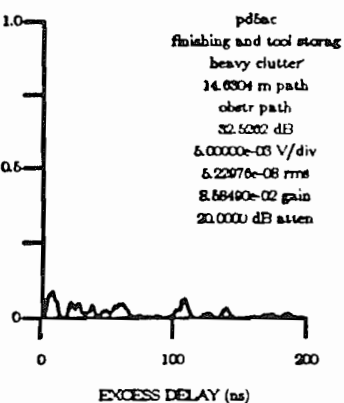
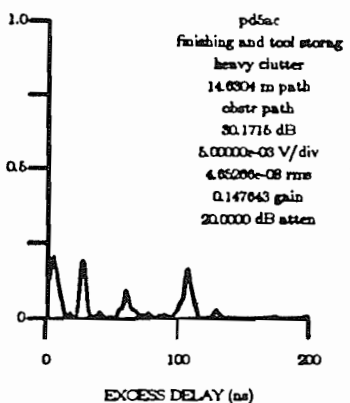
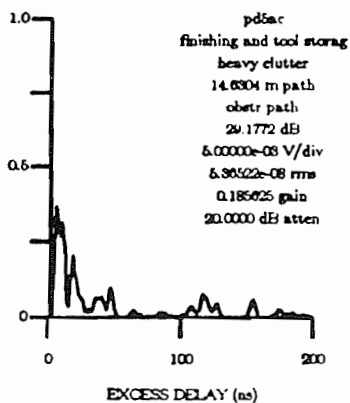


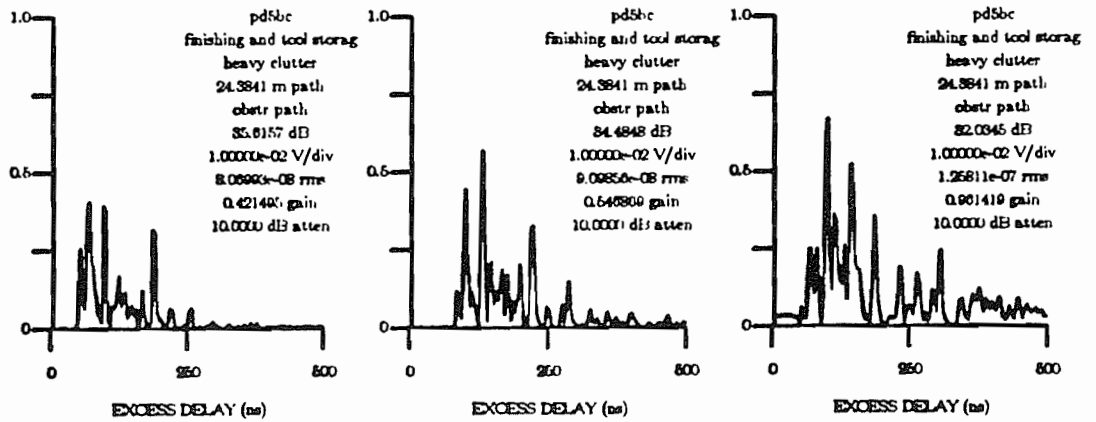
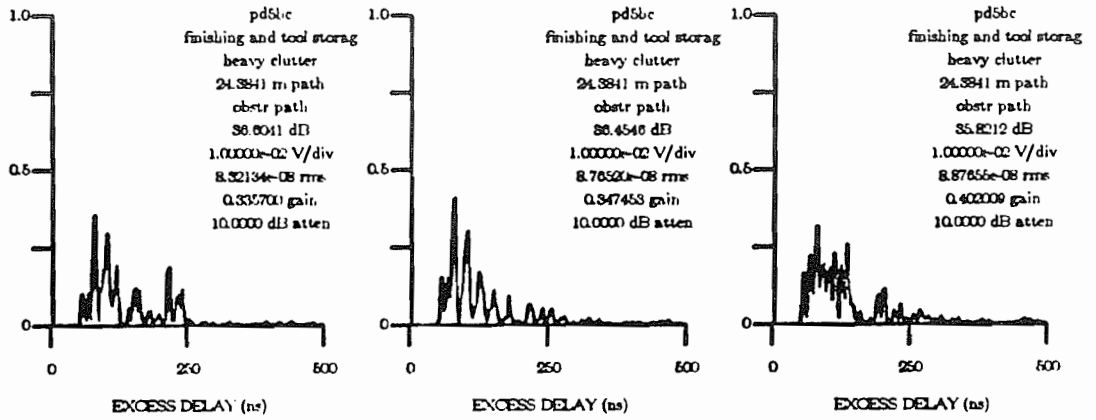
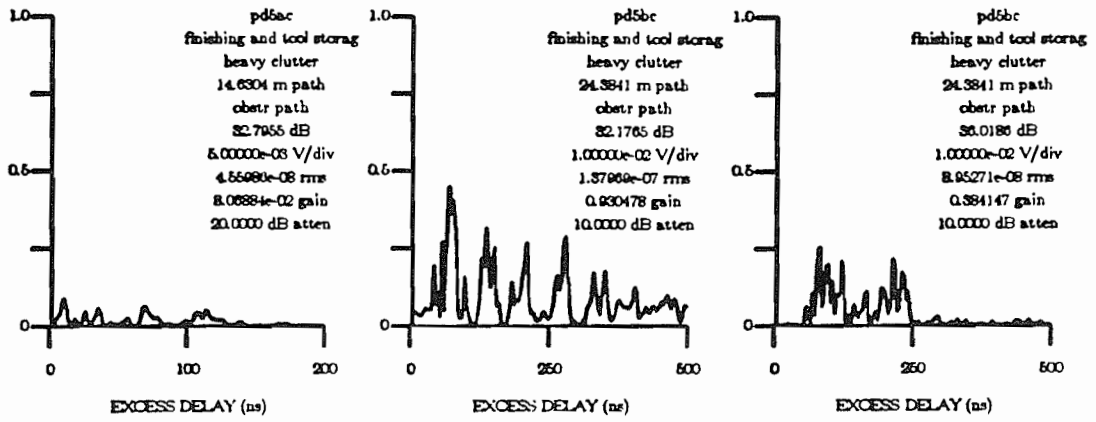


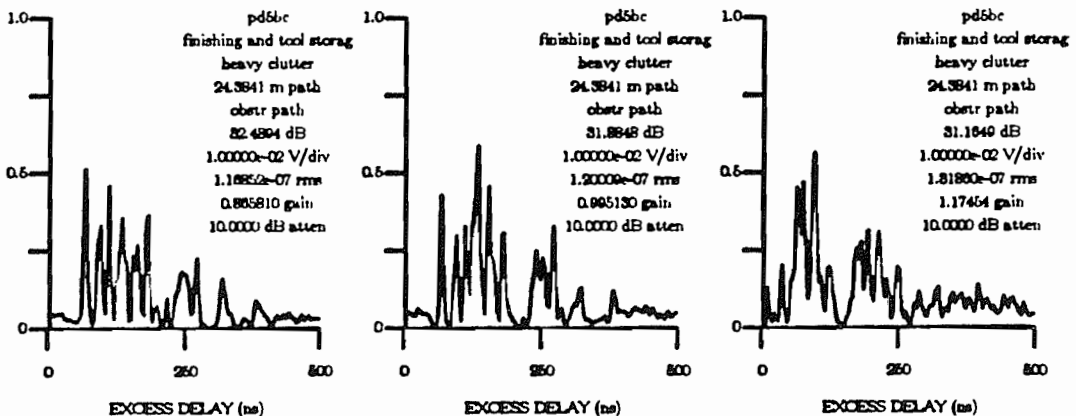
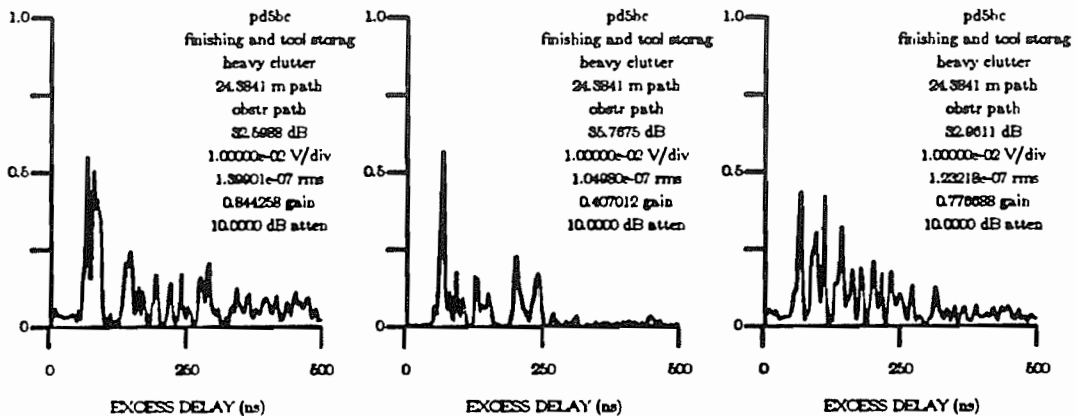
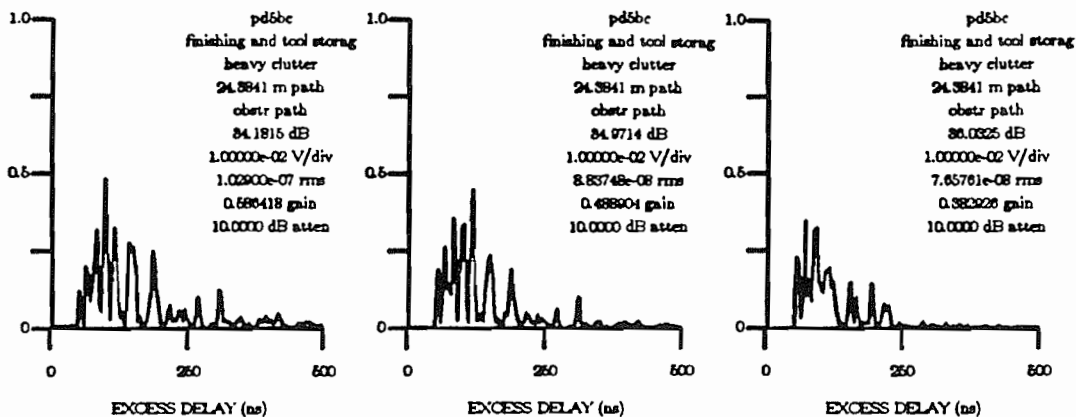


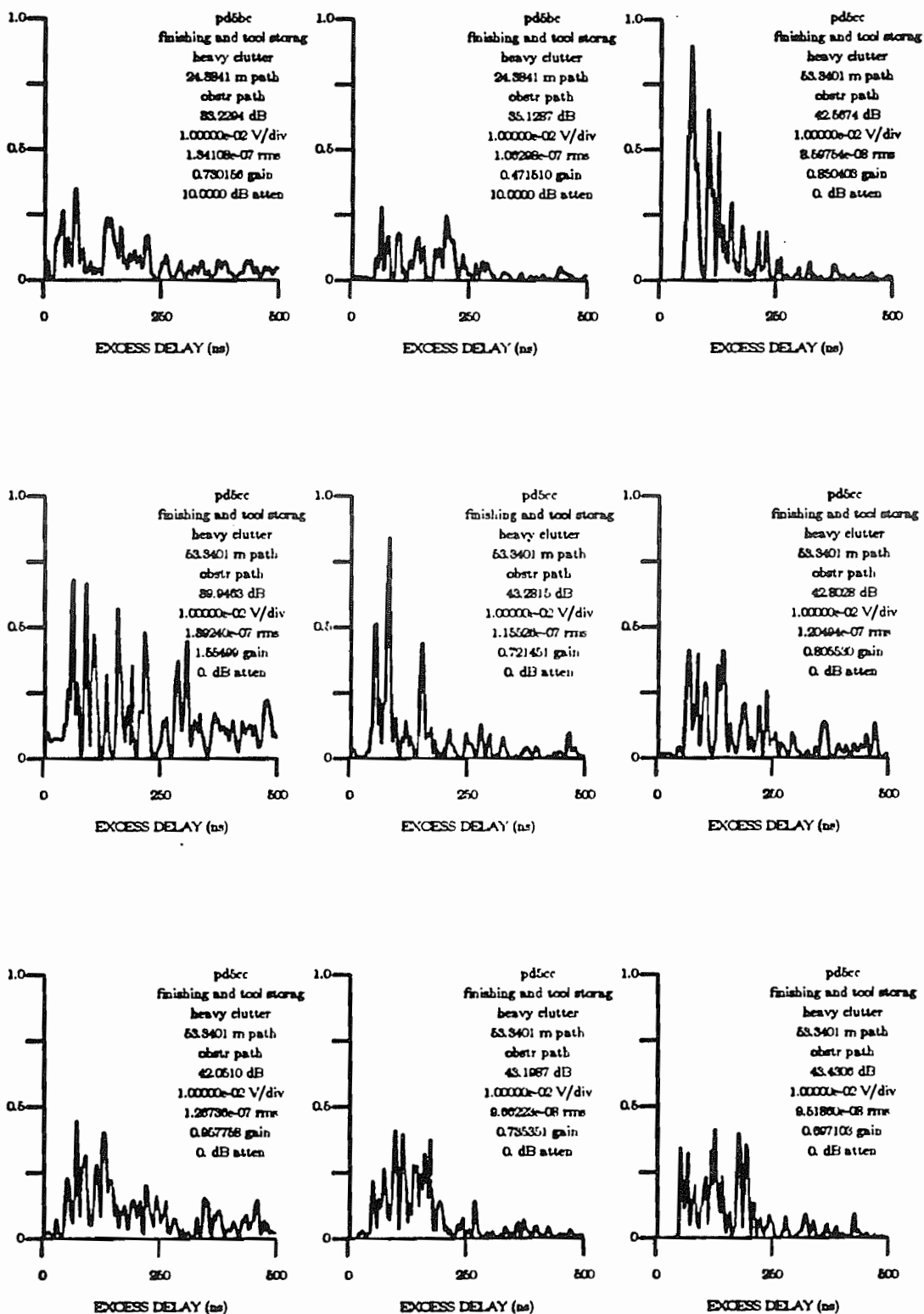




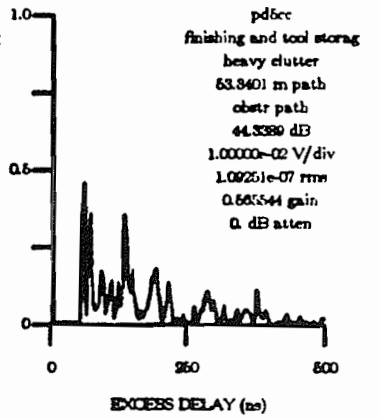
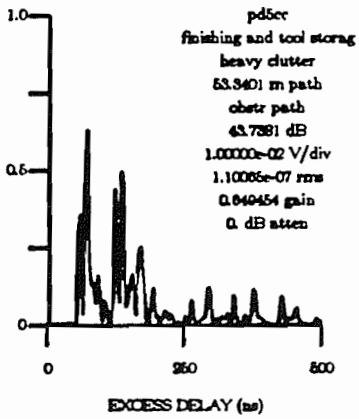
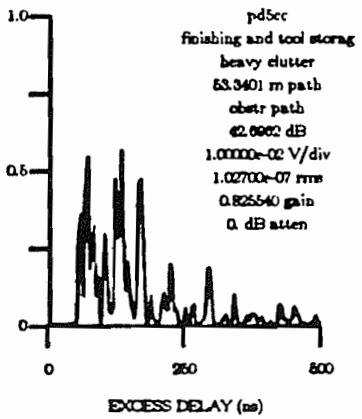
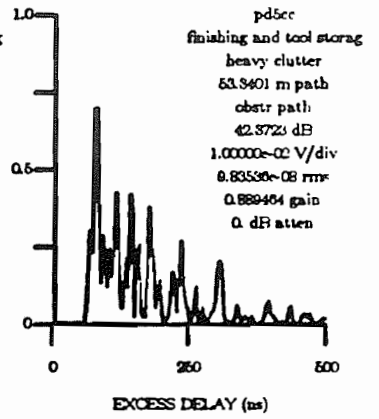
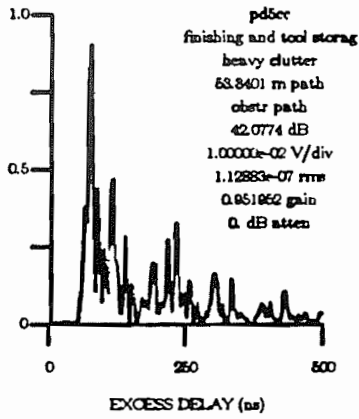
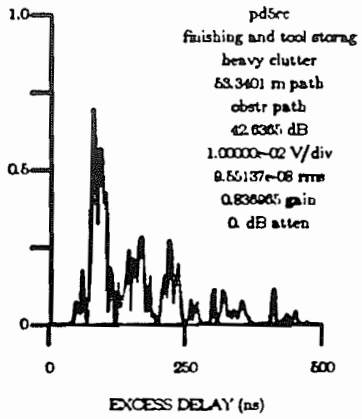
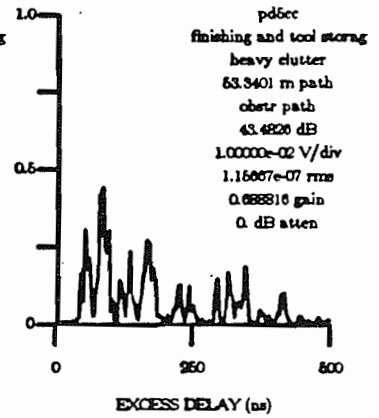
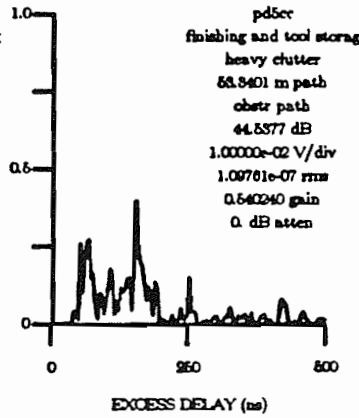
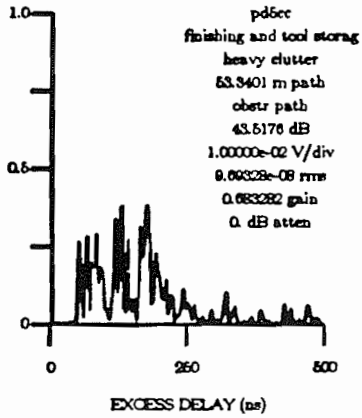


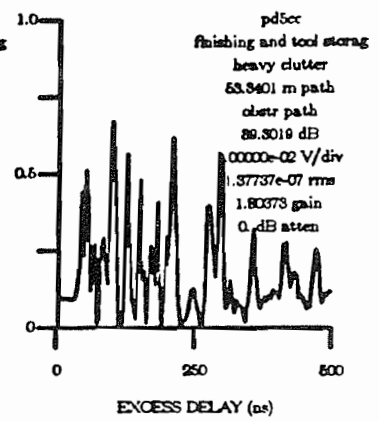
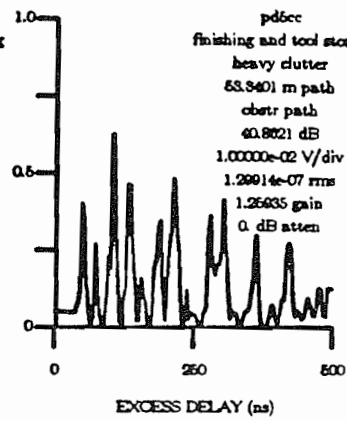
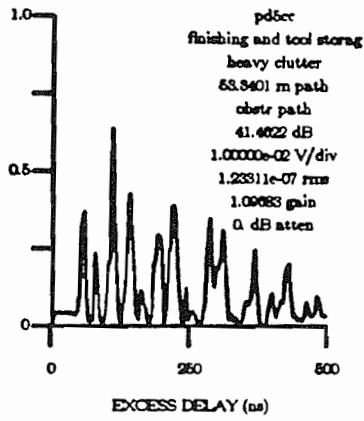


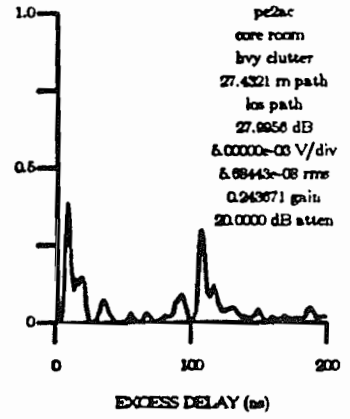
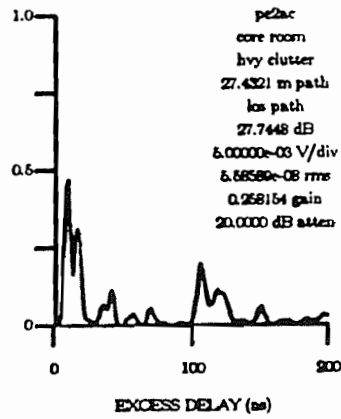
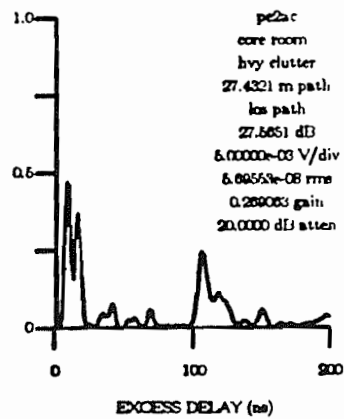
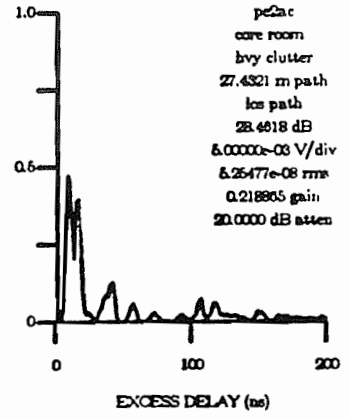
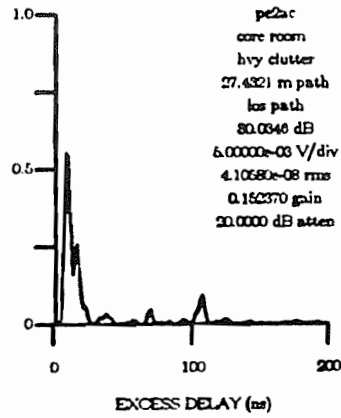
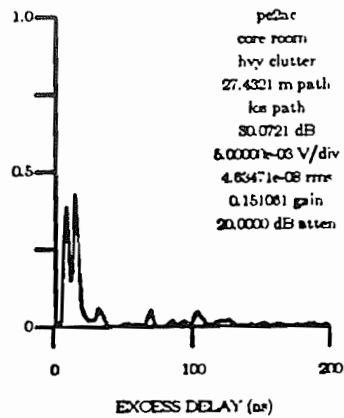
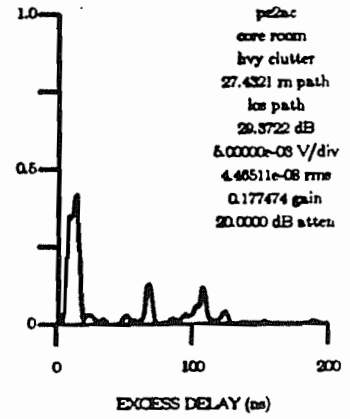
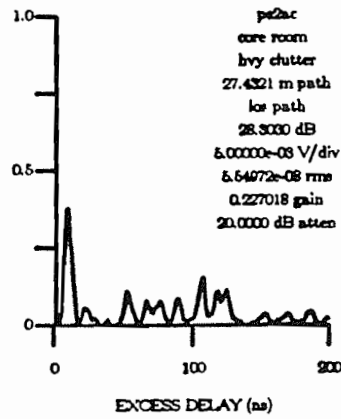
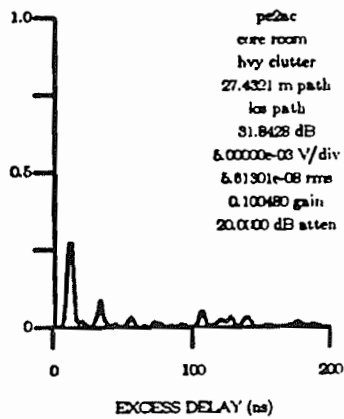


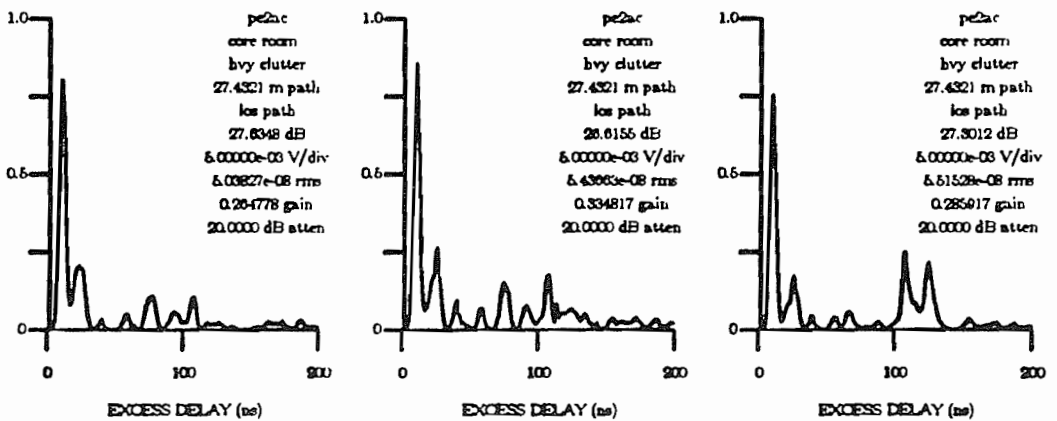
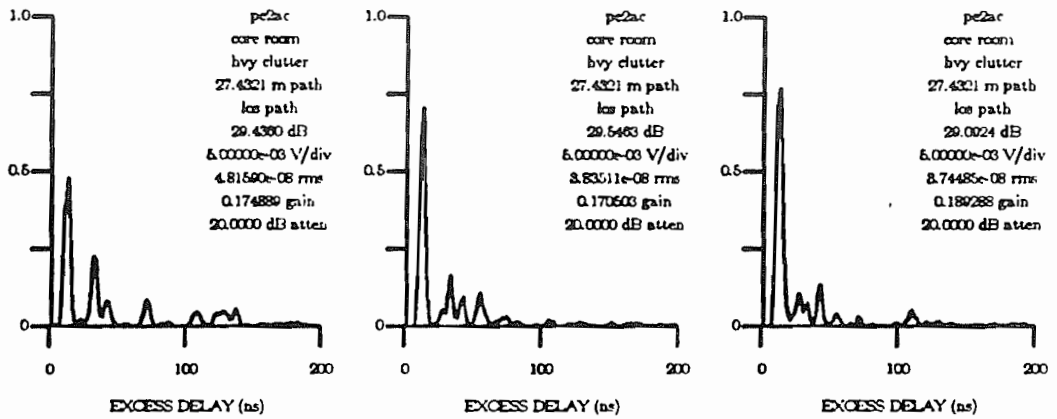
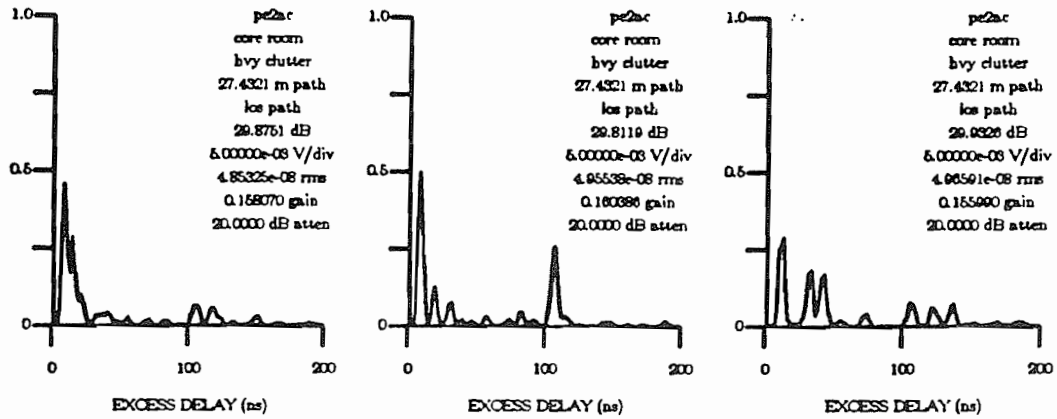


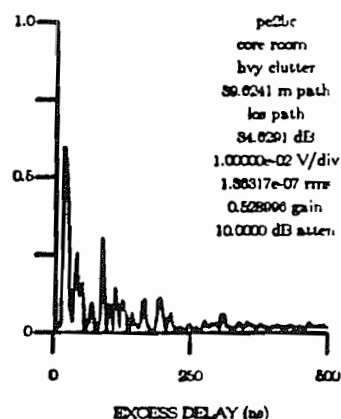
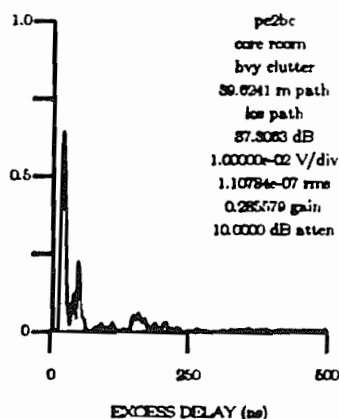
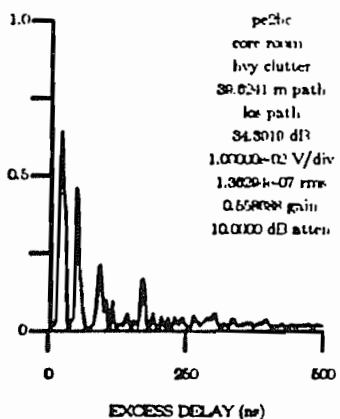
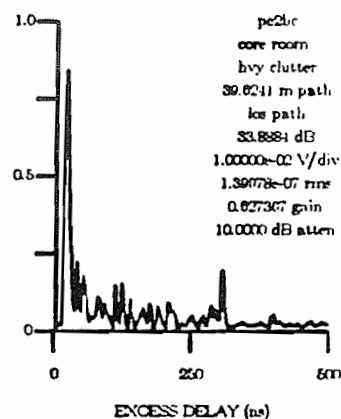
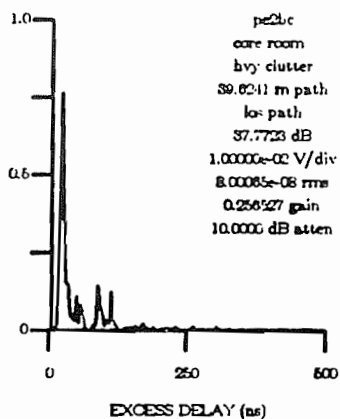
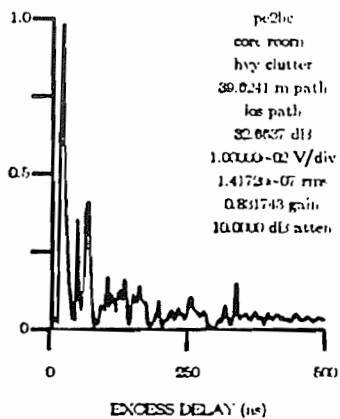
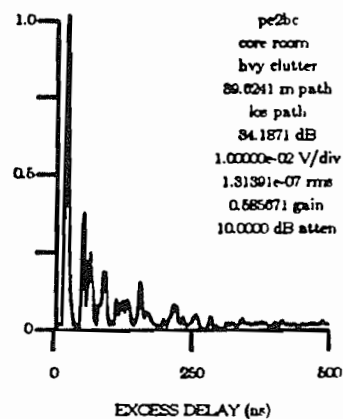
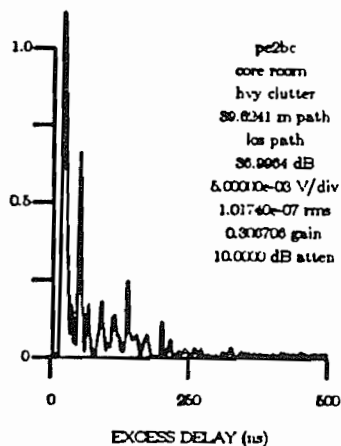
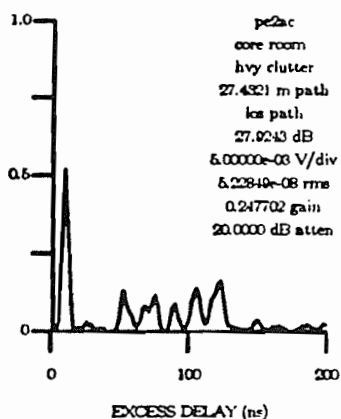


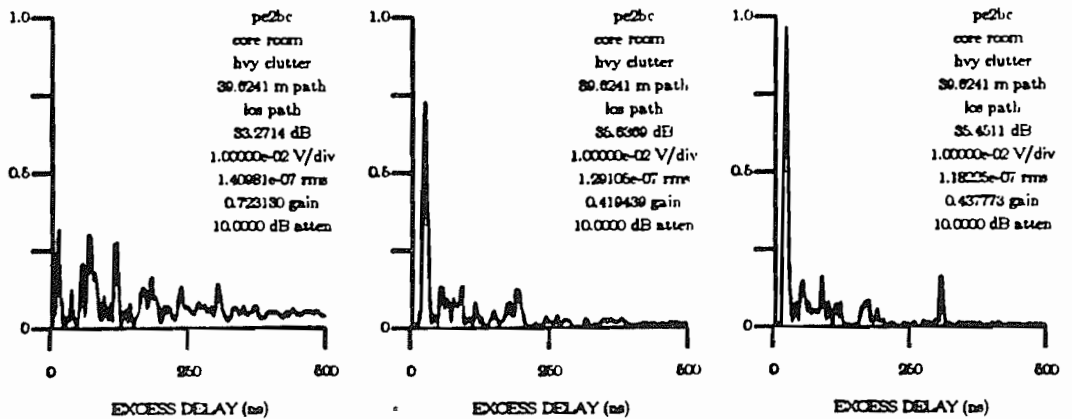
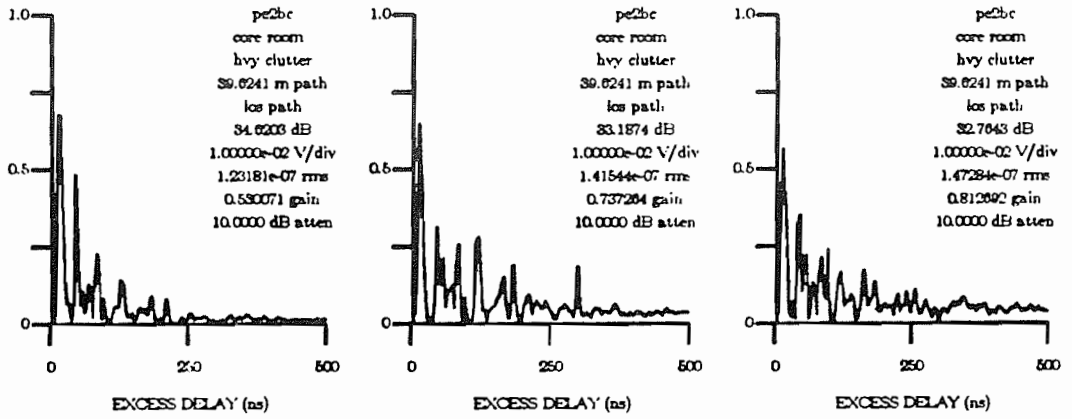
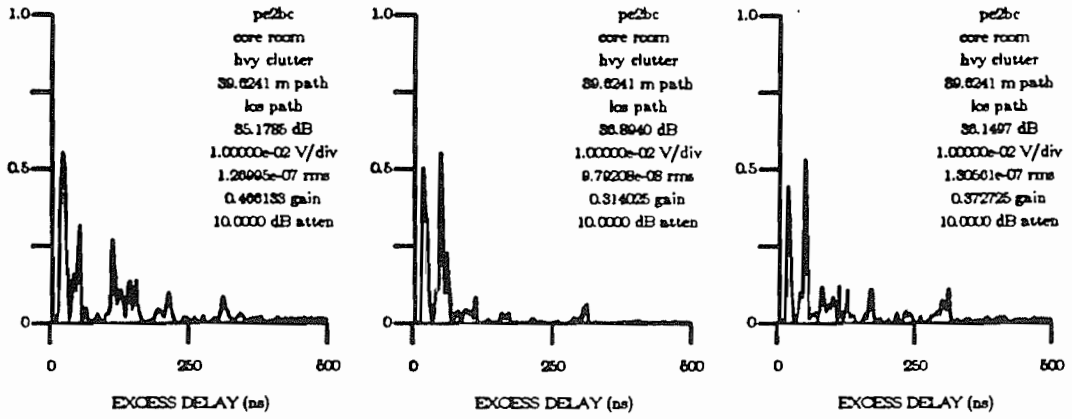


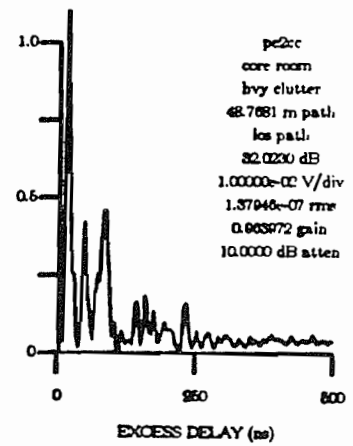
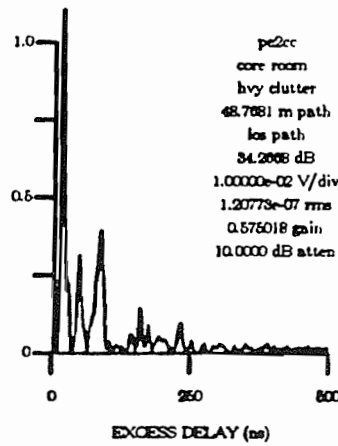
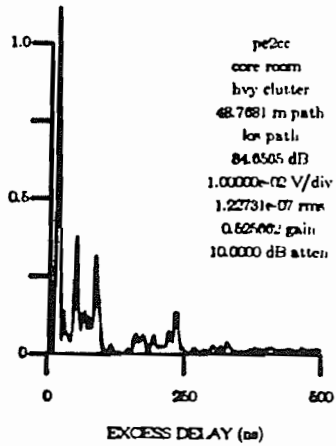
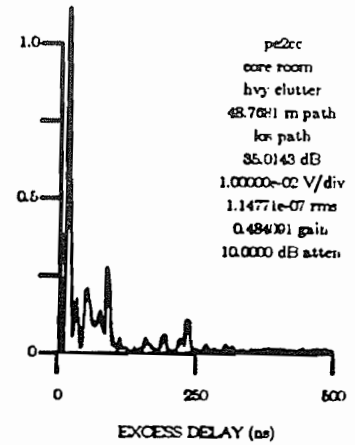
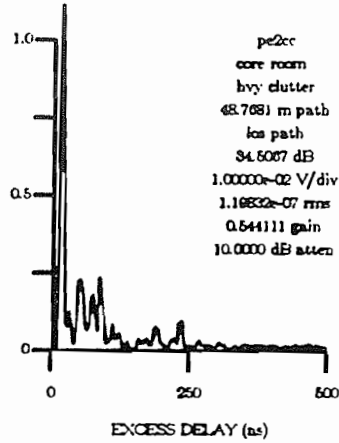
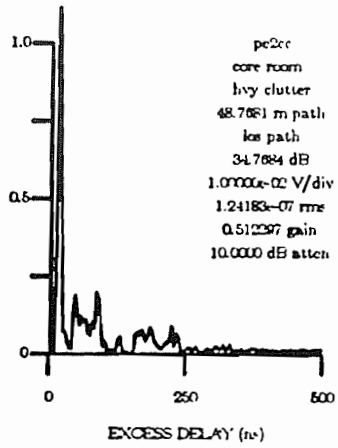
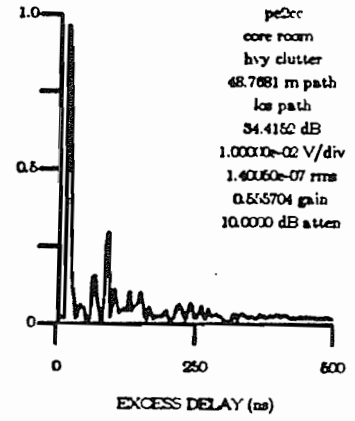
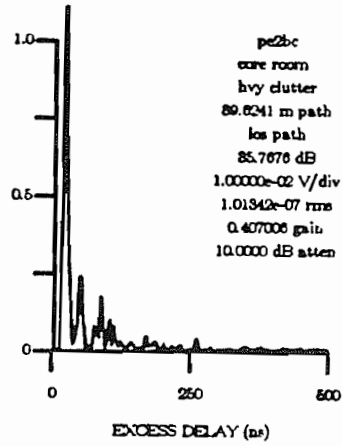
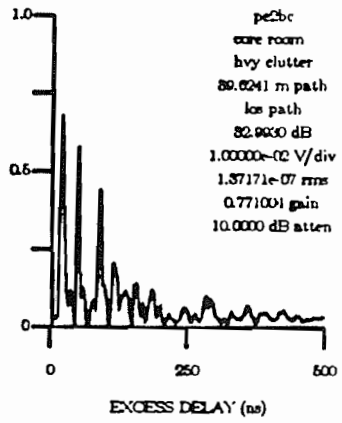


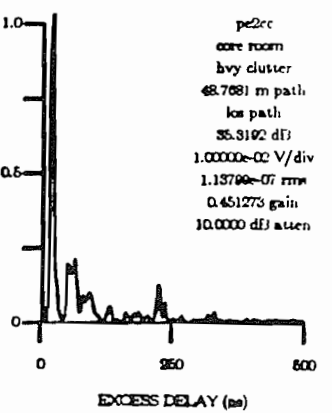
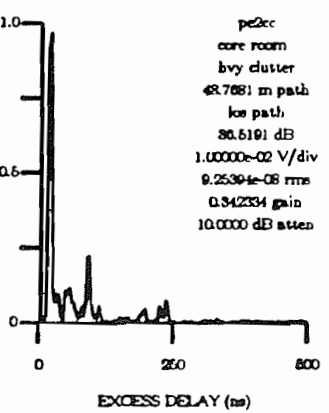
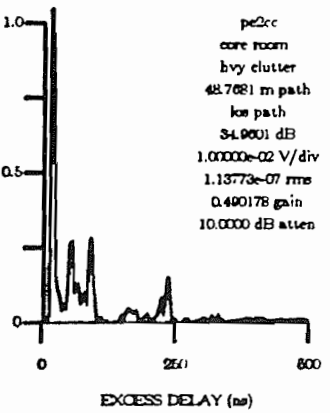
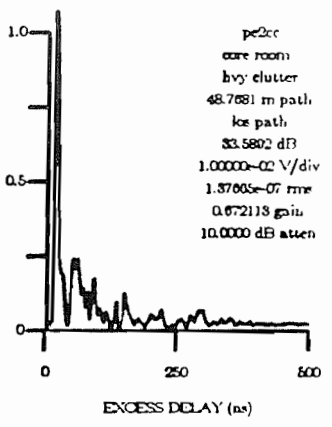
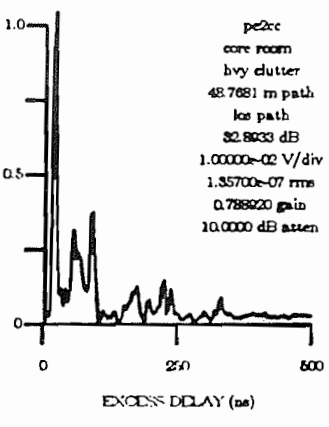
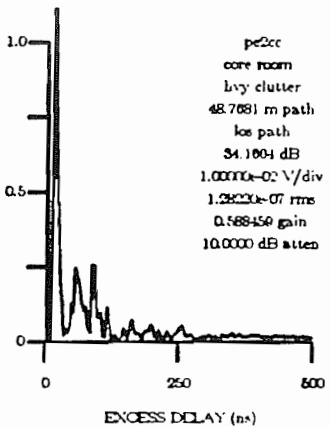
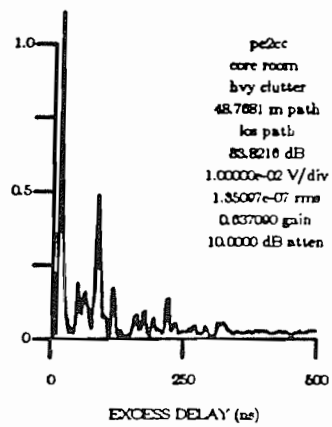
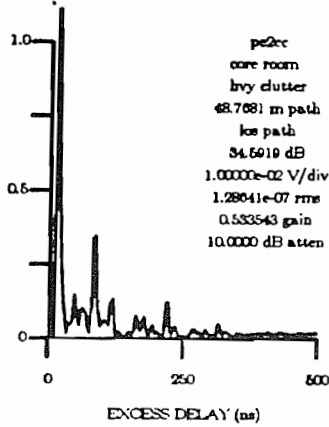
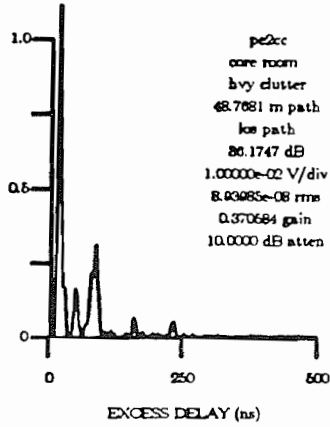




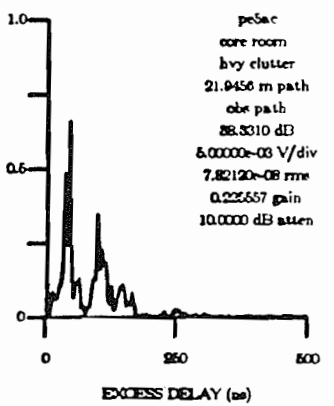
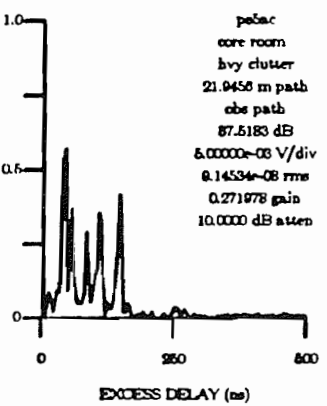
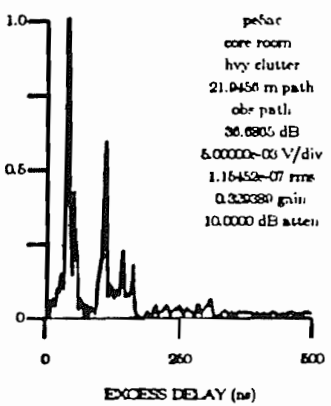
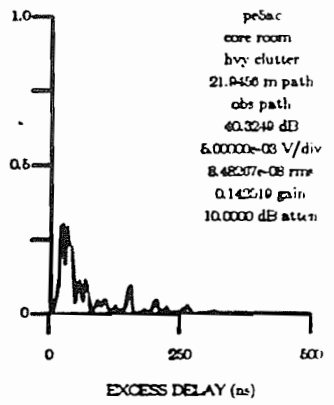
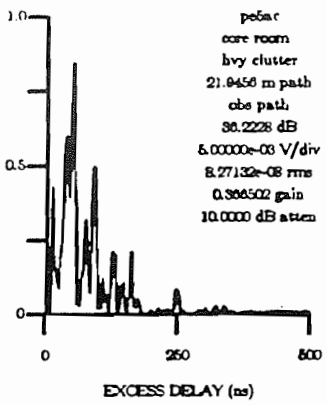
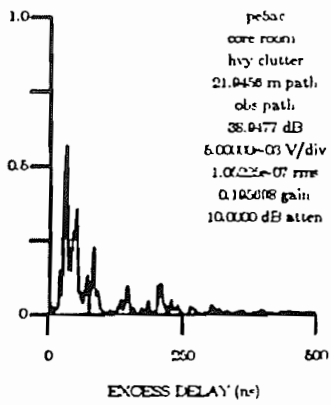
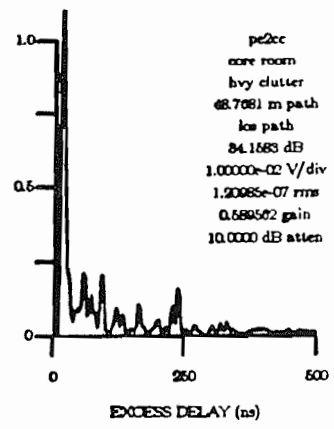
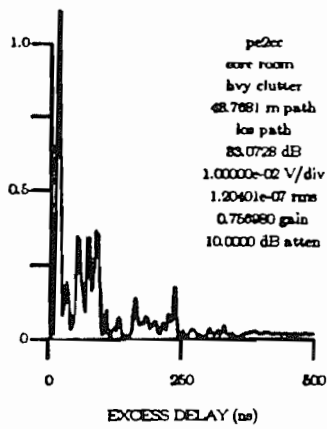
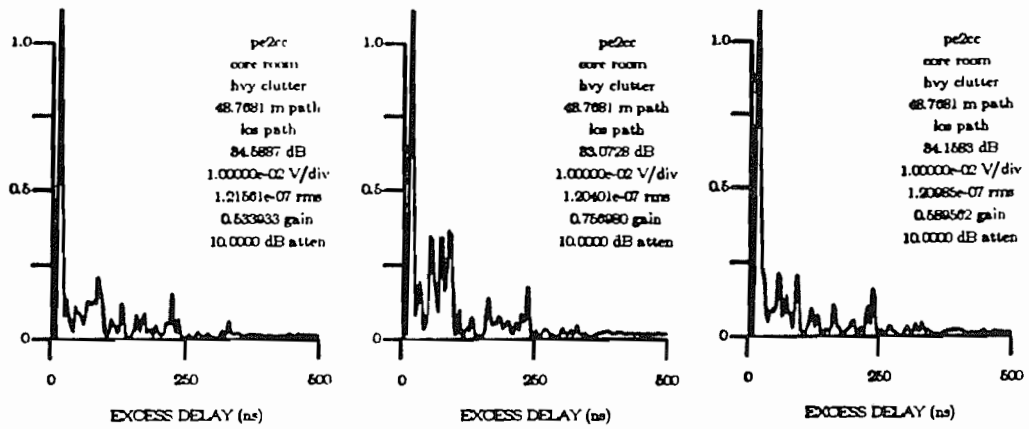


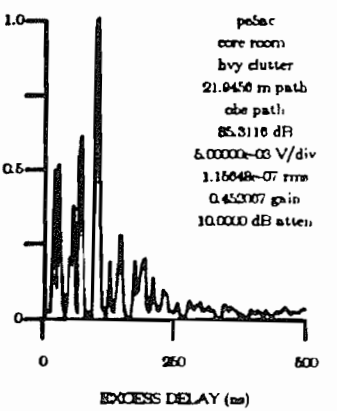
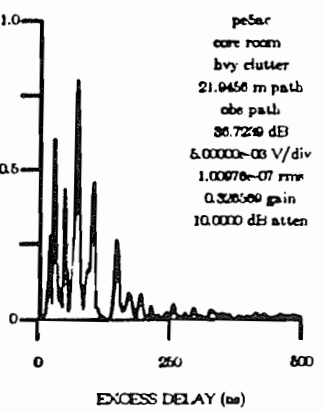
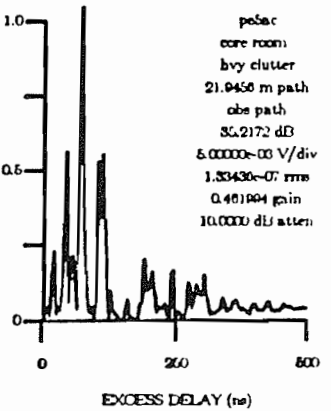
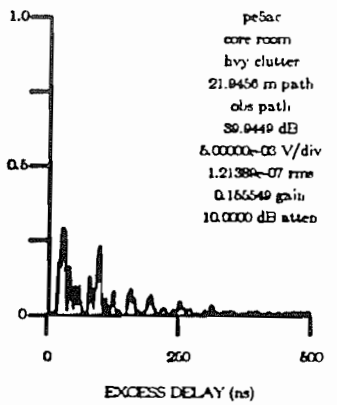
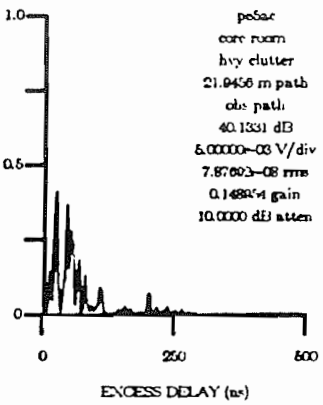
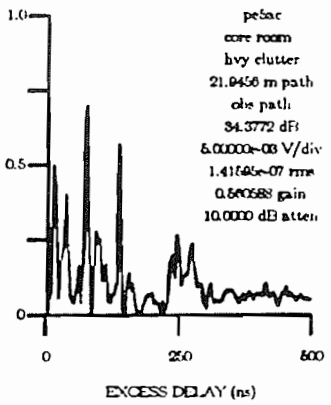
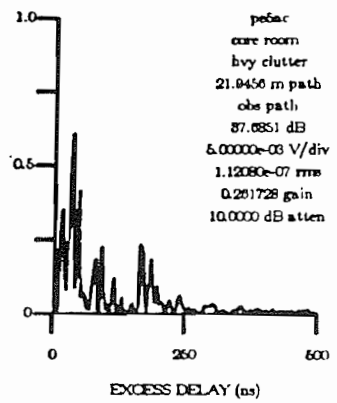
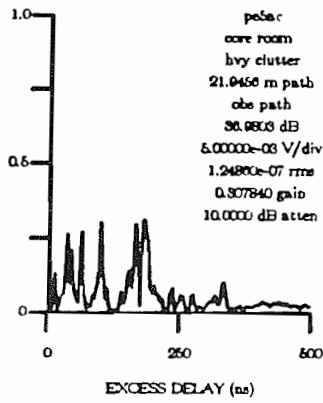
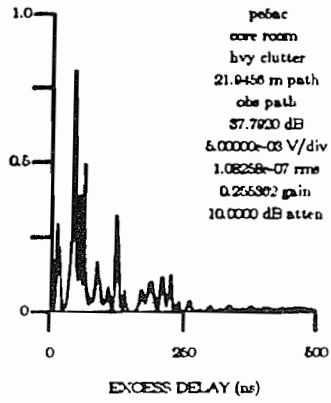


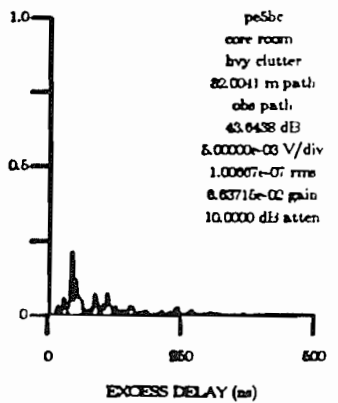
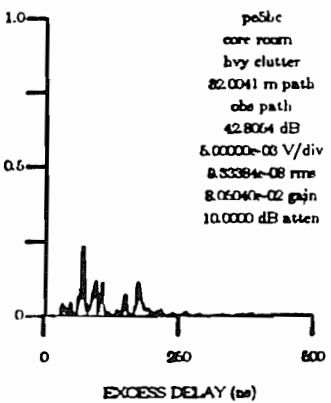
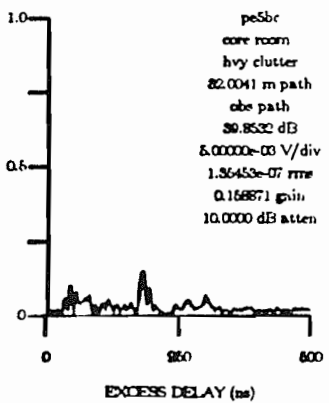
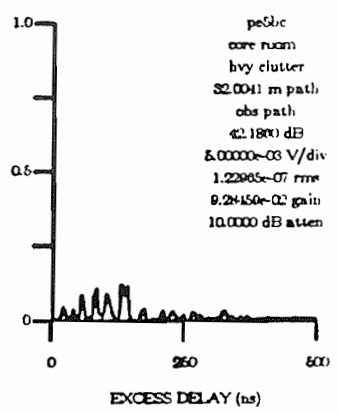
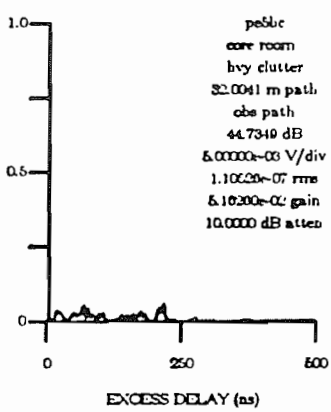
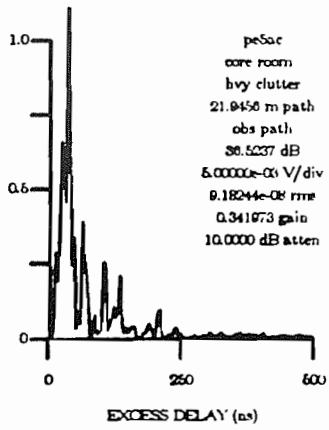
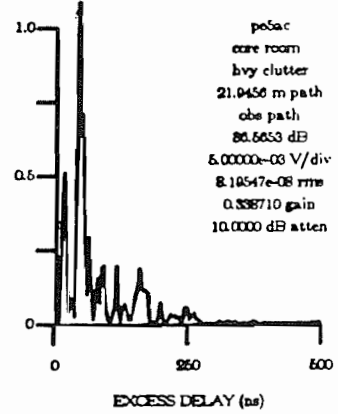
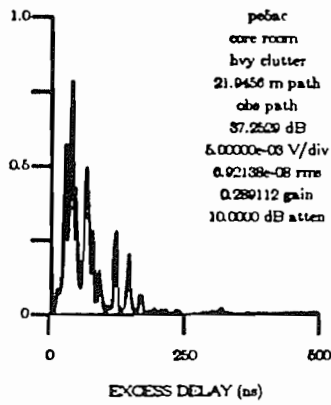
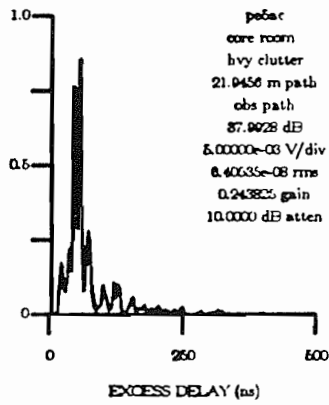


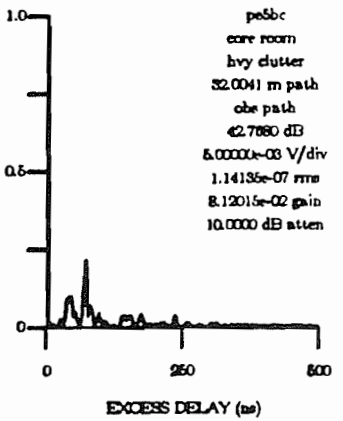
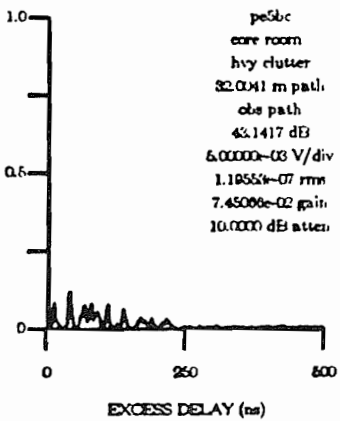
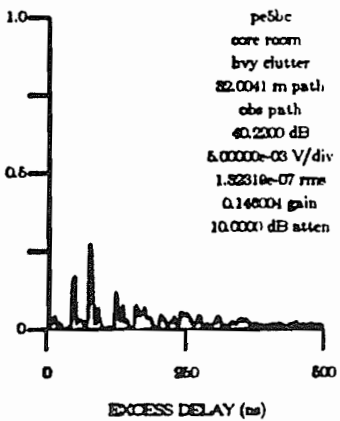
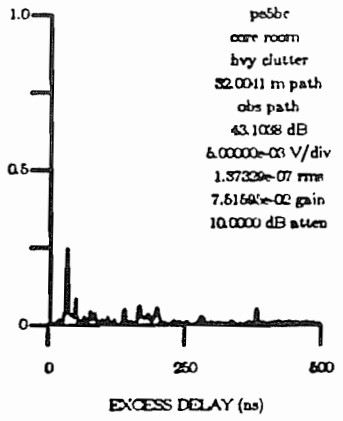
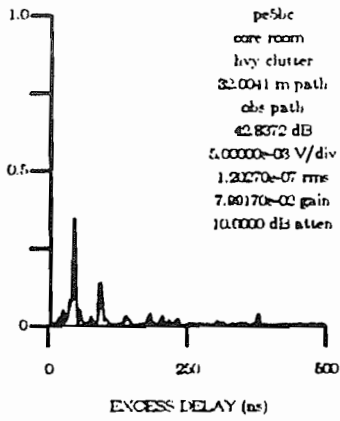
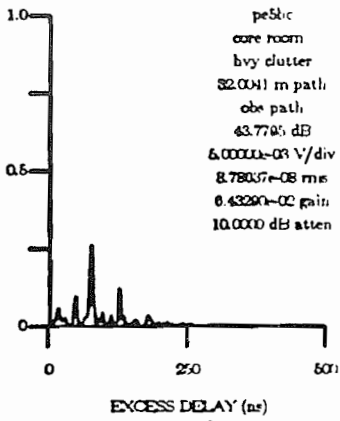
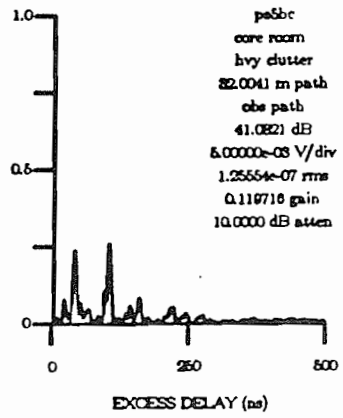
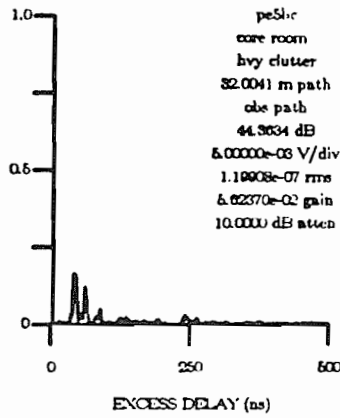
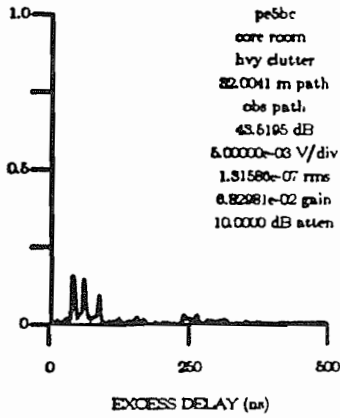


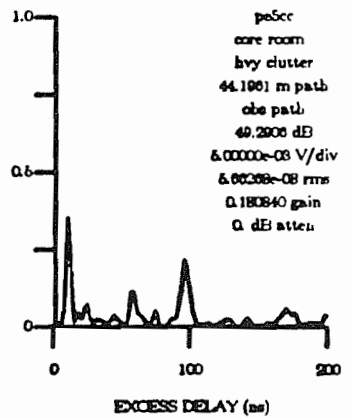
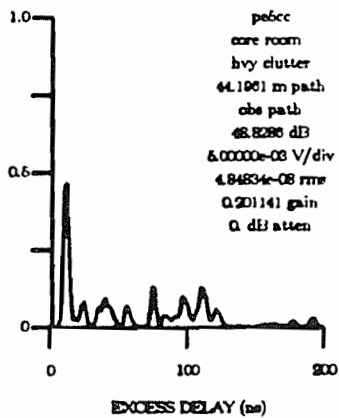
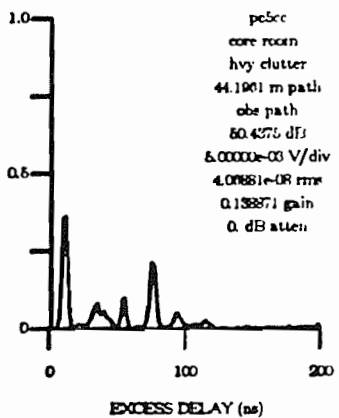
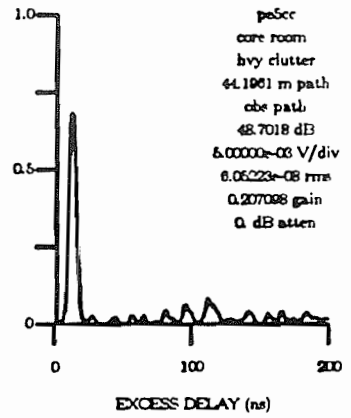
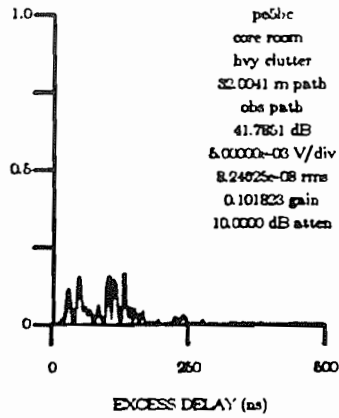
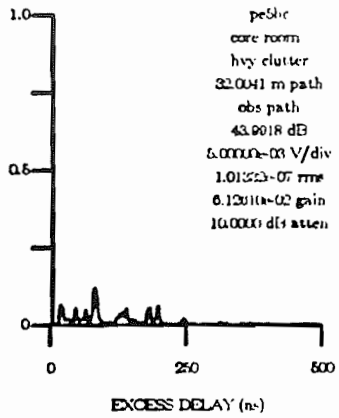
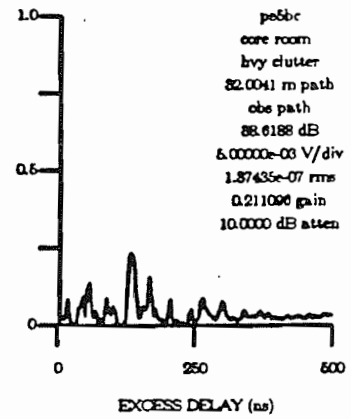
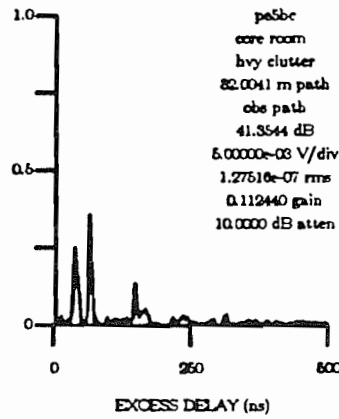
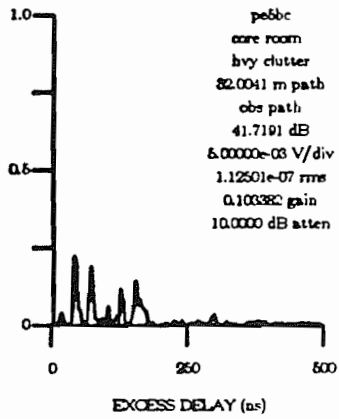


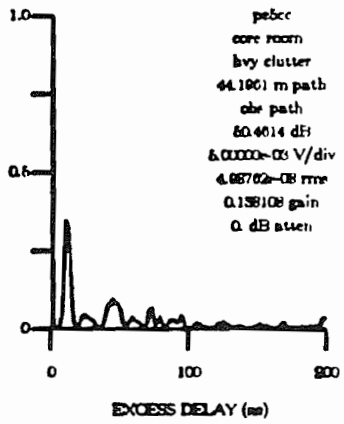
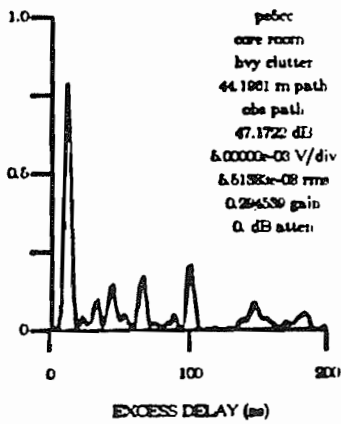
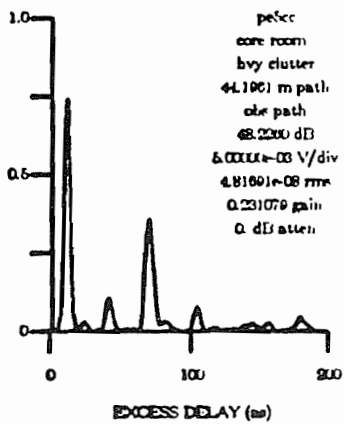
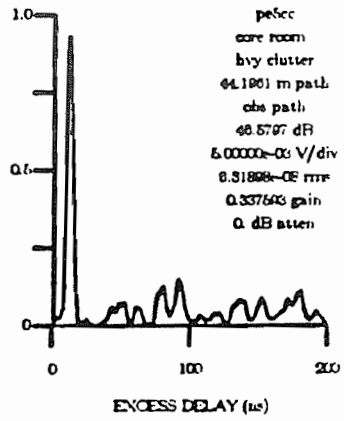
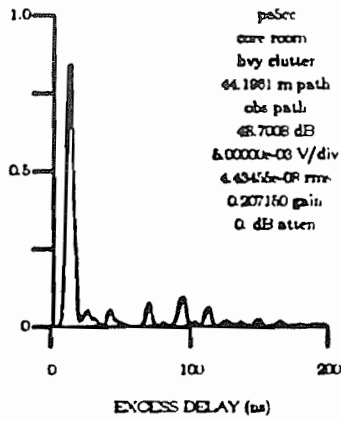
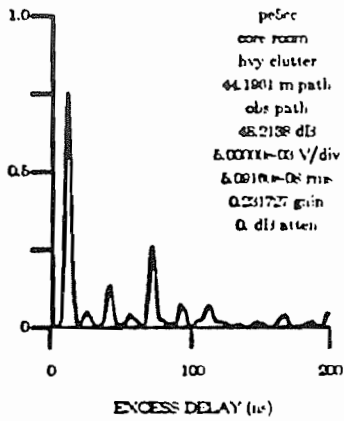
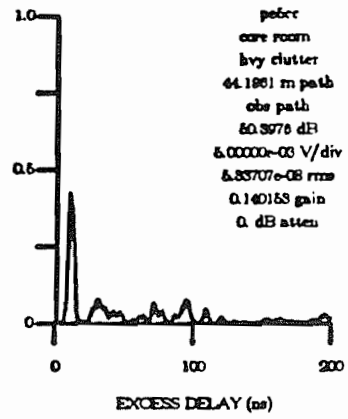
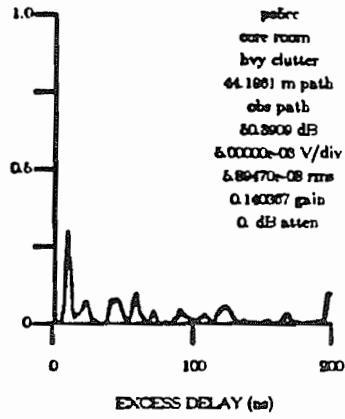
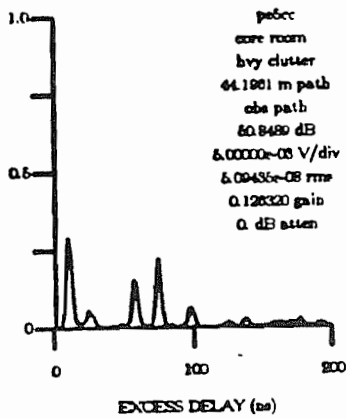


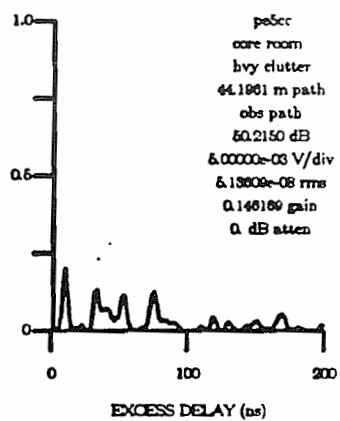
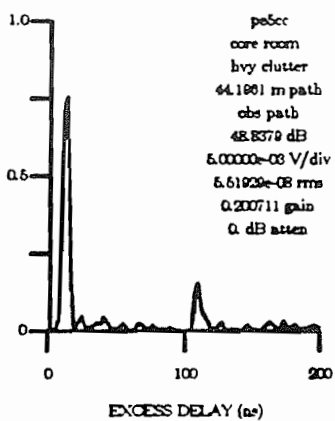
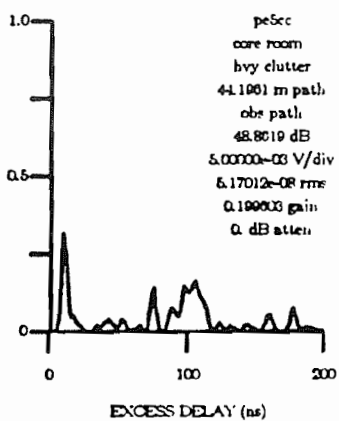
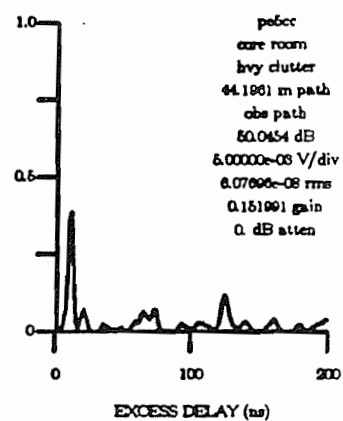
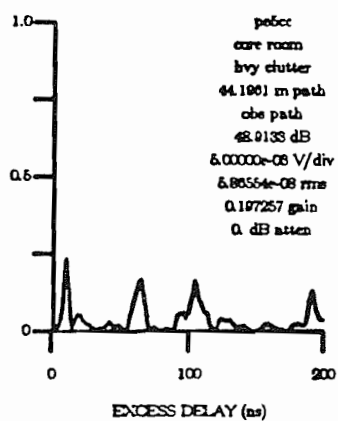
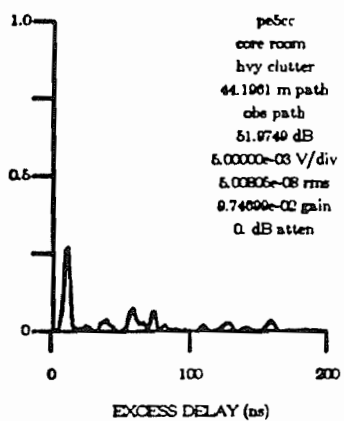


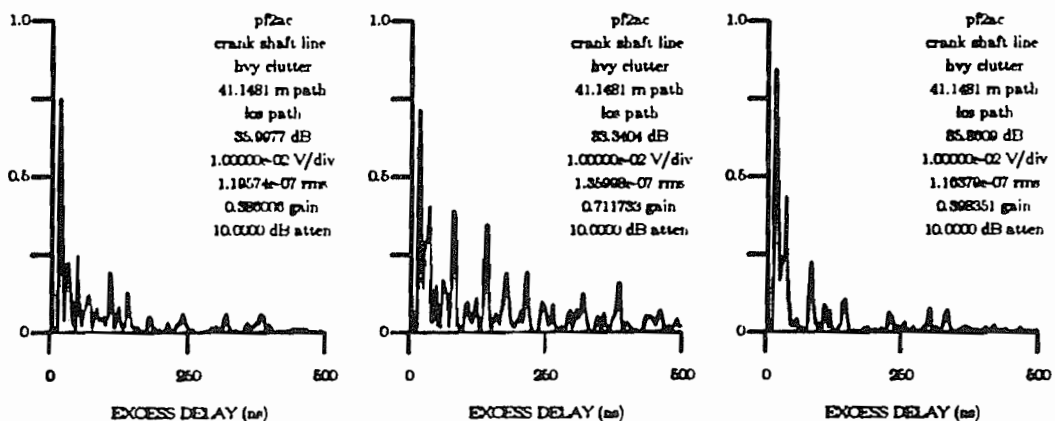
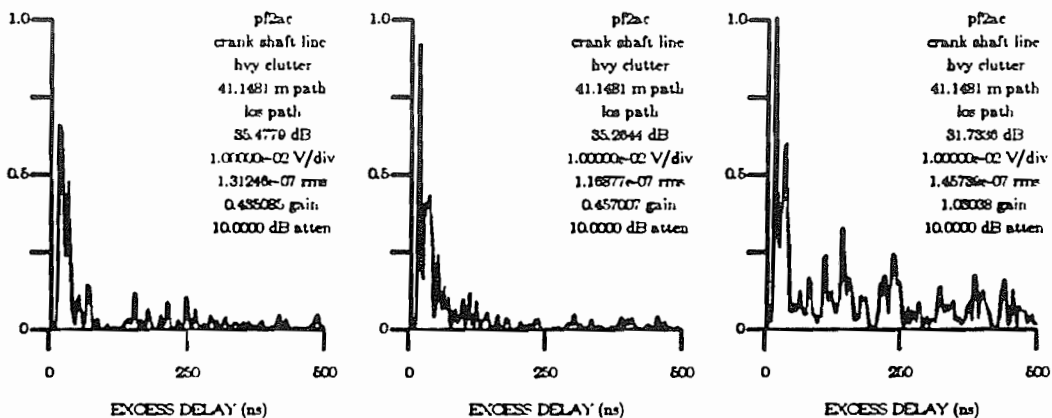
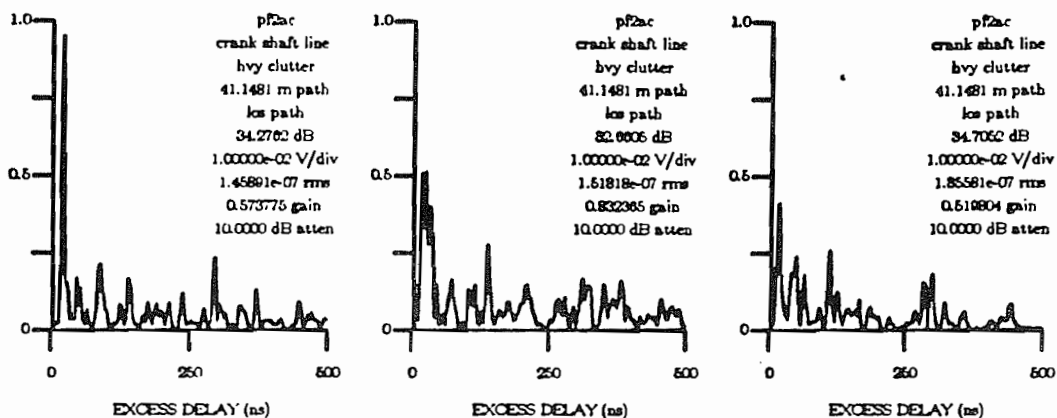




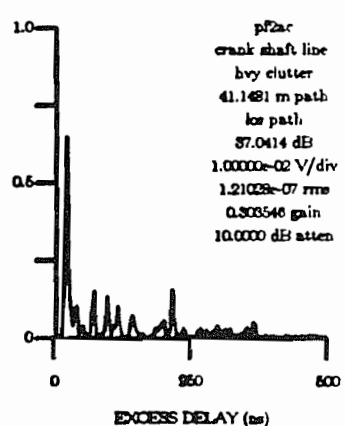
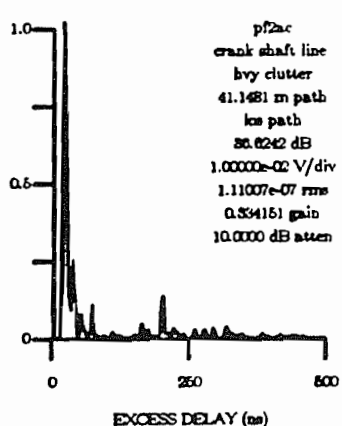
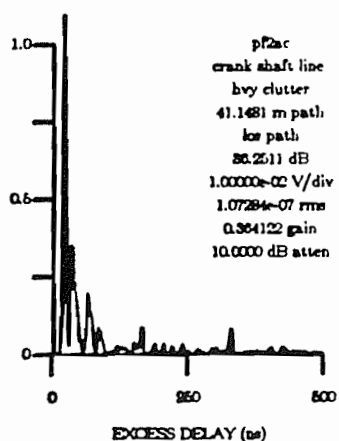
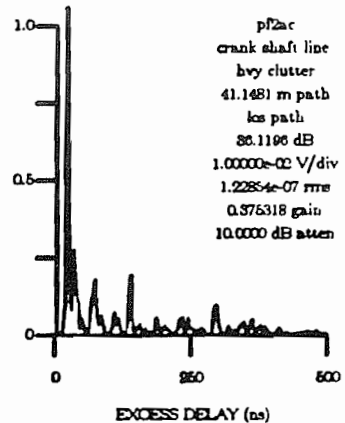
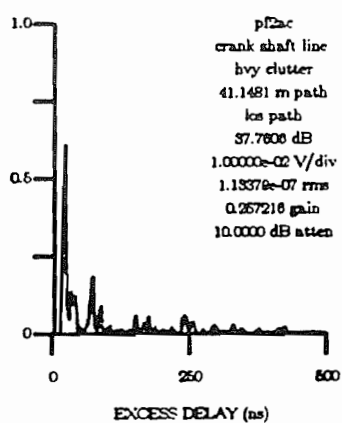
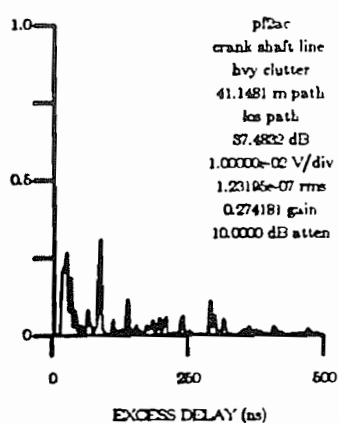
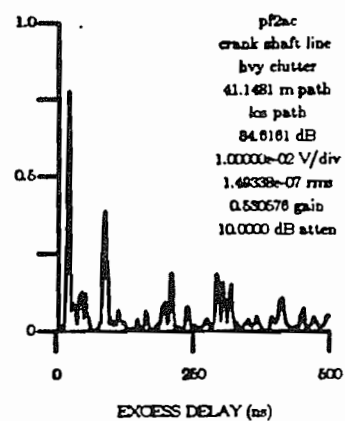
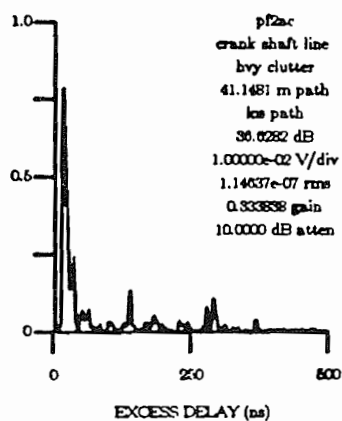
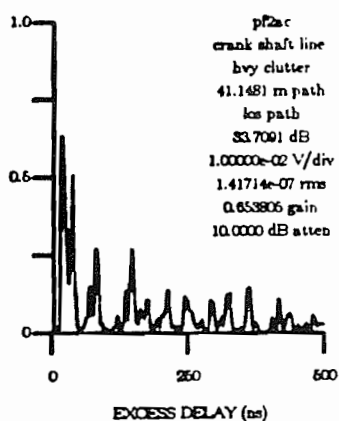


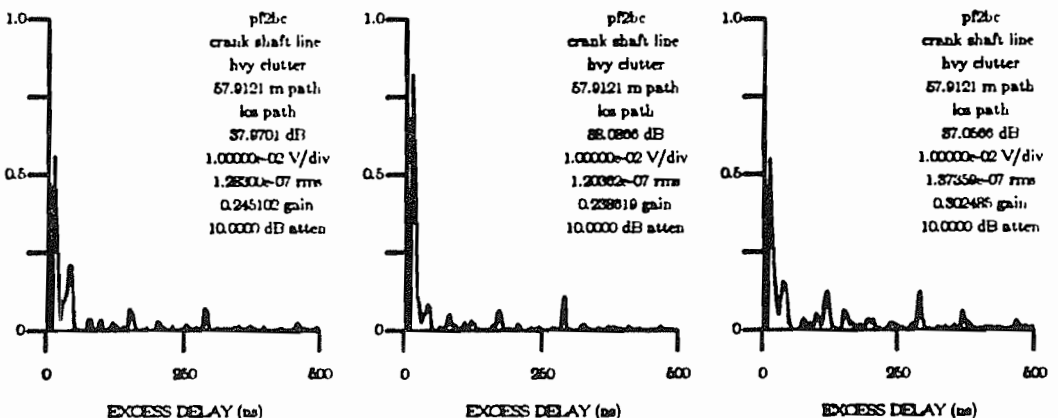
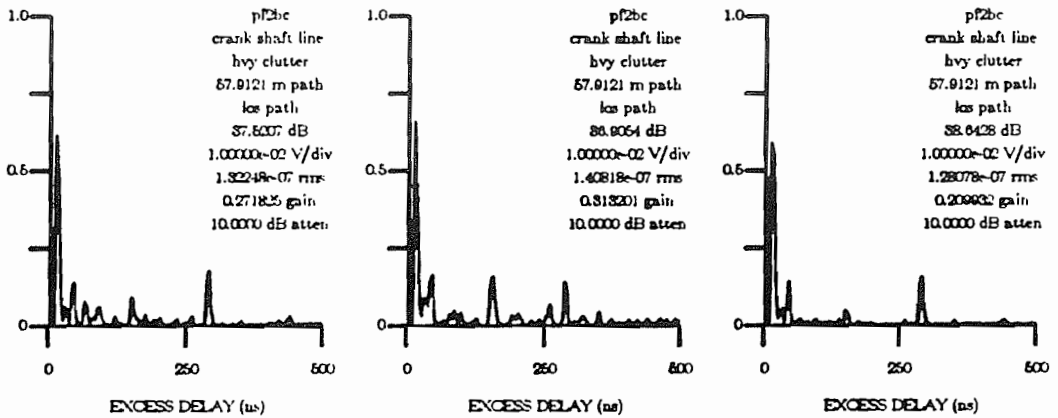
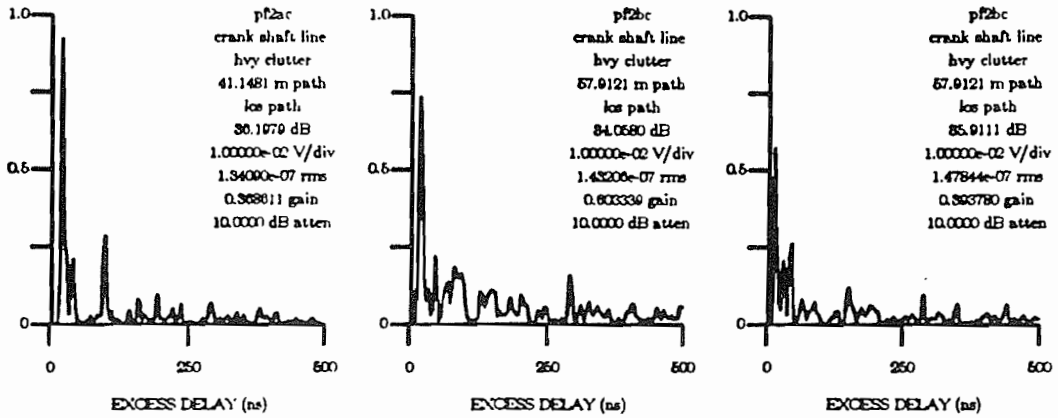


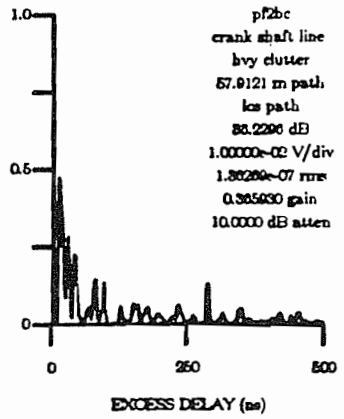
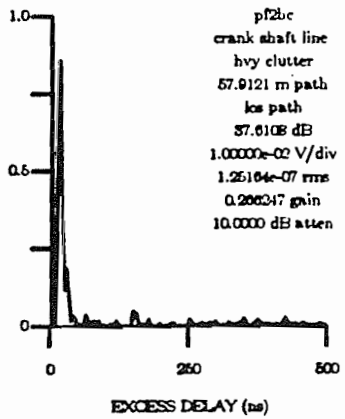
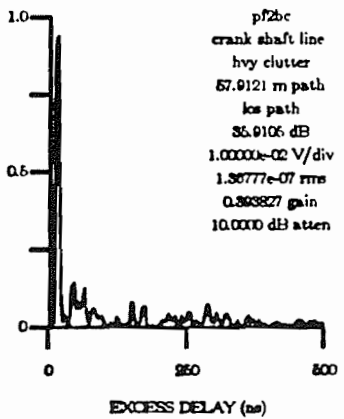
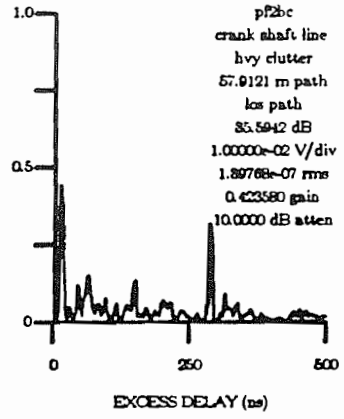
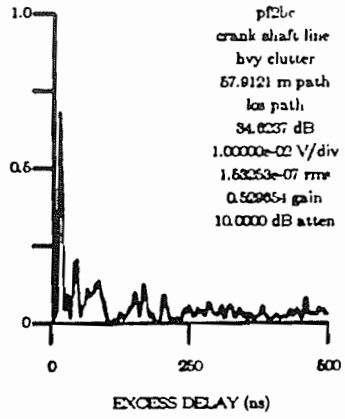
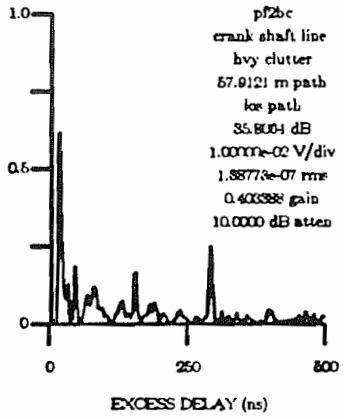
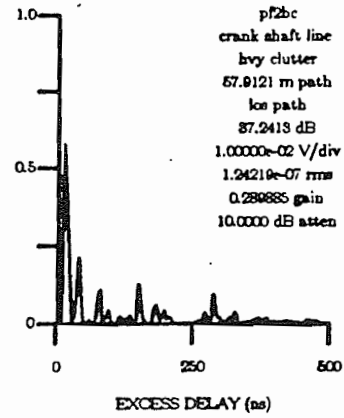
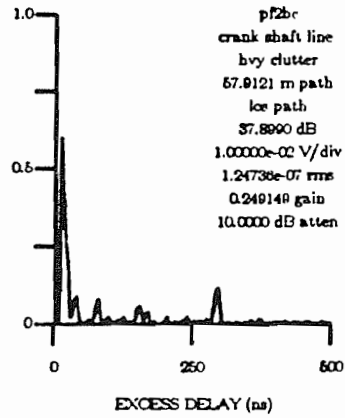
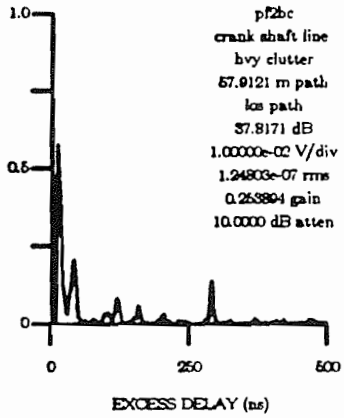


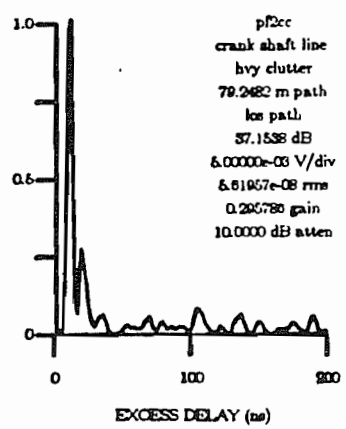
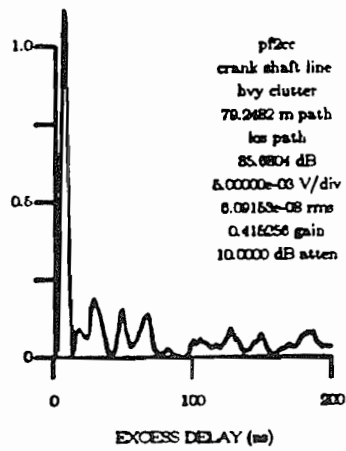
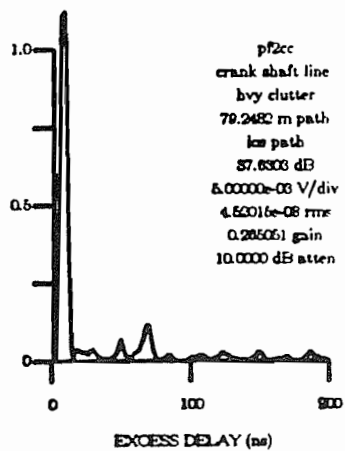
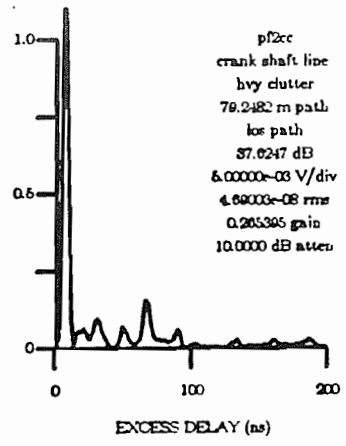
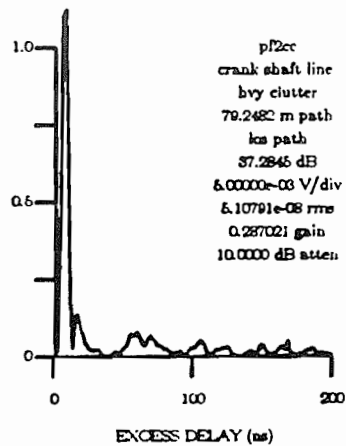
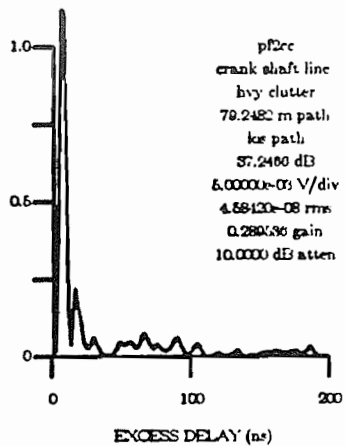
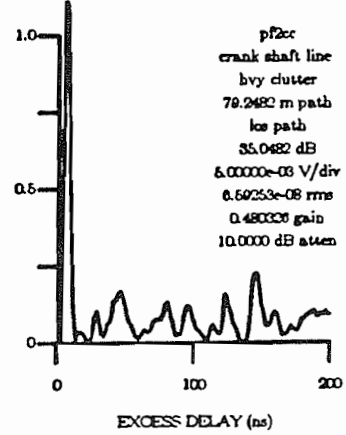
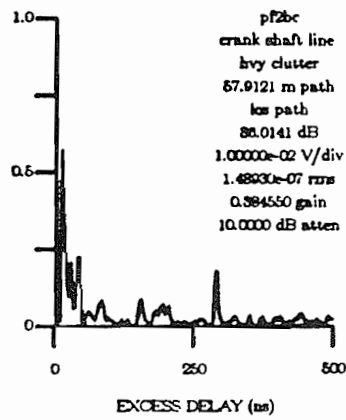
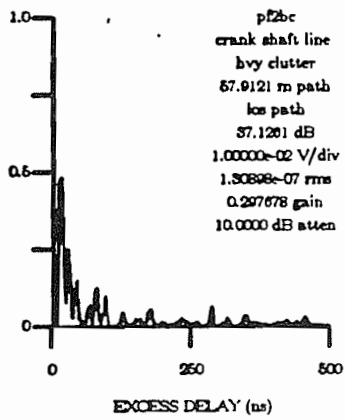


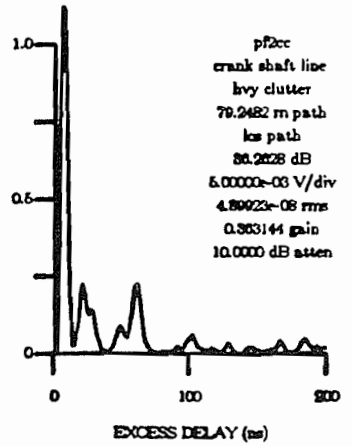
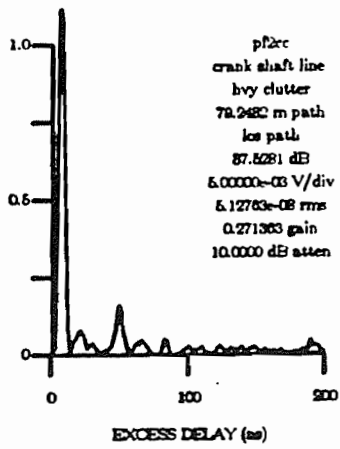
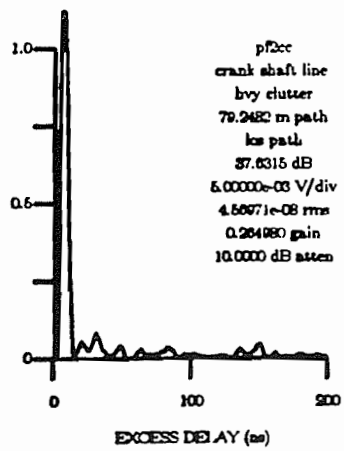
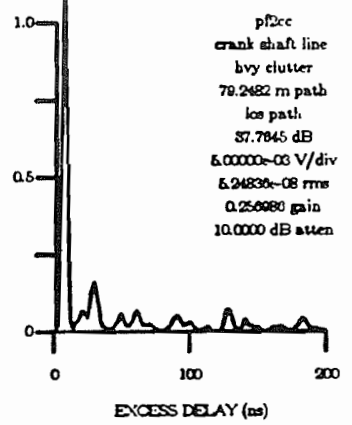
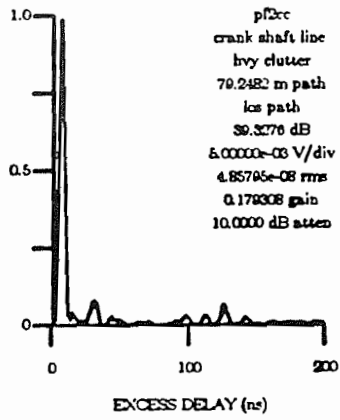
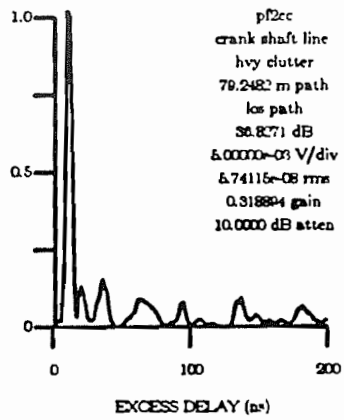
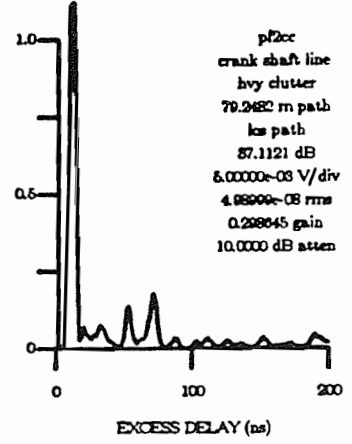
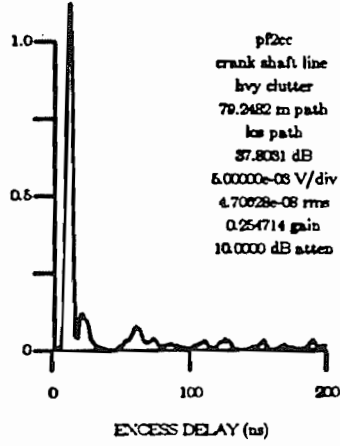
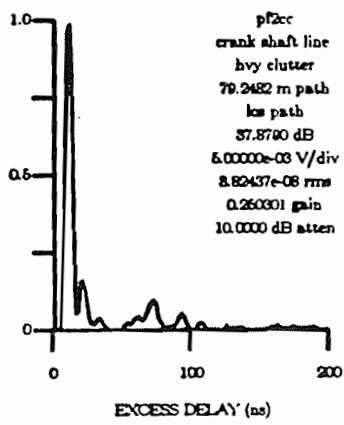


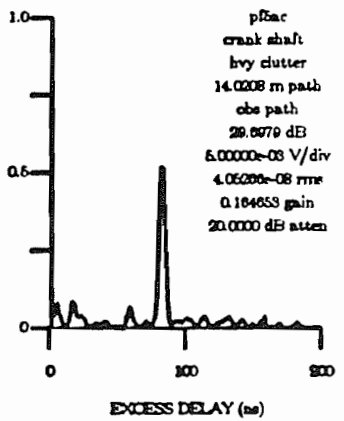
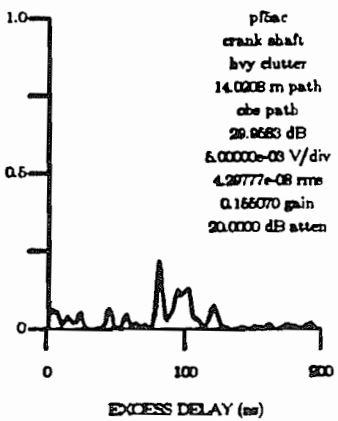
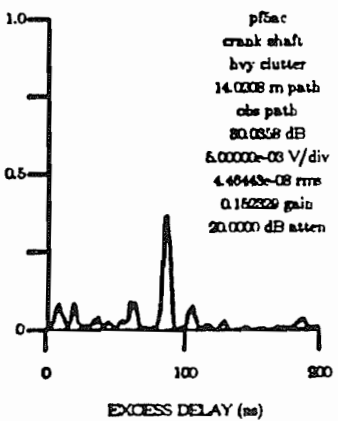
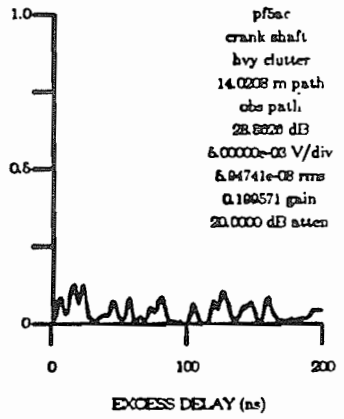
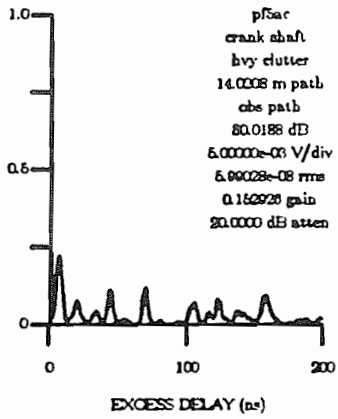
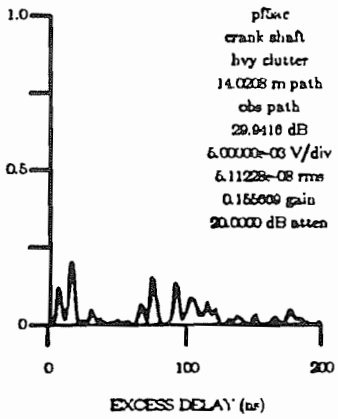
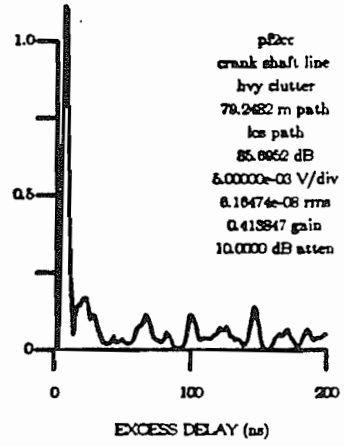
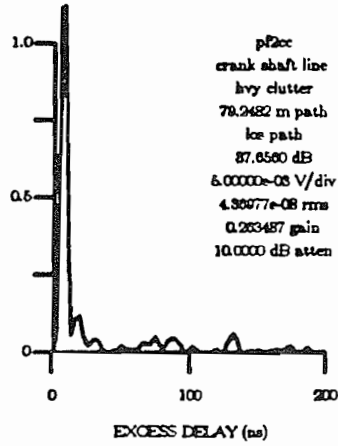
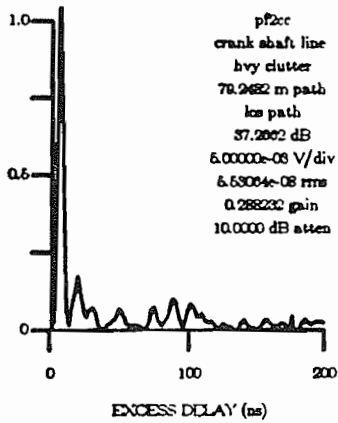


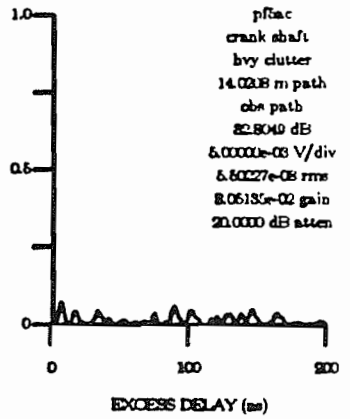
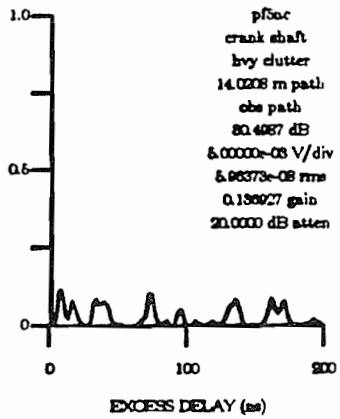
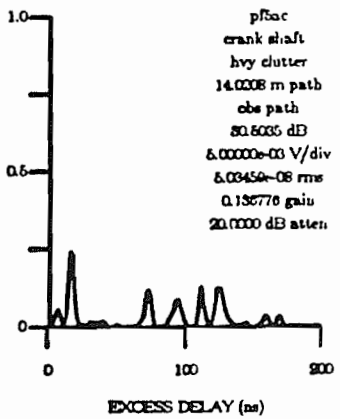
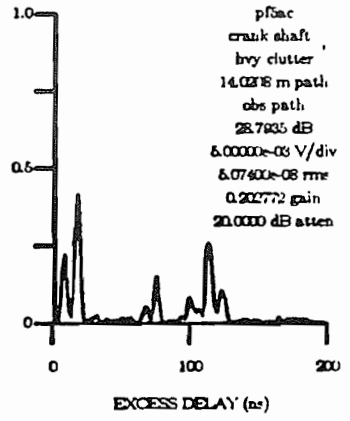
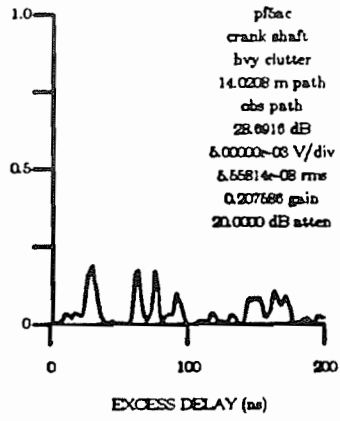
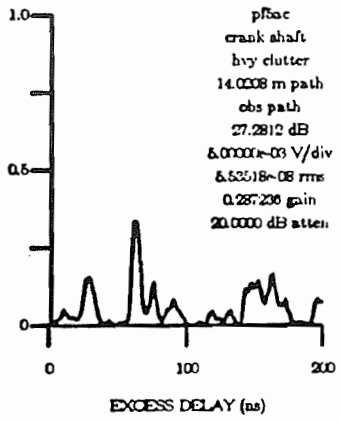
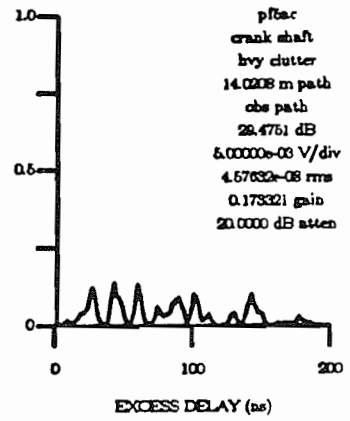
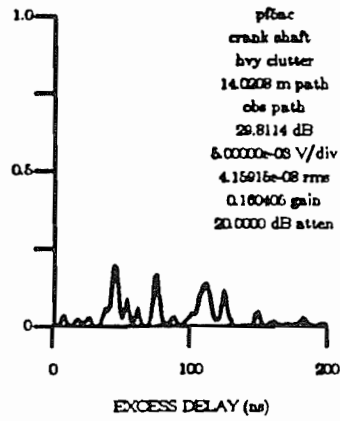
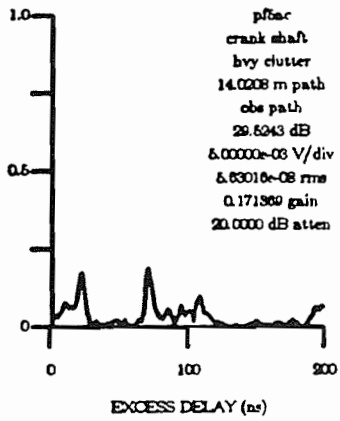


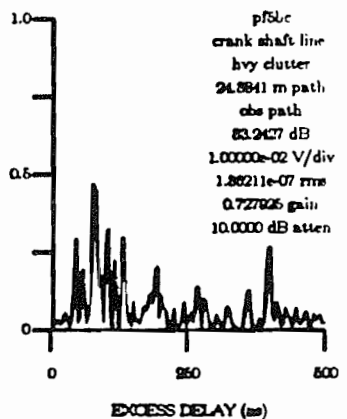
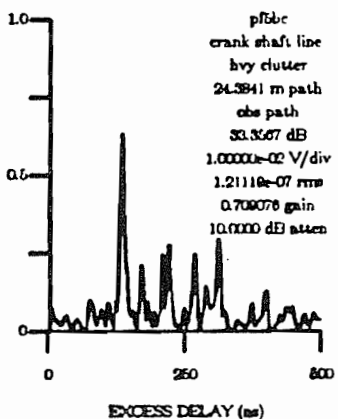
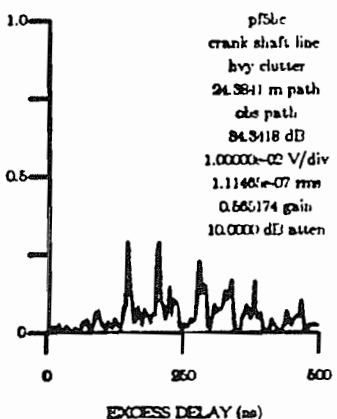
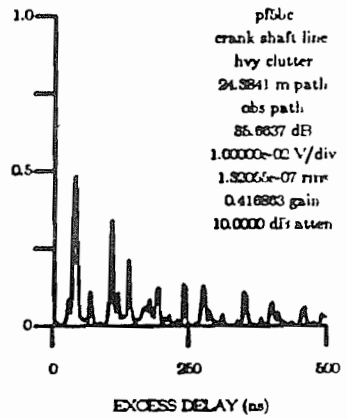
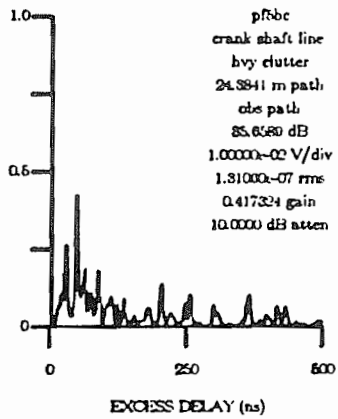
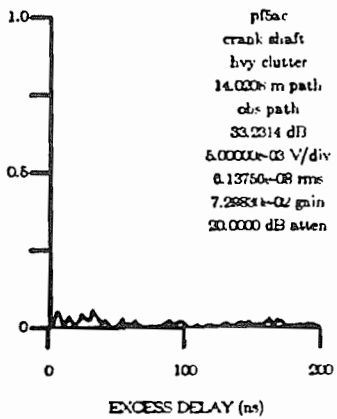
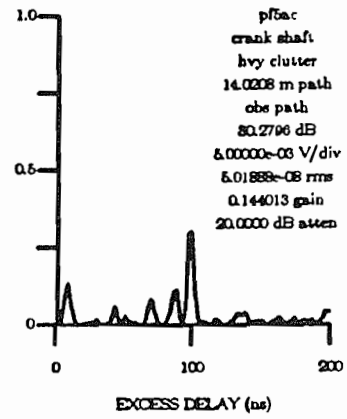
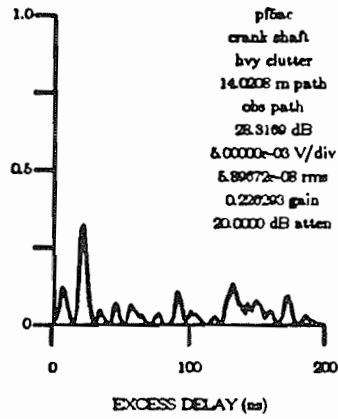
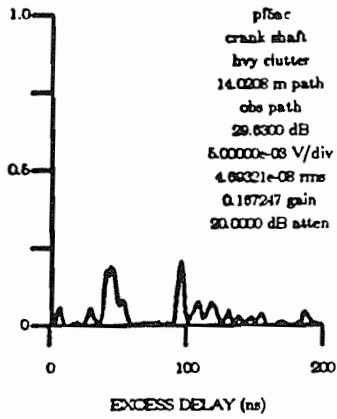




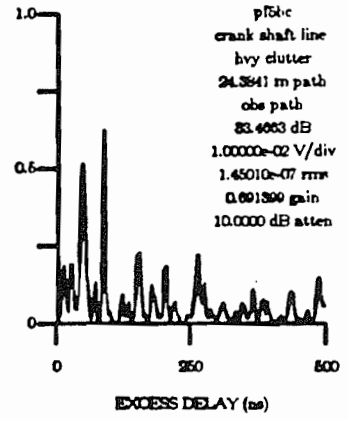
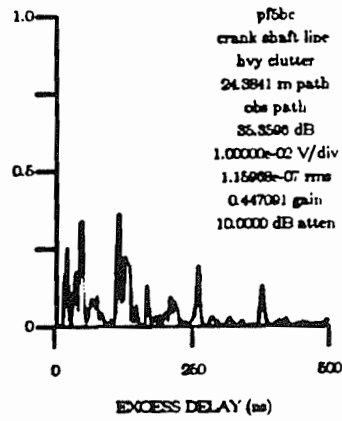
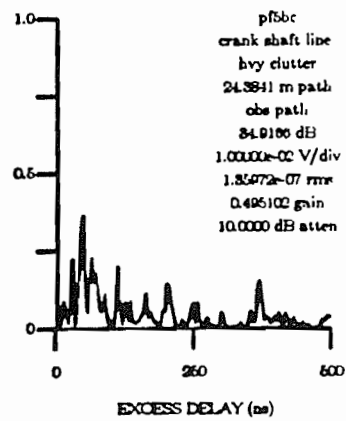
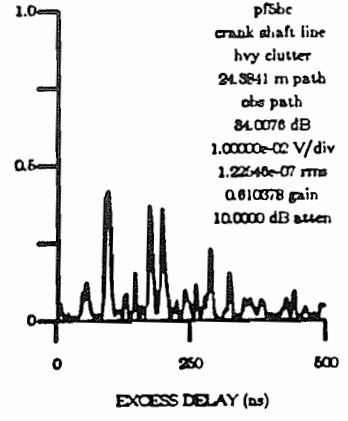
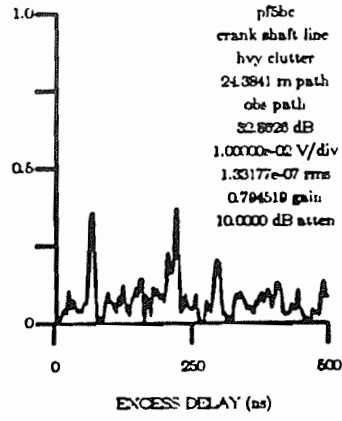
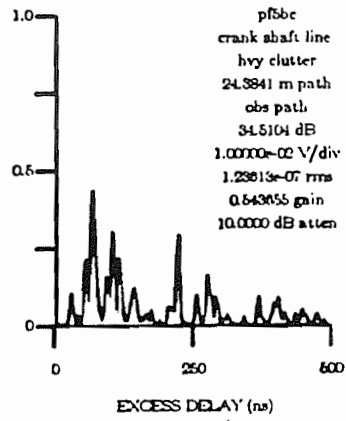
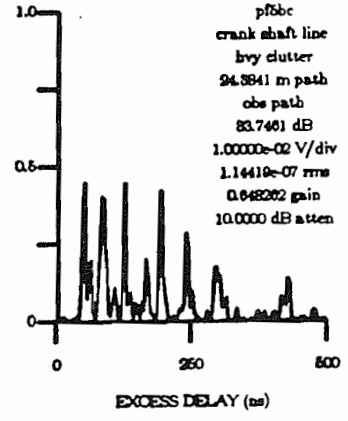
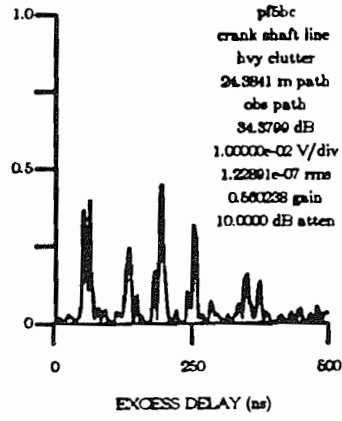
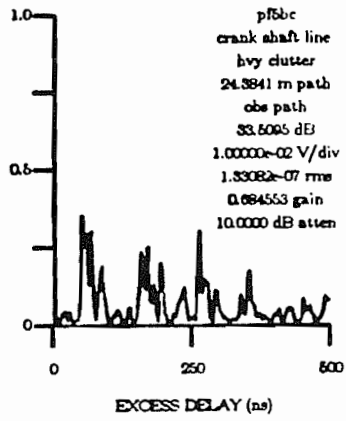


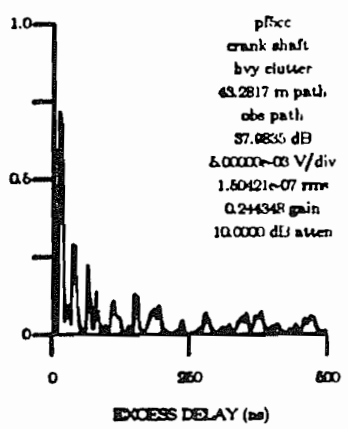
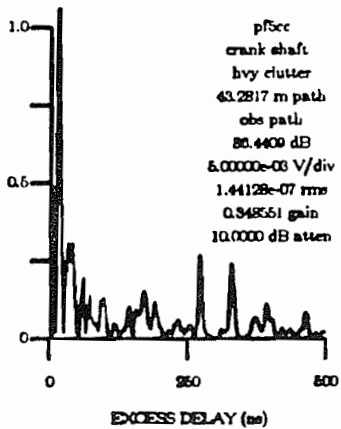
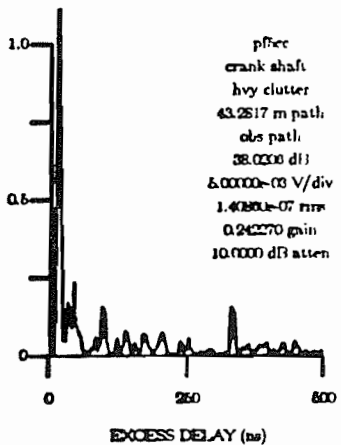
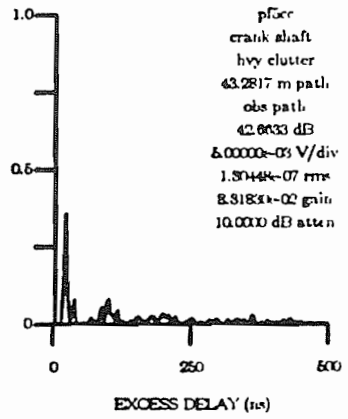
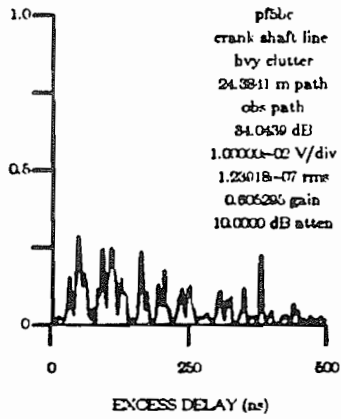
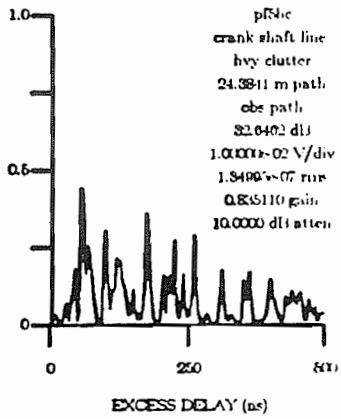
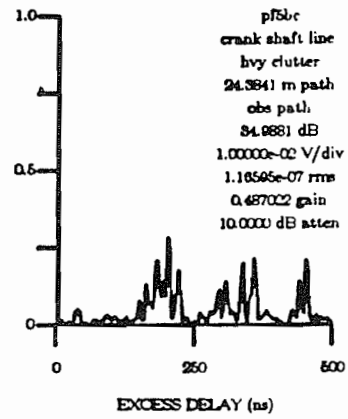
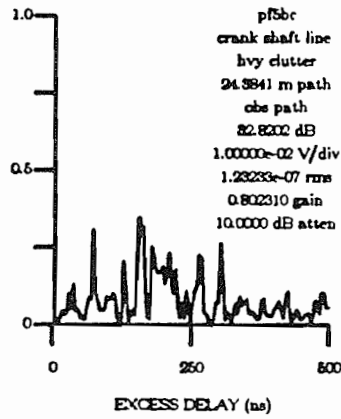
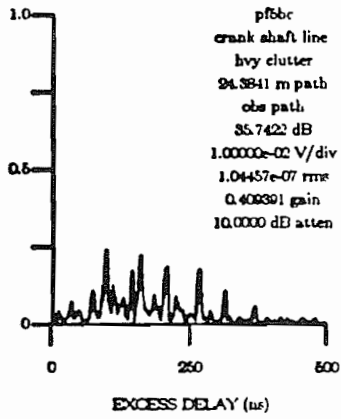


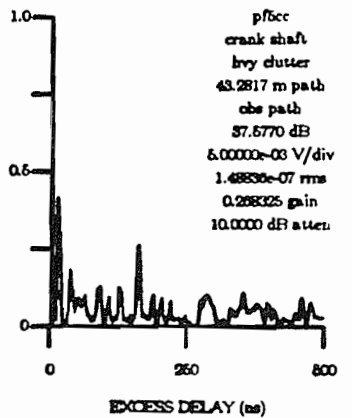
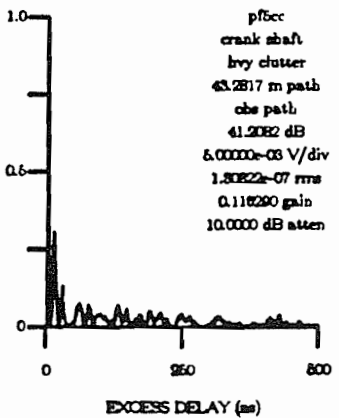
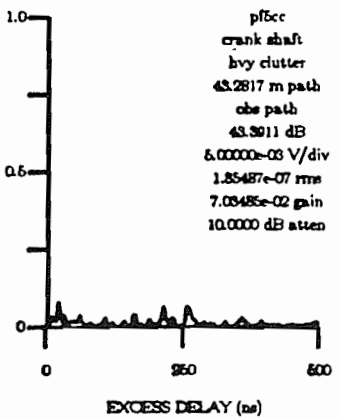
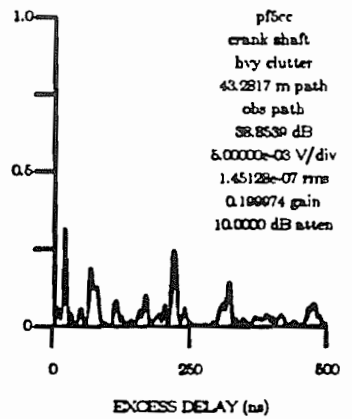
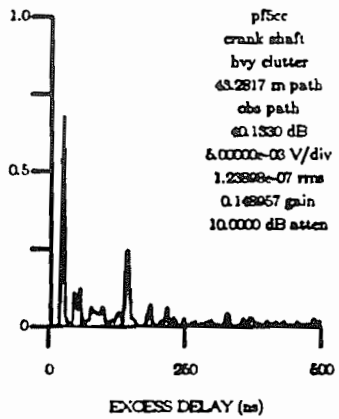
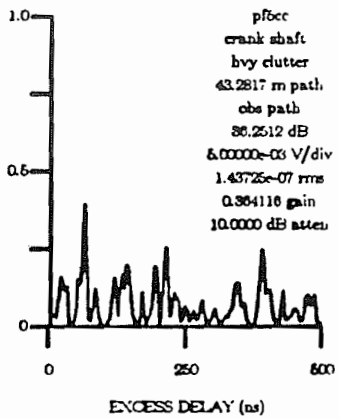
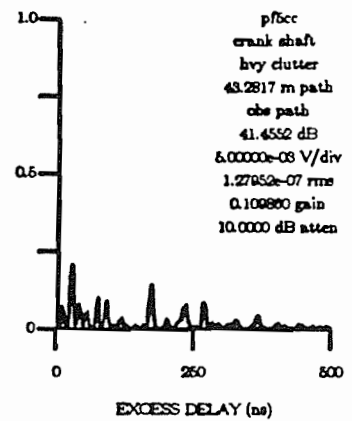
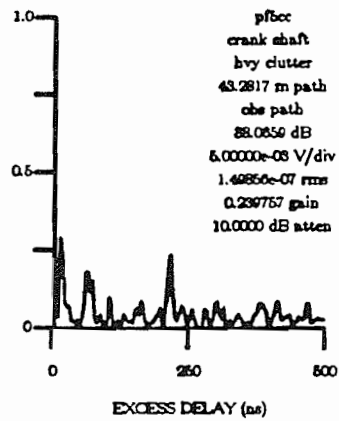
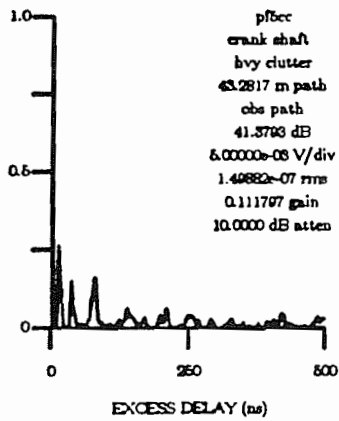


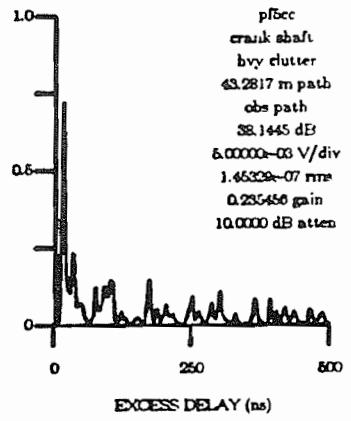
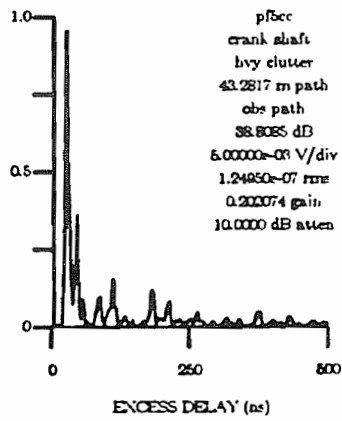
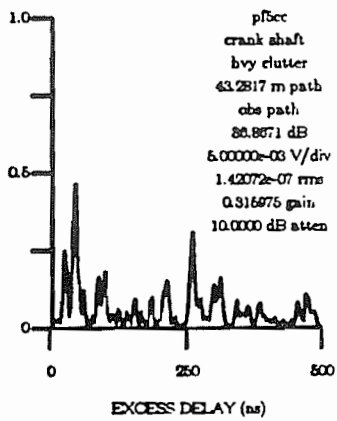
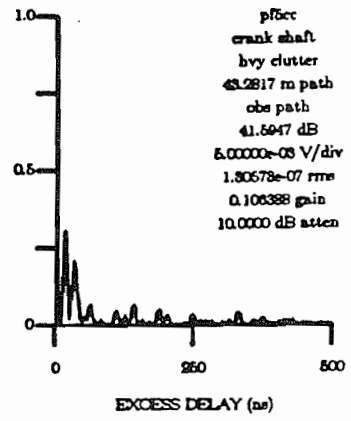
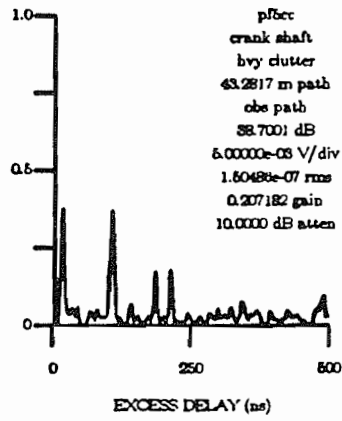
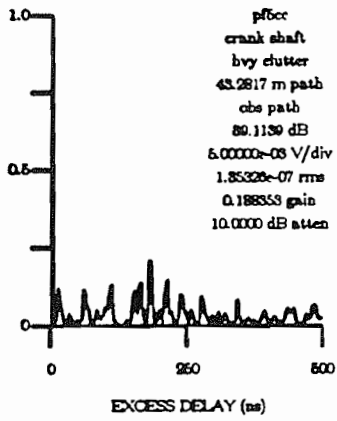






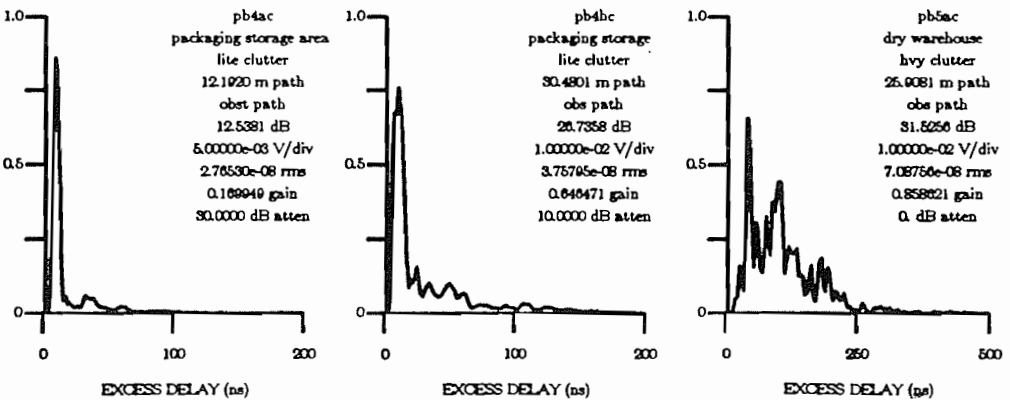
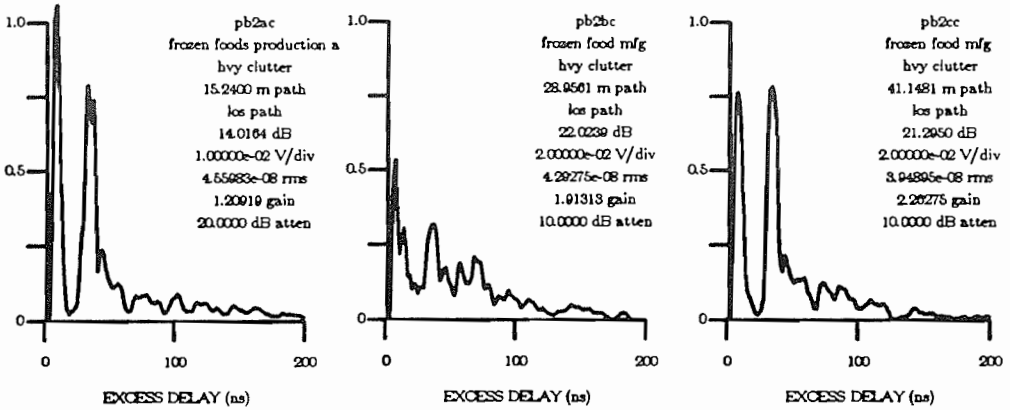
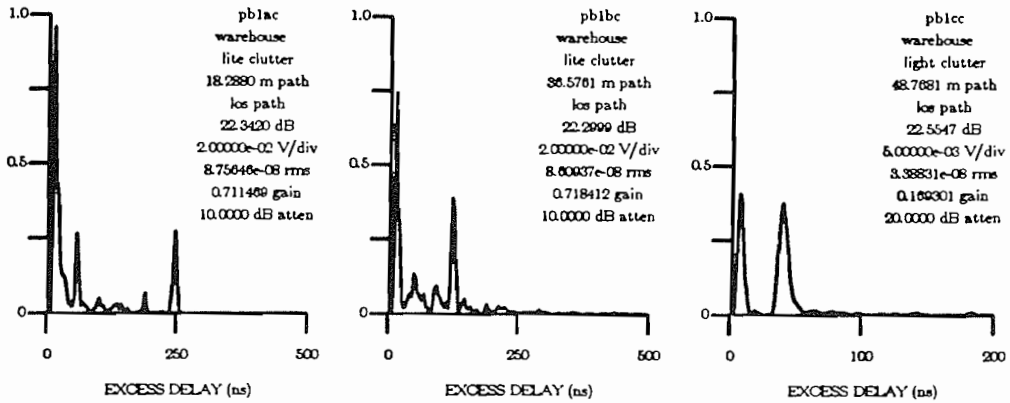


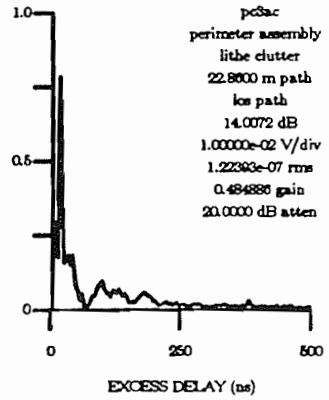
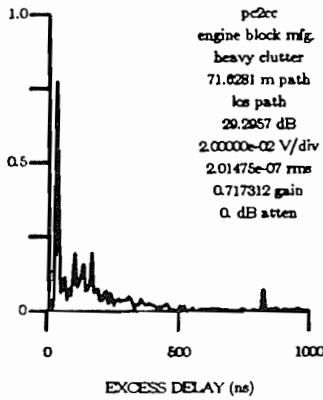
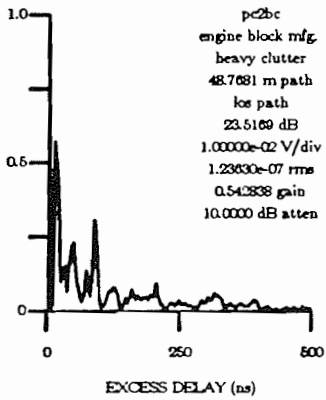
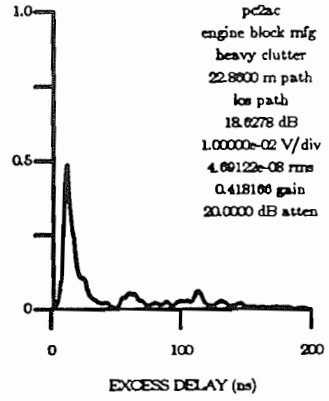
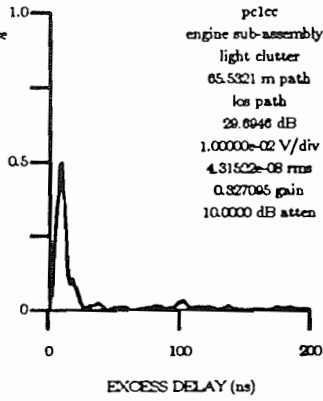
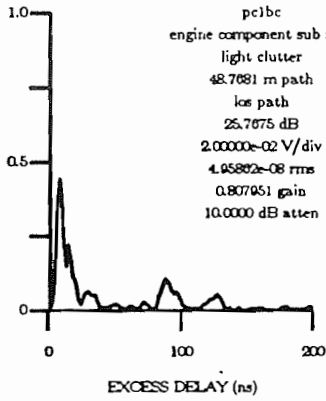
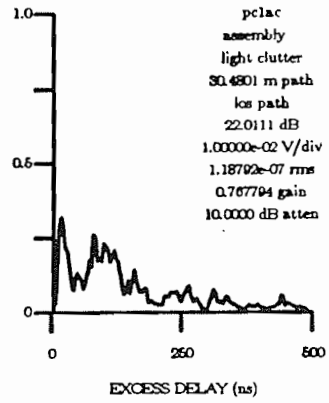
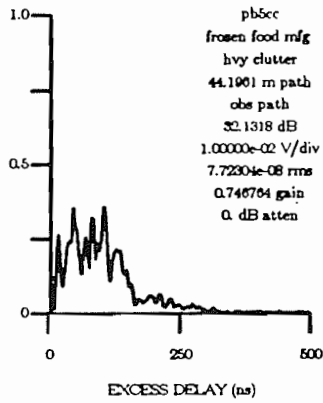
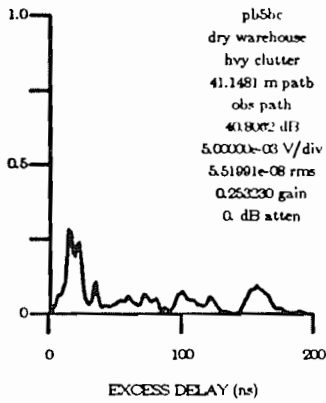


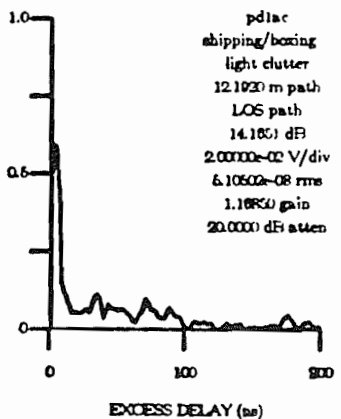
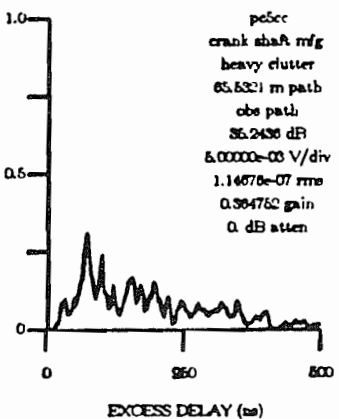
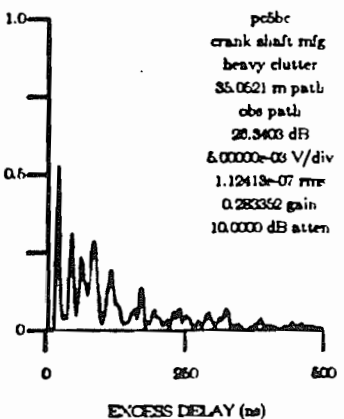
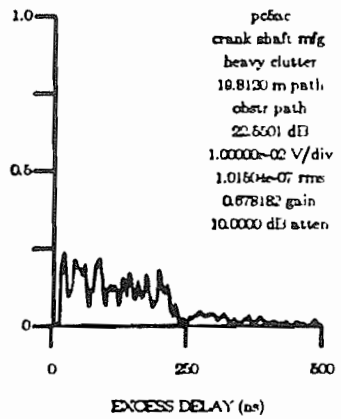
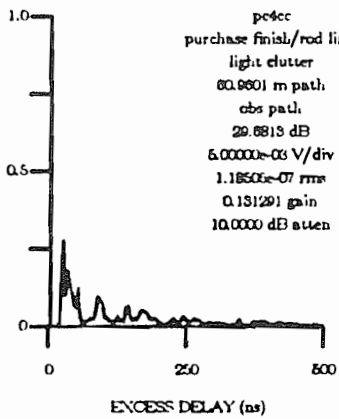
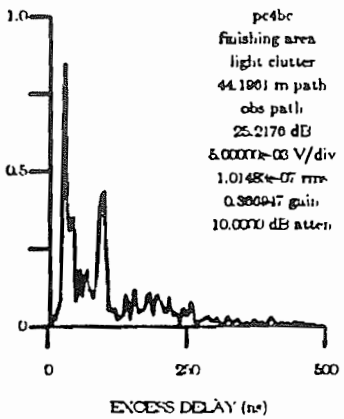
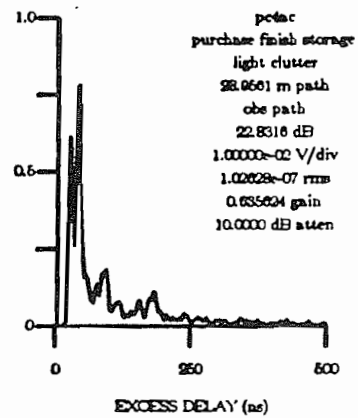
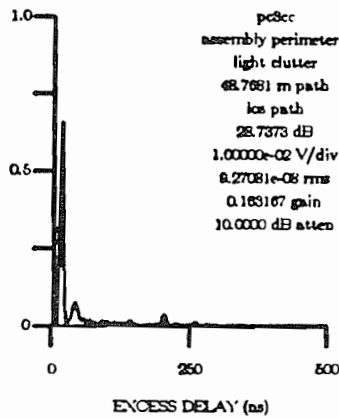
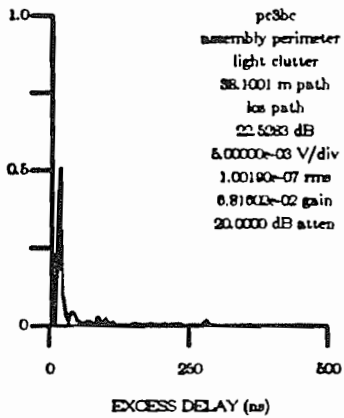


**Appendix E**  
**Spatially Averaged Multipath Power Delay Profiles**

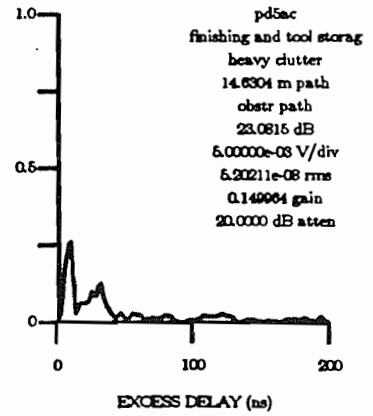
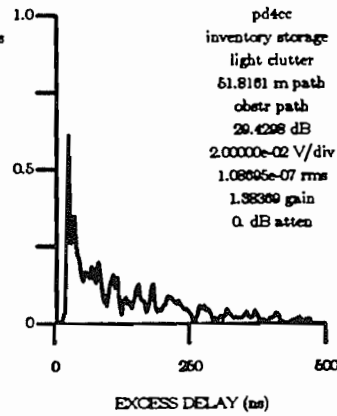
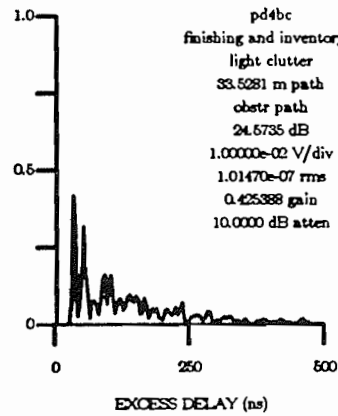
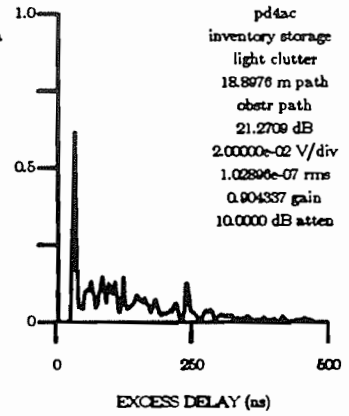
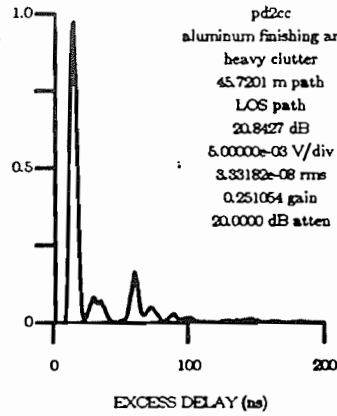
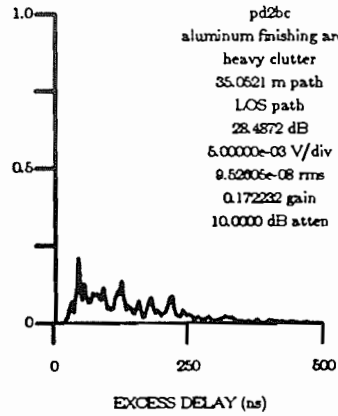
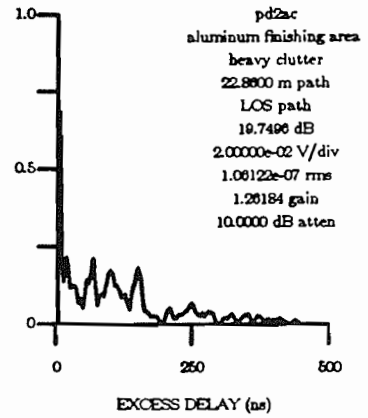
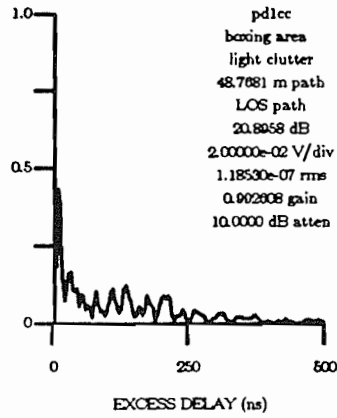
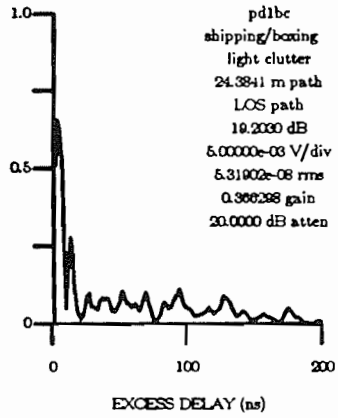
The following are spatially averaged multipath power delay profiles made from the local average of 19 profiles collected at each of 50 measurement locations in 5 factories. The filename is located in the upper right hand corner of each plot and indicates the measurement location (see Figure 3.4). The following data is given from top to bottom on each profile plot: filename, factory area, clutter conditions, T-R separation, LOS or obstructed path, relative path loss, vertical scale setting of oscilloscope, r.m.s. delay spread, relative path gain, transmitter attenuator setting.

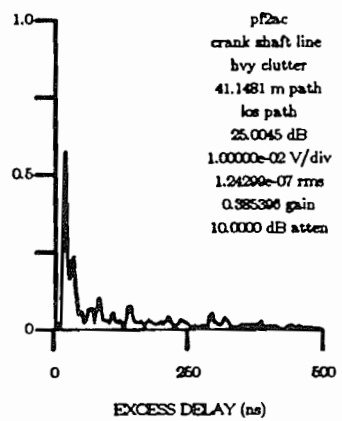
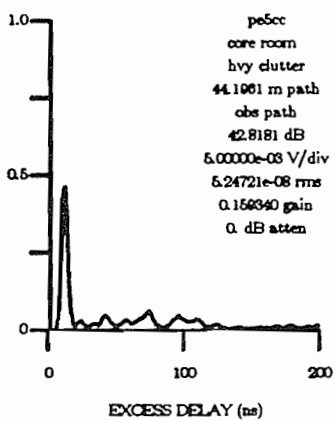
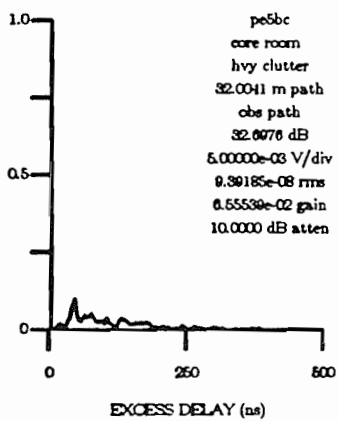
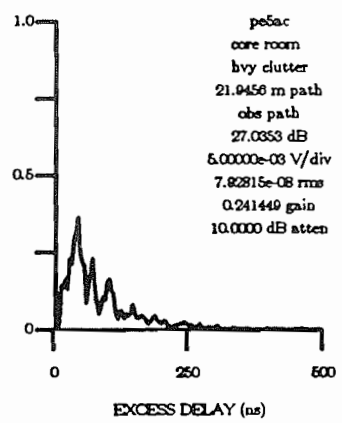
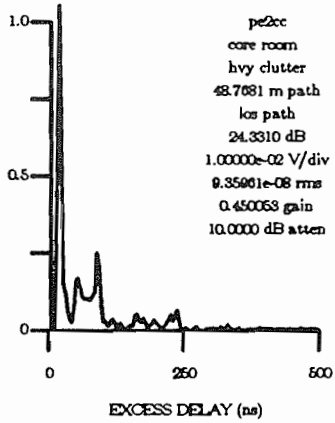
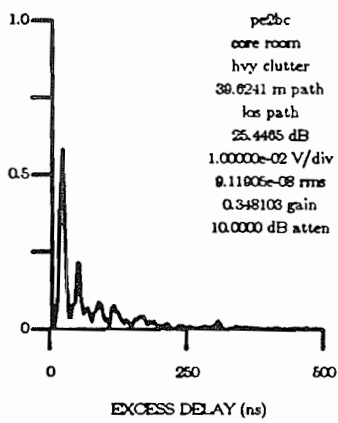
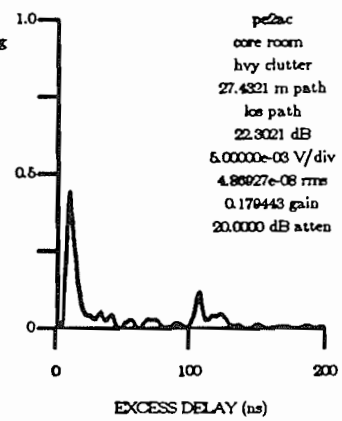
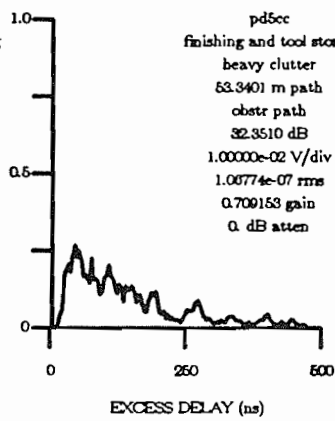
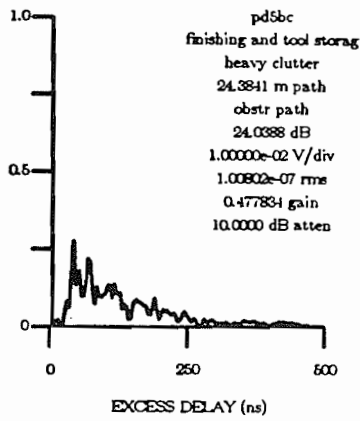


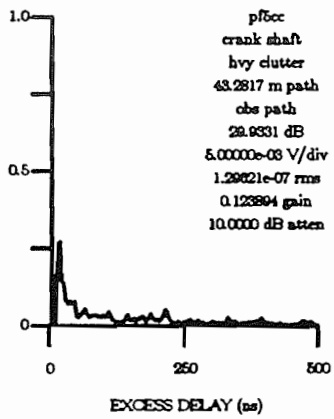
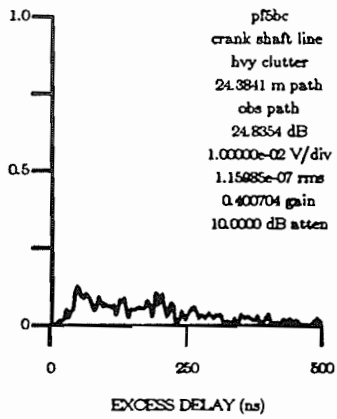
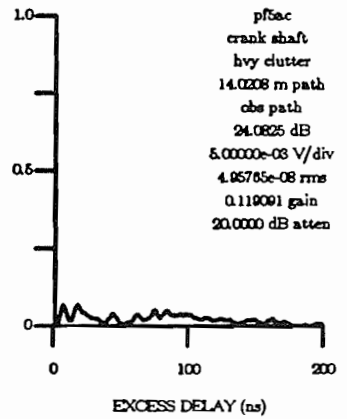
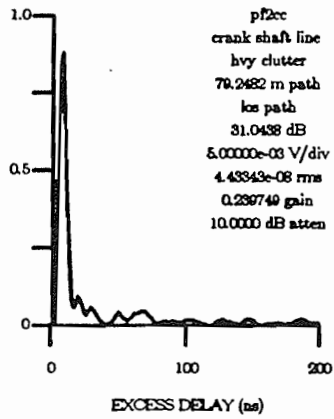
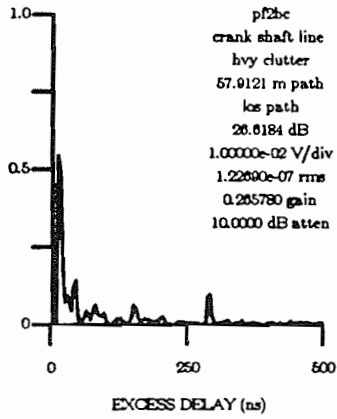






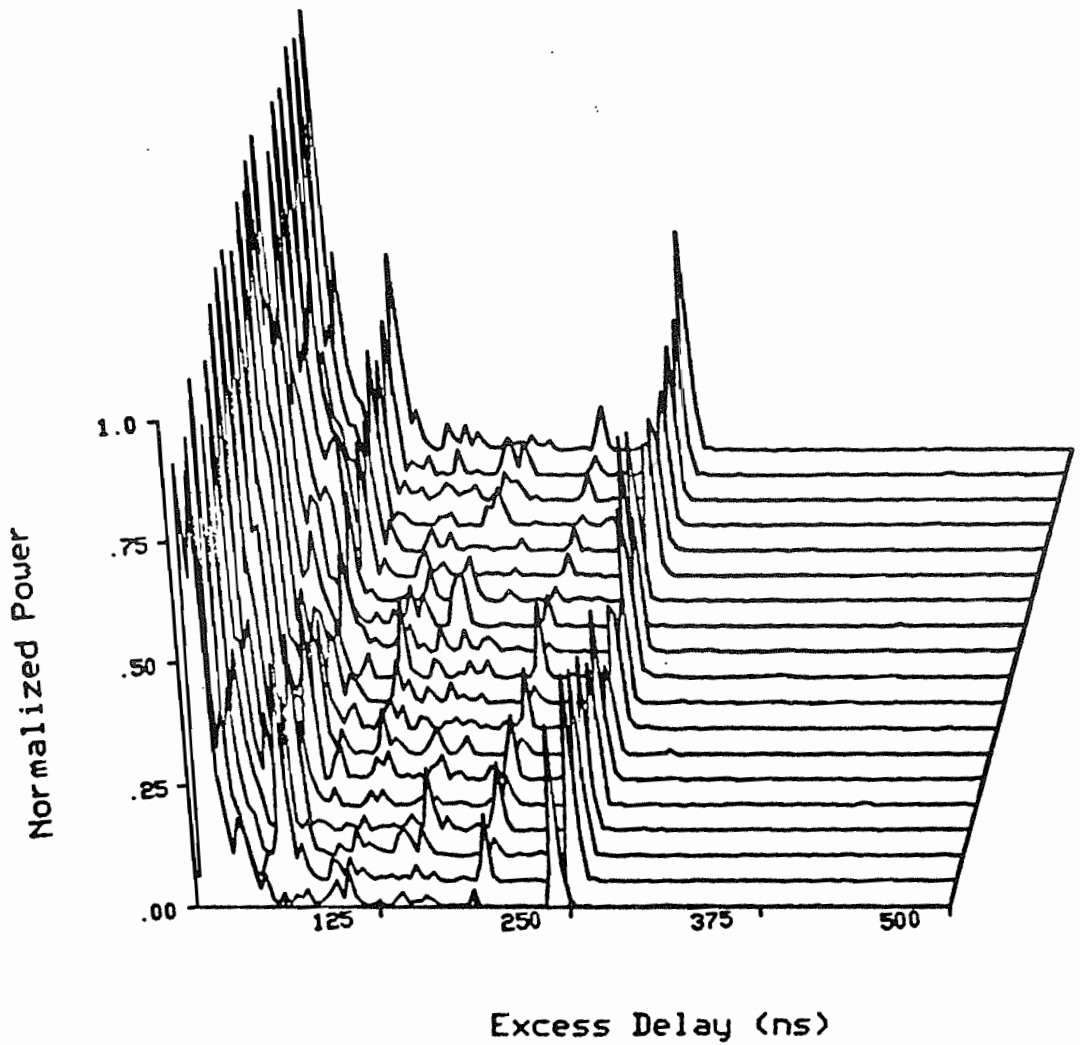




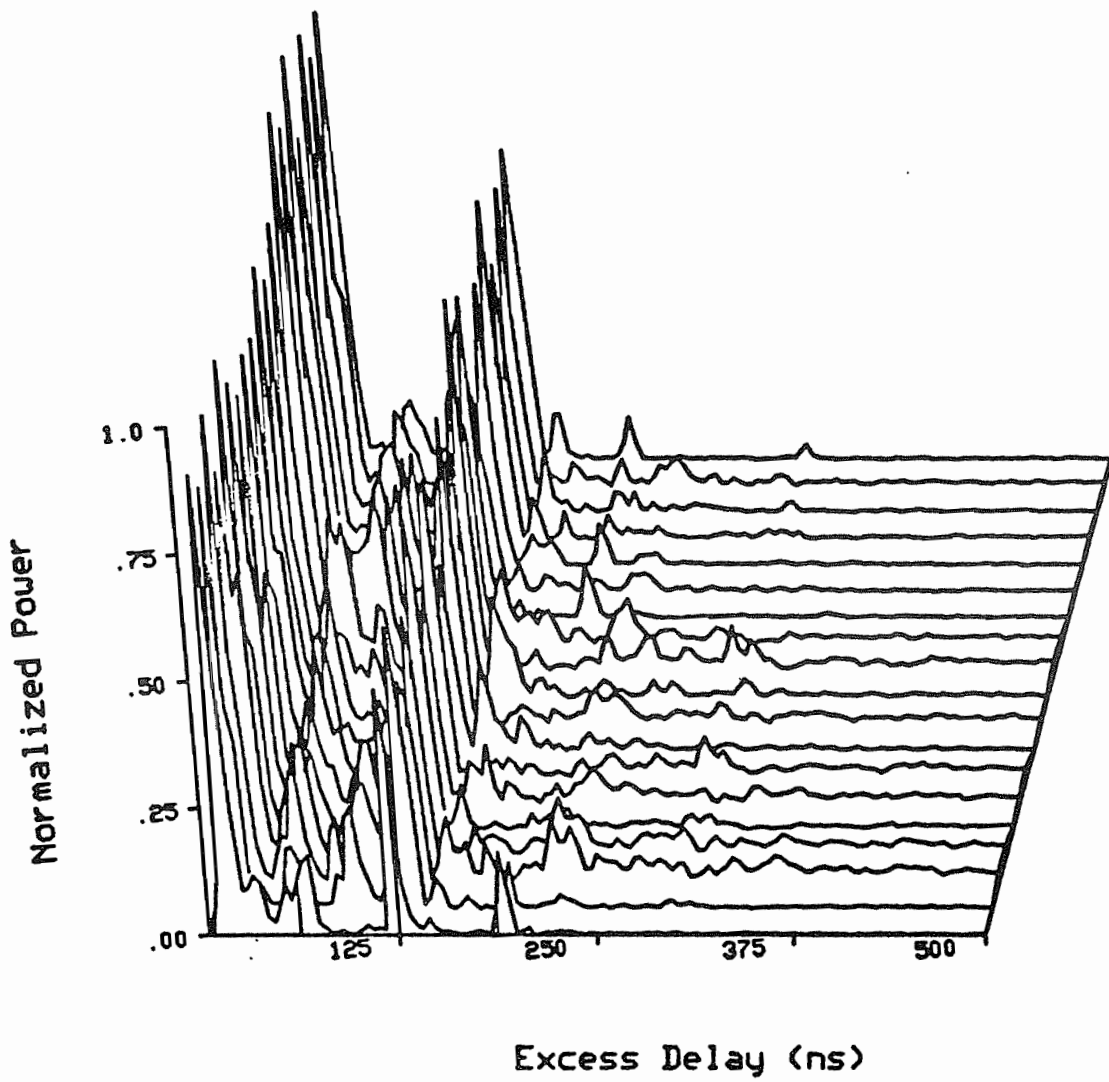


**Appendix F**  
**Spatial Fluctuations of Multipath over a Local Area**

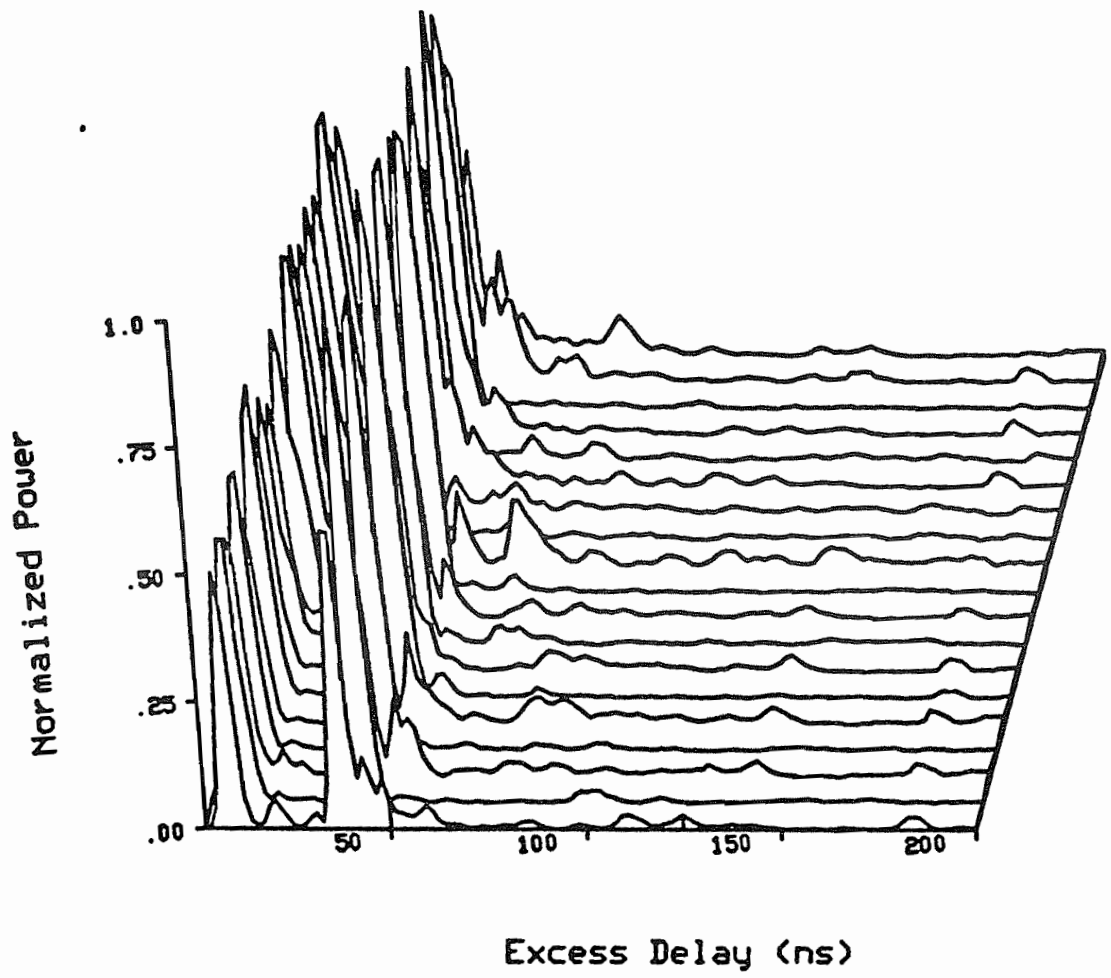
The following are plots made from the multipath power profiles collected from 50 measurement locations in 5 factory sites. The filename is given at the bottom of each plot and indicates the measurement location (see Figure 3.4).



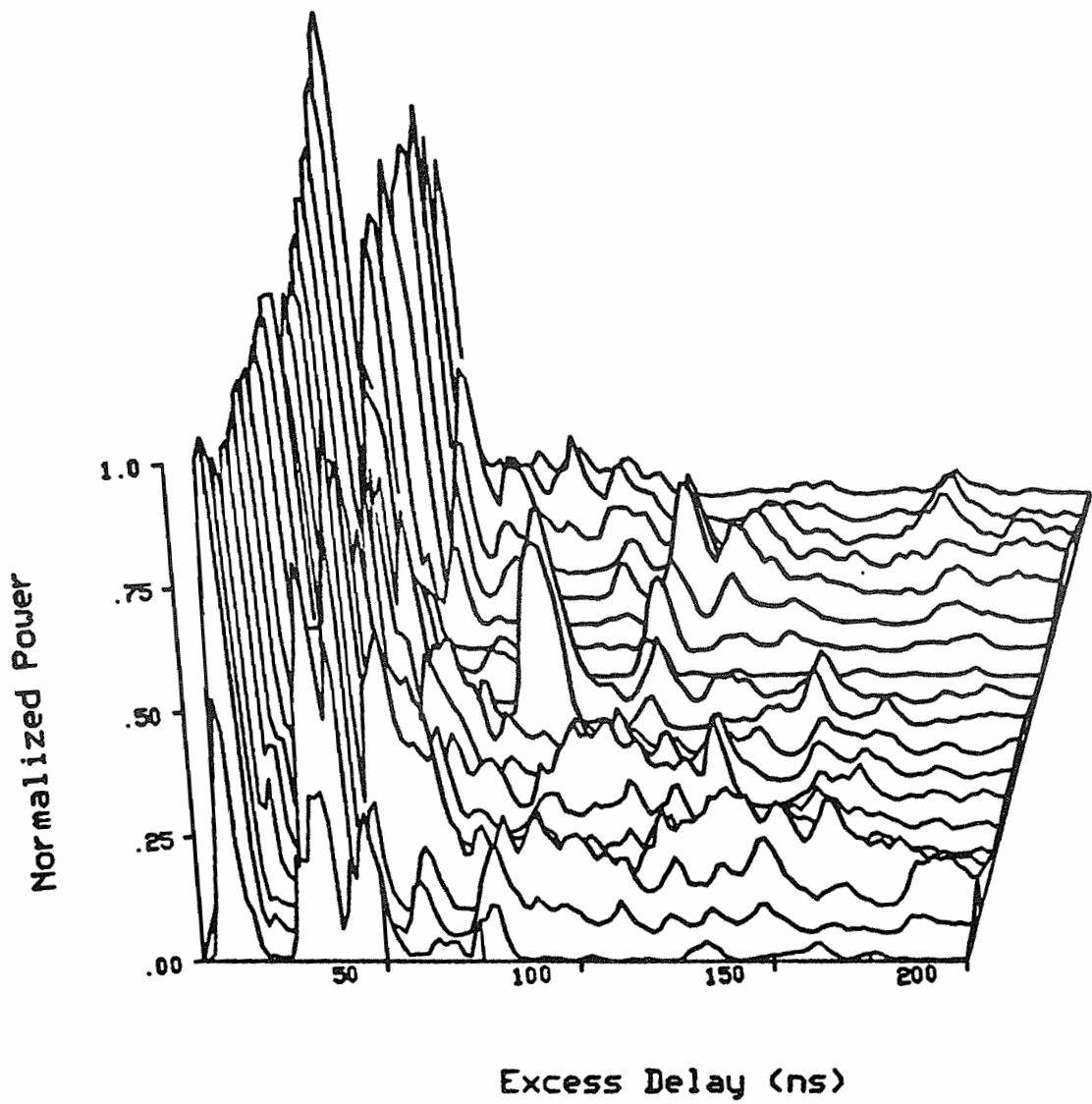
pblac



pb1bc

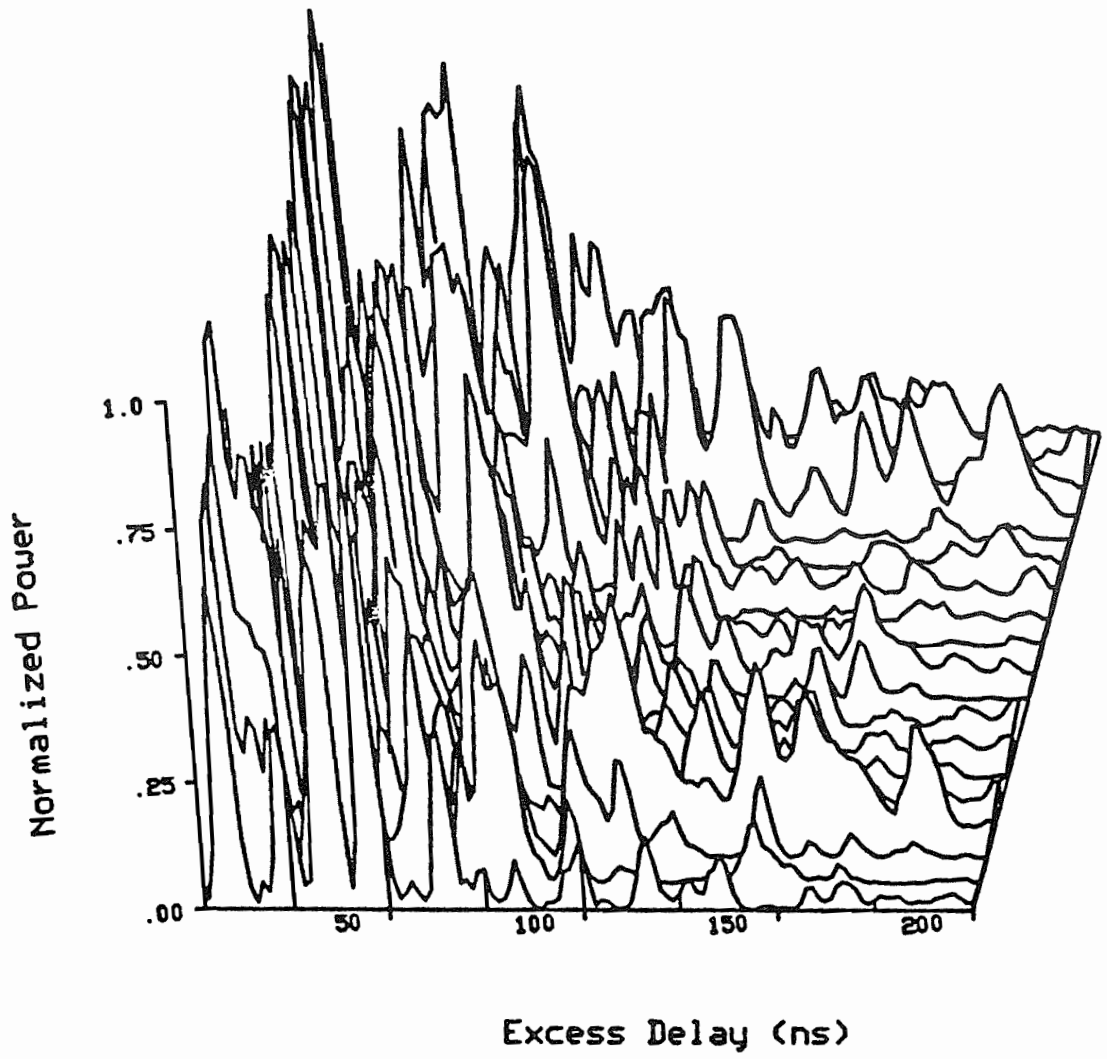


pb1cc

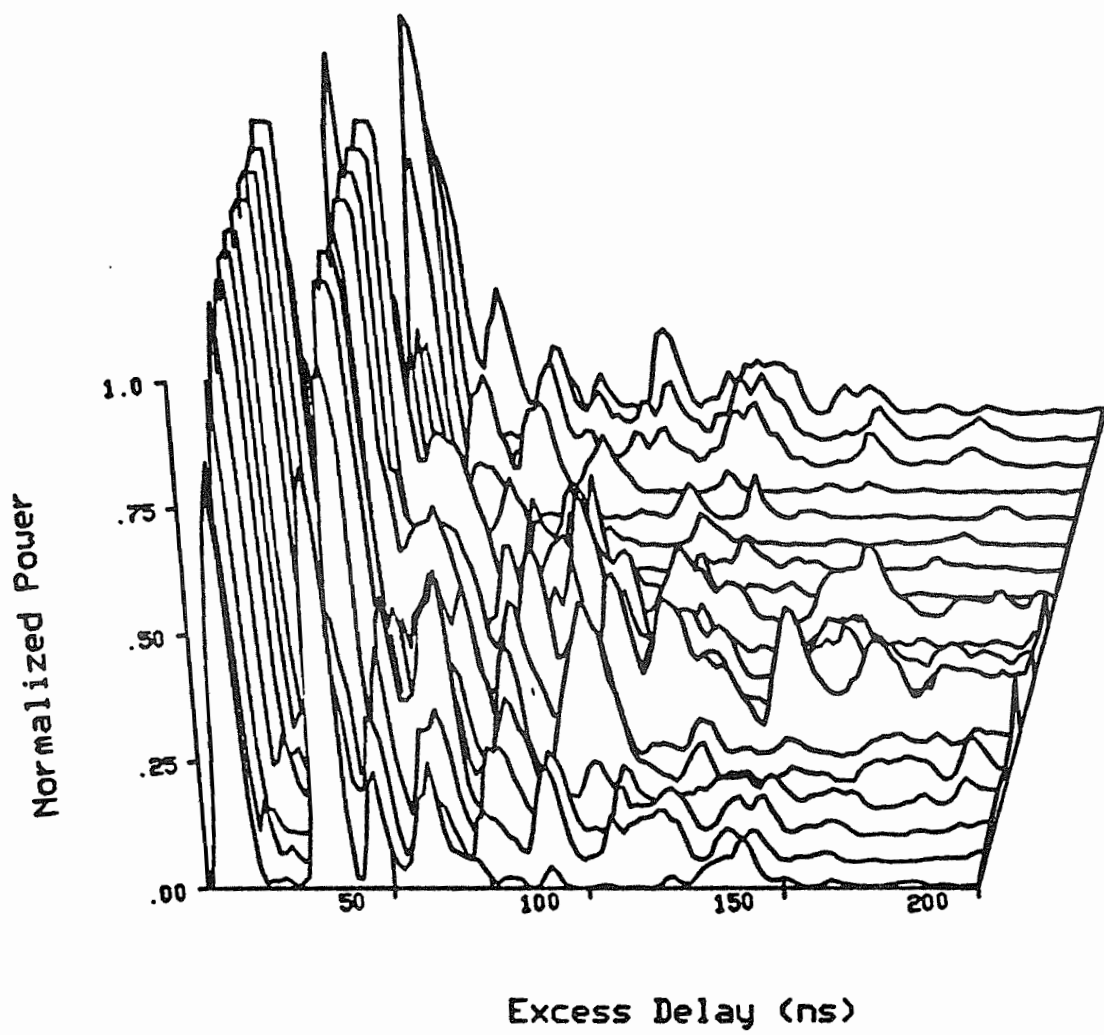


pb2ac

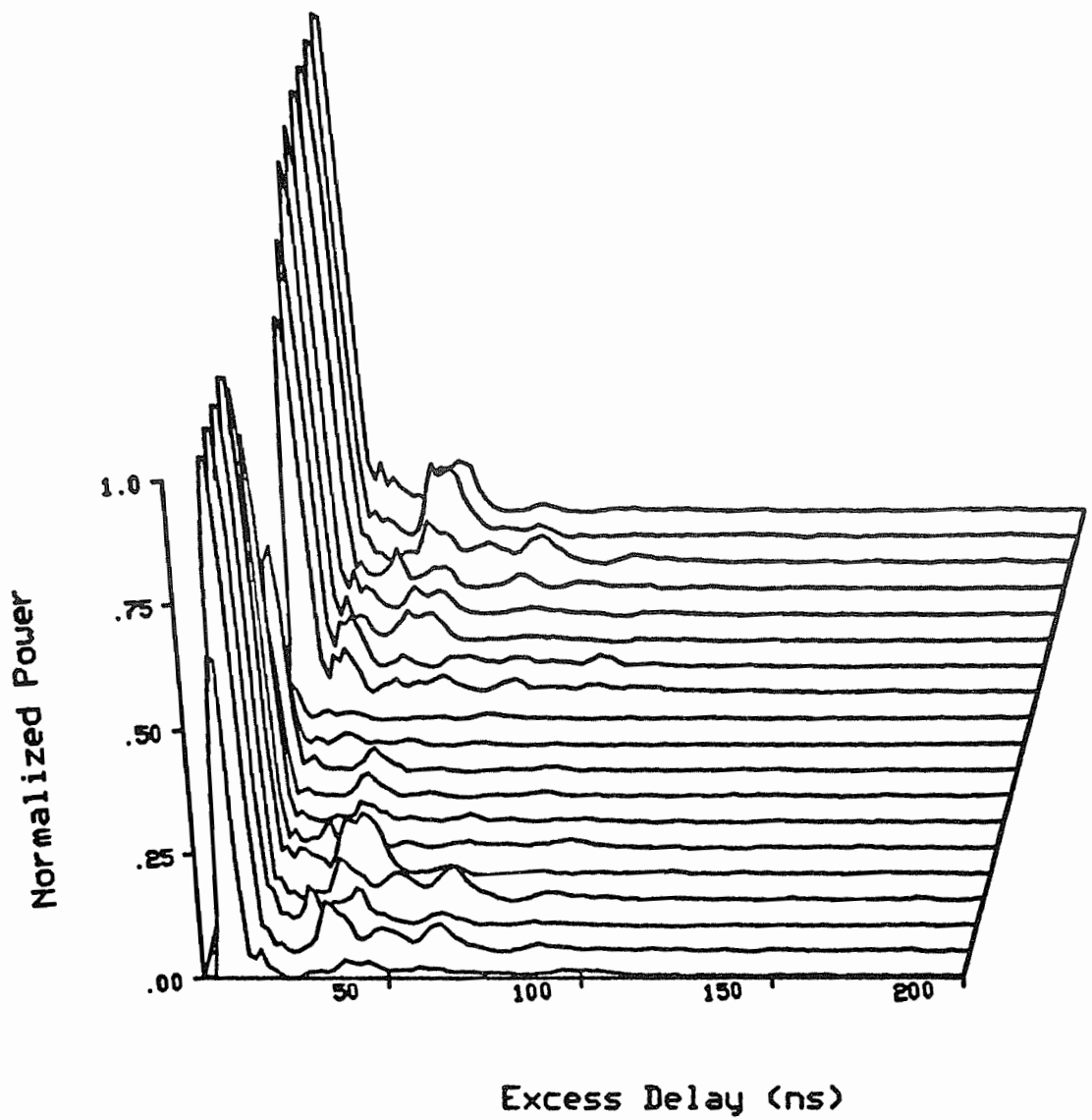




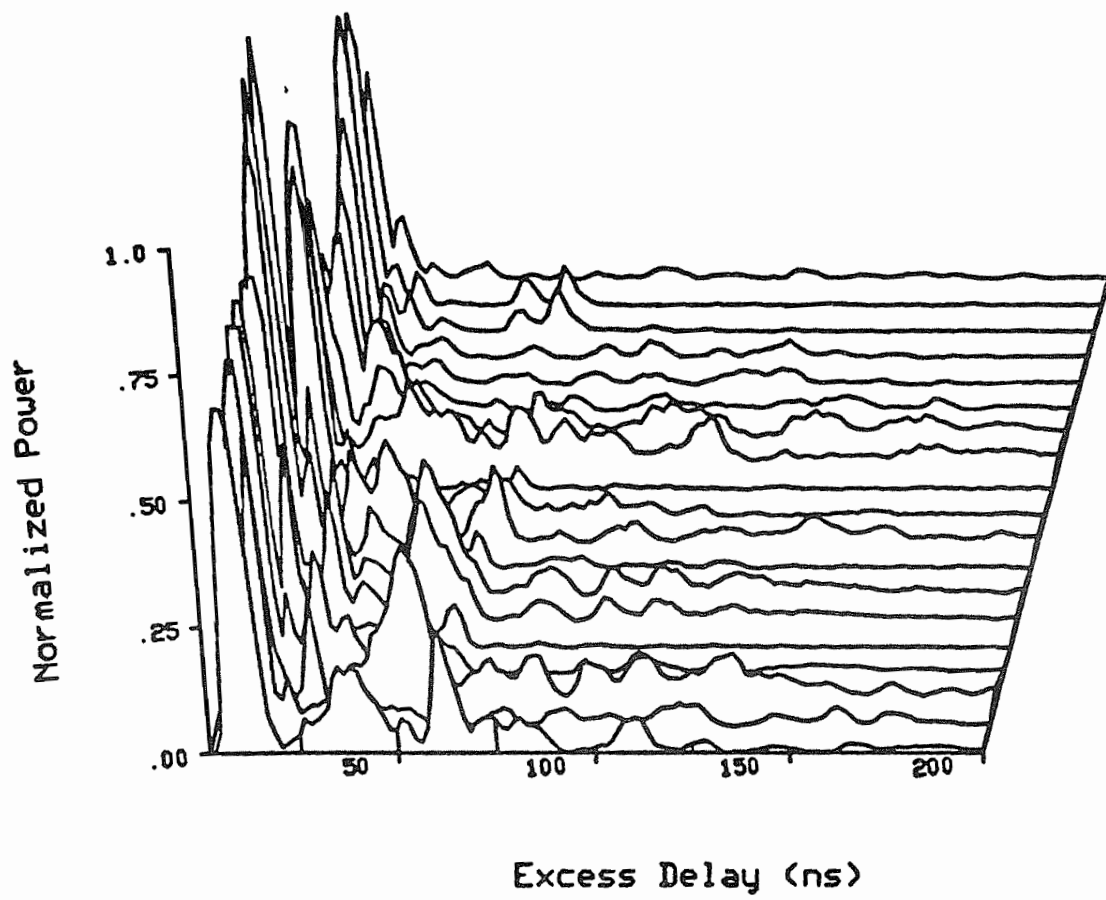
pb2bc



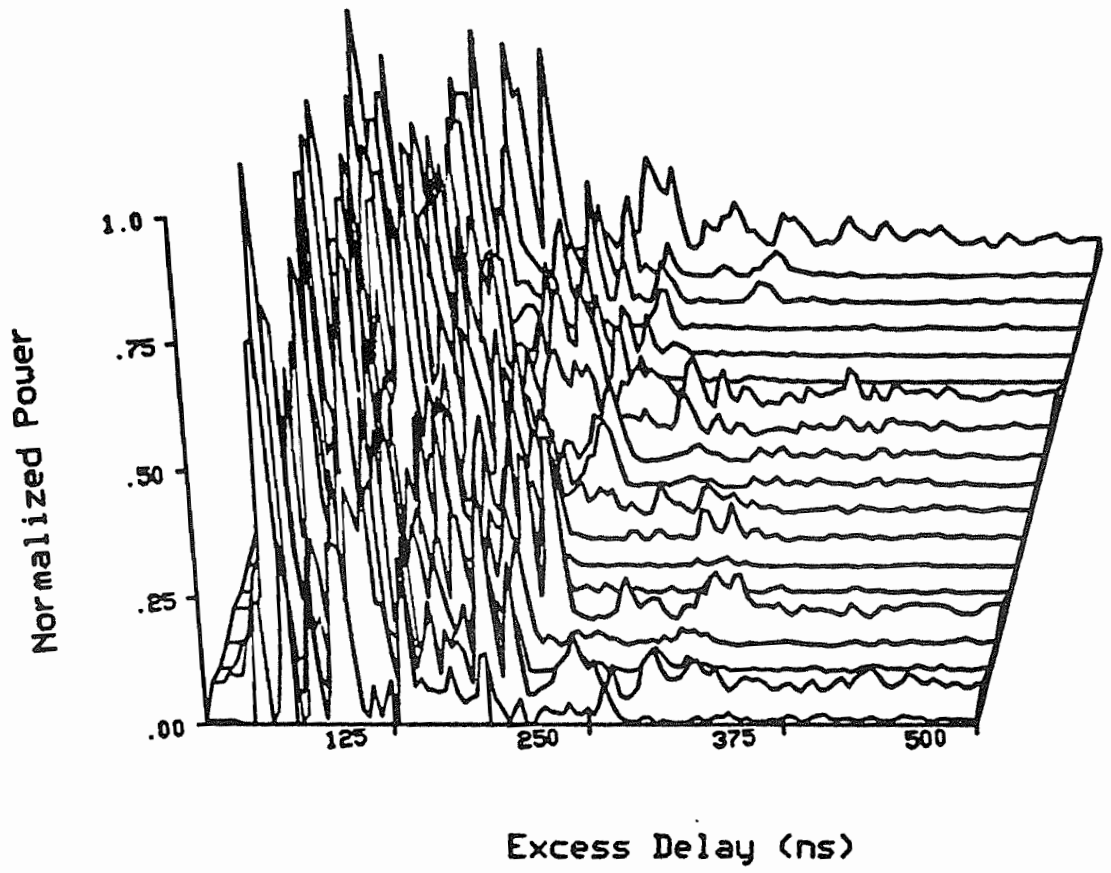
pb2cc



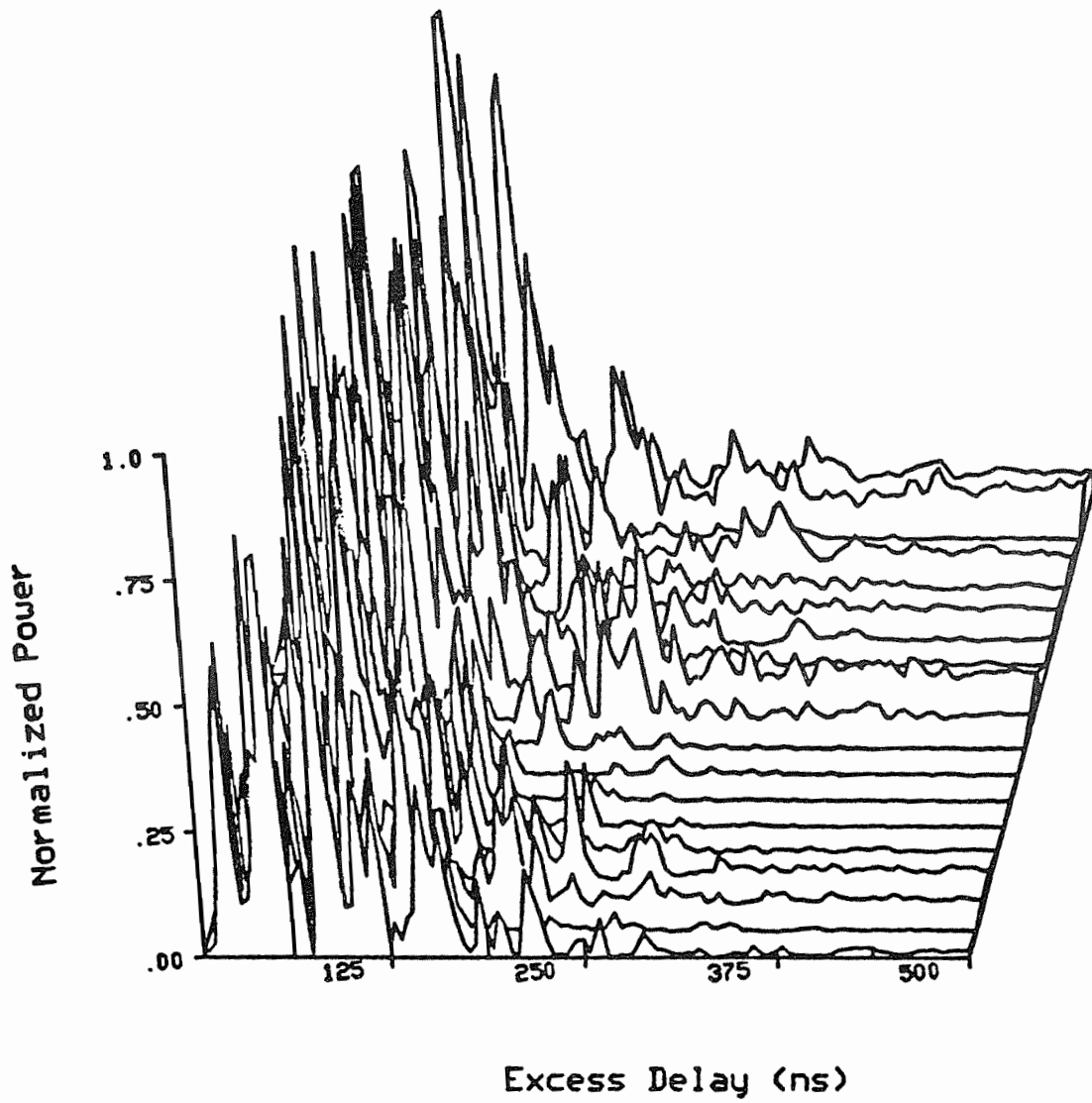
pb4ac



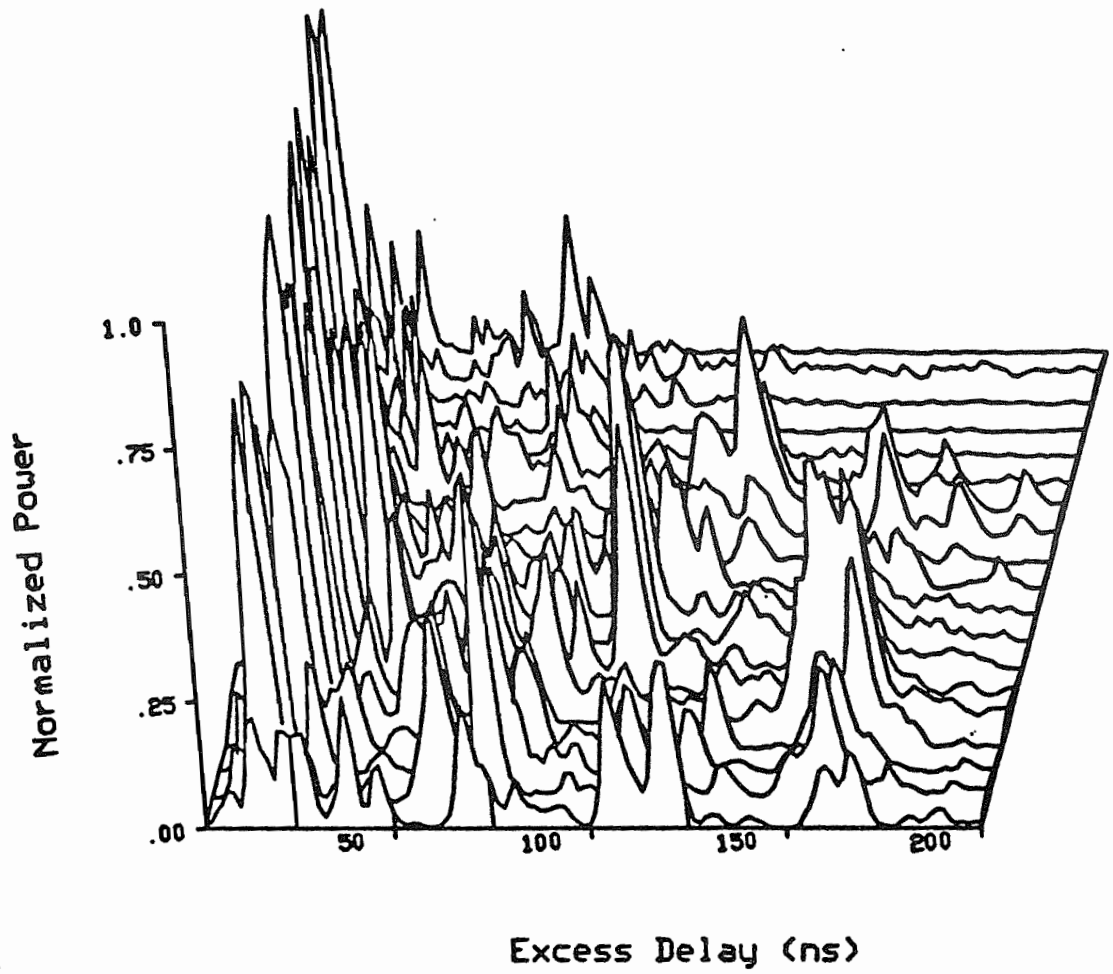
pb4bc



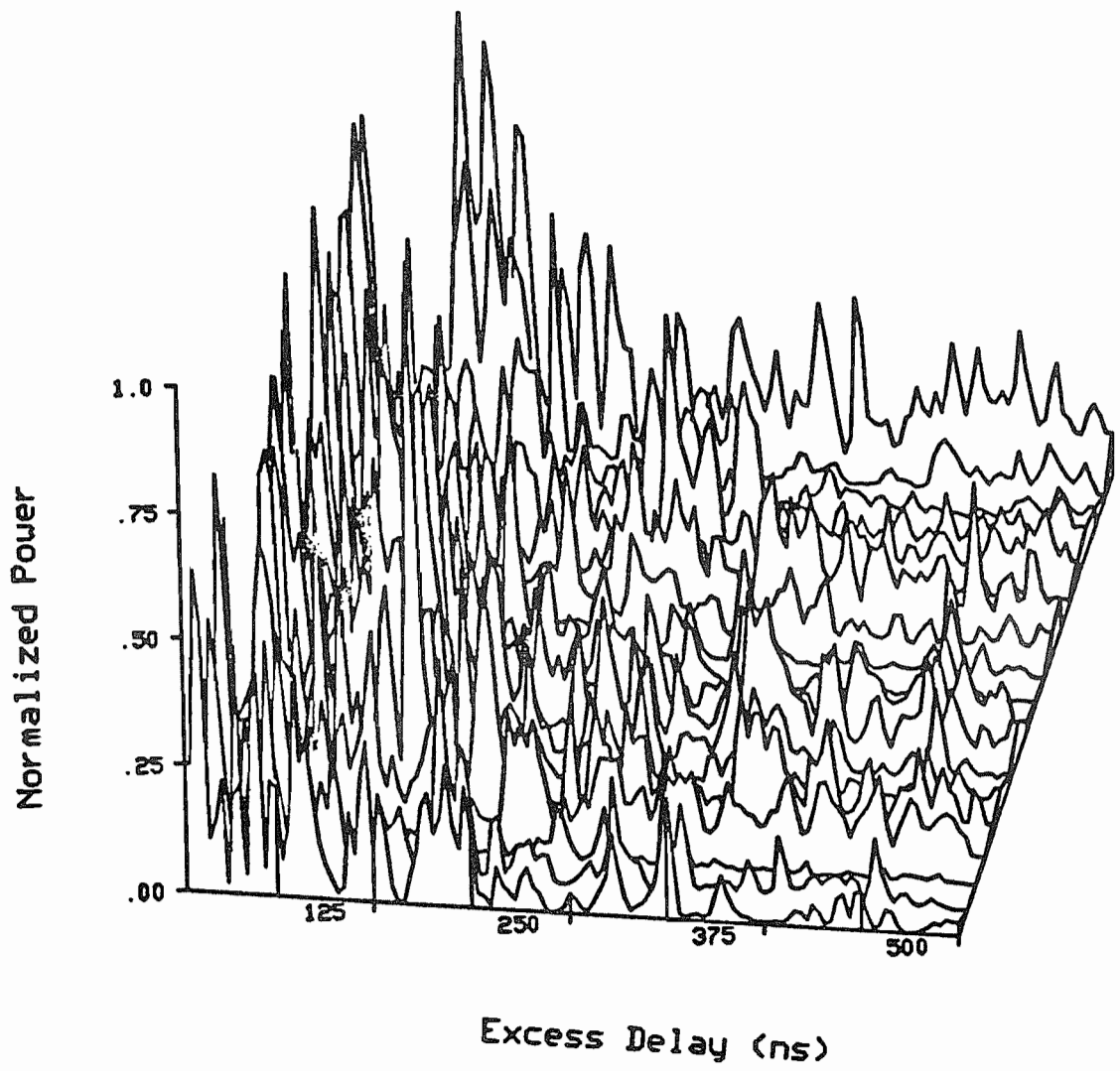
pb5ac



pb5cc

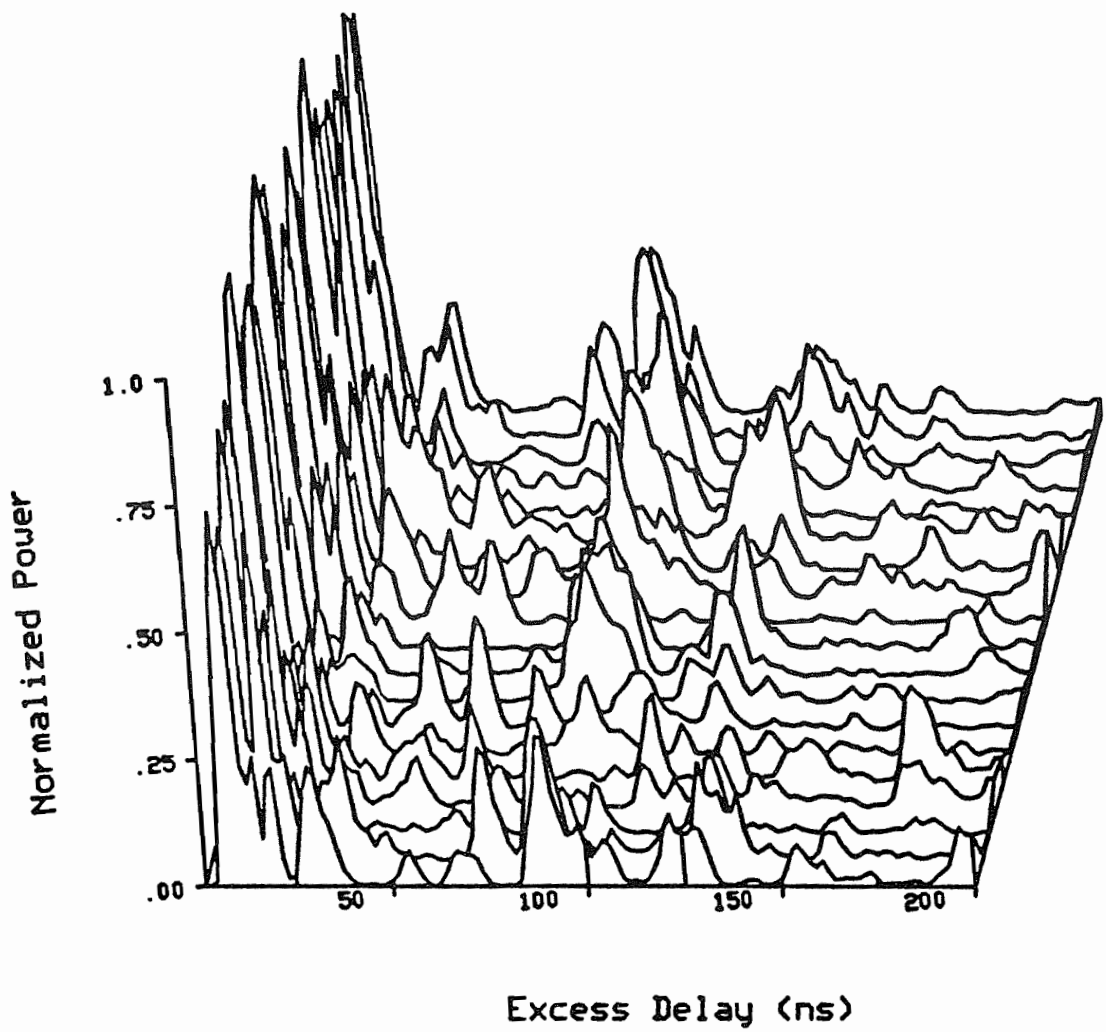


pb5bc

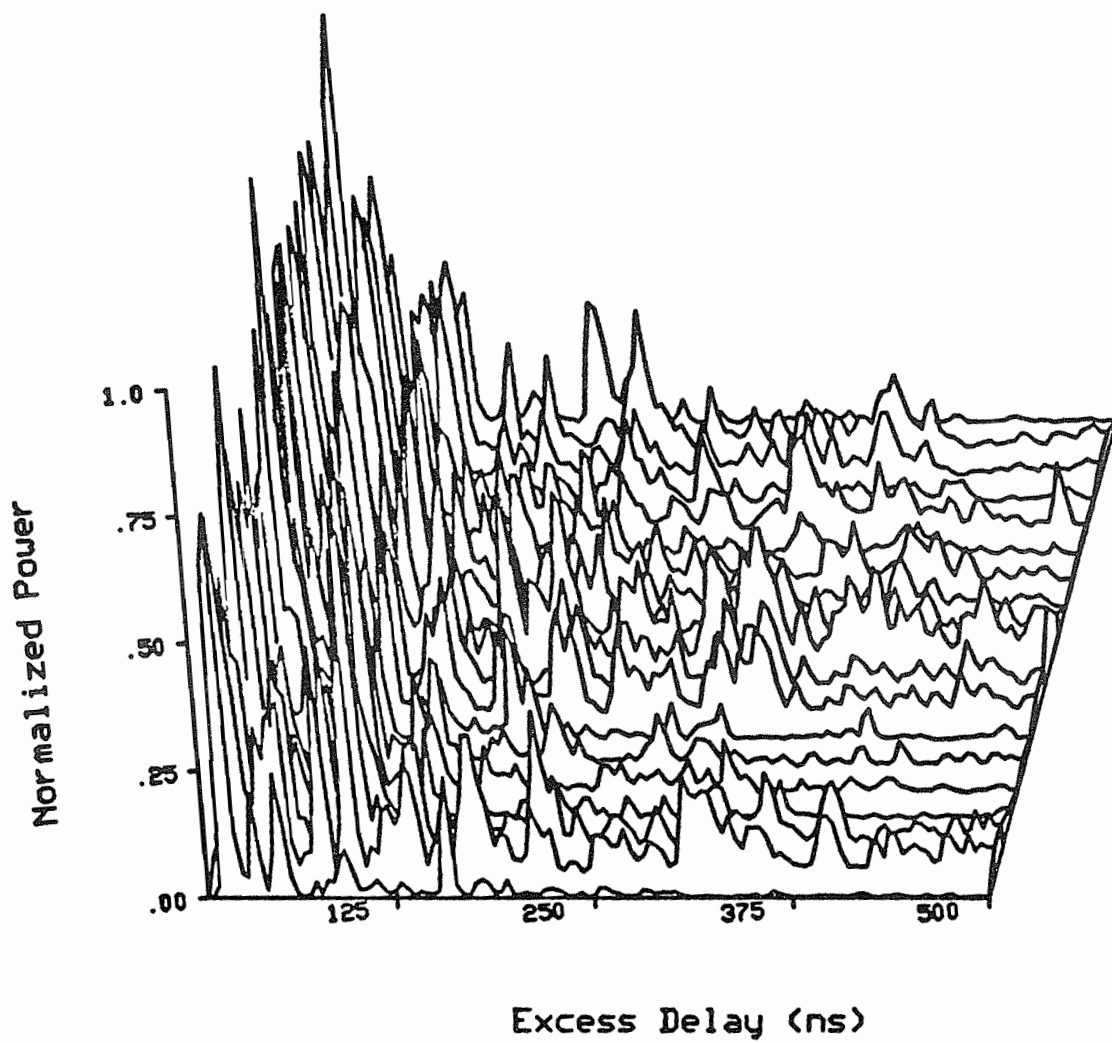


pclac

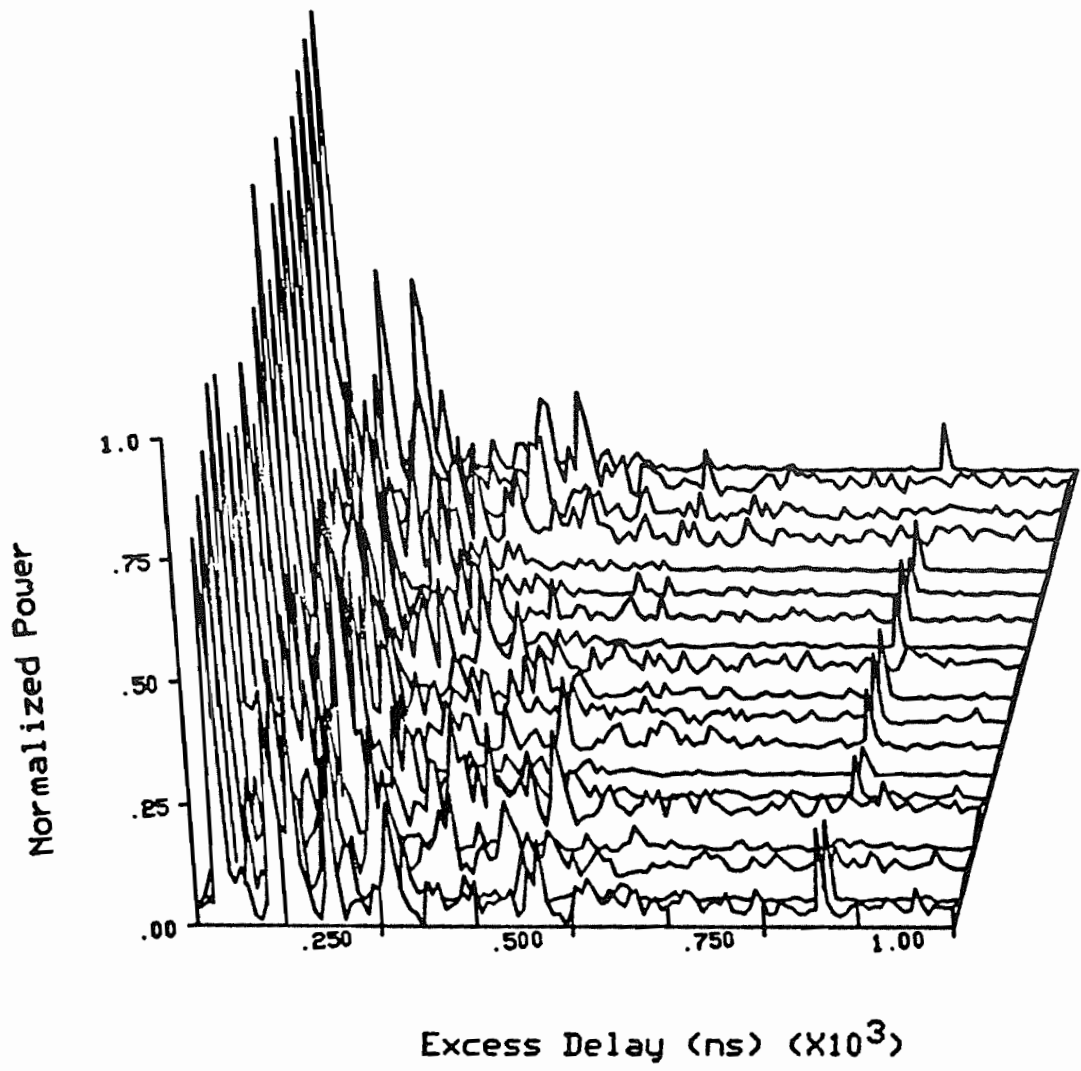




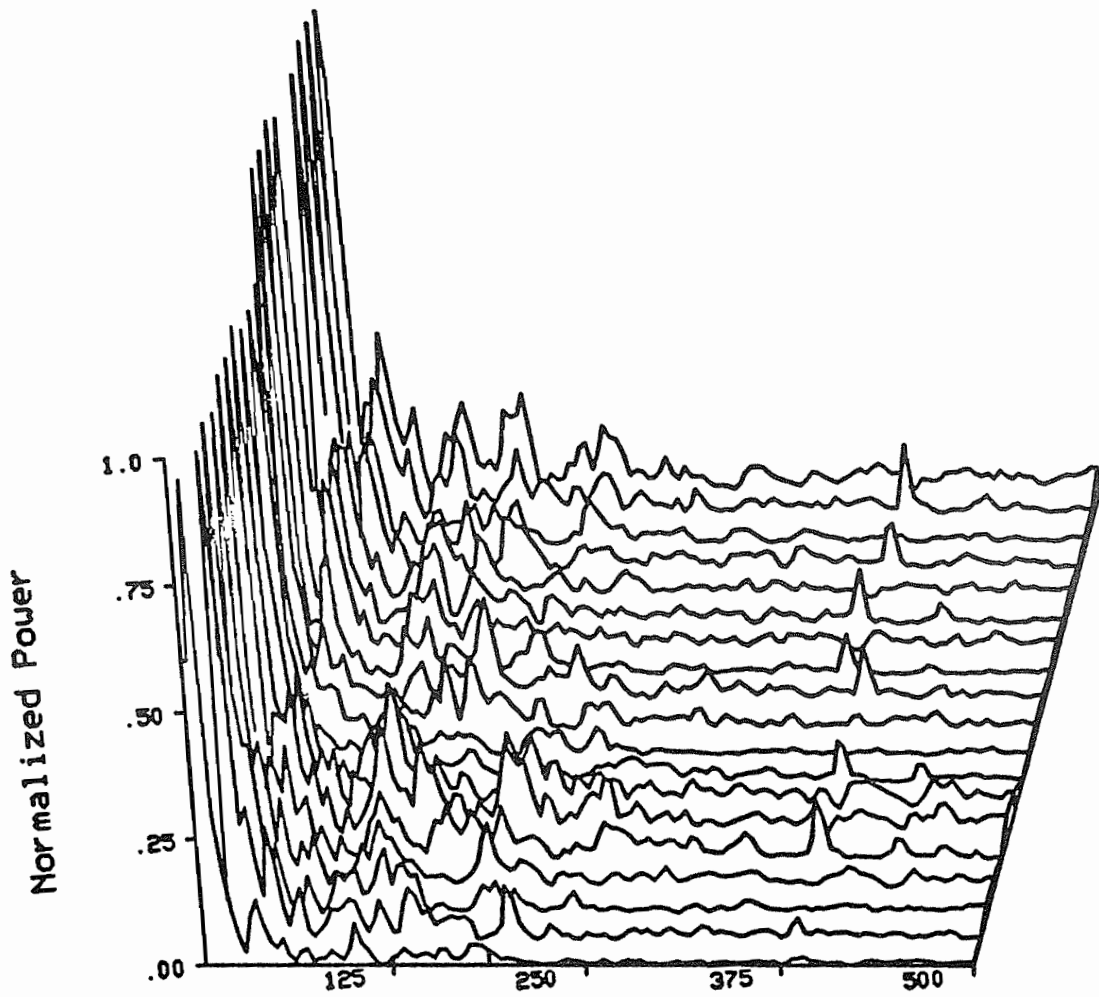
pc1bc



pc2bc

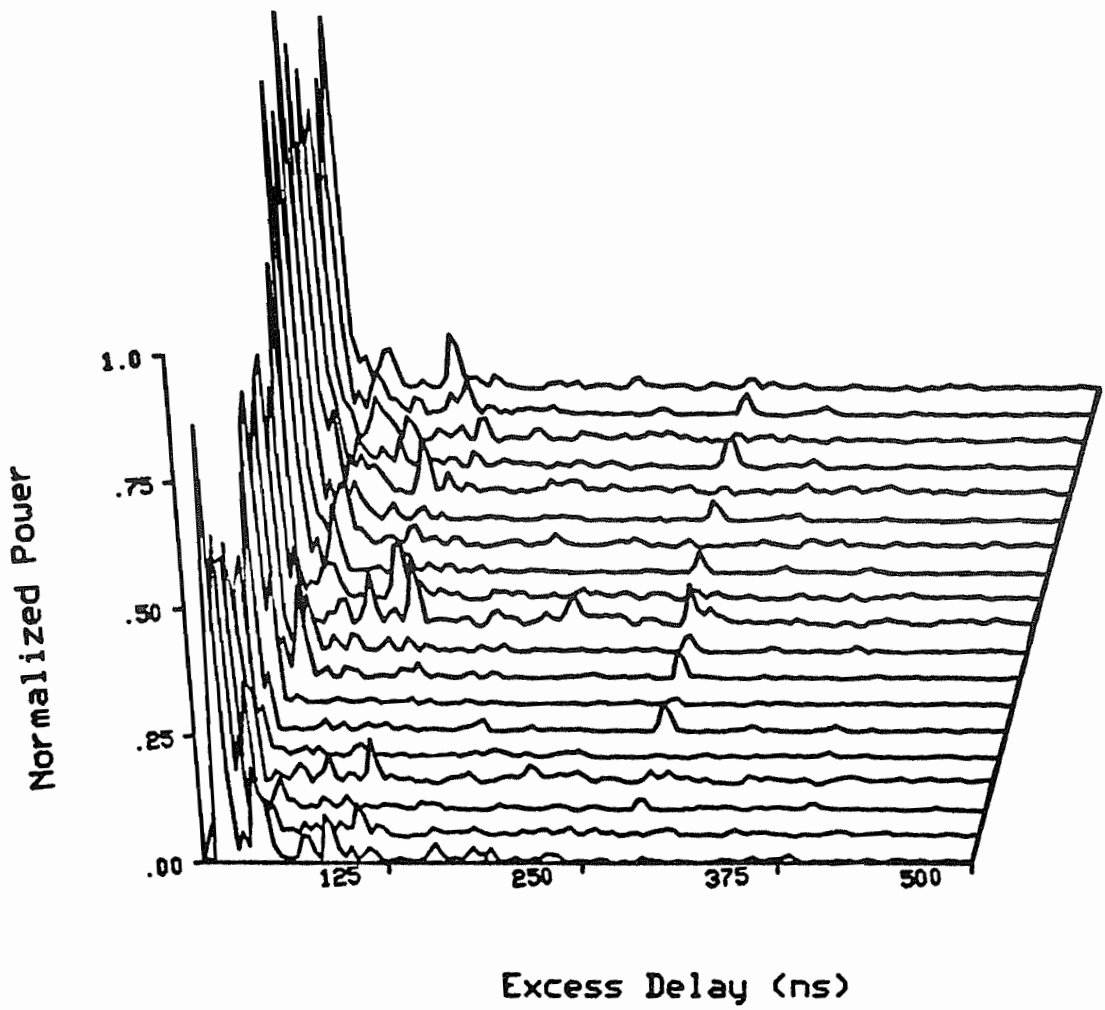


pc2cc

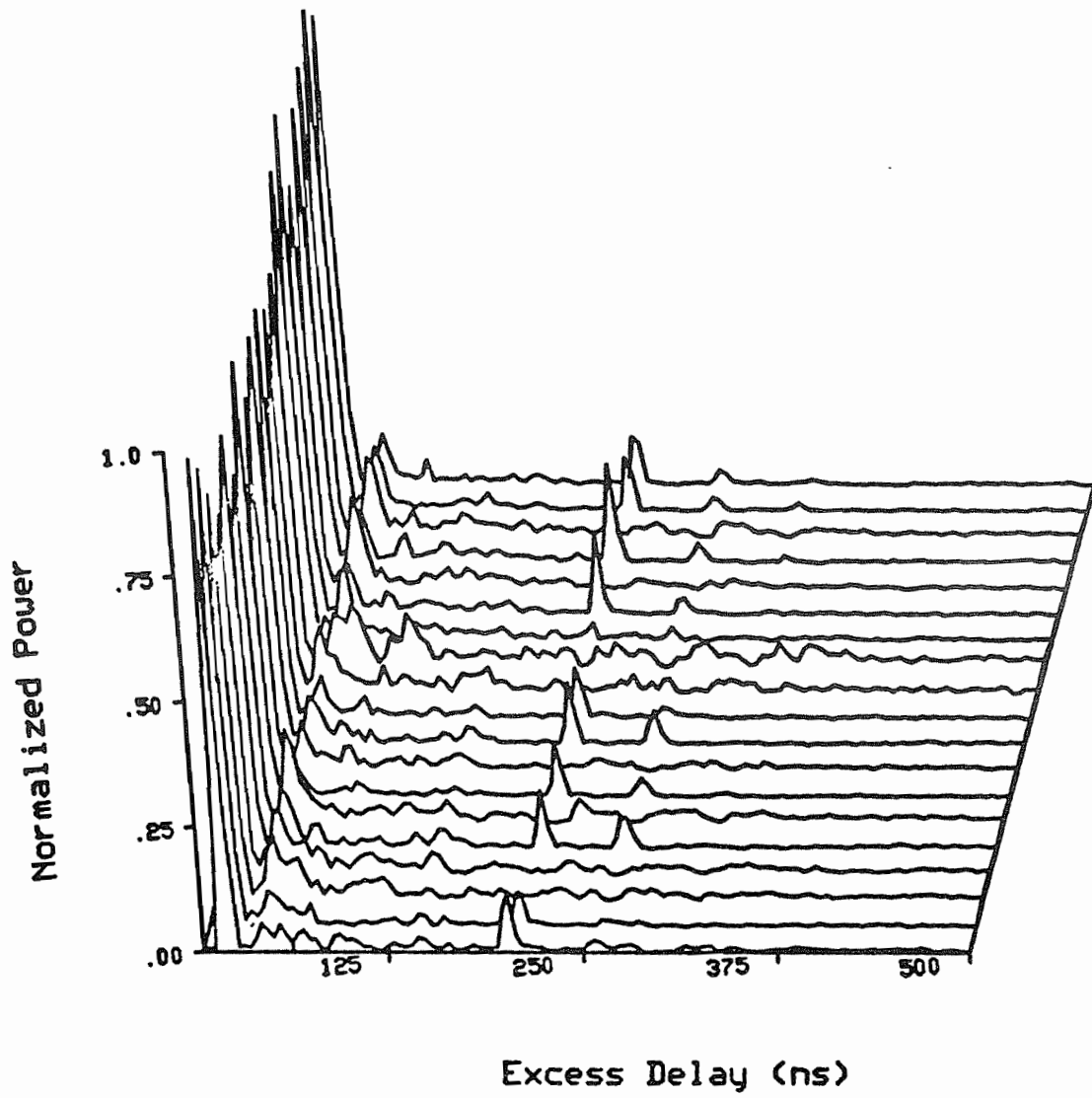


Excess Delay (ns)

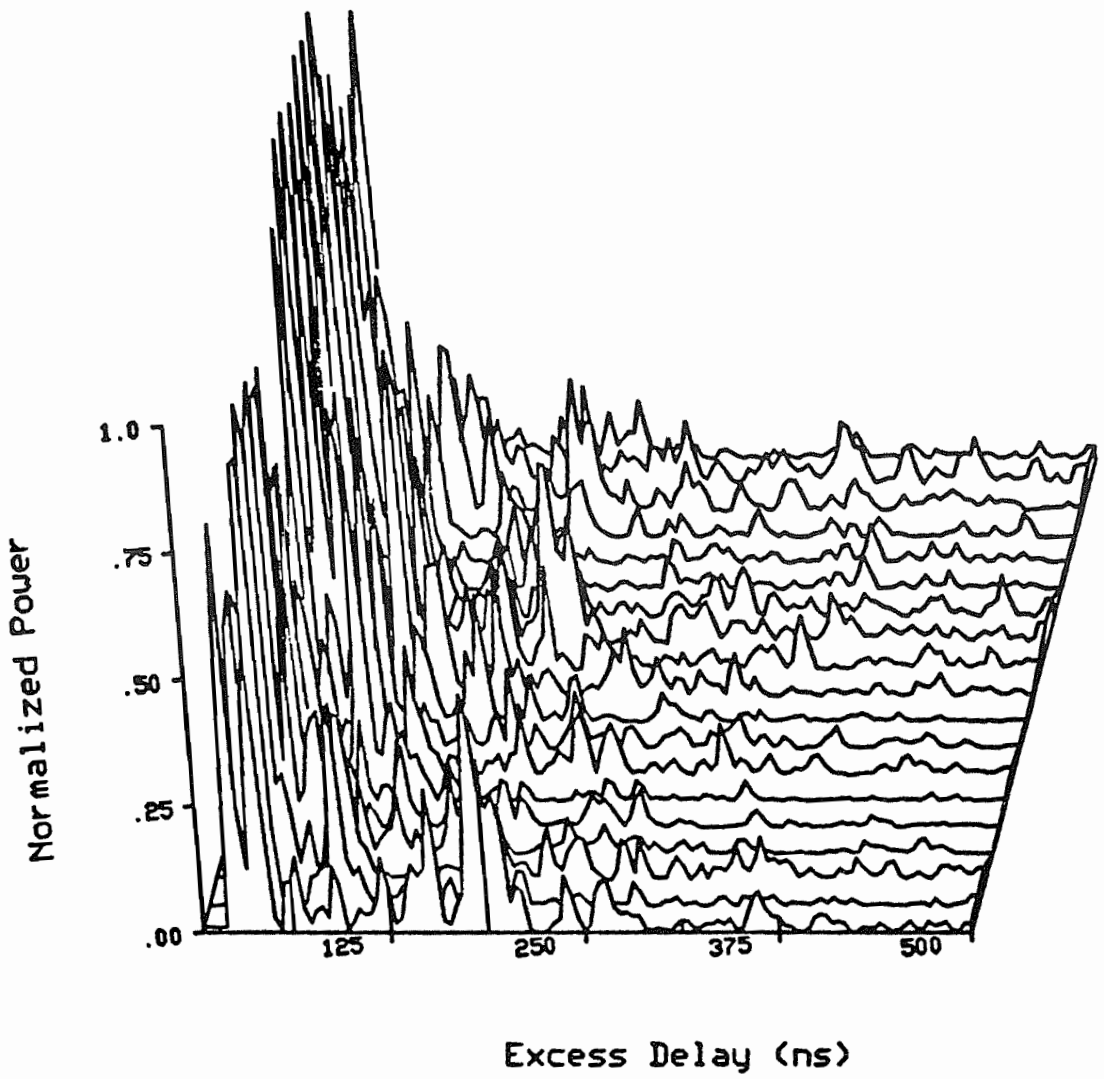
pc3ac



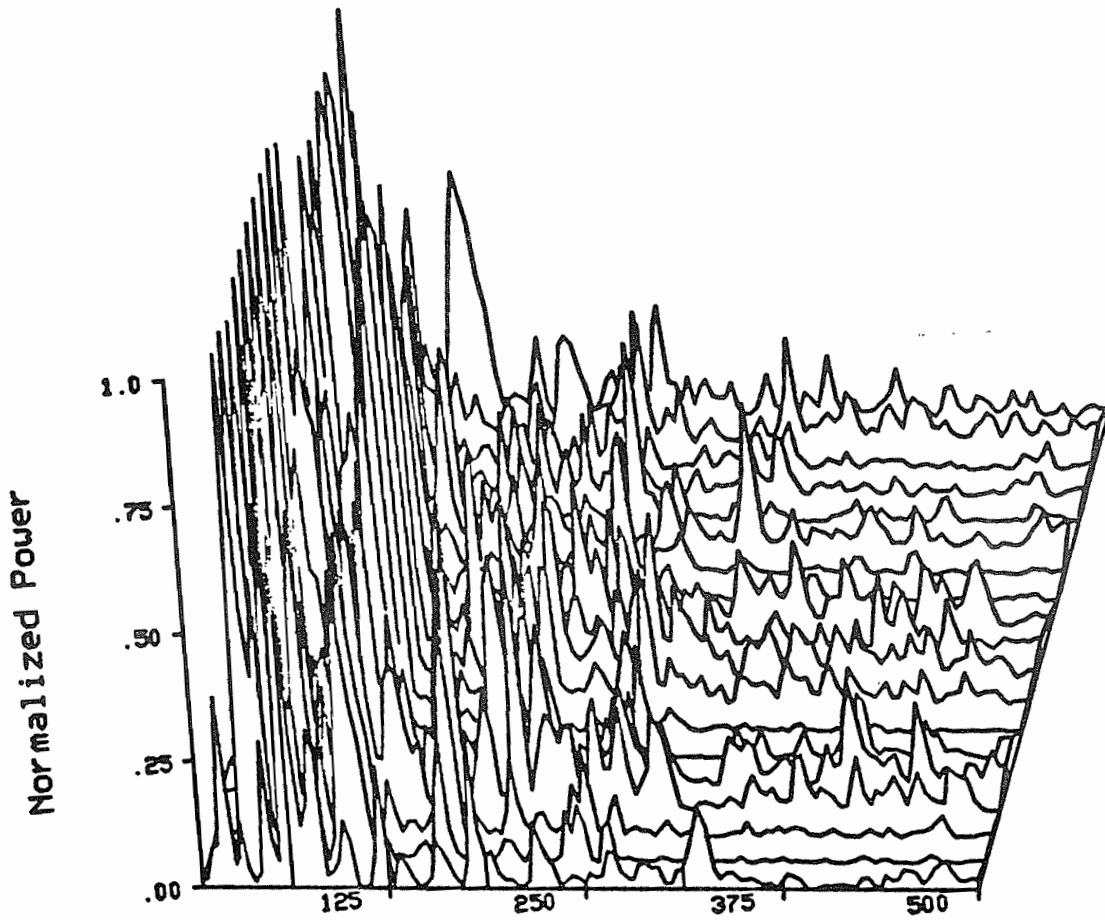
pc3bc



pc3cc



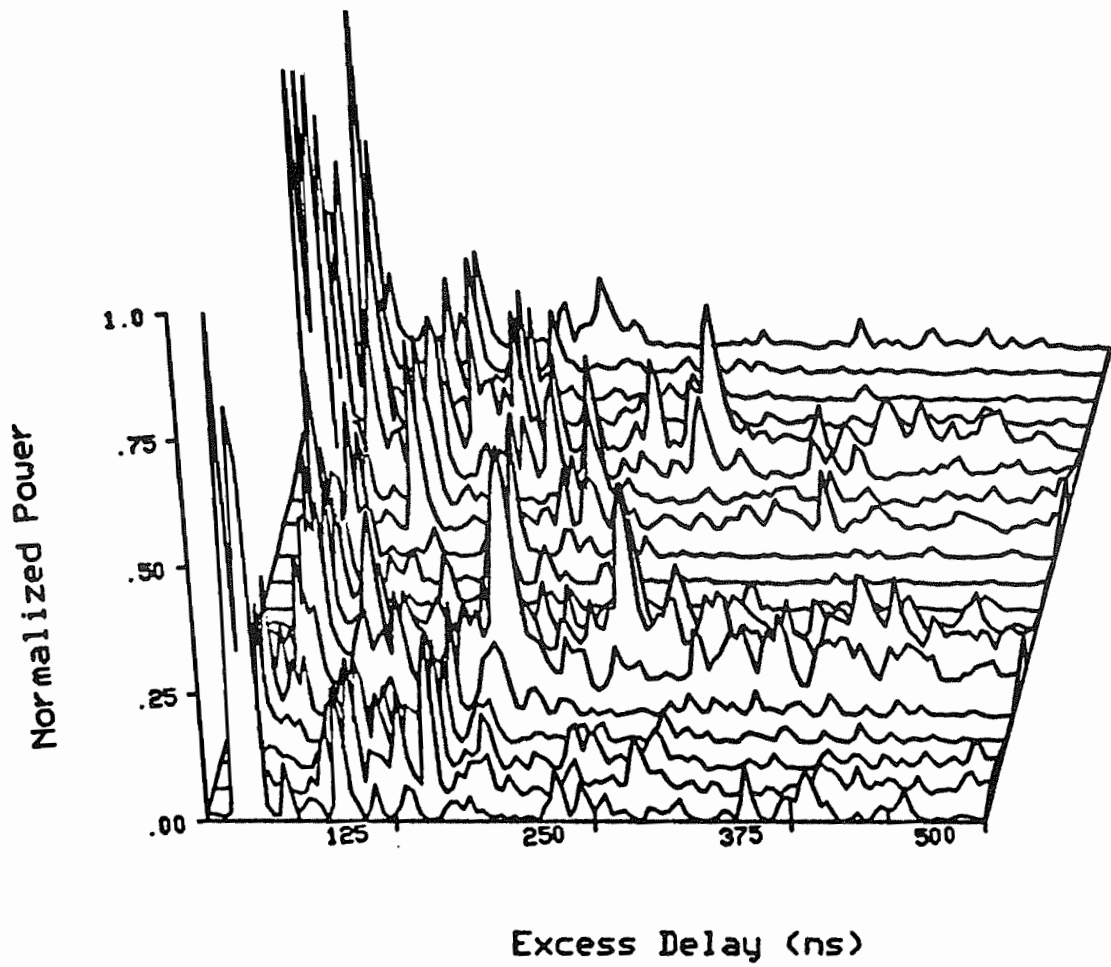
pc4ac



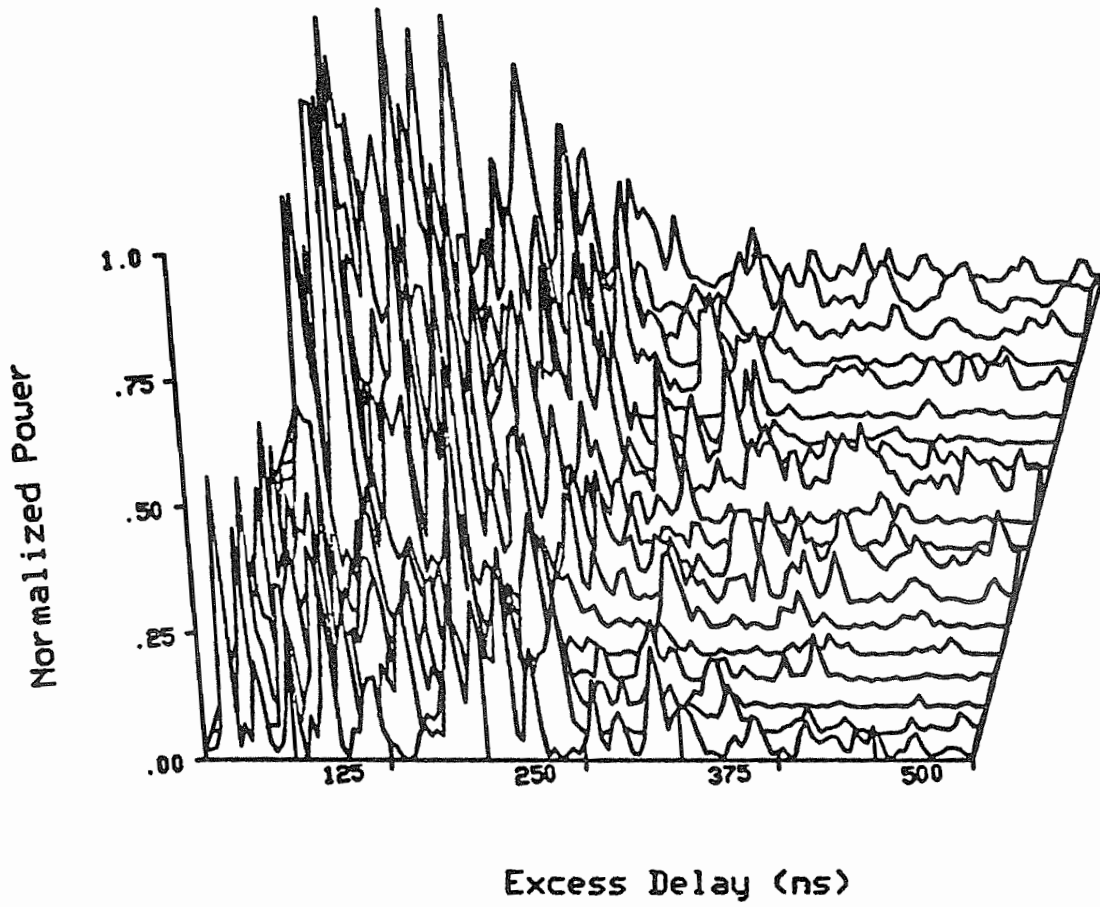
Excess Delay (ns)

pc4bc

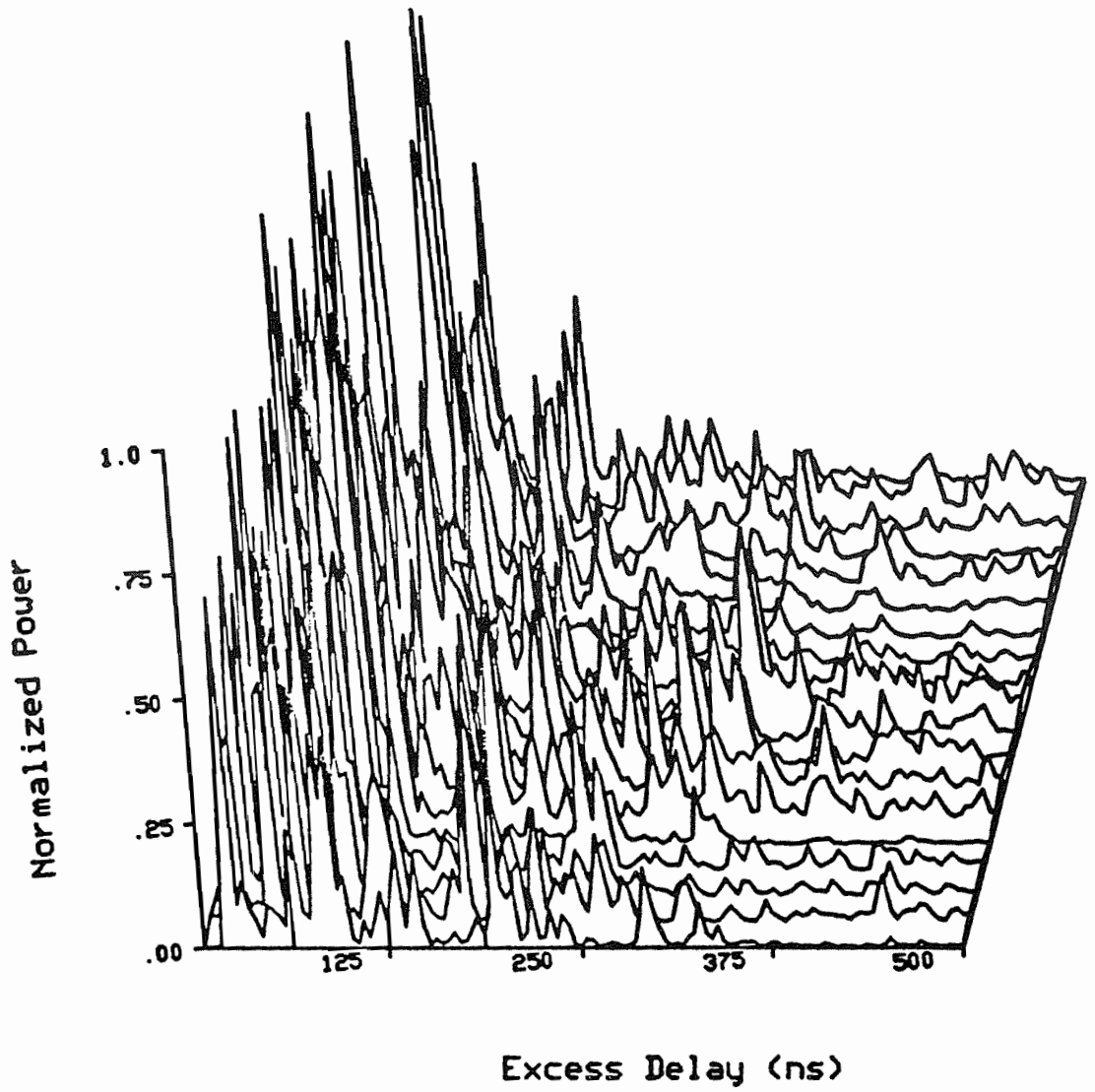




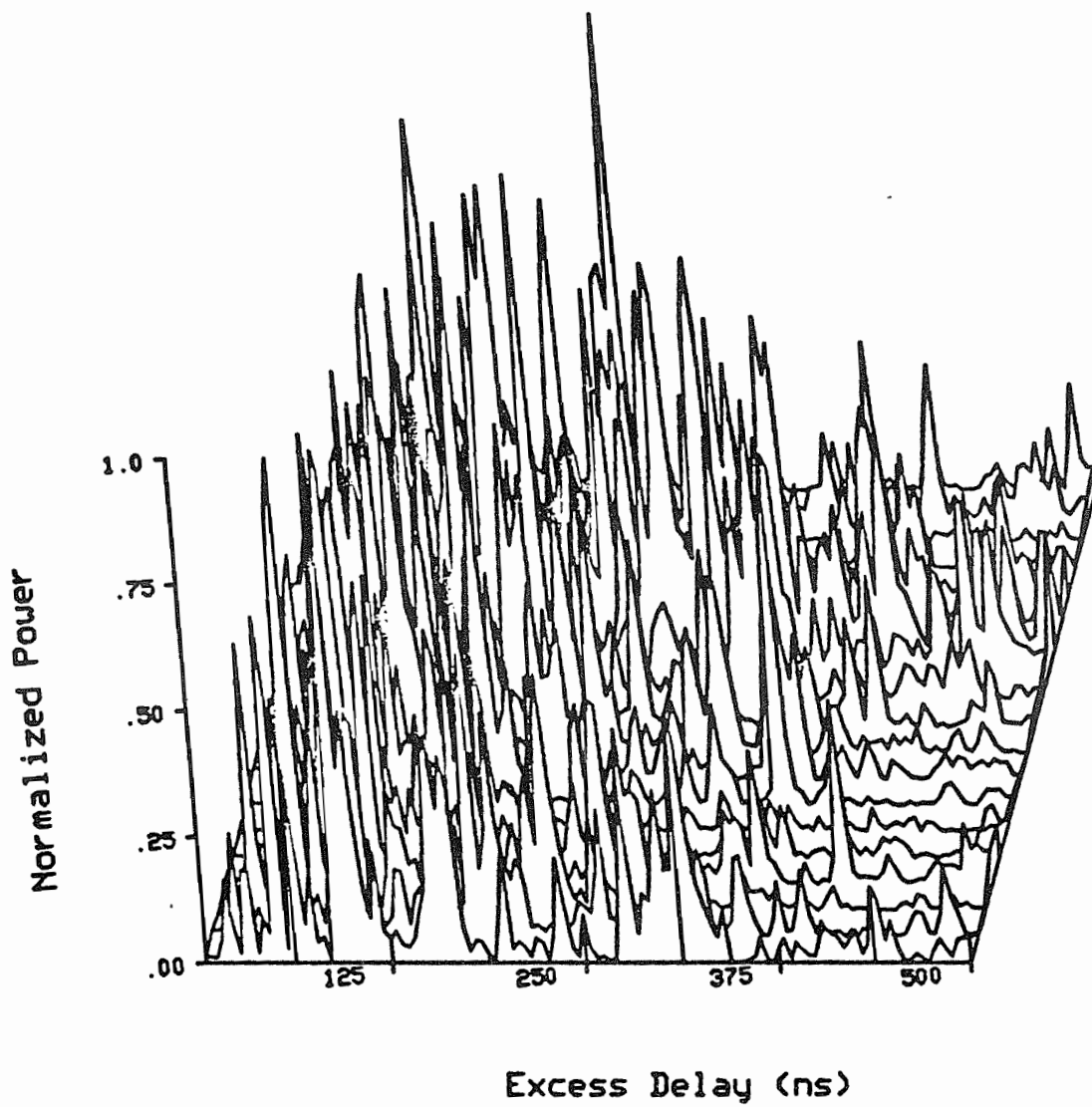
pc4cc



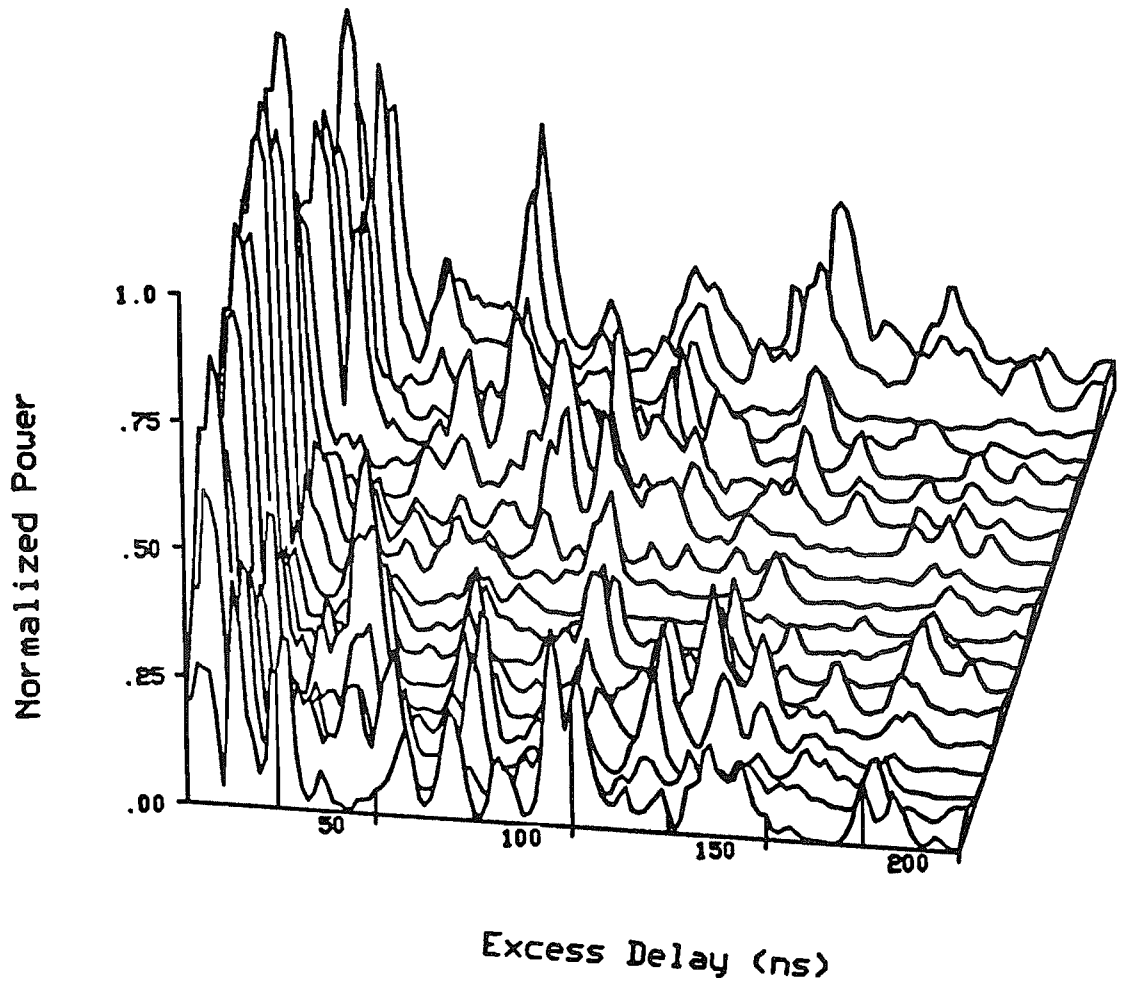
pc5ac



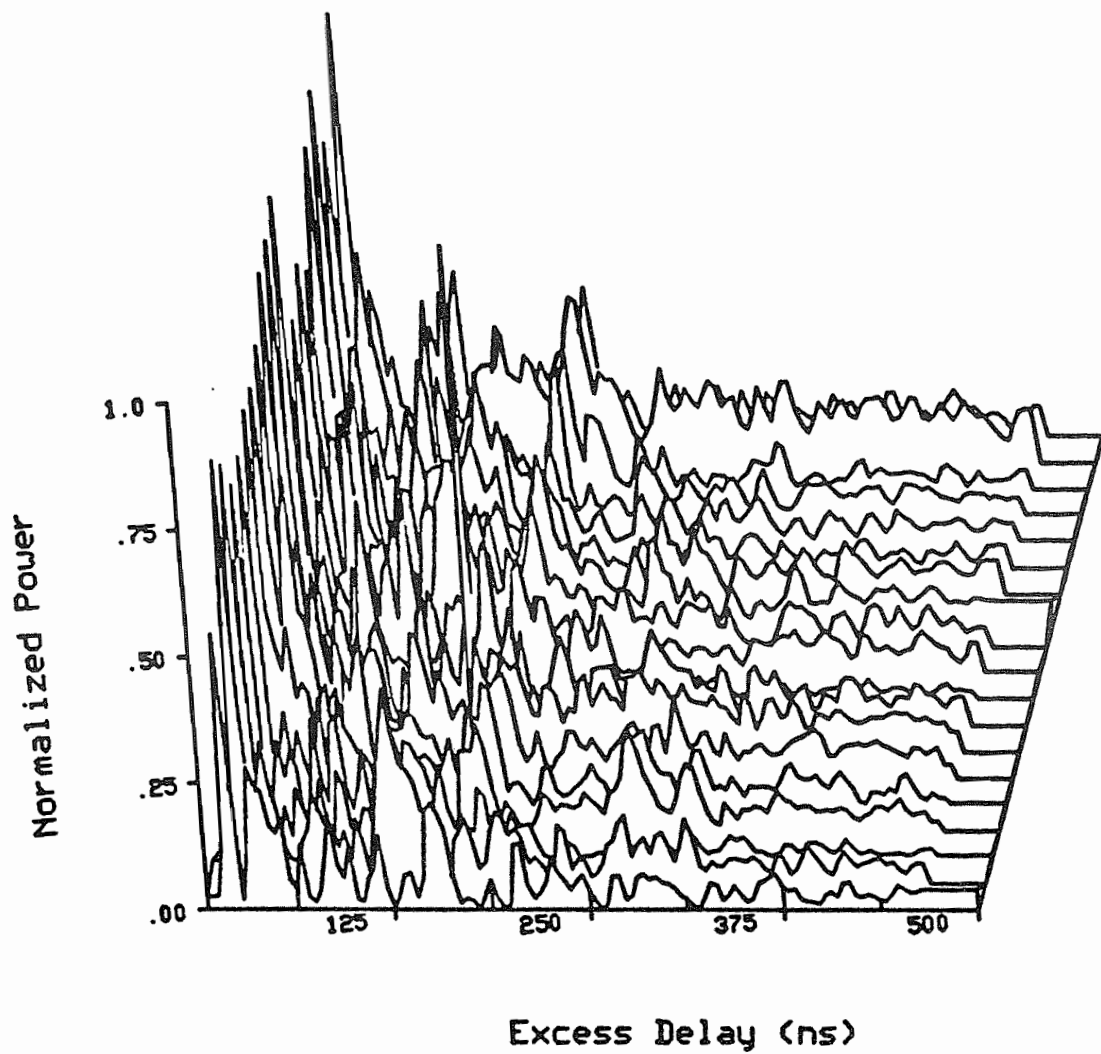
pc5bc



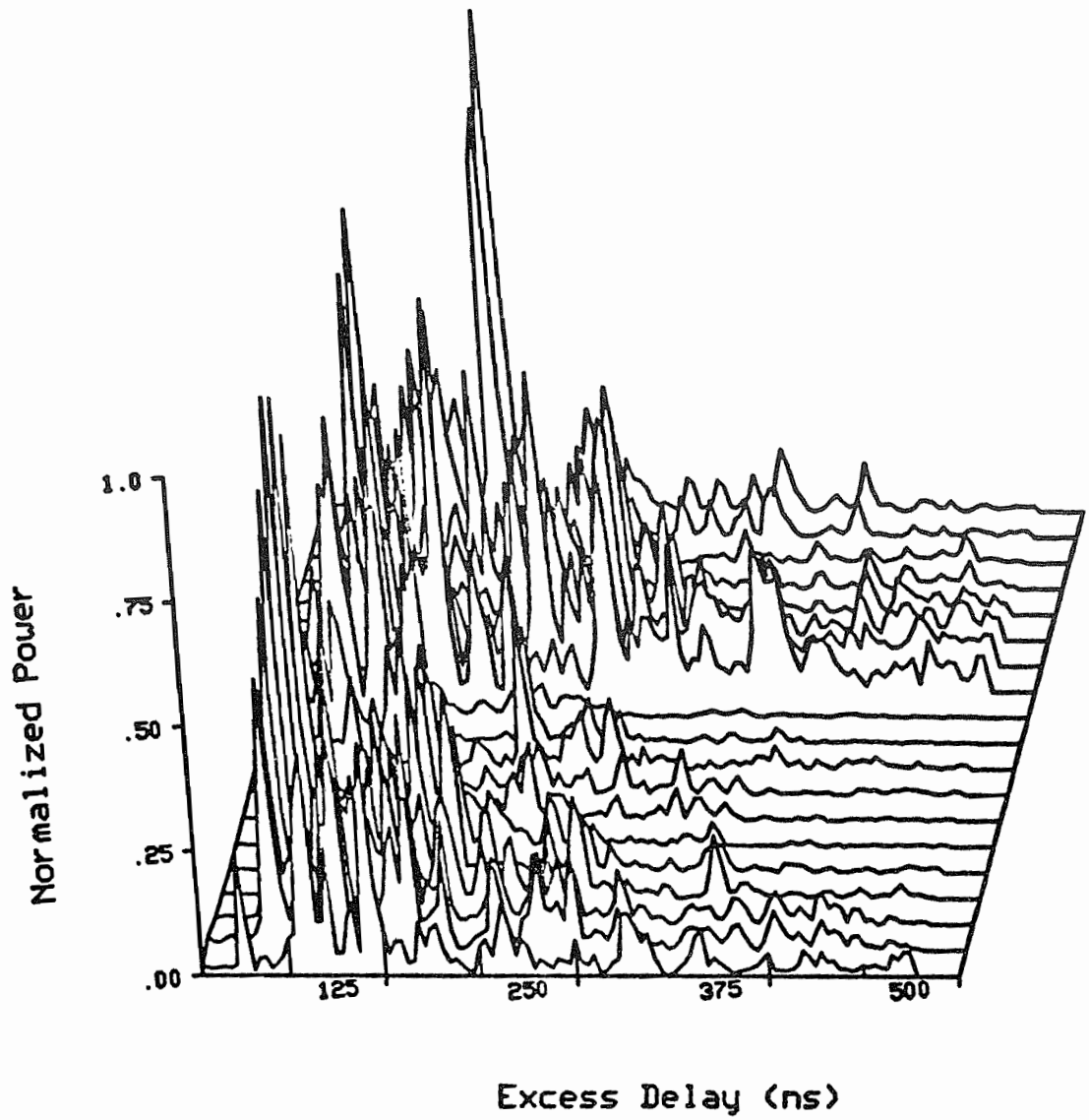
pc5cc



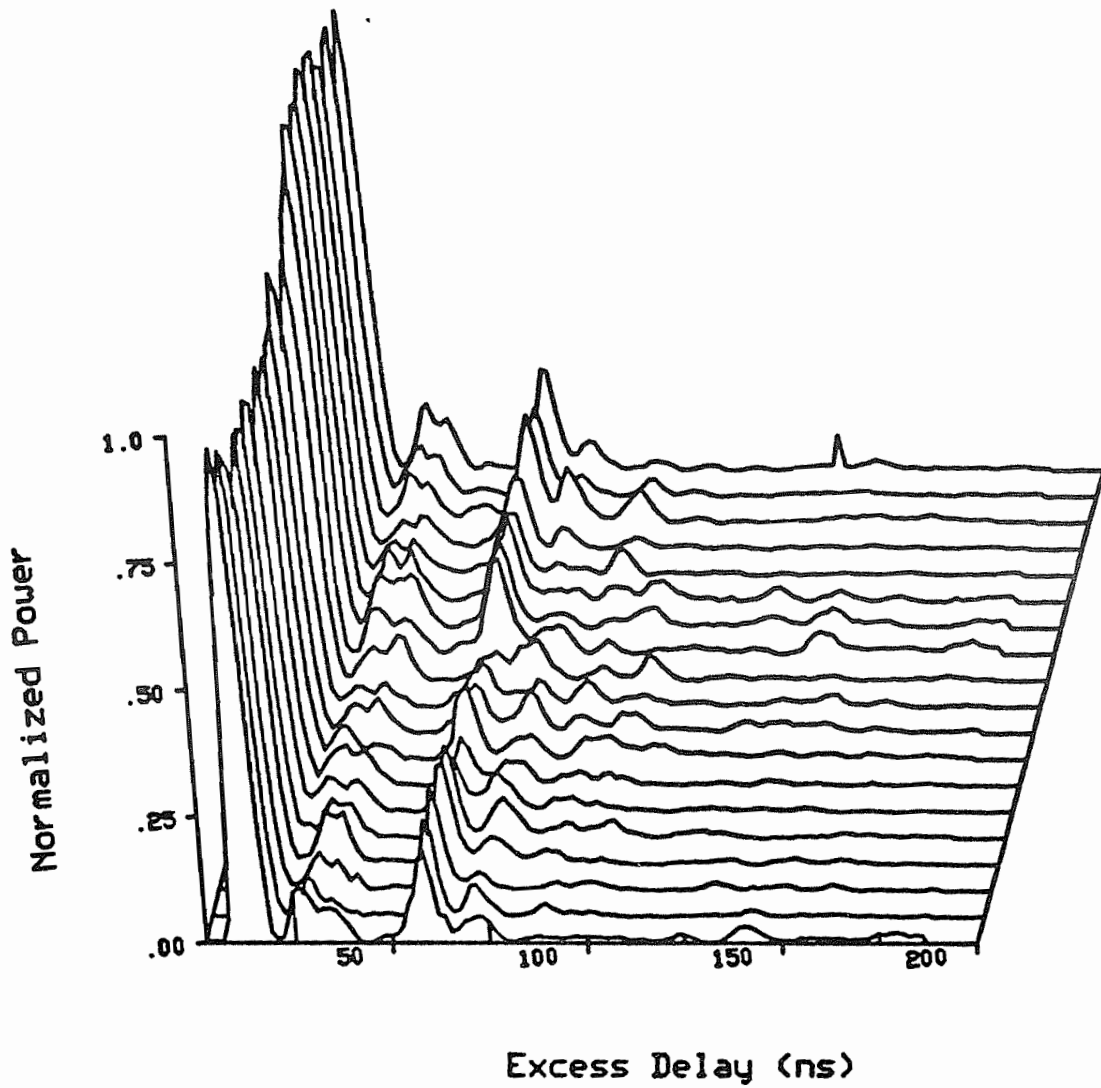
pd1bc



pd2ac

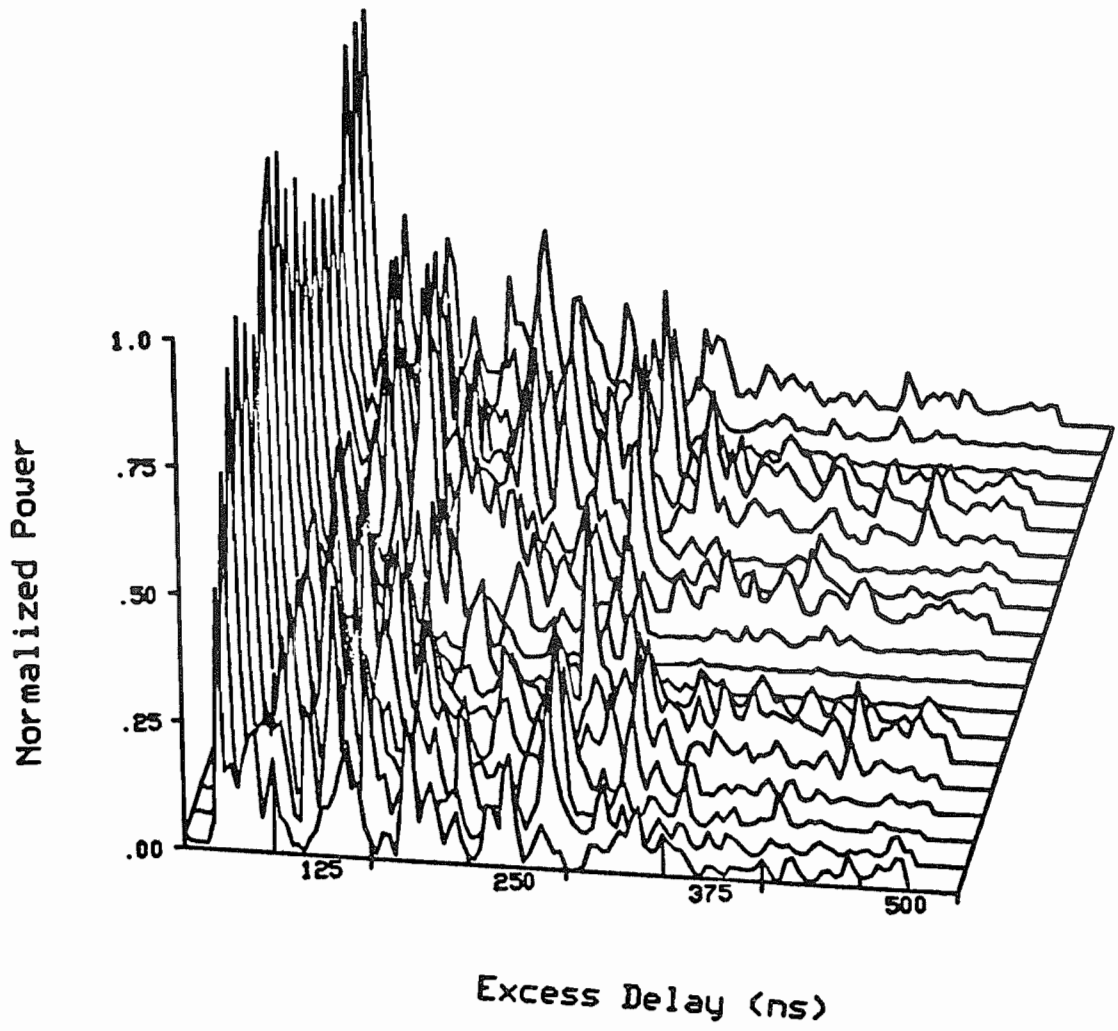


pd2bc

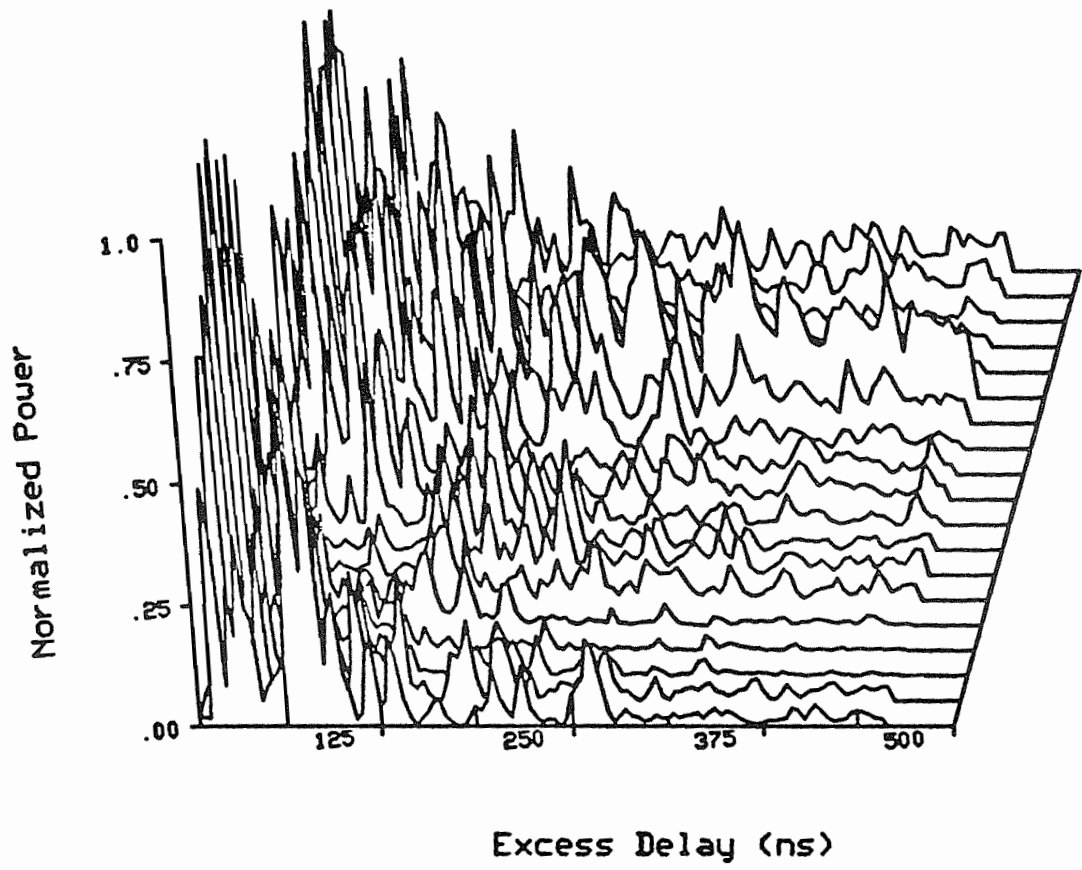


pd2cc

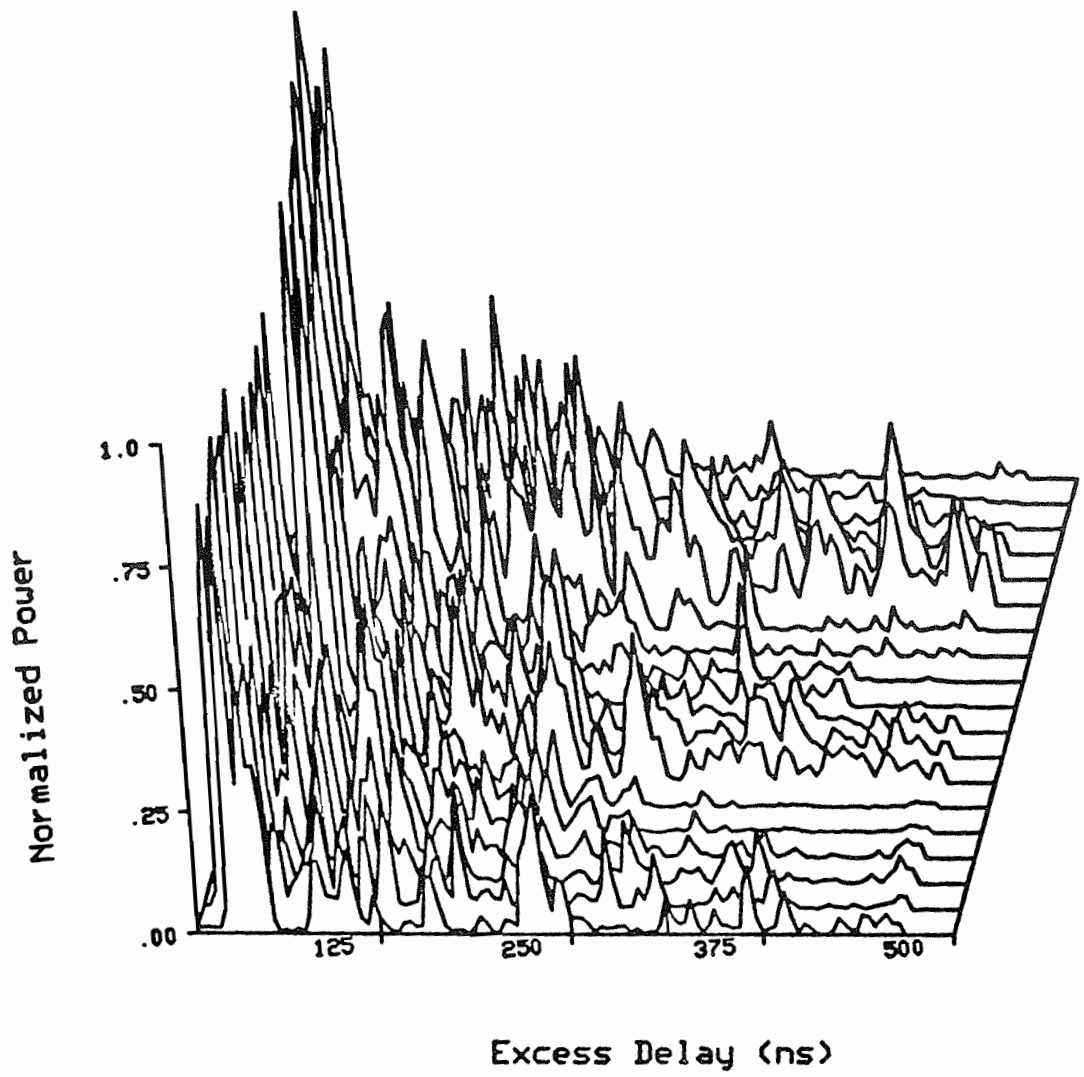




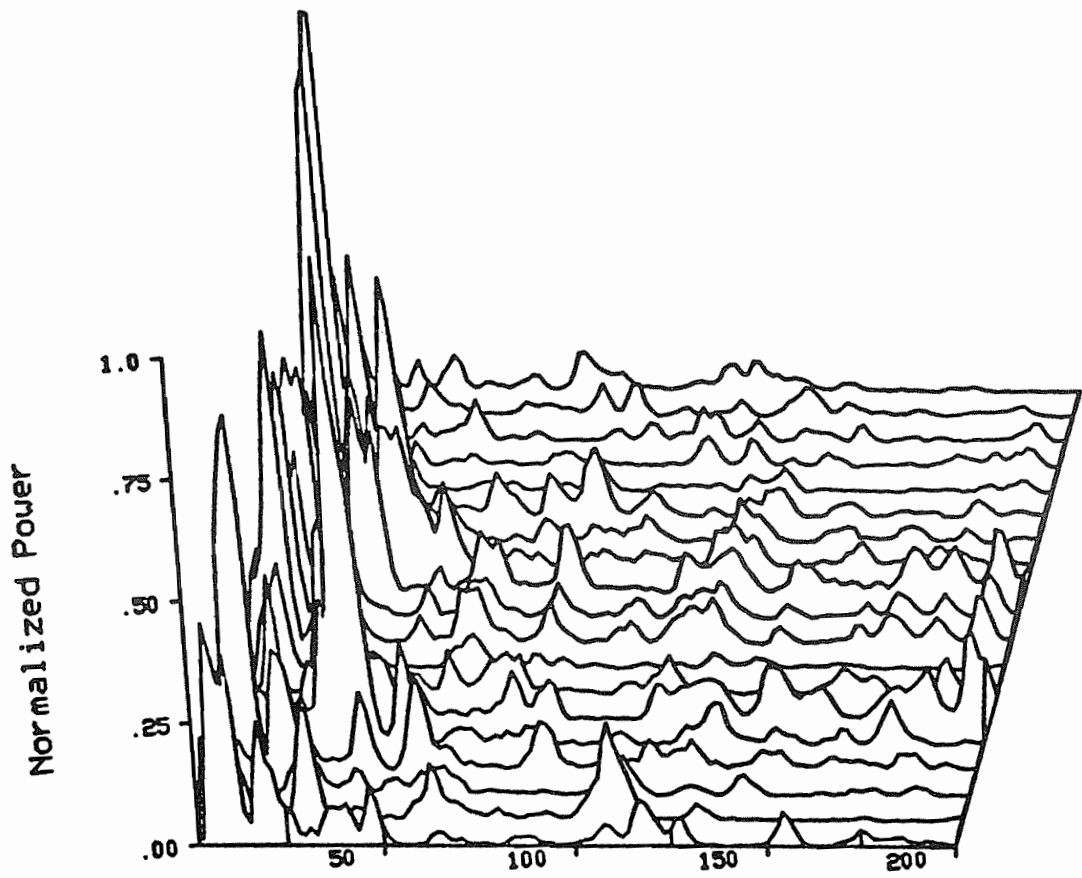
pd4ac



pd4bc

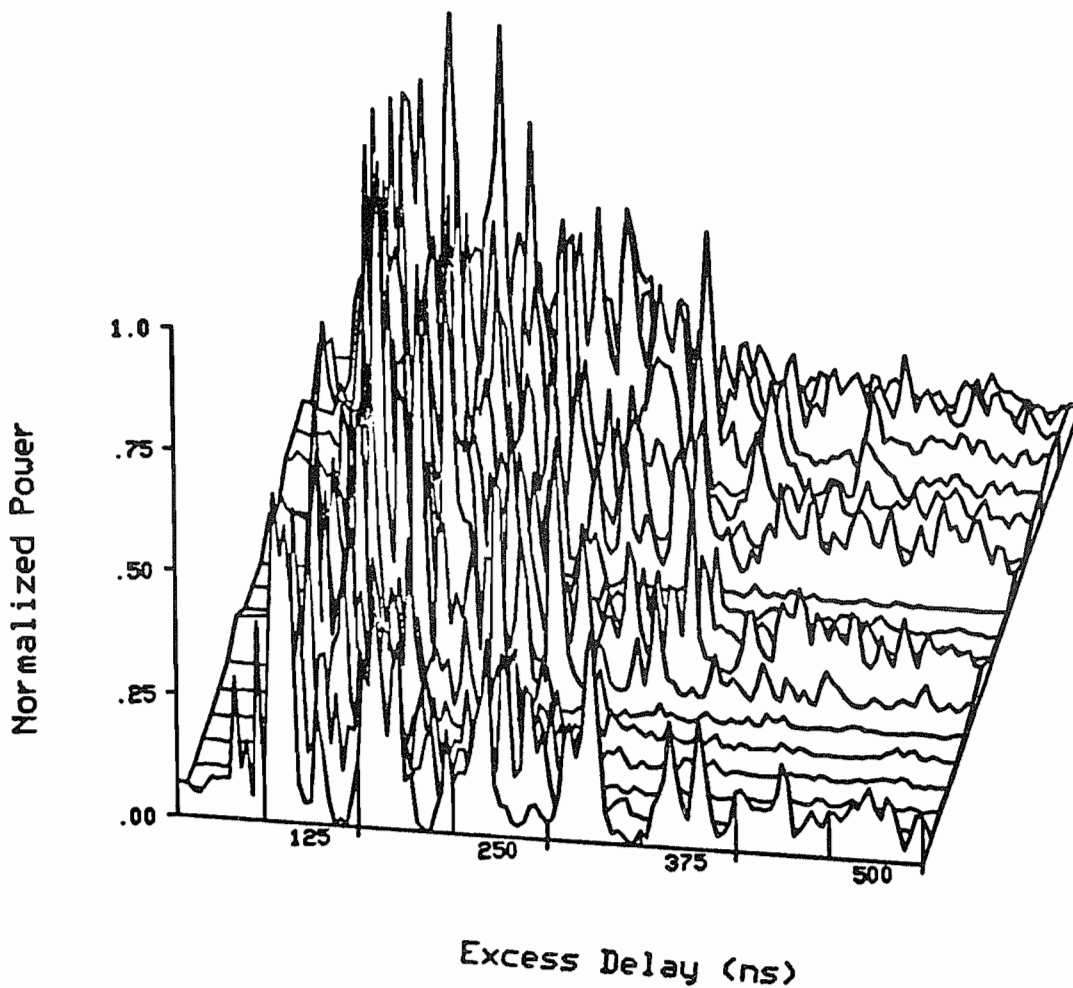


pd4cc

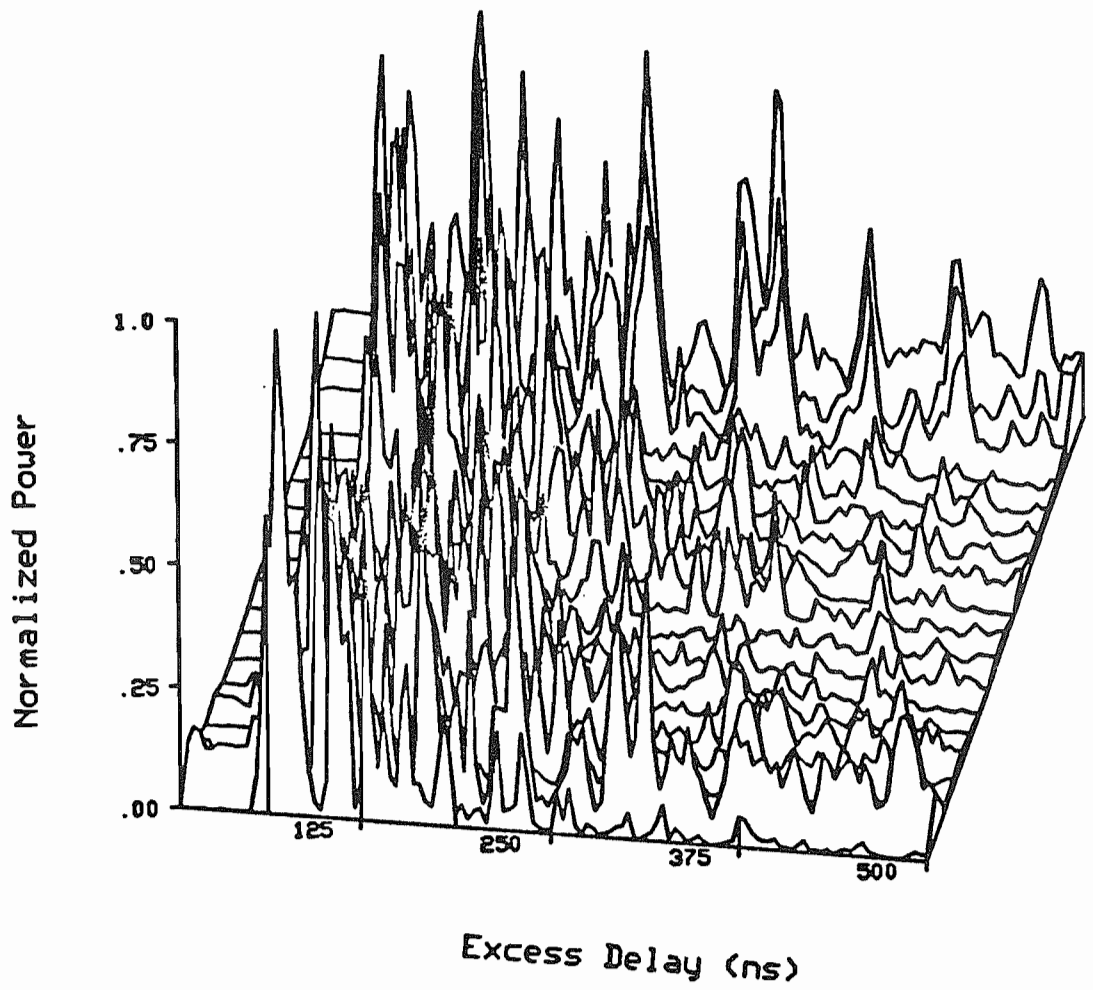


Excess Delay (ns)

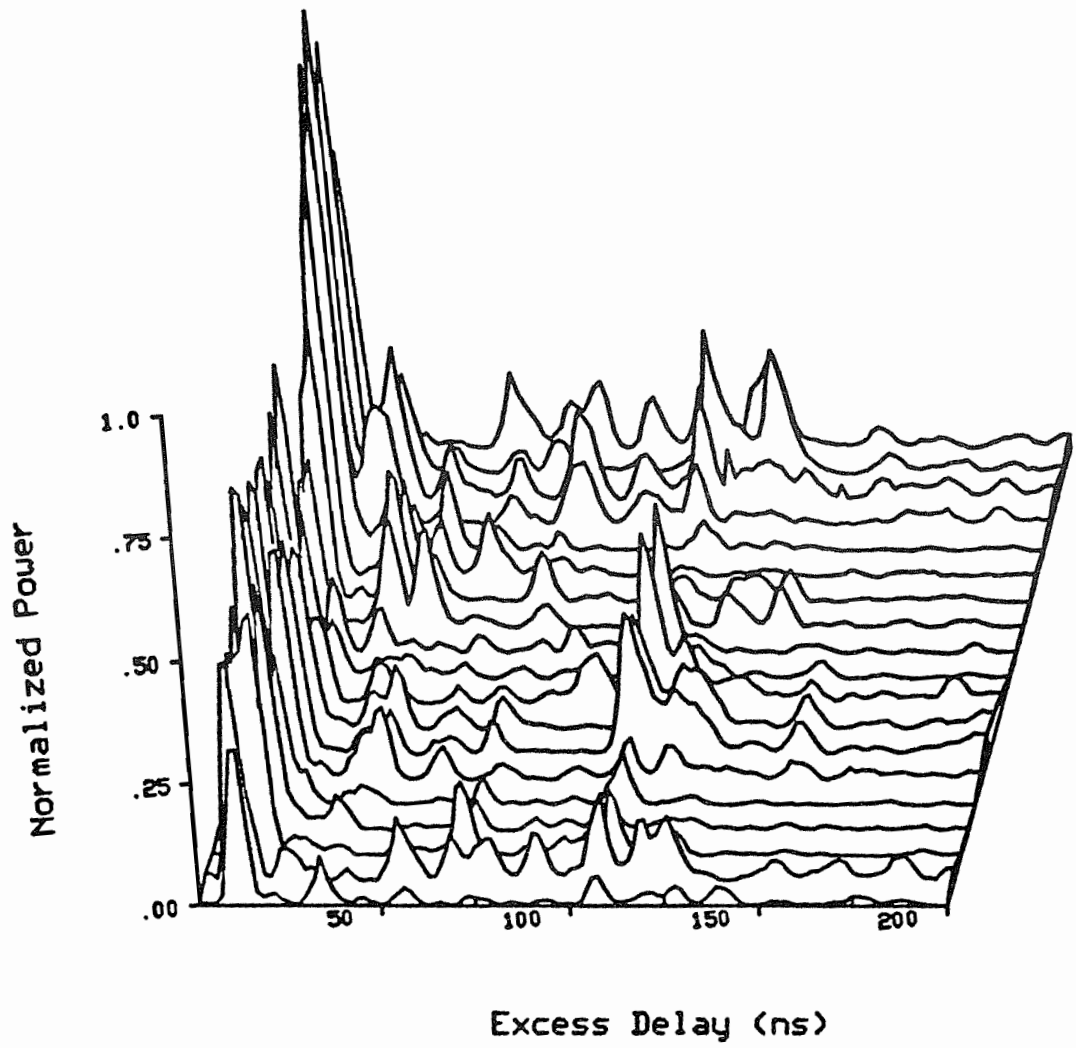
pd5ac



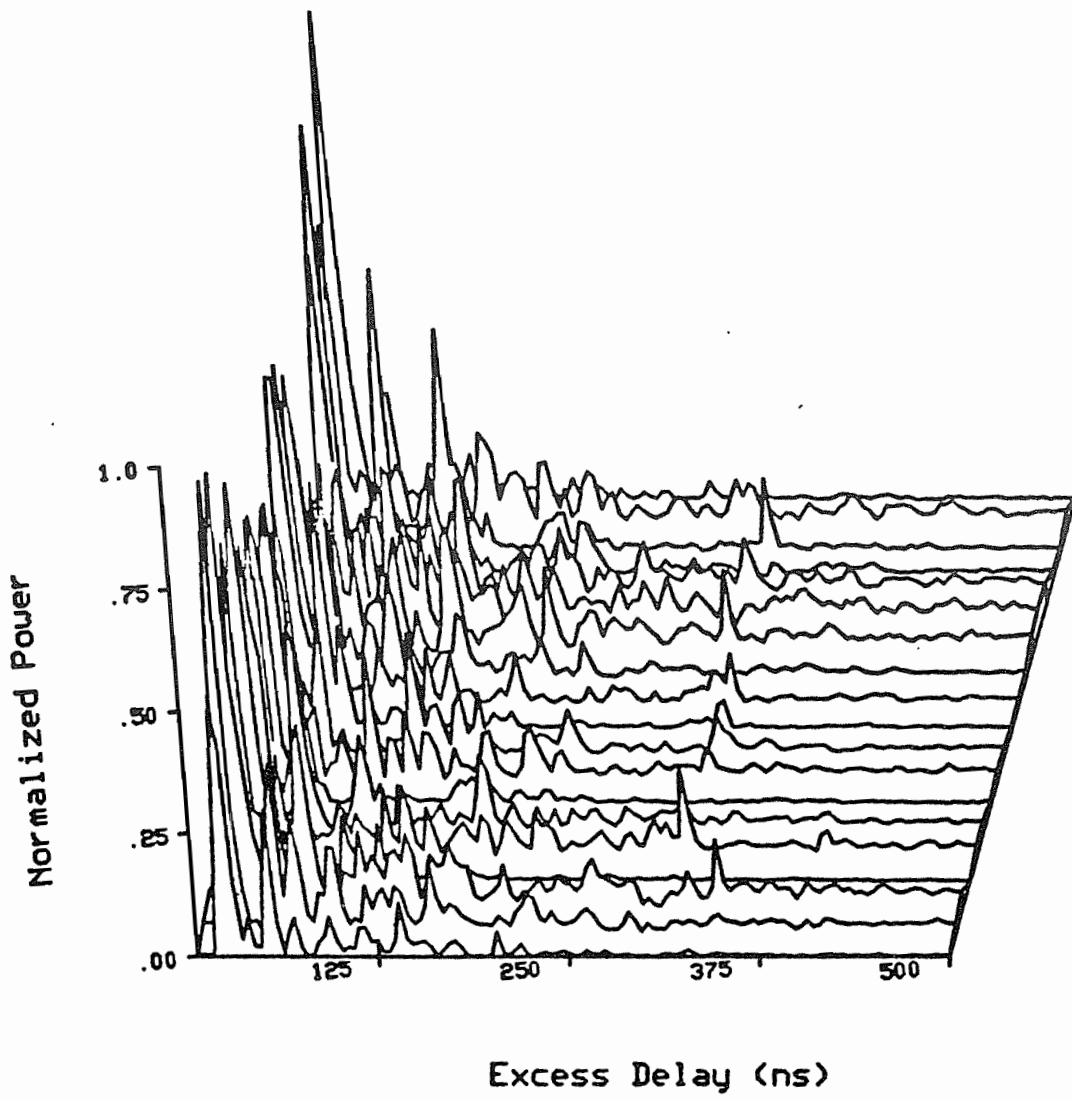
pd5bc



pd5cc

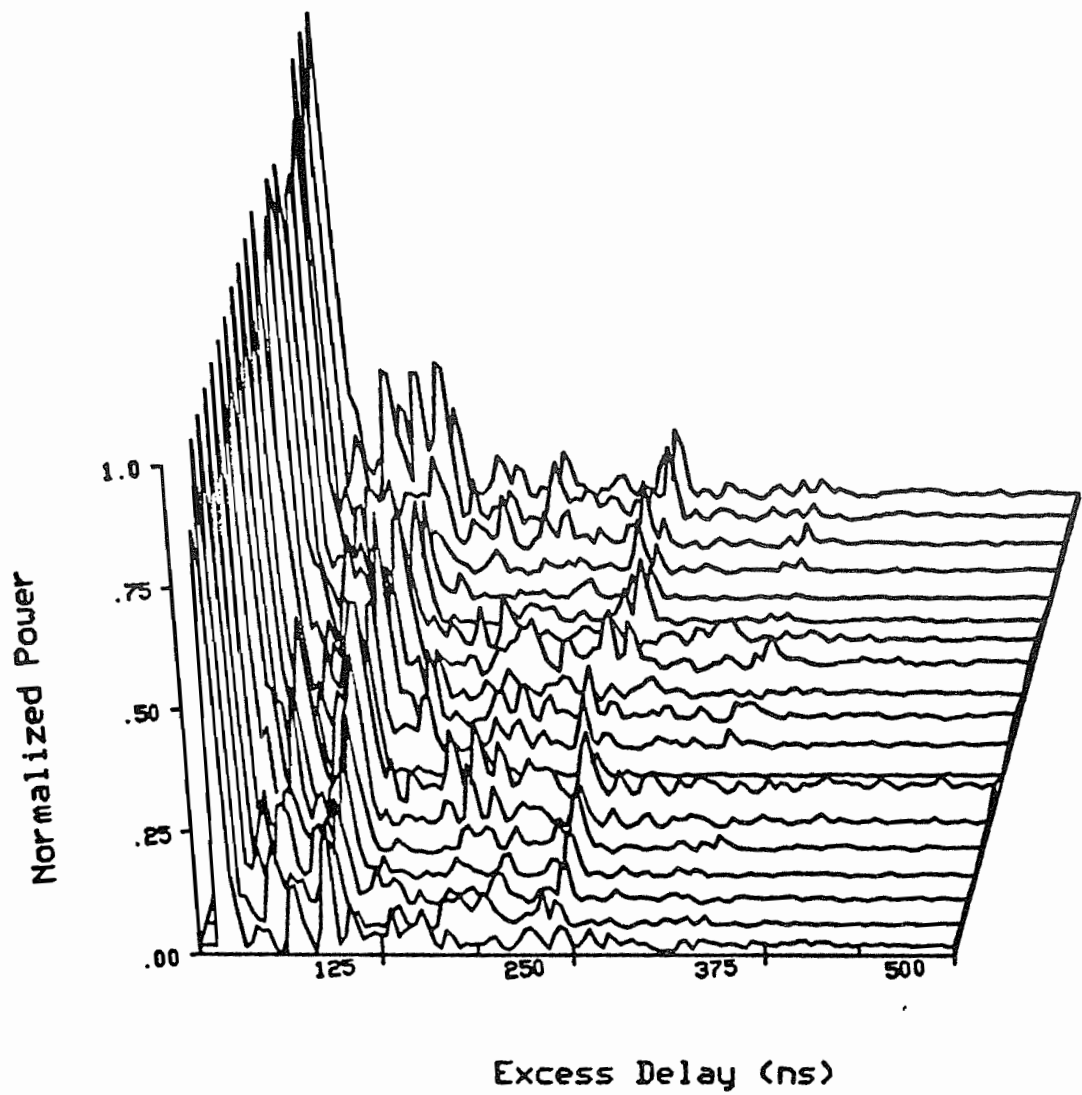


pe2ac

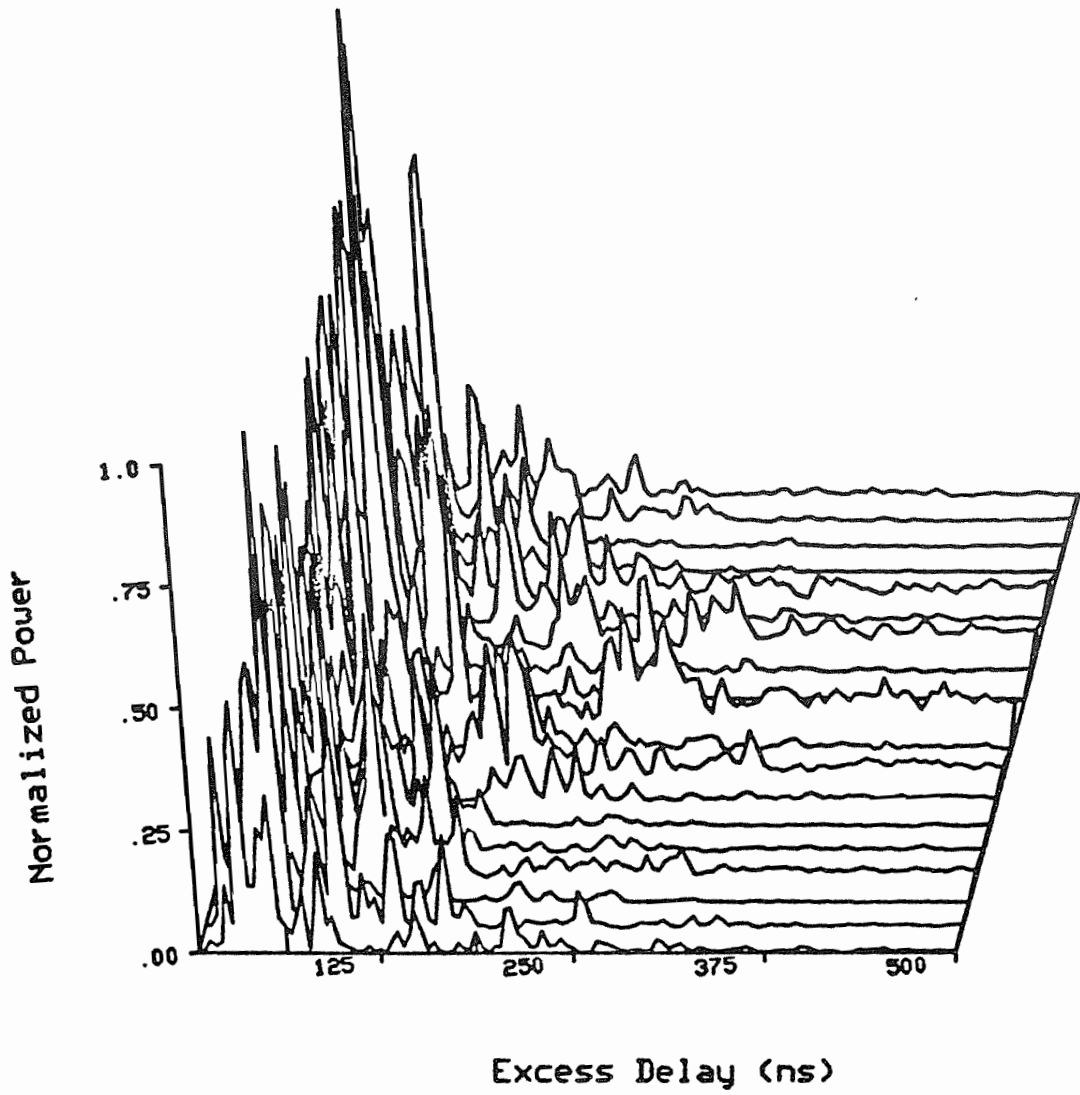


pe2bc

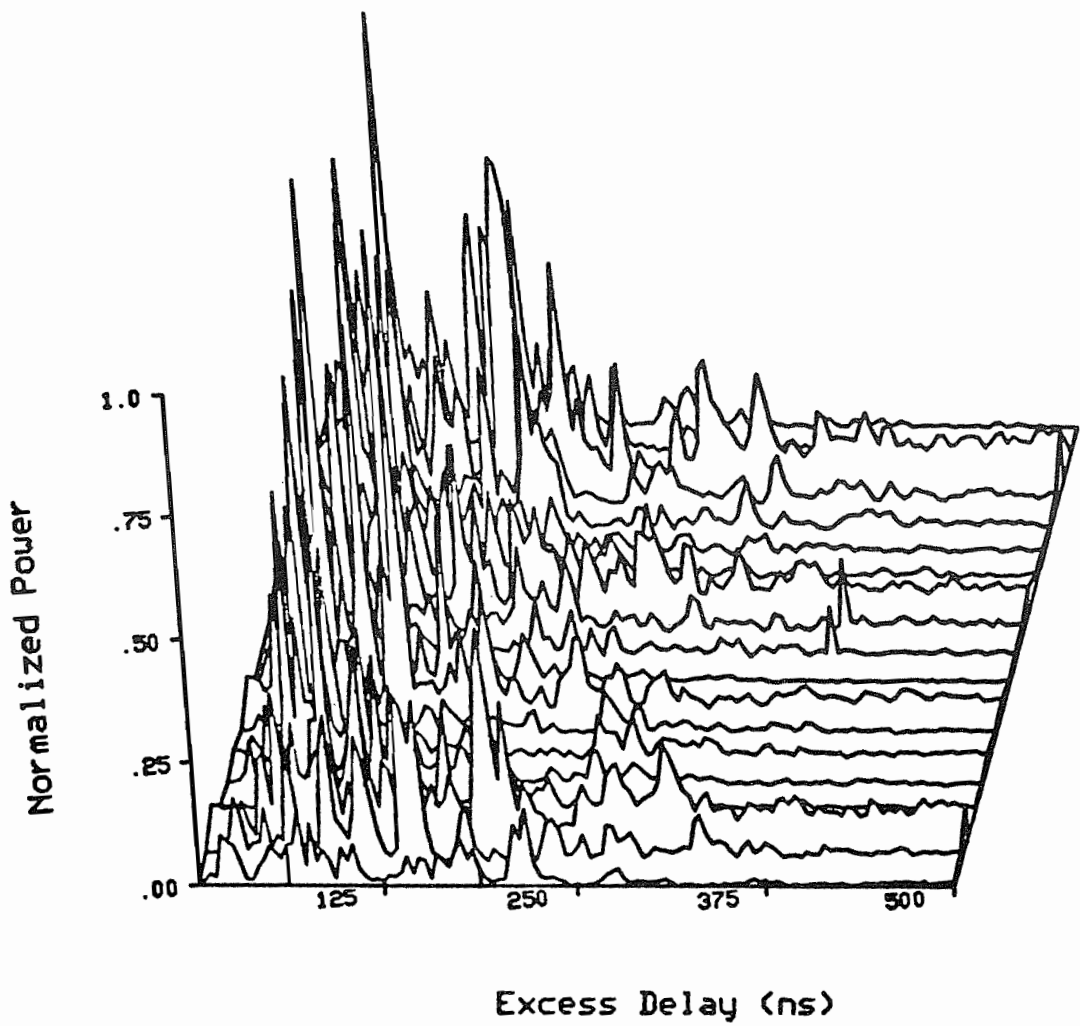




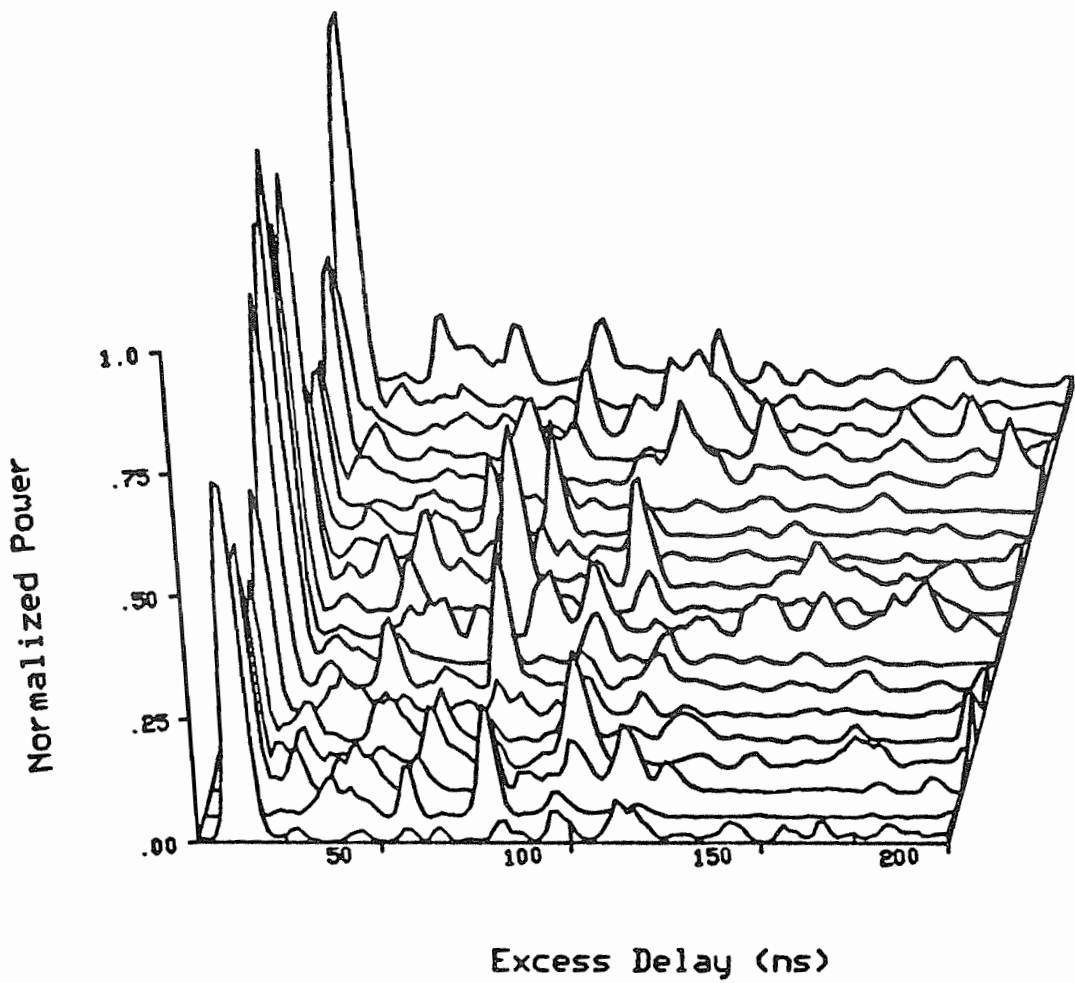
pe2cc



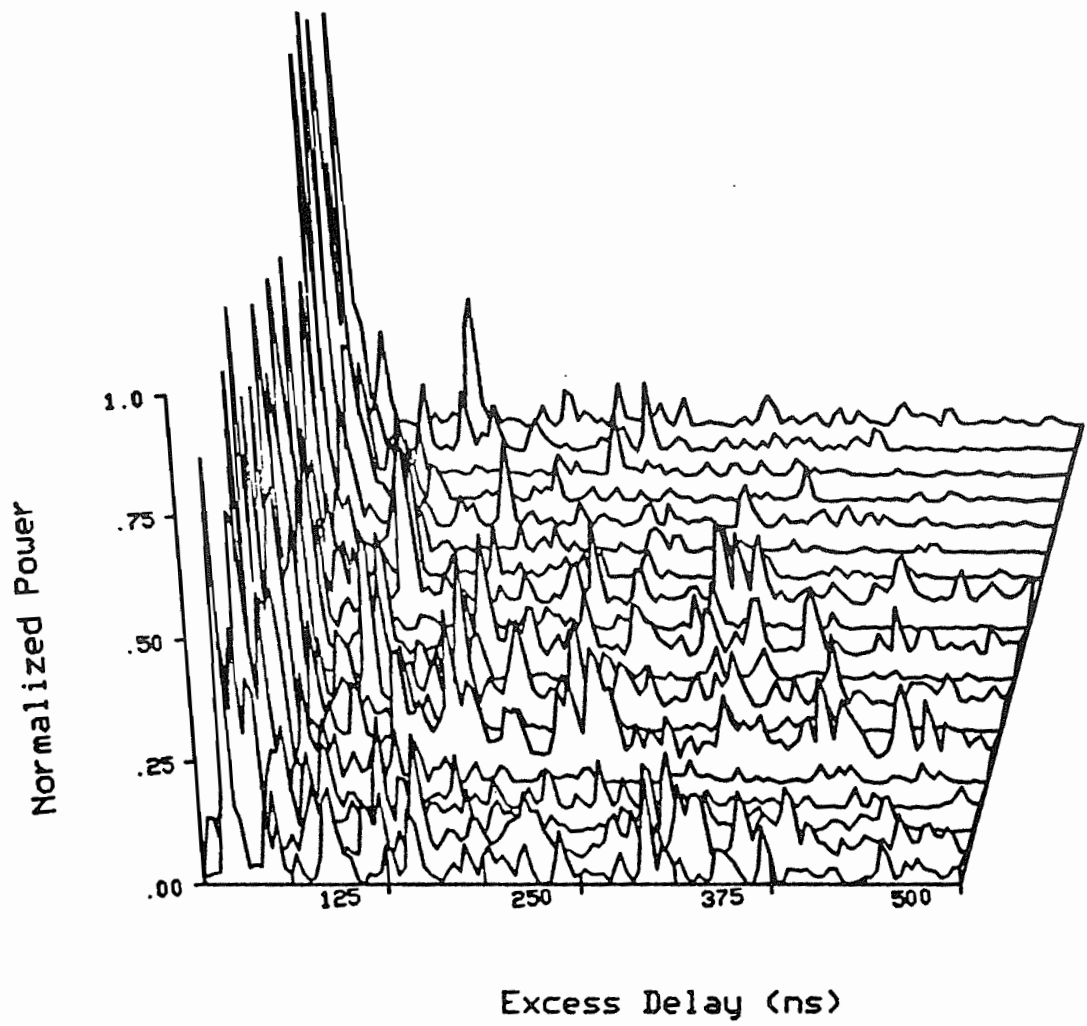
реџас



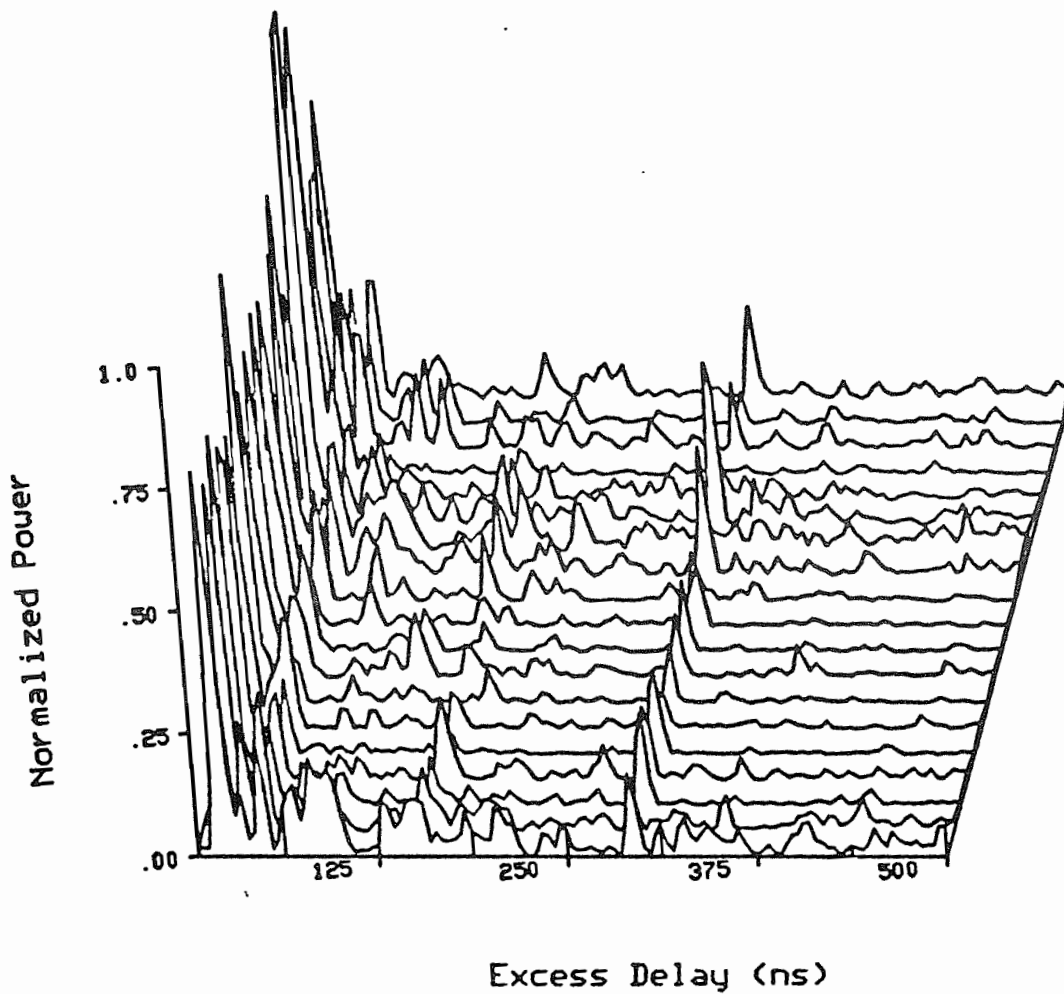
pe5bc



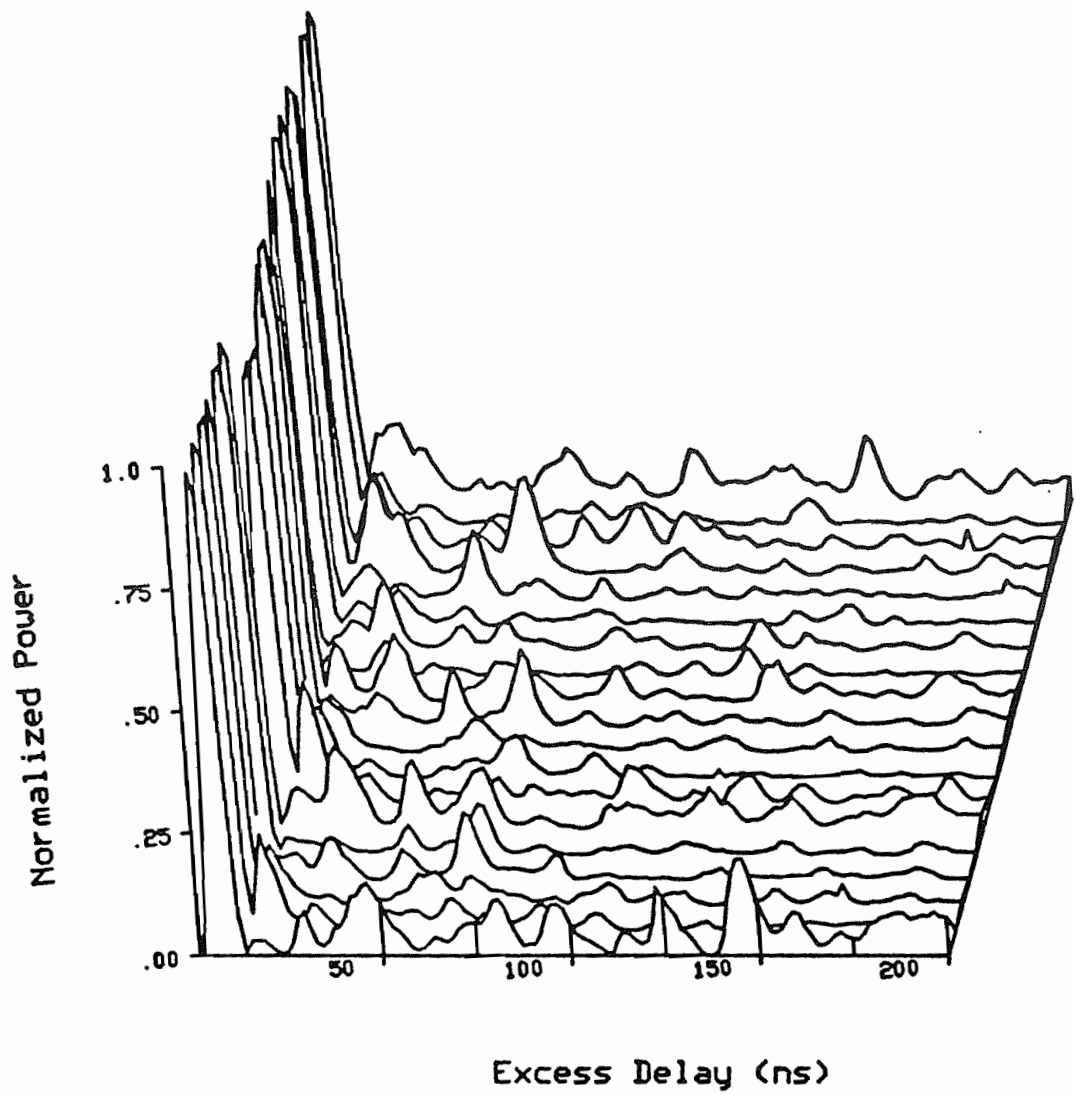
pe5cc



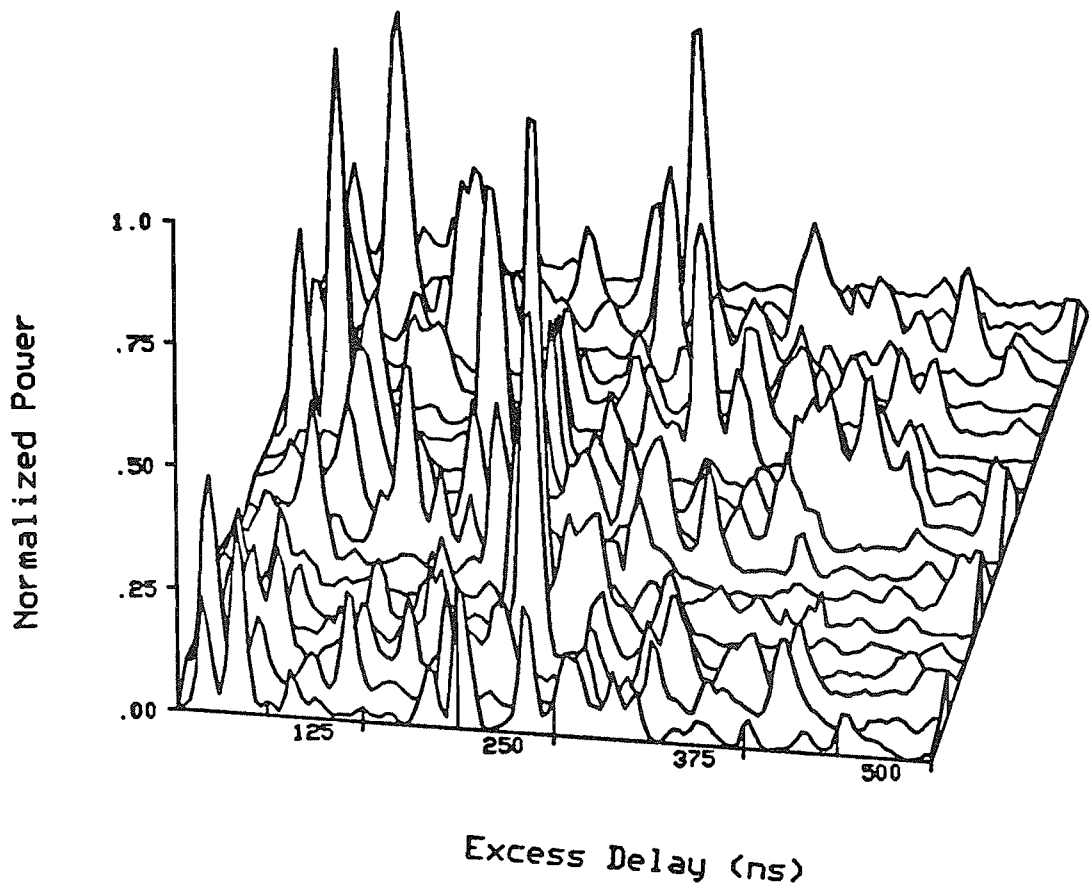
pf2ac



pf2bc

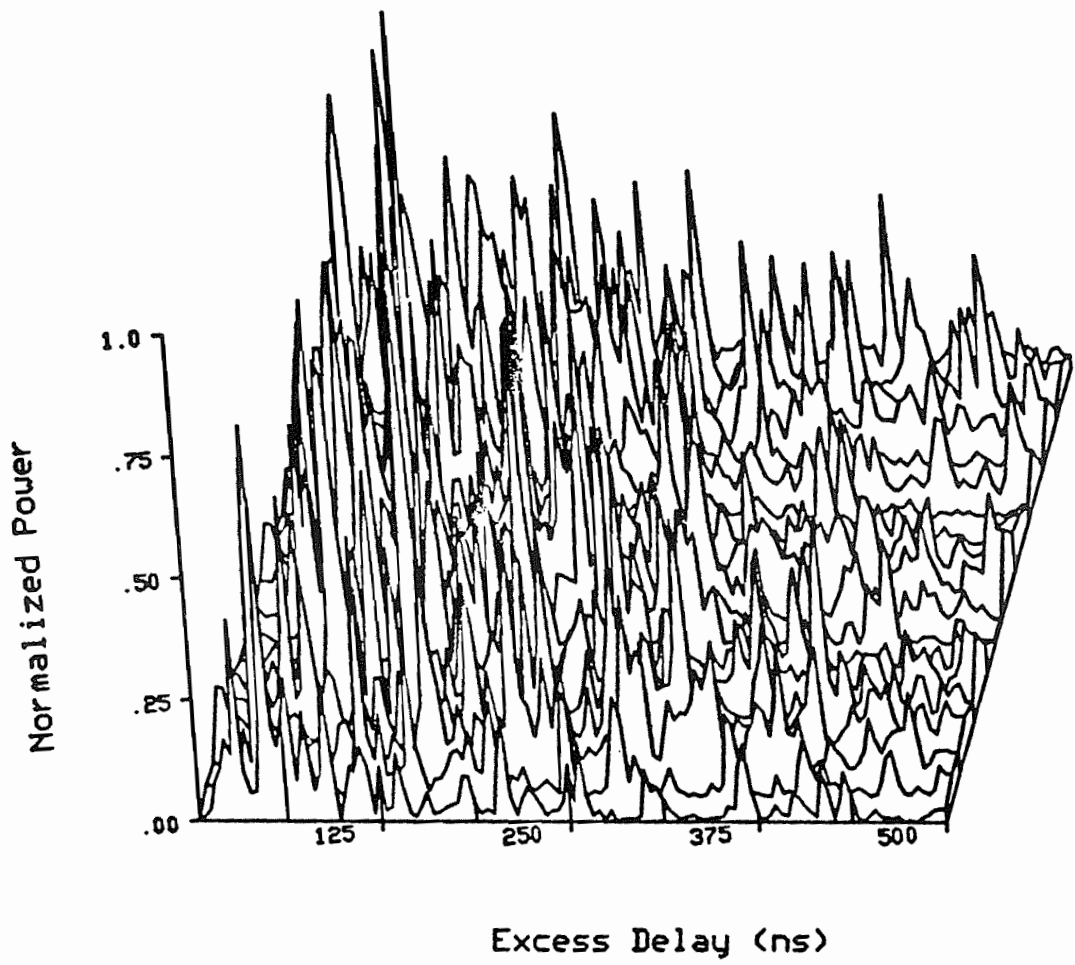


pf2cc

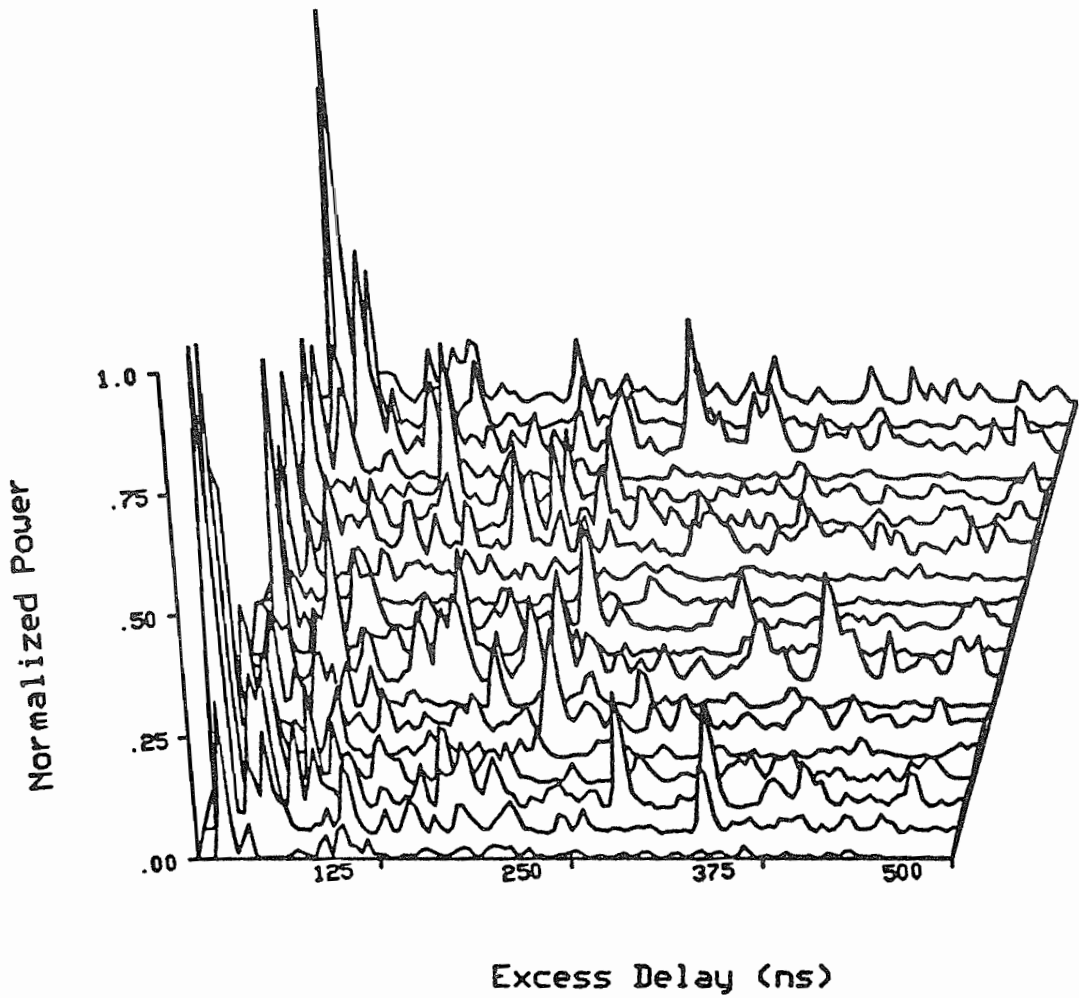


pf5ac





pf5bc



pf5cc

